Vol. 19. No 4, 2017

ISSN 1507-2711
Cena: 25 zł (w tym 5% VAT)

EKSPLOATACJAINIEZAWODNOŚĆ
MAINTENANCEANDRELIABILITY

Polskie Naukowo Techniczne Towarzystwo Eksploatacyjne
Warszawa

Polish Maintenance Society
Warsaw

The Journal is indexed and abstracted in the Journal Citation Reports (JCR Science Edition), Scopus, Science Citation Index Expanded (SciSearch®) and Index Copernicus International.

The Quarterly appears on the list of journals credited with a high impact factor by the Polish Ministry of Science and Higher Education and is indexed in the Polish Technical Journal Contents database – BAZTECH and the database of the Digital Library Federation.

All the scientific articles have received two positive reviews from independent reviewers.

Our 2016 Impact Factor is 1.145

Editorial staff:	Dariusz Mazurkiewicz, PhD, DSc (Eng), Associate Professor (Editor-in-Chief, Secretary of the Editorial Board) Tomasz Klepka, PhD, DSc (Eng), Associate Professor (Deputy Editor-in-Chief) Teresa Błachnio-Krolopp, MSc (Eng) (Editorial secretary) Andrzej Koma (Typesetting and text makeup) Krzysztof Olszewski, PhD (Eng) (Webmaster)
Publisher:	Polish Maintenance Society, Warsaw
Scientific patronage:	Polish Academy of Sciences Branch in Lublin
Address for correspondence:	"Eksploatacja i Niezawodność" – Editorial Office ul. Nadbystrzycka 36, 20-618 Lublin, Poland e-mail: office@ein.org.pl http://www.ein.org.pl/
Circulation:	550 copies

GÓMEZ CQM, GARCÍA FPM, JIMENEZ AJ, CHENG L, KOGIA M, MOHIMI A, PAPAELIAS M. **A heuristic method for detecting and locating faults employing electromagnetic acoustic transducers**. Eksploatacja i Niezawodnosc – Maintenance and Reliability 2017; 19 (4): 493–500, http://dx.doi.org/10.17531/ein.2017.4.1.

The objective of this paper is to demonstrate a novel signal processing for detection, identification and flaw sizing of structural damage using ultrasonic testing with Electromagnetic Acoustic Transducers (EMATs). Damage detection involves the recognition of a defect that exists within a structure. Damage location is the identification of the geometric position of the defect. Defect classification is the cluster of the damage type into multiple damage scenarios. In the absence of external interferences, a good measure of detectability of a flaw is its signal-to-noise ratio (SNR). Although the SNR depends on various parameters such as electronics used, material properties, e.g. homogeneity and damping, and flaw size, it can be improved using advanced signal processing. The main scientific novelties presented in this paper focus on filtering signal noise through advanced digital signal processing; incorporating wavelet transforms for image and signal representation enhancements; investigating multi-parametric analysis for noise identification and defect classification; studying attenuation curves properties for defect localisation improvement and flaw sizing and location algorithm development.

GÓMEZ CQM, GARCÍA FPM, JIMENEZ AJ, CHENG L, KOGIA M, MOHIMI A, PAPAELIAS M. **Heurystyczna metoda wykrywania i lokalizowania usterek z wykorzystaniem elektromagnetycznych przetworników akustycznych**. Eksploatacja i Niezawodnosc – Maintenance and Reliability 2017; 19 (4): 493–500, http://dx.doi.org/10.17531/ein.2017.4.1.

Celem niniejszego artykułu jest omówienie nowatorskiego sposobu przetwarzania sygnałów w celu wykrywania, identyfikacji i oceny uszkodzeń strukturalnych przy użyciu ultrasonograficznych testów za pomocą elektromagnetycznych przetworników akustycznych (EMAT). Wykrywanie uszkodzeń polega na rozpoznaniu istniejących defektów wewnątrz danej struktury. Lokalizacja uszkodzeń sprowadza się do identyfikacji geometrycznego położenia defektu. Klasyfikacja defektu to klaster typu uszkodzenia w wielu scenariuszach uszkodzeń. W przypadku braku zewnętrznych zakłóceń, dobrym wskaźnikiem wykrywalności błędu jest stosunek sygnału do szumu (SNR). Pomimo tego, że SNR zależy od różnych parametrów, takich jak użyta elektronika, właściwości materiału, np. jednorodność i tłumienie, a także wielkość wady, wskaźnik ten można poprawić przy użyciu zaawansowanego przetwarzania sygnałów. Główne nowe zagadnienia naukowe przedstawione w niniejszym artykule skupiają się na filtrowaniu szumu sygnału za pomocą zaawansowanego przetwarzania sygnału cyfrowego, w tym wykorzystując transformaty falkowe w celu ulepszenia obrazu i sygnału; badanie analizy wieloparametrycznej w celu identyfikacji szumów i klasyfikacji defektów; badanie właściwości krzywych osłabiania w celu sprawniejszego wykrywania i oceny wad oraz rozwoju algorytmu lokalizacji.

CHŁOPEK Z, BEBKIEWICZ K. **Model of the structure of motor vehicles for the criterion of the technical level on account of pollutant emission**. Eksploatacja i Niezawodnosc – Maintenance and Reliability 2017; 19 (4): 501-507, http://dx.doi.org/10.17531/ein.2017.4.2.

Inventory of total vehicle pollution emission is only possible through the use of emission modelling. One of the most difficult problems in modelling total emission from motor vehicles is the identification of the structure of vehicle fleet. While it is possible to use vehicle registration data to model the numerosity of elementary vehicle categories, it is very difficult to design representative driving cycles for vehicles in separate categories, in the absence of empirical evidence. The article proposes two models of the structure of motor vehicles for the criterion of technical level on account of pollutant emission. The method of modelling the intensity of use of motor vehicles by elementary categories on account of pollutant emission, outlined in this article, is the first unique undertaking in this field on a global scale. This method was used for inventorying pollutant emission from motor vehicles in Poland, in the years 2000–2015.

CHŁOPEK Z, BEBKIEWICZ K. **Model struktury pojazdów samochodowych dla kryterium poziomu technicznego ze względu na emisję zanieczyszczeń**. Eksploatacja i Niezawodnosc – Maintenance and Reliability 2017; 19 (4): 501-507, http://dx.doi.org/10.17531/ein.2017.4.2.

Inwentaryzacja całkowitej emisji zanieczyszczeń samochodowych jest możliwa tylko dzięki zastosowania modelowania emisji zanieczyszczeń. Jednym z najtrudniejszych problemów modelowania całkowitej emisji zanieczyszczeń z pojazdów samochodowych jest identyfikacja ich struktury. O ile jest możliwe wykorzystanie danych związanych z rejestracją pojazdów samochodowych do modelowania liczności kategorii pojazdów samochodowych, o tyle wyznaczenie reprezentatywnych przebiegów pojazdów elementarnych kategorii jest zadaniem bardzo trudnym ze względu na brak wyników badań empirycznych. W artykule zaproponowano dwa modele struktury pojazdów samochodowych dla kryterium poziomu technicznego ze względu na emisję zanieczyszczeń. Przedstawiony w niniejszym artykule sposób modelowania intensywności użytkowania pojazdów samochodowych kategorii elementarnych ze względu na emisję zanieczyszczeń jest pierwszym unikatowym przedsięwzięciem w tym zakresie w skali światowej. Metodę tę zastosowano do inwentaryzacji zanieczyszczeń pojazdów samochodowych w Polsce w latach 2000–2015.

KOSUCKI A, MALENTA P, STAWIŃSKI Ł, HALUSIAK S. **Energy consumption and overloads of crane hoisting mechanism with system of reducing operational loads**. Eksploatacja i Niezawodnosc – Maintenance and Reliability 2017; 19 (4): 508–515, http://dx.doi.org/10.17531/ein.2017.4.3.

The paper presents the study of the hoisting mechanism for various lifting cases. For the developed method of reducing an operating overloads of the driving system of the hoisting mechanisms, studies of the energy consumption of the cycle and the dynamic overloads of the drive (and bearing structure) have been conducted in comparison with other methods of the payload lifting. The influence of a start-up time on the overloads and energy overloads of the mechanism was determined, taking into account the whole duty cycle time. Using the proposed start-up time, the influence of a lifting height and a weight of the lifted load on the drive overload and duty cycle power consumption were shown. Studies have shown good operating properties of a drive with overloads compensation system.

KOSUCKI A, MALENTA P, STAWIŃSKI Ł, HALUSIAK S. **Energochłonność i przeciążalność mechanizmu podnoszenia suwnicy z układem zmniejszania obciążeń eksploatacyjnych**. Eksploatacja i Niezawodnosc – Maintenance and Reliability 2017; 19 (4): 508–515, http://dx.doi.org/10.17531/ein.2017.4.3.

W artykule przedstawiono badania mechanizmu podnoszenia dla różnych przypadków podnoszenia ładunku. Dla opracowanej metody zmniejszania przeciążeń eksploatacyjnych układu napędowego mechanizmów podnoszenia przeprowadzono badania porównawcze energochłonności cyklu roboczego i przeciążalności dynamicznej napędów (i konstrukcji nośnej) w stosunku do innych sposobów rozruchu. Określony został wpływ czasu rozruchu na przeciążalność i przeciążalność energetyczną mechanizmu z uwzględnieniem czasu całego cyklu roboczego. Przedstawiono badania wpływu wysokości podnoszenia i masy podnoszonego ładunku na przeciążalność mechanizmu i energochłonność cyklu roboczego. Badania wykazały dobre własności eksploatacyjne napędu wykorzystującego metody kompensacji przeciążeń.

TRZMIEL G. **Determination of a mathematical model of the thin-film photovoltaic panel (CIS) based on measurement data**. Eksploatacja i Niezawodnosc – Maintenance and Reliability 2017; 19 (4): 516–521, http://dx.doi.org/10.17531/ein.2017.4.4.

In this paper the author attempted to determine the most accurate mathematical model of the photovoltaic panel composed of a monolithic structure of series connected Copper Indium Diselenide (CIS) based solar cells, based on its actual measurement data. The purpose of this paper has been achieved by implementing the original applications which, using the methods of approximation, made it possible to design the final mathematical model of the tested panel, characterized by the minimum of error modelling. Using the known literature on the operation of similar facilities, the model parameters were determined directly from the collection of random measurement data; then the obtained models were verified by several different statistical methods. As a result, the best model was selected, based on the smallest dispersion of the theoretical values (simulated) calculated from the model relative to the actual measurements. The model will be used in practice in the future to evaluate the condition (inefficiency, use) of photovoltaic panels, what will be the theme of following articles.

TRZMIEL G. **Wyznaczanie modelu matematycznego cienkowarstwowego panelu fotowoltaicznego (CIS) na podstawie danych pomiarowych**. Eksploatacja i Niezawodnosc – Maintenance and Reliability 2017; 19 (4): 516–521, http://dx.doi.org/10.17531/ein.2017.4.4.

W artykule autor dąży do określenia, w oparciu o rzeczywiste dane pomiarowe, najbardziej dokładnego modelu matematycznego panelu fotowoltaicznego, składającego się z monolitycznej struktury połączonych szeregowo ogniw fotowoltaicznych typu CIS. Cel pracy został osiągnięty poprzez wdrożenie oryginalnych aplikacji, które przy użyciu metod aproksymacji umożliwiły zaprojektowanie ostatecznego modelu matematycznego badanego panelu, charakteryzującego się minimalnym błędem modelowania. Wykorzystując literaturę tematu dotyczącą działania podobnych obiektów nieliniowych, parametry modelu zostały określone bezpośrednio z wcześniej zarchiwizowanych losowych danych pomiarowych. Następnie uzyskane modele zweryfikowano kilkoma różnymi metodami statystycznymi. W wyniku tego wybrano najlepszy model, oparty na najmniejszej dyspersji wartości teoretycznych (symulowanych) obliczonej z modelu w stosunku do rzeczywistych pomiarów. Otrzymany model zostanie w przyszłości zastosowany w praktyce do oceny stanu (niesprawności, zużycia) paneli fotowoltaicznych, co będzie tematem kolejnych artykułów.

MERKISZ J, RYMANIAK Ł. **The assessment of vehicle exhaust emissions referred to CO_2 based on the investigations of city buses under actual conditions of operation**. Eksploatacja i Niezawodnosc – Maintenance and Reliability 2017; 19 (4): 522–529, http://dx.doi.org/10.17531/ein.2017.4.5.

The paper discusses the assessment of the exhaust emissions from heavy-duty vehicles following investigations under actual traffic conditions. The environmental characteristics presented thus far were mainly based on unit or road emissions. The paper presents an analysis of exhaust emissions referred to the harmful CO_2, which was assumed as measure of correctness of the combustion process. The parameters determining this way are referred to as emission indexes. The research objects were 18-meter city buses fitted with three types of powertrains: conventional engine, hybrid (electric motor combined with a diesel engine) and a spark ignition engine fuelled with compressed natural gas (CNG). All buses were Euro V–EEV compliant. The measurements were performed according to the SORT 2 driving test procedure on the test route within the Poznan agglomeration. Investigations performed under actual traffic conditions allow a true assessment of environmental performance of a given research object because they cover a much greater engine operating parameter variability range compared to laboratory and homologation tests. The performed road tests and their analysis led to conclusions related to the applicability of the developed method of emission assessment based on emission indexes for vehicles fitted with different powertrains.

MERKISZ J, RYMANIAK Ł. **Ocena emisji zanieczyszczeń z pojazdów w odniesieniu do CO_2 na podstawie badań autobusów miejskich w rzeczywistych warunkach eksploatacji**. Eksploatacja i Niezawodnosc – Maintenance and Reliability 2017; 19 (4): 522–529, http://dx.doi.org/10.17531/ein.2017.4.5.

W artykule przedstawiono rozważania dotyczące oceny emisji zanieczyszczeń z pojazdów ciężkich na podstawie badań realizowanych w rzeczywistych warunkach eksploatacji. Przedstawiane do tej pory charakterystyki ekologiczne silnikowych środków transportu opierały się przede wszystkim na emisji jednostkowej lub drogowej. W pracy przedstawiono analizę emisji związków toksycznych odniesioną do związku szkodliwego CO_2, dla którego założono, że jest miarą poprawności realizacji procesu spalania. Wyznaczone w ten sposób parametry nazwano wskaźnikami toksyczności. Obiekty badawcze stanowiły osiemnastometrowe autobusy miejskie wyposażone w trzy rodzaje układów napędowych: konwencjonalny i hybrydowy z silnikami ZS, a także pojazd zasilany sprężonym gazem ziemnym z silnikiem ZI. Wszystkie autobusy spełniały normę Euro V–EEV. Pomiary wykonano zgodnie z procedurą testu jezdnego SORT 2 oraz na trasie badawczej w aglomeracji poznańskiej. Badania w warunkach rzeczywistej eksploatacji pozwalają dokonać rzetelnej oceny ekologiczności danego obiektu badawczego, ponieważ obejmują znacznie większy obszar zmienności parametrów pracy silników spalinowych w porównaniu z laboratoryjnymi testami homologacyjnymi. Wykonane badania drogowe i ich analiza pozwoliły na sformułowanie wniosków dotyczących słuszności stosowania opracowanej metody oceny emisji zanieczyszczeń, bazującej na wskaźnikach toksyczności, dla pojazdów wyposażonych w różne rodzaje układów napędowych.

WANG ZB, SHANG S, WANG JW, HUANG ZL, SAI F. **Accelerated storage degradation testing and failure mechanisms of aerospace electromagnetic relay**. Eksploatacja i Niezawodnosc – Maintenance and Reliability 2017; 19 (4): 530–541, http://dx.doi.org/10.17531/ein.2017.4.6.

It is difficult to obtain the failure data of high-reliability and long-lifetime aerospace electromagnetic relay (EMR), even if based on the traditional accelerated storage life testing method. Based on the reliability test technique, the scheme of accelerated degradation testing for aerospace EMR was designed. The test system of aerospace electromagnetic relay storage parameters under temperature-accelerated stress was designed and developed. The most past research on storage reliability of relay only focuses on the measurement of contact resistance. The relay time parameters (pick-up time, opening time, overtravel time, rebound duration time, etc.) which reflect main performance function were not monitored. So, in this study the relay time parameters and relay contact resistance were detected simultaneously. According to the analysis on experiment results of contact resistance, relay time parameters, the degradation phenomena of aerospace EMR in long-term storage are investigated, which provides the bases for determining degradation sensitive parameters. Finally, based on the structure and function of aerospace EMR, the storage failure mechanism is investigated by conductive properties themselves. The microscopic morphology and changes in chemical elements for relay contact surface was analyzed by SEM and EDX regularly, which provide references for the relay storage failure mechanism.

WANG ZB, SHANG S, WANG JW, HUANG ZL, SAI F. **Badania przyspieszone degradacji w czasie składowania przekaźników elektromagnetycznych stosowanych w przemyśle lotniczym oraz mechanizmów ich uszkodzeń**. Eksploatacja i Niezawodnosc – Maintenance and Reliability 2017; 19 (4): 530–541, http://dx.doi.org/10.17531/ein.2017.4.6.

Ze względu na wysoką niezawodność i długi cykl życia przekaźników elektromagnetycznych stosowanych w przemyśle lotniczym (EMR), trudno jest uzyskać dane o ich uszkodzeniach, nawet gdy korzysta się z tradycyjnej metody przyspieszonych badań dopuszczalnego okresu składowania. W przedstawionym artykule, opracowano, w oparciu o technikę badania niezawodności, schemat przyspieszonego badania degradacji przekaźników elektromagnetycznych stosowanych w lotnictwie. Zaprojektowano i opracowano system oceny parametrów składowania przekaźników elektromagnetycznych używanych w lotnictwie w warunkach przyspieszonych przy skrajnych temperaturach. Ostatnie badania nad niezawodnością składowania przekaźników koncentrują się wyłącznie na pomiarze rezystancji styku. Nie były w nich monitorowane parametry czasowe przekaźnika (czas załączania, czas otwarcia, czas opóźnienia, czas trwania odbicia itp.), które odzwierciedlają jego główne funkcje. W przedstawionych badaniach mierzono jednocześnie parametry czasowe przekaźników i rezystancję styków. W oparciu o analizę uzyskanych wyników doświadczeń, badano zjawiska degradacji EMR podczas ich długoterminowego składowania, co stanowiło podstawę do wyznaczenia parametrów wrażliwych na degradację. Wreszcie, w oparciu o strukturę i funkcje EMR, badano mechanizm powstawania uszkodzeń podczas ich składowania na podstawie właściwości przewodzących. Prowadzone regularnie metodami SEM i EDX analizy budowy mikroskopowej oraz przemian pierwiastków chemicznych zachodzących na powierzchni styków przekaźnika stanowią odniesienie dla badań mechanizmu powstawania uszkodzeń podczas składowania przekaźników.

PIETRUSIAK D. **Evaluation of large-scale load-carrying structures of machines with the application of the dynamic effects factor**. Eksploatacja i Niezawodnosc – Maintenance and Reliability 2017; 19 (4): 542–551, http://dx.doi.org/10.17531/ein.2017.4.7.

Load-carrying structures of large-scale machines are their key element, mainly due to their size which renders them virtually impossible to replace during operation. Such structures are used for example in the heavy industry, mining, bulk material handling or rock processing. This article presents the most important results of recent research into dynamic loads and design of such structures. Based on these results the article introduces the author's method of evaluating load-carrying structures with the application of the dynamic effects factor and describes the effects of the application of this method.

PIETRUSIAK D. **Ocena wielkogabarytowych ustrojów nośnych maszyn z zastosowaniem współczynnika obciążeń zastępczych**. Eksploatacja i Niezawodnosc – Maintenance and Reliability 2017; 19 (4): 542–551, http://dx.doi.org/10.17531/ein.2017.4.7.

Ustroje nośne maszyn wielkogabarytowych są ich kluczowym elementem, ze względu na ich rozmiar a tym samym niemalże brak możliwości wymiany w trakcie eksploatacji. Ustroje tego typu stosowane są np. w przemyśle wydobywczym, przeładunkowym czy przetwórstwa skalnego. W artykule zebrano i zaprezentowano wyniki najważniejszych badań ostatnich lat dotyczących obciążeń dynamicznych oraz projektowania tego rodzaju obiektów. Na tej podstawie przedstawiono autorską metodę oceny ustrojów nośnych z zastosowaniem współczynnika obciążeń zastępczych oraz efekty jej stosowania.

MARSARO MF, CAVALCANTE CAV. **Random preventive maintenance policy based on inspection for a multicomponent system using simulation**. Eksploatacja i Niezawodnosc – Maintenance and Reliability 2017; 19 (4): 552–559, http://dx.doi.org/10.17531/ein.2017.4.8.

In today's global situation where highly competitive companies demand production efficiently to reduce costs, increase product quality, and customer loyalty, maintenance becomes crucial to achieve this goal by reducing unplanned downtime, reworking of products, and costs. In this sense, the use of models that can represent this type of system, and help managers make decisions more easily, are of vital importance for companies. Thus, a preventive maintenance model for a multicomponent system with different failure mechanisms is proposed in this work. Considering that the objective is to optimize the number and the time of maintenance interventions, that will be done in the system, periodic inspections are carried out in order to minimize the expected costs of maintenance. The optimization was performed with simulation, which proved

MARSARO MF, CAVALCANTE CAV. **Oparta na przeglądach polityka losowej konserwacji zapobiegawczej systemu wieloelementowego z wykorzystaniem symulacji**. Eksploatacja i Niezawodnosc – Maintenance and Reliability 2017; 19 (4): 552–559, http://dx.doi.org/10.17531/ein.2017.4.8.

W dzisiejszej sytuacji globalnej, w której przedsiębiorstwa o wysokim stopniu konkurencyjności wymagają efektywnego obniżania kosztów produkcji, poprawy jakości produktów oraz zwiększania lojalności klientów, konserwacja ma zasadnicze znaczenie dla osiągnięcia tych celów poprzez redukcję nieplanowanych przestojów, oraz zmniejszenie konieczności usuwania usterek produktów a także obniżanie kosztów. W tym sensie, wykorzystanie modeli reprezentujących tego typu systemy i ułatwiające menedżerom podejmowanie decyzji , ma kluczowe znaczenie dla firm. W tej pracy zaproponowano model konserwacji zapobiegawczej dla wieloelementowego systemu o różnych mechanizmach uszkodzeń. Biorąc pod uwagę, że celem jest optymalizacja liczby i czasu trwania zabiegów konserwacyjnych dokonywanych w systemie, przeprowadzane są okresowe przeglądy mające na celu

to be satisfactory, since the decision variables of the model behaved adequately when utilized within the context of an applied case study. In addition, these variables had different performances when analyzed in four different scenarios: the original model of the proposed policy, and three variations attributing costs of penalties.

zminimalizowanie oczekiwanych kosztów utrzymania. Optymalizację przeprowadzono za pomocą symulacji, która okazała się zadowalająca, ponieważ zmienne decyzyjne modelu zachowywały się odpowiednio przy wykorzystaniu ich w kontekście omawianego studium przypadku. Dodatkowo, zmienne te przybierały różne wartości dla czterech różnych scenariuszy: pierwotnego modelu proponowanej polityki konserwacyjnej i trzech wariantów, w których uwzględniono koszty pracy systemu w stanie awaryjnym.

EKIELSKI A, ŻELAZIŃSKI T, DURCZAK K. **The use of wavelet analysis to assess the degree of wear of working elements of food extruders**. Eksploatacja i Niezawodnosc – Maintenance and Reliability 2017; 19 (4): 560–564, http://dx.doi.org/10.17531/ein.2017.4.9.

The paper presents the evaluation of the wear status of the single-screw extruder working elements on the basis of die pressure and screw load toque load values changes. The changes of this parameters were analyzed as frequency spectrum using the tools of wavelet analysis. In the study plan the hypothesis was formulated that the assessment of extruder elements wear level is possible through observation of the frequency of process parameters changes. Due to the dynamic characteristics of the process in the determination of natural frequencies Morlet wavelet transform was used. Research was carried out for three heights of longitudinal wedges: 4, 2 and 1 mm. During experiment the extruder drive line load and the extruder screw speed were changed. It has been found that based on the observation of changes in resonant frequencies, it is possible to accurately assess the wear degree of friction elements in a single screw extruder. Moreover, it has been noted that the wavelet analysis may be an effective tool for the assessment of the extruder working elements wear level.

EKIELSKI A, ŻELAZIŃSKI T, DURCZAK K. **Wykorzystanie analizy falkowej do oceny stopnia zużycia elementów roboczych ekstruderów spożywczych**. Eksploatacja i Niezawodnosc – Maintenance and Reliability 2017; 19 (4): 560–564, http://dx.doi.org/10.17531/ein.2017.4.9.

W pracy przedstawiono ocenę stanu zużycia elementów roboczych ekstrudera jednoślimakowego na podstawie obserwacji zmian składowych częstotliwościowych widma obciążenia układu napędowego ślimaka ekstrudera i ciśnienia w matrycy przy wykorzystaniu narzędzi analizy falkowej. W planie badań sformułowano hipotezę, że możliwa jest ocena stopnia zużycia elementów roboczych ekstrudera przez obserwację częstotliwości zmian parametrów procesowych. Ze względu na dynamiczne cechy procesu przy wyznaczeniu częstotliwości własnych wykorzystano falkę Morlet'a. Badania przeprowadzono dla trzech wysokości klinów wzdłużnych 4, 2 i 1 mm. Podczas eksperymentu zmieniano obciążenia ekstrudera oraz prędkość obrotową ślimaka. Stwierdzono, że na podstawie obserwacji zmian częstotliwości rezonansowych można precyzyjnie oszacować stopień zużycia elementów ciernych w ekstruderze jednoślimakowym. Ponadto zaobserwowano, że analiza falkowa może być skutecznym narzędziem oceny stopnia zużycia elementów roboczych ekstrudera.

SKOCZYLAS L, WYDRZYŃSKI D. **Operational tests of worm gearbox with ZK2 concave profile**. Eksploatacja i Niezawodnosc – Maintenance and Reliability 2017; 19 (4): 565–570, http://dx.doi.org/10.17531/ein.2017.4.10.

The article presents an operational tests of worm gearboxes. Test bench trails were conducted for three gearbox types. Two of these gearboxes were manufactured using modern methods with conical endmills. The only difference between the two is the tooth profile. A ZK2 worm with a concave tooth profile and Archimedes' screw was used in the gearboxes. The third analyzed gearbox was a commercial gearbox with a ZK1 worm. When comparing the results of the analysis, the efficiency and load carrying capacity of the ZK2 worm gearbox is the highest and greatest respectively. The higher load carrying capacity of the ZK2 worm with concave teeth in comparison to the Archimedes' screw is confirmed by Hertz's theory. The results show, that the meshing area for ZK2 worm gearboxes is greater than Archimedes' screw. The confirmed increase of usage indicators of concave profile worm gearboxes can lead to their widespread production and application. The higher efficiency of the gearbox results in lower usage costs.

SKOCZYLAS L, WYDRZYŃSKI D. **Badania eksploatacyjne przekładni ślimakowej z wklęsłym zarysem ZK2**. Eksploatacja i Niezawodnosc – Maintenance and Reliability 2017; 19 (4): 565–570, http://dx.doi.org/10.17531/ein.2017.4.10.

W artykule przedstawiono badania eksploatacyjne przekładni ślimakowych. Badaniom stanowiskowym poddano trzy przekładnie. Dwie z nich zostały wykonane nową technologią z wykorzystaniem stożkowych narzędzi trzpieniowych. Różnica pomiędzy nimi dotyczyła wyłącznie zarysu kół. Zastosowano przekładnie ze ślimakiem ZK2 o wklęsłym zarysie oraz ślimakiem Archimedesa. Trzecią badaną przekładnią była przekładnia handlowa ze ślimakiem ZK1. Z porównania otrzymanych charakterystyk wynika, że sprawność i obciążalność przekładni ze ślimakiem ZK2 jest najwyższa. Wyższa nośność przekładni z wklęsłym zarysem ZK2 w stosunku do zarysu Archimedesa znajduje potwierdzenie w teorii Hertza. Uzyskane charakterystyki pokazują, że obszar zazębienia dla przekładni ze ślimakiem ZK2 jest większy w porównaniu z przekładnią Archimedesa. Potwierdzony wzrost wskaźników eksploatacyjnych przekładni ze ślimakiem o zarysie wklęsłym może przyczynić się do powszechnej ich produkcji i stosowania. Wyższa sprawność przekładni to zarazem niższe koszty jej eksploatacji.

MITURA A, GAWRYLUK J, TETER A. **Numerical and experimental studies on the rotating rotor with three active composite blades**. Eksploatacja i Niezawodnosc – Maintenance and Reliability 2017; 19 (4): 571–579, http://dx.doi.org/10.17531/ein.2017.4.11.

In this paper, the dynamic behaviour of active composite blades were considered. Both numerical and experimental studies were performed. It was assumed that the rotor hub would be rotated at constant velocity. Experimental measurements were made. A special test rig was built which consisted of an active rotor with three composite blades, an electric drive system and a system of Digital Signal Processors. This DSP system was used for the excitation of the blades, control of the hub's rotary velocity and data acquisition. The MFC patch and strain-gauge sensors were used. The influence of the hub's rotary velocity and/or piezoelectric effect on the dynamic behaviour of the blades was determined. The numerical simulations were performed using two commercial simulation programmes: Abaqus and Matlab.

MITURA A, GAWRYLUK J, TETER A. **Badania numeryczne i eksperymentalne wirującego wirnika z trzema aktywnymi łopatami kompozytowymi**. Eksploatacja i Niezawodnosc – Maintenance and Reliability 2017; 19 (4): 571–579, http://dx.doi.org/10.17531/ein.2017.4.11.

W niniejszej pracy przedstawiono dynamikę aktywnych łopat kompozytowych. Przeprowadzono badania numeryczne i eksperymentalne. Założono, że wirnik obraca się ze stałą prędkością obrotową. Pomiary doświadczalne wykonano na stanowisku badawczym, składającym się z aktywnego wirnika z trzema łopatami, elektrycznego układu napędowego oraz procesora sygnałowego DSP. Układ elektroniczny z procesorem wykorzystano do wzbudzania łopat, kontroli prędkości obrotowej oraz pozyskania danych pomiarowych. W badaniach laboratoryjnych użyto elementy aktywne typu MFC oraz czujniki tensometryczne. W pracy określono wpływ prędkości obrotowej piasty oraz efektu piezoelektrycznego na dynamikę łopat. Symulacje numeryczne przeprowadzono z zastosowaniem programów: Abaqus oraz Matlab.

DUAN R, HU L, Lin Y. **Fault diagnosis for complex systems based on dynamic evidential network and multi-attribute decision making with interval numbers**. Eksploatacja i Niezawodnosc – Maintenance and Reliability 2017; 19 (4): 580–589, http://dx.doi.org/10.17531/ein.2017.4.12.

The complexity of modern system structures and failure mechanisms makes it very difficult to locate the system fault. It has characteristics of dynamics of failure, diversity of distribution and epistemic uncertainties, which increase the challenges in the fault diagnosis significantly. This paper presents a fault diagnosis framework for complex systems within which the failure rates of components are expressed in interval numbers. Specifically, it uses a dynamic fault tree (DFT) to model the dynamic fault behaviors and deals with the epistemic uncertainties using Dempster-Shafer (D-S) theory and interval numbers. Furthermore, a solution is proposed to map a DFT into a dynamic evidential network (DEN) to calculate the reliability parameters. Additionally, diagnostic importance factor (DIF), Birnbaum importance measure (BIM) and heuristic information values (HIV) are taken into account comprehensively in order to obtain the best fault search scheme using an improved VIKOR algorithm. Finally, an illustrative example is given to demonstrate the efficiency of this method.

DUAN R, HU L, Lin Y. **Diagnostyka uszkodzeń systemu złożonego oparta na dynamicznych sieciach dowodowych oraz wieloatrybutowej metodzie podejmowania decyzji z wykorzystaniem liczb interwałowych**. Eksploatacja i Niezawodnosc – Maintenance and Reliability 2017; 19 (4): 580–589, http://dx.doi.org/10.17531/ein.2017.4.12.

Złożoność nowoczesnych struktur systemowych oraz mechanizmów uszkodzeń powoduje trudności w lokalizacji uszkodzeń systemu. Systemy złożone charakteryzują się cechami, takimi jak dynamika uszkodzeń, różnorodność rozkładów oraz niepewność epistemiczna, które czynią wyzwania dotyczące diagnostyki uszkodzeń znacznie trudniejszymi. W niniejszym artykule przedstawiono metodę diagnozowania uszkodzeń systemów złożonych, w której intensywność uszkodzeń poszczególnych składników wyraża się za pomocą liczb przedziałowych. W szczególności, podejście to wykorzystuje dynamiczne drzewo błędów (DFT) do modelowania dynamicznych zachowań związanych z uszkodzeniami oraz rozwiązuje problem niepewności epistemicznej przy użyciu teorii Dempstera-Shafera (DS) oraz liczb przedziałowych. W celu obliczenia parametrów niezawodności, zaproponowano rozwiązanie polegające na odwzorowaniu DFT w dynamiczną sieć dowodową (DEN). Dodatkowo, w sposób kompleksowy wykorzystano czynnik ważności diagnostycznej (DIF), miarę ważności Birnbauma (BIM) oraz wartości informacji heurystycznej (HIV),

aby przy użyciu udoskonalonego algorytmu VIKOR uzyskać najlepszy system wyszukiwania błędów. Skuteczność omawianej metody zilustrowano na podstawie przykładu.

KUCZMASZEWSKI J, ZALESKI K, MATUSZAK J, PAŁKA T, MĄDRY J. **Studies on the effect of mill microstructure upon tool life during slot milling of Ti6Al4V alloy parts**. Eksploatacja i Niezawodnosc – Maintenance and Reliability 2017; 19 (4): 590–596, http://dx.doi.org/10.17531/ein.2017.4.13.

Different forms of tool wear occur in the milling process. Mechanical wear, which has a range of varieties, is a typical form of wear connected with mill operating. One of the varieties of mechanical wear, frequently occurring during milling machining-resistant materials, is undesirable catastrophic wear. Avoiding that kind of wear by appropriate selection of technological parameters, sort of burning carbides and their microstructure constitutes basic information about reliability of the tool. This paper presents the findings from the experimental testing of the impact SC grain size in end mills on the cutting tool tooth (bit) service life and surface topography after slot milling Ti6Al4V alloy parts. The tool wear indicator was determined in compliance with PN-ISO 8688:1996. It was demonstrated that ultra fine grain SC milling cutters are the most resistant to chipping, whereas the surfaces machined with these cutting tools reveals the lowest roughness. The coarse grain SC milling cutters are among those with the shortest service life of all tested tools.

KUCZMASZEWSKI J, ZALESKI K, MATUSZAK J, PAŁKA T, MĄDRY J. **Badania wpływu mikrostruktury frezu na trwałość ostrza w procesie frezowania rowków w stopie tytanu TI6Al4V**. Eksploatacja i Niezawodnosc – Maintenance and Reliability 2017; 19 (4): 590–596, http://dx.doi.org/10.17531/ein.2017.4.13.

W procesie skrawania występują różne formy zużycia narzędzi. Zużycie mechaniczne, które ma szereg odmian, jest typową formą zużycia związaną z eksploatacją frezów. Jedną z odmian zużycia mechanicznego, często pojawiającą się podczas skrawania materiałów trudnoobrabialnych jest niepożądane zużycie katastroficzne. Unikanie tego rodzaju zużycia poprzez odpowiedni dobór parametrów technologicznych, gatunku węglików spiekanych oraz ich mikrostruktury stanowi podstawową informację o niezawodności narzędzia. W pracy przedstawiono wyniki badań doświadczalnych wpływu wielkości ziaren węglików spiekanych we frezach walcowo-czołowych na trwałość ostrza i topografię powierzchni po procesie frezowania rowków w stopie tytanu Ti6Al4V. Wskaźniki zużycia wyznaczono w oparciu o normę PN-ISO 8688: 1996. Wykazano, że frezy o strukturze ultradrobnoziarnistej są najbardziej odporne na wykruszenia, a powierzchnia po obróbce charakteryzuje się najmniejszą chropowatością. Najmniejszą trwałością charakteryzują się frezy o strukturze gruboziarnistej.

BRZĘCZEK J, MIKRUT S. **The use of photogrammetry for special flight tests**. Eksploatacja i Niezawodnosc – Maintenance and Reliability 2017; 19 (4): 597–603, http://dx.doi.org/10.17531/ein.2017.4.14.

Carrying out flight tests of de-icing systems of aircraft in real or artificial conditions, apart from the measurement of the temperature of the heated areas, requires the verification of the work of the installations in the form assessment of the places of the formation of ice accretions rate and their size. To measure them in the mentioned about tests the authors applied the photogrammetric method, and the obtained results were verified with flight tests, including certified tests. The application of the photogrammetric method in such analyses with the example of processing of the obtained pictures gives base for the assessment of its usefulness and the directions of development in similar applications.

BRZĘCZEK J, MIKRUT S. **Wykorzystanie fotogrametrii do prób specjalnych w locie**. Eksploatacja i Niezawodnosc – Maintenance and Reliability 2017; 19 (4): 597–603, http://dx.doi.org/10.17531/ein.2017.4.14.

Prowadzenie prób w locie instalacji odlodzeniowych statków powietrznych w warunkach rze-czywistych lub sztucznych, oprócz pomiaru temperatury ogrzewanych powierzchni wymaga weryfikacji pracy instalacji w postaci oceny miejsc osadzania się tworów lodowych i ich roz-miarów. Do ich pomiaru w wymienionych próbach autorzy zastosowali metodę fotograme-tryczną, a uzyskane wyniki zweryfikowali próbami w locie, w tym próbami certyfikacyjnymi. Zastosowanie metody fotogrametrycznej do takich analiz z przykładem przetwarzania uzyski-wanych obrazów daje podstawę do oceny jej przydatności oraz kierunków rozwoju w podob-nych zastosowaniach.

SHEN G, ZENG W, ZHANG Y, HAN C, LIU P. **Determination of the average maintenance time of CNC machine tools based on type II failure correlation**. Eksploatacja i Niezawodnosc – Maintenance and Reliability 2017; 19 (4): 604–614, http://dx.doi.org/10.17531/ein.2017.4.15.

An average maintenance time calculation method based on components failure correlation analysis is proposed to revise the traditional system maintenance time. This paper focus on complex system type II fault correlation, using the Decision-making trial and evaluation laboratory / Interpretative structural model method to divide the fault level of components. And the copula connection function is introduced to calculation of failure rate function of failure correlation components. In addition, the system maintenance time model is established by synthesizing the failure rate function of each unit of the system. Moreover, the average maintenance time under the minimum number of failures is determined. This method shows that the minimum average maintenance time of the proposed system is more reasonable than the traditional one and provides the basis for system and component reliability design.

SHEN G, ZENG W, ZHANG Y, HAN C, LIU P. **Określenie średniego czasu konserwacji obrabiarek CNC w oparciu o korelację awarii typu II**. Eksploatacja i Niezawodnosc – Maintenance and Reliability 2017; 19 (4): 604–614, http://dx.doi.org/10.17531/ein.2017.4.15.

W artykule zaproponowano metodę obliczania średniego czasu konserwacji, opartą na analizie korelacji uszkodzeń elementów składowych systemu. Metoda ta ma na celu rewizję tradycyjnego czasu konserwacji systemu. Głównym tematem pracy jest korelacja awarii typu II występujących w systemach złożonych. Elementy systemu podzielono ze względu na poziom uszkodzenia przy użyciu metody DEMATEL w połączeniu z interpretacyjnym modelowaniem strukturalnym. Funkcję intensywności skorelowanych uszkodzeń elementów systemu obliczono za pomocą funkcji łączącej (kopuły). Dodatkowo, opracowano model czasu konserwacji systemu poprzez syntezę funkcji intensywności uszkodzeń każdej jednostki systemu. Ponadto, określono średni czas konserwacji dla minimalnej liczby uszkodzeń. Metoda ta pokazuje, że minimalny średni czas konserwacji proponowanego systemu jest korzystniejszy niż tradycyjnie przyjęty i stanowi podstawę do projektowania niezawodności systemu i jego składowych.

EPLER I, SOKOLOVIĆ V, MILENKOV M, BUKVIĆ M. **Application of lean tools for improved effectiveness in maintenance of technical systems for special purposes**. Eksploatacja i Niezawodnosc – Maintenance and Reliability 2017; 19 (4): 615–623, http://dx.doi.org/10.17531/ein.2017.4.16.

Today, executives from the system of maintenance of technical systems for special purposes (military combat vehicles), are trying to improve their organizational processes and create competitive advantage through increasing the quality of maintenance services (increase effectiveness), reducing the total cost (increase efficiency) and reduce the maintenance cycle-time. One of the possible ways for improvements in the maintenance system is the application of lean concept of maintenance, by usage of different tools as 5S, Layout, Visual systems, Kanban and new developed "Technical system maintenance" tool. In order to gain a better understanding of this concept, the paper presents a new developed maintenance model for the application of the lean concept in the real maintenance system. The results of empirical and experimental testing of the proposed model are analysed based on Analysed of methods and effects of improvements (IMEA), Benchmarking methods and multi-criteria, 22 analysis by using the statistical software application MINITAB. The special character of experimental testing are obtained regression equations that describe the changes of the duration of the maintenance cycle, depending on the applied lean tools. The obtained results show that the duration of maintenance cycle is reduced for about 23%, the improvement of maintenance effectiveness is around 14% and the efficiency is showing an upward trend.

EPLER I, SOKOLOVIĆ V, MILENKOV M, BUKVIĆ M. **Zastosowanie narzędzi szczupłego utrzymania ruchu do poprawy efektywności obsługi systemów technicznych specjalnego przeznaczenia**. Eksploatacja i Niezawodnosc – Maintenance and Reliability 2017; 19 (4): 615–623, http://dx.doi.org/10.17531/ein.2017.4.16.

W dzisiejszych czasach, kadra kierownicza zarządzająca systemami utrzymania ruchu układów technicznych specjalnego przeznaczenia (np. wojskowych pojazdów bojowych) stara się usprawniać procesy organizacyjne i tworzyć przewagę konkurencyjną poprzez podniesienie jakości usług serwisowych (zwiększenie efektywności), redukcję kosztów całkowitych (zwiększenie wydajności) oraz skrócenie czasu trwania cyklu eksploatacyjnego. Jednym z możliwych sposobów udoskonalenia systemu utrzymania ruchu jest zastosowanie pojęcia szczupłego utrzymania ruchu z wykorzystaniem różnych narzędzi, takich jak 5S, Layout, Visual systems, kanban oraz nowo opracowanego narzędzia "Obsługi Ruchu Systemu Technicznego". Aby lepiej zrozumieć tę koncepcję, w artykule przedstawiono nowo opracowany model obsługi technicznej, który pozwala na zastosowanie koncepcji szczupłego utrzymania ruchu w rzeczywistym systemie obsługi. Wyniki empirycznych i eksperymentalnych badań proponowanego modelu analizowano na podstawie analizy metod i efektów doskonalenia IMEA, metod benchmarkingowych oraz analizy wielokryterialnej 22 przy użyciu oprogramowania statystycznego MINITAB. W badaniach eksperymentalnych otrzymano równania regresji, które opisują zmiany czasu trwania cyklu eksploatacyjnego w zależności od zastosowanych narzędzi. Uzyskane wyniki wskazują, że przy zastosowaniu proponowanej metody czas trwania cyklu eksploatacyjnego ulega skróceniu o około 23%, efektywność utrzymania ruchu wzrasta o około 14%, a wydajność wykazuje tendencję wzrostową.

POGAČNIK B, DUHOVNIK J, TAVČAR J. **Aircraft fault forecasting at maintenance service on the basis of historic data and aircraft parameters**. Eksploatacja i Niezawodnosc – Maintenance and Reliability 2017; 19 (4): 624–633, http://dx.doi.org/10.17531/ein.2017.4.17.

Aircraft maintenance and repair organizations (MROs) have to be competitive and attractive for both existing and new customers. The aircraft ground time at MROs should be as short as possible and cost effective without reducing the quality of the work. Process optimization in MROs requires the continuous improvement of processes and the elimination of non-value-added activities during maintenance checks. There is, on the one hand, an obligation to follow the prescribed procedures and, on the other hand, pressure for time and cost reduction. The aircraft servicing process has been analysed according to a lean methodology. The optimization of logistics processes is recognized as the most promising method for reducing the maintenance service time and costs of spare parts. The probability of aircraft faults is calculated on the basis of historic data from previously completed service projects. Aircraft parameters, such as aircraft type, operator, aircraft age, flight hours, flight cycles, engine type and operation location, are taken into consideration in the fault forecasting. The fault probability is used as an indicator for defining a priority list for the accomplishment of jobs included in the aircraft maintenance service. The proposed methodology was validated and confirmed on four different projects.

POGAČNIK B, DUHOVNIK J, TAVČAR J. **Prognozowanie uszkodzeń statków powietrznych dla celów obsługi konserwacyjnej na podstawie ich parametrów oraz danych z eksploatacji**. Eksploatacja i Niezawodnosc – Maintenance and Reliability 2017; 19 (4): 624–633, http://dx.doi.org/10.17531/ein.2017.4.17.

Organizacje zajmujące się konserwacją i naprawami statków powietrznych (MRO) muszą dbać o swoją konkurencyjność i atrakcyjność zarówno dla istniejących jak i nowych klientów. Czas trwania obsługi naziemnej w MRO powinien być jak najkrótszy a konserwacja powinna pociągać za sobą jak najmniejsze koszty, bez konieczności obniżania jakości pracy. Optymalizacja procesów przeprowadzanych w MRO wymaga ciągłego doskonalenia oraz eliminacji nieuzasadnionych czynności przeglądowych. Z jednej strony pracownicy MRO muszą przestrzegać określonych procedur, z drugiej zaś strony, ciąży na nich presja redukcji czasu i kosztów obsługi. Proces obsługi statku powietrznego analizowano zgodnie z metodologią szczupłego utrzymania ruchu. Optymalizację procesów logistycznych uznaje się za najbardziej obiecujący sposób redukcji czasu obsługi serwisowej oraz kosztów części zamiennych. Prawdopodobieństwo wystąpienia uszkodzeń statku powietrznego obliczano na podstawie danych historycznych z uprzednio przeprowadzonych prac obsługowych. W prognozowaniu uszkodzeń, uwzględniano takie parametry statku powietrznego, jak typ statku, jego operator, wiek, liczba godzin w powietrzu, liczba cykli lotów, typ silnika oraz miejsce stacjonowania. Prawdopodobieństwo wystąpienia uszkodzeń wykorzystano jako wskaźnik do hierarchizacji zadań obsługi technicznej statku powietrznego. Przydatność proponowanej metodologii zweryfikowano i potwierdzono na przykładzie czterech różnych projektów.

CELIK N, GULOKSUZ CT. **A new lifetime distribution**. Eksploatacja i Niezawodnosc – Maintenance and Reliability 2017; 19 (4): 634–639, http://dx.doi.org/10.17531/ein.2017.4.18.

The well-known statistical distributions such as Exponential, Weibull and Gamma distributions have been commonly used for analysing the different types of lifetime data. In this paper, following the idea of the extension of T-X family of distributions, we propose a new type of exponential distribution. We define the survival function, the hazard function and the mean time to failure related to this new distribution. Type II censoring procedure is also considered for this distribution. Additionally, stress-strength reliability and the maximum likelihood (ML) estimators of the unknown parameters are obtained. As an application, a real data set is used to show that the proposed distribution gives best fit than the alternative ones.

CELIK N, GULOKSUZ CT. **Nowy rozkład cyklu życia**. Eksploatacja i Niezawodnosc – Maintenance and Reliability 2017; 19 (4): 634–639, http://dx.doi.org/10.17531/ein.2017.4.18.

Powszechnie znane rozkłady statystyczne, takie jak rozkład wykładniczy, Weibulla czy rozkład Gamma znajdują szerokie zastosowanie w analizie różnych typów danych dotyczących cyklu życia. W niniejszym artykule, zaproponowano nowy typ rozkładu wykładniczego, w oparciu o rozszerzenie rodziny rozkładów TX. Zdefiniowano funkcję przeżycia, funkcję ryzyka (hazardu) oraz średni czas do uszkodzenia w odniesieniu do proponowanego rozkładu. Rozpatrywano także procedurę ucinania typu II dla nowego rozkładu. Dodatkowo określono niezawodność wytrzymałościową oraz estymatory największej wiarygodności nieznanych parametrów. Sposób wykorzystania proponowanego rozkładu zilustrowano wykorzystując rzeczywisty zbiór danych. Wykazano, że daje on lepsze dopasowanie niż modele alternatywne.

SHIM J, RYU H, LEE Y. **Availability analysis of series redundancy models with imperfect switchover and interrupted repairs**. Eksploatacja i Niezawodnosc – Maintenance and Reliability 2017; 19 (4): 640–649, http://dx.doi.org/10.17531/ein.2017.4.19.

This paper considers N+1 series redundancy, where N components are active and 1 component is standby in normal state. The active components execute the service, while the standby component is ready to take over the active role if the active components fail. When an active component fails, the standby, if available, automatically takes over system operations. However, the automatic switchover of the standby component to active mode might not be possible due to hardware or software issues. When a component failure or an imperfect switchover occurs, it immediately begins to be repaired. However, the repair process is possible to be interrupted. The most existing literature of redundancy models has focused on Markovian systems with uninterrupted repairs. This paper considers a non-Markovian redundancy model with interrupted repairs, where the repair time, the non-automatic switchover time, and the interrupted time are generally distributed. Using supplementary variable method and integro-differential equations, we obtain the steady-state availability for the redundancy model.

SHIM J, RYU H, LEE Y. **Analiza gotowości modeli redundancji kaskadowej uwzględniających niedoskonałe przełączanie oraz przerwane naprawy**. Eksploatacja i Niezawodnosc – Maintenance and Reliability 2017; 19 (4): 640–649, http://dx.doi.org/10.17531/ein.2017.4.19.

W niniejszym artykule rozważano przypadek redundancji kaskadowej typu N+1, w której liczba N elementów pozostaje aktywnych, a jeden komponent jest w trybie gotowości w stanie normalnym. Elementy aktywne wykonują usługę, podczas gdy składowa rezerwowa pozostaje w stanie gotowości do przejęcia roli aktywnej w przypadku, gdyby składniki aktywne uległy uszkodzeniu. Gdy element aktywny przestaje działać, element zastępczy, jeśli jest dostępny, automatycznie przejmuje operacje systemowe. Jednak automatyczne przełączenie komponentu zastępczego na tryb aktywny nie zawsze jest możliwe z powodu problemów ze sprzętem lub oprogramowaniem. Jeśli wystąpi awaria komponentu lub niedoskonałe przełączenie, natychmiast rozpoczyna się naprawa. Proces naprawy może jednak zostać przerwany. Większość istniejącej literatury na temat modeli nadmiarowości koncentruje się na systemach Markowa, w których nie dochodzi do przerwania naprawy. W niniejszym artykule rozważano niemarkowowski model nadmiarowości uwzględniający możliwość przerwania naprawy, w którym czas naprawy, czas nieautomatycznego przełączenia oraz czas przerwany mają rozkład ogólny. Wykorzystując metodę dodatkowej zmiennej oraz równania całkowo-różniczkowe otrzymano gotowość stacjonarną dla omawianego modelu redundancji.

FUQING Y, BARABADI A, JINMEI L. **Reliability modelling on two-dimensional life data using bivariate weibull distribution: with case study of truck in mines**. Eksploatacja i Niezawodnosc – Maintenance and Reliability 2017; 19 (4): 650–659, http://dx.doi.org/10.17531/ein.2017.4.20.

An engineering system can exhibit two- or multi-dimensions in its lifetime. As the classical univariate distribution cannot model this multi-dimensional characteristic, it is necessary to extend it to multivariate distribution in order to capture the multi-dimensional characteristics. This paper proposes a bivariate Weibull distribution that combines two classical Weibull models by a common exponent. The common exponent can represent the correlation between the two dimensions. A ratio likelihood test is proposed to test the significance of the correlation between the two dimensions. To solve the parameter estimation problem, this paper suggests a Bayesian method. Moreover, a goodness of fit test method is developed to visually check the fitness of the model. A case study considering mining trucks is presented to apply the bivariate Weibull distribution to model the two-dimensional life data.

FUQING Y, BARABADI A, JINMEI L. **Modelowanie niezawodnościowe dwuwymiarowych danych dotyczących okresu eksploatacji z wykorzystaniem dwuwymiarowego rozkładu Weibulla. Z badań nad wywrotkami kopalnianymi**. Eksploatacja i Niezawodnosc – Maintenance and Reliability 2017; 19 (4): 650–659, http://dx.doi.org/10.17531/ein.2017.4.20.

Systemy inżynieryjne można charakteryzować za pomocą dwóch lub więcej wymiarów dotyczących okresu ich eksploatacji (np. przebieg i czas pracy pojazdu). Ponieważ klasyczny rozkład jednowymiarowy nie wystarcza do zamodelowania tej wielowymiarowej charakterystyki, konieczne jest wykorzystanie rozkładu wielowymiarowego, który pozwala uchwycić wielowymiarowość cyklu życia systemu. W artykule zaproponowano dwuwymiarowy rozkład Weibulla, który łączy w sobie dwa klasyczne modele Weibulla za pomocą wspólnego wykładnika. Wspólny wykładnik może reprezentować korelację między dwoma wymiarami. Zaproponowano test ilorazu wiarygodności, który umożliwia badanie istotności korelacji pomiędzy dwoma wymiarami. Do rozwiązania problemu estymacji parametrów zastosowano metodę bayesowską. Ponadto opracowano metodę badania dopasowania modelu do danych empirycznych służącą do wizualizacji dopasowania modelu. Przedstawiono studium przypadku dotyczące wywrotek kopalnianych, w którym dwuwymiarowy rozkład Weibulla zastosowano do modelowania dwuwymiarowych danych dotyczących okresu eksploatacji tych pojazdów.

Article citation info:
GÓMEZ CQM, GARCÍA FPM, JIMENEZ AJ, CHENG L, KOGIA M, MOHIMI A, PAPAELIAS M. A heuristic method for detecting and locating faults employing electromagnetic acoustic transducers. Eksploatacja i Niezawodnosc – Maintenance and Reliability 2017; 19 (4): 493–500, http://dx.doi.org/10.17531/ein.2017.4.1.

Carlos Quiterio GÓMEZ Muñoz
Fausto Pedro GARCÍA Marquez
Alfredo ARCOS Jimenez
Liang CHENG
Maria KOGIA
Abbas MOHIMI
Mayorkinos PAPAELIAS

A HEURISTIC METHOD FOR DETECTING AND LOCATING FAULTS EMPLOYING ELECTROMAGNETIC ACOUSTIC TRANSDUCERS

HEURYSTYCZNA METODA WYKRYWANIA I LOKALIZOWANIA USTEREK Z WYKORZYSTANIEM ELEKTROMAGNETYCZNYCH PRZETWORNIKÓW AKUSTYCZNYCH

The objective of this paper is to demonstrate a novel signal processing for detection, identification and flaw sizing of structural damage using ultrasonic testing with Electromagnetic Acoustic Transducers (EMATs). Damage detection involves the recognition of a defect that exists within a structure. Damage location is the identification of the geometric position of the defect. Defect classification is the cluster of the damage type into multiple damage scenarios. In the absence of external interferences, a good measure of detectability of a flaw is its signal-to-noise ratio (SNR). Although the SNR depends on various parameters such as electronics used, material properties, e.g. homogeneity and damping, and flaw size, it can be improved using advanced signal processing. The main scientific novelties presented in this paper focus on filtering signal noise through advanced digital signal processing; incorporating wavelet transforms for image and signal representation enhancements; investigating multi-parametric analysis for noise identification and defect classification; studying attenuation curves properties for defect localisation improvement and flaw sizing and location algorithm development.

Keywords: *fault detection and diagnosis, electromagnetic acoustic transducers (EMAT), wavelet transforms, non destructive tests, guided waves.*

Celem niniejszego artykułu jest omówienie nowatorskiego sposobu przetwarzania sygnałów w celu wykrywania, identyfikacji i oceny uszkodzeń strukturalnych przy użyciu ultrasonograficznych testów za pomocą elektromagnetycznych przetworników akustycznych (EMAT). Wykrywanie uszkodzeń polega na rozpoznaniu istniejących defektów wewnątrz danej struktury. Lokalizacja uszkodzeń sprowadza się do identyfikacji geometrycznego położenia defektu. Klasyfikacja defektu to klaster typu uszkodzenia w wielu scenariuszach uszkodzeń. W przypadku braku zewnętrznych zakłóceń, dobrym wskaźnikiem wykrywalności błędu jest stosunek sygnału do szumu (SNR). Pomimo tego, że SNR zależy od różnych parametrów, takich jak użyta elektronika, właściwości materiału, np. jednorodność i tłumienie, a także wielkość wady, wskaźnik ten można poprawić przy użyciu zaawansowanego przetwarzania sygnałów. Główne nowe zagadnienia naukowe przedstawione w niniejszym artykule skupiają się na filtrowaniu szumu sygnału za pomocą zaawansowanego przetwarzania sygnału cyfrowego, w tym wykorzystując transformaty falkowe w celu ulepszenia obrazu i sygnału; badanie analizy wieloparametrycznej w celu identyfikacji szumów i klasyfikacji defektów; badanie właściwości krzywych osłabiania w celu sprawniejszego wykrywania i oceny wad oraz rozwoju algorytmu lokalizacji.

Słowa kluczowe: *wykrywanie i diagnozowanie wad, elektromagnetyczne przetworniki akustyczne, EMAT, transformaty falkowe, badania nieniszczące, fale prowadzone.*

1. Introduction

Non-destructive testing (NDT) for fault detection in structures has received more attention in recent years. Significant advances in instrumentation technology and digital signal processing have been made [16, 17, 19, 25, 30]. Signal processing methods together with structural health monitoring (SHM) permit the identification and diagnosis of faults and their location based on changes in static and

dynamic structural features [14, 22, 23]. In addition, these techniques can be remotely controlled and they should work online, resulting in a reduction of costs associated to manual inspections, downtimes, etc. [11, 20, 28].

Guided waves are a common technique employed for SHM within the NDT field, being particularly useful for structural components based on plate or tube geometries. The technique is based on the excitation of low frequency ultrasonic waves propagating along a structure such as a pipeline over long distances, allowing inspection of large areas without any relocation of the transducers.

The purpose of this paper is to demonstrate a novel fault detection and diagnosis (FDD) approach using ultrasound inputs in conjunction with advanced signal processing methods [4, 10, 21, 31] for monitoring the structural condition of a steel plate. The novel signal processing is based on system identification techniques in discrete time to estimate potential faults. The wavelet and Hilbert transforms are employed to work in conjunction with an automatic peak detection algorithm [5]. The algorithm detects which peaks correspond to echoes from the edges, and which correspond to potential defects. Once a potential crack is detected, the algorithm shows the exact location of the defect, and the crack size is compared with the attenuation curve.

2. Electromagnetic acoustic transducers for condition monitoring

The electromagnetic acoustic transducer (EMAT) is a transducer for non-contact sound generation and reception using magnetostrictive phenomena and the interaction of the Lorenz force with the crystal lattice of the material being inspected. EMATs have been widely used in non-destructive testing in the generation of Shear and Lamb waves [3, 33]. In this study EMATs manufactured by SONEMAT Limited in the UK (Figure 1) have been used to carry out the experiments of interests. The EMATs employed use a specific coil and magnet configuration appropriate for the tests carried out [27].

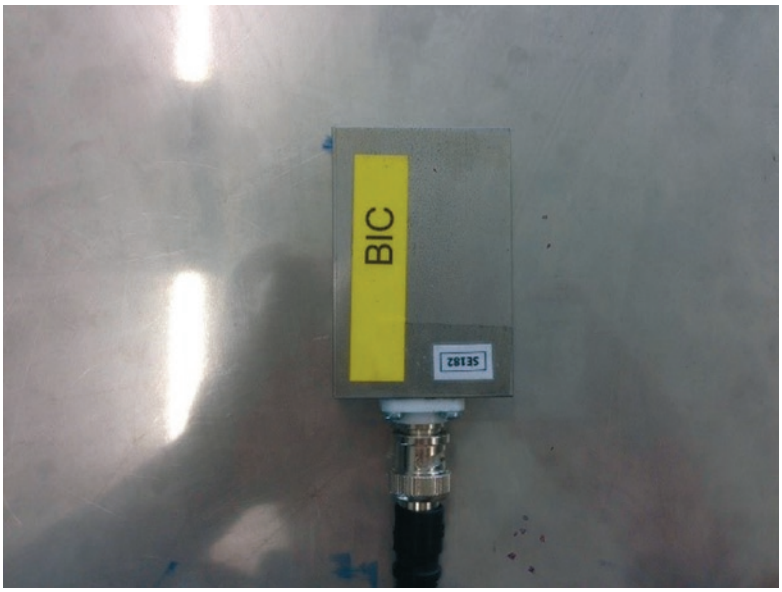

Fig. 1. Electromagnetic Acoustic Transducer manufactured by SONEMAT Limited in the UK

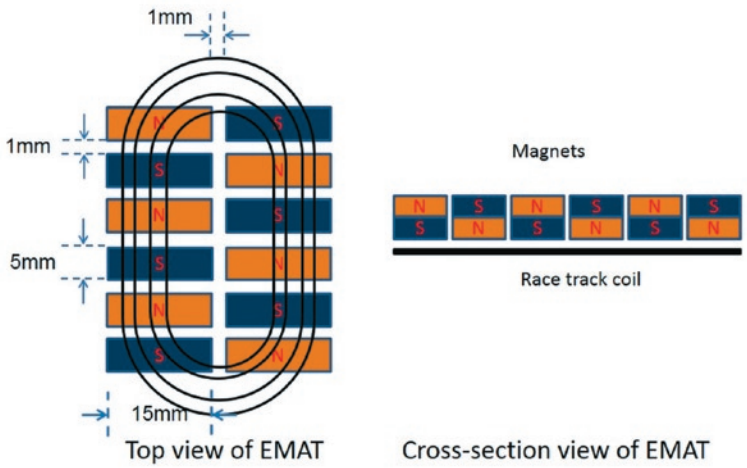

Fig. 2. Configuration of EMAT transducer

A 3 mm thickness plate of 316Ti stainless steel has been employed for the experiments. The EMATs incorporate a race track coil with periodic permanent magnet to generate shear waves (SH0 mode) in the plate. The dimension of each EMAT is 15 mm x 5 mm x 5 mm. The distance between the magnets is 1 mm and the magnetic strength of each magnet is 0.3 T. The diameter of the coil is 0.315 mm, the width 15 mm and length 35 mm, with a lift-off distance of 0.1 mm from the samples surface. The EMAT configuration is shown in the schematic of Figure 2.

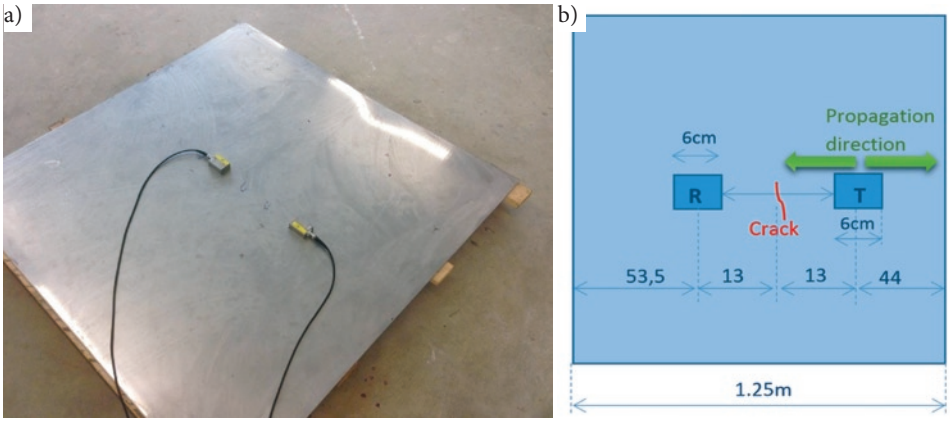

Fig. 3. Actuator and sensor placement in the plate (a) and scheme of the defect location (b).

This type of EMAT configuration is applicable for the detection of transverse defects, such as spiral cracking, blow-out holes, circumferential cracking, bell splitting, etc. Since 316Ti stainless steel has an austenitic microstructure it is paramagnetic and therefore, magnetostriction is not relevant. Ultrasonic waves are produced due to the Lorentz forces acting normal to the plate surface producing ultrasonic waves propagating along the longitudinal direction of the test plate.

3. Experimental Tests

An artificial defect has been induced in the plate using spark erosion to carry out automatic detection and location of defects. Figure 3 shows the experimental configuration employed. The EMAT is excited by a 256 kHz and six-cycle pulse. Shear waves are generated in both directions. The

EMAT (R) receives echoes from the edges and from the crack. Figure 4 shows the four first reflections produced by the boundaries.

Shear waves are non-dispersive signals, i.e. the propagation velocity of these waves is not frequency dependent. The propagation velocity of shear waves depends on the material properties [32]. For the 3 mm austenitic steel plate (316Ti) considered herewith the shear wave velocity is 3020 m/s.

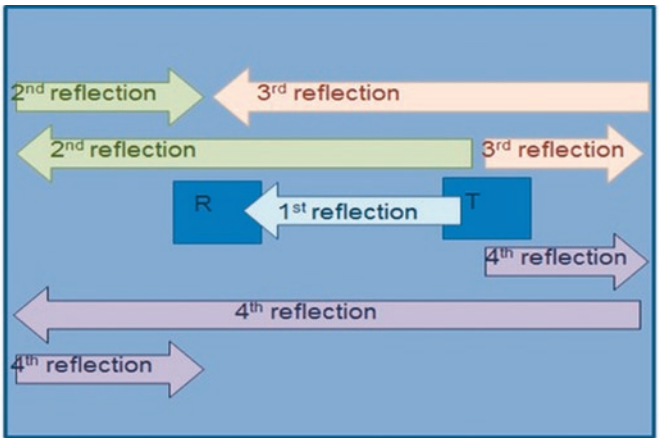

Fig. 4. Reflections from the edges registered by sensor (R)

4. Signal processing

This section presents a novel method based on a wavelet-based algorithm that has been applied to the signals from the EMATs to improve the SNR. A pre-filter has been implemented to extract the low frequency information of the EMAT signals, where it reduces the unexpected frequency components of signals. Then a denoising algorithm has been applied to improve the SNR without introducing time delay in the original signals [15].

4.1. Wavelet pre-filter and de-noising.

The wavelet transform is an analysis method which can be employed to identify the local characteristics of a signal in the time and frequency domain, e.g. with the use of a series of decomposition coefficients at different frequency bands [6, 10]. It is recommended for large time intervals where great accuracy is required at low frequencies and vice versa, e.g. small regions where precision details are required at higher frequencies [7]. The wavelet transform is also a useful method to characterise and identify signals with spectral features, unusual temporary files and other properties related to non-standing waves.

Wavelet transforms are an alternative to the fast Fourier transform (FFT), or to the short-time Fourier transform,

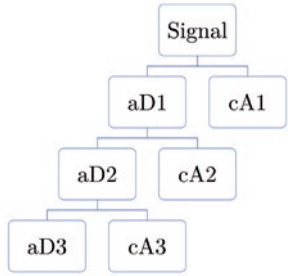

Fig. 5. Wavelet decompositions tree

to obtain results in the time domain [13] and [24]. The signal processing from the time domain to the frequency domain usually implies loss of information, being difficult to determine the appearance of specific frequencies [26].

Signals are divided therefore into low frequency *approximations* (**A**) and high frequency *details* (**D**), where the sum of **A** and **D** is always equal to the original signal. The division is done using low pass and high pass filters [2]. In order to reduce the computational and mathematical costs due to the data duplication, a sub-sampling is usually implemented, containing the half of the collected information from **A** and **D** without losing information.

In the case of the multi-level filters, they repeat the filtering process with the output signals from the previous level. This leads to the wavelet decomposition trees (Figure 5) [1, 9]. Additional information is obtained by filtering at each level. However more decompositions levels do not always mean more accurate results.

The objective of the signal pre-processing is to extract the most important information of the original signal before carrying out signal de-noising. It generates new signals adjusted for the application of filters, providing more robust results and greater similarity between signals obtained under different conditions.

The first filter used to prepare the signal has been employing a Daubechies wavelet transform. Daubechies wavelets were used because they handle with boundary problems for finite length signals, being their biggest advantage over other families [12, 29] and [34].

The decomposition five D5 contains more information of the original signal and a lower signal noise ratio without delay regarding to the original signal.

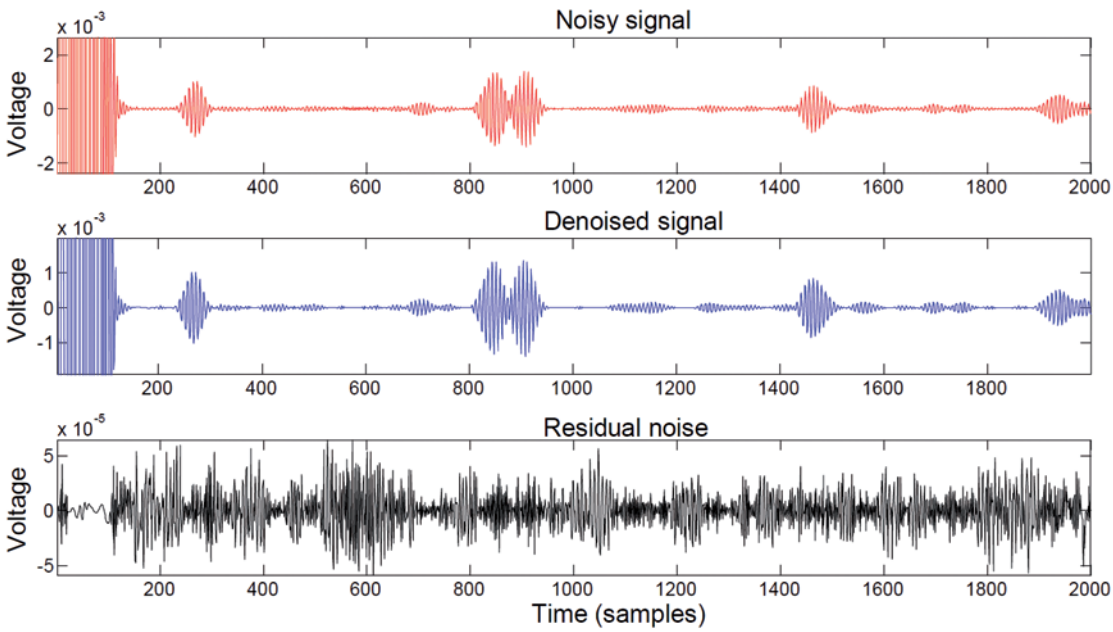

Fig. 6. Decomposition detail five (D5), De-noised D5 and extracted residual noise

Effective filtering should not eliminate any information about the defects, e.g. the peaks with low amplitudes, because it is likely that any of these peaks can be due to a defect. This section describes the approach considered in order to remove noise without compromising the detection of a smaller defect.

The denoising of the signal is performed employing a multilevel 1-D wavelet analysys using Daubechies family. The wavelet decomposition structure of the signal to be de-noised is extracted. The threshold for the de-noising is obtained by a wavelet coefficients selection rule using a penalization method provided by Birgé-Massart. An overly aggressive filtering could eliminate data of interest, such as small echoes that come from defects. Figure 6 shows the original signal and the de-noised signal when it is applied the wavelet de-noised filter. In contrast to other digital filters, the Wavelet de-noising filter does not produce an unwanted signal delay.

It is observed that the filter removes noise significantly, and also does not eliminate information that is related to different structural features.

4.2. Finding events within the signal: Envelope and smooth

Hilbert Transform is employed to obtain the envelope of the filtered signal. It is necessary to smooth the envelope with the aim of finding events in the signal, which usually appear as peaks, i.e. it is desired do not find false alarms. An inadequate window size could produce distortions as "sawtooth" in the signal.

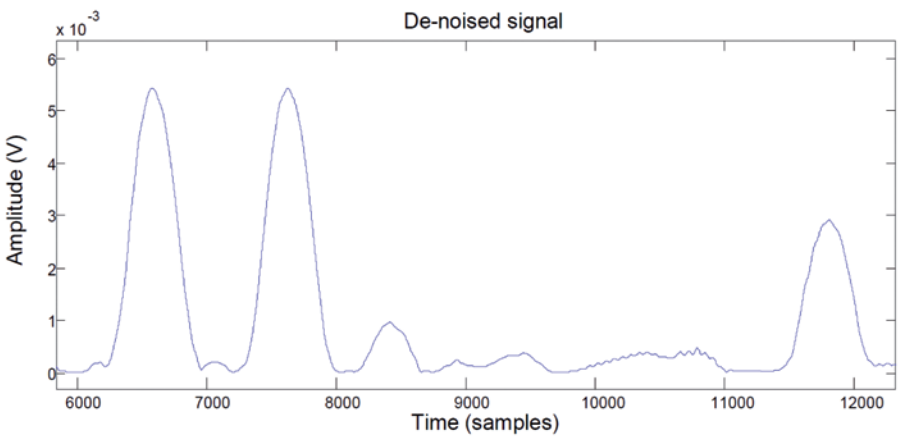

Fig. 7. Smooth of the envelope using Wavelet low pass filter

A good result is achieved by applying again a Wavelet de-noising filter and selecting the low frequency decompositions (approximations). This produces a smoothed function without significantly altering the signal (Figure 7).

4.3. Cracks detection and edges location

The approach identifies the events from the signals that are obtained from elements as boundaries or welds. This process consists of the following steps (see Figure 8):

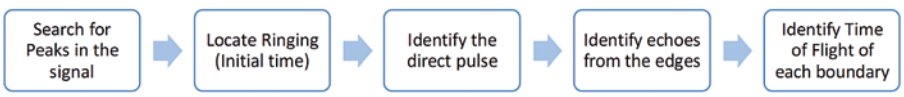

Fig. 8. Identification of edges echoes algorithm

- *Peak search*: It is important to select a proper threshold for this purpose.
- *Identify echoes from the edges*: The time of flight of each echo is obtained and compared with the distances of the sensor and actuator regard to the boundaries.
- *Theoretical and experimental comparison for identification of the boundaries* (Figure 9).

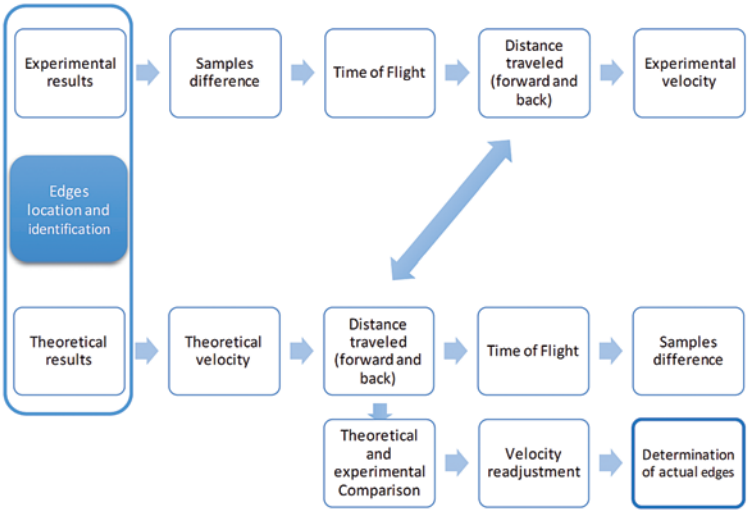

Fig. 9. Theoretical and experimental comparison for edges identification

The obtained information allows the discarding of false cracks, and also provides information such as the attenuation of the ultrasonic wave propagation along the material. The algorithm uses the distance of the EMATs from the edges to perform a self-identification of signal events. The event is located theoretically when the two possible ways of propagation of ultrasound, forward and reverse, are analysed together, taking into account the time of flight (ToF) of each echo. Then the algorithm correlates the theoretical events with the potential events detected in the signal. Finally, the measurement accuracy is checked and validated or not, and each specific event is experimentally located, and obtaining the experimental propagation velocity.

Vector $\mathbf{X}$ contains the position values of the peaks obtained experimentally, $\mathbf{Y}$ the height of the peaks of $\mathbf{X}$, and $\mathbf{X}^*$ the position values of the peaks obtained theoretically.

$$\mathbf{X} = [x_1, \cdots, x_i, \ldots x_n]$$

$$\mathbf{Y} = [y_1, \cdots, y_i, \ldots y_n]$$

$$\mathbf{X}^* = [x_1^*, \cdots, x_j^*, \ldots x_m^*]$$

The matrix $\mathbf{C}$, given by equation (1) contains the absolute difference between each value of $\mathbf{X}$ and each value of $\mathbf{X}^*$

$$\mathbf{C}=\begin{bmatrix} \left|x_1-x_1^*\right| & \cdots & \left|x_1-x_j^*\right| & \cdots & \left|x_1-x_m^*\right| \\ \vdots & & \vdots & & \vdots \\ \left|x_i-x_1^*\right| & \cdots & \left|x_i-x_j^*\right| & \cdots & \left|x_i-x_m^*\right| \\ \vdots & & \vdots & & \vdots \\ \left|x_n-x_1^*\right| & \cdots & \left|x_n-x_j^*\right| & \cdots & \left|x_n-x_m^*\right| \end{bmatrix}, i=1,\ldots n,\ \ j=1,\ldots m \quad (1)$$

The purpose of this approach is to select the real peaks having its homologous in the set of theoretical peaks. For each x_i, the most similar value x_j^* is chosen if the difference between them is less than the tolerance θ, where an alarm could notice that the similitude has not been found. The minimum value of the components of each column $\mathbf{C}_j$ is given by a particular x_i. $\mathbf{X}_{\text{edges}}$ is a subset of $\mathbf{X}$ that contains the minimum values of each column **C**j, i.e.:

$$\mathbf{X}_{edges}=\left[\mathrm{x}_{edges1},\cdots,\mathrm{x}_{edges\,j},\cdots,\mathrm{x}_{edges\,m}\right]$$

$$\mathrm{x}_{edges,j}=x_r,\ x_r\in\mathbf{X}\ \ \forall\, r,j\ :\ c_{rj}=\min\left(\mathbf{C}_j\right)\leftrightarrow c_{rj}<\theta,\ j=1,2\ldots m \quad (2)$$

This method allows the determination of the absolute and relative error between the values obtained and expected for each event. The differences between the experimental and theoretical values are shown in Figure 10.

The peaks that do not have their counterpart with the theoretical peaks are possible echoes that come from a defect ($\mathbf{X}_{cracks}$).

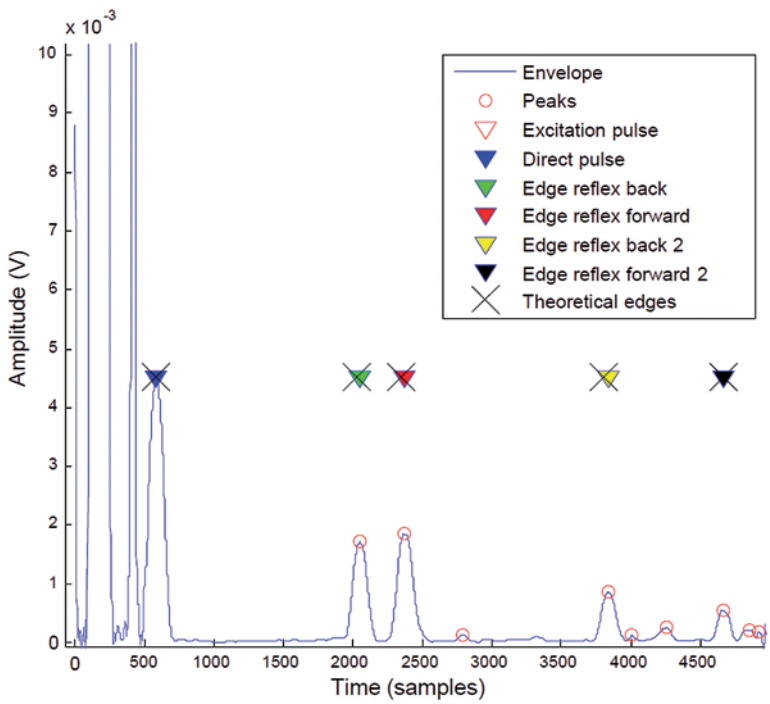

Fig. 10. Boundaries location using an algorithm which compares theoretical (cross) and experimental (triangle) values of ToF

$$\mathbf{X}_{cracks}\subseteq\mathbf{X}:\mathbf{X}_{cracks}\notin\mathbf{X}\cap\mathbf{X}_{edges} \quad (3)$$

$$\mathbf{X}_{cracks}=\left[\mathrm{x}_{cracks\,1},\cdots,\mathrm{x}_{cracks\,k},\cdots,\mathrm{x}_{cracks\,n-m}\right],\quad k=1,2,\ldots n-m$$

where the heights of $\mathbf{X}_{cracks}$ are:

$$\mathbf{Y}_{cracks}=\left[\mathrm{y}_{cracks\,1},\cdots,\mathrm{y}_{cracks\,k},\cdots,\mathrm{y}_{cracks\,n-m}\right],\quad k=1,2,\ldots n-m$$

The potential crack detection and location (see Figure 11) is based on the echoes that are coming from the same crack, where they could

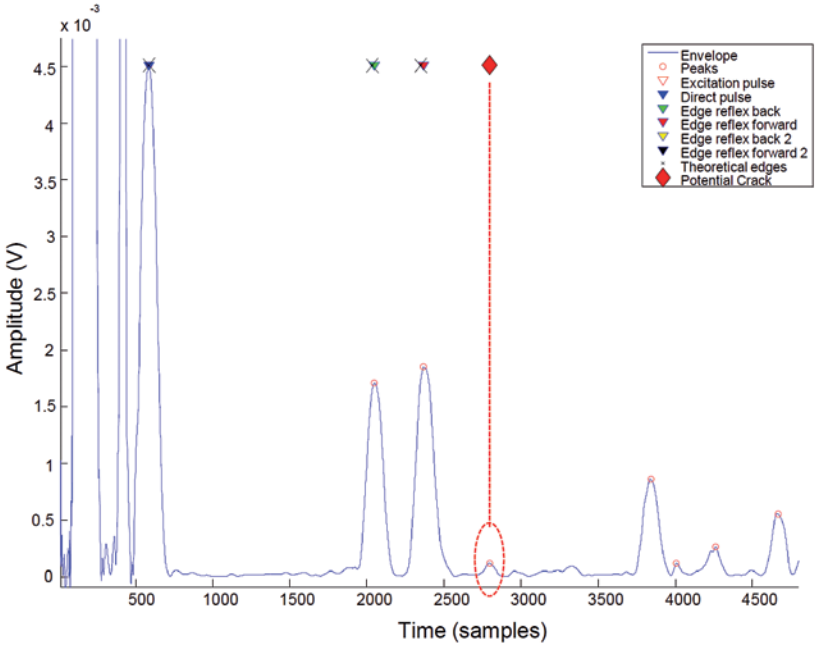

Fig. 11. Potential crack locations establishing relations between the two possible ways.

come from different paths due to the EMAT generate forward and reverse shear waves.

The algorithm considers that if the distance travelled is close, the defect is detected and therefore located. The scheme of this method is shown in Figure 12.

The pattern recognition approach is based on an automatic detection of cracks that compares the ToF employed by the same pulse to travel two different paths [18]. The two shortest paths for detecting a crack between the sensor and transmitter are the path "a" and path "b" shown in Figure 13. The distance travelled by an echo in the path "a", for example d_{echo_a}, is used to determine the distance drc_a between the crack and the receptor. Similarly, the distance travelled by an echo in the path "b" d_{echo_b} is used to determine the distance drc_b. The distances drc_a and drc_b should be close. The method performs a comparison between the distances obtained for each component of $\mathbf{X}_{cracks}$.

The paths are:

Path a:

$$d_{echo_{a,k}}=dtr+2dr+2drc_{a,k} \quad (4)$$

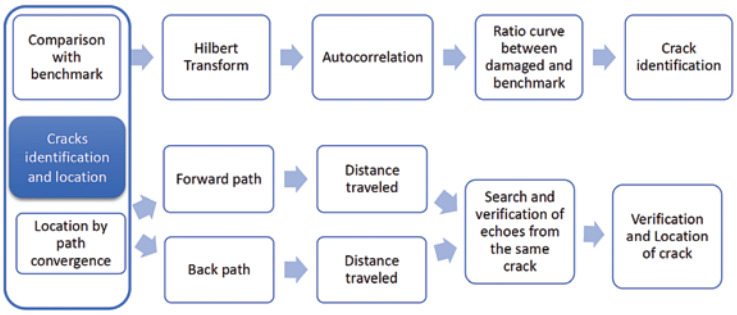

Fig. 12. Location of the crack by two methods: Comparison with "as commissioned" and; location by convergence of different paths

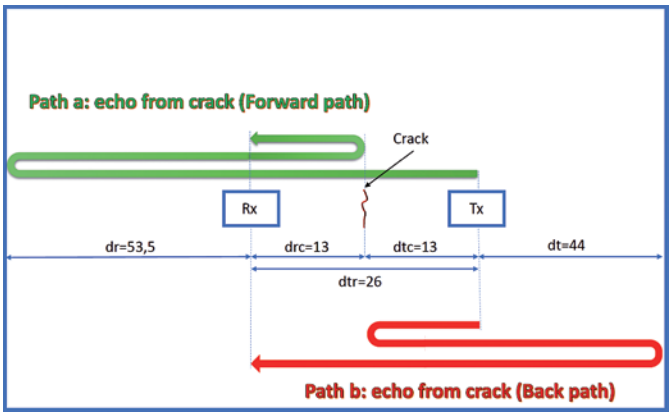

Fig. 13. Two shortest paths from Tx and Rx detecting the defect. The distance is given in centimetres

$$drc_{a,k} = \frac{d_{echo_{a,k}} - dtr - 2dr}{2} \tag{5}$$

$$\mathbf{D}\mathrm{rc}_{\mathrm{a}} = \left[drc_{a,1}, \cdots, drc_{a,k}, \cdots, drc_{a,m-n} \right], k = 1,2 \ldots n-m$$

Path b:

$$d_{echo_{b,k}} = 3dtc + 2dt + drc_{b,k} \tag{6}$$

$$dtc = dtr - drc_{b,k} \tag{7}$$

$$d_{echo_{b,k}} = 3(dtr - drc_{b,k}) + 2dt + drc \tag{8}$$

$$drc_{b,k} = \frac{3dtr + 2dt - d_{echo_{b,k}}}{2} \tag{9}$$

The distance $drc_{a,k}$ is compared with all the echoes that come from the path 2 ($drc_{b,k}$). Therefore, the pair of echoes that provide the most similar distances drc_1 and drc_2 have the greatest likelihood to come from the same defect.

$$\mathbf{D} = \begin{bmatrix} \left| d_{rc_{a,1}} - d_{rc_{b,1}} \right| & \cdots & \left| d_{rc_{a,1}} - d_{rc_{b,l}} \right| & \cdots & \left| d_{rc_{a,1}} - d_{rc_{b,n-m}} \right| \\ \vdots & & \vdots & & \vdots \\ \left| d_{rc_{a,k}} - d_{rc_{b,1}} \right| & \cdots & \left| d_{rc_{a,k}} - d_{rc_{b,l}} \right| & \cdots & \left| d_{rc_{a,k}} - d_{rc_{b,n-m}} \right| \\ \vdots & & \vdots & & \vdots \\ \left| d_{rc_{a,n-m}} - d_{rc_{b,1}} \right| & \cdots & \left| d_{rc_{a,n-m}} - d_{rc_{b,l}} \right| & \cdots & \left| d_{rc_{a,n-m}} - d_{rc_{b,n-m}} \right| \end{bmatrix}, \tag{10}$$

where $k = 1,2,\ldots,n-m, and\ l = 1,2,\ldots,n-m$. In some cases could appear superposition between two echoes that came from paths a and b, and therefore they would present in the signal as a single peak. The main diagonal provides the solution for these cases. The component $e_{crack\,k,l}$ is de minimum difference between both paths, given by:

$$e_{crack\,k,l} = d_{kl} : \quad d_{kl} = \min(\mathbf{D}) \leftrightarrow d_{kl} < \mathrm{t}, \quad \forall k,l. \tag{11}$$

The solution to the problem of location is $f_{crack,a}$, which is the distance of the crack from the sensor.

$$f_{crack,a} = drc_{a,k}, \ \forall\ k : \ d_{kl} = \min(\mathbf{D}) \leftrightarrow d_{kl} < \mathrm{t}, \quad \forall k,l. \tag{12}$$

The main diagonal is not taken into account for all other cases because it is assumed that there are no overlapping echoes. The difference between the $d_{rc_{a,k}}$ and $d_{rc_{b,l}}$ must be within the tolerance.

$$e_{crack} = d_{kl} : \quad d_{kl} = \min(\mathbf{D}) : k \neq l \leftrightarrow \ \mathbf{D}_{kl} < \mathrm{t}, \forall k,l. \tag{13}$$

$$f_{crack,a} = drc_{a,k}, \ \forall\ k : \ d_{kl} = \min(\mathbf{D}) : k \neq l \leftrightarrow d_{kl} < \mathrm{t}, \quad \forall k,l. \tag{14}$$

In some cases, there may be a need to consider the amplitude of each echo to perform the analysis. Theoretically an echo coming from a large transverse crack should have a greater amplitude than the echoes from smaller cracks, because more energy will be reflected.

The equation (15) weights the more similar distances with the amplitude of the two echoes of each path.

$$f^{w}_{crack,a} = drc_{a,k}, \ \forall\ k : \ d_{kl} = \min\left(\frac{\left| d_{rc_{a,k}} - d_{rc_{b,l}} \right|}{\mathrm{y}_{cracks\,k} + \mathrm{y}_{cracks\,l}} \right) : k \neq l, \quad \forall k,l. \tag{15}$$

In most cases the amplitude of the echoes is several orders of magnitude smaller than the 'x' axis.

The equation (16) is a heuristic expression which gives more weight to the amplitude and corrects this problem.

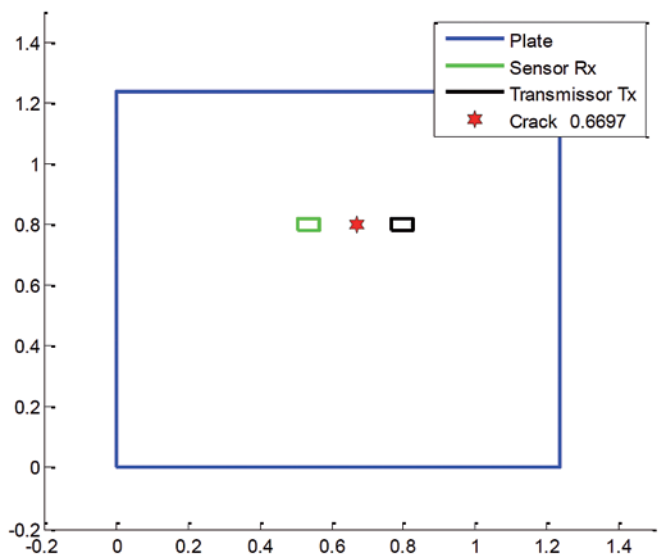

Fig. 14. Crack location relative to the left edge (meters)

$$f^{w}_{crack,a} = drc_{a,k},\ \forall\ k:\ \ d_{kl} = \min\left(\frac{\sqrt[g]{\left|d_{rc_{a,k}} - d_{rc_{b,l}}\right|}}{\left(y_{cracks\,k} + y_{cracks\,l}\right)^{g}}\right) \quad (16)$$

$$: k \neq l,\ \ \forall k,l,g$$

Finally, when the location is determined the crack is shown in a schematic with the actual dimensions of the plate and the position of the sensors (Figure 14).

5. Conclusions

This paper presents a new SHM approach using EMATs and advanced signal processing to automatically identify, locate and determine the severity of a defect in a plate. The technique presented could be used to detect defects in pipes operating under relatively high temperature. The approach employed is based on pre-filtering and denoising using Wavelet methodologies and the Hilbert Transform to detect relevant peaks. The Time of Flight (ToF) of the echoes is calculated theoretically and then compared with the experimental times to determine which echoes come from the plate borders. Any other echo represents a potential crack. Echoes from the same defect travelling on different paths are compared and the defect is located by taking consideration of the amplitude.

Acknowledgements

This work has been supported by the EU project INTERSOLAR (Ref.: FP7-SME-2013-605028) and the MINECO projects Ref.: RTC-2016-5694-3 and DPI2015-67264-P. The authors would like to thank Sonemat UK for their contribution to the manufacture of the EMAT transducers.

References

1. Aktas M, Turkmenoglu V. Wavelet-based switching faults detection in direct torque control induction motor drives. IET Science, Measurement & Technology 2010; 4(6): 303-310, https://doi.org/10.1049/iet-smt.2009.0121.
2. Canal M R. Comparison of wavelet and short time Fourier transform methods in the analysis of EMG signals. Journal of Medical Systems 2010; 34(1): 91-94, https://doi.org/10.1007/s10916-008-9219-8.
3. Chen Y. Acoustical transmission line model for ultrasonic transducers for wide-bandwidth application. Acta Mechanica Solida Sinica 2010; 23(2): 124-134, https://doi.org/10.1016/S0894-9166(10)60014-6.
4. Dai D, He Q. Structure damage localization with ultrasonic guided waves based on a time–frequency method. Signal Processing 2014; 96: 21-28, https://doi.org/10.1016/j.sigpro.2013.05.025.
5. Ruiz R, Garcia F P, Dimlaye V. Maintenance management of wind turbines structures via MFCs and wavelet transforms. Renewable and Sustainable Energy Reviews 2015; 48: 472-482, https://doi.org/10.1016/j.rser.2015.04.007.
6. Ruiz R, Garcia, F P, Dimlaye V, Ruiz D. Pattern recognition by wavelet transforms using macro fibre composites transducers. Mechanical Systems and Signal Processing 2014; 48(1): 339-350.
7. Dong Y, Shi H, Luo J, Fan G, Zhang C. Application of wavelet transform in MCG-signal denoising. Modern Applied Science 2010; 4(6): 20, https://doi.org/10.5539/mas.v4n6p20.
8. Eristi H. Fault diagnosis system for series compensated transmission line based on wavelet transform and adaptive neuro-fuzzy inference system. Measurement 2013; 46(1): 393-401, https://doi.org/10.1016/j.measurement.2012.07.014.
9. García F P, García I. Principal component analysis applied to filtered signals for maintenance management. Quality and Reliability Engineering International 2010; 26(6): 523-527, https://doi.org/10.1002/qre.1067.
10. García F P, Chacón J M, Tobias A M. B-Spline approach for failure detection and diagnosis on railway point mechanisms case study. Quality Engineering 2015; 27(2): 177-185, https://doi.org/10.1080/08982112.2014.933980.
11. García F P, Pedregal D J, Roberts C. Time series methods applied to failure prediction and detection. Reliability Engineering & System Safety 2010; 95(6): 698-703, https://doi.org/10.1016/j.ress.2009.10.009.
12. Genovese L, Neelov A, Goedecker S, Deutsch T, Ghasemi S A, Willand A. Schneider R. Daubechies wavelets as a basis set for density functional pseudopotential calculations. The Journal of chemical physics 2008; 129(1), https://doi.org/10.1063/1.2949547.
13. Jia M T, Wang Y C. Application of wavelet transformation in signal processing for vibrating platform. Journal-Shenyang Institute of Technology 2003; 22(3): 53-55.
14. Light-Marquez A, Sobin A, Park G, Farinholt K. Structural damage identification in wind turbine blades using piezoelectric active sensing. Structural Dynamics and Renewable Energy 2011; 1: 55-65, https://doi.org/10.1007/978-1-4419-9716-6_6.
15. Ljung L. System Identification Toolbox for Use with {MATLAB} 2007.
16. Marquez F P. An approach to remote condition monitoring systems management. Railway Condition Monitoring. The Institution of Engineering and Technology International Conference 2006: 156-160, https://doi.org/10.1049/ic:20060061.
17. Márquez F P. A New Method for Maintenance Management Employing Principal Component Analysis. Structural Durability & Health Monitoring 2010; 6(2): 89-99.
18. Márquez F P, Muñoz J M. A pattern recognition and data analysis method for maintenance management. International Journal of Systems Science 2012; 43(6): 1014-1028, https://doi.org/10.1080/00207720903045809.
19. Márquez F P, Pardo I, Nieto M. Competitiveness based on logistic management: a real case study. Annals of Operations Research 2013: 1-13.
20. Márquez F P G, Pedregal D J, Roberts C. New methods for the condition monitoring of level crossings. International Journal of Systems Science 2015; 46(5): 878-884, https://doi.org/10.1080/00207721.2013.801090.
21. Márquez F P, Pérez, J M, Marugán A P, Papaelias M. Identification of critical components of wind turbines using FTA over the time. Renewable Energy 2016; 87(2): 869–883, https://doi.org/10.1016/j.renene.2015.09.038.
22. Márquez F P, Tobias A M, Pérez J M, Papaelias M. Condition monitoring of wind turbines: Techniques and methods. Renewable Energy 2012; 46: 169-178, https://doi.org/10.1016/j.renene.2012.03.003.
23. Marugán A P, Márquez F P. A novel approach to diagnostic and prognostic evaluations applied to railways: A real case study.

Proceedings of the Institution of Mechanical Engineers, Part F: Journal of Rail and Rapid Transit 2016; 230(5): 1440-1456, https://doi.org/10.1177/0954409715596183.
24. Morsi W G, El-Hawary M E. Novel power quality indices based on wavelet packet transform for non-stationary sinusoidal and non-sinusoidal disturbances. Electric Power Systems Research 2010; 80(7): 753-759, https://doi.org/10.1016/j.epsr.2009.11.005.
25. Muñoz J, Márquez F P, Papaelias M. Railroad inspection based on ACFM employing a non-uniform B-spline approach. Mechanical Systems and Signal Processing 2013; 40(2): 605-617, https://doi.org/10.1016/j.ymssp.2013.05.004.
26. Nieto N, Marcela D. The use of the discrete Wavelet transform in the reconstruction of sinusoidal signals. Scientia et Technica 2008; 38: 381-386.
27. Papaelias M, Cheng L, Kogia M, Mohimi A, Kappatos V, Selcuk C, García F P, Gan T H. Inspection and Structural Health Monitoring techniques for Concentrated Solar Power plants. Renewable Energy2016; 85: 1178-1191, https://doi.org/10.1016/j.renene.2015.07.090.
28. Pedregal D J, García F P, Roberts C. An algorithmic approach for maintenance management based on advanced state space systems and harmonic regressions. Annals of Operations Research 2009; 166(1): 109-124, https://doi.org/10.1007/s10479-008-0403-5.
29. Peng Z K, Chu F L. Application of the wavelet transform in machine condition monitoring and fault diagnostics: a review with bibliography. Mechanical Systems and Signal Processing 2004; 18(2): 199-221, https://doi.org/10.1016/S0888-3270(03)00075-X.
30. Pérez, J. M. P., Márquez, F. P. G., & Hernández, D. R. (2016). Economic viability analysis for icing blades detection in wind turbines. Journal of Cleaner Production, 135, 1150-1160, https://doi.org/10.1016/j.jclepro.2016.07.026.
31. Pliego,A, García F P, Lorente J. Decision making process via binary decision diagram. International Journal of Management Science and Engineering Management 2015; 10(1): 3-8, https://doi.org/10.1080/17509653.2014.946977.
32. Su Z, Ye L. Identification of damage using Lamb waves: from fundamentals to applications Springer Science & Business Media 2009; 48.
33. Wang X, Peter W T, Mechefske C K, Hua M. Experimental investigation of reflection in guided wave-based inspection for the characterization of pipeline defects. NDT & E International 2010; 43(4): 365-374, https://doi.org/10.1016/j.ndteint.2010.01.002.
34. Wu J D, Liu C H. Investigation of engine fault diagnosis using discrete wavelet transform and neural network. Expert Systems with Applications 2008; 35(3): 1200-1213, https://doi.org/10.1016/j.eswa.2007.08.021.

Carlos Quiterio GÓMEZ Muñoz
Ingenium Research Group
European University of Madrid
Tajo street, C Building, C4 office, 28670, Villaviciosa de Odon
Madrid, Spain

Fausto Pedro GARCÍA Marquez
Alfredo ARCOS Jimenez
Ingenium Research Group
Castilla-La Mancha University
Politecnic Building, Camilo José Cela Street, 13071
Ciudad Real, Spain

Liang CHENG
Maria KOGIA
Abbas MOHIMI
Brunel Innovation Centre
TWI, Granta park, Granta Park
Cambridge, CB21 6AL
United Kingdom

Mayorkinos PAPAELIAS
School of Metallurgy and Materials
University of Birmingham
Edgbaston
Birmingham, B15 2TT
United Kingdom

E-mails: carlosquiterio.gomez@universidadeuropea.es, faustopedro.garcia@uclm.es, alfredo.arcos@alu.uclm.es, liang.cheng@brunel.ac.uk, maria.kogia@brunel.ac.uk, abbas.mohimi@brunel.ac.uk, m.papaelias@bham.ac.uk

Article citation info:
CHŁOPEK Z, BEBKIEWICZ K. Model of the structure of motor vehicles for the criterion of the technical level on account of pollutant emission. Eksploatacja i Niezawodnosc – Maintenance and Reliability 2017; 19 (4): 501-507, http://dx.doi.org/10.17531/ein.2017.4.2.

Zdzisław CHŁOPEK
Katarzyna BEBKIEWICZ

MODEL OF THE STRUCTURE OF MOTOR VEHICLES FOR THE CRITERION OF THE TECHNICAL LEVEL ON ACCOUNT OF POLLUTANT EMISSION

MODEL STRUKTURY POJAZDÓW SAMOCHODOWYCH DLA KRYTERIUM POZIOMU TECHNICZNEGO ZE WZGLĘDU NA EMISJĘ ZANIECZYSZCZEŃ*

Inventory of total vehicle pollution emission is only possible through the use of emission modelling. One of the most difficult problems in modelling total emission from motor vehicles is the identification of the structure of vehicle fleet. While it is possible to use vehicle registration data to model the numerosity of elementary vehicle categories, it is very difficult to design representative driving cycles for vehicles in separate categories, in the absence of empirical evidence. The article proposes two models of the structure of motor vehicles for the criterion of technical level on account of pollutant emission. The method of modelling the intensity of use of motor vehicles by elementary categories on account of pollutant emission, outlined in this article, is the first unique undertaking in this field on a global scale. This method was used for inventorying pollutant emission from motor vehicles in Poland, in the years 2000–2015.

Keywords: *motor vehicles, inventory of pollutant emission, motor vehicle categories.*

Inwentaryzacja całkowitej emisji zanieczyszczeń samochodowych jest możliwa tylko dzięki zastosowania modelowania emisji zanieczyszczeń. Jednym z najtrudniejszych problemów modelowania całkowitej emisji zanieczyszczeń z pojazdów samochodowych jest identyfikacja ich struktury. O ile jest możliwe wykorzystanie danych związanych z rejestracją pojazdów samochodowych do modelowania liczności kategorii pojazdów samochodowych, o tyle wyznaczenie reprezentatywnych przebiegów pojazdów elementarnych kategorii jest zadaniem bardzo trudnym ze względu na brak wyników badań empirycznych. W artykule zaproponowano dwa modele struktury pojazdów samochodowych dla kryterium poziomu technicznego ze względu na emisję zanieczyszczeń. Przedstawiony w niniejszym artykule sposób modelowania intensywności użytkowania pojazdów samochodowych kategorii elementarnych ze względu na emisję zanieczyszczeń jest pierwszym unikatowym przedsięwzięciem w tym zakresie w skali światowej. Metodę tę zastosowano do inwentaryzacji zanieczyszczeń pojazdów samochodowych w Polsce w latach 2000–2015.

Słowa kluczowe: *pojazdy samochodowe, inwentaryzacja emisji zanieczyszczeń, kategorie pojazdów samochodowych.*

1. Introduction

The aim of this paper is to present the author's original mathematical model of intensity of using motor vehicles to be applied for inventorying emissions from road transport. The measure of car use intensity, in case of quantifying the release of pollutants within one year, is an annual vehicle mileage. Determining the intensity of motor vehicle use is one of the most difficult tasks in the inventory of pollutant emission from road transport.

Numerous publications, including both scientific papers [6, 7, 18, 24, 25, 27, 31, 35] and methodological manuals, as well as reports from pollutant emission inventories [1, 8, 14–17, 19–21, 23, 28, 30, 32], do not contain any models of intensity of using motor vehicles. In case of quantifying the emission of pollutants at local scale, as e.g. in urban areas, the results of empirical studies made with the use of sensors to identify traffic characteristics and vehicle type (among others: induction loops and camera systems) have often been used to estimate vehicle mileage [24, 25]. In the latter case, the estimation of traffic intensity is only correct for vehicle categories at a very elevated level of aggregation, e.g. for such categories as small vehicles (passenger cars and light duty commercial vehicles) and large vehicles (heavy duty vehicles and buses). Consequently, the latter data is completely useless for application in the software commonly used for inventorying pollution from road transport, e.g. COPERT (Computer Programme for calculating Emissions from Road Traffic [14, 18]. The same is valid when traffic intensity data is applied in a local scale, using traffic simulators such as VISUM, VISSIM, TREM and VADIS [7]. Similarly, the use of complex systems, such as results of empirical research and vehicle traffic modelling, including neural networks [24] or Newell kinematic waveforms for vehicle traffic modelling [35], do not provide opportunities for identifying the intensity of car use, taking into account the different vehicle classification criteria, due to the requirements of software for emission estimation, e.g. COPERT.

Some publications, including, among others, reports from pollutant emission inventories [20, 28, 30, 32], contain only qualitative descriptions of procedures for determining the annual mileage of cars, which are based on data recorded during technical inspection reviews. These data are used to establish the annual mileage of cumulative categories; these mileage are estimated as average values based on vehicle data. However, there are no generalizations, and even more so, attempts to model the intensity of use of motor vehicles. In these reports, there is only a qualitative assessment of motor vehicle use intensity indicating, namely, that newer cars have higher average annual mileage than older cars, and therefore vehicles with better environmental performance due to emissions are more heavily used [20, 28].

(*) Tekst artykułu w polskiej wersji językowej dostępny w elektronicznym wydaniu kwartalnika na stronie ***www.ein.org.pl***

Account taken of the above-mentioned state of knowledge, it was deemed purposeful, for both cognitive and practical reasons, to attempt to generalize knowledge about how the intensity of motor vehicle use depends on vehicle quality due to pollutant emission. The practical aspect of modelling the intensity of use of motor vehicles, according to their environmental characteristics, is unequivocal: it is the only possibility to provide data for the inventory of traffic pollutant emissions in view of the lack of, at least in Poland, empirical data on annual mileage of cars of different ecological categories.

The model of intensity of motor vehicle use, developed by the authors, constitutes the first unique attempt on a global scale to solve the above important problem linked to the use of motor vehicles. The experience gained by both the authors [3–5] and the practitioners in the environmental impact assessment of road traffic, with the use of the developed model, make it possible to formulate positive opinions about its usefulness.

2. Bases for modelling the total pollutant emission from motor vehicles

The total pollutant emission from motor vehicles can only be determined through the use of emission modelling. [1, 3–8, 13–21, 23–25, 27, 28, 30–32, 35]. The same is valid for the total energy consumption by motor vehicles [13]. In case of fuel consumption, however, it is possible to estimate, or at least approximate, this amount [11]. This is why, it is necessary to model pollutant emissions from road transport in order to assess the environmental pollution by motor vehicles.

The model of total pollutant emission is simple: the total pollutant emission constitutes a superposition of emission released from individual vehicles [3, 8, 13–19, 23]. The above is underlain by the following assumptions [3, 8, 13]:

- the intensity of the emission of particular pollutants is an additive,
- inventory of pollutants concerns substances in the state emitted from vehicles, not the substances that are subject to environmental changes.

The intensity of pollutant emissions associated with the use of motor vehicles with internal combustion engines is the sum of pollutant emissions for the states of [3, 8, 13–19, 23]:

- internal combustion engine heated to a stable temperature,
- internal combustion engine warm up,
- fuel evaporation from the car fuel system.

$$E_x = E_{xs} + E_{xh} + E_{xV} \tag{1}$$

where: E_x – the intensity of emission of pollutant „x”,
E_{xs} – the intensity of pollutant emission intensity for internal combustion engine heated up to a stable temperature,
E_{xh} – the intensity of pollutant emission for the engine warm phase,
E_{xV} – the intensity of pollutant emission for evaporation from the car fuel system.

Due to the purpose of the article, further considerations will be made using the example of emissions from diesel engines heated to a stable temperature. The modelling of the structure of vehicle fleet, which is the subject of this work, is also applicable to the remaining two states of the engine [3, 8, 13–19, 23].

The most significant challenge in modelling total emissions from motor vehicles is model identification. Of course, it is impossible to model pollutant emissions from all individual vehicles. First of all, the concept of vehicle categories is introduced in pollution modelling. Category means in philosophy the concept that introduces the structure, and therefore the term denotes a class of objects that have certain characteristics and interrelated relationships. The basic criteria for classifying motor vehicles into respective categories include [3, 8, 13–19, 23]:

- vehicle construction purpose,
- contractual size of vehicle or of internal combustion engine,
- properties resulting from the construction solutions applied,
- fuel type applied,
- technological level, with special regard to pollutant emission.

Taking into account the adopted criterial characteristics, vehicles displaying all the above characteristics qualify to the elementary category of motor vehicles. Whereas, the cumulated category of motor vehicles embraces vehicle types displaying various criterial characteristics. Consequently, there exist different levels of cumulation of motor vehicles within individual categories.

In modelling of pollutant emission, the notion of traffic conditions has been introduced, characterized by the properties of vehicle traffic. Consequently, it is assumed, that the intensity of pollutant emission constitutes a superposition of emissions from individual vehicles under particular traffic conditions which determine pollutant emission.

The conditions for motor vehicle traffic have been modelled, using software for emission inventory, as typical vehicle driving patterns in traffic situations [3, 8, 13–19, 23]:

- in cities – urban,
- outside cities – rural,
- on highways and expressways.

There is also a possibility to separate, from a model accounting for urban driving cycle, a segment pertaining to street congestion situations; in the latter circumstances, models accounting for urban driving cycles have been replaced by models of motor vehicle motion mode [9]:

- in the street congestion situations,
- in cities, disregarding the street congestion situations.

In modelling pollutant emission from motor vehicles, under model traffic conditions, a more specific dependence of pollutant emission on the velocity process is additionally considered [1, 3, 8, 13–19, 21, 23]. Most often, the average value of velocity is assumed as the zero-dimensional characteristics of the velocity process [1, 3, 8, 13–19, 21, 23]. The specific distance emission – a derivative of pollutant emission (mass) with respect to the distance travelled by a vehicle – is utilized in modelling of the total emission of pollutants [3, 13].

Account taken of the assumptions adopted, the intensity of the total pollutant emission, averaged over one year, may be modelled for separate elementary categories, under each of the modelled traffic conditions, as the value proportionate to [1, 3, 8, 13–19, 23]:

- the number of vehicles in a category,
- the distance travelled by a vehicle, representative of a given category, over one year, what constitutes a measure of the vehicle use intensity,
- the characteristics of pollutants specific distance emission for a vehicle representative of a category.

$$E_{ax} = N \cdot p \cdot b_x \tag{2}$$

where: N – the number of vehicles in a given category,
p – the distance travelled by vehicle representative of a given category over one year,
b_x – the specific distance emission of pollutant „x”.

The intensity of the total emission from motor vehicles is a superposition of emissions from individual vehicle categories, under considered particular traffic conditions, which determine pollutant emissions [3, 13].

The intensity of the total annual emission of pollutants with respect to averaging over one year is called annual emission [3–5, 13], while in national reports on yearly emission inventories, the term: 'national annual emission of pollutants' is applied [3–5].

The criteria for classifying motor vehicles include [1, 3, 8, 13–19, 21, 23]:

1. Vehicle purpose:
   - passenger cars,
   - light commercial vehicles (vans),
   - heavy duty trucks,
   - urban buses,
   - coaches,
   - motorcycles,
   - mopeds[1].
2. Contractual size, properties and technical level of motor vehicles:
   - the contractual size is considered with respect to: (i) volume of engine displacement: for passenger cars and light duty vehicles as well as for motorcycles and mopeds, and (ii) maximum vehicle mass – for heavy duty trucks and buses,
   - the type of combustion system of internal combustion engine: spark ignition engines and compression ignition engines,
   - the type of cycle: four stroke and two stroke engines,
   - the technological level of road vehicles with regard to both: the stage of environmental protection regulations concerning effects of motor vehicle operation modes and to the date when the vehicle was first placed on the market,
   - the fuel type applied: motor gasoline, diesel, LPG – Liquefied Petroleum Gas, natural gas (CNG – Compressed Natural Gas and LNG – Liquefied Natural Gas) as well as other non-conventional fuels.

The number of vehicles in the individual elementary categories can be, at least approximately, determined based on the information on registered cars. One of the most significant challenges in identification of models accounting for the total emission from motor vehicles is the assessment of the intensity of use of motor vehicles belonging to individual categories, and particularly to elementary categories. In the framework of developing software to assist with the calculation of road transport emission, by the end of the 20th century, there were undertaken research programmes in the developed countries, aiming at the estimation of annual distances travelled by motor vehicles from elementary categories [8, 15, 19]. Despite that large financing was dedicated to these programmes, only a part of their results found reasonable practical application, among others in Germany and Switzerland [8, 15, 19]. The analysis of results of study on the structure of vehicle fleet in Western Europe, on the basis of reports of the programme CORINAIR (Core Inventory of Air Emissions) [15, 19], made it possible to produce a model of the delay of the condition of motorization in Poland, in relation to the state of motorization in Western Europe [12]. This model, however, can only be used for categories at the highest cumulation level, e.g. passenger cars, light duty vehicles, heavy duty vehicles and buses, as well as motorcycles and mopeds.

The subject of modelling the intensity of use of vehicles by elementary categories was undertaken in view of the lack of sufficient empirical material to determine the annual mileage of vehicles representing elementary categories and, in particular, in view of the technical level of cars in Poland.

1 In accordance with the Law of 20 June 1997: Act on Road Traffic (Official Journal of 2012, item 1137), motor vehicle means any vehicle that is motor powered, except mopeds and rail cars. Irrespective of the above definition, modelling emission from road transport also covers mopeds as elements of the set of motor vehicles.

3. Modelling the intensity of use of motor vehicles by elementary categories

Information pertaining to car registration may provide grounds to develop the description of the vehicle fleet structure. This concerns the purpose of vehicles and their contractual size. In particular, the environmental performance of a motor vehicle is determined by the date of placing the car on the market [2–5]. Of course, there are some difficulties in taking efficient advantage of data from bases on car registration, to the description of the structure of vehicle fleet, since the criteria for vehicle classification are sometimes very demanding with respect to details, as is the case with the COPERT software programme.

Despite these difficulties, the past experience of authors suggests the possibility of effective use of official data on the number of vehicles, contained in the databases of the Central Information System of Vehicles and Drivers (CEPiK) for use in the COPERT software programme [2–5].

The significant challenge in describing the structure of vehicle fleet constitute data on the annual mileage of vehicle, representative of individual elementary categories. Up to now, there are no information systems for collecting data on annual mileage travelled by particular vehicles, despite that such attempts have been undertaken. However, if such an undertaking is successful, then there will be no data on vehicle mileage s in previous years, and the analysis of emission trends of individual pollutants plays an important role in the inventory of pollutant emission from motor vehicles [4, 5].

The up-to-date surveys of annual car mileage s in Poland carried out on sets of vehicles with statistical inertia make it possible, however, to approximate the annual mileage of cumulative vehicle categories, describing the intended use of vehicles and, to a lesser extent, their contractual size and constructional characteristics [11]. The major challenge is the determination of annual mileage for elementary categories of vehicles due to pollutant emission. Consequently, it was undertaken to model the intensity of use of motor vehicles for elementary categories of vehicles due to release of pollutants.

From the information contained in the databases used in the software build for determining vehicle emission characteristics, primarily from the INFRAS AG software [21], results a characteristic feature for the annual mileage of elementary vehicles of different emission classes.

These categories are described by the names of successive stages of motor vehicle homologation regulations with respect to the emission of pollutants [2, 33, 34]:

- for cars with a maximum mass lower than 3.5 Mg for Euro 1 – 4 rules, and a reference weight of less than 2.61 Mg for Euro 5 and 6: Pre Euro (or Conventional), Euro 1, Euro 2, Euro 3, Euro 4, Euro 5 and Euro 6,
- for cars with a maximum mass of more than 3.5 Mg for Euro I – IV, and with a reference mass greater than 2.61 Mg for Euro V and VI: Pre Euro (or Conventional), Euro I, Euro II, Euro III, Euro IV, Euro V and Euro VI.

Sometimes these categories are even more detailed, depending on sub-steps of further Euro regulations, e.g. Pre Euro (ECE 15/00-01, ECE 15/02, ECE 15/03 and ECE 15/04), Euro 5 and Euro 6 (Euro 6 and Euro 6c).

The characteristic feature of the annual mileage of elementary category vehicles of different emission classes is the fact, that newer vehicles have recently been in use, which have a higher class with respect to environmental performance. This fact is also confirmed by the results of review studies conducted in connection with balancing of fuel consumption [8, 20, 21, 28, 30, 32].

The model of the intensity of using motor vehicles, for elementary categories of vehicles with respect to pollutant emission, was decided

to be adopted in the form of a growing function of the values describing successive stages of vehicle approval regulations due to emission of pollutants – these values are growing as more and more recent phases of regulations appear. The proposed model is constructed according to the criterion of functional similarity (behavioral model) [10, 26].

The modeling of the intensity of use of vehicles by elementary environmental performance categories with respect to pollutant emission, consists of the following elements:

1. Arbitrary allocation of non-negative real numbers to individual environmental performance categories, according to the principle that higher quality environmental categories correspond to higher numbers. The way of assigning numbers to individual environmental performance categories of vehicles used in this work is presented in tables 1–4.

Table 1. The way of assigning numbers to individual environmental performance categories of passenger cars

Category	y
Pre ECE	0
ECE 15/00-01	1
ECE 15/02	2
ECE 15/03	3
ECE 15/04	4
Euro 1	5
Euro 2	6
Euro 3	7
Euro 4	8
Euro 5	9
Euro 6	10

Table 2. The way of assigning numbers to individual environmental performance categories of light duty vehicles

Category	y
Coventional	0
Euro 1	1
Euro 2	2
Euro 3	3
Euro 4	4
Euro 5	5
Euro 6	6

Table 3. The way of assigning numbers to individual environmental performance categories of heavy duty vehicles, urban buses and long range coaches

Category	y
Conventional	0
Euro I	1
Euro II	2
Euro III	3
Euro IV	4
Euro V	5
Euro VI	6

Table 4. The way of assigning numbers to individual environmental performance categories of motorcycles and mopeds

Category	y
Coventional	0
Euro 1	1
Euro 2	2
Euro 3	3

2. Adoption of models describing the relative intensity – k – of using of motor vehicles belonging to elementary environmental performance categories with respect to pollutant emission, in the form:

Model 1 is in the form [29]:

$$k_1 = 1 - \exp\left(-a \cdot x^{c+1}\right) \cdot \left(1 - k_{\min}\right) \tag{3}$$

Model 2 was adopted as a function:

$$k_2 = \left\{ \frac{arctg\left[d \cdot (x - 0.5)\right]}{arctg(0.5 \cdot d) - arctg(-0.5 \cdot d)} + 0.5 \cdot \frac{1 + k_{\min}}{1 - k_{\min}} \right\} \cdot \left(1 - k_{\min}\right) \tag{4}$$

whereat:

$$x = \frac{y}{y_{\max}}. \tag{5}$$

where: y_{max} – the maximum value of numbers 'y' from tables 1–4 for a given year of estimating pollutant emission.

The value k_{min} is the relative intensity of using motor vehicles belonging to the lowest category of environmental performance.
The model parameters are:

- for model 1: a, c;
- for model 2: d.

3. Scaling of the average annual mileage of motor vehicles belonging to elementary environmental performance categories, with respect to pollutant emission to the average annual mileage of motor vehicles of cumulative categories.

In figure 1, a comparison is presented of both models for k_{min} = 0.25 as well as model parameters: a = 6.908, c = 2.5 and d = 7.

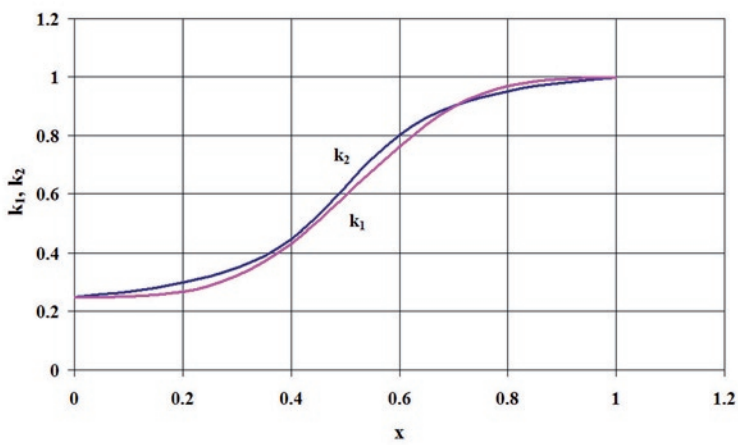

Fig. 1. Models of relative intensity of use of motor vehicles belonging to elementary environmental performance categories with respect to pollutant emission

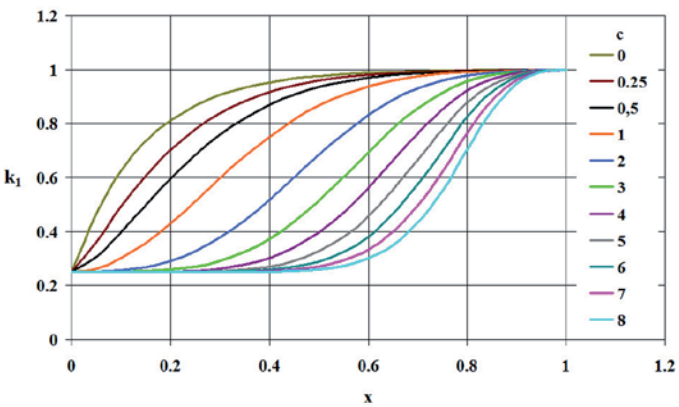

Fig. 2. Results of testing model 1 due to variable parameter 'c'

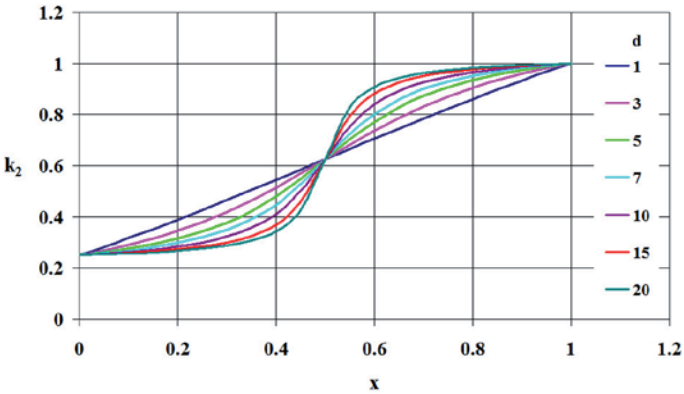

Fig. 3. Results of testing model 2 due to variable parameter 'd'

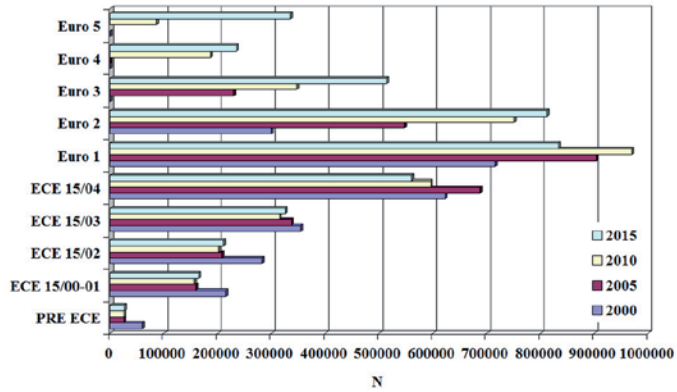

Fig. 4. Number of passenger cars with spark ignition engines and displacement volume contained with the limits (1.4 ÷ 2) dm^3, by environmental performance categories

The models were tested for their parameters. The test results are given in figures 2 and 3.

Model 1 is much more sensitive to parameter 'c'. Regardless of the parameter, antisymmetry is significant for model 2. The existing knowledge, based on the authors' own research and on data from INFRAS AG software as well as from the EU Member State reports under the CORINAIR program, indicates that model 1 is more effective in modeling the intensity of use of motor vehicles due to their category of emission characteristics.

Of course, due to the lack of sufficiently rich empirical evidence, the major challenge is to identify the model. However, this difficulty

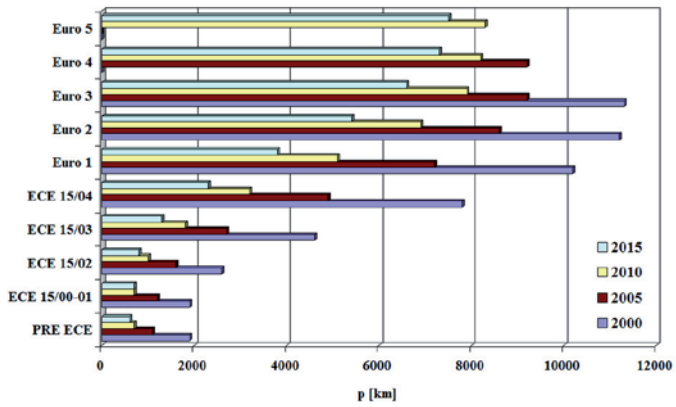

Fig. 5. Average annual mileage of passenger cars with spark ignition engines and displacement volume contained with the limits (1.4 ÷ 2) dm^3, by environmental performance categories

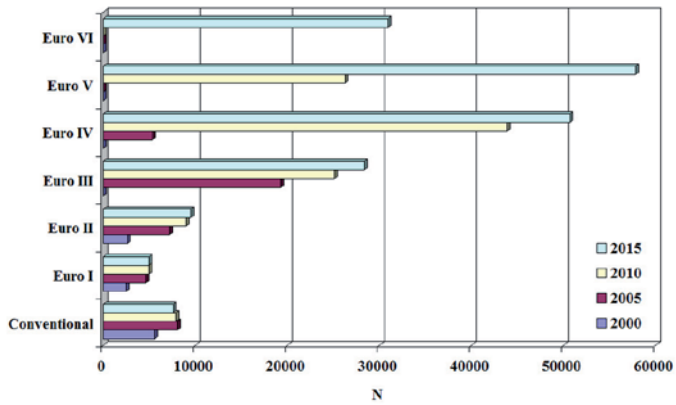

Fig. 6. Number of heavy duty trucks with the maximum mass contained in the limits (34 ÷ 40) Mg, by environmental performance categories.

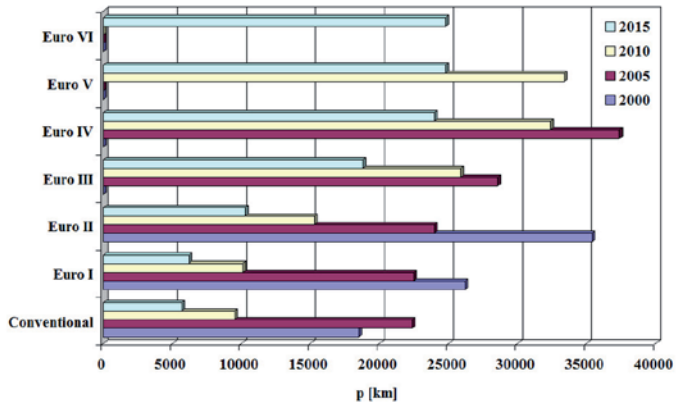

Fig. 7. Average annual mileage of heavy duty trucks with the maximum mass contained in the limits (34 ÷ 40) Mg, by environmental categories.

is greatly mitigated by the fact, that the scope of the model parameters under consideration can be limited, based on the existing knowledge, to the limits:

- for model 1: c = 1 ÷ 4;
- for model 2: d = 7 ÷ 15;

while the sensitivity of the models within the scope of the above values of both parameters is not strong.

It is impossible, in practice, to apply the classic methods of identification [22] of the proposed models. Therefore, the models are tuned, while their verification is performed through the test of compliance of

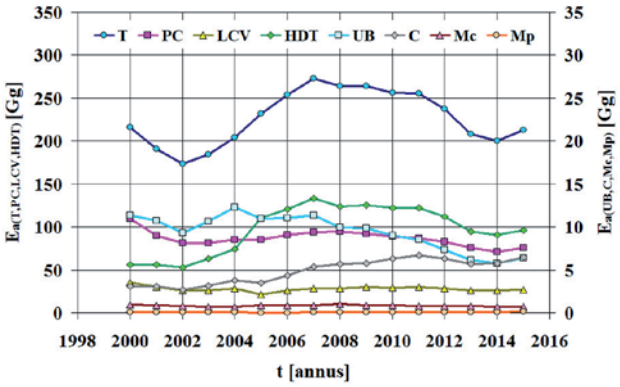

Fig. 8. National annual emission of nitrogen oxides from vehicles of cumulated categories.

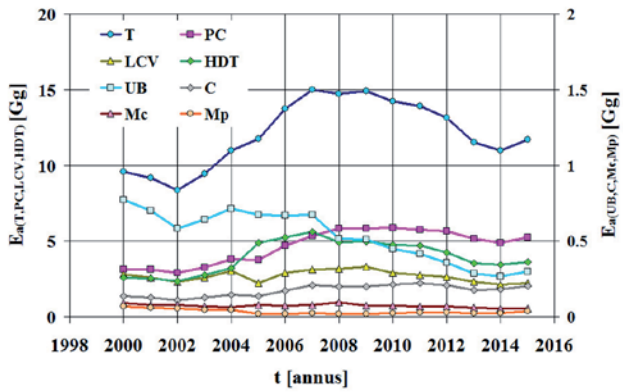

Fig. 9. National annual emission of particulates PM10 from vehicles of cumulated categories.

the total annual fuel consumption by motor vehicles obtained via the modelling with the official data of the Central Statistical Office [3–5].

Figures 4–7 illustrate, for example, the number and annual mileage of vehicles of the two cumulative categories: passenger cars with spark ignition engines and displacement volume contained with the limits (1.4 ÷ 2) dm^3 as well as heavy duty trucks with the maximum mass within the limits (34 ÷ 40) Mg, for the years 2000, 2005, 2010 and 2015. The number of vehicles by environmental performance categories for the years 2000, 2005 and 2010 was determined on the basis of the data contained in CEPiK, while for the year 2015 – the car's numerical structure was estimated based on the data of the Central Statistical Office (due to lack of data from CEPiK). The Model 1 intensity of use of vehicles with the parameters a = 6.908 and m = 2.5 was used to determine vehicle mileage by respective environmental performance categories.

The results of the use of the model clearly show: increasing annual mileage of vehicles of higher environmental performance categories.

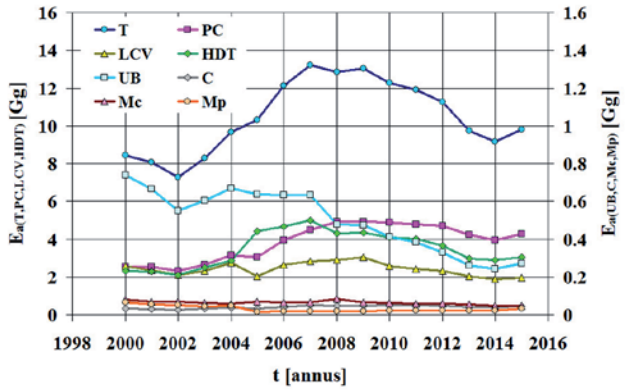

Fig. 10. National annual emission of particulates PM2.5 from vehicles of cumulated categories.

The use of the model 1, accounting for the intensity of using motor vehicles has made it possible to investigate the annual national pollutant emission from motor vehicles in Poland [3–5].

Figures 8–10 show the sample results for the years 2000–2015 – national annual emission – E_a oxides of nitrogen, particulates PM10 and particulates PM2.5 for cumulative categories: all motor vehicles – T, passenger cars – PC, light commercial vehicles – LCV, heavy duty trucks – HDT, urban buses – UB, coaches – C, motorcycles – Mc and mopeds – Mp.

It is clear from figures 8–10 that, for example, the national annual emission of substances which constitute one of the most serious problems in the use of motor vehicles, have been decreasing since around 2007, despite the fact, that the number of vehicles and the intensity of their use have been considerably increasing. This is the result of technical progress in the design of motor vehicles.

4. Recapitulation

The way of modelling the intensity of use of motor vehicles belonging to elementary categories with respect to pollutant emission, outlined in this article, is the first unique undertaking in this field on a global scale. The proposed models are built according to the criterion of functional similarity. Tests on the models show that their sensitivity within the scope of real values of model parameters is not too large, to unable the models to be fine tuned with the use, as the compliance criterion, of the total fuel consumption data from models and those officially published. The presented results of applying one of the developed models are consistent with the state of the art. An example of practical use of one of the developed models is the inventory of pollutant emission from motor vehicles in Poland in the years 2000–2015, made using the COPERT software. These results have been presented in the official reports of the European Union.

References

1. 2006 IPCC Guidelines for National Greenhouse Gas Inventories. http://www.ipcc-nggip.iges.or.jp/public/2006gl/ vol2.html. (2016–12–06).
2. AVL Emission Testing Handbook 2016.
3. Bebkiewicz K, Chłopek Z, Szczepański K, Zimakowska-Laskowska M. Issues of modeling the total pollutant emission from vehicles. Proceedings of the Institute of Vehicles. 2017; 110 (1): 103–118.
4. Bebkiewicz K, Chłopek Z, Szczepański K, Zimakowska-Laskowska M. Results of air emission inventory from road transport in Poland in 2014. Proceedings of the Institute of Vehicles 2017; 110 (1): 77–88.
5. Bebkiewicz K, Chłopek Z, Szczepański K, Zimakowska-Laskowska M. The influence of the properties of vehicles traffic on the total pollutant emission. Proceedings of the Institute of Vehicles 2017; 110 (1): 89–102.
6. Borge R et al. Development of road traffic emission inventories for urban air quality modeling in Madrid (Spain). 21st USEPA International Emission Inventory Conference. April 13–16, 2015. San Diego (California).

7. Borrego C et al. Integrated modelling of road traffic emissions: application to Lisbon air quality management. Cybernetics and Systems. An International Journal 2004; 35(5–6): 535–548.
8. BUWAL (Bundesamt für Umwelt, Wald und Landschaft), INFRAS AG (Infrastruktur-, Umwelt- und Wirtschaftsberatung). Luftschadstoffemissionen des Strassenverkehrs 1950–2010, BUWAL-Bericht 1995; 255.
9. Chłopek Z, Biedrzycki J, Lasocki J, Wójcik, P. Comparative examination of pollutant emission from an automotive internal combustion engine with the use of vehicle driving tests. Combustion Engines 2016; 164 (1): 56–64.
10. Chłopek Z, Piaseczny L. Remarks about the modelling in science researches. Eksploatacja i Niezawodnosc – Maintenance and Reliability 2001; 11 (4): 47–57.
11. Chłopek Z, Waśkiewicz J. Projections of the fuel consumption by the road transport in Poland. Journal of KONES 2013; 20 (2): 33–39.
12. Chłopek Z. Testings of vehicle ecological structure in European Union countries in consideration of emission model adaptation into polish conditions. Journal of KONES 2000: 65–76.
13. Chłopek Z. Zasady modelowania zużycia paliwa i energii oraz emisji zanieczyszczeń związanych z użytkowaniem pojazdów drogowych. (Principles of modeling of fuel and energy consumption and emission of pollutants associated with the use of road vehicles). Technika Transportu Szynowego 2015; 12: 262–267. (In Polish).
14. COPERT Training 5. COPERT 5 vs COPERT 4. European Environment Agency. 2016. http://emisia.com/sites/default/ files/COPERT_5_features.pdf. (2016–12–06).
15. CORINAIR – Coordinated Information on the Environment in the European Community – Air. http://reports.eea.europa.eu/EMEPCORINAIR4/en/page002. html. (2016–12–06).
16. COST 319. Estimation of pollutant emissions from transport. http://lat.eng.auth.gr/ COPERT/. (2016–12–06).
17. EMEP/EEA air pollutant emission inventory guidebook – 2016. European Environment Agency. http://www.eea. europa.eu/publications/emep-eea-guidebook-2016. (2016–12–06).
18. Gkatzoflias D, Kouridis Ch, Ntziachristos L, Samaras Z. COPERT 4 Computer programme to calculate emissons from road transport User manual (version 9.0). European Environment Agency. Emisia SA. 2012. (2016–12–06).
19. http://www.eea.europa.eu/publications/EMEPCORINAIR5. (2014–08–24).
20. Informative inventory report Sweden 2016. Swedish Environmental Protection Agency. Stockholm. 2016.
21. INFRAS AG. Handbook emission factors for road transport 3.2. Quick reference. Version 3.2. Bern, 2014.
22. Mańczak K.: Metody identyfikacji wielowymiarowych obiektów sterowania. Warszawa: Wydawnictwa Naukowo-Techniczne, 1979. (In Polish).
23. MEET. Methodologies for Estimating Air Pollutant Emissions from Transport. http://lat.eng.auth.gr/COPERT/. (2016–12–06).
24. Naranjo J E, Jimenez F, Serradilla F J, Zato J G. Floating car data augmentation based on infrastructure sensors and neural networks. IEEE (Institute of Electrical and Electronics Engineers) Transactions on Intelligent Transportation Systems 2012; 13: 107–114, https://doi.org/10.1109/TITS.2011.2180377.
25. Reynolds A W, Broderick B M. Development of an emissions inventory model for mobile sources. Transportation Research Part D: Transport and Environment 2016; 5: 77–101, https://doi.org/10.1016/S1361-9209(99)00025-5.
26. Rosenbluth A., Wiener N: The role of models in science. Phil. Sci. 1945: 12 (4), https://doi.org/10.1086/286874.
27. Saikawa et al. The impact of China's vehicle emissions on regional air quality in 2000 and 2020: a scenario analysis. Atmospheric Chemistry and Physics 2011; 11: 9465–9484, https://doi.org/10.5194/acp-11-9465-2011.
28. Sandmo T. The Norwegian Emission Inventory 2013. Documentation of methodologies for estimating emissions of greenhouse gases and long-range transboundary air pollutants. Statistics Norway. Oslo-Kongsvinger. 2013.
29. Vibe I I. Nowoje o rabocziem cikle dvigatieliej (Вибе И.И.: Новое о рабочем цикле двигателей – New about working cicle of engines). Sverdlovsk (Свердловск): Mashgiz Moskow (Машгиз Москва), 1962. (In Russian).
30. Wakeling D et al. UK informative inventory report (1990 to 2015). Final Version (v1.0). Ricardo Energy & Environment. March 2017. https://uk-air.defra.gov.uk/ assets/documents/reports/cat07/1703161205_GB_IIR_2017_Final_v1.0.pdf.
31. Wang H Z, Ni D H, Chen C Y, Li J. Stochastic modeling of the equilibrium speed-density relationship. Journal of Advanced Transportation 2013; 1(47): 126–150, https://doi.org/10.1002/atr.172.
32. Winther M.: Danish emission inventories for road transport and other mobile sources. Inventories until the year 2010. National Environmental Research Institute. University of Aarhus. 2012. Scientific Report No. 24. http://www.dmu.dk/Pub/SR24.pdf.
33. Worldwide emission standards. Heavy duty & off-road vehicles. Delphi. Innovation for the real world. 2015/2016.
34. Worldwide emission standards. Passenger cars and light duty vehicles. Delphi. Innovation for the real world. 2016/2017.
35. Zhou X et al. Integrating a simplified emission estimation model and mesoscopic dynamic traffic simulator to efficiently evaluate emission impacts of traffic management strategies. Transportation Research Part D: Transport and Environment 2015; 37: 123–136, https://doi.org/10.1016/j.trd.2015.04.013.

Zdzisław CHŁOPEK
Katarzyna BEBKIEWICZ
Institute of Environmental Protection – National Research Institute in Warsaw
The National Centre for Emissions Management (KOBiZE)
ul. Chmielna 132/134, 00-805 Warsaw, Poland

E-mails: zdzislaw.chlopek@kobize.pl, katarzyna.bebkiewicz@kobize.pl

Article citation info:
KOSUCKI A, MALENTA P, STAWIŃSKI Ł, HALUSIAK S. Energy consumption and overloads of crane hoisting mechanism with system of reducing operational loads. Eksploatacja i Niezawodnosc – Maintenance and Reliability 2017; 19 (4): 508–515, http://dx.doi.org/10.17531/ein.2017.4.3.

Andrzej KOSUCKI
Piotr MALENTA
Łukasz STAWIŃSKI
Sławomir HALUSIAK

ENERGY CONSUMPTION AND OVERLOADS OF CRANE HOISTING MECHANISM WITH SYSTEM OF REDUCING OPERATIONAL LOADS

ENERGOCHŁONNOŚĆ I PRZECIĄŻALNOŚĆ MECHANIZMU PODNOSZENIA SUWNICY Z UKŁADEM ZMNIEJSZANIA OBCIĄŻEŃ EKSPLOATACYJNYCH*

The paper presents the study of the hoisting mechanism for various lifting cases. For the developed method of reducing an operating overloads of the driving system of the hoisting mechanisms, studies of the energy consumption of the cycle and the dynamic overloads of the drive (and bearing structure) have been conducted in comparison with other methods of the payload lifting. The influence of a start-up time on the overloads and energy overloads of the mechanism was determined, taking into account the whole duty cycle time. Using the proposed start-up time, the influence of a lifting height and a weight of the lifted load on the drive overload and duty cycle power consumption were shown. Studies have shown good operating properties of a drive with overloads compensation system.

***Keywords**: hoisting winch, overloads, energy consumption, energetic efficiency.*

W artykule przedstawiono badania mechanizmu podnoszenia dla różnych przypadków podnoszenia ładunku. Dla opracowanej metody zmniejszania przeciążeń eksploatacyjnych układu napędowego mechanizmów podnoszenia przeprowadzono badania porównawcze energochłonności cyklu roboczego i przeciążalności dynamicznej napędów (i konstrukcji nośnej) w stosunku do innych sposobów rozruchu. Określony został wpływ czasu rozruchu na przeciążalność i przeciążalność energetyczną mechanizmu z uwzględnieniem czasu całego cyklu roboczego. Przedstawiono badania wpływu wysokości podnoszenia i masy podnoszonego ładunku na przeciążalność mechanizmu i energochłonność cyklu roboczego. Badania wykazały dobre własności eksploatacyjne napędu wykorzystującego metody kompensacji przeciążeń.

***Słowa kluczowe**: wciągarka, przeciążenia, energochłonność, efektywność energetyczna.*

Introduction

The energy consumption of production processes is more often considered in the context of possible energy savings. The important role during a process of goods making is played by different kinds of transportation devices including gantries. Those devices, equipped with at least three mechanisms, have different characteristics of their work. A winch is the most energy consumable mechanism. The possibilities of energy recuperation (during a payload lowering) or consumption minimization are also most significant in this mechanism. Issues of energy consumption of hoisting mechanisms are currently being considered in the context of energy saving, reduction of steel construction loads (also design guidelines) or possibilities of energy storage.

The authors of [4] describing energy efficiency of goods making processes, underlined the relevant impact of transport operations as one of auxiliary processes in automated production cycles. They assumed that their simplified method of energy consumption assessment could serve as a tool for analyzing different strategies of controlling the transport devices to perform transport operations with minimal energy consumption.

A lot of researchers treat hosting mechanisms as „generators" of steel structures loading and vibrations which impacts on deformation of crane structures. As the example might serve [3] where authors pointed that the hybrid approach of finite element method and system dynamics simulation of the overhead traveling crane in the case of lifting a payload allowed to define dynamic loads of crane structure already during designing phase. Similarly in [1] there was presented the model of a crane used to estimate the dynamic coefficient of structure load caused by lifting operation. The authors had also pointed, that future research should consider an influence of hoisting mechanism on dynamic overloads. In [15], the authors underlined the inevitability of considering an energy consumption during the cranes designing. They focus mainly on the structural aspects of the device using the load probability distribution of the hoisting mechanism. The minimization of overloads and vertical oscillations of crane steel structure caused by a hoisting mechanism operation using control systems with PID regulator were presented in [5].

Research on optimization of crane structure using energy efficiency in regard to dynamic coefficients of a payload lifting was presented in [18]. The effects of research were the reduction of the device mass, what caused less power consumption during horizontal movements.

A lot of research teams were concentrated on crane mechanisms in context of payload trajectory and sway minimisation using proper input function. It was confirmed inter alia in [13], where authors pointed the systems counteracting payload swaying and bridge bevelling as main direction of research and development of control systems of cranes movements.

(*) Tekst artykułu w polskiej wersji językowej dostępny w elektronicznym wydaniu kwartalnika na stronie ***www.ein.org.pl***

Some teams conducted a research of energetic efficiency of motors which were used in hoisting mechanisms fed by inverters. The research presented in [12] showed, that increasing the energetic effectiveness of motors did not make tangible benefits. It was caused by short times of operation and a large share of partial load of the mechanism.

In [2] the necessity of energy saving in lifting devices was pointed. The authors state that energy saving was possible in two manners, energy recuperation during payload lowering and increasing speed (for small masses of lifting payloads). The method of determining the energy consumption by using the calculation of changes of potential energy during lifting operation and the work of horizontal movements was presented in [16]. The method of energy saving using flywheel was also presented. The problems of energy efficiency evaluation of overhead crane using neural nets were presented in [17]. The another method of storage, which was connected with increasing development of supercapacitors was presented inter alia in [10] and [11]. Supercapacitors began to be used as storages of energy recuperated during payloads lowering or braking of cranes.

The research of energetic effectiveness of transport devices exploitation was conducted on many ways, however during lifting phase some savings are possible in methods of payload acceleration. The savings of these area gave huge (in respect with travelling mechanisms) energetic effects, both in the form of minimisation of power consumption and minimisation of dynamic overloads in drive systems and steel structures.

In [8] the authors presented advantages of model research e.g. possibility of increasing the precision of structure optimisation because of geometry and strength and prediction of influence of control methods of mechanisms on vibrations of steel structure and dynamic overloads. They underlined that one of the most important loads which should be considered during designing an overhead cranes were dynamic loads from hoisting mechanism. Both, the dynamic forces and energy consumption of payload lifting were defined using simulation tests taken on experimentally verified model.

The authors of [14], analyzing and forecasting of an evolution of selected crane units, paid attention to the development of transport and transhipment applications, new techniques of cranes control and improvement of safety systems..

The paper presents the continuation of research described in [6] in field of energy consumption in basic methods of payloads lifting, as well as energetic effectiveness of the developed method of dynamic overloads minimization with respect to standard methods of lifting. In addition to the basic methods of payload lifting, the solution to improve the winch operational parameters is included. The method was based on the proper structure of control system and the algorithm of acceleration phase, using linear change of lifting speed and controller of constant power. Presented research allows to estimate advantageous parameters of acceleration phase of hoisting mechanism allowing also to minimize dynamic overloads and improvement of energetic efficiency. The presented analyses allowed to use the method both to the jerk of payloads and another methods of payload lifting. The research described below were presented on experimentally verified model of hoisting winch of overhead crane.

The hoisting mechanism

The considered hoisting mechanism of overhead crane is presented in figure 1. Mechanism was consisted of double rope system with transmission ratio 2, which was driven using geared motor fed by inverter. Mechanism ensured lifting of payload with masses up to 5 t on 7 m. Equipment of the stand allowed measuring of basic parameters of mechanism operation, such as speed of lifting, force in ropes and parameters of the inverter which fed drive.

The stand was used to verify the model of mechanism. The model of hoisting mechanism fed by inverter widely was described inter alia in [6] and model of inverter-motor stator system in [7]. In mechanical

Fig. 1. The hoisting mechanism

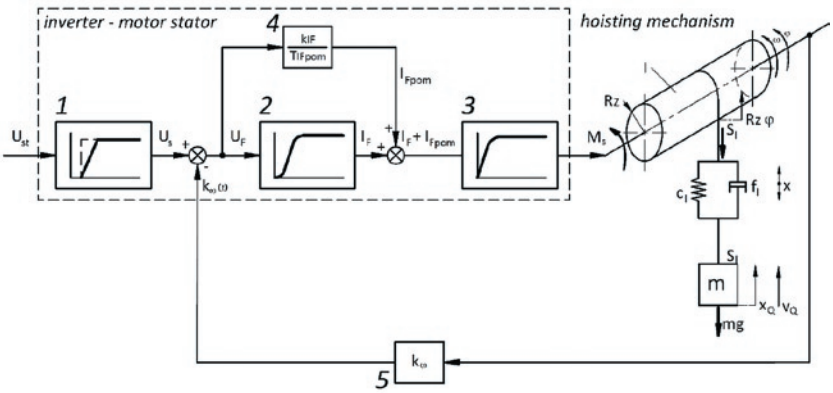

Fig. 2. The model of hoisting winch and inverter-motor stator system

part of the winch known equations of dynamics, described inter alia in [9] were used as well as kinematic dependences of payload and elements connected with a motor. The model is presented in figure 2. The following parameters of elements and variables were defined:

- I - moment of inertia of rotational parts of the winch reduced to the motor shaft
- m - mass of lifting payload
- R_z - effective radius of the mechanism
- c_l - equivalent rigidity of the rope system
- f_l - damping ratio of the rope system
- T_{F1}, T_{F2} - time constants of block 2,
- k_{IF} - conversion factor of blocks 2 and 4,
- k_{wzm} - gain factor,
- T_{IFpom} - time constant of block 4,
- k_ω - conversion factor of angular speed
- k_{Ms} - gain factor of block 3,
- T_{Ms} - time constant of block 3.
- U_F - control voltage signal
- S_l - force in ropes
- x_Q - displacement of the payload
- φ - angular displacement of the motor

The model described in state space notation is shown below:

mechanical part of the hoisting mechanism

$$\begin{aligned}
\frac{d\omega}{dt} &= \frac{1}{I}\cdot M_s - \frac{c_l}{I}\cdot x - \frac{R_z\cdot f_l}{I}\cdot\omega + \frac{f_l}{I}\cdot v_Q \\
\frac{dx}{dt} &= R_z\cdot\omega + v_Q \\
\frac{dv_Q}{dt} &= \frac{c_l}{m}\cdot x - \frac{R_z\cdot f_l}{m}\cdot\omega + \frac{f_l}{m}\cdot v_Q - g
\end{aligned} \tag{1}$$

inverter – motor stator system

$$\begin{aligned}
\frac{dUs}{dt} &= \frac{1}{T_C}\cdot U_{SZ} \\
\frac{dI_F'}{dt} &= \frac{k_{IF}\cdot k_{wzm}}{T_{F1}^2}\cdot\left(U_s - k_\omega\cdot\omega\right) - \frac{T_{F2}}{T_{F1}^2}\cdot I_F' - \frac{1}{T_{F1}^2}\cdot I_F \\
\frac{dI_F}{dt} &= I_F' \\
\frac{dM_s}{dt} &= \frac{k_{Ms}}{T_{Ms}}\cdot\left(I_F + I_{Fpom}\right) - \frac{1}{T_{Ms}}\cdot M_s \\
\frac{dI_{Fpom}}{dt} &= \frac{k_{IF}}{T_{IFpom}}\cdot\left(U_s - k_\omega\cdot\omega\right)
\end{aligned} \tag{2}$$

The following state variables were defined:

- x - elongation of the payload ropes
- v_Q - speed of the payload
- ω - angular speed of the motor.
- I_F - stator current,
- I_F' - auxiliary variable
- I_{Fpom} - auxiliary stator current,
- M_s - torque on the motor stator,
- U_s - control voltage signal

The input value for the model was voltage signal U_{st} which was proportional to the assumed angular motor speed.

Comparative studies

Due to the conditions at the start of the lifting cycle, four cases were considered and described as follows:

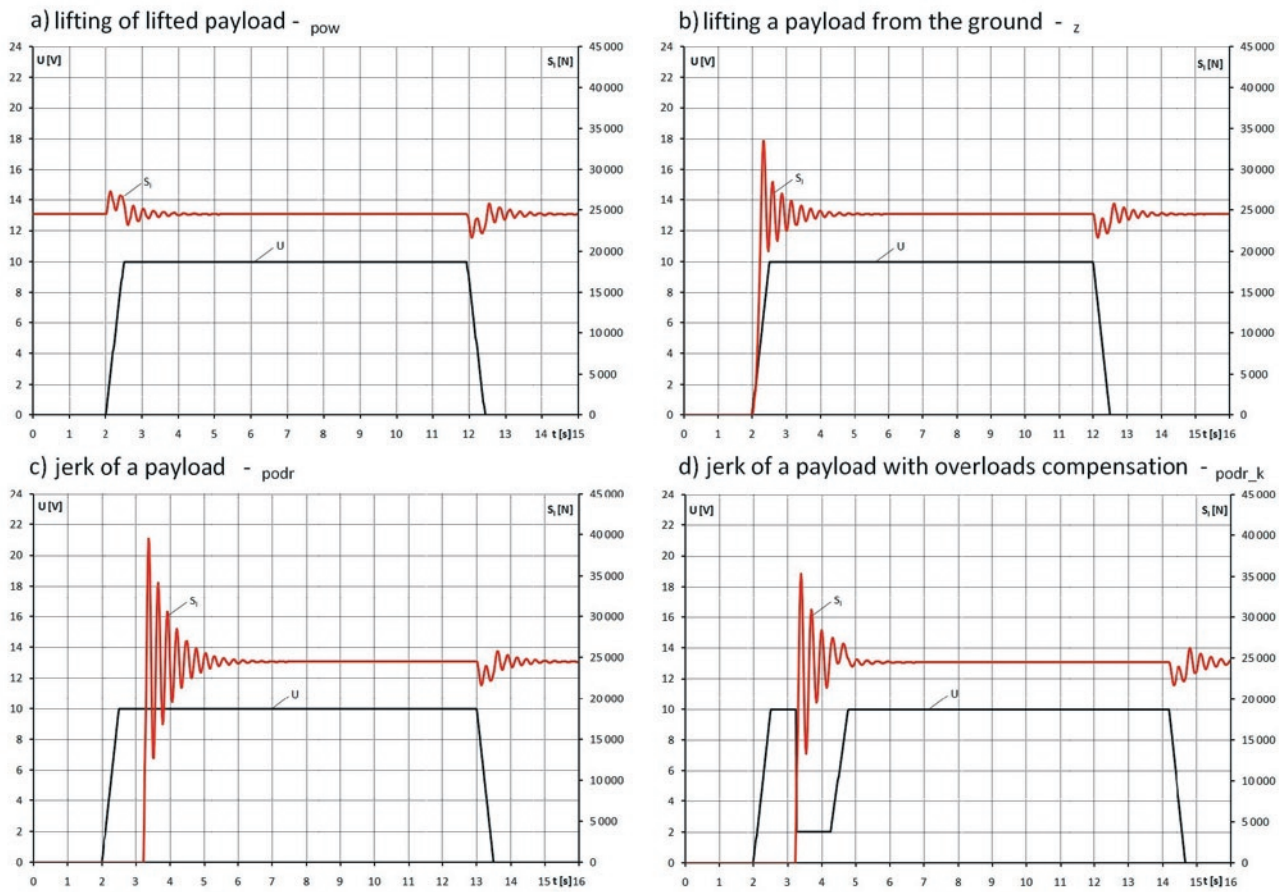

Fig. 3. The methods of payload lifting

– lifting of lifted payload (ropes pre-strained – introduced sign - pow)
– lifting a payload from the ground (ropes not strained – introduced sign - z)
– jerk of a payload (ropes with clearance, straining began when a motor operate with steady speed – introduced sign - podr)
– In addition, the method allowing minimisation of dynamic overloads of the drive using proper shape of input function, described in [6] was considered– introduced sign - podr_k

Exemplary, taken from model tests time charts of input function and force in ropes for considered cases are presented in figure 3.

To define energy consumption of particular cycle the values connected with motor shaft were used, that are angular speed and torque between stator and rotor. These values were continuously measured (3) and calculated (4) and allowed to estimate temporary power consumption of the mechanism.

$$N = M_s \cdot \omega \qquad (3)$$

Due to the fact the work of the system (what means also its equivalent energy) was calculated as the integral of the temporary power due to time, it could be described as follow:

$$E = \int_0^{t_k} N \cdot dt = \int_0^{t_k} M_s \cdot \omega_s \cdot dt \qquad (4)$$

To define the influence of basic parameters of duty cycle such as time or method of acceleration the series of simulation tests were performed. The tests could be carried out thanks to verification tests presented inter alia in [6]. The experimental data acquisited during tests on hoisting winch were used and compared with values calculated numerically with assumption of the same input functions. Figure 4 presents time charts of motor speeds acquired from the experiment (ω_{sreal}) and model (ω_{smod}) forced by defined input function (U_{ref}) operating in cycle of lifting the payload with mass 1130 kg from the ground on height equal 1,6 m. Based on experimental and model data, the total energy consumption of the cycle was calculated of about 17600 J. A high level of compatibility between energy consumption values taken from experiment (E_{real}) and model (E_{mod}) was achieved. The maximum deviation (ΔE) during cycle was less than few percent (in presented case 4,29 %), while difference at the end of the cycle was less than 1 %. Basing on performed verification the presented model was approved for wider research on energy consumption of hoisting mechanism.

Both, a maximum overloads and a time of cycle duration depend on one of important parameters of cycle, the time of acceleration. The research of the influence of acceleration time on energy consumption was carried out when the nominal payloads masses were lifted on 5m height. The times of acceleration were changing from 0 to 3 s. The maximum forces in ropes and energy consumption of whole cycle were registered for compare purposes.

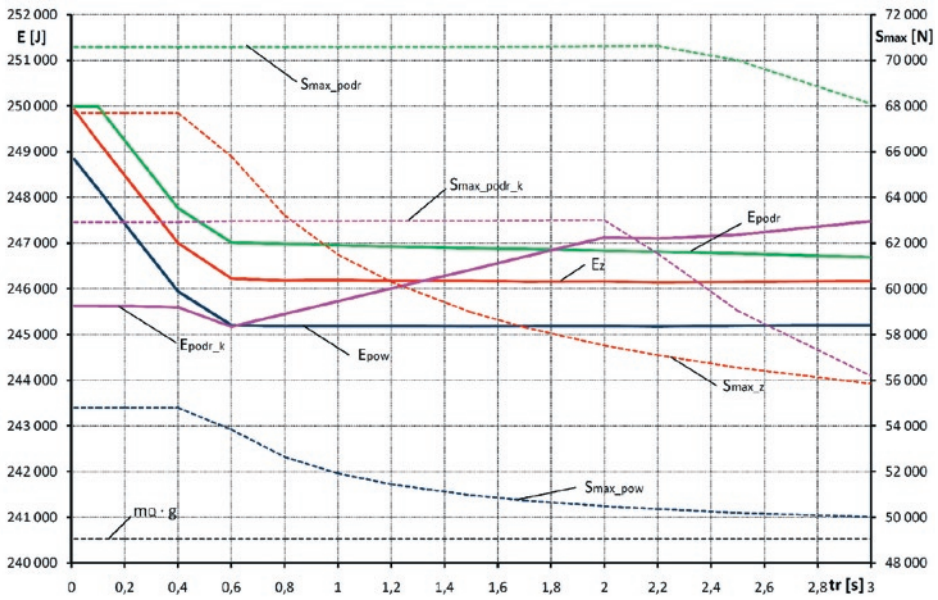

Fig. 5. Dependences of an energy consumption for the payload with mass m_Q= 5 t lifted on 5 m height for cases of lifting from the ground, lifting of lifted payload and jerk of payload

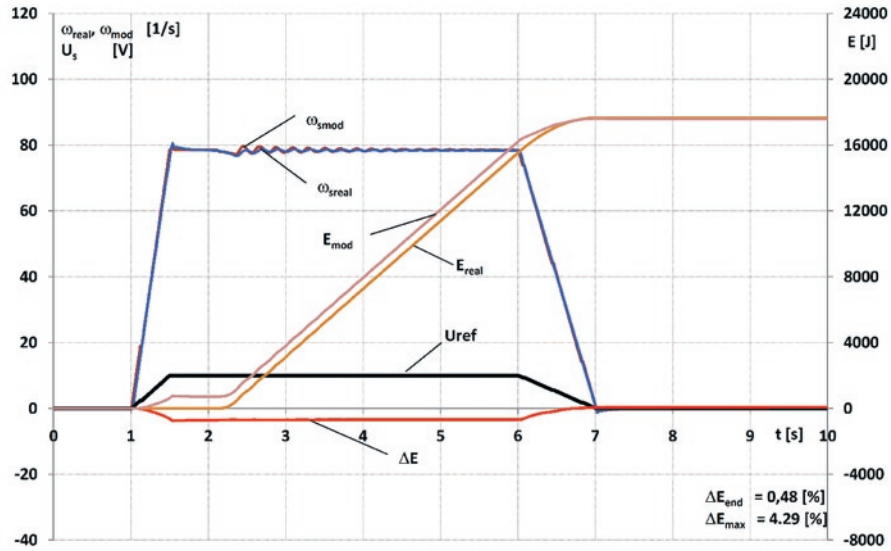

Fig. 4. Comparison of the energy of lifting cycle

Figure 5 presents energy consumption and maximum force in ropes for the cycle of lifting payload with mass 5000 kg on 5 m height depending on acceleration time.

The charts presented in figure 5 shows that increasing the acceleration (and braking) times independently from methods of lifting, for values above about 0,6 s weren't important for energy consumption of duty cycle. For the controlling method which minimized overloads, the energy consumption was smaller for shorter acceleration times and what is more, was smaller or similar with energy consumption in case of lifting of lifted payload. Simultaneously over a dozen percent decrease of the maximum force in ropes emerged.

The coefficients of overloads and energetic overloads used for comparison of effectiveness of particular methods of lifting were defined. The proper analytical dependences were given by equations:

$$p = \frac{S_{max}}{m_Q \cdot g}$$
$$p_E = \frac{E}{m_Q \cdot g \cdot h} \quad (5)$$

where:
p - overload
p_E - energetic overload
S_{max} - maximum force in ropes
E - energy consumption of duty cycle of lifting
m_Q - mass of a payload
h - height of lifting

The comparisons of coefficients are presented in figures 6a and 6b.

The energy overload of lifting cycles did not exceed several hundreds of unity above one for short acceleration times and were approaching unity already from time of approximately 0,6 seconds, which was important in the context of improving the energy efficiency of the entire crane and also possibilities of energy recuperation estimation. According to overloads in ropes system, acceleration times shouldn't be less than 0,8 s, which assures the comparable loads of structure both in case of lifting from the ground and jerk of payload with overload minimization.

Increasing acceleration times had consequences in elongation the time of the whole cycle. The dependences of the duration of whole cycle for particular methods of lifting are presented in figure 7. In case of acceleration time equal 1 s elongation of whole cycle in respect with duration of the cycle of lifting lifted payload was 2,1 s and in respect with jerk of payload was 0,96 s.

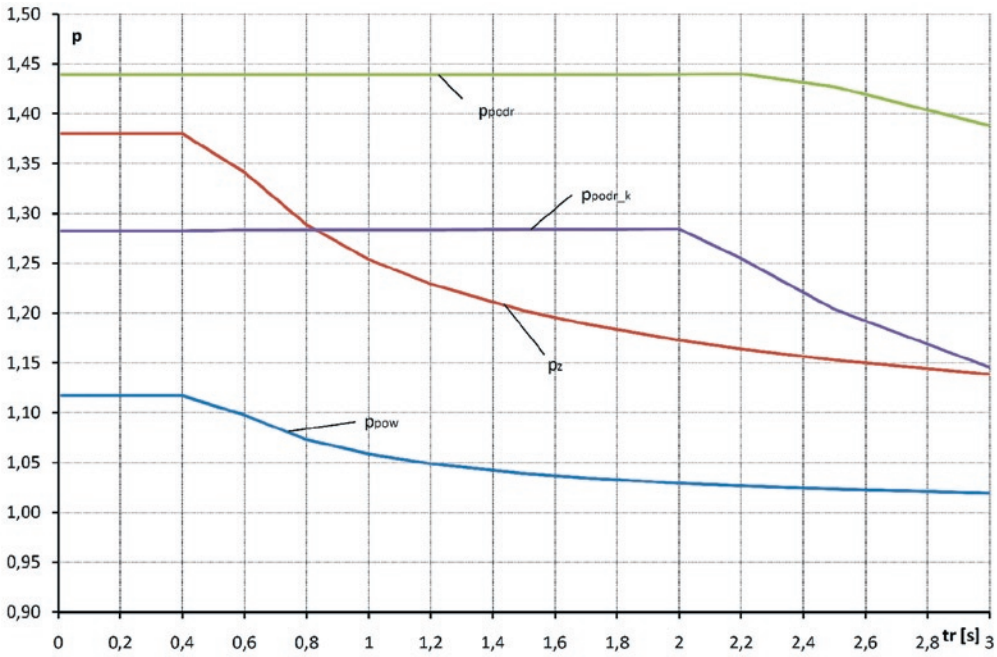

Fig 6a. Overloads (p) in dependence with the lifting method and the acceleration times

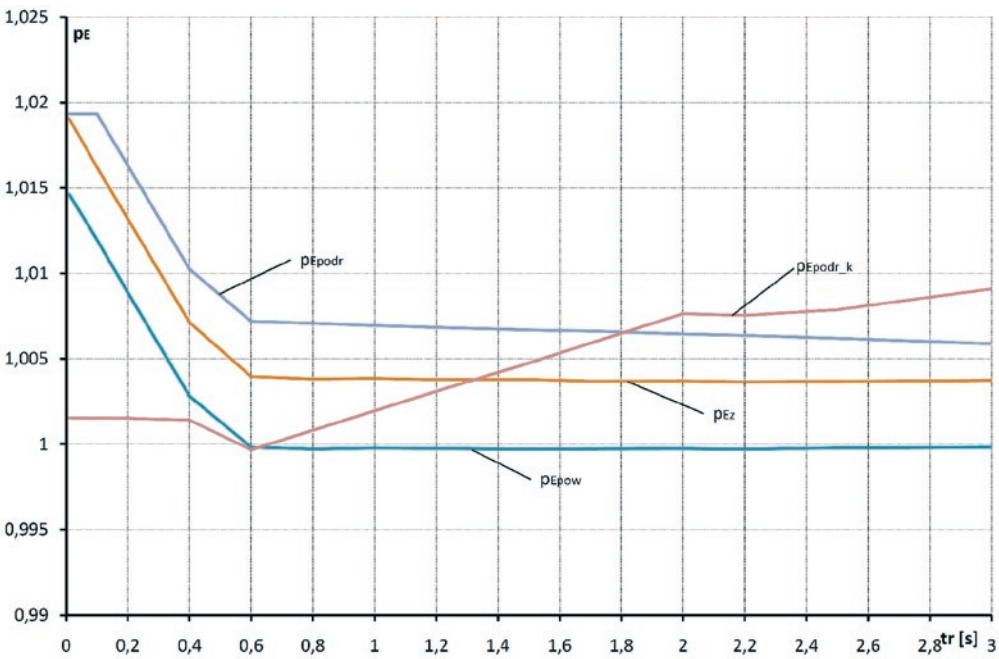

Fig 6b. Energetic overloads (p_E) in dependence with the lifting method and the acceleration times

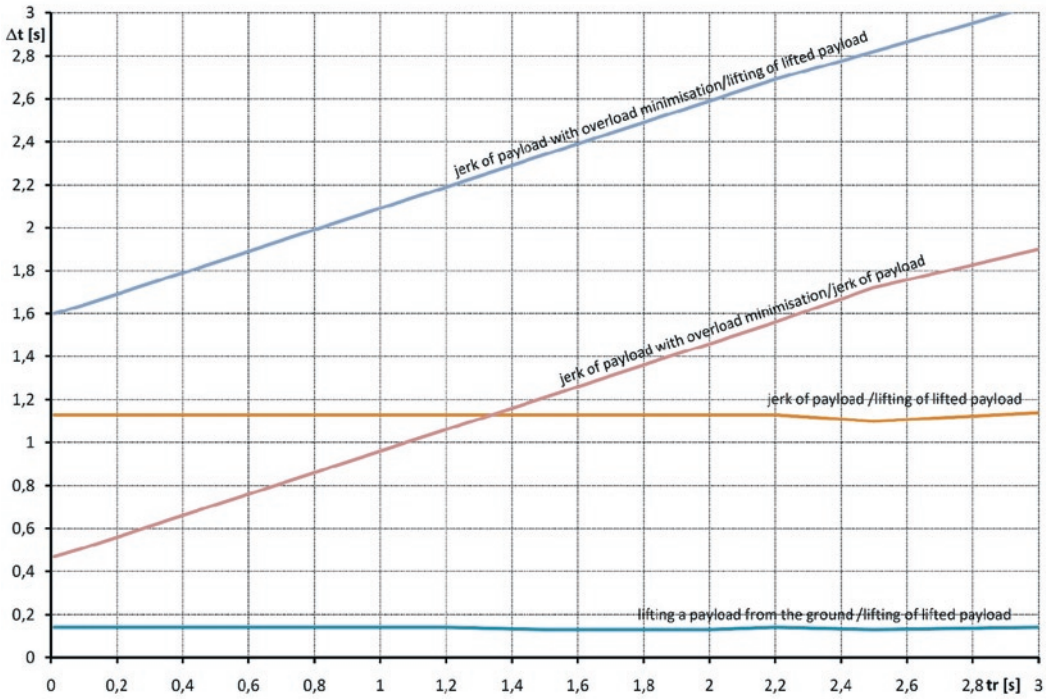

Fig 7. The elongation of cycle in dependence with the method of lifting and acceleration time of the hoisting mechanism

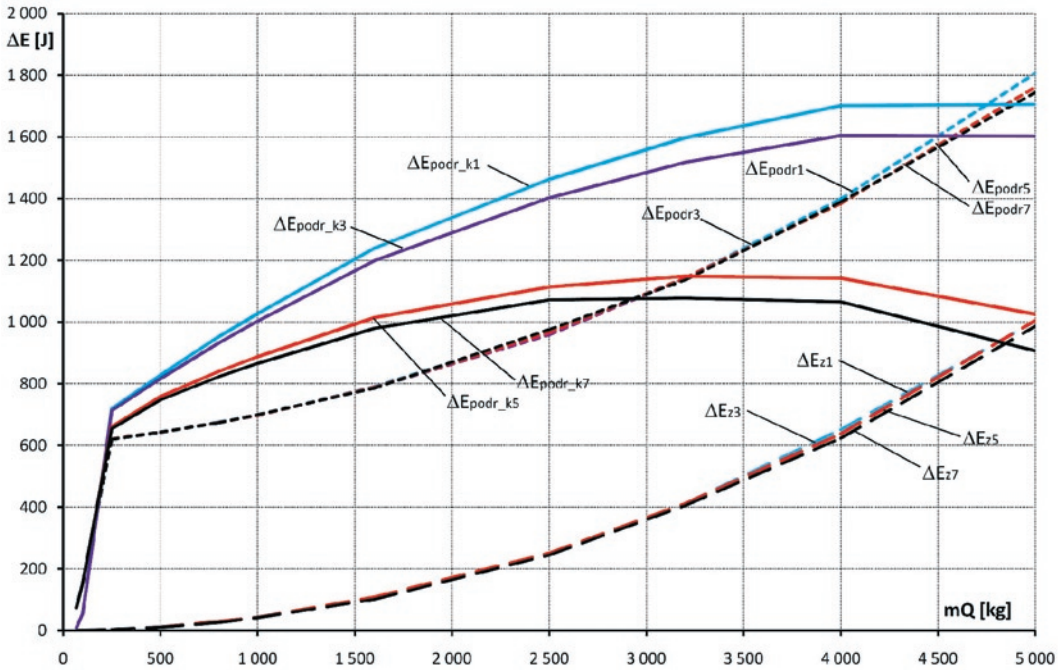

Fig 8. Coefficients of energy consumption increase in cases of lifting from the ground, jerk of a payload and jerk with overload minimization for different masses and heights of lifting

Assuming the constant value of acceleration time equal 1 s the research of energy consumption was conducted out for full spectrum of loads and different heights of payload lifting. The loads from empty hook to nominal load were considered. Calculations were performed for heights of payload lifting equal 1, 3, 5 and 7 m.

Assuming as the reference the energy consumption during lifting of lifted payload, the coefficients of energy consumption increase (ΔE) were introduced and defined as follows:

$\Delta E_z = E_z - E_{pow}$ - for lifting from the ground

$\Delta E_{podr} = E_{podr} - E_{pow}$ - for jerk of a payload

$\Delta E_{podr\_k} = E_{podr\_k} - E_{pow}$ - for jerk of a payload with overload minimisation

Additional indexes 1, 3, 5 and 7 introduced in charts represented proper heights of lifting. The coefficients are presented in figure 8.

In case of small height of lifting, the method of dynamic overloads minimization introduced increased energy consumption in full range of loads. Whereas for greater heights of lifting, for loads above half of nominal the energy consumption was smaller with respect in jerk of a payload. The energetic overload of the hoisting mechanism should be considered together with overload of driving system, especially in

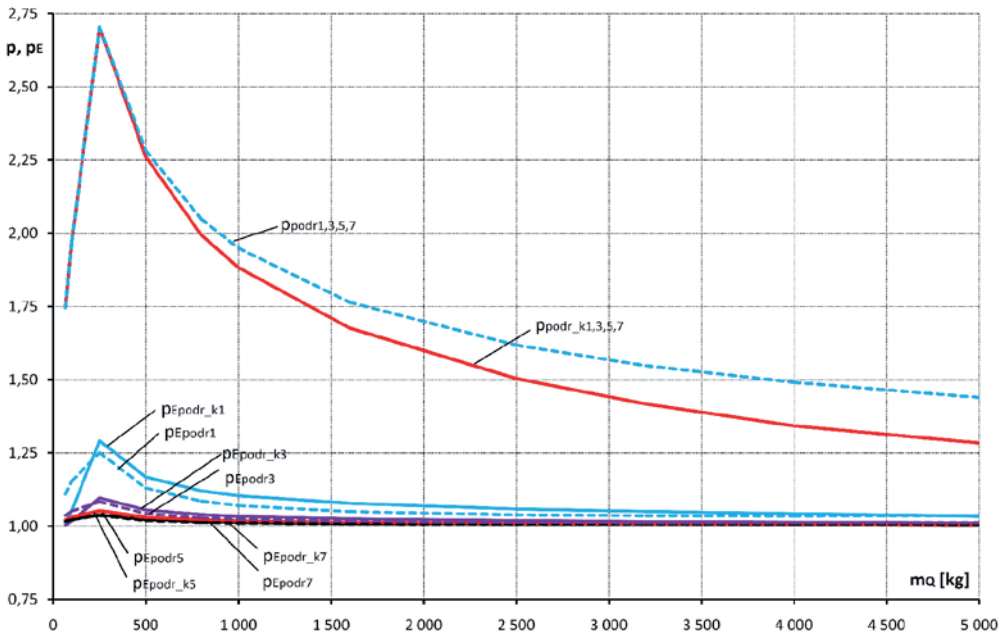

Fig. 9. The comparison of overload and energetic overloads in cases jerk of a payload and jerk with overload minimization for different masses and heights of lifting

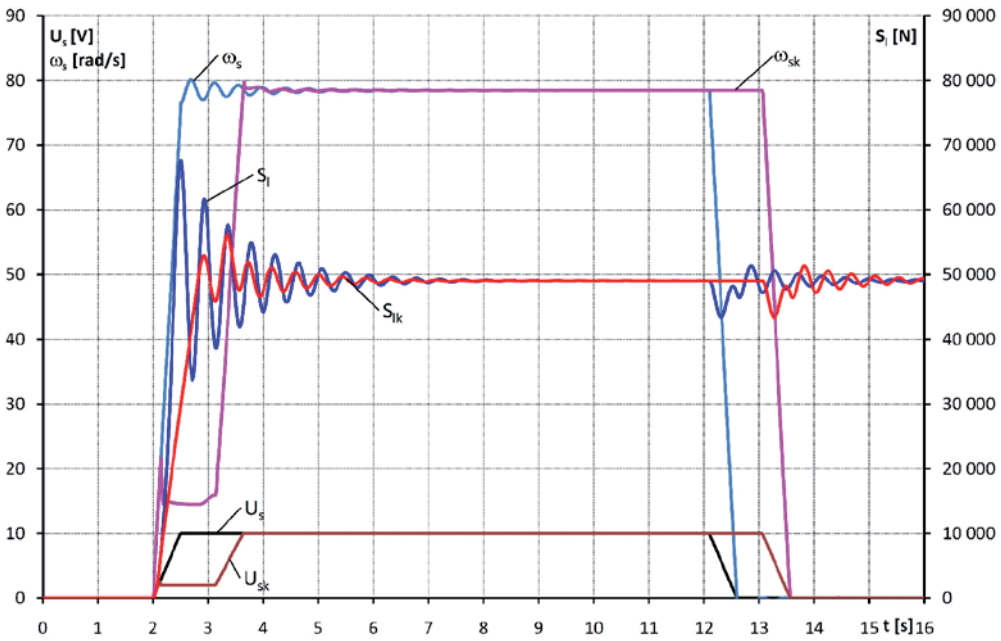

Fig. 10. The comparison of charts of input signals (U_s), speeds of the motor (ω_s) and force in ropes (S_l) in case of lifting from the ground without and with overloads minimization (index $_k$)

cases of jerk of a payload and jerk with overload minimisation. The comparison is shown in Figure 9.

The results showed that overloads during jerk of a payload were independent from heights of lifting, because they depended on the character of mechanism acceleration only. For small loads (up to 10 % of nominal lift), overloads were independent from the method of lifting. For heavier loads, the successive reduction of overloads in cases of the payload jerk with minimization in respect to jerk of a payload were observed. Considering the energetic overloads bigger differences between particular cases were visible only for small masses.

Figure 10 presents example of usage of described method in case of lifting from the ground. The payload with mass 5000 kg was lifted on height 3 m. With minimum increasing of energetic overload (from 1,008 to 1,017), minimizing of dynamic overload from p=1.378 to pk=1.146 was achieved.

Summary

Performed research showed the desirability of dynamic overloads compensation not only because of the significant reduction of dynamic overloads but also because of the energy consumption of the lifting cycle.

Increased energetic overload occurred only for small masses of lifting payload and for low lifting heights. For higher lifting heights and above the half of nominal load, it was visible for used method of minimization in respect with jerk of a payload, the energetic profit.

The acceleration time which was proposed at the level of 1 s was beneficial both because of dynamic overloads of driving system (and steel structure) and energy consumption of cycle or time of cycle duration, independently from method of lifting.

The method of minimization of operational loads could be used independently from method of lifting. The structure of control system did not interfere in other cases of lifting and in case of lifting of lifted payload the improvement of dynamic properties was visible.

The usage of the method gives the possibility to take into account less overloads when calculating crane carrier structures. The method decreases overloads of the structures, so in case of its usage in cranes, it helps to increase their service life as well as improves the reliability of these devices.

The preliminary works are conducted to implement the method using features which are build in inverters related to programming the acceleration phases. It allow usage the method of minimization even in case of manual control.

Visible influence of the motor speed changes during acceleration phase on driving system overloads empowers to continue research using different than presented methods of motor speed shaping, including optimization methods.

Good energetic properties of the system with minimization allows to use it in drive systems of transport devices with storage of recuperated energy e.g. during lowering.

References

1. Gąska D, Margielewicz J, Haniszewski T, Matyja T, Konieczny Ł, Chróst P. Numerical identification of the overhead travelling crane's dynamic factor caused by lifting the load off the ground. Journal Of Measurements In Engineering 2015; 3(1): 1-8.
2. Grygorov O V, Zaytsev Y I, Svirgun V P, Srtyzhak V V.Realization of energy-saving control modes on cranes of great load - carrying capacity. Annals of the University of Petroşani, Mechanical Engineering 2010; 12: 111-118 [3] Haniszewski T.: Hybrid analysis of vibration of the overhead travelling crane. Transport Problems (Problemy Transportu) 2014; 9(2): 89-100.
3. Haniszewski T.: Hybrid analysis of vibration of the overhead travelling crane. Transport Problems (Problemy Transportu) 2014; 9(2): 89-100.
4. Honczarenko J, Berliński A. Modelowanie energochłonności procesów transportowych w zautomatyzowanych systemach montażowych. Technologia i Automatyzacja Montażu 2011;4: 49-52.
5. Kiviluoto S, Eriksson L, Koivo H N. Modelling and control of vertical oscillation in overhead cranes. Proc. of American Control Conference 2015: 1290-1295, https://doi.org/10.1109/acc.2015.7170911.
6. Kosucki A, Malenta P. The possibilities of reducing the operational load of hoisting mechanisms in case of dynamic hoisting. Eksploatacja i Niezawodnosc – Maintenance and Reliability 2016; 18(3): 390–395, https://doi.org/10.17531/ein.2016.3.10.
7. Kosucki A. Badanie transportu ładunków przy wykorzystaniu skojarzonych ruchów mechanizmów suwnic pomostowych. Rozprawy Naukowe. Politechnika Łódzka z. 474; Zeszyty Naukowe. Politechnika Łódzka nr 1175, Łódź: 2013.
8. Margielewicz J, Haniszewski T, Gąska D, Pypno C. Badania modelowe mechanizmów podnoszenia suwnic. Komisja Transportu, Polska Akademia Nauk Oddział w Katowicach. Katowice 2013.
9. Newton I. Mathematical Principles of Natural Philosophy. NY: 1846.
10. Parise G, Honorati A. Port Cranes with Energy Balanced Drive. Proc. of AEIT Annual Conference - From Research to Industry: The Need for a More Effective Technology Transfer (AEIT) 2014: 1-5, https://doi.org/10.1109/aeit.2014.7002047.
11. Plotnikov I, Braslavsky I, Ishmatov Z, Polunin F. About Using the Frequency-Controlled Electric Drives with Supercapacitors in the Hoisting Applications. Proc. of International Siberian Conference on Control and Communications (SIBCON) 2015: 1-9, https://doi.org/10.1109/SIBCON.2015.7147174.
12. Repo A, Montonen J, Sizonenko V, Lindh P, Pyrhönen J. Energy efficiency of hoisting motors. Proc. of International Conference on Electrical Machines (ICEM) 2014: 144-149, https://doi.org/10.1109/icelmach.2014.6960172.
13. Smoczek J, Szpytko J. Sposoby sterowania zautomatyzowanymi pomostowymi suwnicami. Prace Naukowe Politechniki Warszawskiej. Transport, 2010, z. 73: pp. 95-104.
14. Szpytko J, Chodacki J. Analiza ewolucji wybranych zespołów dźwignic, Konferencja LOGITRANS 2010, Logistyka, systemy transportowe, bezpieczeństwo w transporcie, Czasopismo: Logistyka 2010; 2.
15. Tong Yifei, Tang Zhaohui, Mei Song, Shen Guomin, Gu Feng. Research on Energy-Saving Design of Overhead Travelling Crane Camber Based on Probability Load Distribution. Mathematical Problems in Engineering 2014: 1-9.
16. Xinyi Xiao, Shiqing Lu. Study on Measurement of Energy Consumption for Cranes and Designing of Energy Saving Device. Applied Mechanics and Materials 2012; 159: 326-330, https://doi.org/10.4028/www.scientific.net/AMM.159.326.
17. Yifei T, Ruiwen Z, Wei Y, Dongbo L. Research on energy efficiency evaluation for overhead crane. Kybernetes 2016; 45 (5): 788-797, https://doi.org/10.1108/K-09-2015-0225.
18. Yifei T, Zhaohui T, Wei Y, Zhen Y. Research on energy-saving optimization design of bridge crane. Eksploatacja i Niezawodnosc – Maintenance and Reliability 2013; 15 (4): 449–457.

Andrzej KOSUCKI
Piotr MALENTA
Łukasz STAWIŃSKI
Sławomir HALUSIAK
Lodz University of Technology, Department of Vehicles and Fundamentals of Machine Design
ul. Żeromskiego 116, 90-924 Łódź

E-mails: andrzej.kosucki@p.lodz.pl, piotr.malenta@p.lodz.pl, lukasz.stawinski@p.lodz.pl, slawomir.halusiak@p.lodz.pl

Article citation info:
TRZMIEL G. Determination of a mathematical model of the thin-film photovoltaic panel (CIS) based on measurement data. Eksploatacja i Niezawodnosc – Maintenance and Reliability 2017; 19 (4): 516–521, http://dx.doi.org/10.17531/ein.2017.4.4.

Grzegorz TRZMIEL

DETERMINATION OF A MATHEMATICAL MODEL OF THE THIN-FILM PHOTOVOLTAIC PANEL (CIS) BASED ON MEASUREMENT DATA

WYZNACZANIE MODELU MATEMATYCZNEGO CIENKOWARSTWOWEGO PANELU FOTOWOLTAICZNEGO (CIS) NA PODSTAWIE DANYCH POMIAROWYCH

In this paper the author attempted to determine the most accurate mathematical model of the photovoltaic panel composed of a monolithic structure of series connected Copper Indium Diselenide (CIS) based solar cells, based on its actual measurement data. The purpose of this paper has been achieved by implementing the original applications which, using the methods of approximation, made it possible to design the final mathematical model of the tested panel, characterized by the minimum of error modelling. Using the known literature on the operation of similar facilities, the model parameters were determined directly from the collection of random measurement data; then the obtained models were verified by several different statistical methods. As a result, the best model was selected, based on the smallest dispersion of the theoretical values (simulated) calculated from the model relative to the actual measurements. The model will be used in practice in the future to evaluate the condition (inefficiency, use) of photovoltaic panels, what will be the theme of following articles.

***Keywords**: photovoltaic panel, CIS solar cells, approximation, mathematical model, statistical verification.*

W artykule autor dąży do określenia, w oparciu o rzeczywiste dane pomiarowe, najbardziej dokładnego modelu matematycznego panelu fotowoltaicznego, składającego się z monolitycznej struktury połączonych szeregowo ogniw fotowoltaicznych typu CIS. Cel pracy został osiągnięty poprzez wdrożenie oryginalnych aplikacji, które przy użyciu metod aproksymacji umożliwiły zaprojektowanie ostatecznego modelu matematycznego badanego panelu, charakteryzującego się minimalnym błędem modelowania. Wykorzystując literaturę tematu dotyczącą działania podobnych obiektów nieliniowych, parametry modelu zostały określone bezpośrednio z wcześniej zarchiwizowanych losowych danych pomiarowych. Następnie uzyskane modele zweryfikowano kilkoma różnymi metodami statystycznymi. W wyniku tego wybrano najlepszy model, oparty na najmniejszej dyspersji wartości teoretycznych (symulowanych) obliczonej z modelu w stosunku do rzeczywistych pomiarów. Otrzymany model zostanie w przyszłości zastosowany w praktyce do oceny stanu (niesprawności, zużycia) paneli fotowoltaicznych, co będzie tematem kolejnych artykułów.

***Słowa kluczowe**: panel fotowoltaiczny, ogniwa słoneczne CIS, aproksymacja, model matematyczny, weryfikacja statystyczna.*

1. Introduction

The subject of modelling and research of photovoltaic panels is still valid as can be seen in recent publications [1, 6, 9, 10]. Modelling of photovoltaic panels during their operation is essential to control both the systems and current operational activities. An appropriate device model, determined from a certain optimal time step also makes it possible to predict the operation and any possible repairs. It also indicates the need to perform repair works.

A commonly used ideal equivalent circuit model (with three elements shown in Fig. 1) of the photovoltaic cell is shown in Fig. 1, the output current I [A] is as follows [7, 8, 20]:

$$I = I_{ph} - I_D = I_{ph} - I_0\left[\exp\left(\frac{qU}{k_B\left(T+273.15\right)}\right)-1\right] \qquad (1)$$

where: I_0 [A] – diode dark saturation current, q – elementary charge ($1.6\cdot10^{-19}$ C), k_B - Boltzmann constant ($1.38\cdot10^{-23}$ J/K), T [ºC] – temperature.

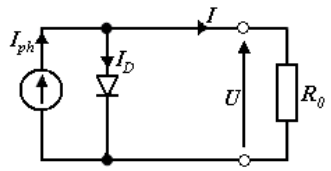

Fig. 1: An ideal equivalent circuit diagram of the photovoltaic cell for the model with three parameters [7, 8, 18]: R_0 [Ω] – termination resistance, I_{ph} [A] – current in the irradiated cell, I_D [A] – current of the diode with large surface, I [A] – load current, U [V] – voltage drop on the receiver R_0

Equally often a five-element model is used, for which the equation (1) is as follows [2, 7, 8]:

$$I = I_{ph} - I_0\left\{\exp\left[\frac{q\left(U+IR_S\right)}{k_B T_K}\right]-1\right\} - \frac{U+IR_S}{R_W} \quad [\mathrm{A}] \qquad (2)$$

where: T_K [K] – temperature.

An equivalent circuit diagram, corresponding to the equation (2) and including five elements of extended model, is shown in Fig. 2.

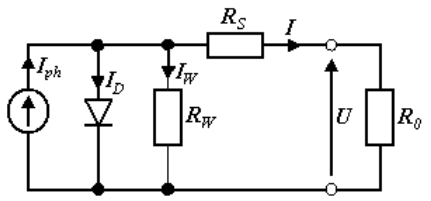

Fig. 2. An equivalent circuit diagram of the photovoltaic cell for the model with five parameters [8, 17]: I_W [A] – current flowing through the shunt resistance

The R_S series resistance includes contact resistance, base resistance, and the resistance of other layers of the cell. The R_W shunt resistance represents the current leakage along the edge of the cell. When designing the cell, small R_S values and the largest R_W values are expected.

Implementation of an equivalent circuit diagram comes down to determining the parameters of a single solar cell, because the resultant current and voltage of photovoltaic modules (Figure 3) are (according to the Kirchoff's first and second law) sums of currents, respectively (for parallel connection), and voltage (for serial connection) of the single photovoltaic cells [3].

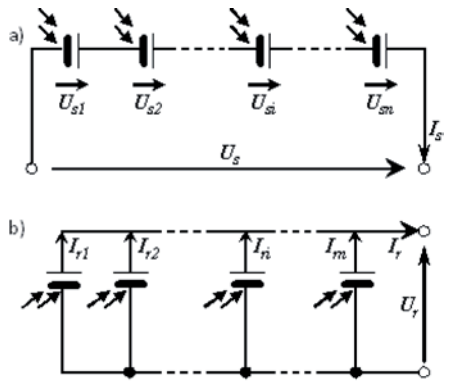

Fig. 3. a) Serial connection and b) parallel connection of the photovoltaic modules [15, 16]: U_{si} [V] – voltage at the i-th module which is connected in series, I_s [A] – current of the serial connection, U_s [V] – resultant voltage of the serial connection, I_{ri} [A] – current generated in the i-th module which is connected in parallel, I_r [A] – resultant current of the parallel connection, U_r [V] – voltage of the parallel connection

2. Materials and Methods

2.1. Modelling of the photovoltaic cell under actual operation conditions

The above-mentioned models from the literature do not include explicitly the essential operation parameters of the tested module. This can lead to large errors in the evaluation of the operating status of such devices. Therefore, an original equivalent circuit model of the photovoltaic cell is suggested, which contains:

- voltage at the terminals of the loaded module – U [V],
- current generated by the module – I [A],
- temperature of the immediate surroundings (of the air layer) around the module – T_K [K],
- % quality of lighting on the surface of the module – D [%] (assuming uniform illumination across the entire surface of the module, which is true for solar power plants).

The temperature T_K [K] and the quality of light D [%] (then the converted directly to the power density of visible radiation (irradiance) D_r [W/m^2]) was measured using the transmitter TH-03 (Pico Technology) sensors, respectively: EL015 (resolution ±0,01°C) and EL031 (resolution: ±0,1 %,). Current I [A] and the voltage U [V] were measured designed by the author of a microcontroller measuring module based of PIC18F8722 microcontroller with built-in AC converter. The measurements were verified: laser / electronic thermometers, professional measure of irradiance PRC Krochmann GmbH and universal digital voltage and current meters. Methods and measurement equipment during the measurement modeling, verification and testing were the same.

Since the photovoltaic panels operate under variable load conditions, their mathematical models can be expressed as the following symbols:

$$I = f(D, T_K, U). \tag{3}$$

The process of determining the mathematical model was held under actual operation conditions of the photovoltaic panels. Due to the repeatability, modelling of the photovoltaic cell will be presented on the example of Shell ST20 panel which is composed of a monolithic structure of series connected Copper Indium Diselenide (CIS) based solar cells [14].

In order to obtain a mathematical model of the tested panel, an application written in Delphi has been designed. The algorithm of the polynomial approximation of functions of several variables was used to determine the model parameters. Sample waveforms of current-voltage characteristics $I=f(U)$ were determined by the final application and based on the manufacturer's data [14]. The designing process of a mathematical model of the tested photovoltaic panel, due to the increasing accuracy of the model, proceeded in several stages.

At first, the ideal model was suggested, and then, after its extension and modification, the final model with the lowest δr_m average relative error was proposed.

Mathematical models were determined using multivariate polynomial approximation (many variables) [4]; the detailed examples of calculation shown later in the paper relate to Shell ST20 photovoltaic panel [14].

It was found that the modelled problem is characterized by the overdetermination, which means that there is a larger number of collected measurement data than the number of parameters to set. In the present proceedings, predominance of the number of measurement data (several hundred thousand) is clear and it is purposeful, designed to obtain the most satisfactory results of the carried out search for an equivalent circuit model.

2.1.1. Simplified model

A simplified mathematical model is based on an ideal model with three parameters (1). It was determined from over a dozen series of measurements for different levels of lighting quality D, load varying from 0 to 400 Ω and the variable temperature T (from 20 up to 50ºC). Measurement intervals for T and R were equal: ΔT = 1ºC and ΔR = 10 Ω. Changes in lighting made it possible to obtain currents of the full range of possible values presented in the manufacturer's documentation [14].

It was assumed that any mathematical model is true for the actual parameters with values in the ranges of variation observed during the modelling process by a method of approximation [19].

For the polynomial approximation of functions of several variables the equation (4) was taken into account. Repeated test samples and different data sets with the same value of current I were rejected by the approximating application.

$$I = I_{ph} - I_0\left[\exp\left(\frac{BU}{(T+273.15)}\right)-1\right] = I_{ph0}D_r - I_0\left[\exp\left(\frac{BU}{(T+273.15)}\right)-1\right], \tag{4}$$

where: I_{ph0} [mA·m²/W] – parameter for short-circuit current in the irradiated cell, D_r [W/m²] – power density of visible radiation (irradiance), B [K/V] – parameter of the simplified model which is determined empirically.

Approximating the collected measurements, the following dependence (5) was obtained. The resulting current I is then expressed in [mA]:

$$I = 1.52 \cdot D_r - 1.0919 \cdot 10^{-6} \left[\exp\left(\frac{325 \cdot U}{(T + 273.15)} \right) - 1 \right], \quad (5)$$

where: I_{ph0} = 1.52 mA·m²/W, I_0 = 1.0919·10^{-6} mA, B = 325 K/V.

The average absolute error of the expressed by the formula (6) was ΔI_{sr}=49,6487 mA:

$$\Delta I_{sr} = \frac{1}{g} \sum_{i=1}^{g} \left| \left| I - \hat{I} \right| \right|, \quad (6)$$

where: g – number of sample measurements during modelling, I [mA] – current actual value (from the measurement), $\hat{I}$ [mA] - current value generated by the model.

The average percentage relative error, calculated according to equation (7), was δI_{sr}=28,03%:

$$\delta I_{sr} = \frac{1}{g} \sum_{i=1}^{g} \left| \frac{I - \hat{I}}{\hat{I}} \right|. \quad (7)$$

It was assumed that the simplified model should be modified in order to reduce the error (7), indicating unsatisfactory accuracy to reflect the actual operation by the resulting model.

2.1.2. Modifications of the model

In the formula (2) I_{ph} current can be expressed using the following dependence [7]:

$$I_{ph} = I_{ph0} D_r + J_0 (T_K - T_0), \quad (8)$$

where: J_0 [A/K] – temperature coefficient, T_K [K] – actual temperature of the cell operation, T_0 – reference temperature – under Standard Test Conditions (STC), i.e. when the power density of radiation is D_r=1000 W/m², T_0=298,15 K.

Next, transformation of the expression (2) gives the following dependence:

$$I = I_{ph0} D_r + J_0 (T_K - T_0) - I_0 \left\{ \exp\left[\frac{q(U + IR_S)}{\alpha k_B T_K} \right] - 1 \right\} - \frac{U + IR_S}{R_W}, \quad (9)$$

where: α – diode quality factor (for ideal photovoltaic cells α=1, in fact usually 1<α<2 for real PV panel [19]).

Experimentally it is found that the diode quality factor α in polycrystalline solar cells is higher than its single crystal value, and it increases with decreasing grain size. The diode quality factor α increases also with increasing insulation layer thickness [5, 13]. For Shell ST20 PV Copper Indium Diselenide (CIS) panel the diode quality factor α is typically in the range (1,2).

Assuming R_W=∞ and R_S=0, which is not very significant error in the construction of the latest photovoltaic panels, the following model (10) is obtained. Assumption of R_S=0 might cause poor agreement between measured and calculated data in lower current exponential region (near open circuit voltage). The intention of the author was, however, obtaining the universality of the method (by performing analogous modeling measurements and evaluation of mathematical models for different geographic locations and installation arrangements). Therefore, by modifying the following mathematical models were minimized these discrepancies. Furthermore, when determining a mathematical model of any panel, some of their parameters are not known explicitly, therefore they are replaced with an additional parameter B_2:

$$I = I_{ph0} D_r + J_0 (T_K - T_0) - I_0 \left\{ \exp\left[\frac{B_2 U}{T_K} \right] - 1 \right\}, \quad (10)$$

$$B_2 = \frac{q}{\alpha k_B}. \quad (11)$$

However, it appears that in order to highlight the qualitative effect of temperature change on the generated current I, the current record I_0 can also be modified according to the formula [7, 12]:

$$I_0 = I_{d0} \left(\frac{T_K}{T_0} \right)^3 \exp\left[\frac{q E_q m_s}{\alpha k_B} \left(\frac{1}{T_0} - \frac{1}{T_K} \right) \right], \quad (12)$$

where: I_{d0} [A] – diode dark current, E_q [V] – potential energy barrier depending on the diode material, k_B – Boltzmann constant (1.381·10^{-23} J/K), m_s – number of cells connected in series.

Considering the still tested panel as an object of known principles of operation, but of the unknown parameters resulting from the construction and other properties, it was decided to replace a number of coefficients from the formula (13) with B_1 constant (14). After implementing all the modifications described, the following formula was obtained:

$$I = I_{ph0} D_r + J_0 (T_K - T_0) - I_{d0} \left(\frac{T_K}{T_0} \right)^3 \cdot \exp\left[B_1 \left(\frac{1}{T_0} - \frac{1}{T_K} \right) \right] \cdot \left[\exp\left(\frac{B_2 U}{T_K} \right) - 1 \right], \quad (13)$$

$$B_1 = \frac{q E_q m_s}{\alpha k_B}. \quad (14)$$

2.1.3. Final model

Based on the model (13) a symbolic form of an approximated polynomial was suggested:

$$I = a_1 D_r + a_2 T_1 + a_3 T_2 \cdot \exp(B_1 T_3) \cdot \left[\exp(B_2 z) - 1 \right], \quad (15)$$

where: a_1, a_2, a_3 – model coefficients determined in the process of approximation, B_1, B_2 – the final model parameters which are selected empirically, T_1, T_2, T_3, z – parameters calculated from the input data:

$$a_1 = I_{ph0}, \quad (16)$$

$$a_2 = J_0, \tag{17}$$

$$a_2 = I_0, \tag{18}$$

$$T_1 = (T_K - T_0), \tag{19}$$

$$T_2 = \left(\frac{T_K}{T_0}\right)^3, \tag{20}$$

$$T_3 = \left(\frac{1}{T_0} - \frac{1}{T_K}\right), \tag{21}$$

$$z = \frac{U}{T}. \tag{22}$$

Approximation was performed for three different basis functions presented in equations (23-25). It is therefore a three-dimensional approximation of the first degree:

$$f_1(D_r) = D_r\ , \tag{23}$$

$$f_2(T_K) = T_1\ , \tag{24}$$

$$f_3(T_K, U) = T_2 \cdot \exp(B_1 T_3) \cdot \left[\exp(B_2 z) - 1\right]. \tag{25}$$

With the approximation performed, the following parameters were obtained: a_1=1.52 mA(W/m^2)$^{-1}$, a_2=−119.80·10^{-3} mA/K, a_3=−10.92·10^{-7} mA, B_1=150 K, B_2=324 K/V. The average percentage relative error, calculated according to equation (7), was δI_{sr}=14,07%.

During the verification of the model (13, 15) unsatisfactory functioning of the T_2 (21) section was found, manifested by a worse waveform representation *I=f(U)* for current values *I* tending to zero. An empirical review of the solutions was made during the T_2 changes and it was decided to introduce a modified T_2' section. The model (15) changed its form into:

$$I = a_1 D_r + a_2 T_1 + a_3 T_2' \cdot \exp(B_1 T_3) \cdot \left[\exp(B_2 z) - 1\right]\ , \tag{26}$$

$$T_2' = \left(\frac{T_C}{T_{C0}}\right)^2\ , \tag{27}$$

where: T_C [ºC] – actual temperature of the cell operation, T_{C0} – reference temperature – under Standard Test Conditions (STC), i.e. when the power density of radiation is D_r=1000 W/m^2, T_{C0}=25ºC.

With the approximation performed, the following parameters were obtained: a_1=1.52 mA(W/m^2)$^{-1}$, a_2=-119.80·10^{-3} mA/K, a_3=-10.92·10^{-7} mA, B_1=150 K, B_2=315 K/V. The average percentage relative error, calculated according to equation (7), was δI_{sr}=13.17%.

3. Results and Discussion

3.1. Verification of the obtained models

The average percentage relative error of the intermediate model after the modification (of the developed model), calculated according to the equation (15) for all the measurement samples is δI_{sr}= 14.07% (footnote: for the simplified model – δI_{sr}= 28.03%). As can be seen, this error is twice smaller than the error obtained during the simplified modelling (10). The average percentage relative error of the final modelling (26), after having introduced a new T_2' parameter (4.27), is δI_{sr}=13.17%. Detailed results of the verification are presented in Table 1.

Table 1. Modelling errors for all measurement samples

Model type Error type	Simplified model	Developed model	Final model
δI_{sr} [%]	28.033	14.070	13.174
W_k [-]	0.921	0.917	0.967
F_S [-]	1100.457	1043.317	2784.994
$\hat{\chi}^2$ [-]	0.157	0.164	0.066

Figure 4 presents examples of mapping current-voltage characteristics calculated using the final model after the modification. Maximum power point P_{max} was marked. The results were limited to the power density of radiation D_r to approx. 600 W/m^2, because according to the literature [8, 11] these values correspond to the maximum levels of the most common levels in Poland (for locations in other latitudes should each case match the measurement ranges when calculating the mathematical model, for example, increasing the power density of radiation D_r to approx. 1200 W/m^2). The temperature during determining the characteristics varied in the range from 25.5 up to 39.4ºC, because of the lit halogen lamps.

The curve of results obtained for D_r = 596 W/m^2 are characterized by comparable accuracy as the results shown in Figure 4 and 5 and have been taken into account in verification of the obtained models. The effect of temperature changes on the curves has been omitted because temperature changes resulted in small changes (at 5%) near open circuit voltage.

An analysis of current-voltage characteristics, as in Figure 4, makes it possible to conclude that the various models differ mainly in their lower exponential parts. Capacities of the photovoltaic cells in this characteristics range, obtained during the operation, are much lower than the point of maximum power. However, in practice they are not so important. Also the listed average percentage values of relative errors are largely associated with these characteristics fragments. Black curves (actual measurement) are a little different from the typical I/V characteristics near V_{oc} shown in the Shell ST20 data sheet [14], which could be caused by many different factors. The test panel was operated from 10 years – probably undergo the aging process (caused eg by weather conditions). It could be characterized by the presence of "hot spots" (which was not separately tested), during the measurements may exist local differences in temperature. Conditions of actual measurements were certainly different from the ideal, which are a reference to the catalog items. Moreover the author's intention was to create a method of designing a mathematical model of the real measurements (modeling) without having to know the technical details (manufacturer's data included in the application).

Similar results of the modeling for generated power as voltage are presented in Figure 5.

Sample results of errors calculation: the average relative error δI_{sr} and comparative errors [21]: W_k (of the multivariate correlation coefficient), F_S (F-Snedecor test) and $\hat{\chi}^2$ (chi-square test) were provided

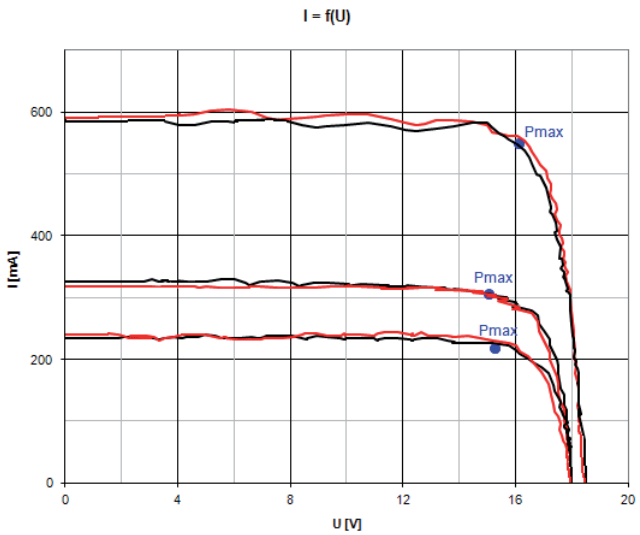

Fig. 4. Sample mapping of the characteristics I=f(U) for three different levels of irradiance D_r [15]: black curves – actual measurements, red curves – a final mathematical model after modification

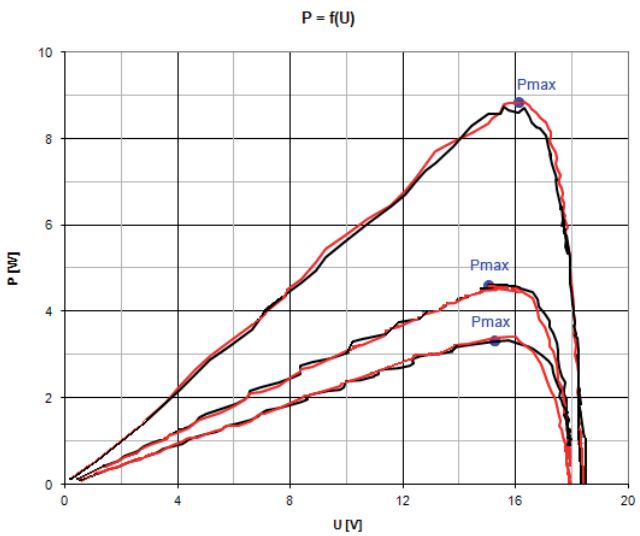

Fig. 5. Sample mapping of the characteristics P=f(U) for three different levels of irradiance D_r [22]: black curves – actual measurements, red curves – the final mathematical model after modification

in Table 1. In order to show their interpretation, the values of individual indicators are placed in subsequent rows of coloured backgrounds: red – the worst, yellow – better, green – the best.

The better model is obtained during the approximation process if the W_k parameter is closer to 1, the F_S parameter is greater in value and the $\hat{\chi}^2$ value is closer to zero. The F_S parameter is designed to evaluate the accuracy of the W_k multidimensional correlation coefficient, and the chi-square test ($\hat{\chi}^2$) is a separate method of assessing the quality of approximation.

In the operation of photovoltaic panels working with the regulators, we seek to use them under conditions as similar as possible to the point of maximum power P_{max}. Assuming the operation in the range of $[0{,}9 \cdot P_{max}, P_{max}]$ we can determine the average relative percentage errors, which provide more useful information about the effectiveness of the model under the most common conditions of their use. For example, the error value δI_{sr} decreases then from 13,174% to 2,816%.

This and similar examples show that the modelling errors δI_{sr} in the assumed power range are much smaller than the errors determined for all samples. Thus, with the development of a mathematical model, their trend is still downward, but the decline is less steep. All the values for the obtained parameters, as in Table 1, showed the best properties of the suggested final model.

4. Conclusion

Modelling of the photovoltaic cells during their operation is essential for their proper maintenance. Operation conditions of such systems are, in fact, characterized by randomness; the parameters are related to each other nonlinearly. Therefore, it is necessary to include this in temporary sets of modelling data from the measurements. One of the effective methods is to use a suitable polynomial approximation of the data, including the coefficients modelling the unknown functional dependencies.

The model of the photovoltaic Copper Indium Diselenide (CIS) panel has been obtained, which satisfactorily reflects the actual operation of the photovoltaic panel, and the applied methodology can be used for any type of panel.

The model will be used in practice in the future to state assessment of photovoltaic panels (cells), what will be the theme of following articles.

References

1. Ahmad H. El Khateb, Nasrudin Abd Rahim, Jeyraj Selvaraj. Fuzzy Logic Control Approach of a Maximum Power Point Employing SEPIC Converter for Standalone Photovoltaic System. Procedia Environmental Sciences (Elsevier) 2013; 17: 529-536, https://doi.org/10.1016/j.proenv.2013.02.068.
2. Ben Salah Ch, Ouali M. Energy management of a hybrid photovoltaic system. International Journal of Energy Research 2012; 36: 130 – 138, https://doi.org/10.1002/er.1765.
3. Celik B, Gokmen N, Karatepe E, Silvestre S. Simple diagnostic approach for determining of faulted PV modules in string based PV arrays. Solar Energy 2012; 86: 3364 – 3377, https://doi.org/10.1016/j.solener.2012.09.007.
4. Dzyubenko G A, Kopotun K A, Prymak A V. Three-monotone spline approximation. Journal of Approximation Theory 2010; 162: 2168–2183, https://doi.org/10.1016/j.jat.2010.07.004.
5. Goel A, Sharma T P. Change in the diode quality factor with insulator layer thickness in a metal-insulator-n-semiconductor solar cell. Journal of Applied Physics 1985; 57: 2973-2974, https://doi.org/10.1063/1.335499.
6. Habbati Bellia, Ramdani Youcef, Moulay Fatima. A detailed modeling of photovoltaic module using MATLAB. NRIAG Journal of Astronomy and Geophysics 2014, 3: 53-61, https://doi.org/10.1016/j.nrjag.2014.04.001.
7. Ikegami T, Maezono T, Nakanishi F, Yamagata Y, Ebipara K. Estimation of equivalent circuit parameters of PV module and its application to optimal operation of PV system. Solar Energy 2001; 67: 389 - 395, https://doi.org/10.1016/s0927-0248(00)00307-x.

8. Kandyda A, Rodacki T. Energy conversion in solar power (in polish). Silesian University of Technology Publisher, Gliwice, Poland 2000.
9. Krismadinata, Nasrudin Abd. Rahim, Hew Wooi Ping, Jeyraj Selvaraj. Photovoltaic Module Modeling using Simulink/Matlab. Procedia Environmental Sciences 2013; 17: 537-546, https://doi.org/10.1016/j.proenv.2013.02.069.
10. Ma Jieming, Man Ka Lok, Ting T. O., et al. Approximate Single-Diode Photovoltaic Model for Efficient I-V Characteristics Estimation. SCIENTIFIC WORLD JOURNAL 2013.
11. Pluta Z. Solar energy installations (in polish). Warsaw University of Technology Publisher, Warsaw, Poland 2003.
12. Rajapakse A. Simulation of Grid Connected Photovoltaic Systems. Cedrat News - Flux Solutions & Mechatronic Products; Inovallée, France 2009; 57: 4.
13. Sen K, Tyagi B P. Diode quality factor in polycrystalline solar cells. Journal of Applied Physics 1984; 56: 1240-1241, https://doi.org/10.1063/1.334059.
14. Shell Solar. Product Information Sheet – Shell ST20 Photovoltaic Solar Module. 2004.
15. Skowronek K, Trzmiel G. Analysis of selected parameters of photovoltaic modules under random operation conditions with regard to the effect of instantaneous disturbances. PELINCEC - Power Electronics and Intelligent Control for Energy Conservation, Warsaw, Poland 2005.
16. Skowronek K, Trzmiel G. Determining the effect of faulty operation on the condition of a photovoltaic matrix. Post-conference Monograph Computer Applications in Electrical Engineering", Poznan, Poland 2006; 182 - 195.
17. Skowronek K, Trzmiel G. Generalized analysis of the effect of statistical scatter of the elements of photovoltaic matrix on its equivalent dynamic parameters by random values of darkening fields. Post-conference Monograph Computer Applications in Electrical Engineering", Poznan, Poland 2005; 238-249.
18. Skowronek K, Trzmiel G. The method for identification of fotocell in real time. ISTET - XIV International Symposium on Theoretical Electrical Engineering, Szczecin, Poland 2007.
19. Skowronek K, Trzmiel G. The model of photovoltaic cell with consideration of load variability, AMTEE - Advanced Methods of the Theory of Electrical Engineering, Cheb, Czech Republic 2009.
20. Smolinski M, Perkowski T, Mystkowski A, Dragašius E, Jastrzebski RP. AMb flywheel integration with photovoltaic system for household purpose – modelling and analysis. Eksploatacja i Niezawodnosc – Maintenance and Reliability 2017; 19 (1): 86–94, https://doi.org/10.17531/ein.2017.1.12.
21. Taylor J R. Introduction to the analysis of measurement error. Polish Scientific Publishers PWN, Warsaw 1999.
22. Trzmiel G. Stochastic analysis of the characteristics of the photovoltaic module. PhD dissertation, Poznan University of Technology, Poland 2010.

Grzegorz TRZMIEL
Faculty of Electrical Engineering
Poznan University od Technology
Piotrowo 3A, 60-965 Poznan, Poland

E-mail: grzegorz.trzmiel@put.poznan.pl

Article citation info:
MERKISZ J, RYMANIAK Ł. The assessment of vehicle exhaust emissions referred to CO_2 based on the investigations of city buses under actual conditions of operation. Eksploatacja i Niezawodnosc – Maintenance and Reliability 2017; 19 (4): 522–529, http://dx.doi.org/10.17531/ein.2017.4.5.

Jerzy MERKISZ
Łukasz RYMANIAK

THE ASSESSMENT OF VEHICLE EXHAUST EMISSIONS REFERRED TO CO_2 BASED ON THE INVESTIGATIONS OF CITY BUSES UNDER ACTUAL CONDITIONS OF OPERATION

OCENA EMISJI ZANIECZYSZCZEŃ Z POJAZDÓW W ODNIESIENIU DO CO_2 NA PODSTAWIE BADAŃ AUTOBUSÓW MIEJSKICH W RZECZYWISTYCH WARUNKACH EKSPLOATACJI*

The paper discusses the assessment of the exhaust emissions from heavy-duty vehicles following investigations under actual traffic conditions. The environmental characteristics presented thus far were mainly based on unit or road emissions. The paper presents an analysis of exhaust emissions referred to the harmful CO_2, which was assumed as measure of correctness of the combustion process. The parameters determining this way are referred to as emission indexes. The research objects were 18-meter city buses fitted with three types of powertrains: conventional engine, hybrid (electric motor combined with a diesel engine) and a spark ignition engine fuelled with compressed natural gas (CNG). All buses were Euro V–EEV compliant. The measurements were performed according to the SORT 2 driving test procedure on the test route within the Poznan agglomeration. Investigations performed under actual traffic conditions allow a true assessment of environmental performance of a given research object because they cover a much greater engine operating parameter variability range compared to laboratory and homologation tests. The performed road tests and their analysis led to conclusions related to the applicability of the developed method of emission assessment based on emission indexes for vehicles fitted with different powertrains.

Keywords: *city bus, emission of CO_2 and other exhaust components, laboratory and actual test conditions, powertrain, emission index.*

W artykule przedstawiono rozważania dotyczące oceny emisji zanieczyszczeń z pojazdów ciężkich na podstawie badań realizowanych w rzeczywistych warunkach eksploatacji. Przedstawiane do tej pory charakterystyki ekologiczne silnikowych środków transportu opierały się przede wszystkim na emisji jednostkowej lub drogowej. W pracy przedstawiono analizę emisji związków toksycznych odniesioną do związku szkodliwego CO_2, dla którego założono, że jest miarą poprawności realizacji procesu spalania. Wyznaczone w ten sposób parametry nazwano wskaźnikami toksyczności. Obiekty badawcze stanowiły osiemnastometrowe autobusy miejskie wyposażone w trzy rodzaje układów napędowych: konwencjonalny i hybrydowy z silnikami ZS, a także pojazd zasilany sprężonym gazem ziemnym z silnikiem ZI. Wszystkie autobusy spełniały normę Euro V–EEV. Pomiary wykonano zgodnie z procedurą testu jezdnego SORT 2 oraz na trasie badawczej w aglomeracji poznańskiej. Badania w warunkach rzeczywistej eksploatacji pozwalają dokonać rzetelnej oceny ekologiczności danego obiektu badawczego, ponieważ obejmują znacznie większy obszar zmienności parametrów pracy silników spalinowych w porównaniu z laboratoryjnymi testami homologacyjnymi. Wykonane badania drogowe i ich analiza pozwoliły na sformułowanie wniosków dotyczących słuszności stosowania opracowanej metody oceny emisji zanieczyszczeń, bazującej na wskaźnikach toksyczności, dla pojazdów wyposażonych w różne rodzaje układów napędowych.

Słowa kluczowe: *autobus miejski, emisja CO_2 i związków toksycznych w spalinach, eksploatacyjne i testowe warunki badań, układ napędowy, wskaźnik toksyczności.*

1. Introduction

The conditions of operation of a combustion engine under actual traffic conditions are characterized with a wide range of engine speeds and torques. This has a direct impact on the vehicle fuel consumption and exhaust emissions that may be expressed with a variety of characteristics. For the PC (passenger car) vehicle category, it is the road emissions that are most frequently used i.e. the mass of a given exhaust component is referred to a given distance covered (e.g. g/km). In the case of HDV (heavy-duty vehicles) vehicles and non-road vehicles, the most efficient way to asses their environmental impact is to use unit exhaust emissions, i.e. the mass of a given exhaust component is referred to performed work (e.g. g/(kW·h)). Heavy-duty vehicles use engines of high torques; therefore, the homologation tests are performed exclusively on engine test beds (measurement cost optimization). To some extent, these tests simulate the actual operating conditions of a vehicle, yet they do not fully reproduce the actual vehicle driving cycle, particularly if city buses are the case [11].

Based on the works carried out in recent years, we know that the qualitative and quantitative measurements of exhaust emissions performed under laboratory conditions may significantly diverge from the actual emissions of a vehicle from a given category. This is also the case for HDV [7, 13]. Therefore, actions are being taken to devel-

(*) Tekst artykułu w polskiej wersji językowej dostępny w elektronicznym wydaniu kwartalnika na stronie ***www.ein.org.pl***

op detailed and universal methods of assessment of exhaust emissions under actual conditions of operation (RDE – real driving emissions) [2, 6, 8–10]. The rapidly advancing PEMS (portable emissions measurement system) equipment and its miniaturization allows carrying out increasingly more accurate tests of vehicle environmental performance under actual operating conditions. Currently, pilot projects are underway worldwide addressing this issue [1, 3, 8, 12].

The homologation standards applied thus far, related to the environmental performance of vehicles of different categories were based on laboratory tests performed only on chassis or engine dynamometers. Legislation introduced in the European Union (Euro VI/6) force the performance of measurements under actual operation [4]. This aims, inter alia, at the assessment of the environmental performance of a given solution at individual points of work of an engine or a vehicle other than that predefined in laboratory tests. It also aims at determining the emission indexes for compliance in operation. Research and development works very often rely on time density characteristics (TD – time density) and 3D emission characteristics created on their basis that present second-by-second emission of a given exhaust component as a function of: engine speed – torque (n–T) or vehicle speed – acceleration (V–a). Given the time of operation, it is possible to characterize motion with a discrete function of coordinates T and n.

To determine the emission characteristics, parameters related to motion or work of a vehicle are utilized. In terms of road emission, it is quite simple to determine the covered distance, which is recorded in both the OBD system (calculated based on instantaneous vehicle speed) and the GPS system (global positioning system) – an inseparable component of the PEMS equipment. The determination of actual work performed by an engine or the entire powertrain (if hybrid vehicles are the case) is more difficult when calculating the unit emission of a given exhaust component. Instantaneous power output is calculated based on the engine speed and load, the values of which can be pulled from the OBD system. The first of the said parameters is obtained directly by induction sensors or Hall effect sensors and the data obtained with this method are sufficient. The torque is obtained from the pressure values in the fuel system and the opening time of the injector, which is critical for the accuracy of the measurement [5]. In homologation tests, the 'net' parameters of power output and load must be considered, i.e. parameters obtained on a test stand at the end of the crankshaft with additional aggregates [14], which is why certain divergence appears compared to the values obtained under actual operating conditions. The reason for this is that the data pulled from the OBD system allow for engine internal resistance. In the calculations, one can allow for this by including the percentage share of friction, but it is some sort of simplification, because the actual resistance is dependent on a variety of factors. These factors are rarely linear and they change with the parameters of the engine operation.

2. The assessment of the exhaust emissions referred to CO_2

As a result of combustion of hydrocarbon fuels in the engine, thermal energy is released along with a variety of components harmful for the environment. Carbon dioxide CO_2 forms as a result of complete oxidation, while CO, THC (total hydrocarbons), NO_x and particulate matter (mass and number) are a result of non-full and incomplete combustion at high temperatures. They are unwanted by-products having great impact on the natural environment. Therefore, in different regions/countries of the world various kinds of emission related restrictions are imposed on motor vehicles. Carbon dioxide is not a toxic component but harmful – it contributes to the greenhouse effect and in higher concentrations is poisonous for the living organisms.

Given the physicochemical course of oxidation inside the combustion chamber, we may assume that CO_2 is a measure of correctness of this process, which is why it is considered useful in the assessment of the exhaust emissions from many types of combustion engines. Besides, when defining a powertrain as a combustion engine together with aftertreatment systems, we may also consider aspects related to the environmental impact of vehicles of different categories, particularly in terms of road tests. To this end, it is necessary to apply a quantitative emission index M defined with the quotient:

$$M_j = b \cdot \frac{e_{real,\,j}}{e_{CO_2}} \tag{1}$$

where: M – dimensionless emission index [–]; j – exhaust component, for which the emission index was determined; b – universal constant (for CO, THC and $NO_x = 10^3$, for PM = 10^5); $e_{real,\,j}$ – unit or road emission or mass of the exhaust component j determined in the test [g/(kW·h); g/(km); g]; e_{CO2} – unit or road emission or mass of CO_2 (tantamount to $e_{real,\,j}$) [g/(kW·h); g/(km); g].

3. Research methodology under actual vehicle operation

Three 18-meter city buses of similar performance were used for the research. Such vehicles are most often used on heavily loaded bus routes, where many passengers are carried. The first research object was fitted with a conventional diesel powertrain, the second research object was a serial hybrid and the third research object was fitted with a CNG-fuelled spark ignition engine (Fig. 1). In the paper, they have been marked: DIESEL, HYBRID and CNG respectively. All buses were homologated, complete and fully operative. Each of the objects was compliant with the Euro V – EEV (Enhanced Environmentally Friendly Vehicle). In order to prepare the vehicles for the tests a dummy load was installed to simulate the passenger load during daily operation – the weight of bus including the load was 24 000 kg.

The exhaust emissions tests performed under actual traffic conditions allow an obtainment of actual environmental and economic indexes. A careful selection of the test routes is extremely important in the process of development of the measurement methodology (Fig. 2). In city traffic, the operating conditions are influenced by many factors (road congestion, traffic organization, traffic lights), which is why it is characterized by a great variability and randomness. During the development of the research methodology, it was assumed that the measurement would be performed on city buses in actual traffic in SORT 2 complex trapezoidal normalized tests (Standardized On-Road Tests 2 – Easy Urban) defined by UITP (Union Internationale des Transports Publics - International Organization for Public Transport) [13]. The characteristics of the test have been presented in Fig. 2a. The tests were carried out on a city route of a local bus operator, classified as one of the most heavily occupied routes (length and number of carried passengers) (Fig. 2b). The total length of the test route was 11.2 km and covered 27 bus stops including bus terminals. The test run started in the northern part of the city and continued through streets of various congestion to the exact downtown area of Poznan.

A portable emissions measurement system (PEMS) was used for the tests under actual traffic conditions: SEMTECH DS and AVL MSS (Fig. 3). The equipment allows carrying out tests on spark ignition and diesel engines compliant with the standard of Euro III and higher. The exhaust gas of the tested vehicle is passed to the mass flow probe, where a sample is taken. The tested volume of the gas is transported through a heated line to a set of SEMTECH DS analyzers. At this point the concentrations of individual gaseous components are measured: THC (FID – flame ionization detector), NO_x (NDUV – non-dispersive detector, ultra violet), CO_x (NDIR – non-dispersive detector infra red), and O_2 (electrochemical sensor). At the same time, a sample of exhaust gas is taken to the portable MSS analyzer, where

a)

Parameter	DIESEL
Type/fuel	4-stroke, CI/ diesel fuel
Displacement [dm^3]	9.2
Compression ratio	17.5
Maximum power output [kW]/[rpm]	265/1900
Maximum torque [N·m]/[rpm]	1450/1100–1700
Aftertreatment	SCR/DPF

b)

Parameter	HYBRID
Type/fuel	4-stroke, CI/ diesel fuel
Displacement [dm3]	6.7
Compression ratio	17.2
Maximum power output [kW]/[rpm]	209/2300
Maximum torque [N·m]/[rpm]	1008/1200–1800
Aftertreatment	SCR/DPF

c)

Parameter	CNG
Type/fuel	4-stroke, SI/ compressed natural gas
Displacement [dm3]	8.9
Compression ratio	12
Maximum power output [kW]/[rpm]	239/2000
Maximum torque [N·m]/[rpm]	1356/1300–1400
Aftertreatment	TWC

Fig. 1. Technical specifications of the research objects

a)

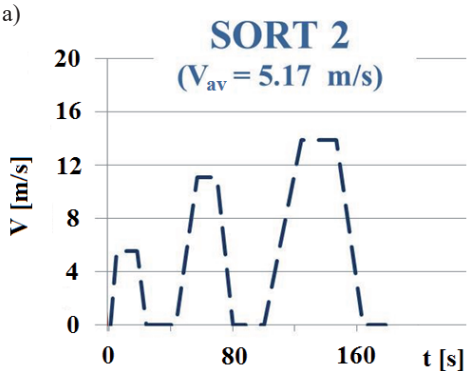

Parameter	SORT 2
Average speed [m/s]/[km/h]	5.17/18.6
Share of stationary vehicle in the test [%]	33.4
Constant speed in profile 1 [m/s]/[km/h]/[m]	5.6/20/100
Constant speed in profile 2 [m/s]/[km/h]/[m]	11.1/40/220
Constant speed in profile 3 [m/s]/[km/h]/[m]	13.9/50/600
Time of stationary vehicle after profile [s]	20/20/20
Distance in the test [m]	20

Fig. 2. RDE research methodology: a) SORT 2 driving cycle, b) city bus route [15]

a)

b)

c)

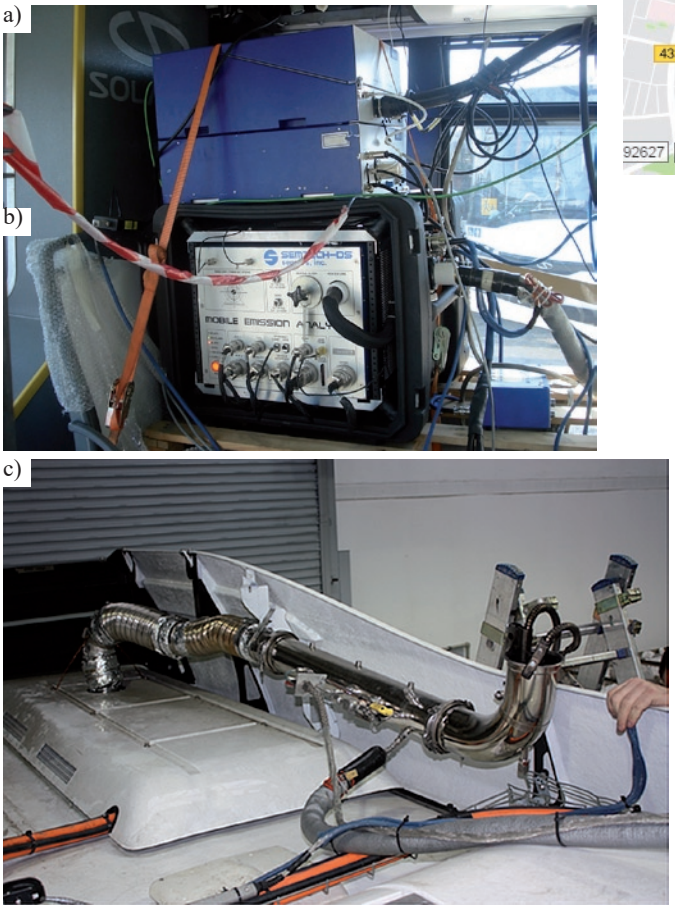

Fig. 3. View of the PEMS equipment during operation on a bus: a) AVL MSS 483, b) SEMTECH DS, c) mass flow meter of the exhaust gas

the concentration of PM is measured based on the photoacoustic method.

b)

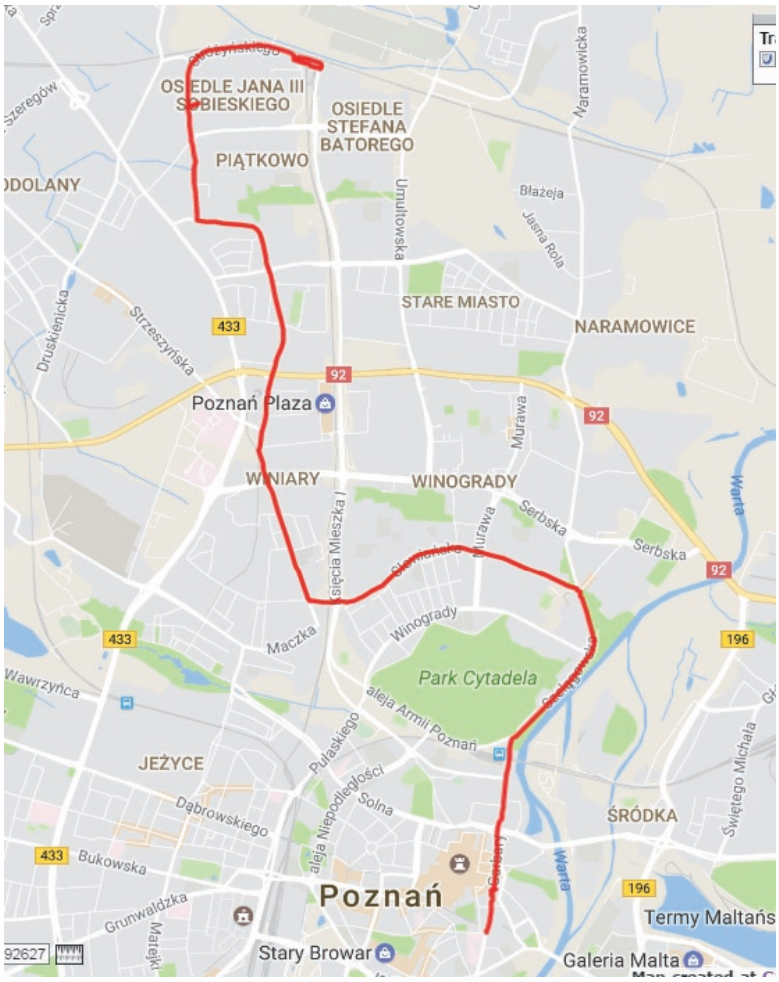

4. Results

4.1. Exhaust emissions referred to CO_2 in the SORT test

Based on the performed tests, a second-by-second emission of individual exhaust components (CO, THC, NO_x and PM) was determined that was referred to the second-by-second emission of CO_2. Individual relations along with the operating parameters of the engines and the speed curves of the diesel vehicle selected for the presentation of results have been shown in Fig. 4. The presentation indicates that always during engine braking, when the engine is propelled by the vehicle wheels and the second-by-second emission of CO_2 is close to zero, a significant increase of the dimensionless index M occurs. This confirms unwanted phenomena inside the engine cylinders – choking the flame, non-full and incomplete combustion as well as very poor performance of the aftertreatment systems. Such a situation always occurs when the gear is reduced, which is confirmed by the engine torque and speed curves. Based on the values obtained for the index M_NO_x/CO_2 (85 during braking in the second profile of the test) it is possible to infer that the efficiency of the SCR, whose operation mainly depends on the temperature and exhaust gas mass flow is reduced. The maximum values of individual indexes were obtained for: M_CO/CO_2 = 191 and M_PM/CO_2 = 31 in the third profile of the SORT 3 test and M_THC/CO_2 = 4.6 that occurred in the first stage of the analyzed cycle.

Consider of the recorded emissions of individual exhaust components, a bar graph of the calculated M indexes for the SORT 2 was drawn (Fig. 5). For CO and THC referred to CO_2 the highest values were obtained by the vehicle fueled with CNG. The vehicle fitted with a spark ignition engine reached a value 8 times higher for

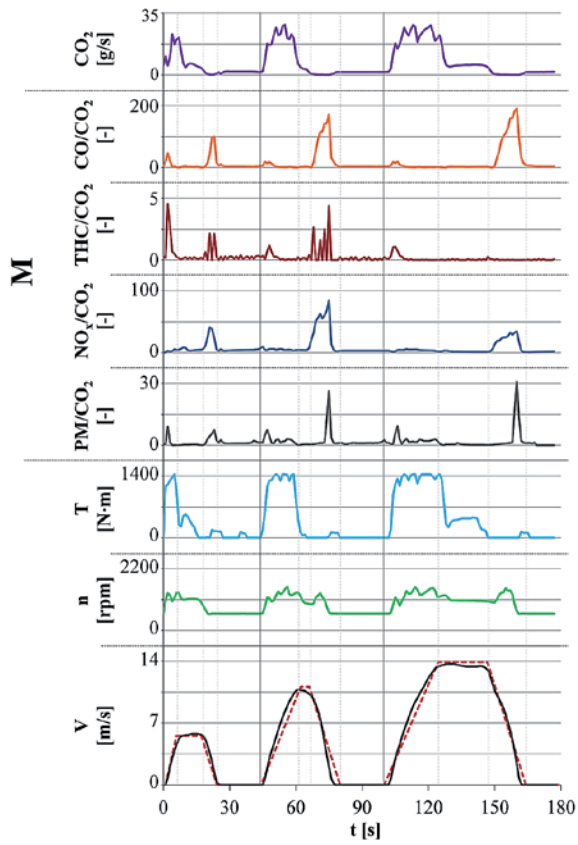

Fig. 4. The curves of vehicle speed, engine speed, engine torque, emission rate of CO_2 and index M for CO, THC, NO_x and PM recorded during the SORT 2 road test

M_THC/CO_2 compared to the other vehicles. It resulted from the characteristics of the applied fuel. It is noteworthy that non-methane hydrocarbons (NMHC) have a significant share of above 98% in these results. NMHC are deemed harmful but not toxic. The highest index of M_NO_x/CO_2 of 6.97 was observed for the hybrid powertrain, where an engine of the lowest maximum torque was applied. The vehicle frequently operated under increased load (higher efficiencies, higher temperature inside the cylinders during combustion), which was impactful on the obtained results. The application of an alternative fuel or a hybrid powertrain, where the electric motor successfully assisted the combustion engine when driving off and accelerating, yielded lower values M_PM/CO_2 values compared to the conventional diesel solution. For this bus the calculated emission index was M_PM/CO_2 = 1.77. Besides, in the third tested vehicle, no PM dedicated aftertreatment system was applied and such low values obtained resulted from the application of a gaseous fuel that very well mixes with air inside the combustion chamber as well as the thermodynamic cycle, in which the engine operated.

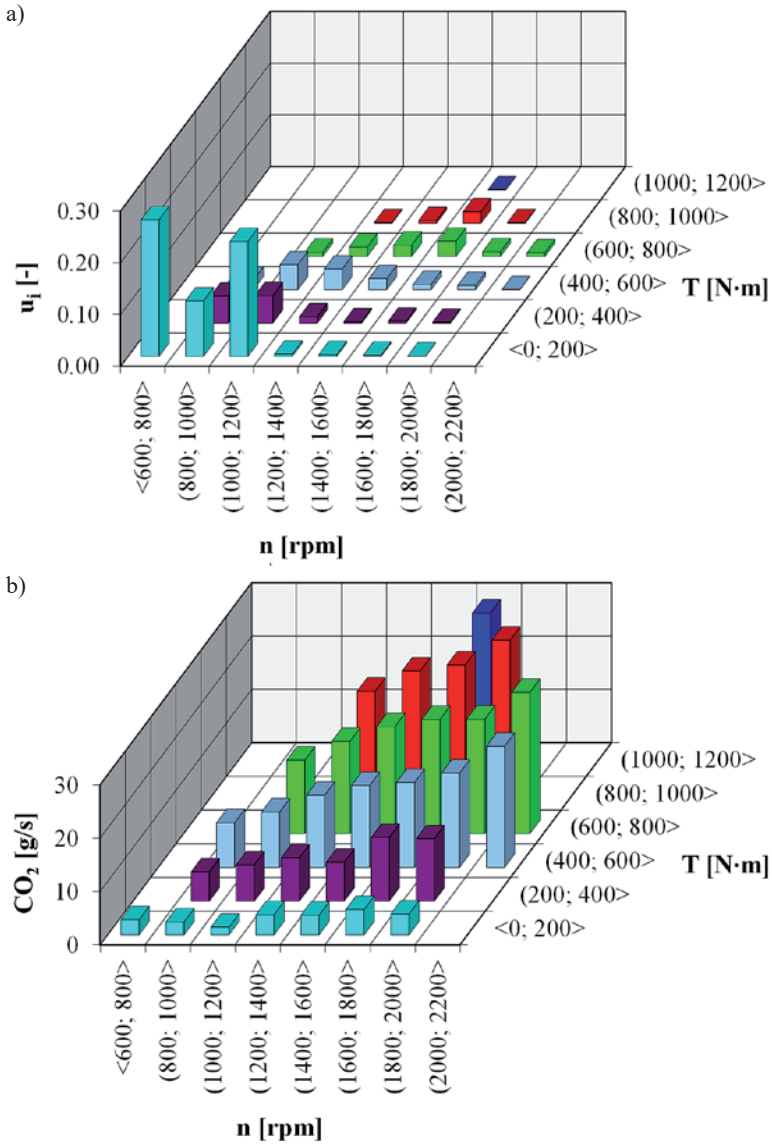

Fig. 6. Characteristics of the hybrid vehicle during the measurements: a) engine operating time share, b) CO_2 emission rate in the speed and torque intervals

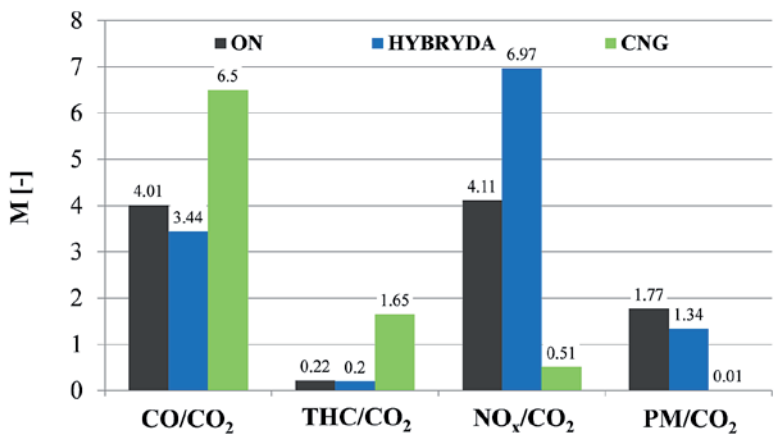

Fig. 5. M emission indexes for CO, THC, NO_x and PM obtained during the normalized SORT 2 test

4.2. Exhaust emissions referred to CO_2 on a city route

Following the analysis of the operating time share of a combustion engine, one may observe that the hybrid bus obtained the highest values of 26.4% for idle speed for the torque in the range ⟨0 N·m; 200 N·m⟩ (Fig. 6a). In the test under analysis, a significant part of the operating time was observed for the parameters (1000 rpm; 1200 rpm⟩ and ⟨0 N·m; 200 N·m⟩ that constituted 22% of the entire test run on the city route. For the test

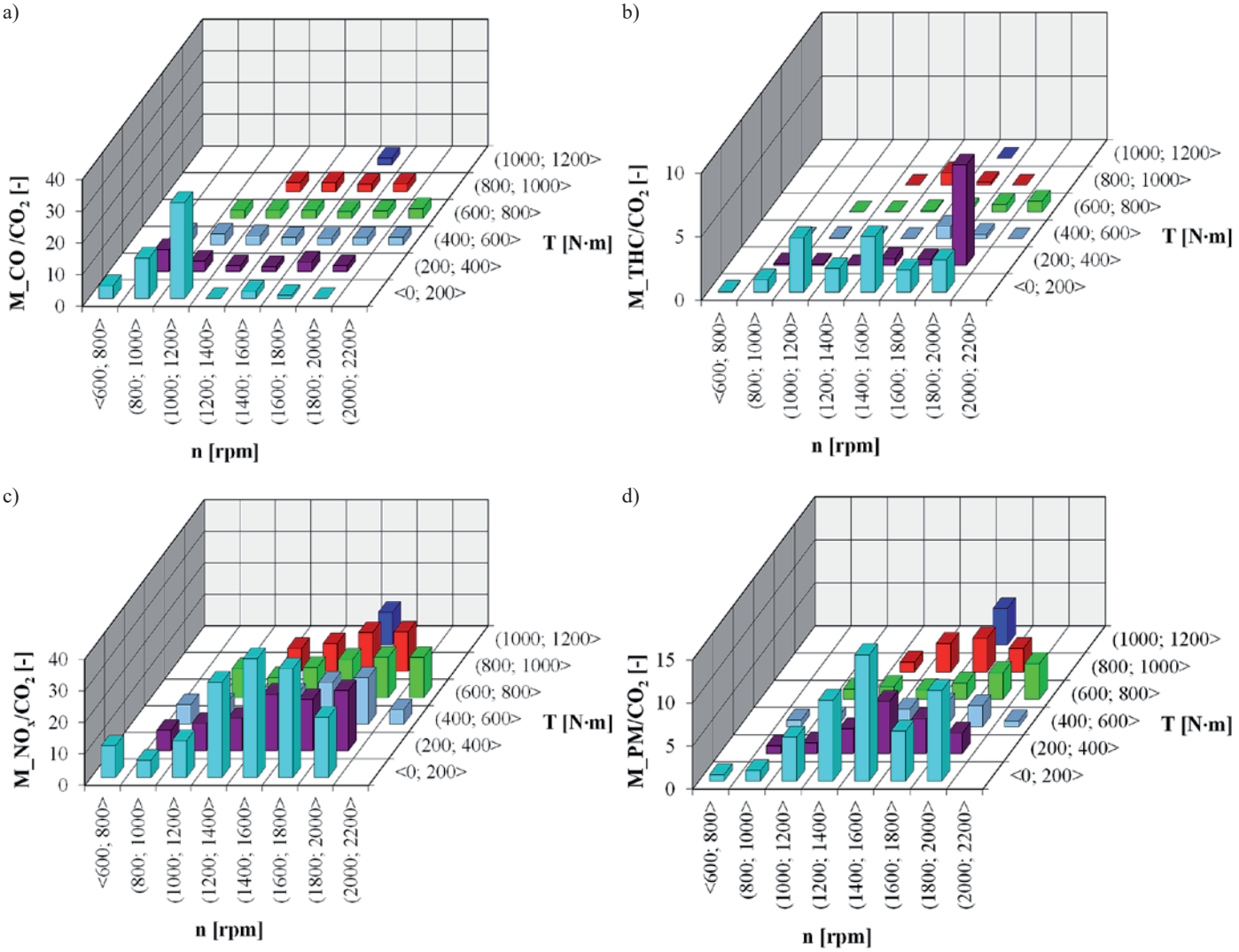

Fig. 7. Characteristics of the dimensionless index M of the hybrid vehicle during measurements of individual exhaust components: a) CO, b) THC, c) NO_x and d) PM

run between the said intervals, an operating time share of 10.7% was determined. The collective operating time share of the engine in the range (800 rpm; 1200 rpm⟩ and (200 N·m; 600 N·m⟩ was 17.2%. For the individual intervals not mentioned in the analysis, the values did not exceed 4%.

For diesel engines, the CO_2 emission rate mainly depends on the load. For the hybrid bus, due to the cooperation of the powertrain components, the values were influenced not only by torques but also engine speeds (Fig. 6b). This was caused by the use of electric energy to assist the vehicle propulsion, particularly during acceleration. The maximum value for the research object under analysis was 28.7 g/s in the range (1600 rpm; 1800 rpm⟩ for the greatest loads. The average for the entire test run was 13.8 g/s and the lowest CO_2 emission rate was obtained in the load range of up to 200 N·m in the entire range of engine speeds.

The emission rate of individual exhaust components recorded during the hybrid bus tests on the city route was referred to the emission of CO_2. For the emission index M_CO/CO_2 the most important values were obtained in the engine speed range (800 rpm; 1200 rpm⟩ at lowest loads, where, in the subsequent individual intervals, the following were obtained respectively: 12.7 and 30.2 (Fig. 7a). In the outstanding intervals, the average was 2.5 and the characteristic distribution was even. Index M_THC/CO_2 reached significant values (3 on average) in the area of the smallest loads up to 200 N·m at the speeds in the range (1000 rpm; 2000 rpm⟩ (Fig. 7b). For the intervals described with parameters (200 N·m; 400 N·m⟩ and (1800 rpm; 2000 rpm⟩ an index of 7.9 was recorded, which may indicate a significant flame choke (fading combustion) inside the engine cylinders. The outstanding intervals were characterized by an index not exceeding 0.97.

The highest values of the emission index M_NO_x/CO_2 (up to 37.7) were determined for the engine speed range (1200 rpm; 2000 rpm⟩ at loads up to 200 N·m (Fig. 7c). This confirms a limited efficiency of the selective catalytic reduction system dosing the reducing agent based on the exhaust temperature and mass flow. In the said area, conditions disadvantageous for high catalytic efficiency occured. In the outstanding engine operating range an even distribution of the index was observed as the engine speed increased – for the outstanding intervals of the characteristics, 10.5 was obtained on average. In the range of engine speeds above 1000 rpm covering the smallest loads, the highest M_PM/CO_2 indexes were obtained in individual intervals from 5.2–14.7 (Fig. 7d). the smallest values of the discussed emission index were recorded in the area of medium torques, in the entire range of engine speeds, which indicates best combustion (complete and full) in this interval of the operating parameters of the tested engine.

Similarly to the measurements performed in the SORT 2 test, the emission indexes of all tested objects indicate that the smallest values of M_CO/CO_2 and M_THC/CO_2 were obtained for the hybrid bus (Fig. 8). The combination of an electric motor with a combustion en-

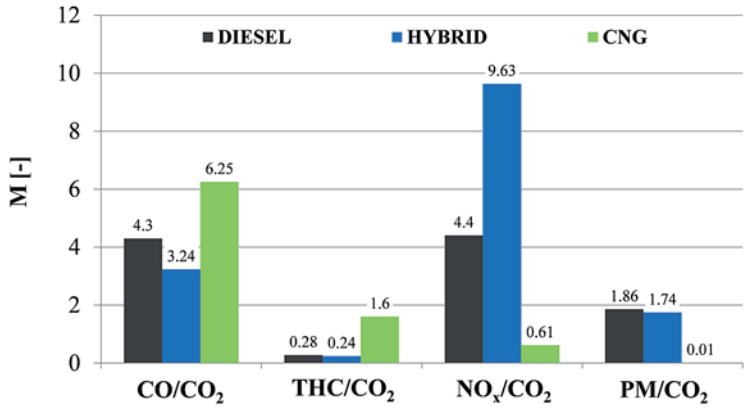

Fig. 8. Emission indexes M for CO, THC, NO_x and PM during road tests on a city route

gine resulted in an increased powertrain efficiency, which positively influenced the analyzed indexes reaching 3.24 and 0.24 respectively. Again, the highest values were obtained for the CNG-fueled vehicle fitted with a three-way catalytic converter characterized by a high conversion rate (NO_x reduction). This contributed to such a low level of M_NO_x/CO_2 reaching 0.61. As for PM, the highest indexes were recorded for the conventional vehicle – 1.86. The hybridization of the powertrain positively influenced the M_PM/CO_2, index, but the application of CNG allows an obtainment of values that are 100 times lower in the analyzed area.

5. Conclusions

The presented assessment of the exhaust emissions from city buses based on tests performed under actual traffic conditions leads to conclusions related to the engine alone as well as the entire powertrain (including aftertreatment systems). The presented and discussed results confirm that applying an emission index, being the ratio of the emission of a given exhaust component to the emission of CO_2, allows considering it in the assessment of exhaust emissions from conventional solutions, hybrid solutions and such based on alternative fuels. The interpretation can be made for all types of characteristics (including discrete ones), which is particularly useful in the research on environmental performance in transport, particularly under actual conditions of operation. The presented coefficient is somewhat a measure of correctness of the fuel combustion inside the engine cylinders and a measure of efficiency of the aftertreatment systems. The emission index M should definitely be used in road tests because, given its dimensionless quality, it provides new explorative opportunities – it is designed to render the final test results independent of the covered distance or performed work during the test. It is possible to limit the number of boundary conditions for the conditions that must be met under actual operation. This is very beneficial in the assessment of environmental performance and completion of measurements because the homologation road tests are difficult to carry out due to a variety of limitations regarding time, speed and acceleration shares, covered distance and work performed by the engine. For the above reasons, the application of the emission index may turn out very useful in the assessment of hybrid powertrains. The analyses presented in the paper are some of the first of this type and their results and conclusions motivate to continue the research on exhaust emissions referred to the emission of CO_2.

Acknowledgement

The research was funded by the National Centre for Research and Development – the INNOTECH Programme (contract No. INNOTECH-K2/IN2/36/182269/NCBR/12).

References

1. Almén J. Swedish In-Service Testing Programme 2010 on Emissions from Heavy-Duty Vehicles. AVL Certification & Regulation Compliance, Södertälje 2010.
2. Bajerlein M, Rymaniak Ł. The Reduction of Fuel Consumption on the Example of Ecological Hybrid Buses. Applied Mechanics and Materials 2014; 518: 96–101, https://doi.org/10.4028/www.scientific.net/AMM.518.96.
3. Bonnel P, Rubino L, Carriero M, Krasenbrink A. Portable Emission Measurement System (PEMS) for Heavy Duty Diesel Vehicle PM Measurement: the European PM PEMS Program. SAE Technical Paper 2009-24-0149.
4. Commission Regulation (EU) No 582/2011 of 25 May 2011 implementing and amending Regulation (EC) No 595/2009 of the European Parliament and of the Council with respect to emissions from HDV (Euro VI) and amending Annexes I and III to Directive 2007/46/EC of the European Parliament and of the Council.
5. Čupera J, Sedlák P. Design and Verification of Engine Power Calculation Model Using the Data of a Digital Bus Built into an Agricultural Tractor. Acta Universitatis Agriculturae et Silviculturae Mendelianae Brunensis, no. 6, Brno 2011.
6. Czerwinski J, Comte P, Zimmerli Y, et al. Testing emissions of passenger cars in laboratory and on-road (PEMS, RDE). Combustion Engines 2016; 166(3): 17–23. https://doi.org/10.19206/CE-2016-326.
7. Fuc P, Lijewski P, Ziolkowski A, Dobrzynski M. Dynamic Test Bed Analysis of Gas Energy Balance for a Diesel Exhaust System Fit with a Thermoelectric Generator. Journal of Electronic Materials 2017; 46 (5): 3145–3155, https://doi.org/10.1007/s11664-017-5280-8.
8. Fulper C. New Measurement Techniques & Procedures for Measuring "Real World" Emissions with PEMS and PAMS. 2013 PEMS Conference & Workshop University of California, Riverside 2013.
9. Kuranc A. Exhaust emission test performance with the use of the signal from air flow meter. Eksploatacja i Niezawodnosc – Maintenance and Reliability 2015; 17 (1): 129–134, https://doi.org/10.17531/ein.2015.1.17.
10. Merkisz J, Kozak M, Lijewski P, Fuć P. Exhaust Emissions from Heavy-Duty Vehicles Under Actual Traffic Conditions in the City of Poznań. SAE Technical Paper 2013-01-0119.
11. Nylund N O, Erkkilä K, Hartikka T. Fuel Consumption and Exhaust Emissions of Urban Buses. VTT Tiedotteita Research Notes 2373, Helsinki 2007.
12. Petrović V S, Janković S P, Tomić M V, Jovanović Z S, Knežević D M. The Possibilities for Measurement and Characterization of Diesel Engine Fine Particles – a Review. Thermal Science 2011: 4(15): 915–938.

13. UITP 2009: UITP Project SORT Standardized On-Road Test Cycles. UITP – International Association of Public Transport, Bruksela 2009.
14. United Nations Economic Commission for Europe: Global technical regulation No. 4: Test procedure for compression-ignition (C.I.) engines and positive ignition (P.I.) engines fuelled with natural gas (NG) or liquefied petroleum gas (LPG) with regard to the emission of pollutants. ECE/TRANS/180/Add.4, 2007.
15. http://gpsvisualizer.com (dostęp: 30.01.2017).

Jerzy MERKISZ
Łukasz RYMANIAK
Institute of Combustion Engine and Transport
Poznan University of Technology
ul. Piotrowo 3, 60-965 Poznan, Poland

E-mails: Jerzy.Merkisz@put.poznan.pl,
Lukasz.Rymaniak@put.poznan.pl

Article citation info:
WANG ZB, SHANG S, WANG JW, HUANG ZL, SAI F. Accelerated storage degradation testing and failure mechanisms of aerospace electromagnetic relay. Eksploatacja i Niezawodnosc – Maintenance and Reliability 2017; 19 (4): 530–541, http://dx.doi.org/10.17531/ein.2017.4.6.

ZhaoBin WANG
Shang SHANG
JiaWei WANG
ZhouLin HUANG
Fu SAI

ACCELERATED STORAGE DEGRADATION TESTING AND FAILURE MECHANISMS OF AEROSPACE ELECTROMAGNETIC RELAY

BADANIA PRZYSPIESZONE DEGRADACJI W CZASIE SKŁADOWANIA PRZEKAŹNIKÓW ELEKTROMAGNETYCZNYCH STOSOWANYCH W PRZEMYŚLE LOTNICZYM ORAZ MECHANIZMÓW ICH USZKODZEŃ

It is difficult to obtain the failure data of high-reliability and long-lifetime aerospace electromagnetic relay (EMR), even if based on the traditional accelerated storage life testing method. Based on the reliability test technique, the scheme of accelerated degradation testing for aerospace EMR was designed. The test system of aerospace electromagnetic relay storage parameters under temperature-accelerated stress was designed and developed. The most past research on storage reliability of relay only focuses on the measurement of contact resistance. The relay time parameters (pick-up time, opening time, overtravel time, rebound duration time, etc.) which reflect main performance function were not monitored. So, in this study the relay time parameters and relay contact resistance were detected simultaneously. According to the analysis on experiment results of contact resistance, relay time parameters, the degradation phenomena of aerospace EMR in long-term storage are investigated, which provides the bases for determining degradation sensitive parameters. Finally, based on the structure and function of aerospace EMR, the storage failure mechanism is investigated by conductive properties themselves. The microscopic morphology and changes in chemical elements for relay contact surface was analyzed by SEM and EDX regularly, which provide references for the relay storage failure mechanism.

Keywords: *electrical contact; electromagnetic relay; failure mechanisms; storage reliability; degradation testing.*

Ze względu na wysoką niezawodność i długi cykl życia przekaźników elektromagnetycznych stosowanych w przemyśle lotniczym (EMR), trudno jest uzyskać dane o ich uszkodzeniach, nawet gdy korzysta się z tradycyjnej metody przyspieszonych badań dopuszczalnego okresu składowania. W przedstawionym artykule, opracowano, w oparciu o technikę badania niezawodności, schemat przyspieszonego badania degradacji przekaźników elektromagnetycznych stosowanych w lotnictwie. Zaprojektowano i opracowano system oceny parametrów składowania przekaźników elektromagnetycznych używanych w lotnictwie w warunkach przyspieszonych przy skrajnych temperaturach. Ostatnie badania nad niezawodnością składowania przekaźników koncentrują się wyłącznie na pomiarze rezystancji styku. Nie były w nich monitorowane parametry czasowe przekaźnika (czas załączania, czas otwarcia, czas opóźnienia, czas trwania odbicia itp.), które odzwierciedlają jego główne funkcje. W przedstawionych badaniach mierzono jednocześnie parametry czasowe przekaźników i rezystancję styków. W oparciu o analizę uzyskanych wyników doświadczeń, badano zjawiska degradacji EMR podczas ich długoterminowego składowania, co stanowiło podstawę do wyznaczenia parametrów wrażliwych na degradację. Wreszcie, w oparciu o strukturę i funkcje EMR, badano mechanizm powstawania uszkodzeń podczas ich składowania na podstawie właściwości przewodzących. Prowadzone regularnie metodami SEM i EDX analizy budowy mikroskopowej oraz przemian pierwiastków chemicznych zachodzących na powierzchni styków przekaźnika stanowią odniesienie dla badań mechanizmu powstawania uszkodzeń podczas składowania przekaźników.

Słowa kluczowe: *Styk elektryczny; przekaźnik elektromagnetyczny; mechanizmy uszkodzeń; niezawodność składowania; badania degradacji.*

1. Introduction

Aerospace electromagnetic relay (EMR) is one kind EMR being required to have the higher technique level and reliablitiy. It has many advantages, such as larger ratio of breaking resistance to making resistance, higher contact power controlled by lower coil power, and simultaneous movement for multi-contacts. And it is one of indispensable electronic devices in the electronic systems of space flight. They differ among themselves with a structure, purpose, and technical parameters [3]. Aerospace EMR is the key mechanical and electrical component in the national defence weapon system or industry to realize the functions of signal transmission, load switching, circuit protection and control, and system isolation.

The reliability of the relay research work can be summarized as reliability analysis, reliability design, and reliability testing.

Professor Lu of Hebei University of Technology opened the relay reliability design precedent. A calculation model of product failure rate based on stress strength interference model provides the basis for the design of electromagnetic system [6]. Zhai studied the influence of the fluctuation of the parameters on the electromagnetic characteristics of the relay by orthogonal test [19]. Wang optimized the calculation method of dynamic characteristics of relay through FEM joint simulation and genetic algorithm, the calculation efficiency is improved, and was verified in actual production [20]. Li tested the contact resistance of the relay by pulse current method, and evaluated the relationship between the variation of contact resistance and contact reliability [4].

It is still in the exploratory stage. Reference [7] firstly tried to apply the accelerated life test to the study of the reliability of the relay, predicted the storage life and achieved preliminary results. But they only gave an exploratory test plan and had a certain exploration component for the selection of accelerated stress, the determination of test time and the selection of test stress level.

In the study of the accelerated life test scheme and simulation evaluation of the relay storage, Li aimed at optimal design of accelerated storage test scheme for relay small sample, they used the MCMC method based on Gibbs sampling and gave a Bayesian estimation method for the parameters of the relay accelerated life test model under the condition of multiple distribution. They presented a test method for evaluating the storage life of sealed relays according to the principle of step stress accelerated life test. In the censored cases, they set up the life distribution of Weibull distribution relay step stress accelerated life test model and used the likelihood method to calculate the life characteristics of the relay under normal stress level, but there is no experimental verification [5].

In the study of the failure mechanism and failure physics modeling, the related research has been carried out. Zang has studied the surface film of sealed relay and the film forming test has been designed. The pollution source which may lead to the increase of contact resistance has been analyzed [18]. According to the known relay failure mechanism, Wan tried to apply the PoF method to the prediction of the storage life of the relay, and the storage life was predicted by the time series method [16].

About the degradation test, Nair pointed out that degradation data is a rich source of information for reliability analysis in 1988 [15]. Reliability method based on product degradation data has become one of the important ways to solve the problem of high reliability and long life products. It is also an inevitable trend of the development of reliability evaluation methods from failure data to performance degradation data [8,17]. There has been a growing literature that is concerned with drawing reliability inferences from degradation data [10].

In view of the traditional reliability test method based on field storage reliability evaluation is very difficult to meet the storage requirements of long-life products, the test conditions, test method and test process of aerospace EMR storage degradation were studied in this paper. The contact resistance and time parameters of the relay are analyzed by using the graph analysis method, the variation law of relay performance parameters with time under storage conditions is obtained, on this basis, the contact resistance and the pick-up time are prescribed as sensitive parameters of storage degradation. Secondly, from the perspective of aerospace EMR function, structure and storage environment stress, the failure mechanism of the relay was analysed. SEM test and EDX analysis were used to analyze the microstructure and chemical composition of relay contacts periodically to provide the basis for analyzing the failure mechanism of relay storage.

2. Accelerated degradation testing methods

2.1. Accelerated degradation testing

Degradation is a physical or chemical process which causes the deterioration of the internal properties or states of the material under environmental stresses. The changing process will lead to product damage after a period of accumulation, which is represented by the changes of product parameters. The products will fail when the parameters reach certain order. One can accelerate the degradation by applying higher stresses (e.g., electrical stress, temperature stress, etc.) which is called accelerated stress [9]. The accelerated degradation test is an alternative to accelerated life testing which counts the time to failure. For the highly reliable and long-lifetime products that experience degradation of their performance, monitoring such degradation with time becomes a more efficient approach to estimate reliability than observing the actual failure time which might not occur during the test time [11, 12]. Namely, accelerated degradation testing method is used when no failure or few failures are expected at normal testing conditions or even at accelerated life testing conditions.

A primary advantage of accelerated degradation test is that multiple degradation measurements can be recorded on each test processing. Compared to traditional accelerated life testing, this method yields plenty more reliability data. As a result, accelerated degradation testing method is suitable for high reliable products. From the standpoint of testing operability and product evaluation, the accelerated degradation sample should meet the following requirements. Firstly, performance degradation must be irreversible. Secondly, performance degradation can be accelerated. From the reliability pre-research test, accelerated storage testing based on parameter degradation for aerospace relay is feasible.

2.2. Procedure of aerospace relay accelerated storage degradation testing (ASDT)

Aerospace relay is one of the most important electromechanical components in weaponry equipments. The structural schematic of a certain aerospace relay is shown in figure 1. This relay is a kind of common switch-type contact relay (one movable contact and two static contacts). The closing process was that when the coil was energized, the armature was moved by electromagnetic force, and the pusher arm pushed moveable spring moving until N.O. contact closed. The opening process was that when the electromagnetic system was power off, movable contact returned by mechanical spring force until N.C. contact closed.

The basic principle of constant stress accelerated degradation test is to separate the same batch of test items to different group, make acceleration test under a constant stress standard, there is a relationship between the product function degeneration and stress, function degeneration would be obviously increased under higher stress, then figure out the life of the products under normal stress from the performance degradation trace of accelerated degradation test.

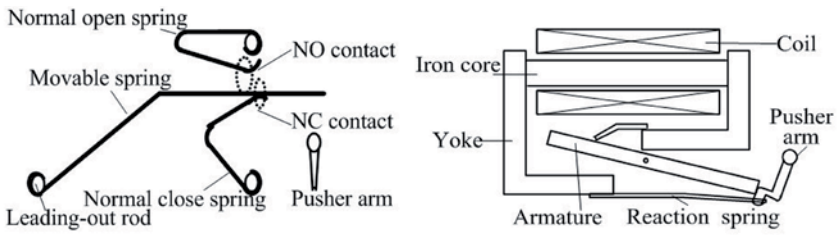

a) Contact system *b) Electromagnetic system*

Fig. 1. Schematic structure of aerospace electromagnetic relay

Aerospace relays are electromechanical elements that the structure is very complex. It will be influenced by many factors .In the period of storage, its failure mechanism is complex. It is better to put multiple stresses than to put single environmental stress, multiple stresses may reflect the real environment, show more limitation of the product. But we must realize that to put multiple stresses will make the experiment more difficult, even bring more interference. These limitations maybe lead to some unexpected results: the data get from experiment may not be dealt. Reference [6] pointed out that the temperature factor is the main influencing factor causing relay failure. Temperature will accelerate physical and chemical process of relay, thus accelerated failure time. So this paper selects the temperature as main accelerated stress, and studies the storage reliability of aerospace relay using the method of constant stress accelerated storage degradation test. The characteristics of storage test are time-consuming, slow degradation. 40 relays were divided into four groups on average and put them in 4 temperature test chambers. The performance degradation parameters are tested and analyzed regularly.

The performance degradation parameters should be able to reflect the aerospace relay storage life, the changes of reliability and have clear physical meanings; in addition they should be measured easily. The performance degradation parameters should have obvious degradation trend, as the accelerated storage life test went on. In order to gain the contact reliability information and contact states as much as possible in contacts storage test, aside from contact resistance this paper also test and analysis time parameters: pick-up time, opening time, overtravel time, and rebound duration time.

Considering the accelerated ability of performance and reliability pre-research test, we determine the lowest stress and highest stress were 80℃ and 170℃. In order to make the middle stresses scattered as far as possible, and the middle stresses were chosen as follows:

$$\Delta = \frac{1}{T_1} - \frac{1}{T_2} = \cdots = \frac{1}{T_{k-1}} - \frac{1}{T_k} = (\frac{1}{T_1} - \frac{1}{T_k}) \Big/ (k-1) \qquad (1)$$

When $k = 4$, therefore, one can get the middle stress are 106℃ and 135℃. The test conditions are as tabled 1.

Table 1. Test conditions of relay accelerated storage degradation test

Temperature stress	80℃, 106℃, 135℃, 170℃
Number of samples	10 relays / temperature
Test frequency	2 days
Current	10mA
parameters test condition	Samples were cooled to room temperature in 2 hours until testing.

The physical map and major structures of the relay ASDT test system are shown in figure 2.This system can monitor relay contact resistances and time parameters of 40 aerospace relays by turns under different temperatures and transmit the test data to the host computer for processing.

3. Results and discussion of aerospace relay accelerated storage degradation testing

3.1. Analysis of storage test results of relay contact resistance

The contact resistance is an important indicator to measure the relay performance. The variations of the average contact resistance of total 40 relays under 4 temperature-accelerated stresses are shown in figure 3, during near 1 year accelerated storage testing process.

a) Physical map of relay testing system

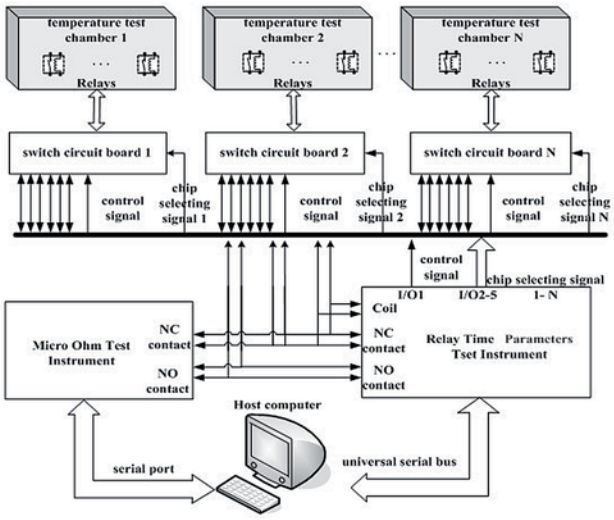

b) Major structures of relay testing system

Fig. 2. Physical map and major structures of relay ASDT test system

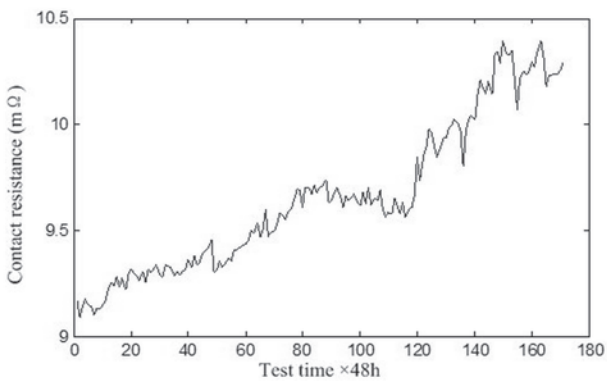

a) 80°C storage test condition

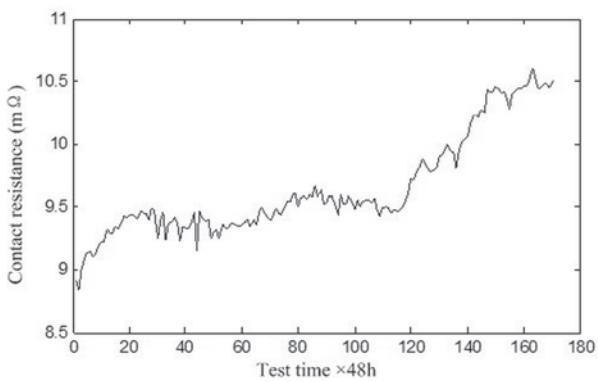

b) 106°C storage test condition

Fig. 3. Scatter plots of average contact resistances for different temperatures

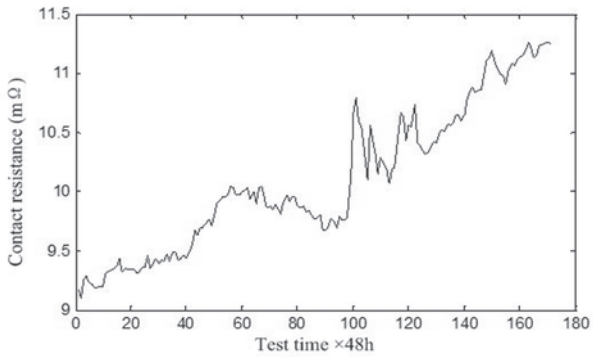

c) 135℃ storage test condition

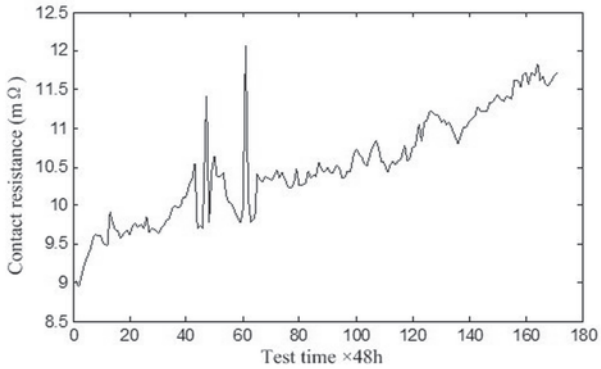

d) 170℃ storage test condition

Fig.3. Scatter plots of average contact resistances for different temperatures

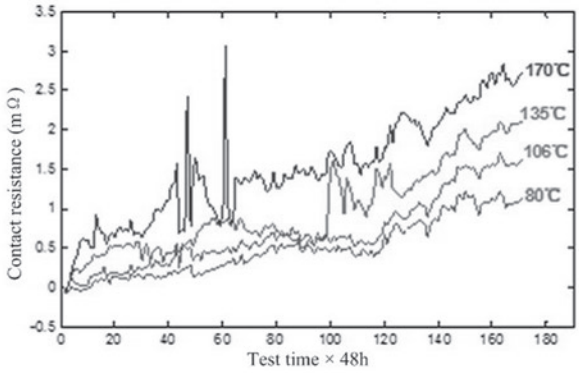

Fig. 4. Scatter plots of average degradation contact resistances with different temperatures

The degradation measures of relay contact resistance under 4 temperature-accelerated stresses in accelerated storage degradation testing are shown in figure 4.

From Figure 3 and Figure 4, it is not difficult to find that in the period the contact resistance is mostly concentrated in 9 mΩ~12 mΩ. Contact resistance is increasing at each temperature. The temperature promotes the degradation of contact resistance. When the temperature-accelerated stress is higher, the rate of contact resistance growth is faster, and the value is also greater.

The variation of contact resistance reflects the cumulative degradation of the contact during relay's accelerated storage period to some extent. The surface of contact will appear the surface oxide film growth and accumulation as the storage time prolongs, the corrosion growth directly reflects the degradation of the relay contact. The contact material of test aerospace relay is Ag-based coated with a thin layer of gold. The gold plating is very thin which is about 1.8μm.

3.2. Analysis of storage test results of relay time parameters

The relay time parameters are described in figure 5 and specific defined as follows:

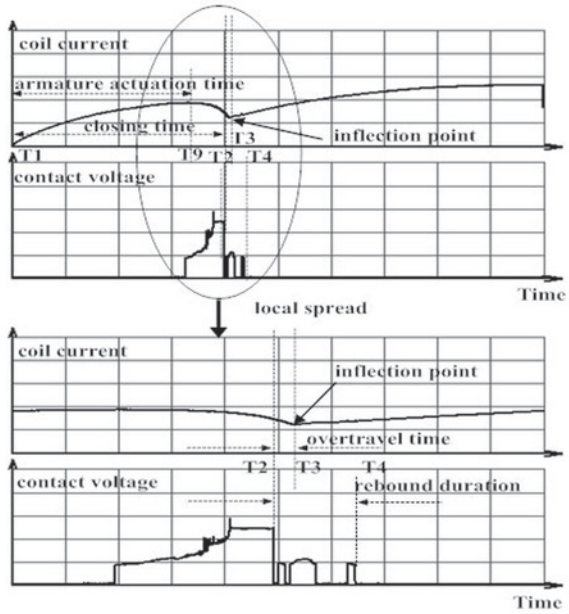

T1 *- Coil energization,* ***T2*** *- Movable contact and N.O. contact first contact,* ***T3*** *- Armature closed* ***T4*** *- Contact rebound finished,* ***T9*** *- Armature actuation*
a) Closing process

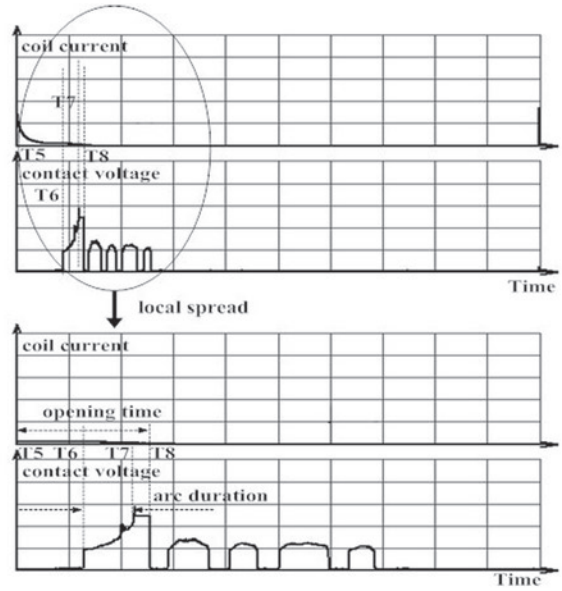

T5 *- Coil power off,* ***T6*** *- Movable contact and N.O. contact part from each other,* ***T7*** *- Movable contact and N.O. contact completely separated,* ***T8*** *- Movable contact and N.C. contact first contact*
b) Opening process

Fig. 5. Oscillograms of coil current and contact voltage during the closing and opening process

- Pick-up time: the time from the power-on of electromagnetic system to the first contact of movable contact and N.O. contact. (T2-T1)
- Opening time: the time from the power-off of electromagnetic system to the first contact of movable contacts and N.C. contact. (T8-T5)
- Overtravel time: the time from the first contact of movable contacts and N.O. contact to full pick-up of the armature. (T3-T2)

- Rebound duration time: the time from the first contact of movable contacts and N.C. contact to the end of rebound during the pick-up period. (T4-T2)

3.2.1. Test results of pick-up time

Pick-up time is the time from the power-on of electromagnetic system to the first contact of movable contact and N.O. contact. With above test system, the relay pick-up time data were obtained by storage accelerated test on 40 relays over 180 days under 4 temperature-accelerated stresses, and the average value of relay pick-up time is shown in figure 6. The degradation measures of pick-up time at 4 temperature-accelerated stresses in accelerated storage degradation testing are shown in figure 7.

It is shown that the pick-up time is on a declining trend under high temperature long term storage. The curve has two steps decrease obviously. The first step declines faster and the second step declines slowly. The most decrease of pick-up time appears on the first step.

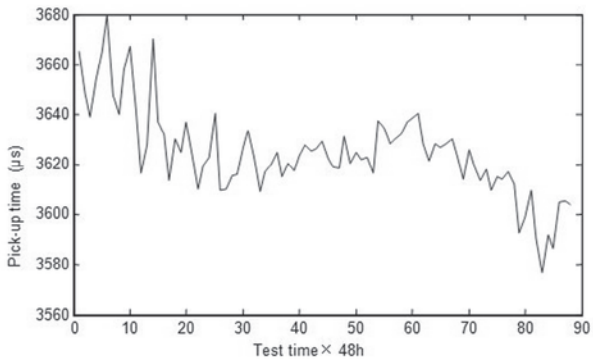

a) 80℃ storage test condition

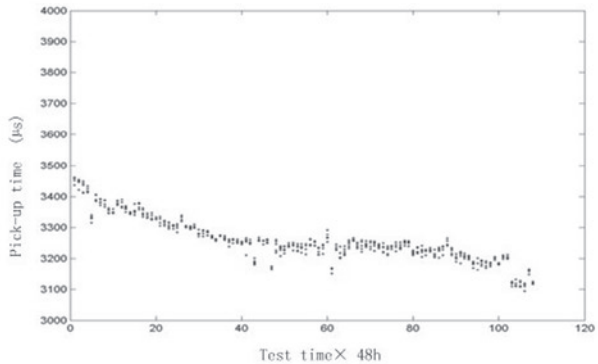

b) 106℃ storage test condition

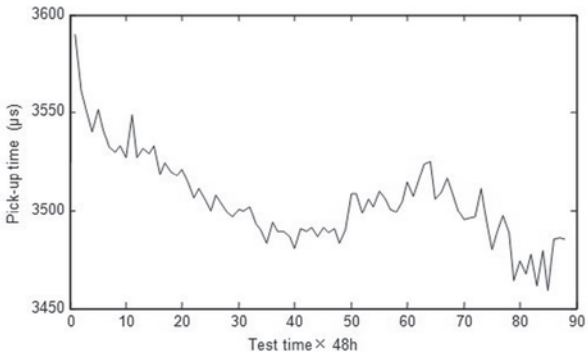

c) 135℃ storage test condition

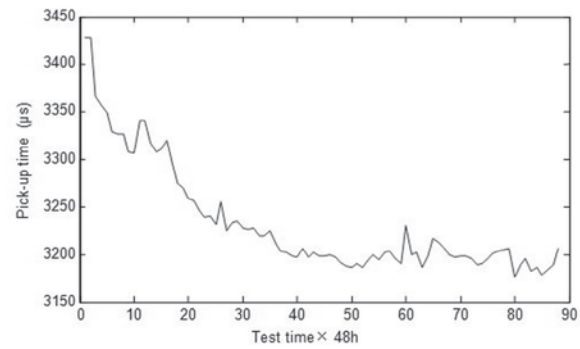

d) 170℃ storage test condition

Fig. 6. Scatter plots of relay pick-up time with different temperatures

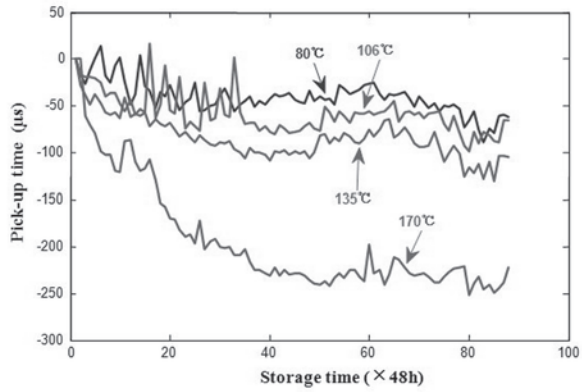

Fig. 7. Scatter plots of average degradation pick-up time with different temperatures

Pick-up time generally including armature actuation time, break time, free travel time, and all of the change of these components will have impact on it.

In figure 5-a), from the oscillograms of coil current during the closing process, we can see T9 is armature actuation time which occupies much time in pick-up time. The relay armature actuation time is mainly influenced by electromagnetic force, reaction force and contact travel. By measuring the coil resistances before and after the test, we found the value of coli resistance has very small change. So, it indicated that the electromagnetic force is basically unchanged. The corrosion film appears between contacts is very thin and can be neglected, we assume contact travel constant. Hence, pick-up time is merely about reaction force. The stress of reaction spring's bending angle may release and thus cause reaction spring pre-pressure decreases during accelerated storage test. This makes armature actuation time decrease, so it has mainly impact on the pick-up time. Of course, there may be some exceptions. Such as N.C. contact may appear cold viscosity during the test, which will lead to the longer armature actuation time.

3.2.2. Test results of opening time

Opening time is the time from the power-off of electromagnetic system to the first contact of movable contacts and N.C. contact. During the release process, only the reaction force spring acts on the armature. Opening time includes initial release time, N.O. contact break time and free travel time.

The opening time is generally related to the contact gap, the contact surface structure and the spring rate. Figure 8 shows the box-and-whisker plots of opening time with different temperatures.

The fluctuation range of opening time curve was higher, and the degradation trend was not obvious. There are a number of outliers in opening time data. After wiping off the abnormity data, there is a little fluctuation in the median of a data set, which means that the opening time would either be not a storage degradation sensitive parameter over time.

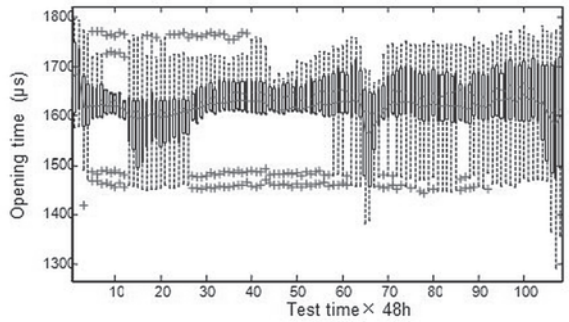

a) 80℃ storage test condition

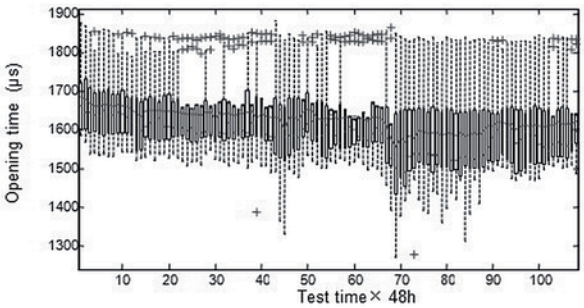

b) 106℃ storage test condition

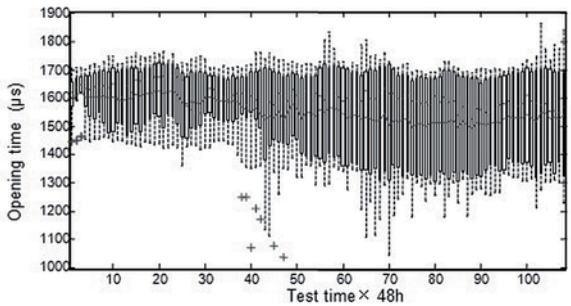

c) 135℃ storage test condition

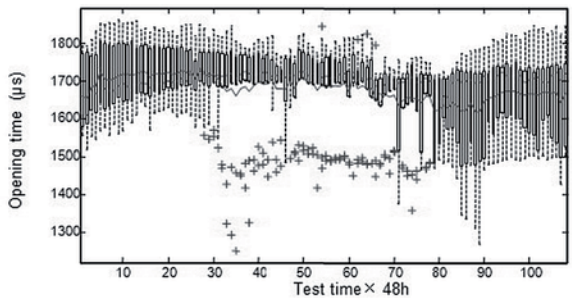

d) 170℃ storage test condition

Fig. 8. Box-and-whisker plots of opening time with different temperatures

3.2.3. Test results of overtravel time

The relay overtravel time data were obtained by storage accelerated test on 40 relays over 180 days under 4 temperature-accelerated stresses, and the Box-and-whisker plots of relay overtravel time is shown in figure 9.

The fluctuation range of overtravel time curve was higher, and the degradation trend was not obvious. There are a number of outliers in overtravel time data. After wiping off the abnormity data, there is a little fluctuation in the median of a data set, which means that the

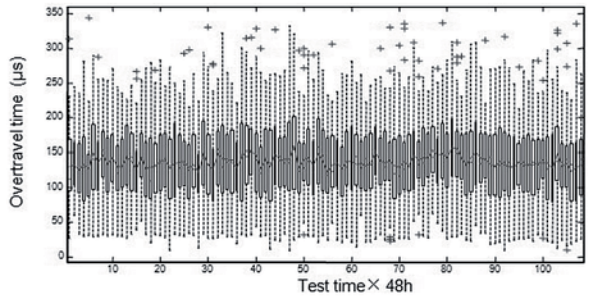

a) 80℃ storage test condition

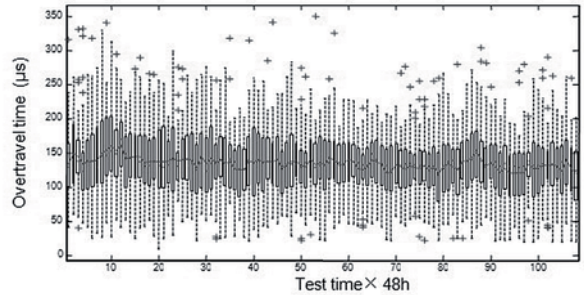

b) 106℃ storage test condition

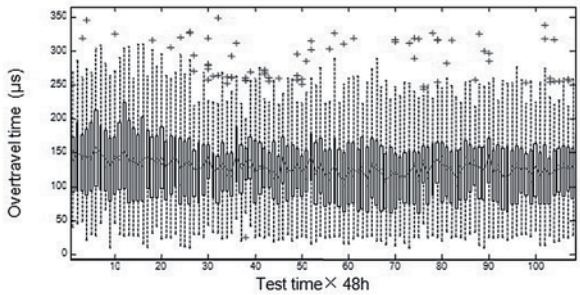

c) 135℃ storage test condition

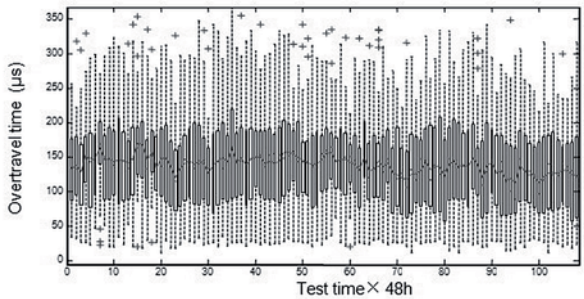

d) 170℃ storage test condition

Fig. 9. Box-and-whisker plots of overtravel time with different temperatures

overtravel time would either be not a storage degradation sensitive parameter over time.

3.2.4. Test results of rebound duration time

The relay rebound duration time data were obtained by storage accelerated test on 40 relays over 180 days under 4 temperature-accelerated stresses, and the scatter diagram of relay rebound duration time is shown in figure 10.

The fluctuation range of rebound duration time curve was higher, and the degradation trend was not obvious. There are a number of outliers in overtravel time data. There is great randomicity and uncertainty of the trend in the overtravel time test data, which means that

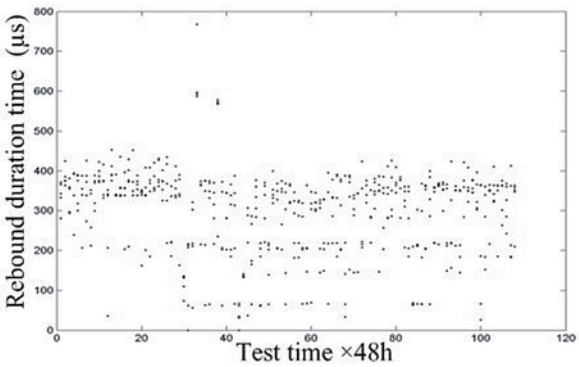

a) 80℃ storage test condition

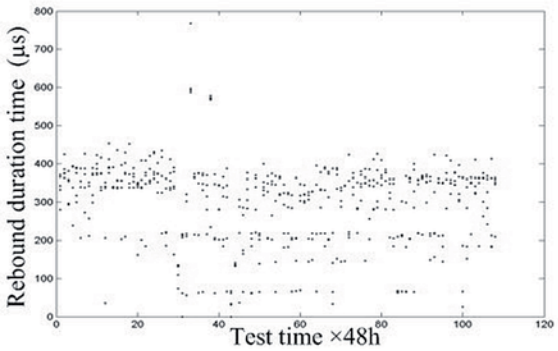

b) 106℃ storage test condition

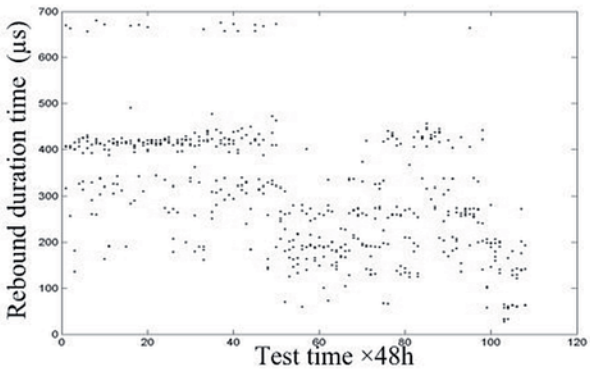

c) 135℃ storage test condition

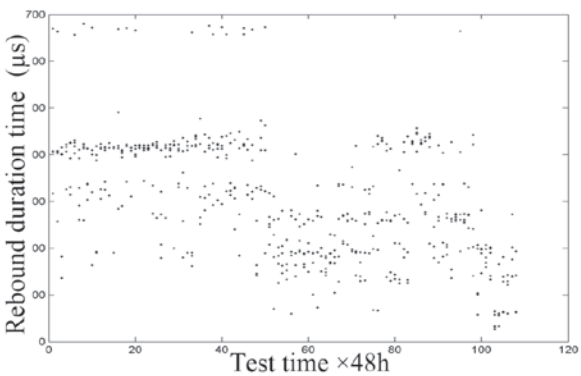

d) 170℃ storage test condition

Fig. 10. Scatter plots of average rebound duration time

the overtravel time would either be not a storage degradation sensitive parameter over time.

3.3. Determination of storage degradation sensitive parameters

From the standpoint of testing operability and product evaluation, to determine the degradation sensitive parameters should note the following points. Firstly, performance degradation must be irreversible. Secondly, performance degradation could be accelerated.

From the analysis of storage test results, when the temperature-accelerated stress is higher, the rate of contact resistance growth is faster, and the value is also greater. When the temperature-accelerated stress is higher, the trend of pick-up time values descend is obvious, and the value is also smaller. The relay contact resistance and pick-up time satisfy two characteristics described in determination degradation sensitive parameters. But, the relay opening time, overtravel time and rebound duration time do not meet the conditions of sensitive parameter's definition.

Finally, the sensitivity parameters such as relay contact resistance as well as pick-up time were determined in accelerated storage degradation testing.

4. Storage failure mechanism analysis of aerospace EMR

4.1. Contact conductive properties of relay

The touching component of aerospace EMR usually consists of silver alloy or copper alloy with a layer of gold of a few microns. The metal surface may be very smooth with the naked eye. However, at the perspective of microscopic , actually is mat and jagged[2].When two metal surface have touch with each other, the really contact only occurs in a few salient points and a part of conducting spots can have the ability of conducting electricity.

In other words, the electrical contact with two solids forms in the some areas among touching surface, the only path of conducting current, as shown in figure 11.When current flows past touching surface and pass through those conducting spots, the current lines begin to constriction resulting resistance values increase correspondingly, which is called constriction resistance[1],expressed as R_s . Because conducting surface among touching surface may be not clear totally, the influences from oxide film, water film, sulfide film, dust or other inorganic membranes change potential distribution of current path and have a influence of distribution of electronics, resulting in the increasing of the other extra resistance, called membrane resistance, the other component constituting contact resistance, expressed as R_f .According to Holm electrical contacting theory, total contact resistance equal to the series resistance of constriction resistance, film resistance and some parts of volume resistances [2]:

$$R = R_s + R_f + R_v == \frac{\rho}{2na} + \frac{\sigma}{\pi na^2} + R_v \tag{2}$$

Formulas ρ – The contacts average resistivity;
σ – Film tunnel resistivity;
n – The number of the contact spots;
a – The radius of the conductive spots;
R_v – Volume resistance.

So, the physical meaning of contact resistance is the sum of an increase in resistance of the metal (constriction resistance) caused by shrinkage effect created by current among conducting spot between contacts, the surface film resistance and body resistance. However, the combined effects for the radius of conducting spot and resistivity, created by the chemical stability of the contact material, the roughness of the contact spot in contact surface, contact pressure and environmental factors outside (temperature, humidity, atmosphere, etc.),lead

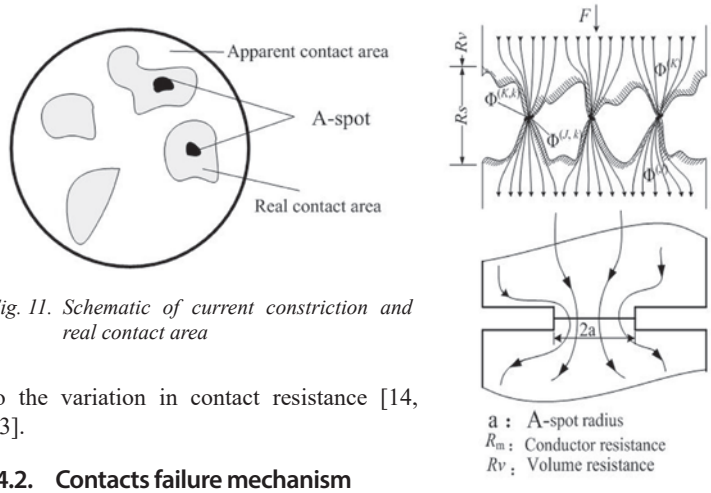

Fig. 11. Schematic of current constriction and real contact area

to the variation in contact resistance [14, 13].

4.2. Contacts failure mechanism analysis of aerospace EMR

Among the structure of aerospace EMR, the contact system is the core part of the relay in the long-term storage. In order to have good conductivity, it is necessary to ensure a stable contact between contacts and contact interfaces; otherwise it may cause the relay contact failure.

According to statistical analysis of historical data based on natural storage of relay manufacturer, during long storage failure, the contacts failure accounted for 62.8% of the total failure .It is the main failure mode, the main form of which is the barrier between contacts and the variation in contact resistance.

Storage reliability of aerospace EMR has a close relation with change of the contact resistance among the relay contacts. Under storage conditions the growth rate of the contact resistance among contacts has a close relation with the growth rate of the corrosion products among contacts. Reference [18] studied the surface film of sealed relay contacts, pointed that contact surfaces of aerospace relay have Ag, Au, O, S, Cl and other elements and analyzed that rosin flux, vacuum plastic, etc. have a great influence on the growth of surface film in contacts.

In this study, the material of contacts in aerospace EMR is gold-plated silver-based alloy and gold plating layer is generally thin (1.8-3.2μm). During the gold-plated contacts process, because the process and other reasons, it will inevitably appear some mechanical scratches, abrasions, micro-cracks, holes or other impurities in the coating, as shown in figure 13.

During the long storage of aerospace electromagnetic relay, the sealing will continue to decline over time, so that atmospheric oxygen and corrosive gases will continue to enter the interior of the housing of the relay, and through the capillary action of cracks and pores [21], penetrate and come into contact with the base metal silver of contacts and deposited to form an electrolyte. The potential difference between the metallic silver and gold so that it forms original battery at the interface of the base metal silver and the coating metal, resulting electronic flows, which occurred a redox reaction, as shown in the following formula:

$$Ag \rightarrow Ag^{+} + e^{-} \tag{3}$$

Because the oxide growth rate of silver is dependent on its lattice disturbed state, and chemical activity of Ag^{+} is strong, its diffusion rate in the solid oxide is much faster than the diffusion rate of oxygen, so its diffusion to the oxide-gas surface is much easier, in other words, the diffusion rate of Ag^{+} from interface of $Au\text{-}Ag$ to the surface of coating much faster than H_2O and. O_2 ,when the atmosphere contains trace corrosive gases, such as SO_2 or H_2S ,then the reduction reaction of the electrochemical reaction takes place on the surface of the gold layer, that is also called the contact surface, and form a high resistivity layer of dark black corrosion film on the contact surface. The chemical reaction is as follows:

$$4Ag^{+} + O_2 + 2H_2S \rightarrow 2Ag_2S + 2H_2O \tag{4}$$

The main component of the formative layer is sulfide and oxide of silver. Both sulfide atmosphere and friction of contact action will promote the formation of sulfides and oxides. Ag_2S has high resistivity, which is about ten thousand times of Cu , the resistivity at room temperature is between 10^7–$10^{18}\Omega\cdot$mm, so the impact on contact resistance is great. The hardness of silver sulfide the oxide is much lower than metal silver, the shear strength is small, therefore it can be easily broken, corrosion film loose. Since redox reaction on the contact surface continues, reactants piled up, such that corrosion film will continue thickening, resulting in increased contact resistance between the contacts, finally resulting in contact failure. Fig. 12 is a comparative morphology of EMR make static contacts for a long-term before and after corrosion.

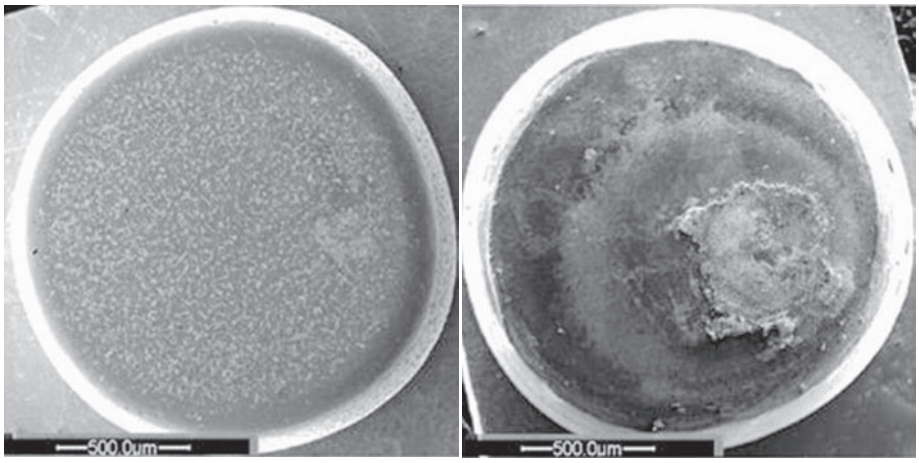

a) Initial state of N.C. contact *b) N.C.contact morphology after corrosion*

Fig. 12. N.C.static contact morphology of electromagnetic

According to the theory of Holm electrical contacts, due to the tunnel effect, increased in the film thickness of the oxides and sulfides can result in increased resistivity of the tunnel, leading to increase in contact resistance, which destroys the electrical contact properties of the gold layer, causing performance of relay contacts declining, such changes caused by environmental factors of contact materials is irreversible, and it is irrecoverable process. When the film thickness is less than 3nm, the increasing thickness L and the tunnel film resistivity σ are substantially linear.

$$\sigma = \eta L \tag{5}$$

Formulas η –scale factor.

Because the membrane resistance can be expressed as $R_f = \sigma / \mathrm{A}$, incremental of contact resistance with time can be expressed as the following formula:

$$R_t = \eta(L - L_0) / \mathrm{A} \tag{6}$$

Formulas L_0 – the original film thickness;
A – Actual contact area of the conductive spots.

It is obviously, in long-term storage environment, aerospace EMR contacts degradation in performance is mainly due to the accumulation of oxides and sulfides generated on the surface, therefore, the growth rate of corrosion products on contact surfaces can be used to evaluate the indirect contact performance of degradation processes.

4.3. Analysis of contact morphology and chemical constitution

In order to further reveal the degradation of long storage of the relay and analyze its storage degradation mechanism, we can use Scanning Electron Microscope (SEM) and Energy Dispersive X-Ray Spectrometer (EDX) to observe the EMR contacts of storage test, observe the changes of surface morphology and chemical changes of the contact surface.

4.3.1. SEM test of relay contacts

Figure 13 shows the static contacts and changeover contact of new aerospace EMR samples with 50 × SEM morphology photograph .

From the figure 12, we can see although it is a new aerospace electromagnetic relay samples, but the contact surface is not completely smooth, there are varying degrees of micro mechanical wear or scratches. These wear scratches are mainly due to the relay assembly process. In the debugging process of structural parameters, many steps require manual debugging, and some mechanical friction is inevitable. The contact area of the wear scratches will damage the contact surface of the gold coating, make the oxygen and other corrosive gases are subjected to oxidation reduction with contact base metal silver by micro capillary action, so that affecting the performance of contacts. During the long storage the relay contact oxidation corrosion more serious parts also occurred in the parts of the mechanical wear.

Figure 14 is the SEM surface morphology of the static contacts in different temperatures in a storage test which lasts nearly a year. From this analysis of SEM morphology of figure 14, it is not difficult to find that as the temperature rises, the relay surface oxidized corrosion severity also increases, and most of them occurs in the wear at the contact surfaces. Moreover, these relay surface oxidized corrosion always centers on the fray and from inside out, these oxidized corrosion is continuously covered annularly. From the phenomena above, we can see that the temperature has the effect to accelerate and boost the oxidized corrosion of the contacts during the process of the relay storage.

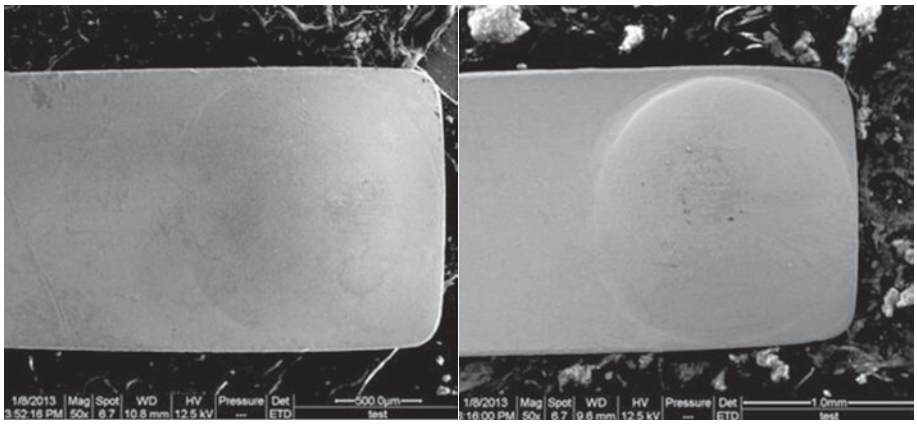

a) 80℃ storage test condition *b) 106℃ storage test condition*

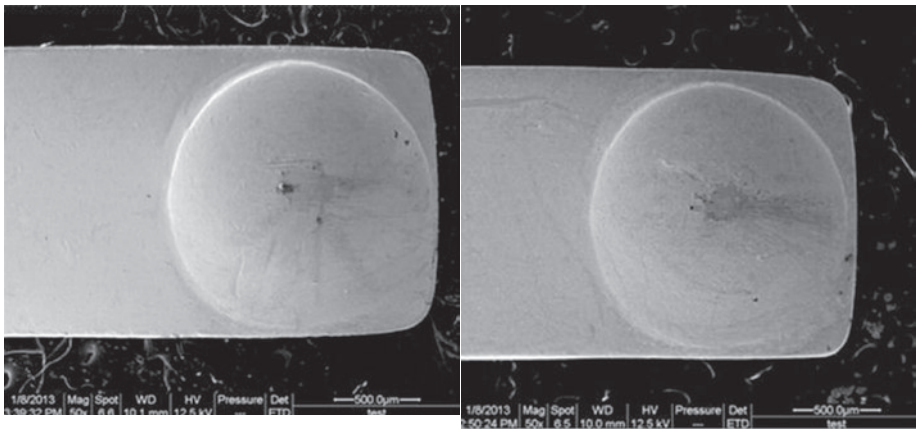

c) 135℃ storage test condition *d) 170℃ storage test condition*

Fig. 14. The N.C.static contact SEM morphologys with different temperatures after 1 year

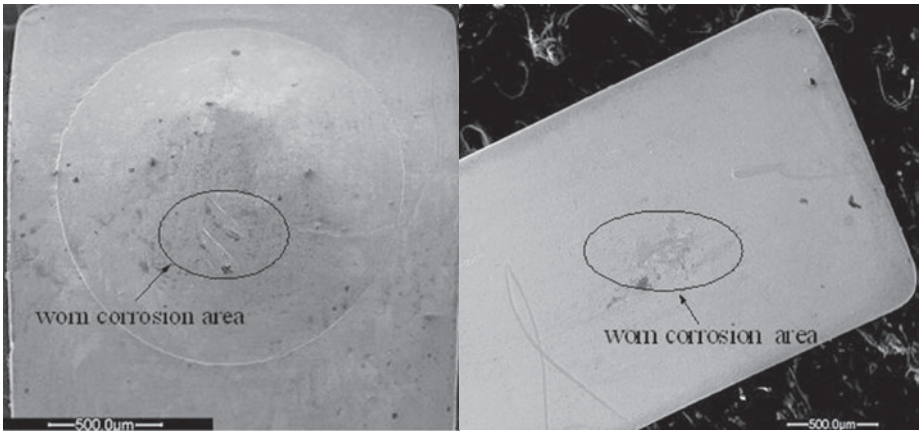

a) N.C.static contact *b) Movable contact*

Fig. 13. The N.C.static contact SEM morphology of new relay sample

The temperature plays the role of promoting and accelerating contacts to degenerate during storage of aerospace relay. In order to further analyze the impact of storage time to the relay contacts degradation, the SEM morphology for each contact of specimen relay at four different temperature stress and different time were analysed. Here we use the storage test at 170℃ temperature stress as example. Its degradation is more evident. Figure 15 a)-d) are relay sample static contact surface SEM morphology photos in the temperature stress

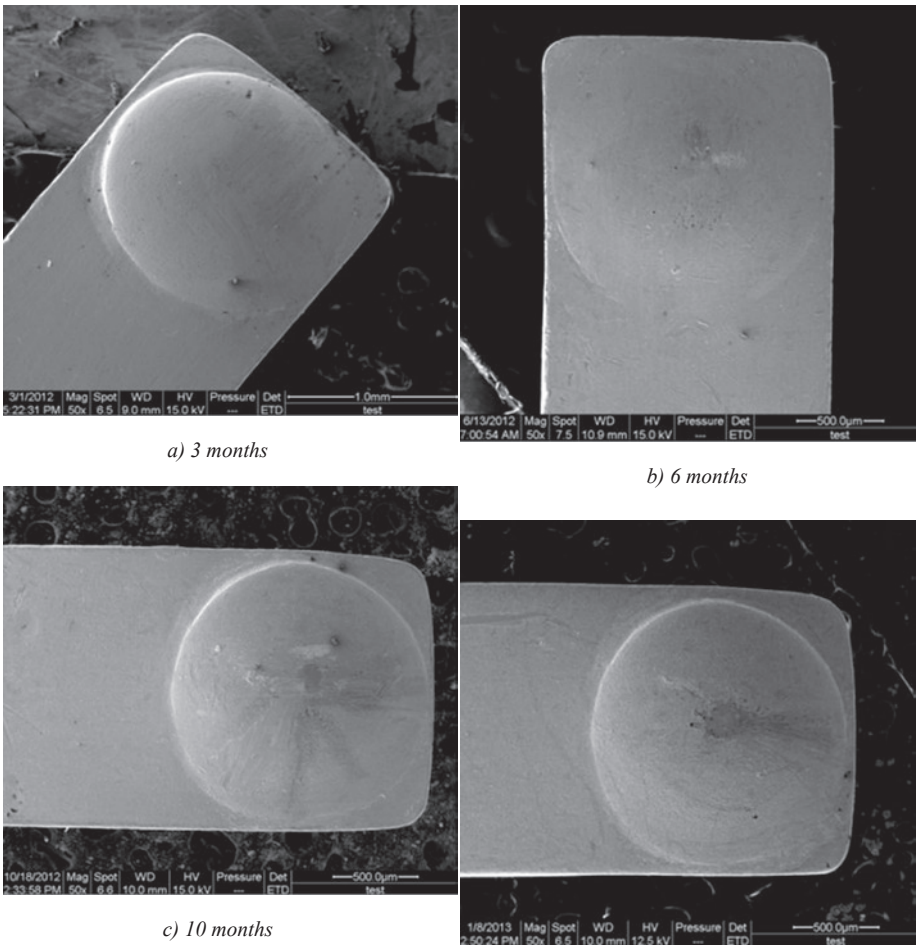

a) 3 months

b) 6 months

c) 10 months

d) 12 months

Fig. 15. The N.C.static contact SEM morphologys in 170℃ with different time

for 3 months, 6 months, 10 months and 12 months. What we can see from the figure is that as the test time increases, the oxidized corrosion of contact is becoming more and more severely.

4.3.2. EDX analysis of relay contacts

The line scan and area scan analysis of EDX for contact samples were test. EDX is an important ancillary instrument for scanning electron microscopy. Combined with SEM, EXD can do the microscopic qualitative and quantitative measurement and analysis for chemical elements of microscopic contact area and its distribution.

Figure 16 is the result of new specimen static contact surface scanned by EDX. We can see that the surface has only one peak of gold (Au) elements. Further we can quantitatively calculate that the mass and atomic number percentage of gold elements is almost 100%. This is mainly because aerospace relay contact surfaces are required to be gold-plated, whose thickness is generally 1.8-3.2μm, and the new test environment is not affected by the oxygen corrosion of environment stress oxygen and other corrosive elements. Therefore, there are no other pollution elements basically.

The 2000× magnified SEM image of N.C. static contact surface after 12 months of storage test in 170℃ is shown in Fig.17.

Through EDX scanning, gold (Au) elements, silver (Ag) elements, oxygen (O) elemental sulfur (S) and other elements can be found in its contact surface. It can be inferred that as the storage time extends, sealing of relay decreased; atmospheric corrosive gases, moisture and micro-cracks through the coating. Infiltrate and contact with the microscopic silver substrate by capillary action, deposited into electrolyte. Potential difference exists between silver and gold, so that the primary battery is formed between the coating metal gold and silver substrate interface, which would cause an oxidation-reduction reaction. Because of strong chemical activity, diffusion velocity of Ag^+ in solid oxide is much greater than that of oxygen, so Ag^+ is easily diffused into the contact surface between oxide and gas , which is mean that diffusion rate of Ag in Au-Ag interface is faster than that of O_2 .Besides when the air contains sulfur contaminants electrochemical reduction reaction occurs at the surface of the gold layer,

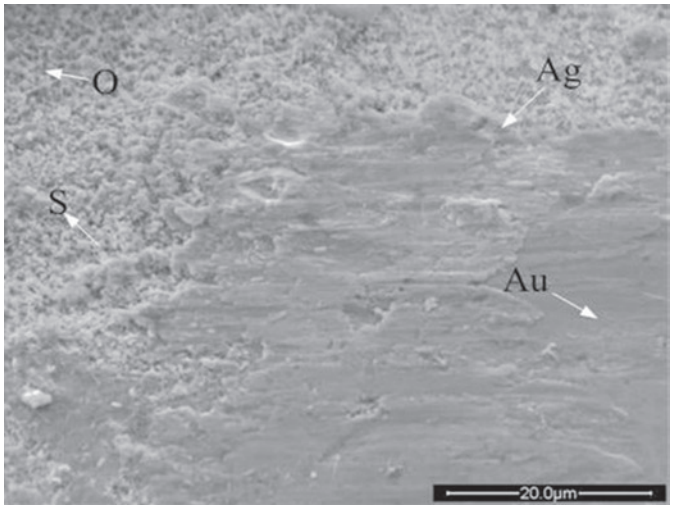

Fig. 17. 2000× magnified SEM image of contact surface after test different time

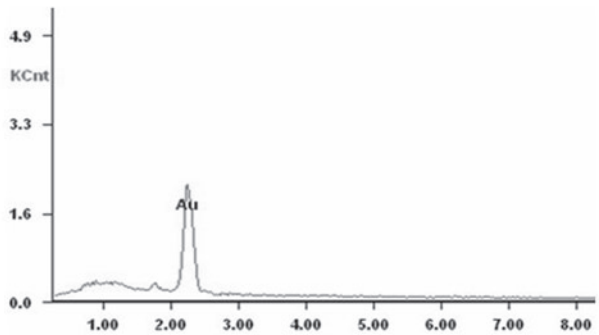

a)Energy dispersive x-ray spectrum

Element	Wt%	At%
AuM	100.00	100.00

b)Chemical composition percentage

Fig. 16. EDX and chemical composition percentage of new-sample N.C. static contact

namely the contact surface and form dark black film of silver sulfide and oxide which has high resistivity.

To further observe contact of base metal, metal plating and film thickness of corrosion etc, we could analyze section of contact by SEM and EDX .As is shown in figure 18, it

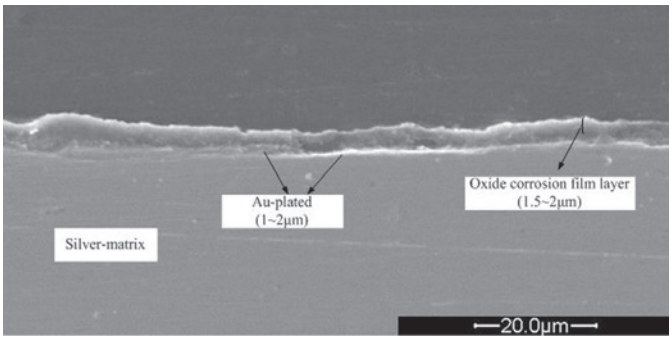

Fig. 18. SEM image of the cross section for the relay N.C. static contact

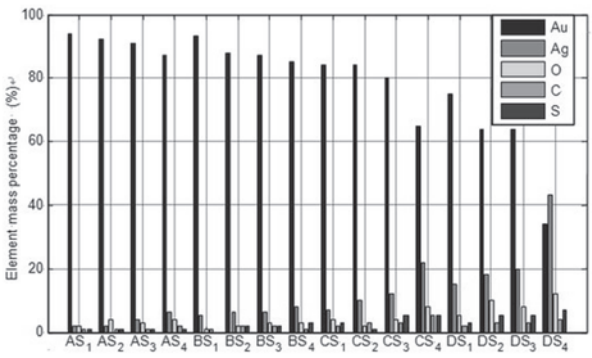

Fig. 19. The weight percentage of N.C. static contact elements of relay samples in storage test

is not difficult to see that after long storage, the surface of aerospace relay contact forms a high resistivity sulfide and oxide film, resulting in increasing of contact resistance, contact performance decline even eventually contact failure.

Figure 19 is the weight percentage of N.C. static contact elements of relay samples in storage test under different test time and stress with different temperatures.

In figure19, A represents the sample under 80℃; B represents the sample under 106℃; C represents the sample under 135℃; D represents the sample under 170℃ in the diagram. S_1 represents 3 months storage time; S_2 represents 6 months storage time; S_3 represents 10 months storage time; S_4 represents 12 months storage time. The figure shows that with the extension of storage time, the surface of the contact emerges base metal silver (Ag) elements, and the proportion continues to grow. Furthermore, oxygen (O) element, carbon (C) element, sulfur (S) element and other elements appears; besides with the increase of test time and temperature stress the proportion of such element has increased differently.

It can be determined from analysis of SEM and EDX test that with the increasing extension of storage time and temperature stress, the contact surface forms a corrosion layer consisting with less conductive oxides, sulfides, and carbides, affecting gradually the contacts contact performance, and may eventually lead to contact failure of the relay contact. Above test results provides a basis and reference of improving storage reliability for relay manufacturers on the micro-level. The storage reliability can be improved by increasing the level of the relay tightness and improving contact spring manual assembly process, reducing personal contact mechanical friction .The analysis of SEM and EDX test provides a microscopic basis for the physics of failure modelling in aerospace EMR storage.

Conclusion

This investigation mainly aims to determine the degradation characteristics and failure mechanisms of aerospace electromagnetic relay in accelerated storage degradation testing. Our results indicate that when the temperature-accelerated stress is higher, the rate of contact resistance growth is faster, and the value is also greater. The trend of pick-up time values descend is obvious, and the value is also smaller. The relay contact resistance and pick-up time satisfy two characteristics described in determination degradation sensitive parameters.

The contact failure mechanism of aerospace EMR in long-term storage is investigated. From analysis of SEM and EDX test, the contact surface forms a corrosion layer consisting with less conductive oxides, sulfides, and carbides, affecting gradually the contacts contact performance, and may eventually lead to contact failure of the relay contact with the increasing extension of storage time and temperature stress. Above test results provides a basis and reference for latter aerospace EMR storage life and storage reliability improving.

Acknowledgement

The authors are grateful to the anonymous reviewers, and the editor, for their critical and constructive review of the manuscript. This study was co-supported by the National Natural Science Foundation of China (Grant No. 51507074), China Postdoctoral Science Foundation (Grant No. 2015M571898), the Natural Science Foundation of Higher Education Institutions of Jiangsu Province (Grant No. 15KJB470003), and the Open Foundation of Zhejiang Provincial Top Key Academic Discipline of Mechanical Engineering and Zhejiang Sci-Tech University Key Laboratory (Grant No. ZSTUME01A02).

References

1. Guo F Y, Chen Z H. Electrical Contacts Theory Applications and Technology, China Electric Power Press, Beijing, 2008.
2. Holm, R. Electrical Contacts . Springer-Verlag Berlin Heidelberg GmbH 1981
3. Książkiewicz A, Janiszewski J. Low voltage relay contact resistance change influence by short-circuit current. Eksploatacja i Niezawodnosc – Maintenance and Reliability 2015; 17 (4): 600–603, http://dx.doi.org/10.17531/ein.2015.4.16.
4. Li K, Lu J G, Zhang G S. The approach to predication of contact reliability for relay. Transactions of China Electrotechnical Society 1999; 14(2): 55-59.
5. Li L , Xu W. Optimum scheme design and analysis of accelerated life test for sealed electromag-netic relay. Low Voltage Apparatus 2010; (4): 13-16.
6. Lu J G, Jin F Q. Reliability design on electromagnetic system of relay. Proceedings of 36th Relay Conference 1988:1-4.
7. Luo Y Y, Lu J G. Li W H, Wang L Z. Study on the accelerated life test of storage life for sealed electromagnetic relays. Acta Armamentarii 2007; 28(8): 997-1001.

8. Ma X B, Wang J Z, Zhao Y. Reliability assessment using constant-stress accelerated degradation data based on pseudo life distribution. Journal of Systems Engineering and Electronics 2011; 33(1): 228-0232.
9. Mcpherson J W. Reliability Physics and Engineering, New York: Springer, 2010, https://doi.org/10.1007/978-1-4419-6348-2.
10. Meeker W Q, Hamada M. Statistical tools for the rapid development and evaluation of high-reliability products. IEEE Transactions on Reliability 1995; 44: 187-198, https://doi.org/10.1109/24.387370.
11. Meeker W Q, Escobar L A, Lu C J. Accelerated degradation tests: Modeling and analysis. Technometrics 1998; 40(2): 89-99.5.
12. Nelson W. Accelerated Testing: Statistical Methods, Test Plans, and data Analysis. New York: John Wiley Press, 1990, https://doi.org/10.1002/9780470316795.
13. Ren W B , Chen Y , Wang Z B, Zhang C and Zhai G F. Investigation of the μN level adhesion force characteristics of gold-coated materials in air. The Journal of Adhesion 2016: 1-16, https://doi.org/10.1080/00218464.2016.1197125.
14. Ren W B, Chen Y, Wang Z B, Xue S J and Zhang X. Electrical contact resistance of coated spherical contacts. IEEE Transactions on Electron Devices 2016; 63(11): 4373-4379, https://doi.org/10.1109/TED.2016.2612545.
15. V N Nair. Discussion of estimation of reliability in field-performance studie. Technometrics 1988; 30(4): 379-383, https://doi.org/10.2307/1269798.
16. Wan B, Fu G C, Li N, Zhao Y H, Wang L. Storage life prediction of electromagnetic relay based on pof analysis. Annual Reliability and Maintainability Symposium 2013: 875-880, https://doi.org/10.1109/RAMS.2013.6517671.
17. Wang Y, Zhang C, Chen X, Tan Y. Lifetime prediction method for electron multiplier based on accelerated degradation test. Eksploatacja i Niezawodnosc - Maintenance and Reliability 2014, 16 (3): 484-490.
18. Zang C Y, He J J, Li J, et al. Contact resistance and surface film of sealed relay contacts . Proceedings of the CSEE 2008; 28(31): 125-130.
19. Zhai G F, Liang H M, Wang H, et al. Research on the parameters optimum design of polarized magnetic system based on orthogonal design. Proceedings of the CSEE 2003; 23(10): 157-163.
20. Zhai G F, Wang Q Y, Yang W Y. Permanent-magnet equivalent model of y,calculating relay's static attractive torque characteristics by finite element method, IEEE Transactions on Magnetics 2012; 48(9): 2467-2471, https://doi.org/10.1109/TMAG.2012.2196705.
21. Zhang J. H., Kong X B.The failure mode analysis of low frequency electrical connectors. Electromechanical Components 1989; 9: 36-43.

ZhaoBin WANG
School of Electronics and Information
Jiangsu University of Science and Technology
No.02 Mengxi Street, Jingkou District
Zhenjiang, Jiangsu, 212003, P.R. China.

Post-doctoral research center, School of Mechanical Engineering and Automation
Zhejiang Sci-Tech University
No.928 Second Avenue, Xiasha Higher Education Zone
Hangzhou, Zhejiang, 310018, P.R. China

Shang SHANG
JiaWei WANG
ZhouLin HUANG
Fu SAI
School of Electronics and Information
Jiangsu University of Science and Technology
No.02 Mengxi Street, Jingkou District
Zhenjiang, Jiangsu, 212003, P.R. China.

E-mail: wangzb@just.edu.cn, shangshang@just.edu.cn, majestyW@126.com, 1535717833qq.com, fusai2015@163.com

Article citation info:
PIETRUSIAK D. Evaluation of large-scale load-carrying structures of machines with the application of the dynamic effects factor. Eksploatacja i Niezawodnosc – Maintenance and Reliability 2017; 19 (4): 542–551, http://dx.doi.org/10.17531/ein.2017.4.7.

Damian PIETRUSIAK

EVALUATION OF LARGE-SCALE LOAD-CARRYING STRUCTURES OF MACHINES WITH THE APPLICATION OF THE DYNAMIC EFFECTS FACTOR

OCENA WIELKOGABARYTOWYCH USTROJÓW NOŚNYCH MASZYN Z ZASTOSOWANIEM WSPÓŁCZYNNIKA OBCIĄŻEŃ ZASTĘPCZYCH*

Load-carrying structures of large-scale machines are their key element, mainly due to their size which renders them virtually impossible to replace during operation. Such structures are used for example in the heavy industry, mining, bulk material handling or rock processing. This article presents the most important results of recent research into dynamic loads and design of such structures. Based on these results the article introduces the author's method of evaluating load-carrying structures with the application of the dynamic effects factor and describes the effects of the application of this method.

***Keywords**: load-carrying structures, numerical simulations, experimental testing, design, dynamic loads.*

Ustroje nośne maszyn wielkogabarytowych są ich kluczowym elementem, ze względu na ich rozmiar a tym samym niemalże brak możliwości wymiany w trakcie eksploatacji. Ustroje tego typu stosowane są np. w przemyśle wydobywczym, przeładunkowym czy przetwórstwa skalnego. W artykule zebrano i zaprezentowano wyniki najważniejszych badań ostatnich lat dotyczących obciążeń dynamicznych oraz projektowania tego rodzaju obiektów. Na tej podstawie przedstawiono autorską metodę oceny ustrojów nośnych z zastosowaniem współczynnika obciążeń zastępczych oraz efekty jej stosowania.

***Słowa kluczowe**: ustroje nośne, obliczenia numeryczne, badania eksperymentalne, projektowanie obciążenia dynamiczne.*

1. Introduction

Because of the enormous size of the undertaking, large-scale load-carrying structures of machines, are designed with long-term operation in mind [36]. Therefore they must satisfy both the ultimate strength requirement as well as the fatigue strength requirement. This is particularly important in the case of mechanical structures, which are likely to undergo variable cyclic loading which, in many cases, directly result from the dynamics of structure [32]. This is the basic difference compared to large-scale load-carrying structures in the construction industry which are usually designed to transfer only static loads and thus only need to fulfill the ultimate strength requirement. Dynamic loads accelerate the progressing degradation of the load-carrying structure, which is manifested in an increasing number of fatigue cracks. Fig 1 shows an example of a fracture and its location.

Such faults are difficult to spot and if the fracture is located in a critical area, it can grow uncontrollably and lead to a catastrophic failure. A fracture similar to the one in Fig. 1 caused the catastrophe of the KWK 1400 excavator (Fig. 2).

Fig. 1. Developing fracture crack

Such load-carrying structures are most often found in the mining, rock processing or bulk material handling industry. The situation in this case is even more special because some of the basic technological processes (e.g. excavating, crushing) are very often subject to large dynamic loads [15, 16]. Due to the environment in which such machines most often operate, it is difficult to use solutions that are effective at reducing vibrations but are not susceptible to damage [2, 48]. In addition, the design of load-carrying structure can be prone to excitation [7,17] (e.g. long-span superstructures of surface mining machines).

Such machines are still being designed in accordance with standards from the 1980s, which define the dynamic effects factor, which, in turn, is used in calculations of fatigue life. Both the definition of this factor and its assumed values, in accordance with the standards, do not reflect the actual operating conditions. This is manifested in the occurrence of numerous cracks in superstructures [1, 12, 37] and undercarriage structures[1, 4, 13, 46]. Over the years several studies have been carried out aimed at solving this problem

(*) Tekst artykułu w polskiej wersji językowej dostępny w elektronicznym wydaniu kwartalnika na stronie ***www.ein.org.pl***

Fig. 2. Catastrophic results of fracture crack [37]

[29]. In his work [24], Kowalczyk proposes to control the assumed values by changing the settings of the protection systems in the machine. The change is carried out in real time during operation. This solution requires that a monitoring system be installed on the machine and connected to its control system. It also restricts the use of the said dynamic effects factor on a standard basis only to cases where the calculated range of stress changes is smaller than the range resulting from the applied static load. On the other hand, in another paper [20], Huss shows the use of dynamic load surpluses in relation to overloads. This paper focuses on identifying impacts and introducing a measure of their effects on the load-carrying structure. In their article, Bosnjak et al. [5] address the influence of rigidity of individual assemblies of the load-carrying structure on the dynamic response of the system. Their analysis is carried out on a flat model with four degrees of freedom. In his doctoral thesis [19], Gnjatovic presents his own reduced, three-dimensional dynamic model. He uses it to measure the response of the system to the loads defined in the DIN standard.

However, the presented approaches require the designer to have comprehensive knowledge and do not correspond to design methods commonly used in the industry. As a result they are either only used occasionally (Kowalczyk [24]) or have never been implemented. Consequently, the machines that have been designed since, are mainly based on outdated literature and standards. Currently, the most commonly used guidelines are international standards:

- German Institute for Standardization (2015) - DIN 22261-2 [18]
- Standards Australia (1995) – AS 4324.1 [47]
- International Organization for Standardization (1994) – ISO 5049.1. [22]

The German standard is the most common point of reference when designing load-carrying structures of large-scale machines. The Polish calculation standard for surface mining machines is a translation of the German standard. This standard was the first to introduce calculations with the application of the dynamic effects factor. The ISO standard, on the other hand, does not provide any specific calculation procedure which would require the use of dynamic loads. It states that the drives and brakes should be designed in such a manner that the acceleration of machine components does not exceed 0,2 m/s^2 (~1/50g). The Australian standard is based largely on the abovementioned DIN and ISO standards. In general, the problems of dynamics are defined exactly as in the DIN standard, i.e. by applying the factor. However, as stated in the AS standard, the values of dynamic effects factors in the DIN standard do not correspond to the values of actual dynamic loads. Therefore, the values of this factor in the AS standard are higher in most cases. What the Australian norm also states is that, as a result, machines designed on the basis of the AS standard will be heavier than those designed on the basis of the DIN standard. Whenever calculations are based on the ISO standard, solutions based on the DIN standard are often used in order to account for the dynamic effects.

To calculate dynamic effects [18] when designing large-scale machines, the German approach defines the dynamic effects factor ψ. Based on the appendix to the standard it can be concluded that the physical interpretation of this factor means the ratio between the measured peak-to-peak acceleration value and the constant value of gravitational acceleration (1):

$$\psi = \frac{\Delta a}{g} \tag{1}$$

$$\Delta a = \max a - \min a$$

where
a – measured value of acceleration
g – value of gravitational acceleration.

This definition raises some doubts due to the high sensitivity to individual events, which may influence the measured value. The application of the ψ factor, defined in this particular manner, would only be justified if the analyzed dynamic process was stationary, which is very difficult to achieve under operational conditions [21, 36].

The values of the factor defined in the DIN standard are presented in Table 1.

It should be pointed out that the information presented above comprehensively covers the issues of dynamics described in the standards. The defined factors are substitute values for the dynamic load and are used in static calculations. Their application only allows for the estimation of the stress of the structure that can cause particular dynamic overloads. Of crucial importance is the application of these factors in fatigue calculations. As many as 3 of 8 components in fatigue load cases are dynamic loads. Unfortunately, the replacement of dynamics with a dynamic effects factor completely overlooks the essence of dynamics in the studied structures. In accordance with the recommendations, or rather due to the absence thereof, no analysis is performed of the structure's dynamic response, nor of the possible resonant excitation e.g. by the overlapping of excitation derived from excavation frequency with mode shapes. Based on both the DIN and ISO standards, the Australian standard introduces new recommendations related to the analysis of possible resonant excitations generated by the digging frequency of buckets. The modernization of existing load-carrying structures in accordance with this recommendation is presented in the research paper [33].

It is also not mandatory to carry out verification by experimental tests. Therefore, there is no method of measurement which would clearly define the procedure for measuring and verifying the assumed dynamic loads. The appendix to the DIN standard does offer sample measurements but there are no recommendations for their implementation, which, in the case of such phenomena, can have a huge impact on the results. As shown in Fig. 3, the grid of measurement points does not cover the entire machine and there is no justification as to why these particular points were selected. Particular attention should

Table 1. Values of ψ coefficient in accordance with DIN standard[18]

Machine type	Machine element	Dynamic effects factors ψ		
		Vertical D_V	Transverse D_Q	Longitudinal D_L
Bucket wheel excavator	Bucket wheel boom	1/10	1/60	0
	Tower or central structure with counter-weight boom	1/25	1/30	0
Bucket-chain excavator	Bucket chain boom with cable supports	1/7	1/30	0
	Main support frame in the hoisting area of the chain boom	1/10	1/30	0
	Central structure	1/30	0	0
	Counterweight boom	1/20	1/50	0
Crawler mounted spreader	Discharge boom	1/10	1/10	0
	Tower - central part	0	0	0
	Counterweight boom	1/20	1/15	0
Crawler mount-ed machines	Connecting bridges	1/20	1/10	1/15
	Cabs for operators	1/2	1/2	1/2

be paid to the points that measure acceleration and are located on the undercarriage. Given the nature of vibrations in the presented structures [11, 28, 30], it can be assumed that the values measured in these points will not be large. Presumably, this is why these values were not included or discussed in the standard. However, it is erroneous to assume that dynamic loads will not act on the undercarriage components.

Dynamic load factors have been used for a long time in the design of cranes [26, 27], with the difference that they apply to the dynamic forces originating from the lifted mass and their value depends on the lifting velocity. Mass forces are determined on the basis of accelerations (dynamic effects) that depend on the characteristics of the drives, which follows the recommendations of the ISO standards.

Based on the above information it can be concluded that the commonly accepted method of designing large-scale machines based on the dynamic effects factor essentially ignores the dynamics of the structures that are being designed. Additionally, even static calculations based on the dynamic effects factor fail to take into account the dynamic effects that machine superstructures have on elements of the undercarriage. Furthermore, there is no well-defined method of experimental tests which could be used to verify the actual values of the assumed factors so as to obtain an approximation of the conditions and time of safe operation.

2. Research on the dynamic effects factor

The aforementioned gaps in knowledge on the dynamics of structures of large-scale machines have become the basis for numerical and experimental studies in recent years. The second chapter presents the author's original studies and their results. These studies were focused on the possibility to develop solutions that could be applied easily to current design guidelines and at the same time could solve the discussed problems related to dynamics of machines.

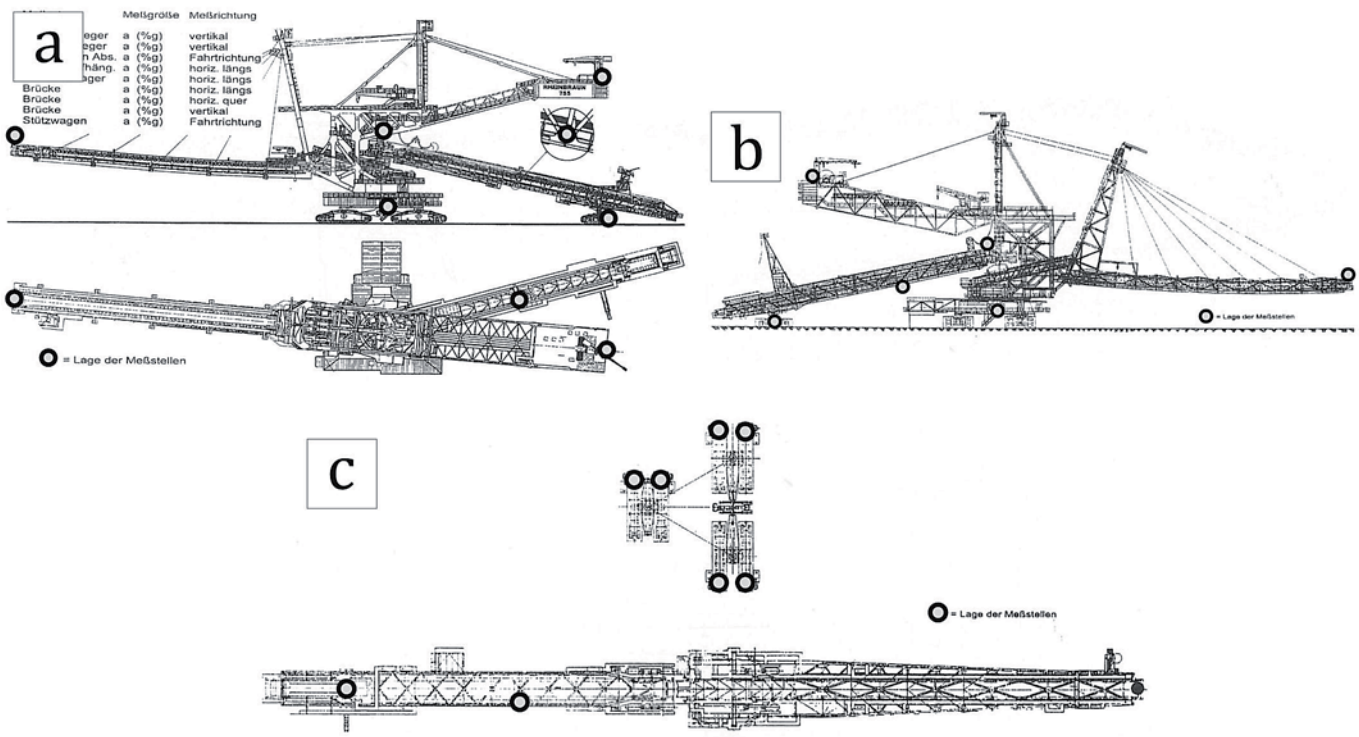

Fig. 3. Distribution of measuring points according to DIN [18]

2.1. Experimental studies of the actual values of the dynamic effects factor

Long-term operation of steel load-carrying structures of large-scale machines has led, in recent years, to the need to assess the technical condition of these structures. This is caused by their decreasing life expectancy. In the absence of recommendations and procedures for such tests, it was necessary to develop a method that could help assess their technical condition. Such an assessment is very complex [8-10, 35, 38] and incorporates verification by numerical calculations of the machine, experimental determination of actual load values, defectoscopic tests, analysis of previous modernizations, repairs and events that could have permanently affected the load carrying capacity of the structure. The conducted studies have shown that the most frequently exceeded operational parameters are the assumed dynamic loads [6, 42-43]. Measurements were performed on more than 20 machines operating in standard conditions. The grid of measurement points was more than twice as dense as the one proposed by the DIN standard. Their distribution for two sample machines is shown in Fig. 4 and Fig. 5.

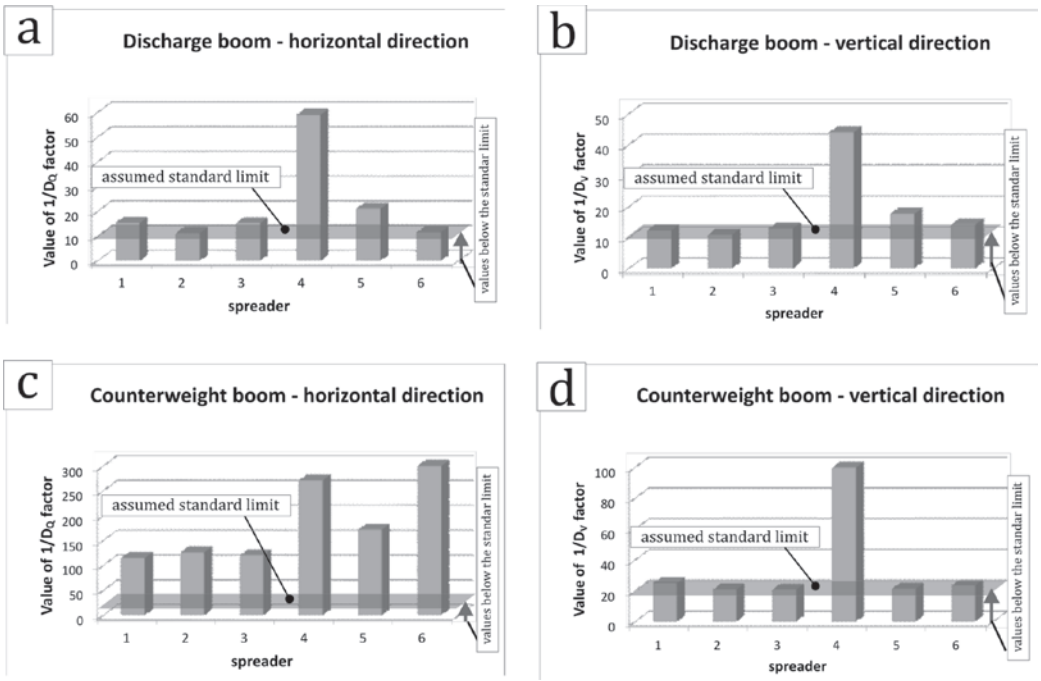

Fig. 6. Comparison of measured values of the dynamic effects factor for bucket wheel excavators

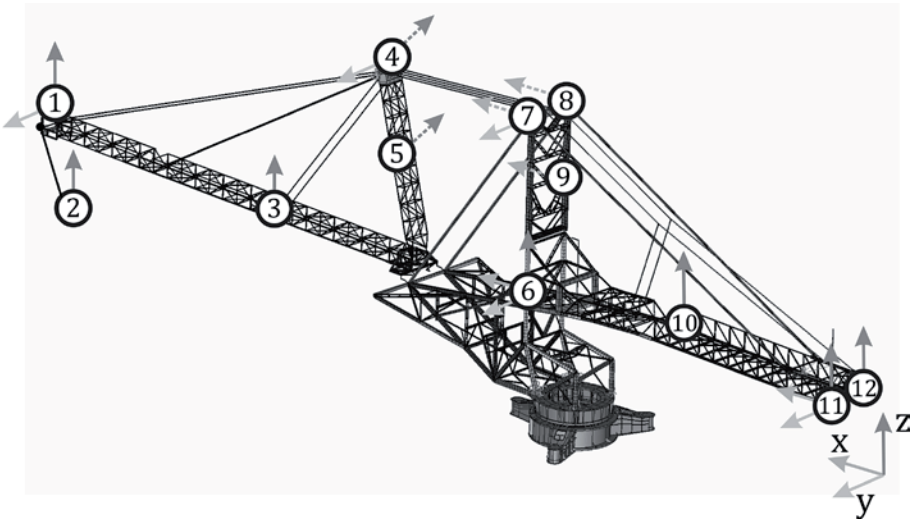

Fig. 4. Grid of measurement points – SchRs 4000.37, 5 excavator

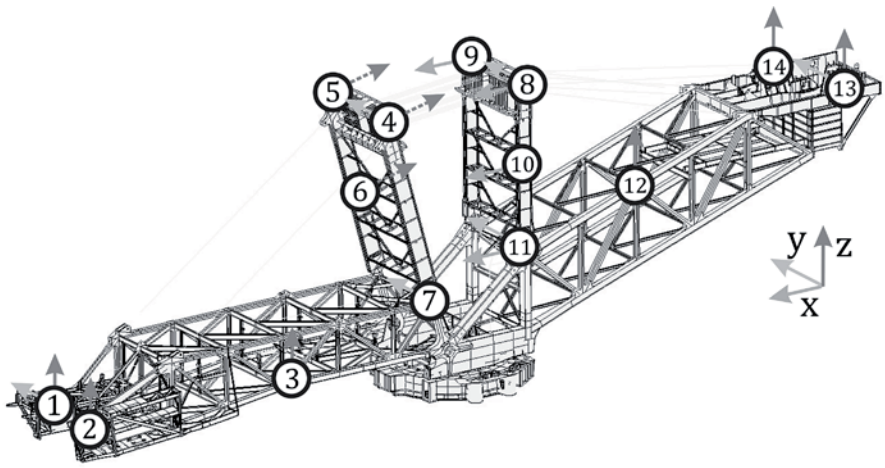

Fig. 5. Grid of measurement points – A_2RsB 12500 stacker

Figure 6 and Figure 7 show a comparison of selected measuring points. Fig. 6 is a comparison of experimentally determined levels of dynamic effects for selected representative measuring points which can be compared to the DIN standard. Fig.6a and Fig.6b represent the horizontal and vertical vibrations of the bucket wheel boom respectively, measured at its end (near the attachment of the bucket wheel). Fig.6c and Fig.6d show vibrations of the counterweight boom measured at its end (near the counterweight ballast). It is clearly visible that the highest number of exceedances were observed in the case of horizontal vibrations of the bucket wheel boom and vertical vibrations of the counterweight boom. What is important is that the vertical vibrations of the counterweight boom actually exceed the limit values only in a few cases. This discrepancy between the vertical vibrations of the booms confirms the influence of the excavated material on dynamic characteristics. This phenomenon was described in detail in [28]. Differenczes in the dynamic loads on counterweight booms in the horizontal direction are mainly due to the class of the machines and, consequently, to their design (compact excavators, C-frame machines, large two-mast machines)[38].

In the case of dynamic loads in stackers [9] (Fig. 7) there are exceedances in almost all pre-

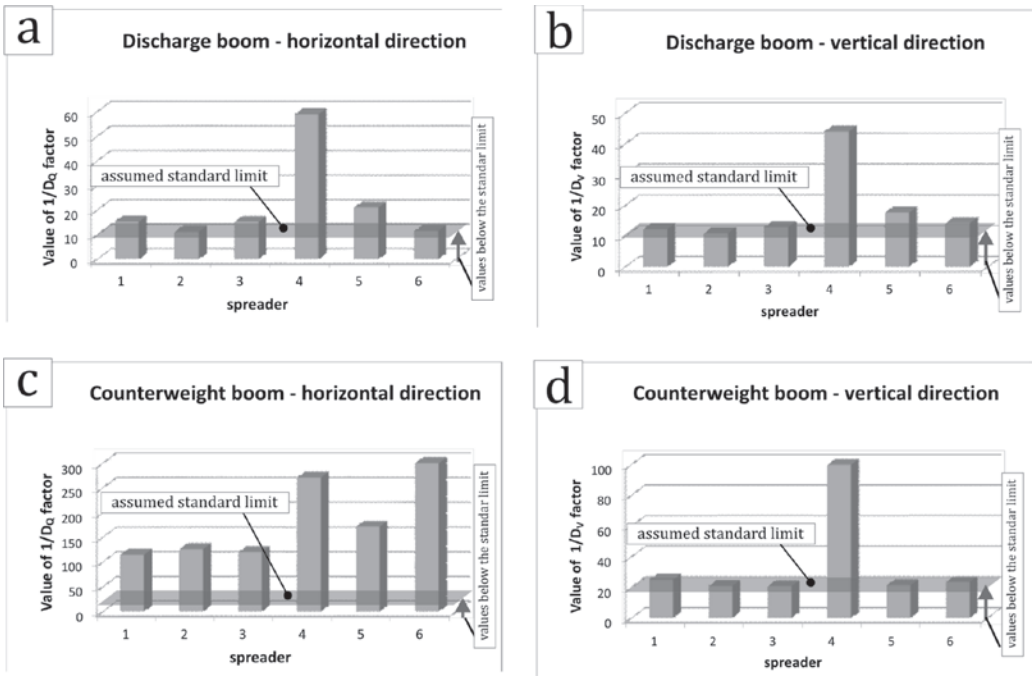

Fig. 7. Comparison of measured values of the dynamic effects factor for spreaders

sented cases and directions. Clearly there are dynamic surpluses in the vertical direction on the discharge boom whose vibrations are not dampened [3] as in the case of excavators, because the boom does not come in contact with the slope of the stockpile. The most relevant values of dynamic surpluses, in comparison to standard values, are those measured on the counterweight boom in the horizontal direction (Fig. 7d).

Additionally, preliminary studies have been carried out on the ŁZKS 1600 stacker-reclaimer, which were designed to verify the actual influence of dynamic loads on the undercarriages of machines. Unlike the method used in the DIN standard, accelerometers were not placed on the elements of the undercarriage, but instead strain gauges were attached to selected elements of the undercarriage. The studies investigated the correlation between the load measured by the strain gauges and the acceleration measured on the bucket wheel boom (Fig. 8). These studies are described in detail in [31]. They show a clear dependency between the loading cycles in the undercarriage, and the main mode of vibrations the superstructure.

Extended studies, still unpublished, have also been carried out on a medium machine (SRs 2000) and a large machine (SchRs 4000.37,5). The applied measuring grid is similar to the one shown in Fig. 4, but complemented by strain gauge measuring points on undercarriage track frame. The results confirm the correlation identified during tests on the ŁZKS 1600 machine. The reason why this is more important is that fatigue calculations for undercarriages have not been recommended before. The identified correlation indicates a new direction for studies on the phenomenon of fatigue of large-scale machines.

Since literature offers little information on verification of dynamic factors by experimental tests [18], the scale of the research project made it necessary, to develop a method of measurement that is identical for each type of machine under study.

In total more than 20 excavators and stackers were tested for superstructure dynamics and for the correlation between undercarriage loads and superstructure dynamics. The results were used to develop and standardize the method of experimental verification of actual values of dynamic load factors. This method establishes the criteria for the selection of measuring points, measurement parameters and signal analysis. The most important guidelines for this method are as follows:

- the measurement points cannot coincide with nodes of natural frequency mode shapes
- when determining the factor that takes into account the loads to elements of undercarriages, the measuring points should be defined in the center of mass of the superstructure elements
- when determining the factor in order to apply load to the undercarriage, the bandwidth range should be limited only to the first mode shape
- in order to analyse the changes in characteristics, the required spectral resolution should be 1/100 of the lowest expected frequency (the first mode shape of the superstructure)
- the goal of data acquisition and signal analysis should be zero loss of signal energy.

In addition, in the studies of the dynamic effects factor, the *peak-to-peak* value was replaced by the RMS value over the entire measurement. Such a definition of the factor makes it insensitive to individual impact overload [23,25]. In contrast to the recommendations in the standard, the tests should also include the dynamic effects factor in the longitudinal direction. This is particularly important in elements that are directly connected with the superstructure platform because, in these cases, even small values of dynamic effects can lead to strain that is relevant in terms of material fatigue. In the case of elements of the load-carrying structure that support other elements (the central section), it

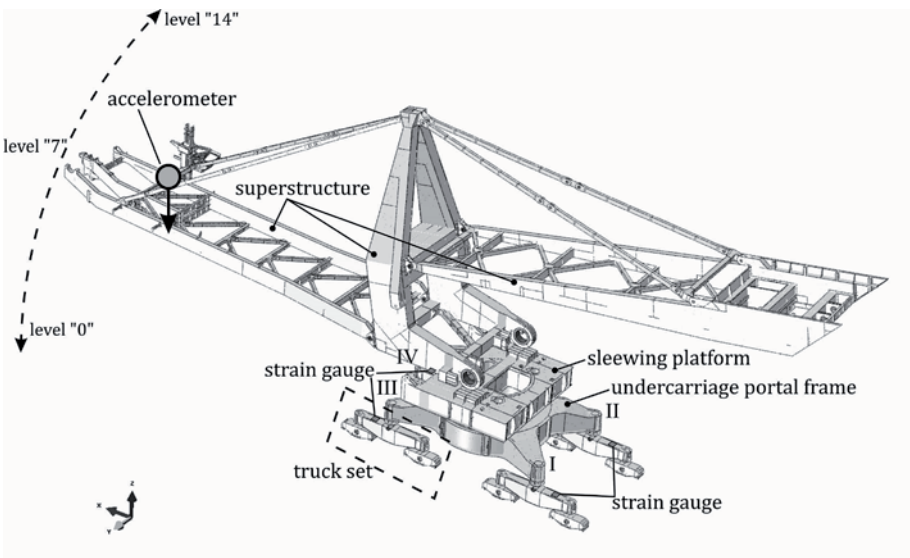

Fig. 8. Studies on the correlation between the dynamics of the superstructure and undercarriage loads [31]

is necessary to define the dynamic effects factor associated with each of the loading elements respectively. It also follows that the measurement point designated on one element can be used to evaluate a different area (central section, undercarriage).

2.2. Development of a designing method that takes into account the dynamic characteristics and the dynamic effects factor

A major concern from the point of view of design is the use of appropriate values for the dynamic effects factor. As shown in the previous section, these values are almost always exceeded during operation. The second important aspect is the fact that the dynamic effects factor in dynamic calculations is basically used to perform quasi-static calculations, which completely ignore the phenomena related to the dynamics of machines. What follows is that the possibility of resonances occurring due to the operation of the excavating unit is not verified, nor are mode shapes identified, which are a significant part of the dynamic response in the non-resonant area.

Thus, the analysis of the aforementioned facts shows considerable inconsistencies in the commonly used method of design. However, in order to solve the presented technical problems, while applying the dynamic effects factor for dynamic calculations, it was necessary to develop a designing approach that meets these objectives. This problem is rather difficult because in order to verify the adopted approach it is necessary to verify its results through experimental tests. In view of the fact that machines such as bucket wheel excavators or stackers are designed to operate for dozens of years they are not built very frequently and the design and construction process takes several years to complete.

It was possible, however, to carry out such a procedure when a new KWK 1500.1 excavator was being built. In the design stage an innovative approach was used which incorporated both the calculations with the application of the dynamic effects factor (mainly to validate fatigue strength) as well as dynamic calculations using modal analysis. The second element of this approach is crucial. As shown in the previous section the standard values of the dynamic effects factor are often exceeded. As a result, the calculations based on these values do not produce correct results in quantitative terms, which is confirmed by the large number of fatigue cracks that appear after many years of operation. The design approach adopted when designing the KWK 1500.1 excavator is based on the use of standard factors, however, what is most important is the optimization of the load-carrying structure in terms of dynamics so as to ensure the most even and lowest possible distribution of the dynamic response of the structure. Therefore, the steel load-carrying structure is optimized with regard to dynamic characteristics, which has not been done before. In the design stage it was assumed that since, thus far, machines have not been optimized in this respect, by carrying out such a process it will be possible to maintain the values of dynamic factors at the intended standard level. A detailed analysis of the modal characteristics of the system was performed and compared with the assumed operational excitation. On this basis, significant changes have been introduced to the kinematics of the counterweight support system. A detailed description of the conducted research and redesign is in the works [34, 39]. What is most important, however, is that the optimization of the load-carrying structure with regard to dynamics takes place already during the preliminary design stage. This introduces completely new possibilities in terms of potential modifications of the structure. Due to its application in fatigue calculations, the dynamic effects factor was applicable only when the final design was completed and followed by the numerical model with all detailed structural nodeconnections, because it is in those connections where potential regions sensitive to overload were located. Unfortunately, given the fact that at this stage the range of possible changes was very limited, the negative effects were merely mitigated instead of solving the underlying cause. It is quite different when optimization of the load-carrying structure is carried out at the preliminary design stage. It is then possible to introduce significant changes such as a change in the support system of individual machine components (Fig. 9).

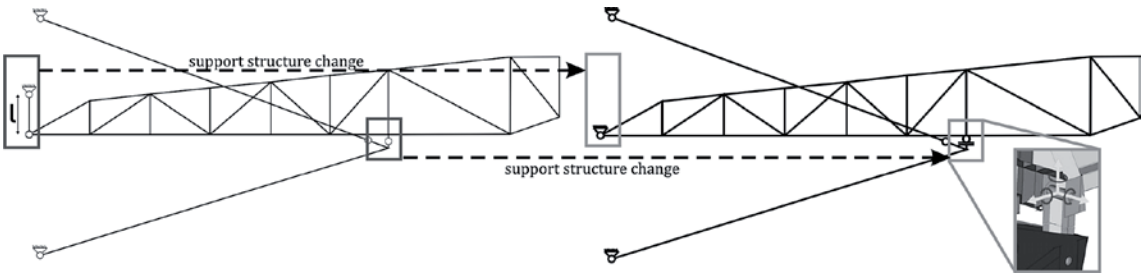

Fig. 9. Conceptual changes during the construction of KWK 1500.1 excavator

The developed design approach is shown in Fig. 10. Its most important advantage is that it is based entirely on the generally accepted design guidelines. The finite element method is used for calculations. It can also be easily implemented for general use. An important difference is in the optimization of the dynamic characteristics of the load-carrying structure. The developed method consists of three stages, each of which involves an analysis of dynamic characteristics. The method used thus far was limited only to the 2nd stage, excluded modal analysis and dynamic response analysis and included only static calculations with the application of the dynamic effects factor.

The above method makes it possible to significantly reduce the dynamic response of the system in actual operating conditions. The recommendations for verification by experimental tests made it pos-

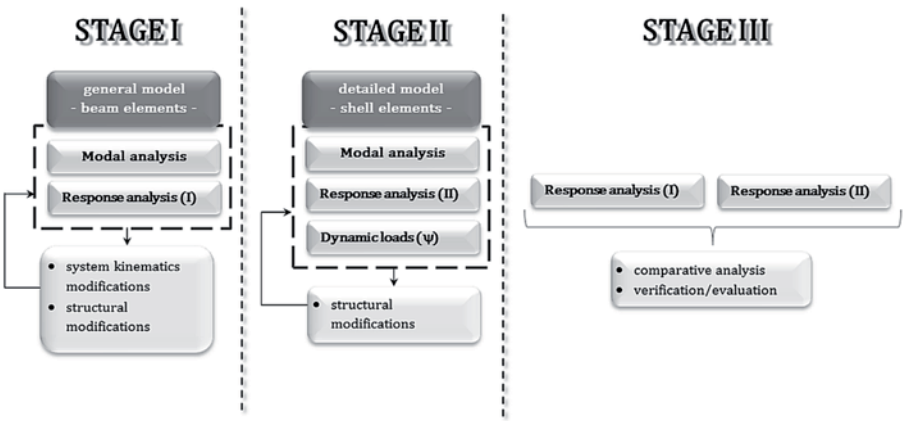

Fig. 10. Design thattakes into account dynamics and the dynamic effects factor

sible to verify the correctness of the proposed calculation model. Experimental studies [34,39] on the new KWK 1500.1 excavator prototype were compared with studies on excavators of the same class and similar structure: KWK 1500 and KWK 1200 (Fig. 11).

Excavators KWK 1500 and KWK 1500.1 are similar structures, with the difference in that the load-carrying structure of excavator KWK 1500.1 was optimized using the method shown in Figure 10.

What is to be expected is a similar behavior in terms of dynamics. An analysis of the results of experimental tests (table 2) showed

Fig. 11. Excavators a) KWK 1500.1, b) KWK 1500, c) KWK 1200

Table 2. Comparison of dynamic factors [34]

machine element	type of D factor	Experimental value 1/D			Standard value $1/D_N$	D_N /D		
		KWK 1200	KWK 1500S	KWK 1500.1		KWK 1200	KWK 1500	KWK 1500.1
bucket wheel boom	average D_Q	45	97	93	60	0,75	1,62	1,54
	average D_V	22	41	20	10	2,20	4,10	2,00
bucket wheel jib	average D_Q	37	45	208	60	0,62	0,75	3,46
	average D_V	35	53	32	10	3,48	5,30	3,18
counterweight boom	average D_Q	132	88	168	30	4,40	2,95	5,61
	average D_V	71	84	30	25	2,84	3,37	1,22

a significant difference in the behavior of the jib, which exhibited approximately five times lower vibrations in comparison to the KWK1500 excavator. This difference results from the optimization of dynamic characteristics that was carried out on the KWK 1500.1 excavator. The modification of the support system of the counterweight boom (Fig. 9) significantly altered the kinematics of the entire system. The counterweight boom is connected to the jib and the bucket wheel boom. It is clear that in the case of the KWK1500.1 machine the measured values of dynamic loads acting on these elements are compliant with the assumed values, which is a direct consequence of the stabilization of the operation of the counterweight boom.

The obtained data can be used to compare the standard values of the factor with the values calculated on the basis of measured acceleration values. The results of such comparison are shown in table 2. D_Q, D_V represent the values of the ψ factor in the lateral and vertical directions respectively, whereas D_N is their corresponding standard value. The recommended standard values used in calculations are exceeded when the measured D factor is smaller than the standard $D_N$factor. For comparison, the table also shows the values of factors for structurally similar KWK1200 and KWK1500 excavators.

Therefore the developed numerical model and the presented calculation method shows that it is possible to optimize the load-carrying structure in such a way as to meet the requirements established in the standard. The proposed model is the only one in the literature, with the calculation method and verification tests.

3. Method of evaluating large-scale load-carrying structures of machines with the application of the dynamic effects factor

The purpose of the studies and analyses presented in the second chapter was to directly address the issues of dynamics of surface mining machines in the design process. The following three basic problems were identified:

- lack of a calculation method that would be reflected both in the dynamic behavior and the dynamic effects factor
- lack of information on the incorporation of variable loads in undercarriages of machines
- lack of an experimental method of verifying the actual value of the dynamic effects factor.

The studies presented in the second chapter solve the problems defined above.

The proposed calculation method was complemented by the possibility to apply the dynamic effects factor in calculations of undercarriages. The model has been validated experimentally. Validation was performed using the experimental method of verification tests developed on the basis of research carried out on over 20 machines.

The presented long-term research and the resulting achievements constitute the author's method of evaluating large-scale load-carrying structures of machines with the application of the dynamic effects factor:

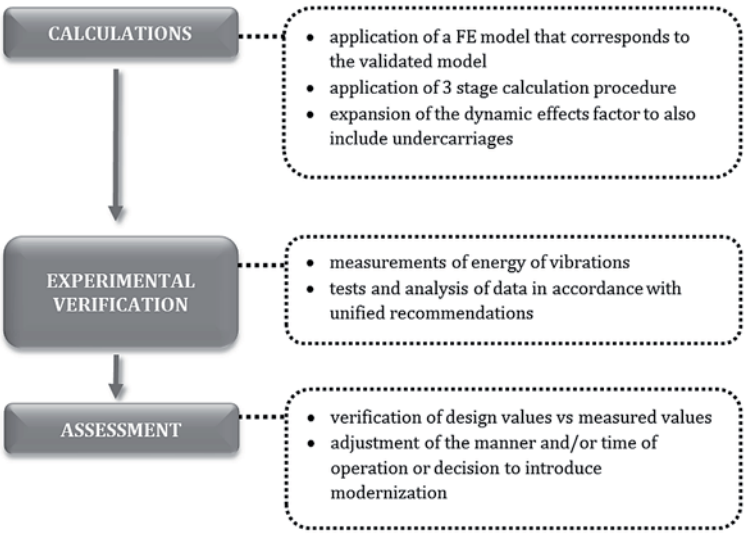

Fig. 12. Method of evaluating large-scale load-carrying structures with the application of the dynamic effects factor

The method consists of 3 basic steps. The first involves calculations based on the 3-stage calculation method presented in the second chapter, which uses the validated model. In addition, this method extends the calculations to also include the loads acting on undercarriages resulting from dynamic effects that have been observed during the studies. The next step of the evaluation method involves validation by experimental studies that are carried out after the structure is built. In this regard the second chapter presents a unified method of validation by experimental studies that offer the possibility to compare the established standard values with the actual ones. Once this information is available, the third step of the evaluation method commences, in which the validity of identified parameters is evaluated. On this basis a decision can be made to the change the manner and/or time of operation or to modernize the completed structure. Such a situation can occur if the verification tests demonstrate that the actual values are still higher than the assumed values. Once the actual values of dynamic loads are known it is possible to correct the estimated operational life. Depending on the obtained results new measures can be taken to limit, to a certain degree, the working loads of the machine and thereby decrease the dynamic loads acting on the load-carrying structure. This solution guarantees that the operational life will remain on the initially assumed level. Modifications can also be introduced to the final load-carrying structure if they are justified and feasible. The fact that actual values of the dynamic effects factor exceed the assumed values may also be a consequence of certain assumptions which were made in the designing stage but which cannot be avoided in the case of systems characterized by this level of complexity. It is also necessary to monitor the loads which are the main cause of excitation of the load-carrying structure and to ensure that their assumed values are not exceeded during operation. Such a situation can be the result of faulty operation, poor technical condition of the machine or operation in conditions (e.g. geological) that are different than those in the design. It is also recommended to continue monitoring the actual values of the dynamic effects factor in later stages of operation. By doing this it will be possible to introduced changes that might be necessary to obtain the required life. The successive steps of the evaluation method with the characteristic elements of each step are shown in figure 12.

4. Conclusions

The proposed evaluation method fills the gap between the scientific calculation methods that are currently being developed in relation to dynamics of large-scale machines and the commonly known and used methods. Because it is based on the dynamic effects factor for dynamic calculations, which, in accordance with standard recommendations is the basis for these calculations, the proposed method is compatible with all current requirements for designers of large-scale machines.

The primary difference, which offers the greatest benefits from the application of this method, is that the result produced by calculations using this method is not only qualitative but also quantitative. Underestimated dynamic loads still lead to the accelerated degradation of load-carrying structures. The presented method makes it possible to apply changes in design in order to customize the load-carrying structure in such a manner that the dynamic response, measured during operation, corresponds to the values assumed in calculations. Dynamic analysis of the structure at the preliminary design stage offers the possibility to develop completely new structures with optimized dynamic characteristics. In addition, if dynamic characteristics are maintained at the appropriate level, operation becomes easier and not only precise technical and operational parameters related to extraction can be obtained but the precision of estimation of durability can be improved.

Also no indication has been made thus far of a direct correlation between variable loads acting on elements of undercarriages and superstructure vibrations. The presented studies clearly show that such a correlation exists and, in addition, indicate the possibility to approach this phenomenon with the dynamic effects factor, which is also an important element of the method. The demonstrated correlation also offers the possibility to develop other alternative methods for estimating fatigue life of undercarriages of large-scale machines.

To verify the actual values of dynamic loads, a unified method for conducting experimental research has been developed. It is also an integral part of the method of evaluating large-scale load-carrying structures.

The proposed method of evaluating large-scale load-carrying structures with the application of the dynamic effects factor as well as the studies on the basis of which it has been developed, are of high value in the field of technical sciences and applied research. Because the method is based on the commonly used dynamic effects factor it has a great potential for quick application in practice. This is confirmed by theKWK 1500.1 excavator, which was designed and built using the described method.

References

1. Babiarz S, Dudek D. Failures and catastrophes in Polishsurfacemining – In Polish. Wroclaw University of Technology Publishing House 2007.
2. Bialas K. Electrical Elements in Reduction of Mechanical Vibrations. Applied Mechanics and Materials, 2013; 371: 657-66.
3. Bocian M, Jamroziak K, Kulisiewicz M. The identification of nonlinear damping of the selected components of MDOF complex vibratory systems. [in:] A. Cunha, E. Caetano, P. Ribeiro, G. Müller (eds.), Proceedings of the 9th International Conference on Structural Dynamics, EURODYN 2014, Porto, Portugal, 30 June - 2 July 2014; 3365-3372.
4. Bosnajk S, Petkovic Z, Simonovic A, Zrnic N, Gnjatovic N. Designing-in failures and redesign of bucket wheel excavator undercarriage. Engineering Failure Analysis 2013; 35: 95–103, https://doi.org/10.1016/j.engfailanal.2012.12.007.
5. BosnjakS M, Oguamanam D C D, Zrnic N D. The influence of constructiveparameters on responsepfbucketwheelexcavatorsuperstructure. Archives of Civil and Mechanical Engineering 2015; 15: 977-985.
6. Brkić A Đ, Maneski T, Ignjatović D, Jovančić P, SpasojevićBrkić V K. Diagnostics of bucket wheel excavator discharge boom dynamic performance and its reconstruction. Eksploatacja i Niezawodnosc – Maintenance and Reliability 2014; 16 (2): 188–197.
7. Cristea D. In Situ Modal Testing Methods For Huge Structures Applications to Surface Mining Machines Annals of the University of Petroşani, Mechanical Engineering 2007; 9: 97-102.
8. Czmochowski J, Kowalczyk M, Pietrusiak D, Przybyłek G, Rusiński E. Metodyka oceny stanu technicznego maszyn górniczych w kopalniach odkrywkowych. Problemy rozwoju maszyn roboczych / red. Andrzej Kosucki. Łódź : Wydawnictwo Politechniki Łódzkiej; 2015: 65-76.
9. Czmochowski J, Moczko P, Pietrusiak D, Przybyłek G, Rusiński E. Selected Aspects of Technical Condition State Assessment of Spreaders Operating in Lignite Mines. Proceedings of the 13th International Scientific Conference Computer Aided Engineering, Polanica Zdrój,

Poland, June 22-25, 2016: 89-98.
10. Czmochowski J, Moczko P, Pietrusiak D, Rusiński E. Numeryczno-Eksperymentalna Analiza Drgań Zwałowarki w Stanach Nieustalonych. Materiały Konferencyjne – XXX Konferencja Problemy Rozwoju Maszyn Roboczych, 24-27.01.2017, Zakopane; 2017.
11. Czmochowski J. Identification of modal models of brow coal excavation machines – In Polish. Wroclaw University of Technology Publishing House; 2008.
12. Danicic D, Sedmak S, Ignjatovic D, Mitrovic S. Bucket wheel excavator damage by fatigue fracture – case study. Procedia Materials Science 2014;3: 1723 – 1728. https://doi.org/10.1016/j.mspro.2014.06.278
13. Derlukiewicz D, Kowalczyk M, Moczko P, Smolnicki T. Selected Aspects Of Loads Identification In Caterpillar Undercarriage Of Bucket Wheel Excavator, 25th Danubia-Adria Symposium On Advances In Experimental Mechanics 2008: 55-56.
14 Equipment in Brown Coal Open Cu tMines Part 2 Calculation Principals Technischen Normen, Gütevorschriftenund Lieferbedingungen, TGL 13472 Stahlbau Stahltragwerke der Hebezeuge; Berechnung, bauliche Durchbildung1974.
15. Fiebig W, Wróbel J. Two stage vibration isolation of vibratory shake-out conveyor. Archives of Civil and Mechanical Engineering 2017; 17: 199-204, https://doi.org/10.1016/j.acme.2016.10.001.
16. Filizikowski J, Macko M. Method of estimation of efficiency of quasi-cutting of recycled opto-telecommunication pipes. Polimery 2001; 46(1): 53-59.
17. Flizikowski J, Macko M. Competitive design of shredder for plastic in recycling, Tools And Methods Of Competitive Engineering 2004; 1/2: 1147-1148.
18. German Institute for Standardization, DIN 22261-2 Excavators, Stackers and Auxillary Equipment in Brown Coal Open Cut Mines Part 2 Calculation Principals 2015.
19. Gnjatovic N. Influence of constructional parameters and parameters of excitation on response of the bucket wheel excavator with two masts in the out-of-resonance region. PhD Thesis, University of Belgrade, 2016.
20. Huss W. Metoda identyfikacji stanów nieustalonych ustroju nośnego koparki kołowej przy obciążeniach losowych. Politechnika Wrocławska, Rozprawa Doktorska, 2012.
21. Idehara S J, Junio . D. Modal analysis of structures under non-stationary excitation. Engineering Structures 2015; 99: 56–62, https://doi.org/10.1016/j.engstruct.2015.04.035.
22. International Organization for Standardization, ISO5049.1: Mobile Equipment for the Continuous Handling of Bulk Materials Part 1 Rules for the Design of Steel Structures, 1994.
23. Jabłoński M, Ozga A. Determining the distribution of values of stochastic impulses acting on a discrete system in relation to their intensity. Acta Physica Polonica A; 2012: 121(1): 174-178, https://doi.org/10.12693/APhysPolA.121.A-174.
24. Kowalczyk M. Wymiarowanie spawanych konstrukcji nośnych maszyn podstawowych górnictwa odkrywkowego w zakresie trwałości zmęczeniowej, Rozprawa Doktorska, Politechnika Wrocławska, 2010.
25. Pach J, Pyka D, Jamroziak K, Mayer P. The experimental and numerical analysis of the ballistic resistance of polymer composites. Composites Part B: Engineering; 2017; 113: 24-30, https://doi.org/10.1016/j.compositesb.2017.01.006.
26. Piątkiewicz A, Sobolski R. Dźwignice, tom 1, WNT 1978.
27. Piątkiewicz A, Sobolski R. Dźwignice, tom 2, WNT 1978.
28. Pietrusiak D. Assessment of the bucket wheel excavators load carrying structures dynamics with use of the modal analysis (Doctoral dissertation – In Polish), Wroclaw University of Technology Institute of Machine Design and Operation, 2013.
29. Pietrusiak D, Moczko P, Rusiński E. Recent achievements in investigations of dynamics of surface mining heavy machines. 24th World Mining Congress : mining in a world of innovation - proceedings, October 18-21, 2016, Rio de Janeiro, Brazil. Rio de Janeiro : IBRAM, 2016: 295-308.
30. Pietrusiak D, Moczko P, Rusiński R. World's largest movable mining machine vibration testing - numerical and experimental approach. Proceedings of ISMA2016 International Conference on Noise and Vibration Engineering, USD2016 International Conference on Uncertainty in Structural Dynamics 19 to 21 September, 2016 / eds. P. Sas, D. Moens, A. van de Walle. Leuven : Katholieke Universitet Leuven, 2016: 2287-2299.
31. Pietrusiak D, Smolnicki S, Stańco M. The influence of superstructure vibrations on operational loads in the undercarriage of bulk material handling machine. Archives of Civil and Mechanical Engineering, https://doi.org/10.1016/j.acme.2017.03.001.
32. Płaczek M, Buchacz A, Wróbel A. Use of piezoelectric foils as tools for structural health monitoring of freight cars during exploitation. Eksploatacja i Niezawodnosc – Maintenance and Reliability 2015; 17 (3): 443–449, http://dx.doi.org/10.17531/ein.2015.3.16.
33. Rusinski E, Dragan S, Moczko P, Pietrusiak, D. Implementation of experimental method of determining modal characteristics of surface mining machinery in the modernization of the excavating unit. Archives of Civil and Mechanical Engineering, 2012; 12(4):, 471–476, https://doi.org/10.1016/j.acme.2012.07.002.
34. Rusinski E, Moczko P, Pietrusiak D. Low frequency vibrations of the surface mining machines caused by operational loads and its impact on durability. Proceedings of International Conference on Noise and Vibration Engineering (ISMA2014) and International Conference on Uncertainty in Structural Dynamics (USD2014), 2014: 683-694.
35. Rusiński E, et al. Ocena Stanu Technicznego Maszyn Podstawowych Górnictwa Odkrywkowego. Oficyna Wydawnicza Politechniki Wrocławskiej, 2015.
36. Rusiński E, Czmochowski J, Moczko P, Pietrusiak D. Challenges and strategies of long-life operation and maintenance of technical objects, FME Transactions 2016; 44: 219-228.
37. Rusiński E, Czmochowski J, Iluk A, Kowalczyk M. An analysis of the causes of a BWE counterweight boom support fracture. Engineering Failure Analysis 2010; 1(17): 179–191, https://doi.org/10.1016/j.engfailanal.2009.06.001.
38. Rusiński E., Czmochowski J., Moczko P., Pietrusiak D.SurfaceMiningMachines – Problems of Maintenance and Modernization, Springer Nature, 2017
39. Rusiński E, Moczko P, Pietrusiak D. Analiza dynamiki wielonaczyniowych koparek kołowych typu KWK, Górnictwo Odkrywkowe 2014; 55(4/5): 197-202.
40. Rusiński E, et. al. Analiza techniczno-ekonomiczna możliwości zastosowania w odkrywce Złoczew maszyn podstawowych pracujących w

KWB Bełchatów. Raporty Wydziału Mechanicznego Politechniki Wrocławskiej. 2016,, Ser. SPR ; nr 133, 2015.
41. Rusiński E, et al. Badania, ekspertyza i diagnostyka maszyn podstawowych KWK-1200M (K-27), ARsP-6500 (Z-45). Raporty Inst. Konstr. Ekspl. Masz. PWroc. 2010, Ser. SPR; nr 87, 88, Politechnika Wrocławska, 2010.
42. Rusiński E, et. al. Badania, ekspertyzy i diagnostyka maszyn podstawowych KWK-1500s (K-9), KWK-1200M (K-14), SchRs-1200 9K-22). Raporty Inst. Konstr. Ekspl. Masz. PWroc. 2009,, Ser. SPR ; nr 90, 91, 92, Politechnika Wrocławska, 2009.
43. Rusiński E, et. al. Badanie ustrojów nośnych maszyn podstawowych. Raporty Wydziału Mechanicznego Politechniki Wrocławskiej 2015, Ser. SPR ; nr 164, 2015.
44. Rusiński E, et al. Ocena stanu technicznego zużycia maszyn podstawowych pracujących w KWB Konin. Etap 1, Ocena stanu technicznego i wykonanie badań na koparkach SchRs-800 i SchRs-1200 pod kątem określenia dalszej możliwości ich pracy Raporty Inst. Konstr. Ekspl. Masz. PWroc. 2010, Ser. SPR; nr 56, Politechnika Wrocławska, 2010.
45. Rusiński E, et al. Ocena stanu technicznego zużycia maszyn podstawowych pracujących w KWB Konin. Etap II, Ocena stanu technicznego i wykonanie badań na koparkach SRs 1200/5 i SRs 1200/6 pod kątem określenia możliwości pracy jednej z nich na O/Ościsłowo. Raporty Inst. Konstr. Ekspl. Masz. PWroc. 2011, Ser. SPR; nr 39, Politechnika Wrocławska, 2010.
46. Rusiński E, Dudek K, Moczko P. Degradation of undercarriage portal frames of surface mining machines – In Polish. Transport Przemysłowy 2006; 2(24): 40-43.
47. Standards Australia AS4324.1: Mobile equipment for continuous handling of bulk materials Part 1 - General requirements for the design of steel structures, 1995.
48. Weber F, Feltrin G, Maślanka M, Fobo W, Distl H. Design of viscous dampers targeting multiple cable modes. Engineering Structures 2009; 31: 2797–2800, https://doi.org/10.1016/j.engstruct.2009.06.020.

Damian PIETRUSIAK
Department of Machine Design and Research
Faculty of Mechanical Engineering
Wrocław University Of Science Technology
ul. Łukasiewicza 7/9, 50-371 Wrocław, Poland

E-mail: damian.pietrusiak@pwr.edu.pl

Article citation info:
MARSARO MF, CAVALCANTE CAV. Random preventive maintenance policy based on inspection for a multicomponent system using simulation. Eksploatacja i Niezawodnosc – Maintenance and Reliability 2017; 19 (4): 552–559, http://dx.doi.org/10.17531/ein.2017.4.8.

Mônica Frank MARSARO
Cristiano Alexandre Virgínio CAVALCANTE

RANDOM PREVENTIVE MAINTENANCE POLICY BASED ON INSPECTION FOR A MULTICOMPONENT SYSTEM USING SIMULATION

OPARTA NA PRZEGLĄDACH POLITYKA LOSOWEJ KONSERWACJI ZAPOBIEGAWCZEJ SYSTEMU WIELOELEMENTOWEGO Z WYKORZYSTANIEM SYMULACJI

In today's global situation where highly competitive companies demand production efficiently to reduce costs, increase product quality, and customer loyalty, maintenance becomes crucial to achieve this goal by reducing unplanned downtime, reworking of products, and costs. In this sense, the use of models that can represent this type of system, and help managers make decisions more easily, are of vital importance for companies. Thus, a preventive maintenance model for a multicomponent system with different failure mechanisms is proposed in this work. Considering that the objective is to optimize the number and the time of maintenance interventions, that will be done in the system, periodic inspections are carried out in order to minimize the expected costs of maintenance. The optimization was performed with simulation, which proved to be satisfactory, since the decision variables of the model behaved adequately when utilized within the context of an applied case study. In addition, these variables had different performances when analyzed in four different scenarios: the original model of the proposed policy, and three variations attributing costs of penalties.

***Keywords**: random preventive maintenance; inspection; simulation; sugarcane plant.*

W dzisiejszej sytuacji globalnej, w której przedsiębiorstwa o wysokim stopniu konkurencyjności wymagają efektywnego obniżania kosztów produkcji, poprawy jakości produktów oraz zwiększania lojalności klientów, konserwacja ma zasadnicze znaczenie dla osiągnięcia tych celów poprzez redukcję nieplanowanych przestojów, oraz zmniejszenie konieczności usuwania usterek produktów a także obniżanie kosztów. W tym sensie, wykorzystanie modeli reprezentujących tego typu systemy i ułatwiające menedżerom podejmowanie decyzji , ma kluczowe znaczenie dla firm. W tej pracy zaproponowano model konserwacji zapobiegawczej dla wieloelementowego systemu o różnych mechanizmach uszkodzeń. Biorąc pod uwagę, że celem jest optymalizacja liczby i czasu trwania zabiegów konserwacyjnych dokonywanych w systemie, przeprowadzane są okresowe przeglądy mające na celu zminimalizowanie oczekiwanych kosztów utrzymania. Optymalizację przeprowadzono za pomocą symulacji, która okazała się zadowalająca, ponieważ zmienne decyzyjne modelu zachowywały się odpowiednio przy wykorzystaniu ich w kontekście omawianego studium przypadku. Dodatkowo, zmienne te przybierały różne wartości dla czterech różnych scenariuszy: pierwotnego modelu proponowanej polityki konserwacyjnej i trzech wariantów, w których uwzględniono koszty pracy systemu w stanie awaryjnym.

***Słowa kluczowe**: losowa konserwacja zapobiegawcza; przeglądy; symulacja; zakład przetwórstwa trzciny cukrowej.*

1. Introduction

Many of today's technological systems, such as airplanes, nuclear power plants, military installations, advanced industrial, and medical equipment, involve high levels of complexity in their maintenance and operation and require a high level of availability and reliability [10]. Furthermore, technological companies have been focusing their activities to achieve operational efficiency in a highly competitive global economy.

So, maintenance has been highlighted as a tool for this. It can be said then, that maintenance are technical and administrative actions that can maintain or restore the state of a system, so that the system can perform its required functions to keep it in full operation. These actions classically fall into two categories: preventive maintenance (PM), and corrective maintenance (CM) [1].

PM activities are typically planned to help prevent the deterioration and failure of the system [24], especially when serious consequences due to failure occurs, which may incur very high costs. Besides this, maintenance actions can reduce maintenance costs, and improve the production efficacy of the system, and reliability and availability. However, excessive PM itself can be expensive and time consuming. Therefore, it is important to perform adequate and effective PM practices to balance maintenance activities and cost [27].

An efficient way to perform PM is through inspections. They can have a variable depth level according to the system, and provide information about the system's operating state to perform repairs or replacements [24, 18]. Zhang et al. [26] developed a PM model based on inspection for mechanical components in three states with competing failure modes using an age limit and degradation for the system. Scarf and Cavalcante [20] established a model based on inspection, however for a single component that has three states: good, defective and fail.

Many authors have been using Condition Based Maintenance (CBM) to create models that take into account inspection, among them Lam and Banjevic [16], Chen et al. [5], Zhu et al. [30], Dieulle et al. [9], and Jardine et al. [14]. Other authors have also developed models for maintenance optimization through inspections in different

segments of, industry such as considering a high-speed milling tool wear by Yan et al. [25], in pipes that undergo corrosion by Sahraoui et al. [21], in reparable multicomponent hospital systems by Golmakani and Moakedi [13], and for the equipment that are inspected by the manufacturers in the warranty period with a cost charged to them, and after this period with the cost charged to the customer [8].

Golmakani and Moakedi [13] were among who developed a maintenance cost optimization model based on periodic inspections for a reparable multicomponent system. Therefore, the main difference between systems with a single component and systems with more than one is that there normally exist some kind of dependence, structure or economic dependence, between them that can be related to the failure mechanism [4, 15].

The economic dependence is related to the fact that there can be economic costs when maintenance is performed; the structural dependence is related to the fact that the components form a part, and that maintenance in one implies the maintenance of the other [23]. In addition, the dependency related to the degradation occurs when the failure rates in one component can affect the incidence in another [7, 28].

In view of the complexity of the multicomponent systems, the construction of analytical models becomes a very difficult task. Many times, it needs simplifications that affect the ability to represent the main aspects of the real problem. In this sense, what has been seen is a rise in the use of simulation for maintenance optimization. The simulation allows modeling a complex behavior and requires fewer assumptions in relation to analytic modeling.

Although the simulation is well established for representation of the operation of productive systems in general, it is still developing in the maintenance area [3]. Simulation has traditionally been used as a tool to understand and perform experiments with a system. However, combining the simulation model with the optimization model ensures better and faster results [2, 11, 12, 18].

The simulation may incur a number of benefits, among them are experimentation in shorter time, because the model uses a computer; reduced analytical requirements; and more easy demonstration of models. But some disadvantages can also be cited: simulation cannot generate accurate results, when the input date is not accurate as well; and it may not be easy to generate answers to complex problems [6].

In this way, the present paper intends, through the simulation, to obtain performance metrics about one policy, in order to evaluate the effectiveness of a policy that establishes simple procedures for the maintenance manager. Once variations of this policy are shown to be effective, we intend to optimize the policy decision variables for different scenarios, which depict very feasible peculiarities of production systems. The maintenance policy is based on inspections and replacement taking into account opportunities for a system composed of two components whose failure characteristics are different, and which have economic and structural dependency. We used the simulation to find the lowest expected maintenance cost evaluating some decision variables of the model described.

This paper is divided as follows: presentation and description of the proposed maintenance model, with the characteristics of each of the components, an experimental application of the model through a case study in the sugarcane industry, showing the main results for the adopted maintenance policy, and a sensitive analysis about the results to evaluate the variables behavior.

2. Model Description

For this model, the follow variables and parameters are used:

Decision variables:

T: inspection time in A (Cumulative);

τ: threshold of system age;

N: Number of inspections in B before τ;

Costs

c1: inspection cost of equipment A.

c2: inspection cost of equipment B.

cp: replacement cost of A.

cr: system replacement cost (*cp* << *cr*)

cF: failure cost of equipment B – large loss due to the need for aggressive maintenance, besides the lost profit.

cdt: downtime cost.

cB: cost of defect penalty in B – is counted from the time of the arrived the defect in B until the moment it is replaced.

Refer to equipment A

k: number of inspections in A (k = 1, 2, ...).

q: number of failures in A.

y_A: time to arrival the failure in equipment B.

Refer to equipment B

T_B: time to inspection in equipment B (Cumulative).

x: time to arrival of the defect in equipment B.

h: delay time.

y_B: time to arrival the failure in equipment B, defined as $y_B = x + h$.

Refer to system

SL: System Life

C: Maintenance Cost

Consider a system with two units, or a system composed of two basic sets, in parallel, in which the system only stops when component B stops working. Each of the components has a series of particulars characteristics, as shown below.

Equipment A:

1. The failures have an abrupt form. That is, there is not a slow degradation that allows intermediate states before the failure. Component A is working, and suddenly stops.
2. The failure of component A is not pronounced, because the system does not stop working. For this reason, it is only detected by inspection. This type of failure can be considered as a soft failure [4], because it can reduce the system reliability and increase the risk of damage due to malfunctioning of the system, despite not causing immediate failure of the system.

   By the failure characteristics presented previously, they can be classified as hidden failure. According to Taghipour and Banjevic [22], this kind of failure does not stop the system, at the moment that it happens; however, it can cause various types of losses, such as performance (working inefficiently) or economic (low production level or rework). This is because there is a time difference between the occurrence of the failure and its detection [13, 29].
3. Component A is inspected at times *kT*, with *k* = 1, 2, ..., so there is a schedule of inspections to be performed on it in order to identify whether it has already failed or not.
4. The inspection is simple and low cost, and it can be performed visually without using a complex equipment.
5. When a failure occurs, the system has a performance loss, increasing the costs.

Equipment B:

1. The failure occurs in a slower way, so it is possible to identify intermediate states. That is, before the failure, the equipment presents a defect. In this way, a component type B can undergo three possible states: (1) Operational, (2) Defective, and (3) Fail.
2. Only it is possible to identify that component B is defective in state 2 by an inspection.
3. However, when component B fails, the identification is immediate, because this failure is catastrophic, that is, it brings a damaging consequence to the system. This type of failure is called hard failure [4].
4. Component B is opportunistically inspected. This occurs on inspection of A when it is identified as fail.
5. The inspection in this component is more complex and incurs higher costs than the inspection of A.

In view of the characteristics of the equipment that comprises the system presented previously, and the fact that the inspection of equipment A is cheaper, as well, due to equipment type B presenting defects, these allows the failures in equipment B to be avoided. So, the following maintenance policy was established:

Equipment A is inspected at times kT, where $k = 1, 2, \ldots$. If this equipment is in the failed state, equipment B is inspected. If equipment A does not present failure, then equipment B is not inspected. The system is replaced when equipment B failed, or when this is found in a defective state by an inspection, whichever happens first. When an inspection reveal that equipment A failed, but the equipment is in operational state, only equipment A is replaced with a new one.

Taking into account that equipment B failure has repercussions of serious consequences, some maintenance actions are specified for the equipment B, in order to not reach the defective state. The maintenance actions that are performed in equipment B are:

- Inspection when a failure in equipment A is found;
- Preventive replacement when $N + 1$ successive failures have already occurred in equipment A;
- Preventive replacement at the failure time of A, when on failure of A the dispositive B already operated for a longer time than τ.

It is observed that despite the existence of three decisions variables (N, τ, and T), the operation of the model, in practice, is quite simple: there is no pre-scheduled action for both items. It is only subject to corrective maintenance, whereas B will be preventively replaced, when some conditions related to the state of A or the number of failures presented by the item shows an opportunity to replace B.

Here are the ways that the system is renewed:

1. In failure of B

Figure 1 represents the arrival of the failure moments of equipment A, the time inspection of A (T), the time inspection of B (T_B), the defect arrival of B, and the failure time of B when the system is renewed.

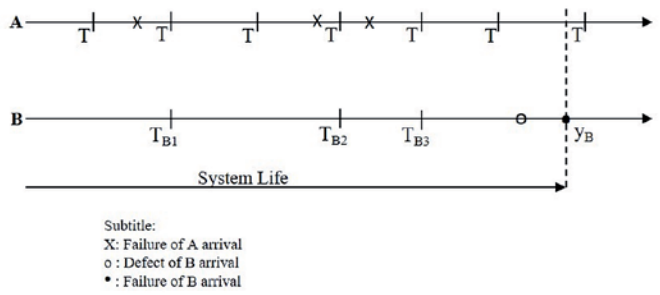

Fig. 1. Representation of the first case of the policy

The System Life (SL) in this case can be presented as follows in Equation 1. It occurs only if the defect and failure of component B happens after the last inspection of B (T_{Bq}). It is also observed that the condition is linked to the fact that the time of the inspection of A occurs before or after the limit τ. Therefore, q represents the quantity of inspections in A, pointing out again that the failure of B is the sum of the defect time in B and the delay time.

$$SL = y_B \; if \; x \geq T_{Bq} \cap q < N+1 \cap \begin{cases} y_A \geq T_{k-1} \leq y_B \leq T_k \; if \; T_k > \mathrm{t} \\ T_{k-1} \leq y_B \leq T_k \; if \; T_k \leq \mathrm{t} \end{cases}, k = 1,2,\ldots \tag{1}$$

We can also study the maintenance costs associated in this case. It is the sum of the inspection costs of A, the replacement cost of A, the inspection costs of component B, the failure cost of component B, and the system replacement cost.

$$C = \sum_{1}^{k} c1 + q\left(cp + c2\right) + cF \tag{2}$$

2. When q is equal to N+1

Taking into account that for equipment B to be inspected a failure in equipment A must have be occurred to generate an opportunity to inspect B, and the number of times that the equipment B was inspected is called N, an excessive number of failure may occur in the system without find a defect in B. In this way, to avoid performance losses, in the next failure of A, when q is equal to $N+1$, the system will be renewed without perform inspection in B. This case is showed in Figure 2, where N equals 3.

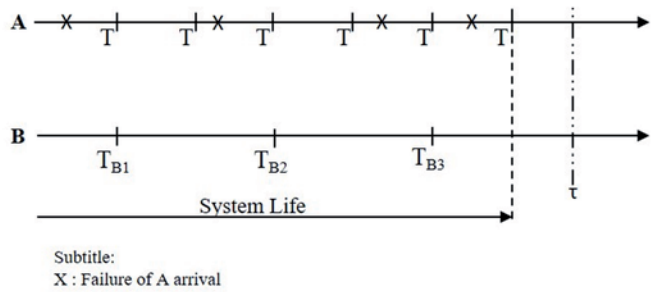

Fig. 2. Representation the second case of the policy

The SL in this case can be presented in this way:

$$SL = T_k \; if \; T_k \leq \mathrm{t} \cap x > T_k \cap q = N+1, k = 1,2,\ldots \tag{3}$$

The system life will be equal to the last time of inspection of A (T_k). It occurs if the inspections of B did not find a defect in the dispositive, and also if the time of the $N + 1$ inspection of A is less than the limit τ. We can analyze the maintenance costs for this case, in this way:

$$C = \sum_{1}^{k} c1 + N\left(cp + c2\right) + cr \tag{4}$$

As highlighted in Equation 4, there is no failure cost added, since it is considered that PM of the system is performed. Consequently, the

inspection costs of A and replacement costs of A, together with the inspection costs of B and the system replacement cost, are all added. Note that the number of times that the inspection costs of B and the replacement costs of A are equal to N, because in the $N + 1$ failure of A, the policy affirms that the system is replaced, not requiring an inspection of B.

3. In the first failure of A after τ

A life threshold τ of the system is specified due to the fact that there occurs a major performance loss after this time. Besides, it is observed that the probability is great that a defect in B occurs after this limit, and, therefore, a preventive replacement is performed in the first opportunity that A provides. This replacement is performed at the time that A is inspected, because its failures are only detected in these conditions. This case of the policy is presented in Figure 3.

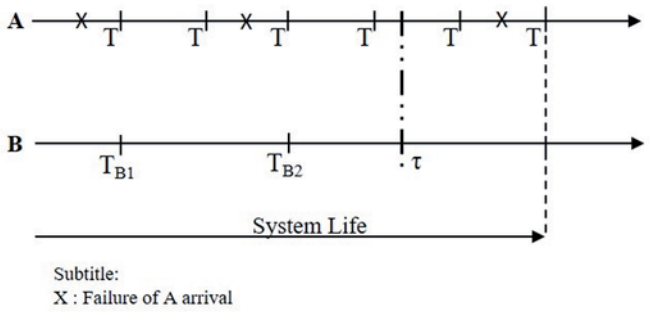

Fig. 3. Representation of the third case of the policy

The SL (equation 5) will be equal to the time of the k-th inspection of A, since it is greater than the time threshold τ, and for this to occur, the arrival time of the defect and the failure of A should be higher than the time of the last inspection. We could analyze the maintenance costs for this case, using the equation 6:

$$SL = T_k \; if \; q < N+1 \cap x > T_k > \mathrm{t} < y_A, k = 1,2,\ldots \tag{5}$$

$$C = \sum_{1}^{k} c1 + (q-1)(cp + c2) + cr \tag{6}$$

In equation 6, we do not consider the failure cost of B, because we are proposing PM when B reaches a certain age. Accordingly, the cost is composed of the sum of the inspection costs of A, $q - 1$ times the inspection costs of B, and the replacement cost of A (because in the last inspection of A, the system is replaced, therefore not needing to inspect B due to A is only changed). Besides that, the replacement cost of the system is added.

4. When to identify a defect in B

This case is characterized when a defect is found on component B through inspection, which is caused by a gradual mechanism of failure that characterizes it. Figure 4 represents this case in which we can identify the defect arrival and the system replacement being performed at T_{B3}.

The SL for this case can be represented in equation 7 below:

$$SL = T_k \; if \; q < N+1 \cap y_A \langle \mathrm{t} \rangle T_k \cap T_{B(q-1)} < x \le T_k < y_B, k = 1,2,\ldots \tag{7}$$

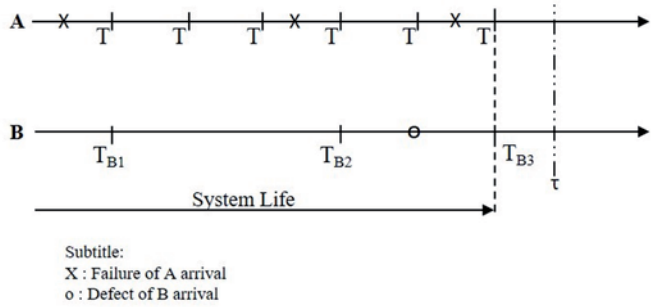

Fig. 4. Representation of the fourth case of the policy

Thus, the SL will be equal to the time of the last inspection of A, which will give an opportunity to carry out an inspection of B, and in that inspection, a defect in device B is found. In addition, it is necessary that the failure of B does not occur. The maintenance costs associated in this case can be expressed by the following equation:

$$C = \sum_{1}^{k} c1 + (q-1)cp + qc2 + c_r \tag{8}$$

It is possible to verify that the cost of an inspection in A is the sum k times the replacement cost of A, added $q - 1$ times, and the inspection cost of B is the sum of q times. This is due to the fact that during the last inspection of B, a defect is found, and therefore the whole system is replaced, not needing to replace only A. In addition, the system replacement cost is added given that there is no failure cost, because we are working with PM in this case.

According Scarf et al. [21], the search for the optimum value of the policy considering the cost minimization, can be calculated by dividing the expected value for the policy cost by the expected value of the cycle size. Thus, the present paper finds the expected value for the cost *E(C)* and the expected value to the size of the cycle *E(SL)* by a simulation process (in a free programming software), through the flowchart shown in Figure 5. In addition, we have used a process to optimize the three decision variables of the model: N (number of failures in A), T (time interval of inspections in A), and τ (threshold of system age), to minimize the total cost of maintenance.

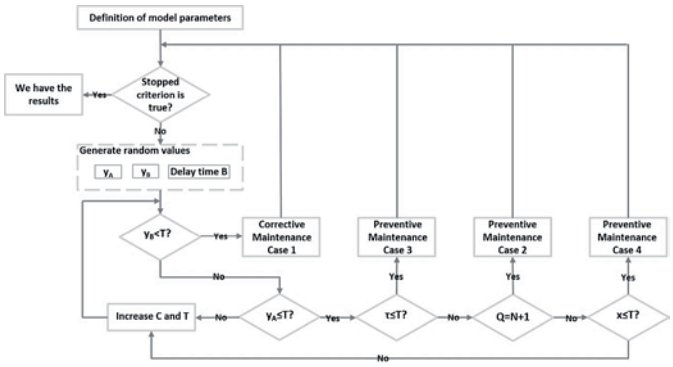

Fig. 5. Flowchart of the simulation process

3. Case Study

For this paper we consider a sugarcane plant, whose production of sugar is 40 tons by an hour. For the extraction of the broth of sugarcane, it is first necessary to perform a washing process, then it is minced and defibrated; generally, this set of operations is considered as the process of preparation of the raw material. A machine, namely a sugarcane shredder, is used to open a sugarcane cell, so that the extraction of the broth in the next step of the production process is carried out with greater efficiency.

The sugarcane shredder is formed by a rotor, to which a set of rotating hammers is attached, so as to force the passage of the sugarcane through a small aperture along a shredder plate. For this study, the set of hammers is called equipment A, whereas the rotor is called equipment B.

The system treated here involves the manufacturing process that uses a perishable raw material, the sugarcane, and as the time interval between the harvest and the beginning of processing increases, the quality of the processed product decreases. After 10 hours, the deterioration begins to have a much steeper curve. Thus, a system shut down by a failure in the set of the system that we are studying can cause a loss of production, both due to the loss of raw materials and the loss of production of the finished product. We can verify the need for periodic inspections of these systems.

A failure in component A may be caused by foreign materials entering with the sugarcane, which was not properly removed during the washing at the beginning of the process, in addition to the natural wear by the effort made by the hammers to defibrate the cane. This failure can generate excessive vibrations and imbalance due to the hammers, causing problems in other equipment such as oil pumps or the rupture of welds in pipes that may lead to loss of steam and oil, and can also cause the accumulation of mass on the sides of the equipment. So, these failures can be characterized by hidden failures, because it can only detected by an inspection on hammers.

Due to the structural dependency between the two components, a failure of the hammer opens an opportunity for the rotor to be inspected to check the existence of a defect. Whereas the failure of the rotor causes the total shutdown of the system, it is the equipment that causes the assembly to rotate for the passage of the sugarcane that will be defibrated. So, due to the characteristics cited above, like the significant failure mechanism, the maintenance cost significant and the dependency, this set is analyzed separately of the whole system.

So, some assumptions of the system are presented:

- The failure of equipment A occurs by an exponential distribution, with parameter λ_1, in which the unit of measurement of failure arrival is months;
- The defect of equipment B is a random variable X that occur by a Weibull distribution, with parameters η (scale) and β (shape), evaluated in months;
- The delay time of equipment B is a random variable H that occurs by an exponential distribution, with parameter λ_2 evaluated monthly;
- The failure of equipment B occurs by $y_B = x + h$;
- The inspections, for both equipment are perfect;
- The inspections times are not significant;
- A failure in equipment B is immediately identified and corrected by a replacement of new equipment, renewing the system;
- On the replacement of equipment B, the system is restored to a new condition.

For the more proper analysis of the maintenance policy shows here, some scenarios were created that are considered possible events in the system presented above. These scenarios can be characterized in this way:

Scenario 1: The failure of equipment A does not cause a loss of performance in the system. This is the general model of the policy, incurring costs according to what showed in the description previously presented.

Scenario 2: The failure in equipment A causes a loss of performance in the system. For this scenario, we consider that equipment A is working in a failure state, that is, there may be some hammer in the set that is not performing the job correctly, causing an accumulation of sugarcane in the corners, as well as not defibrating it correctly. This can result in a loss of quality and quantity of the final product, resulting in more maintenance-related costs.

Scenario 3: The failure in equipment A does not cause a loss of performance (or can be considered null given the low expressiveness), but the defect in equipment B causes a loss of performance. Because of this, the equipment will work much more in this state, with major costs being the penalty for this situation, for example, rotation set with minor velocity.

Scenario 4: The failure in equipment A causes a loss of performance and a defect in B, too.

The data corresponding to the parameters of the model were collected, and are summarized in Table 1. The units of measurement for the parameters related to time were months and for the monetary costs units per month ($/month).

The optimal results for the maintenance policy for the four scenarios is in Table 2.

Table 1: Values of the model parameters

Parameter	Value	Unit
c1	0.1cp	$/month
c2	0.5cp	$/month
cp	1	$/month
cr	10cp	$/month
cF	25cp	$/month
cdt	1	$/failure time
cB	10	$/defect time
λ_1	1	Failure/month
λ_2	0.66	Failure/month
η	5	
β	2	

For Scenario 1, the optimum policy will be dealing with a cost $4.759/month, doing periodic inspections in equipment A in a time interval of 0.9 months, where N would be equal to 4 and τ equal to 4.5 months. Therefore, for Scenario 2, in that the failure of A causes losses during the process, it is considered that the best policy would have a maintenance cost of $4.931/month, with inspection intervals of 0.4 months, where N would be equal to 9 and τ equal to 4.9 months. For Scenario 3, the optimum would be to have a maintenance cost of $5.856/month, and inspections should be done at intervals of 0.8 months, where N is equal to 3 and the limit of τ equal to 3.2 months. In addition, for Scenario 4, the best value of cost is $6.017/month, an inspection interval of A equal to 0.4 months, N equal to 7, and a threshold τ equal to 3.2 months.

Table 2. Results

	Scenario 1		Scenario 2		Scenario 3		Scenario 4	
	Cost (C*)	Parameters	Cost (C*)	Parameters	Cost (C*)	Parameters	Cost (C*)	Parameters
Values	4.759	T=0.9 N=4 τ=4.5	4.931	T=0.4 N=9 τ=4.9	5.856	T=0.8 N=3 τ=3.2	6.017	T=0.4 N=7 τ=3.2

With this, it is possible to identify when the failure of the hammer assembly results in an additional cost, such as a penalty for working

in a failure state, the expected optimum maintenance cost increases, and by contrast, the interval between inspections is shortened. This is because the cost of working with failed equipment is greater than the cost of doing the inspection, which is natural in these types of cases.

In addition, when analyzing an inclusion of cost penalties for the set of rotors to work in a defective state, there is an increase in the expected maintenance cost compared with the original model and the second scenario. This is because sometimes the system will operate with this set in the defective state, for the reason that this defect is only identified in an inspection. Therefore, the time between inspections that was 1.9 months in Scenario 1 decreases to 0.8 in Scenario 3, that is, equipment A (Hammers) is further inspected to provide more opportunities of inspections for equipment B (Rotor) to decrease this added penalty cost. By decreasing the inspection time interval, the amount of times the rotors are inspected may be higher.

If both sets of equipment are working poorly, in a failure state (for A) and in a defective state (for B), this generates additional costs, and the optimal cost expected for the policy increases considerably. The time between inspections decreases in only half a month, because of the fact that the inspection cost is well below the penalty cost.

4. Sensitive analysis

To analyze the variation of the optimal values of the policy, one of the fixed parameters was maintained and the other two were varied. The results of these variations are presented below.

Figure 7 presents a variation for the optimal values of the policy for Scenario 1. It is necessary to understand that the interval time between inspections is dependent on the time of τ and N, once there is sufficient time before τ so that $N + 1$ inspections can be carried out, as previously shown in policy description. In this way, when we change the N value for 3, the maximum time between inspections will be equal 1.1 months, and for N equal to 4, the time should be lower, until 0.7 months. It can be verified in Figure 6 that there is an apparent variation in the optimum expected cost of maintenance, with the variation of only one N for more and one for less. This is not so evident given the variation of the limit of τ, where the curves overlap.

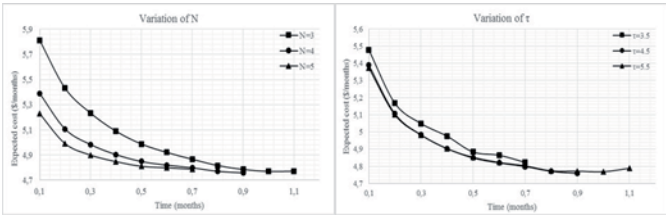

Fig. 6. Sensitive analysis of Scenario 1

As can be seen in Figure 7, the variation in Scenario 2 behaves differently than Scenario 1. By varying the value of N, the cost curves end up overlapping, with a very small variation in cost. When the value of τ is changed, a significant difference is observed when its value decreases, while when it increases, the expected value of the cost is very close to the optimum value. What we can observe is that despite the modifications, the lowest cost remains for the optimally presented value of T, N, and τ.

Behavior similar to this is observed in Scenario 4 (Figure 9). When you change the value to N, there is an overlap of the expected cost curves. While the variation of τ gives an apparent difference in the curve, especially for a smaller value.

Figure 8 shows the variation for the expected cost curves for Scenario 3, in which its behavior is similar to that presented in the Scenario 1 analysis. There is a distance between the curves for both the N variation and the variation of τ, but the latter when it is increased, is closer to the optimum curve.

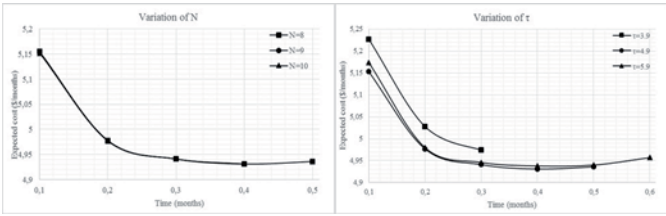

Fig. 7. Sensitivity Analysis of Scenario 2

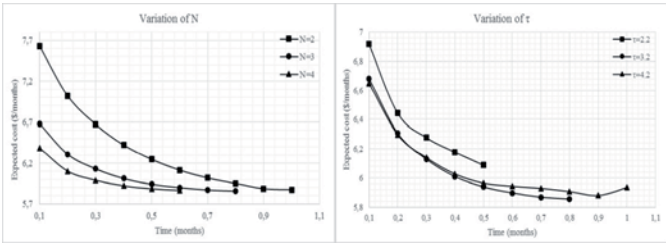

Fig. 8. Sensitivity analysis of Scenario 3

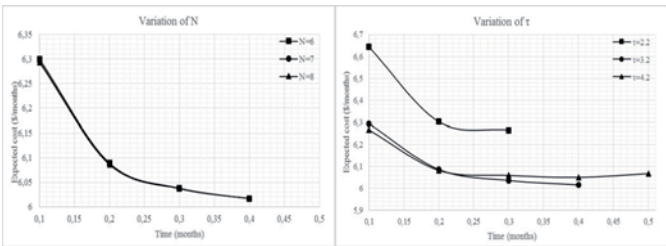

Fig. 9. Sensitivity analysis of Scenario 4

It should be emphasized that when there is a penalty cost, a greater variation in costs is obtained when the decision variables are modified. In addition, it should be noted that the curves have different sizes when related to T values, since the decision variables are related to each other; increasing or decreasing one of them implies restricting values to the others.

Table 3 shows the behavior of the model according to variations in its input parameters.

It can be emphasized that, as expected, when changing cost values (*cp*, *cB*, or *cdt*), only the maintenance cost value for the scenario in which this cost appears is modified. For example, by varying the value of the penalty cost of B, the behavior of the model remains the same for Scenarios 1 and 2, whereas for Scenario 3 when it is increased, a decrease in the time between inspections is observed as the limit τ. While for Scenario 4, the time between inspections remains the same, but the limit τ and N are decreased. A similar fact occurs in the variation for the cost penalty related to equipment A.

Also worth mentioning is the behavior related to parameter λ_1 that represents the number of failures that occur per month. When this quantity was increased, that is, if there were more failures of A in one month, it was observed that the expected cost of maintenance and the time between inspections suffered decay. It is believed that this occurs because since A fails more, there is greater opportunity to perform inspections in B, thus reducing the time it works in the defective state, in addition to preventing the occurrence of failure at the same time, which has a high cost impact for the model, whereas, the limit τ and N increased.

In relation to the variations made in the parameters of B, it can be verified that when β is increased there is a tendency to decrease the intervals between inspections, concentrating the maintenance actions in a shorter lifetime. This is due to the characteristics of this parameter, in that when increasing its value, they are more concentrated on the origin in the time axis and more elongated in the axis of the values. In relation to the scale parameter of the Weibull distribution that

Table 3. Behavior of model according variation of the parameters

PARAMETERS											SCENARIO 1				SCENARIO 2				SCENARIO 3				SCENARIO 4			
λ_1	λ_2	β	η	*c1*	c2	cp	cr	cF	cB	cdt	C*	T	τ	N	C*	T	τ	N	C*	T	τ	N	C*	T	τ	*N*
1	**0.66**	**2**	**5**	**0.1Cp**	**0.5Cp**	**1**	**10**	**25**	**10**	**1**	**4.759**	**0.9**	**4.5**	**4**	**4.931**	**0.4**	**4.9**	9	5.856	0.8	3.2	3	6.017	0.4	3.2	7
	0.5										4.418	1.4	5.7	3	4.606	0.4	5.7	10	5.649	0.8	3.2	2	5.816	0.4	3.6	7
	1										5.267	0.9	3.6	3	5.427	0.4	4	7	6.172	0.7	2.8	3	6.334	0.4	3.2	6
3											4.475	0.5	5.6	10	4.634	0.4	5.7	10	5.199	0.3	4.8	10	5.304	0.3	5.2	10
2											4.562	0.5	5.6	10	4.685	0.3	5.8	10	5.413	0.5	4	7	5.513	0.2	4.5	10
0.66											4.849	2.3	4.7	1	5.042	0.5	4	7	6.07	0.9	2.7	2	6.252	0.5	2.5	4
0.5											4.925	2.3	4.7	1	5.123	0.6	3.6	5	6.252	0.8	2.4	2	6.413	0.6	2.4	3
			4								5.62	2	4	1	5.888	0.5	4	7	6.999	0.8	2.4	2	7.18	0.5	2.5	4
			4.5								5.168	2.2	4.5	1	5.36	0.4	4.4	10	6.361	0.7	2.8	3	6.539	0.3	3	9
			5.5								4.417	1	5.1	4	4.568	0.5	5.6	10	5.428	0.6	3.6	5	5.571	0.4	3.6	6
			6								4.09	0.8	5.7	6	4.232	0.3	5.8	10	5.032	0.7	3.5	4	5.171	0.4	4	9
		1.5									5.574	1.3	5.3	3	6.926	0.7	5.7	7	8.342	1	4	3	8.553	0.5	4.5	8
		2.5									4.292	0.8	4	4	4.443	0.4	4.4	8	5.206	0.7	2.8	3	5.361	0.4	3.2	7
		3									4.024	0.8	4	4	4.159	0.3	4.2	10	4.817	0.6	3	4	4.96	0.5	3	5
						0.5					2.373	1.2	4.9	3	2.502	0.3	5.2	10	3.376	0.6	2.4	3	3.508	0.3	2.7	7
						2					9.493	0.9	4.5	4	9.706	0.6	4.9	7	10.644	0.9	3.6	3	10.854	0.6	3.6	5
						3					14.265	0.9	4.5	4	14.491	0.8	4.9	5	15.445	0.8	4	4	15.665	0.8	4	4
									5		4.755	0.9	4.5	4	4.922	0.4	4.9	9	5.322	0.9	3.6	3	5.496	0.4	4	9
									15		4.755	0.9	4.5	4	4.922	0.4	4.9	10	6.315	0.7	2.8	3	6.482	0.4	2.8	6
										0.5	4.755	0.9	4.5	4	4.853	0.5	5.1	9	5.84	0.8	3.2	3	5.943	0.3	3	5
										5	4.755	0.9	4.5	4	5.179	0.2	5.3	10	5.84	0.8	3.2	3	6.292	0.2	3.6	9

represents the arrival of the defect for this equipment, a standard in the modification of the results regarding the decision variables is not observed. This can be a result of the randomness characteristic of the distribution, although decreasing the value of η shows an increase in maintenance costs, since the arrival of the defect of B occurs before, and a decrease in that cost when this parameter is increased.

Still evaluating parameters related to equipment B we have λ_2, which represents the mean time between the arrival of the defect and the failure of this equipment through an exponential distribution. It can then be verified that as the arrival time of the fault increases, the maintenance cost decreases and, generally, the interval between inspections increases, as well as the limit τ. In relation to N, sometimes it holds and other times it decreases, because it is dependent on the values of the other decision variables as justified above.

5. Conclusion

The present paper showed maintenance based on random maintenance policy and simulation. It was possible verify that when a penalty cost is involved, the time required to perform a periodic inspection in the components is lowered, and consequently, the expected maintenance costs for the policy are higher. It was verified that the results obtained through a simulated procedure of parameters are satisfactory and occurs as expected, thus emphasizing the possibility of producing models for maintenance policies using simulated processes.

This was verified by applying the model in a real case, in which the behavior of this model was evaluated and tested. This real evaluation is important because it can be said that when the costs deal with large amounts of money, any savings realized could be a gain for the company, even gains that are not measurable such as consumer satisfaction through non-fulfillment of rework.

In the future, it is possible to suggest the aggregation of this model with other types of analysis, such as spare parts, besides considering imperfect maintenance through inspection failures.

Acknowledgements

The authors of the paper thank for CAPES – Coordenação de Aperfeiçoamento de Pessoal de Nível Superior – for the financial support to the research, and FAPEMA – Fundação de Amparo à Pesquisa e ao Desenvolvimento Científico e Tecnológico do Maranhão.

References

1. Alaswad S, Xiang Y. A review on condition-based maintenance optimization models for stochastically deteriorating system. Reliability Engineering & System Safety 2017; 157: 54-63, https://doi.org/10.1016/j.ress.2016.08.009.
2. Alrabghi A, Tiwari A. State of the art in simulation-based optimisation for maintenance systems. Computers & Industrial Engineering 2015; 82: 167-182, https://doi.org/10.1016/j.cie.2014.12.022.
3. Alrabghi A, Tiwari A. A novel approach for modelling complex maintenance systems using discrete event simulation. Reliability Engineering & System Safety 2016; 154: 160-170, https://doi.org/10.1016/j.ress.2016.06.003.
4. Babishin V, Taghipour S. Optimal maintenance policy for multicomponent systems with periodic and opportunistic inspections and preventive

replacements. Applied Mathematical Modelling 2016; 40: 10480-10505, https://doi.org/10.1016/j.apm.2016.07.019.
5. Chen N, Ye Z-S, Xiang Y, Zhang L. Condition-based maintenance using the inverse Gaussian degradation model. European Journal of Operational Research 2015; 243:190-199, https://doi.org/10.1016/j.ejor.2014.11.029.
6. Chung C A. Simulation modelling handbook: a practical approach. United States of America: CRC Press LLC, 2004.
7. Dao C D, Zuo M. J. Selective maintenance of multi-state systems with structural dependence. Reliability Engineering & System Safety 2017; 159: 184-195, https://doi.org/10.1016/j.ress.2016.11.013.
8. Darghouth M N, Chelbi C, Ait-kadi D. A profit assessment model for equipment inspection and replacement under renewing free replacement warranty policy. International Journal of Production Economics, 2012; 135: 899-906, https://doi.org/10.1016/j.ijpe.2011.10.029.
9. Dieulle L, Bérenguer C, Grall A, Roussignol M. Sequential condition-based maintenance scheduling for a deteriorating system. European Journal of Operational Research 2003: 150: 451-461, https://doi.org/10.1016/S0377-2217(02)00593-3.
10. Ding S-H, Kamaruddin S. Maintenance policy optimization—literature review and directions. International Journal of Advanced Manufacturing Technology 2015; 76:1743-1756, https://doi.org/10.1007/s00170-014-6341-2.
11. Duffua S O, Ben-Day M, Al-Sultan K S, Andijani A A. A generic conceptual simulation model for maintenance system. Journal of Quality in Maintenance Engineering 2001; 7: 207-219, https://doi.org/10.1108/13552510110404512.
12. Geng J, Azarian M, Pecht M. Opportunistic maintenance for multi-component systems considering structural dependence and economic dependence. Journal of Systems Engineering and Electronics 2015; 26: 493-501, https://doi.org/10.1109/JSEE.2015.00057.
13. Golmakani H R, Moakedi H, Optimal nonperiodic inspection scheme for a multicomponent repairable system with failure interaction using A* search algorithm. International Journal of Advanced Manufacturing Technology 2013; 67: 1325-1336, https://doi.org/10.1007/s00170-012-4569-2.
14. Jardine A T J, Banjevic D. Optimizing condition-based maintenance decisions for equipment subject to vibration monitoring. Journal of Quality in Maintenance Engineering 1999; 5: 192-202, https://doi.org/10.1108/13552519910282647.
15. Laggoune R, Chateauneuf B, Aissania D. Opportunistic policy for optimal preventive maintenance of a multi-component system in continuous operating units. Computers & Chemical Engineering 2009; 33: 1499-1510, https://doi.org/10.1016/j.compchemeng.2009.03.003.
16. Lam J Y J, Banjevic D. A myopic policy for optimal inspection scheduling for condition based maintenance. Reliability Engineering & System Safety 2015; 144: 1-11, https://doi.org/10.1016/j.ress.2015.06.009.
17. Nourelfath M, Nahas M, Ben-Daya M. Integrated preventive maintenance and production decisions for imperfect processes. Reliability Engineering & System Safety 2016; 148: 21-31, https://doi.org/10.1016/j.ress.2015.11.015.
18. Rezg N, Chelbi A, Xie X-L. Modelling and optimizing a joint buffer inventory and preventive maintenance strategy for a randomly failing production unit: analytical and simulation approaches. International Journal of Computer integrated Manufacturing 2005, 18: 225-235, https://doi.org/10.1080/0951192052000288152.
19. Sahraoui Y, Khelif R, Chateauneuf A. Maintenance planning under imperfect inspections of corroded pipelines. International Journal of Pressure Vessels and Piping 2013; 104: 76-82. https://doi.org/10.1016/j.ijpvp.2013.01.009
20. Scarf P A, Cavalcante C A V. Modelling quality in replacement and inspection maintenance. International Journal of Production Economics 2012; 135: 371-381, https://doi.org/10.1016/j.ijpe.2011.08.011.
21. Scarf P A, Cavalcante C A V, Dwight R A, Gordon P. An Age-Based Inspection and Replacement Policy for Heterogeneous Components. IEEE Transactions on reliability 2009; 58: 641-648, https://doi.org/10.1109/TR.2009.2026796.
22. Taghipour S, Banjevic D. Periodic Inspection Optimization Models for a Repairable System Subject to Hidden Failures. IEEE Transactions on Reliability 2011; 60: 275-285, https://doi.org/10.1109/TR.2010.2103596.
23. Thomas L C. A Survey of Maintenance and Replacement Models for Maintainability and Reliability of Multi-Item Systems. Reliability Engineering 1986; 16: 297-309, https://doi.org/10.1016/0143-8174(86)90099-5.
24. Yang L, Ma X, Zhai Q, Zhao Y. A delay time model for a mission-based system subject to periodic and random inspection and postponed replacement. Reliability Engineering & System Safety 2016; 150: 96-104, https://doi.org/10.1016/j.ress.2016.01.016.
25. Yan H-C, Zhou J-H, Pang C K. Machinery Degradation Inspection and Maintenance Using a Cost-Optimal Non-Fixed Periodic Strategy. IEEE Transactions on Instrumentation and Measurement 2016; 65: 2067-2077, https://doi.org/10.1109/TIM.2016.2563998.
26. Zhang J, Huang X, Fang Y, Zhou J, Zhang H, Li J. Optimal inspection-based preventive maintenance policy for three-state mechanical components under competing failure modes. Reliability Engineering & System Safety 2016; 152: 95-103, https://doi.org/10.1016/j.ress.2016.02.007.
27. Zhang X, Zeng J. A general modelling method for opportunistic maintenance modelling of multi-unit systems. Reliability Engineering & System Safety 2015; 140: 176-190, https://doi.org/10.1016/j.ress.2015.03.030.
28. Zhao L, Chen M, Zhou D. General (N, T, τ) Opportunistic Maintenance for Multicomponent Systems With Evident and Hidden Failures. IEEE Transactions on Reliability 2016; 65: 1298-1313, https://doi.org/10.1109/TR.2016.2570547.
29. Zhao X, Al-Khalifa K N, Nakagaw T. Approximate methods for optimal replacement, maintenance, and inspection policies. Reliability Engineering & System Safety 2015; 144: 68-73, https://doi.org/10.1016/j.ress.2015.07.005.
30. Zhu W, Fouladirad M, Bérenguer C. Condition-based maintenance policies for a combined wear and shock deterioration model with covariates. Computers & Industrial Engineering 2015; 85:268-283, https://doi.org/10.1016/j.cie.2015.04.005.

Mônica Frank MARSARO
Department of Mechanical and Production Engineering
State University of Maranhão – UEMA
University City Paulo VI – post office box 09, São Luís – MA – Brazil – Zip Code: 65055-970

Cristiano Alexandre Virgínio CAVALCANTE
Department of Production Engineering
Federal University of Pernambuco – UFPE
Professor Moraes Rego Avenue, 1235 – University City, Recife – PE – Brazil – Zip Code: 50670-901

E-mails: mmarsaro@gmail.com, cristianogesm@gmail.com

Article citation info:
EKIELSKI A, ŻELAZIŃSKI T, DURCZAK K. The use of wavelet analysis to assess the degree of wear of working elements of food extruders. Eksploatacja i Niezawodnosc – Maintenance and Reliability 2017; 19 (4): 560–564, http://dx.doi.org/10.17531/ein.2017.4.9.

Adam EKIELSKI
Tomasz ŻELAZIŃSKI
Karol DURCZAK

THE USE OF WAVELET ANALYSIS TO ASSESS THE DEGREE OF WEAR OF WORKING ELEMENTS OF FOOD EXTRUDERS

WYKORZYSTANIE ANALIZY FALKOWEJ DO OCENY STOPNIA ZUŻYCIA ELEMENTÓW ROBOCZYCH EKSTRUDERÓW SPOŻYWCZYCH*

The paper presents the evaluation of the wear status of the single-screw extruder working elements on the basis of die pressure and screw load toque load values changes. The changes of this parameters were analyzed as frequency spectrum using the tools of wavelet analysis. In the study plan the hypothesis was formulated that the assessment of extruder elements wear level is possible through observation of the frequency of process parameters changes. Due to the dynamic characteristics of the process in the determination of natural frequencies Morlet wavelet transform was used. Research was carried out for three heights of longitudinal wedges: 4, 2 and 1 mm. During experiment the extruder drive line load and the extruder screw speed were changed. It has been found that based on the observation of changes in resonant frequencies, it is possible to accurately assess the wear degree of friction elements in a single screw extruder. Moreover, it has been noted that the wavelet analysis may be an effective tool for the assessment of the extruder working elements wear level.

***Keywords**: wavelet analysis, Short Time Fourier Transformation, Continuous Wavelet Transformation, extruder barrel.*

W pracy przedstawiono ocenę stanu zużycia elementów roboczych ekstrudera jednoślimakowego na podstawie obserwacji zmian składowych częstotliwościowych widma obciążenia układu napędowego ślimaka ekstrudera i ciśnienia w matrycy przy wykorzystaniu narzędzi analizy falkowej. W planie badań sformułowano hipotezę, że możliwa jest ocena stopnia zużycia elementów roboczych ekstrudera przez obserwację częstotliwości zmian parametrów procesowych. Ze względu na dynamiczne cechy procesu przy wyznaczeniu częstotliwości własnych wykorzystano falkę Morlet'a. Badania przeprowadzono dla trzech wysokości klinów wzdłużnych 4, 2 i 1 mm. Podczas eksperymentu zmieniano obciążenia ekstrudera oraz prędkość obrotową ślimaka. Stwierdzono, że na podstawie obserwacji zmian częstotliwości rezonansowych można precyzyjnie oszacować stopień zużycia elementów ciernych w ekstruderze jednoślimakowym. Ponadto zaobserwowano, że analiza falkowa może być skutecznym narzędziem oceny stopnia zużycia elementów roboczych ekstrudera.

***Słowa kluczowe**: analiza falkowa, STFT, skalogram CWT,cylinder ekstrudera.*

1. Introduction

The extrusion treatment of food products is one of the most popular production processes of processing starch in the processing industry [12]. The principal process parameters of this process are the die pressure and temperature profile inside the extruder barrel. Those operational parameters have further significant influence on the extruder drive line load [10]. From the technological point of view the outlet die pressure in screw extruders is a function dependent on extrusion process parameters such as: raw material type and their moisture, screw configuration and wear of extruder working elements (screws, barrel) [3, 8]. The outlet die pressure also impacts the quality parameters of obtained products, thus maintaining the stable pressure value level during whole process time is a key factor in industrial production processes. During proper operation of extruder working elements and with constant process parameters, the pressure value change should impact the extruder drive line load change. Pressures generated inside of an extruder barrel are however result variables, which depend on the extrusion process parameters and work quality of extruder elements, among others the wear level of those elements. In single screw extruders transport properties depend on friction forces difference between friction generated by transported material and inner barrel surface from one side and friction generated by transported material and screw surface other side.

Transported material will be able to move along the barrel, only when tangent friction force of the material on inner barrel surface will be greater than the tangent friction force of the material on a screw surface [14]. This is of key importance, both for extrusion process stability and the quality of final products. In case of single screw extruders to ensure the good transport conditions, the grooves milled are done on the inner surface of barrel or in longitudinal trapezoidal shape channels longitudinal wedges are mounted. Both mentioned solutions may be used to improve friction between moved material and barrel surface.

In the observed extruder, constructors used the second solution to improve friction - he mounted longitudinal wedges made from a hard cast steel on the inner barrel surface [Fig.1]. During working the working wedges are gradually being worn down, and along with the reduction of their height, extruder transport properties get worse. As a consequence, this leads to the worsening of the quality of the extrudated product.

(*) Tekst artykułu w polskiej wersji językowej dostępny w elektronicznym wydaniu kwartalnika na stronie ***www.ein.org.pl***

Currently, the measurement of absolute height of wedges during standard check procedures is the effective method, but for many cases this leads to premature replacement (or regeneration) of the extruder barrel. That procedures are the result of lack of the reliable methods to estimate the influence of wear degree of the extruder wedges on transport properties.

There are methods of verification of their wear level in the literature, however, usually they refer to specific, homogenous materials. For technological reasons, the information on transport properties of the extruder would be important, also for more diverse materials.

Each element or set elements has got their own vibration frequencies which is called "natural frequency". The frequency generated resulting from the shape extruder elements and operating conditions [4, 6]. Extruder load parameters presented as: screw load torque variation and die outlet pressure fluctuations have been shown to depend on working mechanical elements cooperation, the amount and features of treated materials. Thus, in studies of this type hitherto carried out, for the analysis of signals, the Fast Fourier transformation (FFT) was used to extract the frequency components of the process parameters fluctuation [5, 11]. The Fourier transformation, specially FFT is the most common technique used in signal analysis, but FFT assumes that measured signal is stationary, which, in case of non-stationary processes leads to the loss of the information about signal frequency changes in the time domain. The cyclic Fourier transformation have been more reliable method of analysis of non-stationary signal than pure FTT, its procedure consists in segmenting the observed signal into narrow time intervals and then, using the FFT for each range of measured signals.

For that reasons the signal spectrum was observed in the narrow range of time window. The presented method called windowing has been proposed by Gabor [9]. The windows adjacent to each other allow to observe the frequency signal spectrum within time domain. That transformation called Short Time Fourier Transformation (STFT), shows the measured signal frequency spectrum for 3D coordinates: frequency and time [2]. The serious disadvantage of STFT method is the compromise with respect to window size selection, to find non-stationary signal features (then the window should be as narrow as possible), on the other hand, the narrow window size caused the loss of information about the low signal frequencies. So for better frequency resolution the window size should be longer in the time domain.

The main drawback of the constant size window as mentioned is possibility of loss of frequency and time information, so a lot of measure signals need another methods, one of the ways is to employ the changeable window size and overlap windows method. Complementary to the method described above is continuous wavelet transformation (CWT), the CWT uses a window technique also but with variable size windows [13, 15]. The CWT allows the use of large (long time) windows where low frequency signals are treated or small- shorter time windows where high frequency signals are sought for. Owing to the CWT features, some essential information will be found during observation of the non-stationary signals, ignored by other measurement methods, such as: the failure points, discontinuities of higher derivatives or self-similarity [1].

The aim of this work was to present the assessment of wear level of the extruder working elements (height of barrel wedges). The wedges height were evaluated by means of wavelet continuous transformation of the extruder screw load toque and die pressure oscillation.

2. Materials and methods

Measurements were carried out using frequency component of the relative extruder die pressure changes and screw load torque fluctuation. The object of the study was the extrusion process of corn grit processed in the KZM-2 single screw food extruder. The processed corn grit moisture was 14%. Extruder barrel temperatures settings were fixed at: 130, 110, and 80°. The technical data of KZM-2 extruder are shown in Table 1.

Table 1. KZM-2 single screw extruder specification, basic data

ID	Parameter	
1.	Drive motor power	22 (kW)
2.	Extruder screw speed n	200÷500 rpm^{-1}
3.	Die diameter	5 mm
4.	Length to screw diameter ratio L/D	6:1
5.	Compression degree	1.5

The longitudinal grooves on inner extruder barrel surface are used to lock the trapezoidal cross-section longitudinal wedges [Fig.1].

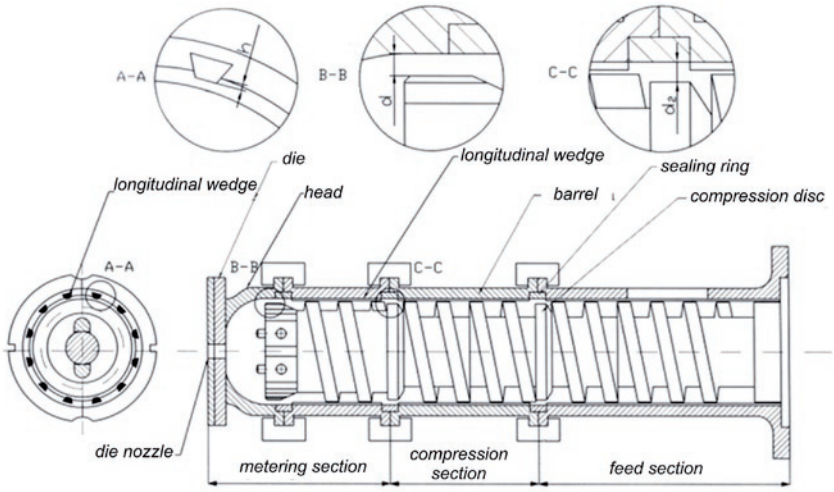

Fig. 1. Diagram of the working part of the extruder KZM-2 [7]

For the acquisition of measurement data (pressure in the matrix and extruder drive line load) National Instruments set was used (measurement sheet – PCI-6024E, module NI SCXI-100 and NI SCXI-1302) and LabView 7.1 software. Data was recorded in 10 Hz frequency.

Wedges protruding beyond the surface of the wall form characteristic grooves. The height of the longitudinal wedges h [Fig. 1, section A-A] was differentiated by replacement of wedges to elements enabling to obtain diversification of friction against inner surface of the extruder barrel. Research was carried out for three working wedges of the extruder: 4, 2 and 1 mm. Also extruder load was changed by means of increase of the mass of the input raw material in time (from 50 $kg \cdot h^{-1}$ to 80 $kg \cdot h^{-1}$) and screw rotation speed (from 200 rpm^{-1} to 300 rpm^{-1}).

For data analysis the continuous wavelet transform (CWT) analysis was used, which analysis was performed using the algorithm realised at the Matlab platform. Wavelet analysis consists in matching the courses of the basic wavelet courses to the course of the examined signal $x(t)$. CWT transformation was also described with an equation (1), [15]:

$$CWT_x^{\psi}(a,b) = W(a,b) = \frac{1}{\sqrt{a}} \int_{-\infty}^{\infty} x(t) \cdot \psi^* \left(\frac{t-b}{a} \right) dt \qquad (1)$$

where:

a – scale,
b – wavelet shift,
ψ – mother wavelet.

Final effect of CWT transform is the obtaining of values of wavelet coefficients A, dependent on the value of scale a and shift b of the mother wavelet. Value of coefficient A determines the matching ratio of the wavelet imposed on a signal to the course of the examined signal. Its higher values means better matching ratio. Monitoring of the coefficient A value change within time domain and frequency enables the observation of non-standard frequencies occurring during the operation of the device.

Research results are presented in diagrams in the form of scaleograms, i.e. wavelet maps. Due to simplified method of generation, Morlet wavelet has been used here.

3. Results and discussion

In Figure 2, the course of changes of pressure and drive line load using the wedges with height of $h = 4$ mm (unused wedges) has been presented.

Drive line load presents the value of the aggravating moment of the extruder shaft in relations to the value of the moment causing the disconnection of the drive through overload clutch.

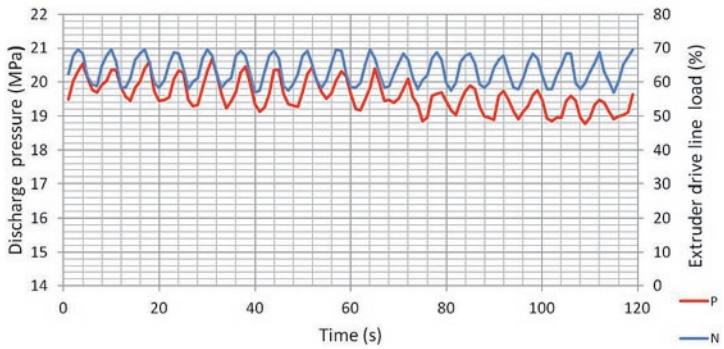

Fig. 2. The course of changes in the pressure P and the load drive system extruder N during constant speed snail n = 200 rpm and the intensity of the feedstock Q = 55 kg·h^{-1}; the height of the grooves inside the housing extruder h = 4 mm

It has been ascertained that in these conditions, both the pressure values and drive line load of the machine have stable course. Moreover, the course of both diagrams is similar, which means that this is the correct character of extruder operation, which is dependent both on construction features of the device and the process parameters set forth at the beginning.

When using barrels, wedges of which were worn in 50% ($h = 2$ mm), clear differences in the course of pressure values change have been noted [Fig. 3].

Thus, in order to change the parameters of the material course within the device, the rotational speed of the extruded was increased. Increase of the rotational speed of the screw is a typical reaction of the device operation, enabling to extend the operation time of the extruder. In case of starch products, too high wedges (more than 4 mm) as well as too low ones (less than 1 mm) are disadvantageous. When the wedges profile is too high, it gets glued by the material, and if it is too low – too low friction against transported material occurs. Manufacturer of the examined extruder model recommends regeneration of its sleeve or replacement of wedges, if the wedges height is smaller than 1 mm. However, in case of material with high value of coefficient of friction against the barrel, the correct operation of the extruder, even with the lower wedges profile, is possible. Unfortunately, in case of extrusion of the raw materials compounds, very often it can be stated only after the process is initiated.

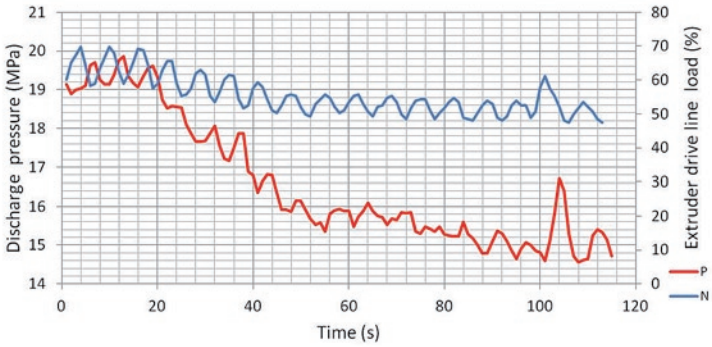

Fig. 3. Number of changes in the pressure P and the extruder drive system load N at which a transient state when changing the screw speed from 200 rpm to 300 rpm and at a constant flow of the feedstock ratio Q = 55 kg·h^{-1}; the amount of grooves within the housing of the extruder h = 2 mm. snail n = 200 rpm and the intensity of the feedstock Q = 55 kg·h^{-1}; the height of the grooves inside the housing extruder h = 4 mm

Experienced operator may define the status of such process and assess further transport possibilities of the extruder by observing the process course. Thus, it can be assumed that it is possible to determine the current status of the transporting system through analysis of the frequency of oscillations of the torque value changes loading the transporting screw drive shaft.

Results of wavelet analysis depicting the changes of the scale (CWT) in the function of time and value of the oscillations interval at different settings of the extrusion process parameters have been shown in figures. The diagrams present the results of the wavelet analysis for the drive line load of the extruder N and changes of the pressure values P. Analysing diagrams 4a and 4b it has been noted that both, for the courses of changes of pressure frequencies and drive line load, no frequency with long oscillations interval has been observed.

Thus, the observed oscillations referred mainly to the changes within the scope og high frequencies , which could also constitute so called "noises". Also no change in the frequency at the change of load has been observed. In the 4b diagram ($n = 300$ rpm^{-1}) frequency spectrum moved towards lower values (longer interval). With these settings of the extruder, it has been noted that both, the change of the drive line load of the extruder, resulting from the change of the mass flow of the raw material supplied to the extruder and the change of the rotational speed, did not negatively affect the course of the extrusion process. Such course of the pressure changes is confirmed by the correctness of the process handling.

The use of barrels with wedges worn in 50% ($h = 2$ mm) caused significant changes in the course of wavelet diagrams [Fig. 5a and 5b].

In the lower part of the diagram, the oscillations interval equalling ca. 64 s may be observed; this interval occurs at the mass raw material flow of 55 kg·h^{-1}. Increase of the mass flow of the raw material to 80 kg·h^{-1} causes the disappearance of these frequencies. Such course of changes was observed for frequency changes P and N at two extruder screw speeds.

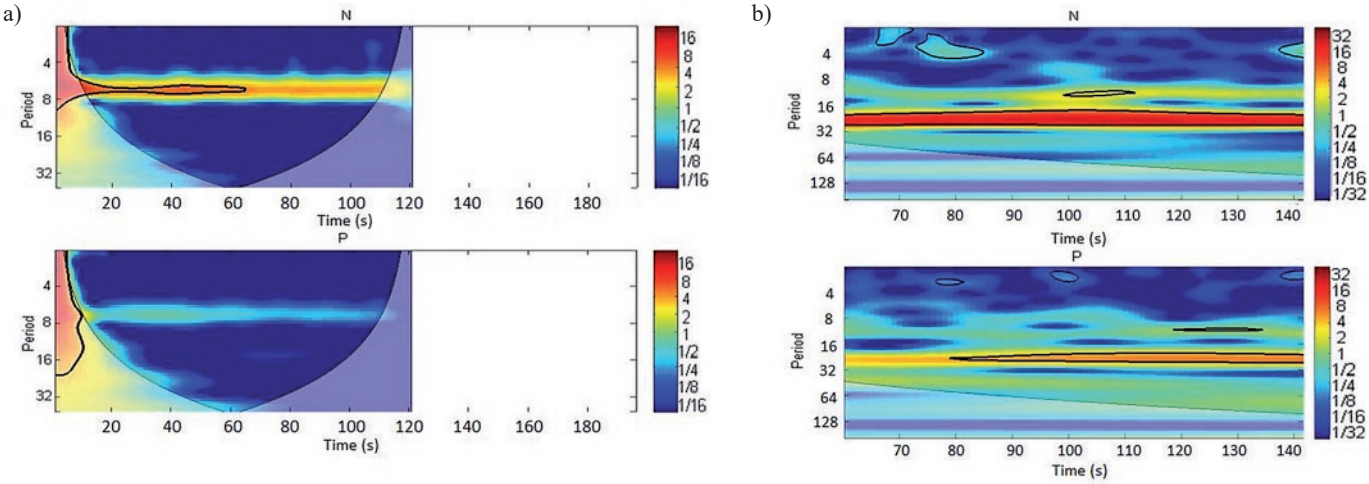

Fig. 4. Scaleogram CWT. h = 4 mm, change in a load of 50 kg·h^{-1} to 80 kg·h^{-1} feed material: a) 200 rpm, b) 300 rpm

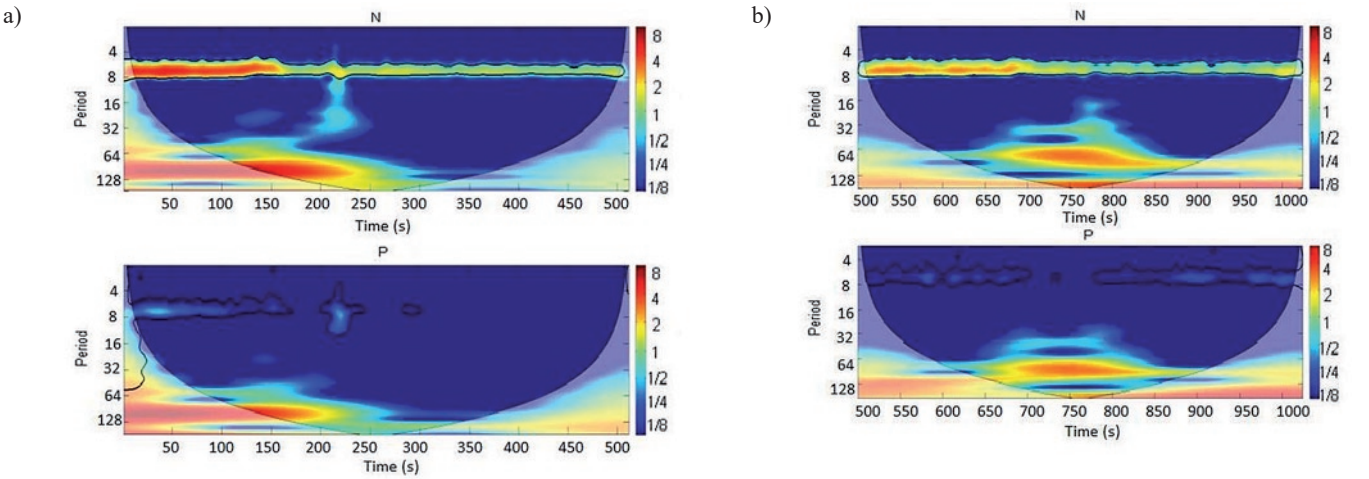

Fig. 5. Scaleogram CWT. h = 2 mm, change in a load of 50 kg·h^{-1} to 80 kg·h^{-1} feed material: a) 200 rpm, b) 300 rpm

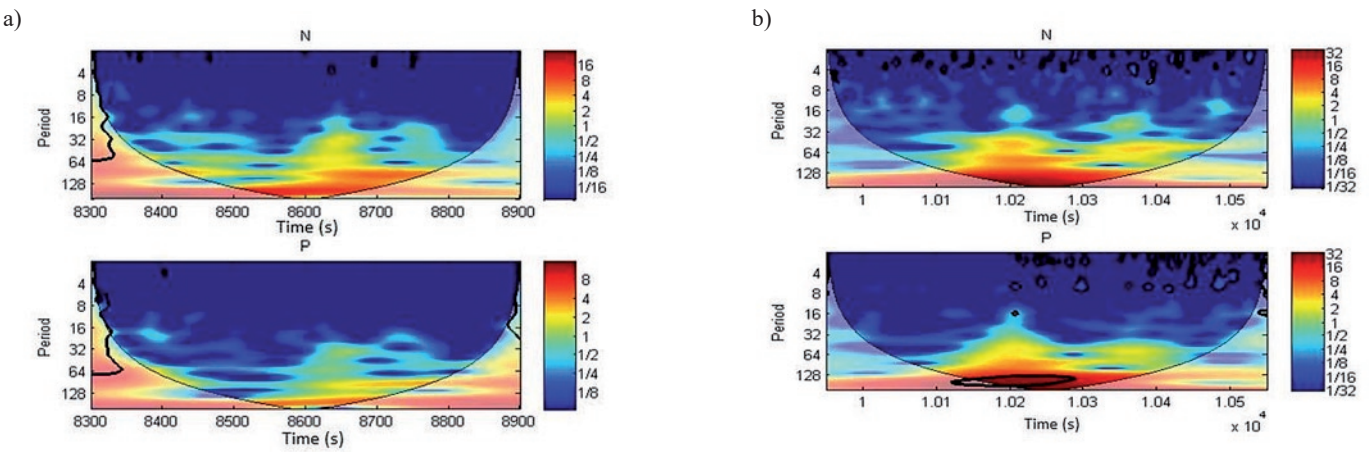

Fig. 6 Scaleogram CWT. h = 1 mm, change in a load of 50 kg·h^{-1} to 80 kg·h^{-1} feed material: a) 200 rpm, b) 300 rpm a) 200 rpm, b) 300 rpm

When using the extruder barrels with wedges of 1 mm in height, it has been noted that short-term oscillations disappeared [Fig. 6a and 6b].

In the examined case, the spectrum with high correlation with studied wavelets may be clearly observed within the scope of long-term oscillations equalling ca. 120 s. Increase of the rotational speed of the screw drive shaft causes the increase of the matching degree of the spectrum to the basic wavelet course. Just as in the diagrams above, changes of values *P* and *N* have similar courses.

To simulate the greater wear level of the operating wedges of the extruder barrel, in point marked as 1.07 [Fig. 7], 2% of the vegetable fat has been added.

A clear frequency changes spectrum within the scope of long-term oscillations connected with the disappearance of the transport proper-

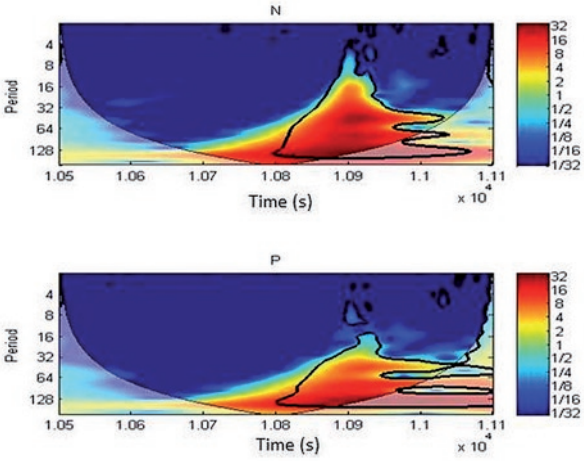

Fig. 7. Scaleogram CWT. h = 1 mm, load of 80 kg·h-1 feed material, 300 rpm

ties of the extruder, may be observed. Such course suggests that in the case of further wear of operating wedges of the extruder, it will be possible to note clearer process frequencies changes.

4. Conclusions

Based on the performed study, the following conclusions have been formulated:

1. Wavelet analysis may be an effective tool for assessment of wear level of operational elements of the extruder (operational wedges).
2. Based on the observation of changes in resonant frequencies, the wear level of friction elements in the single-screw extruder may be assessed.
3. Along with the reduction of height of the working wedges, resonant frequency decreases. At the 2 mm high wedges, the oscillations with an interval of 64 s appear in the spectrum. Oscillations' intensity decreases and it disappears in case of further wear of the wedges. In case of critical (h=1mm) wear of friction elements, oscillations interval exceeded 64 s with a tendency for further growth to ca. 128 seconds [Fig. 6]. Particularly good matching of the native wavelet within the interval of 64 to 126 s took place during long-term work with considerable load [Fig. 7]. Typical measured value of the oscillations interval of the fitted basic wavelet for new elements did not exceed 8-12 s.

References

1. Abu-Zahra N, Seth A. In-process density control of extruded foam PVC using wavelet packet analysis of ultrasound waves. Mechatronics 2002; 12(9), 1083-1095, https://doi.org/10.1016/S0957-4158(02)00016-8.
2. Balazs P, Bayer D, Jaillet F, Søndergaard P. The pole behavior of the phase derivative of the short-time Fourier transform. Applied and Computational Harmonic Analysis 2016; 40(3): 610-621, https://doi.org/10.1016/j.acha.2015.10.001.
3. Bouzaza D, Arhaliass A, Bouvier J M. Die design and dough expansion in low moisture extrusion-cooking process. Journal of Food Engineering 1996; 29(2): 139-152, https://doi.org/10.1016/0260-8774(95)00076-3.
4. Burdzik R. Implementation of multidimensional identification of signal characteristics in the analysis of vibration properties of an automotive vehicle's floor panel. Eksploatacja i Niezawodnosc – Maintenance and Reliability 2014; 16 (3): 458–464.
5. Cremer D R, Kaletunç G. Fourier transform infrared microspectroscopic study of the chemical microstructure of corn and oat flour-based extrudates. Carbohydrate Polymers 2003; 52(1): 53-65, https://doi.org/10.1016/S0144-8617(02)00266-7.
6. Ding Y, He W, Chen B, Zi Y, Selesnick I. W. Detection of faults in rotating machinery using periodic time-frequency sparsity. Journal of Sound and Vibration 2016; 382: 357-378, https://doi.org/10.1016/j.jsv.2016.07.004.
7. Ekielski A, Majewski Z. Effect of dimension of selected elements of the single screw extruder on energy consumption in the maize grit extrusion process. Materiały IX Międz. Kongr. Mech. I Energii w Roln. 2005: 27-29.
8. Ekielski A, Osiak J. Wpływ stopnia zużycia elementów ekstrudera na wybrane parametry ekstruzji. Inżynieria Rolnicza 2003; 7(49): 39-46.
9. Gabor D. Theory of communication, Journal IEE 1947; Vol.93: 429-457, https://doi.org/10.1049/ji-1.1947.0015.
10. Janssen L P B M, Moscicki L, Mitrus M. Energy aspects in food extrusion-cooking. International Agrophysics 2002; 16(3): 191-196.
11. Kaito A, Kyotani M, Nakayama K. Applications of fourier transform infrared microspectroscopy to the analysis of microscopic orientation in liquid crystalline polymer sheets. Polymer 1992; 33(13): 2672-2678, https://doi.org/10.1016/0032-3861(92)90437-2.
12. Pérez A A, Drago S R, Carrara C R, De Greef D M, Torres R L, González R J. Extrusion cooking of a maize/soybean mixture: Factors affecting expanded product characteristics and flour dispersion viscosity. Journal of Food Engineering 2008; 87(3): 333-340, https://doi.org/10.1016/j.jfoodeng.2007.12.008.
13. Storath M, Demaret L, Massopust P. Signal analysis based on complex wavelet signs. Applied and Computational Harmonic Analysis 2015.
14. Thewessen A, Moraru C I, Kokini J L. Effects of fats with different melting points on starch extradite expansion and comparison with microwave expansion. In IFT Annual Meeting Book of Abstracts 2002; 15-19.
15. Wrana B, Czado B. Zastosowanie transformaty falkowej do określenia defektów pali. Górnictwo i Geoinżynieria 2010; 34: 647-653.

Adam EKIELSKI
Tomasz ŻELAZIŃSKI
Department of Production Management and Engineering
Warsaw University of Life Sciences
ul. Nowoursynowska 164, 02-787 Warsaw, Poland

Karol DURCZAK
Institute of Biosystems Engineering
Poznań University of Life Sciences
ul. Wojska Polskiego 50, 60-627 Poznań, Poland

E-mails: adam_ekielski@sggw.pl, tomasz_zelazinski@sggw.pl, kdurczak@up.poznan.pl

Article citation info:
SKOCZYLAS L, WYDRZYŃSKI D. Operational tests of worm gearbox with ZK2 concave profile. Eksploatacja i Niezawodnosc – Maintenance and Reliability 2017; 19 (4): 565–570, http://dx.doi.org/10.17531/ein.2017.4.10.

Leszek SKOCZYLAS
Dawid WYDRZYŃSKI

OPERATIONAL TESTS OF WORM GEARBOX WITH ZK2 CONCAVE PROFILE

BADANIA EKSPLOATACYJNE PRZEKŁADNI ŚLIMAKOWEJ Z WKLĘSŁYM ZARYSEM ZK2*

The article presents an operational tests of worm gearboxes. Test bench trails were conducted for three gearbox types. Two of these gearboxes were manufactured using modern methods with conical endmills. The only difference between the two is the tooth profile. A ZK2 worm with a concave tooth profile and Archimedes' screw was used in the gearboxes. The third analyzed gearbox was a commercial gearbox with a ZK1 worm. When comparing the results of the analysis, the efficiency and load carrying capacity of the ZK2 worm gearbox is the highest and greatest respectively. The higher load carrying capacity of the ZK2 worm with concave teeth in comparison to the Archimedes' screw is confirmed by Hertz's theory. The results show, that the meshing area for ZK2 worm gearboxes is greater than Archimedes' screw. The confirmed increase of usage indicators of concave profile worm gearboxes can lead to their widespread production and application. The higher efficiency of the gearbox results in lower usage costs.

***Keywords**: worm gearbox, worm, wormwheel, ZK2 concave profile.*

W artykule przedstawiono badania eksploatacyjne przekładni ślimakowych. Badaniom stanowiskowym poddano trzy przekładnie. Dwie z nich zostały wykonane nową technologią z wykorzystaniem stożkowych narzędzi trzpieniowych. Różnica pomiędzy nimi dotyczyła wyłącznie zarysu kół. Zastosowano przekładnie ze ślimakiem ZK2 o wklęsłym zarysie oraz ślimakiem Archimedesa. Trzecią badaną przekładnią była przekładnia handlowa ze ślimakiem ZK1. Z porównania otrzymanych charakterystyk wynika, że sprawność i obciążalność przekładni ze ślimakiem ZK2 jest najwyższa. Wyższa nośność przekładni z wklęsłym zarysem ZK2 w stosunku do zarysu Archimedesa znajduje potwierdzenie w teorii Hertza. Uzyskane charakterystyki pokazują, że obszar zazębienia dla przekładni ze ślimakiem ZK2 jest większy w porównaniu z przekładnią Archimedesa. Potwierdzony wzrost wskaźników eksploatacyjnych przekładni ze ślimakiem o zarysie wklęsłym może przyczynić się do powszechnej ich produkcji i stosowania. Wyższa sprawność przekładni to zarazem niższe koszty jej eksploatacji.

***Słowa kluczowe**: przekładnia ślimakowa, ślimak, ślimacznica, zarys wklęsły ZK2.*

1. Introduction

Worm gearboxes belong to a group a screw transmissions with non-intersecting axes. In contrast to different types of gear transmission, they are characterized by their ability to transfer large ratios under beneficial conditions with high loading in a compact form. The kinematics in contrast to other types of transmissions differs because of the high level of meshing slip caused by concurrent meshing of a greater number of teeth. Due to the high loads carried and the type of meshing in the gear set, special attention must be paid to the phenomenon that occur during their operation, especially those that have a significant effect on wear [3, 5, 15, 19]. The main types of wear in the case include: teeth breaking, fatigue cracking and abrasion. Bending of the worm and the heat generated during operation are also considered in a wider scope due to their effect on transmission efficiency. Among the factors that affect wear in a correctly designed and used worm gearbox, the most significant ones are worm wheel tooth abrasion and surface fatigue wear. The factors that affect abrasive wear besides load include, slip direction and velocity between teeth and the surface finish of the gearwheel teeth.

The widespread use of worm gearbox has resulted in an increased amount of research being done on the topic. Several publications concern the material aspects and their effect on the gear set meshing conditions. Due to the significant role of slip in worm gear teeth, it is necessary to use materials that ensure a low coefficient of friction for worm wheels and worm screws. Fontanari and coauthors [14] present a tribological wear mechanism of a gear set made of steel-bronze. The resulting research shows that the identified wear occurrences are dependent on the applied load to the transmission. Additionally, Fontanari and coauthors [13] describe the possibility of using gearwheels made of spheroidal iron and hardened steel. The authors observed changes in the destruction of samples that resulted from pitting. Both the method of lubrication and the microstructure of the material exhibited a strong influence on the initiation and propagation of fractures. On the other hand, Simon [25-27] analyzes the load distribution in a worm drive in a steel-bronze configuration. They suggest to discretely divide the adhesion line into small segments, which allows for calculating the stress distribution and improving the usage parameters.

Besides research on the topic material applications or wear simulation and stress distribution where the teeth mesh, multiple studies on the tooth shape and meshing analysis. Chen and Tsay [4] analyze the geometry and meshing of ZN profile in worm drives in contrast to ZA profiles using their own mathematical model. The developed mathematical model enables the testing of potential further analysis in the realms of sensitivity analysis, kinematic errors, and contact stress analysis. The resulting data is useful for designing. and generating and selecting operating parameters for the gearbox. A computerized approach for determining the contact surface and analyzing meshing in a Klingenberg parallel axes gear set was presented by Litvina and coauthors [17]. The present theory minimizes the error sensitivity re-

(*) Tekst artykułu w polskiej wersji językowej dostępny w elektronicznym wydaniu kwartalnika na stronie ***www.ein.org.pl***

sulting from not being coaxial. Dong et al. [10] describe a method of design a ZI worm screw while analyzing installation errors in a worm drive. The authors present a developed drive design method where they pay special attention to the parameters of the worm screw, which when selected in the correct range cause minimal translation of the contact line that result from installation errors. Tsay et al. [29] present a mathematical model ZE worm drive meshing that was prepared in a CAD environment.

Not only are issues related to geometry being covered in publications, methods of manufacturing are also being discussed. Unfortunately, the topic focuses solely around the use of hobbing tools for the manufacturing of worm drive gearwheels. The use of hobbing cutters in the manufacturing of a worm wheel is presented in the work by Fang and Tsay [12]. They suggested a mathematical model of a worm screw with a ZN profile based on the profile and machining parameters of a hobbing tool. Countless publications are dedicated to the machining of worm screws on universal CNC machines. Nieszporek and Boca [21] analyze the method of machining worm screws using spherical end mills. This approach permits for any profile regardless of the tool profile. On the other hand, Albu [1] and Albu and Bolos [2] developed an approach for creating tool paths for the machining of worm screws using cylindrical end mills on CNC lathes. Kacalak et al. [16] develops an methodology for analysis and modeling helical surface grinding processes using CAD/CAM systems and Matlab. The resulting methodology allows for conducting simulation tests in order to determine the precision of grinding while considering the positioning and geometric deviations of the set up and the run-out of the chuck and work.

Not including ZA, ZN, ZI, and ZK profiles, there are also concave profile worm screws used in worm drives [23]. Non-intersecting positioning of a tool with a linear profile enables the machining of this type of profile. Skoczylas and Pawlus [28] present a method of shaping worm screws with a concave profile by using special tooling. They demonstrated the superiority of a transmission with a concave profile worm screw over the traditional linear profile. In concave profiles, it is possible to transfer greater loads while maintaining lower k_H stress values on the surface.

There are practically no publications dedicated to testing the operating properties in worm drives. Czerniec et al. [8] present a method of calculating the effect of tooth correction of a worm drive with an Archimedes' screw on the contact strength, wear, and durability of the worm gearwheel teeth. The results of the study establish the correctness of the correction effect on the contact parameters and tribological contact. Czerwiec and Kiełbiński developed a method of analyzing the wear kinematics of a worm drive with an Archimedes' screw [7]. Based on the aforementioned method of testing the wear kinematics of materials due to slip friction, they present a method of estimating the lifespan of a worm drive with an Archimedes' screw. Based on the numerical solution, a relationship between the drive resource and wear was determined. Also, Czerwiec and Kiełbiński present a method of calculating the lifespan of a worm drive with a involute worm screw [8]. The result of the numerical solution was used to determine the characteristics of the dependency between the lifespan of the transmission and the linear wear of the worm gearwheel teeth. They determined that changes in the wear of worm gearwheel teeth along the profile, where the maximum contact pressure and slip velocity was. The effect of the module and diameter indicator on select parameters. In turn, Waqar and Demetgul [30] use Fourier transform and neural network to diagnose the damages of toothed elements in worm drives. Vibrations and sound waves that arise during the operation of the transmission are detected using sensors. The data is then used to teach the network. The use of neural networks for the prognosis of damages in the drive system is used by Shao et al. [24]. In order to reduce the variability of vibrations and the accuracy of counteracting the residual durability of the drive system, a method of predicting was proposed, which combines a neural network of radial base functions and recurrent initial processing. The results of the study show that the presented method can be used to optimize traditional prediction methods. The use of the research techniques is a effective way of extracting valuable operation properties. Early acquired information of ongoing degradation processes allow for planing service intervals and repairs correctly. Thus, improving the reliability of all of the elements in the kinematic chain. Developing methods that can be used for early identification of damage in the form of pitting of work surfaces, face chipping, tooth root cracking and partial fracturing was the topic of the paper by Łazarz et al. [18]. They conducted a study on the effectiveness of selected methods on the processing of vibroacoustic signals in the process of detecting faults in gearwheel with concurrent bearing damage of drive systems working in various conditions. Initially the converted vibration signals were analyzed in the framework of time and frequency to be the basis for developing a diagnostic metric that is sensitive to earlier tooth damage. Elforjani et al. [11] indicate that using acoustic emission techniques offers more diagnostic capability of worm drives during operation than vibration analysis. Monitoring the research has shown that the acoustic emission parameters and energy are more reliable, durable, and capable of detecting defects than the corresponding vibration parameters.

The literature covering worm drives consists of many titles that approach the issue in a purely theoretical approach. The papers in this field describe mathematical issues related with the analysis of meshing geometry of worm drives with various worm screw profiles. Very little attention is placed on the possibility of shaping concave profiles that demonstrate a significant level of usefulness when improving the operating parameters of drive system. The descriptions of the machining methods lack information regarding manufacturing issues related with the effects of surface and the precision of the machined work surface. There is also a very small number of publications that approach the issues of analyzing the operating properties of worm dirve with various worm screw profiles that has a significant effect on the durability and reliability of the codependent toothed parts.

2. The effects helical geometry of the worm screw on gearbox usage problems

When looking at fatigue, the factors that affect abrasive wear (load, gearwheel material) should include the curvature of the teeth and the length of the contact line. It can be noticed that some of the aforementioned factors are dependent on the geometry of the gear screw and gearwheel teeth. Improper manufacturing of the worm screw can lead to accelerated tooth wear of the worm gearwheel. The result can be observed in fig. 1.

Fig. 1. Wormwheel tooth damage resulting from excessive loads.

The shape of the teeth determines the length and position relative slip velocity of the contact line. This effectively changes the lubrication conditions in contact area, the efficiency and gearbox wear

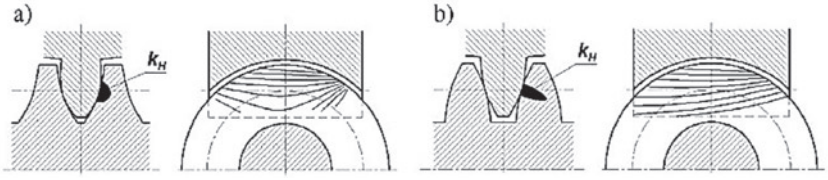

Fig. 2. The meshing of worm gearbox teeth for: a) concave profiles b) convex profiles.

rate. The shape of the teeth also affect the substitute radius curvature, which is an important parameter because of the large contact stress. Thus, the correct shape of the teeth can significantly affect the usage parameters of a gearbox.

The ability to modulate the shape of the helical surface of the worm screw is greatly increased by the non-intersecting positioning of the end mill in relation to the axis of the worm screw. The shape of the profile is the result of proper tool positioning. The advantages of a concave profile in comparison to a convex one are presented in fig. 2

The greater load carrying capacity of a concave profile worm screw results primarily from the lesser contact stress values on the tooth surfaces of the gearwheels. In addition, the large angle between the contact line and the circumferential speed of the worm screw is beneficial for lubricating the contact area.

The maximum stress resulting from cylinder contact can be calculated using the following formula (1) [20]:

$$k_H = \frac{F_N}{2L\mathrm{r}_{zr}} \tag{1}$$

where: F_N – normal force at the contact point, L – contact line length, ρ_{zr} – reduced curvature radius contacting the surface.

Based on this and when the normal forced is accepted, the magnitude of pressure depends on the product of the contact line length and the reduced curvature radius of the cylinders. The area of contact of gearwheels in the transmission can be considered to be very variable. The contact line of the teeth, along with the change of the curvature radius, will change its shape and length. However, the value of reduced curvature radius change along the analyzed contact line. The load carrying capacity will be determined by the minimal value of the aforementioned parameters (calculations are required for the whole meshing range).

3. Meshing characteristics of the analyzed worm screw profiles

Test bench studies were preformed for three gearboxes. Two of them were manufactured using new techniques that use conical end mills. The difference between these gearboxes is limited to the profiles of the gearwheels (gearboxes with concave ZK2 worm screw profiles and an Archimedes' screw). The third gearbox was a commercial transmission with a ZK1 worm screw. The basic parameters of the analyzed gearwheels, in accordance with their respective standards[9, 22], are listed in Table 1.

The decision to analyze ZK2 profiles results primarily from the large possibility of a non-intersecting tool position affecting the thread profile of the worm screw, including shape of concave profiles. Assuming a constant worm screw axial angle profile, calculations were done for the concave ZK2 worm screw profile with the parameters listed in Table 1. The tool parameters and its position angle in specific shaping cases along with the helix angle and thread curvature angle on the pitch diameter of the resulting worm screw are presented in Table 2.

Table 1.
Analyzed worm drive gearwheel parameters.

#	Parameter	Value
	worm gear	
1	Axial module	4 mm
2	Diametrical indicator	10
3	Thread start count	1
4	Tip height factor	1
5	Root height factor	1.2
6	Axial angle profile	20°
7	Helix angle	5.7106°
	Wormwheel	
8	Number of teeth	30
9	Tooth correction factor	0
10	Tip height factor	1
11	Root height factor	1.2
12	Tooth heigh	2mm
13	Width	30mm

Table 2. Tool parameters and positioning angles.

Profile type	Tool				Worm screw
	α_N	d_N	ϕ_N	χ_N	α_o
	[°]	[mm]	[°]	[°]	[°]
Concave	8	5	-36	9,92	20
Linear	8	5	12	90	20

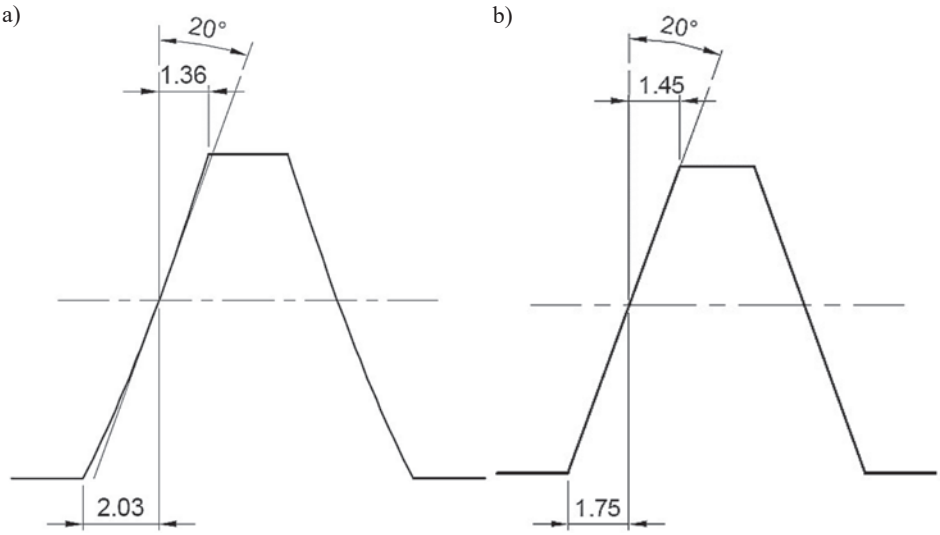

Fig. 3. Axial tooth profile: a) concave b) linear

Positioning the tool in regards to the axis of the worm screw was done to achieve profile that is as concave as possible and to avoid undercutting during meshing with the gearwheel. In order to more precisely visualize the change in shape of the ZK2 profile, fig. 3 presents the concave profile with a Achimedes' profile (ZA). Figure 3a show the visible difference in shape between the concave profile in comparison to the linear profile displayed in fig. 3b.

The most characterizing dimensions are the tip diameters and root diameters. In neither of the aforementioned cases does the thread profile angle match the angle of the tool of 20°.

4. Materials and gearbox loading analysis

4.1. Test bench

The complexity of the phenomena describing the meshing of worm drive results in loading tests being the most objective evaluation of the effect of worm screw profile on the operating parameters. In order to accomplish this, a test bench that assessed actual worm drive was prepared. The block diagram representing this setup and test bench are presented in fig. 4.

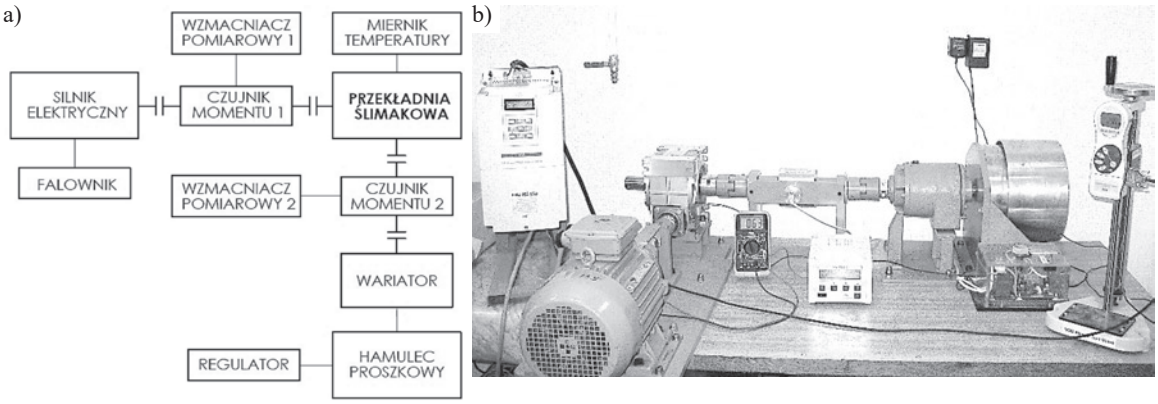

Fig. 4. Gearbox loading test bech: a) block diagram b) actual view

The configuration of the test bench assumes that only the gear set geometries will be variable during the tests. The propulsion and measurement systems were selected in order to appropriate to the size of the gearboxes. The commercial housing was modified to enable visual observation of the gearwheel condition. The housing of the gearbox (fig. 5) is made from aluminum with an axis base of 80mm. The housing material is a standard choice for mass produced gearboxes of this size.

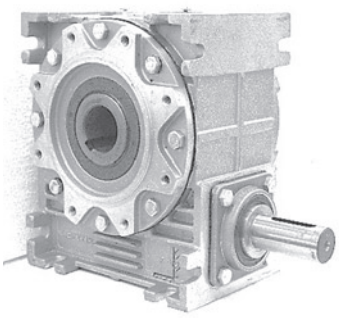

Fig. 5. Analyzed worm drive

A 4kW 3-phase induction motor with nominal speed of 2815 RPM was selected as the propulsion unit of the test bench. The motor control was done using an inverter. The inverter allows for linear scalar control (U/f) as well as sensorless and sensor based controlling of torque and speed. The load was provided by a powder brake with dispersion power of 2kW. The torque of the brake is proportional to the voltage of the electromagnetic coil that is regulated by an electronic system. The brake properties enables constant work with slip that allows for long term tests. Due to the fact that resulting speed out of the worm drive was lower than the recommended operating speed of the brake (50 RPM), the test bench was equipped with an additional gearbox that functioned as a variator. All of the shafts in the drive and loading systems were connected using elastic Rotex clutches (KTR).

The torque before and after the worm gearbox was measured on the test bench as well as the operating temperature. Measuring the torque enables the monitoring of the load levels on the gearbox and limiting power loss. A measuring shaft with a torque sensor was using to measure the rotational moment of the gearbox. Connecting both measuring shafts with a computer allows for electronic registering of torque values before and after the gearbox. The operating temperature measurements were done using a resistance sensor located on the housing of the gearbox.

The described test bench is prepared primarily for tests that determine the size of a worm drive, where the modular design permits quick modifications for testing different gearboxes.

4.2. Research object

Manufacturing the gearwheels makes it possible to conduct experimental gearbox tests. Two worm screw profiles were manufactured and both were shaped using cylindrical end mills. The worm screws were made of 42CrMo4 steel intended for heat treating. The chemical composition of the selected steel alloy is presented in Table 3. This steel is intended for the manufacturing of machine parts with high strength, ductility, and variable loading such as: axles, cranks, gearwheels, discs, rotors, levers and other similar items.

Table 3. Alloy composition [%] of 42CrMo4 steel.

C	Mn	Si	P	S	Cr	Ni	Mo	W	V	Co	Cu
0,38 – 0,45	0,4 – 0,7	0,17 -0,37	max 0,035	max 0,035	0,8 – 1,2	max 0,3	0,15 – 0,25	max 0,2	max 0,05	-	max 0,25

The manufacturing process included centering, roughing, shaping, heat treatment, re-centering, and finishing of the teeth and cylindrical surfaces for bearing seating and clutch fitment. The heat treatment included hardening that was done by heating the metal to 840°C and quenching in oil and annealing at 550°C followed by oil quenching. The resulting hardness was 55HRC. The finishing was done on a five-axis Haas VF-2 mill.

The meshing of concave and linear profile worm screws requires the manufacturing of two worm gearwheels. The blank for the worm gearwheels was heterogeneous and made of a tin-phosphorus bronze

ring cast on a iron hub. The chemical composition of the material is presented in Table 4.

Table 4. Alloy composition[%] of CuSn10P bronze.

Sn	Pb	Mn	Al	P	Zn
9,0 – 11,0	–	–	–	0,8 – 1,2	–

The manufacturing process was mostly traditional besides the tooth cutting operation. The tooth cutting was done on a five-axis Haas VF-2 mill with universal cylindrical and spherical end mills.

4.3. Preparing the test bench

The assembled gearboxes, after filling it with Synlube CLP 220 oil, underwent further test on the loading test bench. The effect of tooth profile on the operating parameters of the gearbox were assessed, where the primary indactor was selected to be gearbox efficiency. The test bench trials were conducted for one gearbox size with an axis base of 80mm. The selected gear set parameters enabled testing in a commercial gearbox housing.

The efficiency tests were also done for the commercial gearbox. The aim was to compare the results of the manufactured gear sets with the mass produced gearbox with comparable parameters. The gear ratio of the commercial gearbox was 31 using a ZK1 worm screw profile. Efficiency testing was done following a break in period of 400 hours. This process was conducted at 1000 RPM and load that results in operating temperatures around 65°C. The efficiency measurements were done at constant worm screw RPM of 1400 RPM and ambient temperature of 23°C. The load level was gradually increased. After every change and when the temperature stabilized, an efficiency measurement was done. The trails were ended when the gearbox oil temperature reached 110°C.

5. Results

The efficiency test results (solid line) and temperature measurements (dashed line) of the gearbox is presented in fig. 6.

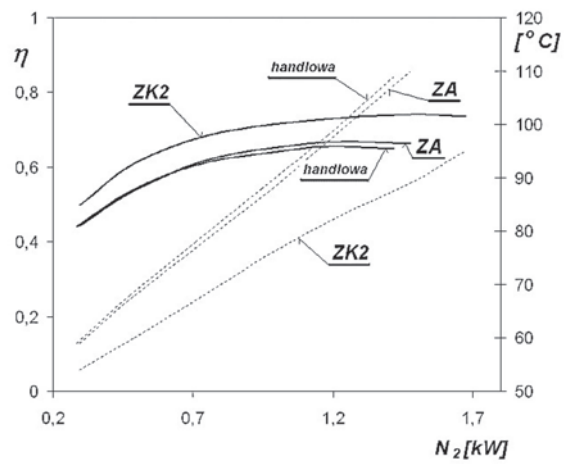

Fig. 6. Gearbox efficiency as a function of load

Comparing the characteristics of the graph (fig. 6), it shows that the efficiency and load carry carrying capacity of the ZK2 gearbox is the greatest. This phenomenon was noticeable during the break in period, when the gearbox with the concave profile had 20% greater load while maintaining the same temperature levels. The efficiency of the commercial gearbox in comparison to the gearbox with Archimedes' screw, besides the similarities of both worm screws, is significantly smaller. This probably results from lesser stiffness of the commercial worm drive, which due to the high gear ratio had a smaller diameter. The temperature characteristics show that the main limiting factor of the Archimedes' screw and commercial gearboxes was temperature. Only the concave profile gearbox did not reach the temperature barrier and could undergo greater loads. Further tests exceeded the possibilities of the brake. The test range was sufficient, which can be observed by the extremes in efficiency.

The greater load carrying capacity of the ZK2 concave profile in comparison to the Archimedes' screw can be confirmed by Hertz's theory. Using a specially developed program, calculations were done to find the product value of the contact line curve and reduced curvature radius of the gearbox teeth. The results of these calculations are presented in fig. 7.

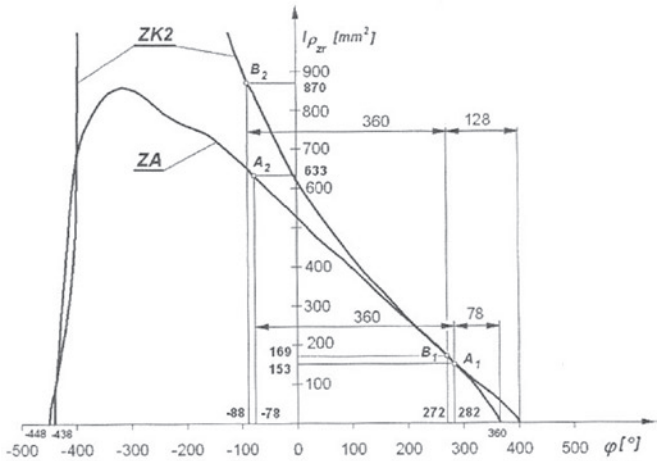

Fig. 7. The dependency of contact line length and curvature radius from worm screw rotation

To maintain the readability of the graph, part of the ZK2 parameter product values were excluded because they reached a few thousand. In the area of decoupling the separation between the lines in lesser, and even comparable. The resulting characteristics show that the meshing area for ZK2 worm screw gearbox is greater that Archimedes' screw drives. The complete meshing indicator for ZK2 is 2355 while ZA is 2216. In relation to the load carrying capacity, the greatest pressure occurs at points with two pair engagement with the lowest contact line length and reduced curvature radius product. For ZA gearbox these are A_1 and A_2, while B_1 and B_2 for ZK2. The total product value for the ZA worm screw is 786mm^2, while it was 1039mm^2 for the ZK2 worm screw. In conclusion, this illustrates the greater load carrying capacity of the ZK2 worm screw compared to the ZA worm screw.

6. Conclusion

Besides long standing use of worm drives, the majority is manufactured using a profile that is easy to shape. These are mostly involute worm screws or conically shaped ZK1 that have a helical thread shaped by a hobbing tool with a linear profile.

The trails show that convex profiles do not ensure a gearbox with maximum power transmission or efficiency. This evidenced by the greater efficiency and load carrying capacity of new concave ZK2 profile worm screws, which illustrate their usefulness. It should be noted that the test bench trails were conducted on a basic variat of the gearbox. Modifying the parameters of the gearbox can additionally affect an increase in usage indicators, which require further experimental trails.

The confirmed increase in usage parameters of the concave worm screw gearbox can lead to its widespread production and use. The higher efficiency of the gearbox results in lower operating costs.

References

1. Albu S C. Roughing helical flanks of the worms with frontal – cylindrical milling tools on NC lathes. Procedia Technology 2014; 12: 448–454, https://doi.org/10.1016/j.protcy.2013.12.513.
2. Albu S C, Bolos V. Considerations regarding a new manufacturing technology of cylindrical worms using NC lathes. Acta Technica Napocensis, Series: Applied Mathematics and Mechanics 2013; II (56).
3. ANSI/AGMA 6022-C93 (R2014), Design manual for cylindrical wormgearing, 2014.
4. Chen K Y, Tsay CH B. Mathematical model and worm wheel tooth working surfaces of the ZN-type hourglass worm gear set. Mechanism and Machine Theory 2009; 44: 1701–1721, https://doi.org/10.1016/j.mechmachtheory.2009.02.003.
5. Crosher W P. Design and Application of the Worm Gear. Bratislava: SME Press, 2002, https://doi.org/10.1115/1.801780.
6. Czerniec M, Kiełbiński J. Calculation method longevity of worm gear with evolventary worm. Tribologia 2013; 2: 31–43.
7. Czerniec M, Kiełbiński J. The investigation method of kinetics wear of a worm gear with an archimedean worm. Tribologia 2009; 3: 31–39.
8. Czerniec M, Kiełbiński J, Czerniec J. The Efect of teeth correction in an Archimedes worm gear on the contact strength, wear, and life the worm gear teeth. Tribologia 2017; 1: 31–34.
9. DIN 3976 – Zylinderschnecken. Zuordnung von Achsabstanden und Ubersetzungen in Schneckeradsatzen.
10. Dong L, Liu P, Wei W, Dong X, Li H. Study on ZI worm and Helical gear drive with large transmission ratio. Mechanism and Machine Theory 2014; 74: 299–309, https://doi.org/10.1016/j.mechmachtheory.2013.12.014.
11. Elforjani M, Mba D, Muhammad A, Sire A. Condition monitoring of worm gears. Applied Acoustics 2012; 73 (8): 859–863, https://doi.org/10.1016/j.apacoust.2012.03.008.
12. Fang H S, Tsay C B. Mathematical model and bearing contacts of the ZN – type worm gear set cut by oversize hob cutters. Mechanism and Machine Theory 2000; 35: 1689–1708, https://doi.org/10.1016/S0094-114X(00)00024-0.
13. Fontanari V., Benedetti M., Girardi Ch., Giordanino L. Investigation of the lubricated wear behavior of ductile cast iron and quenched and tempered alloy steel for possible use in worm gearing. Wear 2016; 350–351: 68–73. https://doi.org/10.1016/j.wear.2016.01.006
14. Fontanari V, Benedetti M, Straffelini G, Girardi Ch, Giordanino L. Tribological behavior of the bronze - steel pair for worm gearing. Wear 2013; 302: 1520–1527, https://doi.org/10.1016/j.wear.2013.01.058.
15. ISO/TR 14521:2010, Gears - calculation of load capacity of worm gears, 2010.
16. Kacalak W, Budniak Z, Szafraniec F. Analisys of the forming proces of conical - like helical surfaces with roller tools. International Journal of Applied Mechanics and Engineering 2017; 22 (1): 101–110, https://doi.org/10.1515/ijame-2017-0006.
17. Litvin F L, Yukishima K, Hayasaka K, Gonzalez–Perez I, Fuentes A. Geometry and investigation of Klingelnberg-type worm gear drive. Journal of Mechanical Design 2007; 129: 17–22, https://doi.org/10.1115/1.2359477.
18. Łazarz B, Wojnar G, Czech P. Early fault detection of toothed gear in exploitation conditions. Eksploatacja i Niezawodnosc – Maintenance and Reliability 2011; 1: 68–77.
19. Marciniak T. Cylindiral worm drive. Warszawa: Handbook. PWN Press, 2013, (in Polish).
20. Marciniak T. Obciążalność zazębienia przekładni ślimakowych. Zeszyty Naukowe Politechniki Łódzkiej, nr 934, Łódź 2004.
21. Nieszporek T, Boca V. A new method of manufacturing the worm gear with concave profile. Annals of MTeM for 2011 & Proceedings of the 10th International Conference 2011: 218–221.
22. PN–93/M–88527 – Przekładnie i reduktory ślimakowe walcowe ogólnego przeznaczenia. Parametry podstawowe.
23. PN–93/M–88509/03 – Przekładnie zębate. Przekładnie ślimakowe. Terminologia i oznaczenia.
24. Shao Y, Li X, Mechefske V K, Chen Z. Rear axle gear damage prediction using vibration signal preprocessing coupled with RBF neural networks. Eksploatacja i Niezawodnosc – Maintenance and Reliability 2009; 4: 57–64.
25. Simon V. Load Distribution in cylindrical worm gear. Journal of Mechanical Design 2003; 125(2): 356–364, https://doi.org/10.1115/1.1561043.
26. Simon V. Load Distribution in double enveloping worm gears. Journal of Mechanical Design 1993; 115: 496-501, https://doi.org/10.1115/1.2919217.
27. Simon V. Stress analysis in worm gears with ground concave worm profile. Mechanism and Machine Theory 1996; 31: 1121–1130, https://doi.org/10.1016/0094-114X(96)84603-9.
28. Skoczylas L, Pawlus P. Geometry and machnining of concave profiles of the ZK – type worm thread. Mechanism and Machine Theory 2016; 95: 35–41, https://doi.org/10.1016/j.mechmachtheory.2015.08.017.
29. Tsay C B, Jeng J W, Feng H S. A mathematical model of the ZE-type worm gear set. Mechanism and Machine Theory 1995; 30: 777, https://doi.org/10.1016/0094-114X(95)00006-K.
30. Waqar T, Demetgul M. Thermal analysis MLP neural network based fault diagnosis on worm gears. Measurement 2016; 86: 56–66, https://doi.org/10.1016/j.measurement.2016.02.024.

Leszek SKOCZYLAS
Dawid WYDRZYŃSKI
Faculty of Mechanical Engineering and Aeronautics
Rzeszow University of Technology
al. Powstańców Warszawy 12, 35-959 Rzeszów, Poland

E–mails: lsktmiop@prz.edu.pl, dwydrzynski@prz.edu.pl

Article citation info:
MITURA A, GAWRYLUK J, TETER A. Numerical and experimental studies on the rotating rotor with three active composite blades. Eksploatacja i Niezawodnosc – Maintenance and Reliability 2017; 19 (4): 571–579, http://dx.doi.org/10.17531/ein.2017.4.11.

Andrzej MITURA
Jarosław GAWRYLUK
Andrzej TETER

NUMERICAL AND EXPERIMENTAL STUDIES ON THE ROTATING ROTOR WITH THREE ACTIVE COMPOSITE BLADES

BADANIA NUMERYCZNE I EKSPERYMENTALNE WIRUJĄCEGO WIRNIKA Z TRZEMA AKTYWNYMI ŁOPATAMI KOMPOZYTOWYMI

In this paper, the dynamic behaviour of active composite blades were considered. Both numerical and experimental studies were performed. It was assumed that the rotor hub would be rotated at constant velocity. Experimental measurements were made. A special test rig was built which consisted of an active rotor with three composite blades, an electric drive system and a system of Digital Signal Processors. This DSP system was used for the excitation of the blades, control of the hub's rotary velocity and data acquisition. The MFC patch and strain-gauge sensors were used. The influence of the hub's rotary velocity and/or piezoelectric effect on the dynamic behaviour of the blades was determined. The numerical simulations were performed using two commercial simulation programmes: Abaqus and Matlab.

***Keywords**: MFC actuator, laminate, stiffening effect, softening effect, FEM.*

W niniejszej pracy przedstawiono dynamikę aktywnych łopat kompozytowych. Przeprowadzono badania numeryczne i eksperymentalne. Założono, że wirnik obraca się ze stałą prędkością obrotową. Pomiary doświadczalne wykonano na stanowisku badawczym, składającym się z aktywnego wirnika z trzema łopatami, elektrycznego układu napędowego oraz procesora sygnałowego DSP. Układ elektroniczny z procesorem wykorzystano do wzbudzania łopat, kontroli prędkości obrotowej oraz pozyskania danych pomiarowych. W badaniach laboratoryjnych użyto elementy aktywne typu MFC oraz czujniki tensometryczne. W pracy określono wpływ prędkości obrotowej piasty oraz efektu piezoelektrycznego na dynamikę łopat. Symulacje numeryczne przeprowadzono z zastosowaniem programów: Abaqus oraz Matlab.

***Słowa kluczowe**: Aktywator MFC, laminat, efekt usztywniający, efekt zmiękczający, MES.*

1. Introduction

Systems with rotating blades are used in many engineering applications. Composite blades can be used in a drone, a helicopter, a wind turbine and many others. Active rotors are the most interesting because one can change the dynamic behavior of such structures in the real time. In the literature of the subject, one can find many solutions for active rotor design. More details can be found in the monograph by Chopra and Sirohi [6]. The researchers from the Department of Applied Mechanics at the Lublin University of Technology, Poland, built the experimental setup of a rotor with three composite blades. In the paper [16], the experimental modal analysis and the numerical modal analysis of this stand were compared. The experimental study was performed by two independent methods. The first was the non-contact method. To this end, a laser vibrometer system was used. The other was the contact method, where an acceleration sensor and a modal hammer were applied. The experimental results were compared with numerical modal analysis performed by the finite element method using the Abaqus software. In this study, the rotor was fixed. Therefore, the influence of the rotor's rotational velocity on the behaviour of the blades was not examined. The relationship of natural frequency versus rotational velocity of the rotor is discussed in the papers [5,17] for a wind turbine blade and a helicopter blade, respectively. The finite element method was applied. In the literature, authors did not find experimental validation of this type solutions. The main problem lies in the experimental verification of numerical results for rotating structures. The rotating structures create difficulties in the implementation of the measurement system. NASA [4] presents the solution dedicated to rotating blades. In a rotating system the vibration of the blades was detected by strain-gauges and optical motion sensors. Special 100 channels slip ring assembly for strain-gauge leads were mounted at the bottom of the multi-blade rotor. The authors of this paper presented their test stand, where a similar solution with slip rings was applied. It enabled performing tests with non-zero rotational velocity.

Experimental studies of active blades can be conducted using piezoelectric (PZT) elements, the so-called Macro Fiber Composite (MFC) elements [15]. Such elements can be used as actuators or sensors. More information about these elements can be found in the papers [2, 12, 14] or books [3,6]. An interesting problem concerns the impact of the stiffening effect on the natural frequencies of the laminated beam with piezoelectric actuators. Kuo [9] indicated that piezoelectric elements can be used to increase or decrease the first natural frequency depending on the sign of the applied DC voltage. He presented the results of the numerical analysis for a simply supported beam. This problem was more thoroughly discussed in the papers [18-19]. Waisman and Abramovich investigated the simply supported and clamped-free beams with one and two sets of the PZT actuators. They concluded that the stiffening effect generated by the piezoelectric actuators ensures the control of the natural frequency and mode shapes of the tested beams. A similar analysis is presented

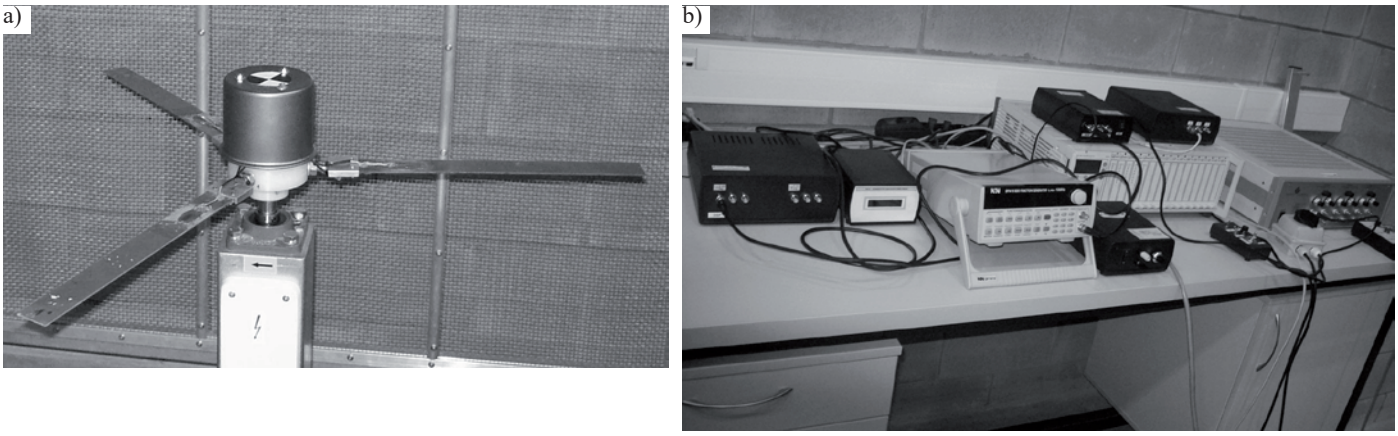

Fig. 1. Views of the tested rotor (a) and electronic equipment(b)

in the paper [8], but the object of the research was a thin plate with PZT actuators.

The aim of this paper is to determine the relation between the dynamics of a rotor blade with MFC elements in relative motion and the rotational movement of the hub. Constant angular velocity can generate undesired changes in the natural frequencies and/or eigenmodes of the active composite blades. The aim of the experimental research was to demonstrate the possibility of using the MFC actuator for reducing these changes.

2. The experimental setup

The experimental studies were performed using a specially designed test stand which is shown in Fig. 1. This stand was built at the Department of Applied Mechanics at the Lublin University of Technology. The rotor (Fig. 1) consisted of a hub with three composite blades which were located 120 degrees relative to each other. The rotor blades were beams with a rectangular cross-section made of glass-epoxy laminate.

The mechanical properties of the glass-epoxy laminate were as follows:

- Young's modulus in fibre direction (i.e., direction 1): 46.43 GPa and in transverse direction of the fibers (i.e., direction 2): 14.926 GPa, respectively,
- Poisson's ratio in plane 1-2: 0.27,
- shear modulus in plane 1-2: 5.233 GPa,
- density: 2032 kg/m^3.

Each blade was composed of six layers. The lay-up configuration of the laminate was: $[\pm 45/90]_S$. The geometry of the rotor blades is given in Table 1.

Table 1. Geometrical dimensions of rotor blades in mm

Length	Width	Thickness
350	34	1.80

The rotor hub was driven by a DC motor. In addition, the sensors and actuators were fixed on the opposite surfaces of the beams. The strain-gauges and piezoelectric actuators were used to measure and control the dynamics of the rotor blades in their relative motion. In our case, the Macro Fiber Composite active elements were used as actuators. They were MFC elements type M-8528-P1. In this case, the piezoelectric d_{33} effect occurs [15]. Each element can be powered by electric current in the range of -500 to 1500 volts.

The piezoelectric properties of the MFC element depend on its dimensions. According to the literature [16], the optimal value of the d_{33} parameter for MFC M-8528-P1 elements is $1.01*10^{-7}$ m/V. The coefficient of permittivity is $8*10^{-9}$ F/m. The mechanical properties of the MFC element were:

- Young's modulus in fibre direction (i.e., direction 1): 15.857 GPa and in transverse direction of the fibers (i.e., direction 2): 30.336 GPa, respectively,
- Poisson's ratio in plane 1-2: 0.31,
- shear modulus in plane 1-2: 5.515 GPa,
- density: 5440 kg/m^3.

Fig. 1(b) shows the electronic equipment which was used to control the power of the electrical motor and piezoelectric transducers. Additionally, the DSP subsystem was used.

3. The numerical model of the rotor

The numerical model of the rotor was designed by the finite elements method using the commercial system Abaqus [1]. The FE model of the rotor is shown in Fig. 2.

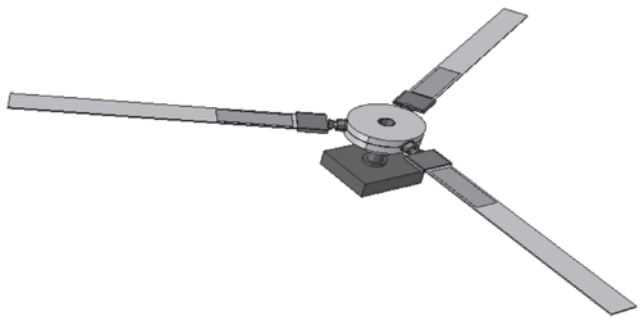

Fig. 2. Numerical model of the active rotor

The model consists of a base with electric drive, the hub with a drive shaft, a blade handle, three composite blades and MFC active elements [16]. The hub and the base of the rotor were built of 10-node tetrahedral, solid elements having three translational degrees of freedom at each node (i.e., C3D10 elements in the Abaqus system). The FE model of the blade handle was built using 20-node (2nd order) solid elements having three translational degrees of freedom at each node (i.e., C3D20R elements). The numerical model of the composite blade was made using 8-node (2nd order) continuum shell elements having three translational degrees of freedom at each node with reduced integration (i.e., SC8R elements). The layup-ply technique was used to made individual layers of the blades. The FE model of the MFC element was constructed using 20-node (2nd order) solid elements, having three translational degrees of freedom at each node and one extra degree of freedom associated with the piezoelectric properties (i.e., C3D20E elements). The combination of all parts of the model was

realized by defining interactions as "TIE" [1]. Mechanical boundary conditions of the model were realized by restraining the nodes located at base translational degrees of freedom. The rotation of the shaft were possible but the base of the rotor was fixed.

4. Influence of the hub rotary velocity on the blade dynamics

The influence of the centrifugal force on the blade dynamics was tested in relative motion. In the experimental studies, the rotating system had a constant rotational velocity denoted as n. The piezoelectric actuator was used to excite the system. The Single Input Single Output procedure was applied, which means that only one blade was excited and its response was measured at one point. In this paper, the experimental results for one blade are reported. The blade was excited using an MFC element powered by a sine sweep signal. Generally, supply voltage can be written as a function:

$$U_A(t) = A\sin\left(\omega_0 t + \frac{1}{2}\varepsilon_A t^2\right) \tag{1}$$

where: A is the amplitude of a sine signal, t is time, ω_0 and ε_A are the initial frequency and angular acceleration, respectively. Both parameters describe the change in the frequency of the signal realized by the MFC actuator. The frequency ω_A of the sine function changes linearly, in the following way:

$$\omega_A(t) = \omega_0 + \varepsilon_A t \tag{2}$$

In the experimental studies, the realization of the time sweep sine was defined as: $t \in \langle 0,30 \rangle s$. In this time, the range of frequency was slowly changed from 8 Hz to 15 Hz (i.e., $\omega_0 = 16\pi$ rad/s, $\varepsilon_A = \frac{7\pi}{15}$ rad/s^2 in Eq. (2)). The frequency range of the MFC excitation signal is illustrated in Fig. 3. The amplitude of the voltage supply signal denoted as A in Eq.(1) was 400 V. The obtained final time series of the voltage supply signal is presented in Fig. 4.

The rotation of the blades caused measurement problems. In the first step, the fast speed cameras were used as a non-contact system. However, this test method did not enable taking precise measurements of the rotating blades. In the second step, the strain-gauges were used. The Wheatstone bridge circuit was located on the hub (Fig. 5a). The signals from the rotor were transmitted through the slip rings (Fig. 5b). Therefore, in this paper the strain-gauge signal (denoted as U_S) is given in volts.

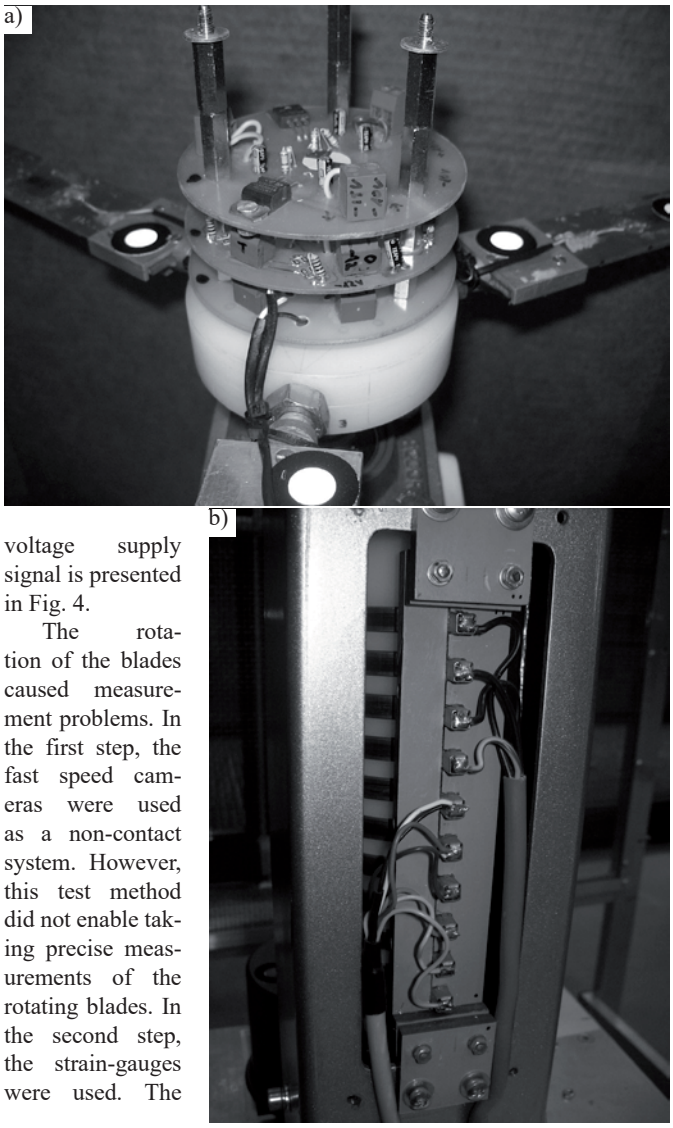

Fig. 5. Views of selected elements of the test stand: (a) electronics system, (b) slip rings

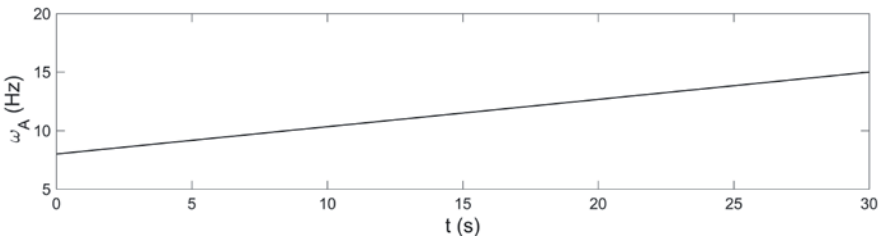

Fig. 3. Frequency change in the MFC excitation signal

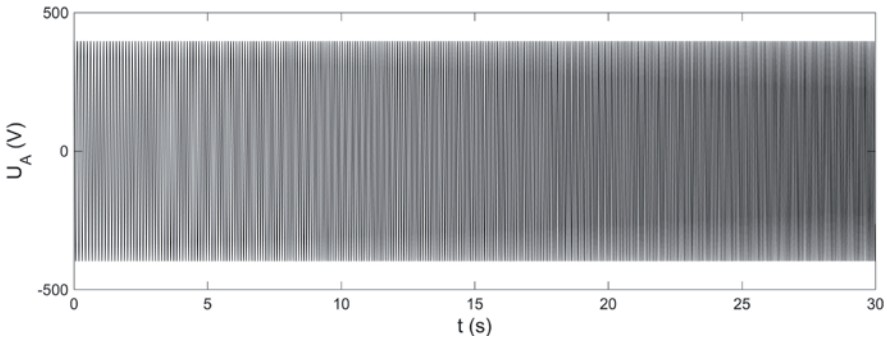

Fig. 4. Time series of the voltage supply of the MFC actuator

The experimental studies were performed with the constant rotational velocity set to 0, 100 rpm, 200 rpm, 300 rpm, 400 rpm, 500 rpm. The response of the blades forced by the MFC element was changing with increasing the rotational velocity (Fig. 6). In the first case, the maximum response of the strain-gauge signal was at 5.49 s (Fig. 6a). In the second case, the maximum response of the strain-gauge signal was at 10.0217 s (Fig. 6b). The natural frequency of the first bending mode (denoted as ω_1) was determined as follows:

$$\omega_1 = \omega_0 + \varepsilon_A t_m \tag{3}$$

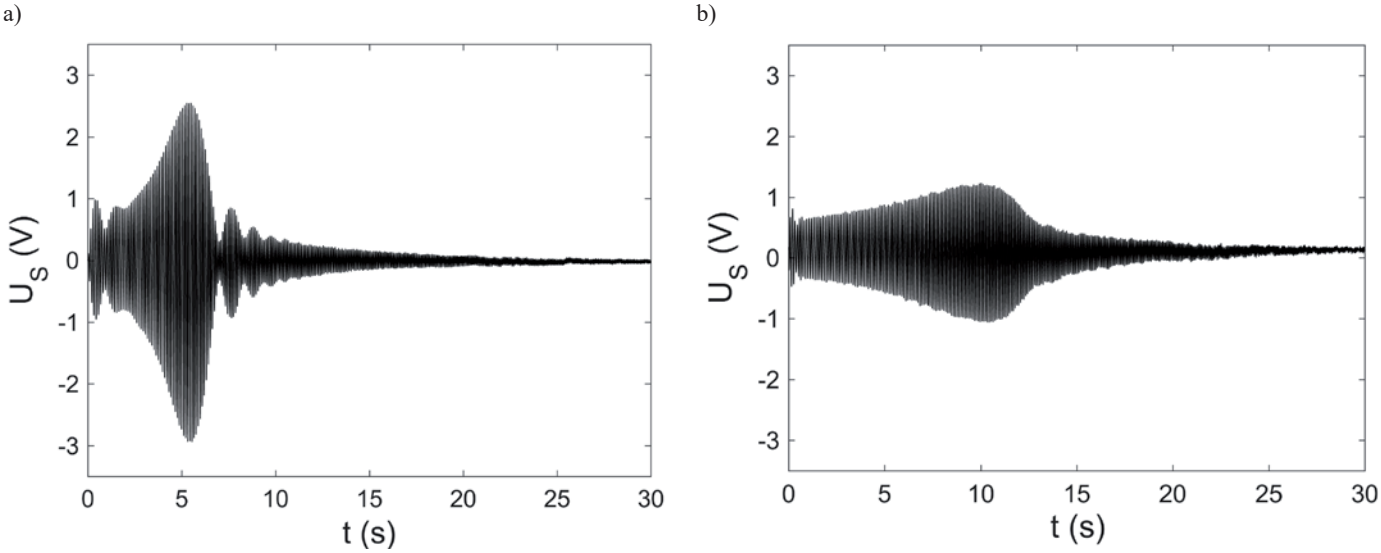

Fig. 6. Strain-gauge signal vs. time, when the rotational velocity was: (a) 0 (b) 200 rpm

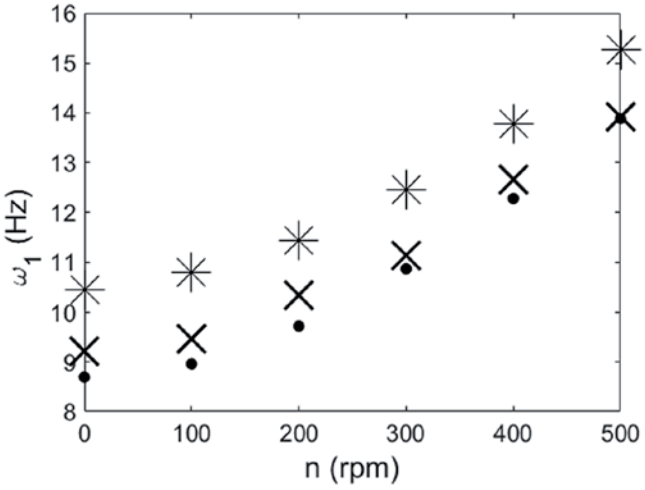

Fig. 7. First bending natural frequency vs. rotational velocity. The numerical solutions are marked by stars (FE-model with MFC elements) and dots (FE-model without MFC elements), respectively. The experimental results are marked by crosses

where: t_m is a time when the amplitude of blade vibration is the maximum.

The obtained experimental values of the first bending natural frequency are shown in Fig. 7. Next, a comparison of the experimental results and the numerical solutions for the lowest bending mode of free vibration was made (Fig. 8). In the FE analysis, the eigen-frequencies and the corresponding modes of free vibration were determined using the Lanczos method [1]. Rotation with a constant angular velocity generates a constant centrifugal force. This effect was taken into account in the FE model by introducing mechanical load. The simulations were made for a selected angular velocity. The FE results for the first five vibration modes, when the angular velocity was 500 rpm, are illustrated in Fig. 8.

The FE results are given in Table 2. These results reveal the impact of the centrifugal force on the resonance area shift. An increase in the natural frequencies was calculated when the angular velocity was 500 rpm (denoted as $\omega_{\max}^{FEM}$) or 0 (denoted as $\omega_{\min}^{FEM}$). The percentage increase in the frequencies was defined as:

$$\delta\omega^{FEM} = \frac{\omega_{\max}^{FEM} - \omega_{\min}^{FEM}}{\omega_{\min}^{FEM}} \quad 100\% \tag{4}$$

In this case, the percentage increase in the frequencies was: 46 %, 9 %, 4 % for the first, second and third vibration modes (Figs. 8a, b, c and Table 2) and 0 % for other modes (Figs. 8 d, e and Table 2), respectively.

The experimental findings are closer to the numerical results when the piezoelectric elements are not included in the FE model. A very good agreement for all methods was achieved. The details are given in Fig. 7. The obtained characteristic demonstrates that the natural frequency of the first bending mode increases with increasing

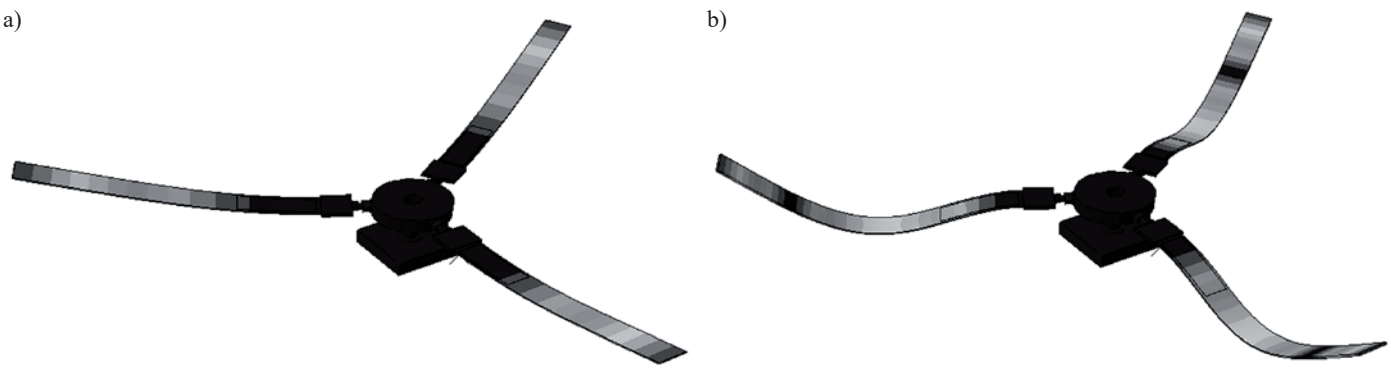

Fig. 8. Free vibration modes when the angular velocity is 500 rpm (a) (b) - first, second in plane bending modes

c)

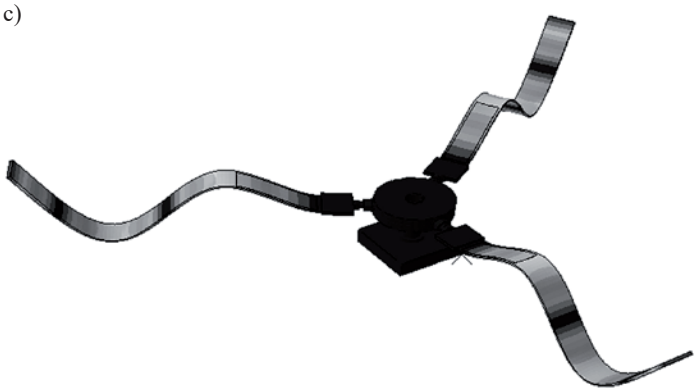

d)

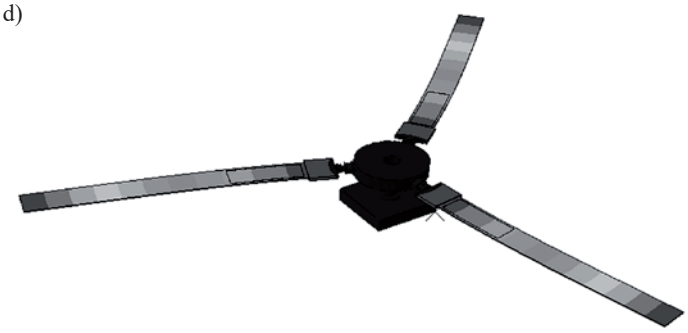

e)

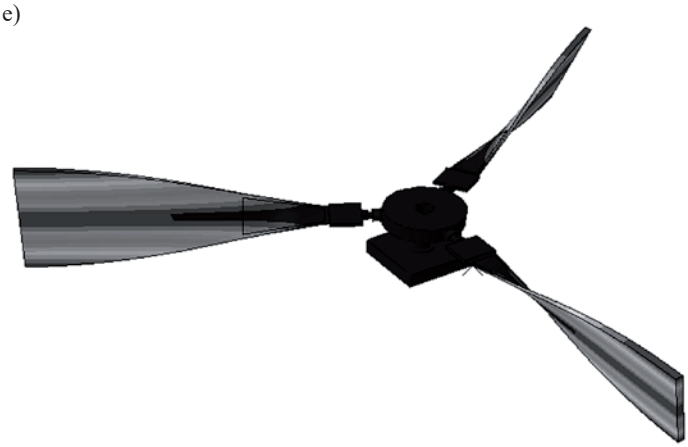

Fig. 8. Free vibration modes when the angular velocity is 500 rpm (c) - third in plane bending modes, (d) - first out of plane bending mode and (e)- first torsion mode

the rotational velocity. This is the centrifugal stiffening effect. Unfortunately, the strain-gauge can only verify the first mode vibrations. For higher natural frequencies, the signal from the strain-gauge is close to the level of noise. In the case of the experimental studies, the increase in the value of the first natural frequency versus the rotational velocity [7] can be described by:

$$\omega_1(n) = \sqrt{\omega_{\min}^2 + \left(\frac{n}{n_{\max}}\right)^2 \left(\omega_{\max}^2 - \omega_{\min}^2\right)} \tag{5}$$

where: n is the analyzed rotational velocity, ω_{min} is the experimental value of the natural frequency when the rotor is fixed, ω_{max} is the experimental value of the natural frequency when the tested angular velocity is maximum n_{max}= 500 rpm.

Both values can be read from Fig. 7. The final form of Eq. (5) can be written as:

$$\omega_1(n) = \sqrt{a + bn^2} \tag{6}$$

where: a and b are new constants.

Table 3 lists the values of the parameters a and b calculated by Eq. (5). These parameters were called strict values in Table 2. They were calculated based on two experimental points when the angular velocity was 0 or 500 rpm (Fig. 7). Further, these parameters were estimated using the nonlinear least squares solver in the Matlab software (lsqcurvefit function) [13]. In this case, all experimental points were taken into account. Both methods can be applied because the parameters a and b are almost the same. Eq. (5) helped describe the centrifugal stiffening effect very well.

Table 3. Comparison of the parameters a and b

Parameter	Strict values $a = \omega_{\min}^2$, $b = \frac{\omega_{\max}^2 - \omega_{\min}^2}{n_{\max}^2}$	Values estimated by Matlab	Error in %
FE model with MFC actuator			
a	109.1816	110.7562	1.4
b	0.0004953	0.000491	0.9
FE model without MFC actuator			
a	75.6117	75.7407	0.17
b	0.0004686	0.0004687	0.03
Experimental results			
a	84.9715	86.4554	1.7
b	0.0004351	0.00043799	0.7

Table 2. Natural frequencies vs. rotational velocity in FE analysis

Rotational velocity in rpm	Natural frequency ω^{FEM} in Hz				
	First in plane bending mode	Second in plane bending mode	Third in plane bending mode	First out of plane bending mode	First torsion mode
0	10.5	58.6	157.6	94.6	209.1
100	10.8	58.8	158.9	94.6	209.1
200	11.5	59.5	159.5	94.6	209.1
300	12.5	60.5	160.5	94.6	209.2
400	13.8	61.9	161.8	94.6	209.4
500	15.3	63.7	163.6	94.6	209.5

5. Influence of the MFC actuator on the blades dynamics

A change in the dynamic properties of the blades during rotation may be undesired. So, the initial stress and deflection of the blades can be induced using MFC elements. In this case, the piezoelectric actuator was powered by constant voltage. When placed asymmetrically (only on one side of the beam), the actuator produces a bending effect. It may have an impact on the beam dynamics. Therefore, successive tests were performed when one MFC actuator was powered by the following signal:

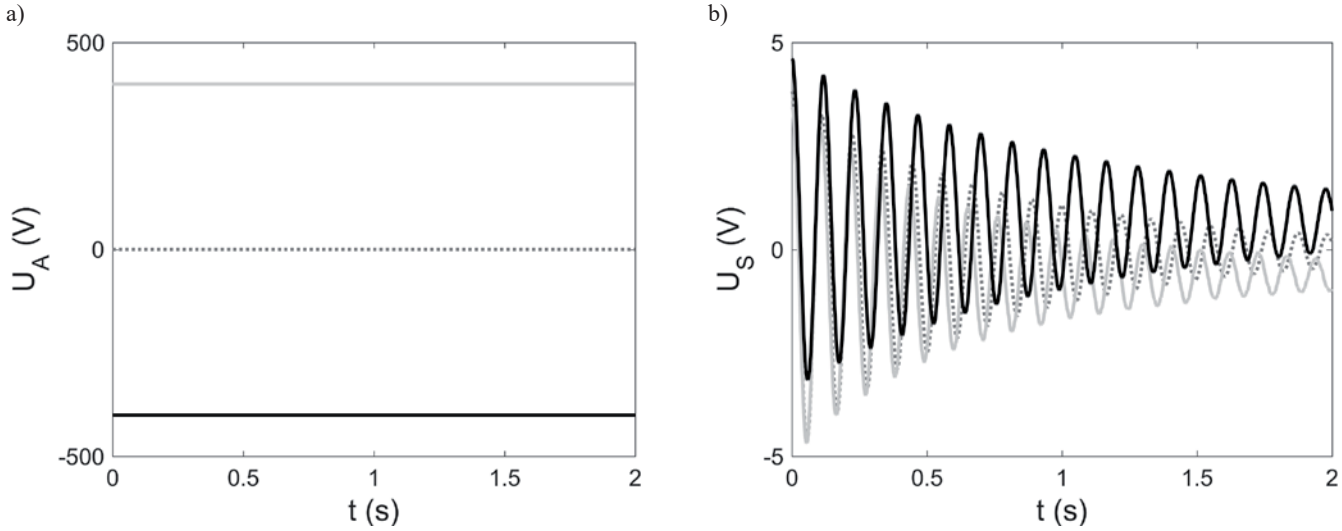

Fig. 9. Power supply voltage of the MFC element (a) and beam responses during the impact test (b) where: gray line - A_0= 400 V, dot line - A_0= 0 and black line - A_0= −400 V

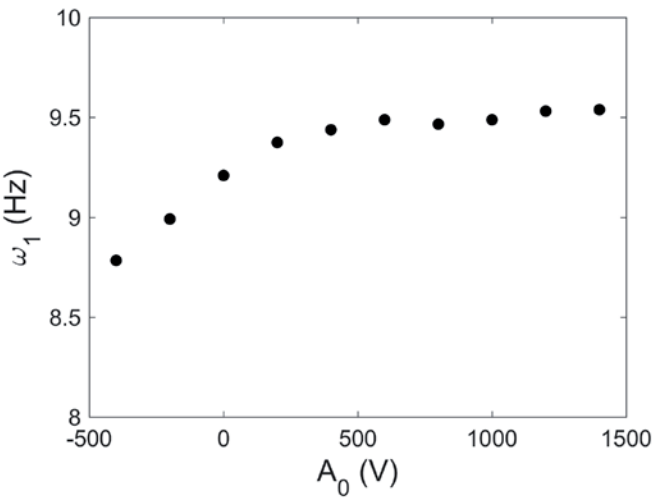

Fig. 10. First natural frequency of the blade vs. voltage parameter A_0 in the impact test

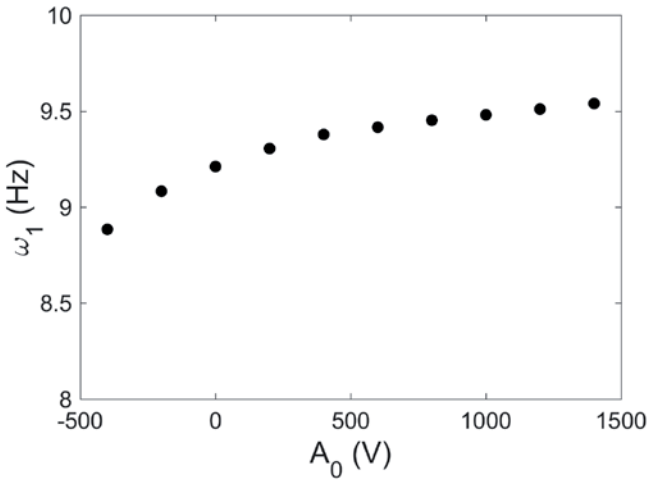

Fig.11. First natural frequency vs. voltage parameter A_0 in the sine sweep test

$$U_A(t) = A_0 \tag{7}$$

where: A_0 is a constant term, offset of the voltage.

The effect of the constant voltage parameter A_0 (Eq.(7)) on the first natural frequency was determined using the impact test. This test was performed when the constant value A_0 was changed from −400 V to +1400 V at 200 V. During the tests, the rotor was fixed. The actuator was supplied with constant voltage (Fig. 9a). The blade was excited using a modal hammer. A short fragment of the recorded signals from the selected impact tests is shown in Fig. 9b. Different voltage levels cause a change in the vibration period. A negative voltage led to an increase in the period of oscillation, in contrast to the case when the voltage parameter A_0 is 0. This can be called a softening effect (Fig. 9b). On the other hand, a positive voltage made this period decrease. This is a stiffening effect (Fig. 9b). All results are shown in Fig. 10. In the considered object, the use of the MFC actuator led to changing the frequency of free vibration by about ±0.5 Hz.

Next, the MFC actuator was used simultaneously for the control of the natural frequency (Eq.(7)) and vibration excitation (Eq.(1)). It is a sine sweep test. The supply voltage can be written as a function:

$$U_A(t) = A_0 + A\sin\left(\omega_0 t + \frac{1}{2}\varepsilon_A t^2\right) \tag{8}$$

The following parameters were applied: A_0 was changed from −400 V to 1400 V at 200 V, A was 100 V, $\omega_0 = 16\pi$ rad/s, $\varepsilon_A = \frac{7}{15}\pi$ rad/s^2. A selection of the applied signals U_A is given in Fig. 12a, whereas the blade responses are shown in Fig. 12b. Natural frequencies were determined using a time series. The results are shown in Fig. 11. The rotor was fixed.

Both methods led to obtaining a similar relation between the first natural frequency and the voltage parameter A_0 (see Figs. 10 and 11).

The possibility of control of the first bending natural frequency by the application the MFC actuator should ensure a partial reduction of the centrifugal stiffening effect. Therefore, the final stage of testing was to analyze the experimental case taking into consideration the above two. Thus, the rotor had a constant angular velocity and the MFC actuator was used for vibration excitation and the control of resonant frequency. The applied voltage signals U_A are shown in Fig. 12a. The following parameters were applied: A_0, was -400 V, 0 or

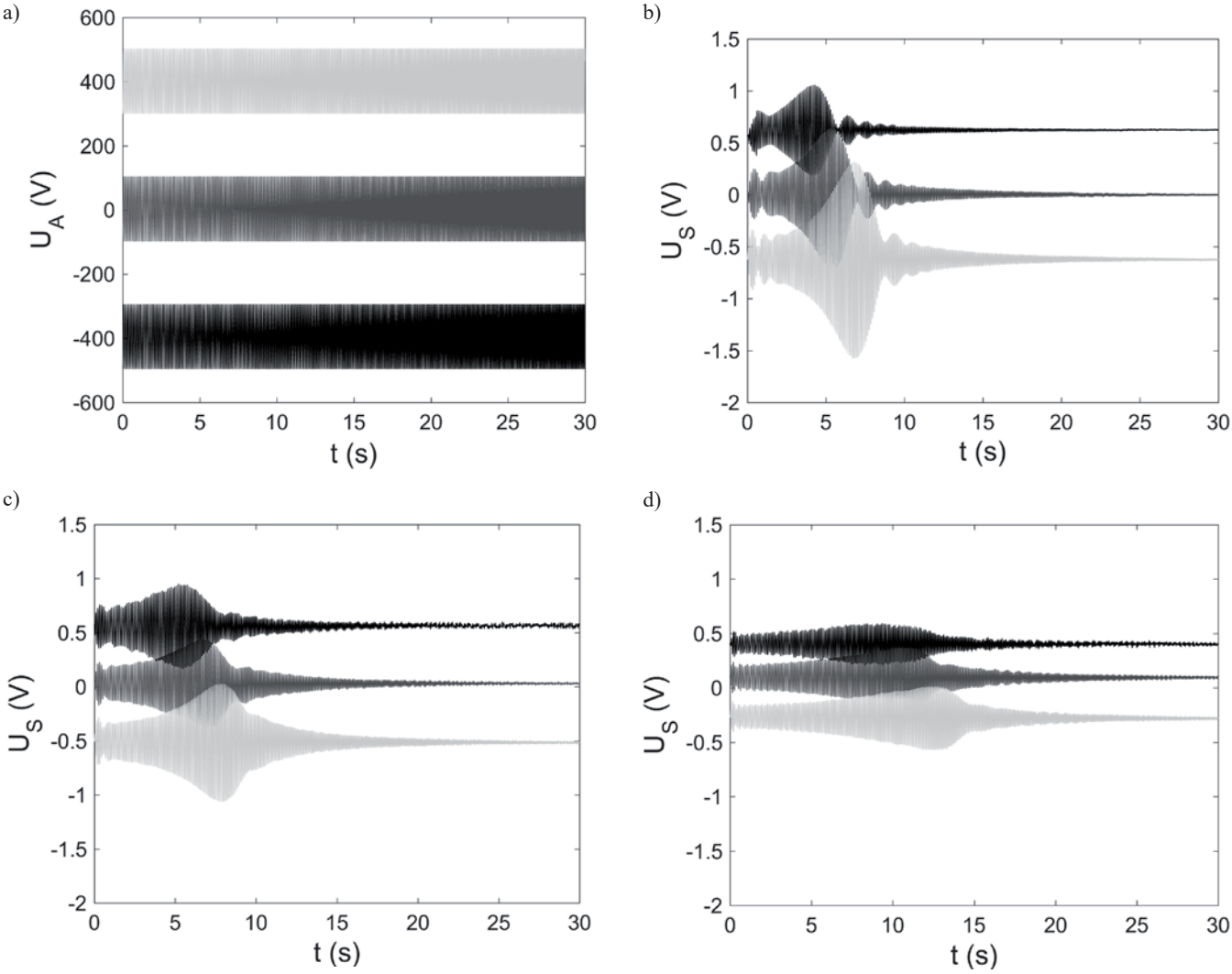

Fig. 12. Experimental results: supply of the MFC actuator (a) and blade response when the angular velocity was: 0 (b), 100 rpm (c) and 200 rpm (d)

+400 V, A was 100 V, $\omega_0 = 16\pi$ rad/s, $\varepsilon_A = \frac{7}{15}\pi$ rad/s^2 and the time window: $t \in \langle 0,30 \rangle s$. The signals from the strain-gauge at different angular velocities are given in Figs. 12b, c, d.

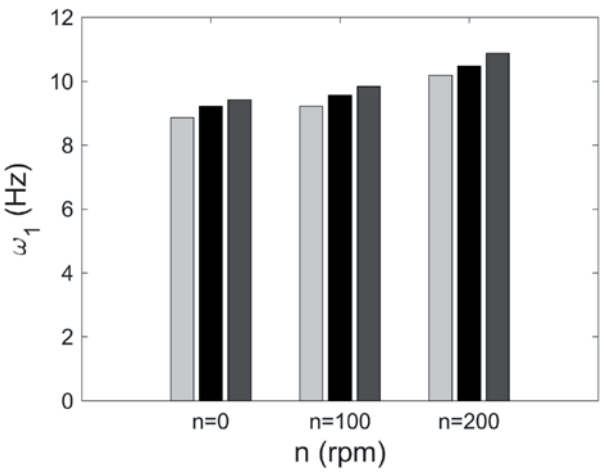

Fig.13. First natural frequency vs. rotational velocity n and control voltage parameter A_0 black color - A_0= 0, brown color - A_0= 400 V, gray color - A_0= -400 V

Using the previously described procedure (Eq. (3)), the natural frequencies were determined for a selected voltage parameter A_0 and rotating velocity. The results are shown in Fig. 13. The value of the voltage parameter A_0 was important and shifted the resonance area. The initial stresses and displacements contributed to a small change in the value of the first bending natural frequency [8, 9, 18, 19]. The active stiffening/softening effect depended on the size and position of the piezoelectric actuator. In our case, the MFC was small and was installed on one side of the blade. This may influence the results given in Fig. 13.

In the numerical study, the MFC actuator was modeled as a deformable body. It was a solid where two opposite walls were electrodes. Piezoelectric material was defined using the standard procedure in the Abaqus software [1]. This approach described the piezoelectric element in a macro scale, but the MFC actuator was not a monolithic crystal. In fact, it was a very complex structure where the PZT fibers as electrodes produce many cells. For example, the active element M-8503-P1 consists of 170 sections distant by 0.5 mm from each other [11]. The equivalent model based on the linear constitutive equation [6, 10]:

$$\begin{aligned} \varepsilon &= S\sigma + dE \\ D &= d\sigma + \xi E \end{aligned} \tag{9}$$

The mechanical phenomenon is described by: strain – ε, stress – σ and compliance – S. In the electrical domain, the following physical

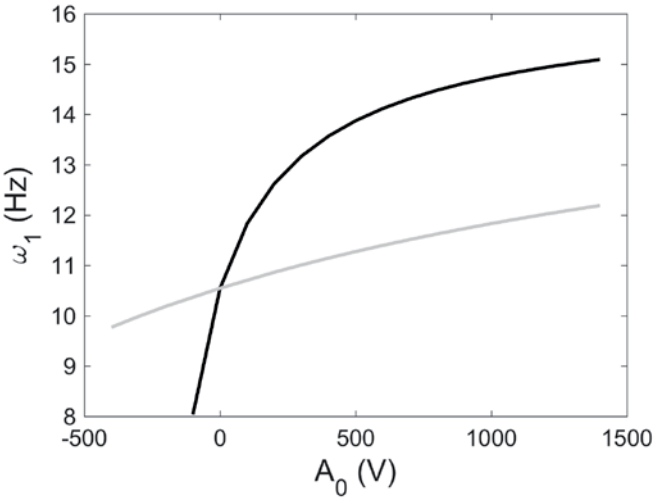

*Fig. 14. First natural frequency vs. parameter d_{33}. Black color – d_{33}= 1.01*10^{-7} m/V, gray color – d_{33}= 1.01*10^{-8} m/V*

parameters are applied: electrical field – E, electric charge – D and permittivity – ξ.

Both equations are coupled by an electromechanical coupling coefficient. The numerical modal analysis was performed, where one MFC actuator was powered by constant voltage. In the numerical model, the voltage-powered MFC element was defined by electrical boundary conditions. Fig. 14 shows the natural frequency of the first mode from the numerical analysis for different values of the coupling coefficient d_{33}. These curves reveal that the active stiffening effect depends on the value of the parameter d_{33}. In the literature [16], this parameter for MFC-8528-P1 was 1.01*10^{-7} m/V. Its value was estimated using the free strain test and the blocking force test. Finally, in the paper [11] this parameter was validated by a comparison of the maximum static deflection using numerical and experimental studies. However, the experimental results (Figs. 10 and 11) are closer to the numerical solution, when the parameter d_{33} was 1.01*10^{-8} m/V. This may be due to the fact that the applied model does not consider phenomena in a micro-scale. Additionally, this parameter cannot be maintained constant in the static and dynamical studies.

6. Conclusions

In the paper, the model of three blade rotor was presented. The experimental and numerical studies were conducted. The analysis investigated the phenomena of the centrifugal stiffening effect and piezoelectric stiffening/softening effects. The following conclusions were formulated:

a) When the rotational velocity was increased, the value of the first bending natural frequency of the blades increased too. The maximum change induced by the centrifugal stiffening effect was 4.7 Hz (Fig. 7, experimental data), when the angular velocity was changed from 0 to 500 rpm.
b) A constant voltage supply to the MFC actuator caused initial stresses/deflections, their value depending on the parameter A_0. This piezoelectric effect can generate a change in the value of natural frequency. The observed change in the first bending mode of the blade was about ±0.5 Hz. The nature of the changes (i.e., increase or decrease) depends on the voltage sign (Figs. 10 and 11).
c) The rotational velocity and the control voltage parameter A_0 are vital . Both parameters can interact with each another and can change the frequency of the first vibration mode. This effect was demonstrated in Fig. 13. However, the applied control voltage parameter A_0 is hardly effective.

The experimental findings were compared and confirmed by the results of the numerical anaZlysis by the finite elements method. The simulations were performed by the Abaqus software package. The studies on the active rotor will be continued in the future.

Acknowledgment

This research is financially supported by the Polish National Science Center under the research grant no. DEC2012/07/B/ST8/03931.

References

1. Abaqus 6.14 documentation.
2. Bilgen O, Wang Y, Inman D J. Electromechanical comparison of cantilevered beams with multifunctional piezoceramic devices. Mechanical Systems and Signal Processing 2012; 27: 763-777, https://doi.org/10.1016/j.ymssp.2011.09.002.
3. Brockmann T H. Theory of Adaptive Fiber Composites >From Piezoelectric Material Behavior to Dynamics of Rotating Structures. Springer Dordrecht Heidelberg London New York, 2009.
4. Brown G V, Kielb R E, Meyn E H, Morris R E, Posta S J. Lewis research center spin rig and its use in vibration analysis of rotating systems. NASA technical paper 2304, 1984.
5. Chaudhari N.B. Dynamics characteristics of wind turbine blade. International Journal of Engineering Research & Technology 2014; 3: 168-173.
6. Chopra I, Sirohi J. Smart structures theory. First edition. New York: Cambridge University Press, 2013. https://doi.org/10.1017/CBO9781139025164.
7. Chromek L. Design of the blisk of an aircraft turbojet engine and verification of its resonance free operation. Applied and Computational Mechanics 2016; 10: 17-26.
8. Hernandes J A, Almeida S F M, Nabarrete A. Stiffening effects on the free vibration behavior of composite plates with PZT actuators. Composite Structures 2000; 49: 55-63, https://doi.org/10.1016/S0263-8223(99)00125-7.
9. Kuo S Y. Stiffening effects on the natural frequencies of laminated beams with piezoelectric actuators. Journal of Aeronautics, Astronautics and Aviation 2010; 42: 67-72.
10. Latalski J. Modelling of a rotating active thin-walled composite beam system subjected to high electric fields. W: Advanced Methods of Continuum Mechanics for Materials and Structures, K. Naumenko, M. Assmus (eds.), Springer, Singapore 2016; 435-455, (ISBN 978-981-10-0958-7), https://doi.org/10.1007/978-981-10-0959-4_24.
11. Latalski J. Modelling of macro fiber composite piezoelectric active elements in Abaqus system. Eksploatacja i Niezawodnosc - Maintenance and Reliability 2011; 52(4): 72-78.
12. Latalski J, Bocheński M, Warmiński J, Jarzyna W, Augustyniak M. Modelling and simulation of 3 blade helicopter's rotor model. Acta Physica Polonica A 2014; 125(6): 1380-1383, https://doi.org/10.12693/APhysPolA.125.1380.
13. MathWorks documentation. <http://www.mathworks.com/help.html> (28.12.2016).

14. Sodano H A, Park G, Inman D J. An investigation into the performance of macro fiber composites for sensing and structural vibration applications. Mechanical Systems and Signal Processing 2004; 18: 683-697, https://doi.org/10.1016/S0888-3270(03)00081-5.
15. Smart Material. <http://www.smart-material.com/MFC-product-main.html> (28.12.2016).
16. Teter A, Gawryluk J. Experimental modal analysis of a rotor with active composite blades. Composite Structures 2016; 153: 451-467, https://doi.org/10.1016/j.compstruct.2016.06.013.
17. Truong K V, Yeo H, Ormiston R A. Structural dynamics modeling of rectangular rotor blades. Aerospace Science and Technology 2013; 30: 293-305, https://doi.org/10.1016/j.ast.2013.08.014.
18. Waisman H, Abramovich H. Active stiffening of laminated composite beams using piezoelectric actuators. Composite Structures 2002; 58: 109-120, https://doi.org/10.1016/S0263-8223(02)00035-1.
19. Waisman H, Abramovich H. Variation of natural frequencies of beams using the active stiffening effect. Composites Part B: Engineering 2002; 33: 415-424, https://doi.org/10.1016/S1359-8368(02)00031-8.

Andrzej MITURA
Jarosław GAWRYLUK
Andrzej TETER
Department of Applied Mechanics
Faculty of Mechanical Engineering
Lublin University of Technology
ul. Nadbystrzycka 36, PL-20-618 Lublin, Poland

E-mails: a.mitura@pollub.pl, j.gawryluk@pollub.pl, a.teter@pollub.pl

Article citation info:
DUAN R, HU L, LIN Y. Fault diagnosis for complex systems based on dynamic evidential network and multi-attribute decision making with interval numbers. Eksploatacja i Niezawodnosc – Maintenance and Reliability 2017; 19 (4): 580–589, http://dx.doi.org/10.17531/ein.2017.4.12.

Rongxing DUAN
Longfei HU
Yanni LIN

FAULT DIAGNOSIS FOR COMPLEX SYSTEMS BASED ON DYNAMIC EVIDENTIAL NETWORK AND MULTI-ATTRIBUTE DECISION MAKING WITH INTERVAL NUMBERS

DIAGNOSTYKA USZKODZEŃ SYSTEMU ZŁOŻONEGO OPARTA NA DYNAMICZNYCH SIECIACH DOWODOWYCH ORAZ WIELOATRYBUTOWEJ METODZIE PODEJMOWANIA DECYZJI Z WYKORZYSTANIEM LICZB INTERWAŁOWYCH

The complexity of modern system structures and failure mechanisms makes it very difficult to locate the system fault. It has characteristics of dynamics of failure, diversity of distribution and epistemic uncertainties, which increase the challenges in the fault diagnosis significantly. This paper presents a fault diagnosis framework for complex systems within which the failure rates of components are expressed in interval numbers. Specifically, it uses a dynamic fault tree (DFT) to model the dynamic fault behaviors and deals with the epistemic uncertainties using Dempster-Shafer (D-S) theory and interval numbers. Furthermore, a solution is proposed to map a DFT into a dynamic evidential network (DEN) to calculate the reliability parameters. Additionally, diagnostic importance factor (DIF), Birnbaum importance measure (BIM) and heuristic information values (HIV) are taken into account comprehensively in order to obtain the best fault search scheme using an improved VIKOR algorithm. Finally, an illustrative example is given to demonstrate the efficiency of this method.

Keywords: *diagnosis strategy, D-S theory, interval numbers, dynamic evidential network, VIKOR.*

Złożoność nowoczesnych struktur systemowych oraz mechanizmów uszkodzeń powoduje trudności w lokalizacji uszkodzeń systemu. Systemy złożone charakteryzują się cechami, takimi jak dynamika uszkodzeń, różnorodność rozkładów oraz niepewność epistemiczna, które czynią wyzwania dotyczące diagnostyki uszkodzeń znacznie trudniejszymi. W niniejszym artykule przedstawiono metodę diagnozowania uszkodzeń systemów złożonych, w której intensywność uszkodzeń poszczególnych składników wyraża się za pomocą liczb przedziałowych. W szczególności, podejście to wykorzystuje dynamiczne drzewo błędów (DFT) do modelowania dynamicznych zachowań związanych z uszkodzeniami oraz rozwiązuje problem niepewności epistemicznej przy użyciu teorii Dempstera-Shafera (DS) oraz liczb przedziałowych. W celu obliczenia parametrów niezawodności, zaproponowano rozwiązanie polegające na odwzorowaniu DFT w dynamiczną sieć dowodową (DEN). Dodatkowo, w sposób kompleksowy wykorzystano czynnik ważności diagnostycznej (DIF), miarę ważności Birnbauma (BIM) oraz wartości informacji heurystycznej (HIV), aby przy użyciu udoskonalonego algorytmu VIKOR uzyskać najlepszy system wyszukiwania błędów. Skuteczność omawianej metody zilustrowano na podstawie przykładu.

Słowa kluczowe: *strategia diagnostyczna, teoria Dempstera–Shafera, liczby przedziałowe, dynamiczna sieć dowodowa, VIKOR.*

1. Introduction

With the development of science and technology, the functional requirement and modernization level of modern equipments are increasing, which makes these systems become more and more complex and raises some challenges in fault diagnosis. These challenges are shown as follows. (1) Failure dependency of components. Modern engineering systems are becoming increasingly complex, which makes components interact with each other. So, dynamic fault behaviors should be taken into account to construct the fault model. (2) The life distributions of components are different. Modern systems include a variety of components, and they may have different life distributions. Some classical static modeling techniques, including reliability block diagram model [12], fault tree (FT) model [20], and binary decision diagrams (BDD) model [23] have been widely used to model static systems. But these models assume that all components follow the exponential distribution. However, in the practical engineering, different components may have different distributions. For complex systems, a mixed life distribution should be used to analyze these systems. (3) There are a large number of uncertain factors and uncertain information. Many complex systems have adopted a variety of fault tolerant technologies to improve their dependability. However, high reliability makes it difficult to get sufficient fault data. In the case of the small sample data, the traditional methods based on the probability theory are no longer appropriate for complex systems. Aiming at these challenges mentioned above, many efficient diagnostic methods have been proposed. In order to model the dynamic failure characteristics, DFT [6], Markov model [28] and dynamic Bayesian networks (DBN) [9, 26] have been proposed to capture the above mentioned dynamic failure behaviors. DFT is widely used to model the dynamic systems as the extensions of the traditional static fault trees with sequence- and function-dependent failure behaviors. Ge et al. present an improved sequential binary decision diagrams (SBDD) method for highly coupled DFT where different dynamic gates often coexist and interact

by repeated events [7]. A new approach was proposed by Merle et al. to solve DFT with priority dynamic gate and repeated events [17]. Chiacchio et al. presented a composition algorithm based on a Weibull distribution to address the resolution of a general class of DFT [2]. However, these methods assume that all components obey to the same distribution and cannot handle the challenge (2). Furthermore, these methods, which are usually assumed that the failure rates of the components are considered as crisp values describing their reliability characteristics, have been found to be inadequate to deal with the challenge (3) mentioned above. Therefore, fuzzy sets theory has been introduced as a useful tool to handle the challenge (3). The fuzzy fault tree analysis model employs fuzzy sets and possibility theory, and deals with ambiguous, qualitatively incomplete and inaccurate information [8, 16, 18]. To deal with the challenge (1) and (3), fuzzy DFT analysis has been introduced [13-14] which employs a DFT to construct the fault model and calculates the reliability results based on the continuous-time BN under fuzzy numbers. However, these approaches cannot handle the challenge (2). For this purpose, Mi et al. proposed a new reliability assessment approach which used a DFT to model the dynamic characteristics within complex systems and estimated the parameters of different life distributions using the coefficient of variation (COV) method [19]. To a certain extent, this method can meet the above challenges. But it is confined to the reliability analysis and cannot be used for the fault diagnosis. Dugan introduced a diagnostic importance factor (DIF) to determine the diagnosis sequence using DFT analysis [1]. However, the solution for DFT is based on Markov Chain which has an apparent state space explosion problem. In the work of [3], a hybrid fault diagnosis approach was proposed based on fault tree analysis and Bayesian network. Nevertheless, it used a static fault tree model and could not capture the dynamic failure behaviors. Furthermore, diagnosis strategies of these methods are only based on DIF and usually could not do decision making when there were many attributes for consideration. In addition, these diagnostic methods are usually assumed that the failure rates of components are regarded as crisp values and cannot deal with the challenge (3). To overcome these difficulties and limitations, Duan et al. proposed a diagnosis method based on fuzzy sets theory and DFT, which used fuzzy sets theory to estimate the failure rates of basic events and solved the DFT based on discrete-time Bayesian networks [5]. However, this approach could not handle the challenge (2). In addition, all the diagnosis algorithms are based on the single attribute decision making, and usually cause minimal cut sets with a smaller DIF to be diagnosed first [24], thereby influencing the diagnosis efficiency.

Motivated by the problems mentioned above, this paper presents a novel diagnosis strategy for complex systems based on DEN and an improved VIKOR algorithm shown in Fig. 1. It pays close attention to meeting above three challenges. In view of the challenge (1), it uses a DFT to capture the dynamic failure mechanisms. For the challenges (2) and (3), a mixed life distribution is used to analyze complex systems, and the COV method is employed to estimate the parameters of life distributions for components with interval numbers. Furthermore, relevant reliability parameters can be calculated by mapping a DFT into a DEN in order to avoid the aforementioned problems. At last, components' DIF, BIM and HIV are taken into account comprehensively to design a novel diagnosis strategy using an improved VIKOR algorithm. The proposed method takes full advantages of DFT, interval numbers for handling uncertainty, DEN for inference and VIKOR for the best fault search scheme, which is especially suitable for fault location of complex systems.

The remaining of this paper is organized as follows: In section 2, a DEN modeling is introduced and the conversion process from a DFT to a DEN is also provided; Section 3 presents a new fault diagnosis method based on an improved VIKOR algorithm; An illustrative example is provided to demonstrate the proposed method in Section 4; Finally, conclusions are made in Section 5.

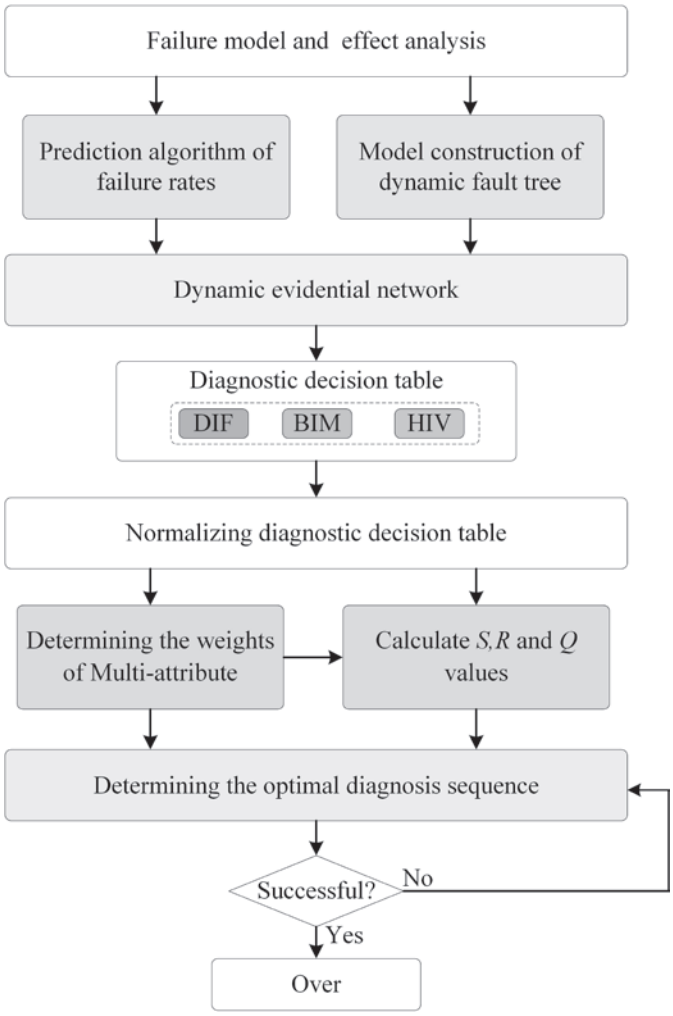

Fig. 1. A novel fault diagnosis framework for complex systems

2. DEN

D-S evidence theory has a unique ability in the expression of epistemic uncertainties. The evidence theory can be well compatible with the theory of probability. This section will describe how to compute the reliability parameters using DEN. The following simply introduces the relevant definitions and theorems in this paper, and more information can be referred to literatures [4,10,22]. Evidential Network is based on graph theory and D-S theory. It is a promising graphical tool for representing and managing uncertainties. Each node represents a variable, and arcs indicate direct conditional relations between the connected nodes. DEN, an extension of evidential network, takes into account the time by defining different nodes to model variables with respect to different time slices [21]. It includes the initial network and the temporal transition network. Each time slice corresponds to a static evidential network, and the time slices are a directed acyclic graph $G_T = < V_T, E_T >$ corresponding to the conditional probabilities. The V_T and E_T are respectively nodes of time T and directed arcs. A directed arc linked two variables belonging to different time slices.

In evidence theory, $\Theta = \{W_i, F_i\}$ is the knowledge framework of the component i and the focal elements are given by:

$$2^{\Theta} = \{\{\varnothing\}, \{W_i\}, \{F_i\}, \{W_i, F_i\}\} \tag{1}$$

where $\{W_i\}$ and $\{F_i\}$ denote the working and the failure state respectively. The state of $\{W_i, F_i\}$ corresponds to the epistemic uncertainty.

Belief measure (Bel) defines the lower bound of the probabilities that the focal element exists, and plausibility measure (Pl) defines the upper bound of the probabilities that the focal element exists. The basic belief assignment in the system state expresses an epistemic uncertainty, where *Bel* and *Pl* measures are not equal and bound the system reliability. Therefore, the basic probability assignment (BPA) of component *i* can be computed as:

$$\begin{aligned} &m(\{W_i\}) = Bel(\{W_i\}) \\ &m(\{F_i\}) = 1 - Pl(\{W_i\}) \\ &m(\{W_i, F_i\}) = Pl(\{W_i\}) - Bel(\{F_i\}) \end{aligned} \tag{2}$$

Presumably, the upper and lower bounds of the component reliability [$\underline{P(x)}, \overline{P(x)}$] is equivalent to the BPA in the DEN:

$$\begin{aligned} &m(\{W_i\}) = 1 - \overline{P(x)} \\ &m(\{F_i\}) = \underline{P(x)} \\ &m(\{W_i, F_i\}) = \overline{P(x)} - \underline{P(x)} \end{aligned} \tag{3}$$

where $Bel(\{F_i\}) = \underline{P(x)}, Pl(\{F_i\}) = \overline{P(x)}$.

2.1. Mapping a static fault tree into a DEN

The conditional probabilities of each node in the static evidential network have been discussed in detail in [25]. Fig. 2 shows an AND gate and its equivalent DEN. Equation 4 and 5 give the conditional probability of each node.

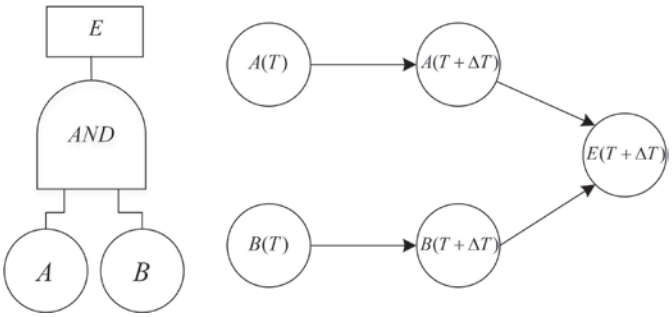

Fig. 2. An AND gate and its equivalent DEN

$$\begin{cases} P(A(T+\Delta T) = 1 \mid A(T) = 0) = 1 - \overline{P(x)} \\ P(A(T+\Delta T) = \{0,1\} \mid A(T) = 0) = \overline{P(x)} - \underline{P(x)} \\ P(A(T+\Delta T) = 1 \mid A(T) = 1) = 1 \\ P(A(T+\Delta T) = 1 \mid A(T) = \{0,1\}) = 1 - \overline{P(x)} \end{cases} \tag{4}$$

$$\begin{cases} P(E = 1 \mid A(T+\Delta T) = 1, B(T+\Delta T) = 1) = 1 \\ P(E = \{0,1\} \mid A(T+\Delta T) = 1, B(T+\Delta T) = \{0,1\}) = 1 \\ P(E = \{0,1\} \mid A(T+\Delta T) = \{0,1\}, B(T+\Delta T) = 1) = 1 \\ P(E = \{0,1\} \mid A(T+\Delta T) = \{0,1\}, B(T+\Delta T) = \{0,1\}) = 1 \\ P(E = 1 \mid else) = 0 \\ P(E = \{0,1\} \mid else) = 0 \end{cases} \tag{5}$$

2.2. Mapping a DFT into a DEN

DFT extended the traditional fault tree by defining some dynamic gates to capture the sequential and functional dependencies. Usually, there are six types of dynamic gates defined: the Functional Dependency Gates (FDEP), the Cold Spare Gates (CSP), the Hot Spare Gates (HSP), the Warm Spare Gates (WSP), the Priority AND Gates (PAND), and the Sequence Enforcing Gates (SEQ).

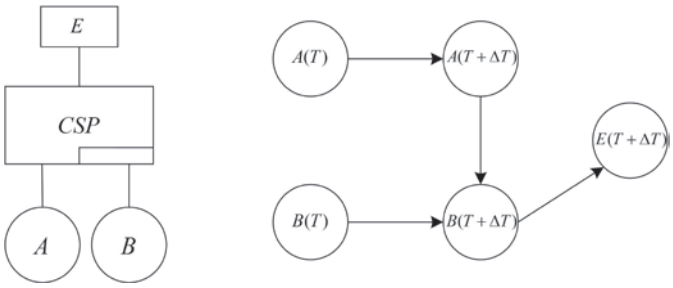

Fig. 3. CSP gate and its equivalent DEN

The following section briefly discusses a CSP gate as it is used later in the example. The CSP gate includes one primary input and one or more alternate inputs. Fig. 3 shows a CSP gate and its equivalent DEN. Suppose that *A* and *B* follow the same distribution, then $\underline{P(x)}$ and $\overline{P(x)}$ denote the lower probability and upper probability of the nodes respectively. At this point, node *A* has the same conditional probability with the AND gate of the node *A* and the conditional probability of other node *B* can be calculated by the following equations:

$$\begin{cases} P(B(T+\Delta T) = 0 \mid A(T+\Delta T) = 0) = 0 \\ P(B(T+\Delta T) = 1 \mid A(T+\Delta T) = 1, B(T) = 0) = \underline{P(x)} \\ P(B(T+\Delta T) = 1 \mid A(T+\Delta T) = 1, B(T) = 1) = 1 \\ P(B(T+\Delta T) = 1 \mid A(T+\Delta T) = 1, B(T) = \{0,1\}) = \underline{P(x)} \\ P(B(T+\Delta T) = \{0,1\} \mid A(T+\Delta T) = \{0,1\}) = \overline{P(x)} - \underline{P(x)} \end{cases} \tag{6}$$

$$\begin{cases} P(E = 0 \mid B(T+\Delta T) = 0) = 1 \\ P(E = 1 \mid B(T+\Delta T) = 1) = 1 \\ P(E = \{0,1\} \mid B(T+\Delta T) = \{0,1\}) = 1 \end{cases} \tag{7}$$

2.3. Calculating reliability parameters

After a DFT model is built, The DFT is converted into an equivalent DEN using the proposed method. Once the structure of the DEN is known and the probability tables are filled, the reliability parameters of the system can be calculated using the DEN inference algorithm. These reliability parameters mainly include system unreliability, DIF, BIM and HIV, which are used for fault diagnosis in the proposed method.

2.3.1. System unreliability

Calculating the system unreliability is very simple using the following equation:

$$P_S = [\underline{P_S}, \overline{P_S}] = [Bel(\{F_S\}), Pl(\{F_S\})] \tag{8}$$

where $[Bel(\{F_S\}), Pl(\{F_S\})]$ represents the failure probability of system.

2.3.2. DIF

DIF is defined conceptually as the probability that an event has occurred given that the top event has also occurred. DIF is the cornerstone of reliability based diagnosis methodology [1]. DIF can be used to locate the faulty components in order to minimize the system checks and diagnostic cost. It is given by:

$$DIF_i = P(i \mid S) = [Bel(\{F_{i|S}\}), Pl(\{F_{i|S}\})] \tag{9}$$

where i is a component of system S; $P(i \mid S)$ is the probability that the basic event i has occurred given the top event has occurred.

Suppose the system has failed at the mission time, we input the evidence that system has failed into DEN and get the DIF of components using the inference algorithm.

2.3.3. BIM

Birnbaum first introduced the concept of a components' reliability importance in 1969. This measure was defined as the probability that a component is critical to system failures. i.e. when component i fails it causes the system to move from a working to a failed state. BIM of a component i can be interpreted as the rate at which the system's reliability improves as the reliability of component i is improved [21]. Analytically, Birnbaum's importance interval measure of a component i can be defined using D-S theory by the following equation:

$$\begin{aligned}[I^B(i)] &= [Bel(\{W_S\} \mid \{W_i\}), Pl(\{W_S\} \mid \{W_i\})] - [Bel(\{W_S\} \mid \{F_i\}), Pl(\{W_S\} \mid \{F_i\})] \\ &= [\underline{P}_{S|Wi}, \overline{P}_{S|Wi}] - [\underline{P}_{S|Fi}, \overline{P}_{S|Fi}]\end{aligned} \tag{10}$$

where $Bel(\{W_s\} \mid \{W_i\})$ and $Pl(\{W_s\} \mid \{W_i\})$ denote respectively the belief and plausibility measures that the system is functioning when it is known that component i is in a working state. Whereas $Bel(\{W_s\} \mid \{F_i\})$ and $Pl(\{W_s\} \mid \{F_i\})$ denote respectively the belief and plausibility measures that the system is functioning when component i is in a failed state.

2.3.4. HIV

The heuristic function plays an important role in the diagnostic sequence [11]. Owing to the different complexity of components their test cost is different, a balance should be taken into account between the DIF and test cost. Therefore, a new heuristic function for complex systems, HIV is proposed. HIV represents the value of the heuristic information contained in each fault search path and the influence degree of the fault search on the next optimal fault search. With the combination of DIF and the test cost, HIV is defined by the following expression:

$$HIV_i = \frac{DIF_i}{T_i} = \frac{P(i \mid s)}{T_i} \tag{11}$$

Table 1. Evaluation standards of the test cost

Linguistic expression for test cost	Interval values
Very High	[0.9 1.0]
High	[0.7 0.9]
Moderate	[0.5 0.7]
Low	[0.3 0.5]
Very Low	[0.1 0.3]

The test cost of the components is usually very difficult to express as crisp values because of uncertainties. So the linguistic assessments are used for generating criteria and alternative ratings, which are transformed into interval numbers to describe test cost of the components for treatment by VIKOR. Table 1 shows the evaluation criteria and alternative ratings of the test cost.

3. Fault diagnosis strategy based on an improved VIKOR algorithm

The basic information provided by reliability analysis can be used to construct the diagnostic decision table for fault diagnosis. Assume that the DEN has n root nodes, each root node represents a diagnostic scheme, $x_i (i = 1, 2, \cdots, n)$ represents the diagnostic scheme and each root node has k reliability parameters. DIF enables us to discriminate between components by their importance from a diagnostic point of view. BIM is used to quantify the contributions of components' reliability to the systems' reliability and HIV plays an important role in the diagnostic sequence. DIF, BIM, and HIV are treated as attribute v1, v2 and v3 respectively. These attributes can be considered comprehensively to obtain the best faulty search scheme using an improved VIKOR algorithm [27].

3.1. Normalizing diagnostic decision table

Fault diagnosis is a process to optimize multi-attribute decision making. After the search scheme for fault diagnosis is defined, we can construct the diagnostic decision table by the corresponding evaluation attributes. However, different evaluation attributes usually have different values and dimensions, which are not directly comparable, so we should normalize the diagnostic decision table. Evaluation attributes can be divided into two classes: benefit attributes and cost attributes. There are three attributes in the diagnostic decision table, DIF, BIM and HIV, which belong to the benefit attributes. For the different data, we use the following formula to normalize them.

When the attribute x_{ij} is a benefit attribute, we use the following formula to normalize them:

$$\tilde{f}_{ij}^t = [\underline{f}_{ij}^t, \overline{f}_{ij}^t] = [\frac{\underline{x}_{ij}^t}{\sum_{i=1}^{m} \overline{x}_{ij}^t}, \frac{\overline{x}_{ij}^t}{\sum_{i=1}^{m} \underline{x}_{ij}^t}] \tag{12}$$

where x_{ij} is the jth attribute value of the ith component.

When the attribute x_{ij} is a cost attribute, we normalize them by using the following formula:

$$\tilde{f}_{ij}^t = [\underline{f}_{ij}^t, \overline{f}_{ij}^t] = [\frac{\frac{1}{\overline{x}_{ij}^t}}{\sum_{i=1}^{m} \frac{1}{\underline{x}_{ij}^t}}, \frac{\frac{1}{\underline{x}_{ij}^t}}{\sum_{i=1}^{m} \frac{1}{\overline{x}_{ij}^t}}] \tag{13}$$

3.2. Determining the weights of attributes

Shannon Entropy is a measure of uncertainty of information formulated in terms of probability theory [15]. It is well suited for measuring the relative contrast intensities of criteria to represent the average intrinsic information transmitted to the decision makers. Entropy weighting is a multi-attribute decision making (MADM) method used to determine the important weights of decision attributes by directly relating a criterion's importance weighting relative to the information transmitted by that criterion. However, because the elements of the

decision matrix are interval numbers, the Entropy method cannot be used directly. Therefore, before the entropy method is put into use, the decision matrix needs to be quantized.

The diagnosis decision table needs to be normalized before the positive and negative ideal solutions are being calculated. The positive ideal solutions are made of all the best performance scores, and the negative solutions are made of all the worst performance scores at these measures in the diagnostic decision table. To compute the positive and negative ideals, by the relations:

$$f_j^+ = \max_{i\in M} \overline{f}_{ij}, f_j^- = \min_{i\in M} \underline{f}_{ij} \quad j \in N \tag{14}$$

Suppose that $a=[a^-,a^+]$ and $b=[b^-,b^+]$ are two interval numbers, the interval deviation degree distance $D(a,b)$ between $a=[a^-,a^+]$ and $b=[b^-,b^+]$ is :

$$D(a,b)=\sqrt{(a^- - b^-)^2 + (a^+ - b^+)^2} \tag{15}$$

The larger the interval deviation degree distance $D(a,b)$, the greater the degree of phase separation will be. In particular, when $D(a,b)=0$, then $a = b$, which means that a and b are equal.

The diagnostic decision table is the interval numbers, which are difficult to directly compare. In order to determine the weight of attributes, the concept of the interval deviation degree distance is used. The objective weights of attributes can be calculated based on the Entropy concept through the following steps:

Step 1: Transform the normalization matrix $\tilde{f}_{ij}^t = [\underline{f}_{ij}^t, \overline{f}_{ij}^t]$ into the interval deviation degree distance matrix $D=(d_{ij})_{n\times m}$, where $d_{ij}=D(f_{ij},f_j^*)$; $f_j^*=[f_j^-,f_j^+]$.

Step 2: Normalize the evaluation criterion for the interval deviation degree distance matrix through:

$$p_{ij} = \frac{d_{ij}}{\sum_{i=1}^{n} d_{ij}} \tag{16}$$

where $\sum_{i=1}^{n} p_{ij} = 1, j=1,2,\cdots,m$.

Step 3: Obtain the entropy $H_j H_j$ value of the attributes j as follows:

$$H_j = -K\sum_{i=1}^{n} p_{ij} \ln p_{ij} (j=1,2,\cdots,m) \tag{17}$$

where $K=1/\ln n$ $(K>0, 0\le p_{ij}\le 1)$ and assume $p_{ij}=0$, then $p_{ij}\ln p_{ij}=0$.

Step 4: Define the value of α_j through:

$$\alpha_j = 1 - H_j \tag{18}$$

Where α_j is the divergence degree of the intrinsic information of the attributes j. The greater the value of α_j, the more important the attribute is in the decision making process.

Step 5: Calculate the weights of attributes using the following equation:

$$\omega_j = \frac{\alpha_j}{\sum_{j=1}^{m} \alpha_j} \tag{19}$$

3.3. Calculating the values $S_i=[\underline{S}_i,\overline{S}_i]$ and $R_i=[\underline{R}_i,\overline{R}_i]$

The value $S_i=[\underline{S}_i,\overline{S}_i]$ of all the decision-making program group is calculated by the linear programming mothed:

$$\min S_i' = \sum_{j=1}^{n} \omega_j' \left(\frac{f_j^+ - \overline{f}_{ij}}{f_j^+ - f_j^-} \right)$$
$$s.t. \begin{cases} \underline{\omega}_j \le \omega_j' \le \overline{\omega}_j, j\in N \\ \sum_{j=1}^{n} \omega_j' = 1 \end{cases} \tag{20}$$

$$\max S_i'' = \sum_{j=1}^{n} \omega_j'' \left(\frac{f_j^+ - \underline{f}_{ij}}{f_j^+ - f_j^-} \right)$$
$$s.t. \begin{cases} \underline{\omega}_j \le \omega_j'' \le \overline{\omega}_j, j\in N \\ \sum_{j=1}^{n} \omega_j'' = 1 \end{cases} \tag{21}$$

Suppose the optimal solutions of model (20) and (21) are $\omega' = (\omega_1', \omega_2', \cdots, \omega_n')$ and $\omega'' = (\omega_1'', \omega_2'', \cdots, \omega_n'')$ $S_i=[\underline{S}_i,\overline{S}_i]$ respectively, then we can compute the interval values $S_i=[\underline{S}_i,\overline{S}_i]$ by the linear programming method. where $\underline{S}_i$ and $\overline{S}_i$ are defined by:

$$\underline{S}_i = \sum_{j=1}^{n} \omega_j' \left(\frac{f_j^+ - \overline{f}_{ij}}{f_j^+ - f_j^-} \right) \tag{22}$$

$$\overline{S}_i = \sum_{j=1}^{n} \omega_j'' \left(\frac{f_j^+ - \underline{f}_{ij}}{f_j^+ - f_j^-} \right) \tag{23}$$

Similarly, the interval values $R_i=[\underline{R}_i,\overline{R}_i], i\in M$ can also be computed by the linear programming method. where $\underline{R}_i$ and $\overline{R}_i$ are given by:

$$\underline{R}_i = \max_{j\in N} \left\{ \omega_j' \left(\frac{f_j^+ - \overline{f}_{ij}}{f_j^+ - f_j^-} \right) \right\} \tag{24}$$

$$\overline{R}_i = \max_{j\in N} \left\{ \omega_j'' \left(\frac{f_j^+ - \underline{f}_{ij}}{f_j^+ - f_j^-} \right) \right\}, i\in M \tag{25}$$

3.4. Calculating the values $Q_i=[\underline{Q}_i,\overline{Q}_i]$

We can calculate the values of $Q_i=[\underline{Q}_i,\overline{Q}_i]$ by the relations:

$$\underline{Q}_i = v\frac{\underline{S}_i - S^-}{S^+ - S^-} + (1-v)\frac{\underline{R}_i - R^-}{R^+ - R^-} \tag{26}$$

$$\overline{Q}_i = v\frac{\overline{S}_i - S^-}{S^+ - S^-} + (1-v)\frac{\overline{R}_i - R^-}{R^+ - R^-} \tag{27}$$

where $S^- = \min_i \underline{S}_i, S^+ = \max_i \overline{S}_i, R^- = \min_i \underline{R}_i, R^+ = \max_i \overline{R}_i$ and v is introduced as the weight for the strategy of maximum group utility, whereas $1-v$ is the weight of the individual regret. Usually, v can take any value from 0 to 1 and the value of v is set to 0.5 in the paper.

3.5. Determining the optimal diagnosis sequence

After the value of $Q_i = [\underline{Q}_i, \overline{Q}_i]$ expressed in interval numbers is obtained, the possibility matrix should be built to rank the alternatives. The possibility matrix can be defined as:

$$p = \begin{bmatrix} 0.5 & p(Q_1 \geq Q_2) & \cdots & p(Q_1 \geq Q_m) \\ p(Q_2 \geq Q_1) & 0.5 & \cdots & p(Q_2 \geq Q_m) \\ \cdots & \cdots & \ddots & \cdots \\ p(Q_m \geq Q_1) & p(Q_m \geq Q_2) & & 0.5 \end{bmatrix} \tag{28}$$

Then the corresponding possibility $p(x_i)$ can be obtained using the following equation.

$$p(x_i) = \sum_{j=1}^{m} p(Q_k \geq Q_i), i,k \in M \tag{29}$$

Obviously, the smaller the value $p(x_i)$, the better the diagnostic scheme. Therefore, we can determine the optimal ranking order by the value $p(x_i)$ and choose the diagnostic scheme with the minimum value $p(x_i)$.

4. Numerical Application

An illustrative example is given to illustrate how the proposed method can be used to perform the diagnosis strategy analysis for the braking system using multi-attribute decision making with interval numbers. Suppose all components follow the exponential distribution or two-parameter Weibull distribution. For the components with an exponential distribution, the interval failure rates of the basic events for the braking system can be calculated using the expert elicitation and the fuzzy sets theory. For the components with a two-parameter Weibull distribution, the interval failure rates are calculated using the COV method [19]. DFT of the braking system is shown in Fig. 4. The interval failure rates of basic events are shown in Table 2. We can map the DFT into the equivalent DEN shown in Fig. 5.

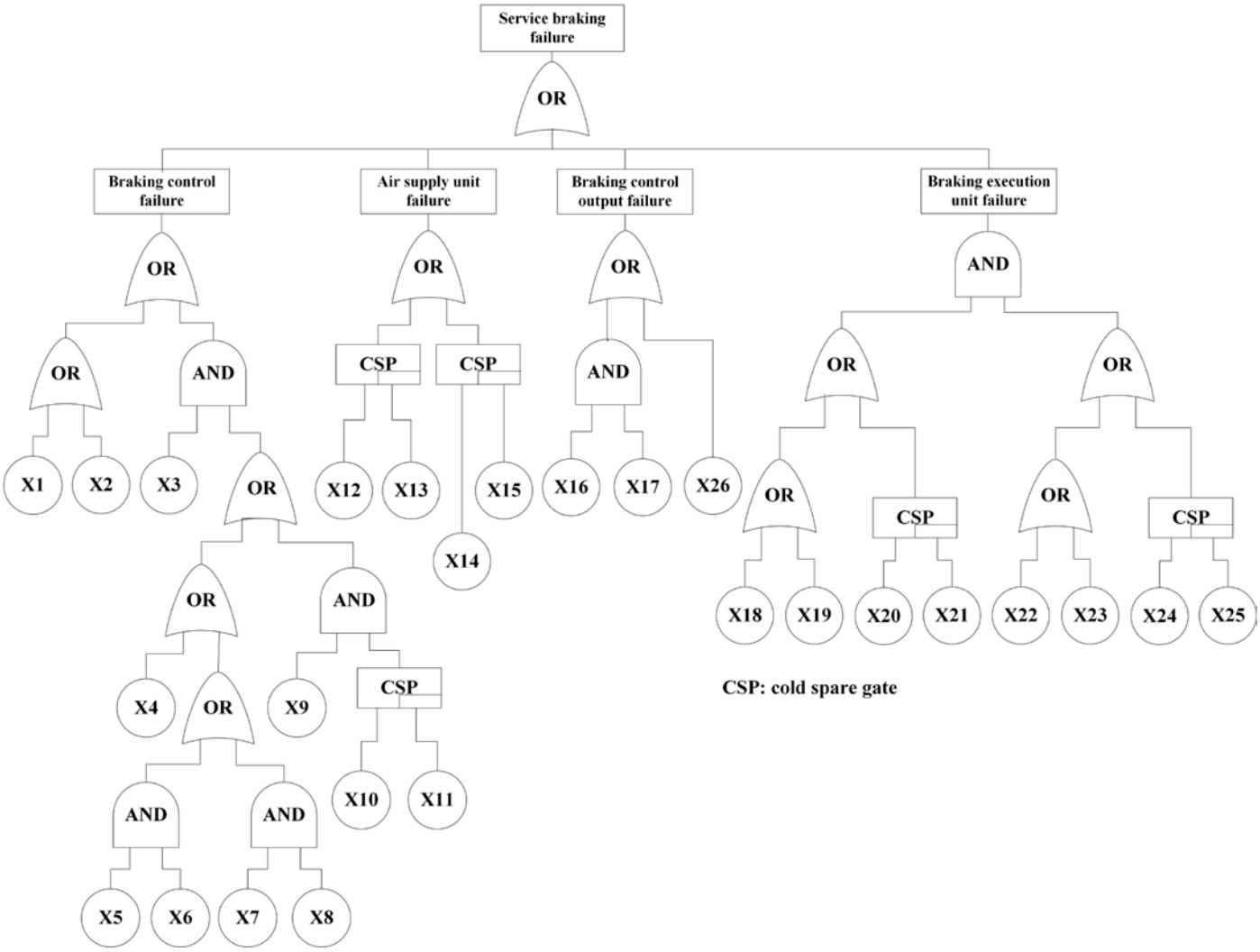

Fig. 4. A DFT for service braking failure of braking syste

Table 2. The interval failure rates of basic events

Components	Failure rate/ hour	Components	Failure rate/hour
X1	[2.88e-6 4.20e-6]	X12, X13	[6.96e-6 1.04e-5]
X3, X9	[6.08e-7 9.12e-7]	X14, X15	[5.68e-6 8.52e-6]
X10, X11	[6.08e-7 9.12e-7]	X16, X17	[5.44e-7 8.16e-7]
X4	[3.28e-7 4.92e-7]	X18, X19	[3.84e-5 5.76e-5]
X5	[1.12e-5 1.68e-5]	X20, X21	[3.84e-5 5.76e-5]
X6	[0.80e-6 1.20e-6]	X22, X23	[3.04e-5 4.56e-5]
X7	[0.88e-5 1.32e-5]	X24, X25	[3.04e-5 4.56e-5]
X8	[7.12e-6 1.07e-5]	*X26*	[6.24e-6 9.36e-6]

Table 3. Occurrence probabilities of failure at the different mission time

Mission time (h)	Interval occurrence probability
500	[0.00644 0.01321]
1000	[0.01550 0.03322]
1500	[0.02690 0.05857]
2000	[0.04035 0.08805]

In this numerical example, component *X2* follows a two-parameter Weibull distribution with parameters η and β, and the distribution function is calculated as follows:

$$F(t) = P(T \le t) = \begin{cases} 1 - exp\{-(\frac{\Delta t}{\eta})^{\beta}\}, t > 0 \\ 0 \qquad\qquad t \le 0 \end{cases} \tag{30}$$

Table 4. Components' test cost and HIV of the components

Components	Test cost T_i	HIV
X1	[0.9 1.0]	[0.14233 0.16066]
X2	[0.5 0.7]	[0.06333 0.08992]
X3	[0.1 0.3]	[0.00413 0.01850]
X4	[0.7 0.9]	[0.00074 0.00143]
X5	[0.7 0.9]	[0.02461 0.04720]
X6	[0.7 0.9]	[0.00178 0.00343]
X7	[0.7 0.9]	[0.01939 0.03723]
X8	[0.7 0.9]	[0.01572 0.03020]
X9	[0.1 0.3]	[0.00407 0.01820]
X10	[0.1 0.3]	[0.00407 0.01820]
X11	[0.1 0.3]	[3.08e-06 0.00610]
X12	[0.9 1.0]	[0.01664 0.02607]
X13	[0.9 1.0]	[0.00297 0.01099]
X14	[0.9 1.0]	[0.00111 0.00183]
X15	[0.9 1.0]	[1.83e-5 0.00062]
X16	[0.1 0.3]	[0.00373 0.01660]
X17	[0.1 0.3]	[0.00373 0.01660]
X18	[0.5 0.7]	[0.42227 0.64426]
X19	[0.5 0.7]	[0.42227 0.64426]
X20	[0.3 0.5]	[0.13046 0.31073]
X21	[0.3 0.5]	[0.01766 0.01284]
X22	[0.5 0.7]	[0.42227 0.64426]
X23	[0.5 0.7]	[0.42227 0.64426]
X24	[0.3 0.5]	[0.13046 0.31073]
X25	[0.3 0.5]	[0.01766 0.12837]
X26	[0.5 0.7]	[0.43907 0.62332]

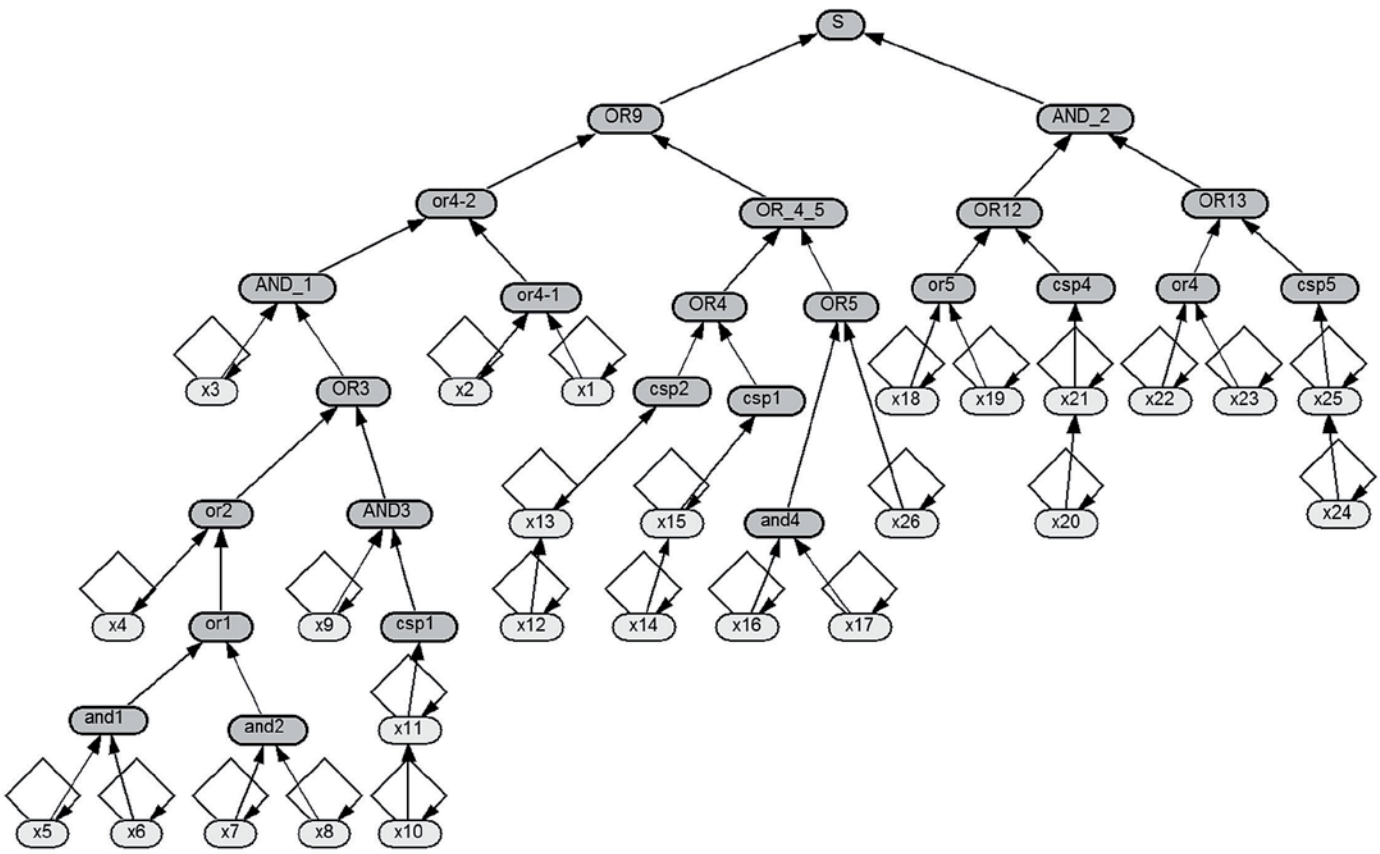

Fig. 5. A DEN of the braking system

Table 5. The diagnostic decision table for the braking system

Components	DIF	BIM	HIV
X1	[0.14233 0.14459]	[0.91965 0.965196]	[0.14233 0.16066]
X2	[0.04433 0.04496]	[0.91419 0.961368]	[0.06333 0.08992]
X3	[0.00124 0.00185]	[-0.04679 0.049173]	[0.00413 0.01850]
X4	[0.00067 0.00100]	[-0.04653 0.049354]	[0.00074 0.00143]
X5	[0.02215 0.03304]	[-0.04770 0.047695]	[0.02461 0.04720]
X6	[0.00160 0.00240]	[-0.04767 0.047745]	[0.00178 0.00343]
X7	[0.01745 0.02606]	[-0.04768 0.047724]	[0.01939 0.03723]
X8	[0.01415 0.02114]	[-0.04768 0.047734]	[0.01572 0.03020]
X9	[0.00122 0.00182]	[-0.04770 0.047695]	[0.00407 0.01820]
X10	[0.00122 0.00182]	[-0.04770 0.047695]	[0.00407 0.01820]
X11	[9.23e-7 0.00061]	[-0.04770 0.047695]	[3.08e-06 0.00610]
X12	[0.01664 0.02346]	[-0.03301 0.05561]	[0.01664 0.02607]
X13	[0.00297 0.00989]	[0.91843 0.95976]	[0.00297 0.01099]
X14	[0.00111 0.00165]	[-0.04654 0.048318]	[0.00111 0.00183]
X15	[1.83e-05 0.00056]	[0.91245 0.959648]	[1.83e-5 0.00062]
X16	[0.00112 0.00166]	[-0.04665 0.049183]	[0.00373 0.01660]
X17	[0.00112 0.00166]	[-0.04665 0.049183]	[0.00373 0.01660]
X18	[0.29559 0.32213]	[0.09422 0.228649]	[0.42227 0.64426]
X19	[0.29559 0.32213]	[0.09422 0.228649]	[0.42227 0.64426]
X20	[0.06523 0.09322]	[-0.03775 0.054004]	[0.13046 0.31073]
X21	[0.00883 0.03851]	[0.07898 0.219255]	[0.01766 0.12837]
X22	[0.29559 0.32213]	[0.09422 0.228649]	[0.42227 0.64426]
X23	[0.29559 0.32213]	[0.09422 0.228649]	[0.42227 0.64426]
X24	[0.06523 0.09322]	[-0.03775 0.054005]	[0.13046 0.31073]
X25	[0.00883 0.03851]	[0.07898 0.219255]	[0.01766 0.12837]
X26	[0.30735 0.31166]	[0.91919 0.971704]	[0.43907 0.62332]

Table 6. Interval values of S, R and Q for all components

Components	$S_i = [\underline{S}_i, \overline{S}_i]$	$R_i = [\underline{R}_i, \overline{R}_i]$	$Q_i = [\underline{Q}_i, \overline{Q}_i]$
X1	[0.4365 0.6208]	[0.2503 0.2896]	[0.5827 0.7376]
X2	[0.5777 0.7352]	[0.2873 0.3140]	[0.7120 0.8338]
X3	[0.9620 0.9974]	[0.3320 0.3328]	[0.9776 0.9969]
X4	[0.9718 0.9989]	[0.3329 0.3333]	[0.9840 0.9985]
X5	[0.9153 0.9723]	[0.3091 0.3326]	[0.9721 0.9866]
X6	[0.9697 0.9980]	[0.3317 0.3329]	[0.9183 0.9839]
X7	[0.9277 0.9782]	[0.3142 0.3326]	[0.9326 0.9868]
X8	[0.9364 0.9823]	[0.3179 0.3326]	[0.9427 0.9889]
X9	[0.9627 0.9976]	[0.3320 0.3328]	[0.9780 0.9971]
X10	[0.9627 0.9976]	[0.3320 0.3328]	[0.9780 0.9971]
X11	[0.9702 1.0000]	[0.3333 0.3339]	[0.9838 1.0000]
X12	[0.9336 0.9767]	[0.3200 0.3295]	[0.9445 0.9812]
X13	[0.6554 0.7903]	[0.3278 0.3326]	[0.8145 0.8908]
X14	[0.9971 0.9984]	[0.3326 0.3332]	[0.9832 0.9980]
X15	[0.6705 0.7952]	[0.3333 0.3339]	[0.8307 0.8953]
X16	[0.9632 0.9976]	[0.3322 0.3329]	[0.9785 0.9972]
X17	[0.9632 0.9976]	[0.3322 0.3329]	[0.9785 0.9972]
X18	[0.2466 0.5716]	[0.2466 0.3023]	[0.4797 0.7322]
X19	[0.2466 0.5716]	[0.2466 0.3023]	[0.4797 0.7322]
X20	[0.7144 0.8985]	[0.3045 0.3305]	[0.8086 0.9428]
X21	[0.8107 0.9595]	[0.2940 0.3281]	[0.8415 0.9703]
X22	[0.2466 0.5716]	[0.2466 0.3023]	[0.4797 0.7322]
X23	[0.2466 0.5716]	[0.2466 0.3023]	[0.4797 0.7322]
X24	[0.7134 0.8985]	[0.3045 0.3305]	[0.8080 0.9428]
X25	[0.8107 0.9595]	[0.2940 0.3281]	[0.8415 0.9703]
X26	[0.0217 0.3798]	[0.0109 0.1980]	[0 0.4727]

Table 7. The value of $p(x_i)$ for all components

Components	$p(x_i)$	Components	$p(x_i)$	Components	$p(x_i)$
X1	5.1472	X10	17.7954	X19	3.5006
X2	9.0748	X11	17.9431	X20	13.4062
X3	17.7862	X12	16.9198	X21	14.6798
X4	17.9213	X13	12.4142	X22	3.5006
X5	16.4790	X14	17.8992	X23	3.5006
X6	17.8562	X15	12.8610	X24	13.3949
X7	16.8035	X16	17.8063	X25	14.6798
X8	17.0278	X17	17.8063	X26	0.5000
X9	17.7954	X18	3.5006		

The interval life $[t_{R=0.95} \quad t_{R=0.5}]$ of $X2$ is [2100 4200] using the general accelerated life test. Other components follow an exponential failure distribution with parameter λ, and the distribution function is calculated as follows:

$$F(t) = P(T \le t) = 1 - \exp(-\lambda \Delta t) \tag{31}$$

Supposing that the mission time is T=2000 hours and ΔT =500 hours, we can calculate the system unreliability using the Eq. (8). Table 3 shows the top event occurrence probabilities at the different mission time.

Considering to the different complexity of components their test cost is different. According to the evaluation standards of the test cost in Table 1, we can calculate HIV using the Eq. (11). Table 4 shows the components' test cost and HIV of the components. Solving the DEN using the inference algorithm gives the DIF and BIM of components for the braking system. The diagnostic decision table for the braking system is shown in Table 5.

Based on the entropy methodology, the weights of the three attributes, ω_1=0.3339, ω_2=0.3326, ω_3=0.3335 are obtained using the Eq. (12) - (19). Table 6 presents the interval values of S, R and Q for all components. And the values of $p(x_i)$ as shown in Table 7 are calculated using the Eq. (29). It can be seen from the results of Table 7 that the optimal diagnosis sequence of the braking system is:
X26≻ X18(X19 X22 X23) ≻ X1≻X2≻ X13≻ X15≻ X24≻ X20≻X25≻ X21 ≻ X5≻ X7≻ X12≻ X8≻ X3≻ X10≻ X9≻ X16(X17) ≻ X6≻ X14≻ X4≻ X11.

5. Conclusions

In this paper, we have discussed the use of DFT, DEN and an improved VIKOR algorithm to locate complex systems failure. Specifically, it has emphasized three important issues that arise in engineering diagnostic applications, namely the challenges of failure dependency, different life distributions and epistemic uncertainty. In terms of the challenge of epistemic uncertainty, the failure rates of the basic events for complex systems are expressed in interval numbers; In terms of the challenge of failure dependency, DFT is used to model the dynamic behaviors of system failure mechanisms. In terms of the challenge of multiple life distributions, a mixed life distribution is used to analyze complex systems. Furthermore, we calculate some reliability results by mapping a DFT into an equivalent DEN in order to avoid some disadvantages. In addition, we take DIF, BIM and HIV into account and obtain the optimal diagnostic ranking order using an improved VIKOR algorithm. The proposed method takes full advantage of DFT for modeling, interval numbers for handling uncertainty and VIKOR for the best fault search scheme, which is especially suitable for fault diagnosis of complex systems.

In the future work, we will focus on how to incorperate sensors data to optimize the diagnosis efficiency.

Acknowledgement

This work was supported by the National Natural Science Foundation of China (71461021), the Natural Science Foundation of Jiangxi Province (20151BAB207044), the Science and Technology Foundation of Department of Education in Jiangxi Province (GJJ14166), the China Postdoctoral Science Foundation (2015M580568) and the Postdoctoral Science Foundation of Jiangxi Province (2014KY36).

References

1. Assaf T and Dugan J.B. Design for diagnosis using a diagnostic evaluation measure. Instrumentation & Measurement Magazine 2006; 9(4): 37-43, https://doi.org/10.1109/MIM.2006.1664040.
2. Chiacchio F, Cacioppo M, D'Urso D, et al. A Weibull-based compositional approach for hierarchical dynamic fault trees. Reliability Engineering & System Safety 2013; 109: 45-52, https://doi.org/10.1016/j.ress.2012.07.005.
3. Chiremsel Z, Said R N, Chiremsel R. Probabilistic fault diagnosis of safety instrumented systems based on fault tree analysis and Bayesian network. Journal of failure analysis and prevention 2016; 16(5): 747-760, https://doi.org/10.1007/s11668-016-0140-z.
4. Dempster A P. Upper and Lower Probabilities Induced by a Multi-Valued Mapping. Annals of Mathematical Statistics 1967; 38(2): 325-339, https://doi.org/10.1214/aoms/1177698950.
5. Duan Rongxing, Zhou Huilin. Diagnosis strategy for micro-computer controlled straight electro-pneumatic braking system using fuzzy set and dynamic fault tree. Eksploatacja i Niezawodnosc - Maintenance and Reliability 2014; 16 (2): 217–223.
6. Dugan J B, Bavuso S J, Boyd M A. Dynamic fault-tree models for fault-tolerant computer systems. IEEE Transactions on reliability 1992; 41(3): 363-377, https://doi.org/10.1109/24.159800.
7. Ge D, Lin M, Yang Y, et al. Quantitative analysis of dynamic fault trees using improved Sequential Binary Decision Diagrams. Reliability Engineering & System Safety 2015; 142: 289-299, https://doi.org/10.1016/j.ress.2015.06.001.
8. Kabir S, Walker M, Papadopoulos Y, et al. Fuzzy temporal fault tree analysis of dynamic systems. International Journal of Approximate Reasoning 2016; 77: 20-37, https://doi.org/10.1016/j.ijar.2016.05.006.
9. Khakzad N. Application of dynamic Bayesian network to risk analysis of domino effects in chemical infrastructures. Reliability Engineering & System Safety 2015; 138: 263-272, https://doi.org/10.1016/j.ress.2015.02.007.

10. Kohlas J, Monney P A. A mathematical theory of hints: an approach to the Dempster-Shafer theory of evidence. Springer Science & Business Media, 2013.
11. Lee J, Lee J S. Heuristic search for scheduling flexible manufacturing systems using lower bound reachability matrix. Computers & Industrial Engineering 2010; 59(4): 799-806, https://doi.org/10.1016/j.cie.2010.08.006.
12. Lisnianski A. Extended block diagram method for a multi-state system reliability assessment. Reliability Engineering & System Safety 2007; 92(12): 1601-1607 ,https://doi.org/10.1016/j.ress.2006.09.013.
13. Li Y F, Huang H Z, Liu Y., et al. A new fault tree analysis method: Fuzzy dynamic fault tree analysis. Eksploatacja i Niezawodnosc - Maintenance and Reliability 2012; 14(3): 208-214.
14. Li Y F, Mi J, Liu Y. et al. Dynamic fault tree analysis based on continuous-time Bayesian networks under fuzzy numbers. Proceedings of the Institution of Mechanical Engineers, Part O: Journal of Risk and Reliability 2015; 229(6): 530-541, https://doi.org/10.1177/1748006X15588446.
15. Liu H C, You J X, You X Y, et al. A novel approach for failure mode and effects analysis using combination weighting and fuzzy VIKOR method. Applied Soft Computing 2015; 28: 579-588, https://doi.org/10.1016/j.asoc.2014.11.036.
16. Mahmood Y A, Ahmadi A, Verma A K, et al. Fuzzy fault tree analysis: A review of concept and application. International Journal of System Assurance Engineering and Management 2013; 4(1): 19-32, https://doi.org/10.1007/s13198-013-0145-x.
17. Merle G, Roussel J M, Lesage J J, et al. Probabilistic algebraic analysis of fault trees with priority dynamic gates and repeated events. IEEE Transactions on Reliability 2010; 59(1): 250-261, https://doi.org/10.1109/TR.2009.2035793.
18. Mhalla A, Collart Dutilleul S, Craye E. Estimation of failure probability of milk manufacturing unit by fuzzy fault tree analysis, Journal of Intelligent and Fuzzy Systems 2014; 26(2): 741-750.
19. Mi J, Li Y F, Yang Y J, et al. Reliability assessment of complex electromechanical systems under epistemic uncertainty. Reliability Engineering & System Safety 2016; 152: 1-15, https://doi.org/10.1016/j.ress.2016.02.003.
20. Rahman F A, Varuttamaseni A, Kintner-Meyer M, et al. Application of fault tree analysis for customer reliability assessment of a distribution power system. Reliability Engineering & System Safety 2013; 111: 76-85, https://doi.org/10.1016/j.ress.2012.10.011.
21. Sallak M, Schon W, Aguirre F. Extended component importance measures considering aleatory and epistemic uncertainties. IEEE Transactions on Reliability 2013; 62(1): 49-65, https://doi.org/10.1109/TR.2013.2240888.
22. Shafer G. A mathematical theory of evidence. Princeton: Princeton University Press, 1976.
23. Shrestha A, Xing L. A logarithmic binary decision diagram-based method for multistate system analysis. IEEE Transactions on Reliability 2008; 57(4): 595-606, https://doi.org/10.1109/TR.2008.2006038.
24. Tao Yongjian, Dong Decun, Ren Peng. An improved method for system fault diagnosis using fault tree analysis. Journal of Harbin Institute of Technology 2010; 42(1): 143-147.
25. Weber P, Simon C. Dynamic evidential networks in system reliability analysis: A Dempster Shafer approach. 2008 16th IEEE Mediterranean Conference on Control and Automation 2008; Ajaccio, France, 603-608, https://doi.org/10.1109/med.2008.4602011.
26. Wu X, Liu H, Zhang L, et al. A dynamic Bayesian network based approach to safety decision support in tunnel construction. Reliability Engineering & System Safety 2015; 134: 157-168, https://doi.org/10.1016/j.ress.2014.10.021.
27. Wu Z, Ahmad J, Xu J. A group decision making framework based on fuzzy VIKOR approach for machine tool selection with linguistic information. Applied Soft Computing 2016; 42: 314-324, https://doi.org/10.1016/j.asoc.2016.02.007.
28. Yevkin O. An Efficient Approximate Markov Chain Method in Dynamic Fault Tree Analysis. Quality & Reliability Engineering International 2015; 32(4):1509-1520, https://doi.org/10.1002/qre.1861.

Rongxing DUAN
Longfei HU
Yanni LIN
School of Information Engineering
Nanchang University
Xuefu Rd., 999 Jiangxi, China

E-mails: duanrongxing@ncu.edu.cn, hulongfeinc@126.com, Nikkilin@yeah.net

Article citation info:
KUCZMASZEWSKI J, ZALESKI K, MATUSZAK J, PAŁKA T, MĄDRY J. Studies on the effect of mill microstructure upon tool life during slot milling of Ti6Al4V alloy parts. Eksploatacja i Niezawodnosc – Maintenance and Reliability 2017; 19 (4): 590–596, http://dx.doi.org/10.17531/ein.2017.4.13.

Józef KUCZMASZEWSKI
Kazimierz ZALESKI
Jakub MATUSZAK
Tomasz PAŁKA
Janusz MĄDRY

STUDIES ON THE EFFECT OF MILL MICROSTRUCTURE UPON TOOL LIFE DURING SLOT MILLING OF Ti6Al4V ALLOY PARTS

BADANIA WPŁYWU MIKROSTRUKTURY FREZU NA TRWAŁOŚĆ OSTRZA W PROCESIE FREZOWANIA ROWKÓW W STOPIE TYTANU Ti6Al4V*

Different forms of tool wear occur in the milling process. Mechanical wear, which has a range of varieties, is a typical form of wear connected with mill operating. One of the varieties of mechanical wear, frequently occurring during milling machining-resistant materials, is undesirable catastrophic wear. Avoiding that kind of wear by appropriate selection of technological parameters, sort of burning carbides and their microstructure constitutes basic information about reliability of the tool. This paper presents the findings from the experimental testing of the impact SC grain size in end mills on the cutting tool tooth (bit) service life and surface topography after slot milling Ti6Al4V alloy parts. The tool wear indicator was determined in compliance with PN-ISO 8688:1996. It was demonstrated that ultra fine grain SC milling cutters are the most resistant to chipping, whereas the surfaces machined with these cutting tools reveals the lowest roughness. The coarse grain SC milling cutters are among those with the shortest service life of all tested tools.

***Keywords**: titanium alloys, milling, wear, roughness.*

W procesie skrawania występują różne formy zużycia narzędzi. Zużycie mechaniczne, które ma szereg odmian, jest typową formą zużycia związaną z eksploatacją frezów. Jedną z odmian zużycia mechanicznego, często pojawiającą się podczas skrawania materiałów trudnoobrabialnych jest niepożądane zużycie katastroficzne. Unikanie tego rodzaju zużycia poprzez odpowiedni dobór parametrów technologicznych, gatunku węglików spiekanych oraz ich mikrostruktury stanowi podstawową informację o niezawodności narzędzia. W pracy przedstawiono wyniki badań doświadczalnych wpływu wielkości ziaren węglików spiekanych we frezach walcowo-czołowych na trwałość ostrza i topografię powierzchni po procesie frezowania rowków w stopie tytanu Ti6Al4V. Wskaźniki zużycia wyznaczono w oparciu o normę PN-ISO 8688: 1996. Wykazano, że frezy o strukturze ultradrobnoziarnistej są najbardziej odporne na wykruszenia, a powierzchnia po obróbce charakteryzuje się najmniejszą chropowatością. Najmniejszą trwałością charakteryzują się frezy o strukturze gruboziarnistej.

***Słowa kluczowe**: stopy tytanu, frezowanie, zużycie, chropowatość powierzchni.*

1. Introduction

The operation of cutting tools renders their teeth (or bits) gradually worn out, leading to the loss of cutting performance. The service life of tool teeth has an impact on the manufacturing cost of items due to the pricing of worn out cutting tools, the costs of reconditioning worn out cutting tools, and the costs of processing machine standstill required for retooling.

The main factors of tool tooth service life include the machined material, the tooth material, the wear protection coating type, the machining parameters and the cooling lubricant type [5, 8, 13, 17]. The tool tooth materials should be chosen with cost effectiveness and technical (processing) considerations [18, 20]. Tool tooth wear is damaging to machining processes. If the machining path length is increased (and hence the tooth wear grows), the cutting force and amplitude value must also increase [10]. As the tool tooth wear grows, the temperature within the machining zone is increased to a point that may result in hazards to machining safety [11, 21]. This relationship also increased the internal tensile stresses within the superficial layer of the workpiece [4].

Titanium alloys are materials the machining of which results in fast wearing of tool teeth [1, 2, 9]. The high tool wear rates are caused by the properties of titanium alloys: extremely low thermal conductivity, relatively high machining resistance, and the affinity for forming deposits and friction adhesion due to high superficial energy levels. The investigation into the process of wearing TiAlN coated SC tooth bits (tool plates) with a counter-sample made of Ti6Al4V demonstrated that the tool wear is caused by adhesive reactions that are combined with high friction reaction of the titanium alloy. The tool wear also increases with feed force and slip velocity [6]. The tool tooth wear process was also studied during milling a Ti-6242S alloy workpiece with SC milling cutters with and without a TiN, TiC or TiCN coating [1].

When machining a titanium alloy, the highest force in the process is the thrust force that negatively affects the geometric accuracy of the workpiece. When compared to cutting force and feed force values, the

(*) Tekst artykułu w polskiej wersji językowej dostępny w elektronicznym wydaniu kwartalnika na stronie ***www.ein.org.pl***

thrust force shows a higher increase with the increase of the tool wear [9]. Hence, given a relatively small Young modulus values of titanium alloy, an increase of a tool tooth wear is expected to result in an increasing scope and number of shape errors in workpieces.

A major quality indicator of machined workpieces is surface roughness. This parameter affects the performance of machine parts, including their fatigue strength, tribological wear resistance and corrosion resistance. The main factors affecting machined surface roughness include feed, corner radius, contact angle, and workpiece material. The paper [7] demonstrated that the machined surface roughness of the TA15 alloy also depends on the tool tooth material and the tool tooth wear. The paper [19] shows the findings of an investigation of the impact of machining parameters on the quality of the Ti6Al4V and pure titanium machined surfaces. Optimal milling technical parameters were selected in the aspect of obtaining minimal roughness and accurateness. During turning spherical surface, due to lower milling speed, higher roughness values were obtained nears the axis of the machined object.

The surface roughness formed by machining may affect the downstream operations on workpieces. It was found that the effectiveness of peening, an operation frequently applied after machining and evaluated with the restitution coefficient values, depends on machined surface roughness [3]. The research completed as discussed in [14] proved that the surface roughness of workpieces milled with various feed rates affects the strength of adhesive bonds.

In the recent years, there has been a trend for manufacturing integrated components (especially in the aerospace industry), which are functional substitutes for assemblies comprising anywhere between dozens or hundreds of individual parts. An integrated component usually features a very complex design and its manufacturing usually involves subtraction of several dozen percent of the intermediate or blank material. The thin wall sections typical of integrated components make their manufacturability difficult due to a high risk of machining instability. The removal of successive solid material layers changes the workpiece geometry and the stability factor [12, 15].

Most papers concerning titanium alloy milling focus on machining of planes. The machine cutting of planes is far easier than slot milling, and slots are frequent features of integrated components. Slotting of a solid material includes a cutting width equal to the slot width, and the cutter contact angle is 180º. This inhibits effective heat dissipation from the machining zone and causes the cutting tool to heat more, resulting in an accelerated wear of its teeth. High feed force values deform shank-mounted milling cutters, which may increase machined surface roughness or tool failure wear if the conditions become extremely unfavourable. Special supports can be used to counter these effects – especially when the cutter reach to diameter ratio is very large, as in deep and narrow slot milling [16].

The shape of milled slots usually requires solid (monolithic) milling cutters, which are most often made of sintered carbide (SC). The properties of SC depend on the chemical composition and the grain size. The reference literature research suggests that the service life testing of milling cutter teeth used for slotting of titanium alloys have not included the criterion of SC grain size so far. The objective of the testing contemplated herein was to determine the impact of the grain size in solid SC milling cutters on the tooth service life and machined surface roughness during slotting of workpieces made of Ti6Al4V.

2. Research methodology

The experiment covered herein was carried out on test samples made of annealed Ti6Al4V, a material which is widely used aerospace, automotive, medical and other industries, thanks to its properties. The Ti6Al4V chemical composition and physical properties are listed in Table 1.

Table 1. Ti6Al4V chemical composition and physical properties

Chemical composition, %					Physical properties		
Al	V	C	Fe	Ti	R_m	HRC	E
6,25-6,31	4,09-4,12	0,026-0,027	0,18-0,21	other	1014 MPa	33	120 GPa

The experimental test involved slot milling the test specimen with a cutting width equal to the cutter diameter, i.e. $a_e = D$. These machining conditions usually put a relatively high strain on the tool. An alternative application consists in a milling cutter the diameter of which is less than the slot width and various machining strategies: equidistant, trochoidal, etc. However, given a known slot depth, the tool rigidity is reduced inversely proportional to the L/D ratio (the tool reach to diameter), and the machining time is extended. Fig. 1 shows an example of the test sample and its model with marked dimensions.

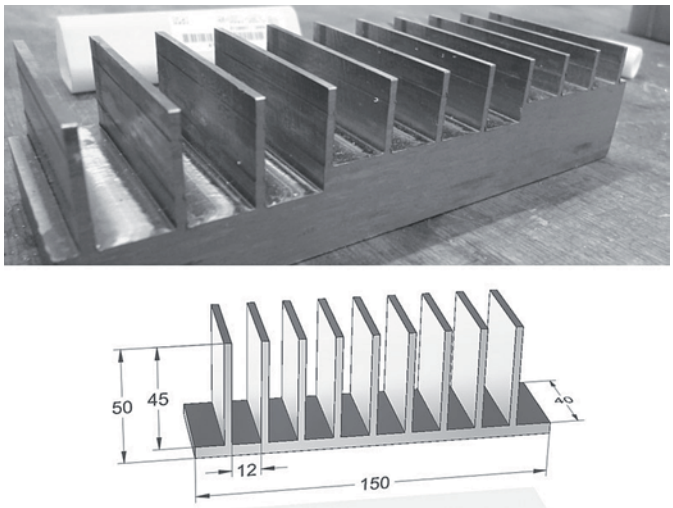

Fig. 1. Test sample form and dimensions

The experimental tests were done on an Avia VMC-800HS machining centre. This machine was equipped with a Heidenhain controller and dedicated to HSM (high-speed machining) with a 25 kW spindle and the maximum speed of 24,000 rpm.

The tests were carried out on SC milling cutters made with D = 12 mm. 4-tooth cutters were used with a geometry adjusted to poorly machinable materials. The variable of these tests was the SC grain size within a cobalt binder matrix. The first test group of milling cutters had an ultra fine grain SC substrate. The second test group included milling cutters with a fine grain SC substrate. The third test group included milling cutters with a coarse grain SC substrate. For the studies tools of ultra fine-grained and coarse-grained structure were used, four pieces of each, as well as six pieces of tools of fine-grained structure. Table 2 shows the photographic images of the microstructure of the cutters from the test groups at 1000x of magnification.

The SC grain size largely affects the cutter wear rate, especially if the wear conditions are dynamic (variable). Another factor of tool material strength is the cobalt percentage share in the binder phase which may vary from several do ca. 30% in cutting tools. The test tools were mounted in tool holders at a constant tool reach length.

Given the dynamics of machining processes, the tool wear is a process complex in nature and may include a combination of any of the following: mechanical wear, adhesive wear, diffusive wear, thermal wear or chemical wear. The experimental tests discussed herein

Table 2. Microstructures of specific cutter test groups (magnification: 1000x)

Ultra fine grain structure	Fine grain structure	Coarse grain structure
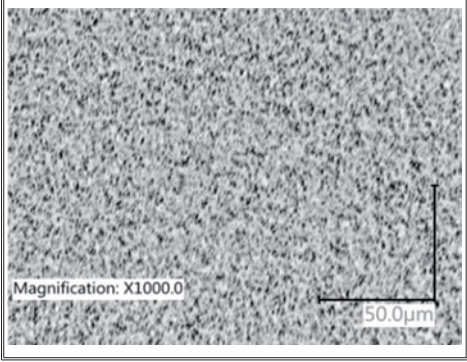	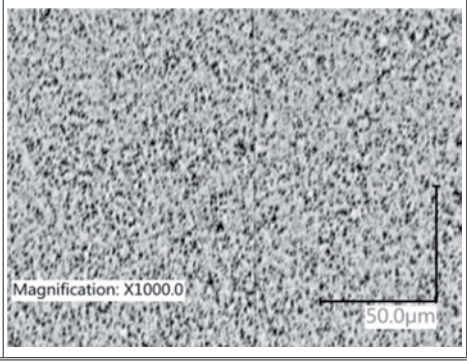	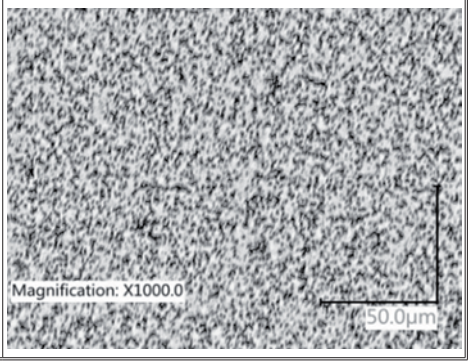

focused on mechanical wear, which can be divided into the subcategories of abrasive wear and strength (emergency or fatigue) wear. Several tool tooth wear criteria can be applied: geometric, processing, physical and economic. Geometric criteria are applied to measure the wear that is directly related to the condition of the cutting tool tooth. The tool tooth wear indicators were determined in compliance with PN-ISO 8688:1996. The test measurements included tool service life, cutting path, and slot bottom surface roughness. The tooth tool wear indicators were measured under a Keyence VHX 5000 digital imaging microscope.

The experimental tests had constant machining values. The cutting speed was $v_c = 30$ m/min and the feed per tooth was $f_z = 0.14$ mm/tooth. The cutting depth selected for slot milling was $a_p = 2$ mm at a cutting width of $a_e = 12$ mm, equal to the diameter of the test milling cutters. The parameter values were assumed from the range of those recommended by manufacturers of tools used during the experiment.

The surface roughness was measured with a HOMMEL-ETAMIC T8000 RC120 machine for roughness, 3D topography and contour mapping.

To analyse the tool wear and its effect on the machined surface quality, the milling process was interrupted at predetermined time steps to measure the tool wear and surface roughness. The time steps were: 0.1; 0.5; 1; 3; 5; 8; 11; 15 min.

3. Test results

Of all the mechanical wear forms defined in PN-ISO 8688:1996, three wear types were witnessed during the experimental tests: localized flank wear, *VB3*, localized chipping, *CH3*, and catastrophic failure, *CF*. Table 3 shows a graphical representation of the discovered wear types with actual images thereof.

Fig. 2 shows a comparative view of a milling cutter after the machining time t = 15 min (Fig. 2a) and a new milling cutter (Fig. 2b). This milling cutter is made of fine grain SC.

Several wear types usually occurred on the studied tool teeth. A tool tooth initially revealed localized flank wear *VB3*. Small defects of the materials change the machining conditions and the localized stress concentration. A consequence of these factors was the emergence of localized chipping *CH3*. A chipping area may thus form a "new" cutting edge the geometry of which was random and undefined (this phenomenon occurs in abrasive machining and it is caused by grain fissility). Once the critical wear *VB3+CH3* is reached as determined for a given tool, the tool wear results in failure wear CF. These effects cannot always be witnessed, which is due to the dynamic nature of machining. A failure wear of one tooth without interruption of the rotational movement of a milling cutter usually results in fracture of all remaining teeth. If a CNC machine tool has no systems to immediately interrupt the machining process upon a tool failure, the feed

Table 3. Found wear types

ISO code	**localized flank wear** ***VB3***	**localized chipping** ***CH3***	**catastrophic failure** ***CF***
Graphical representation	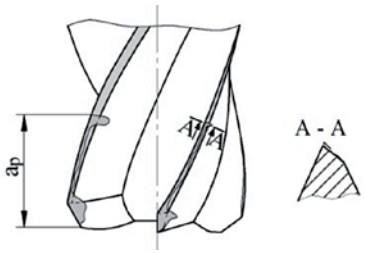	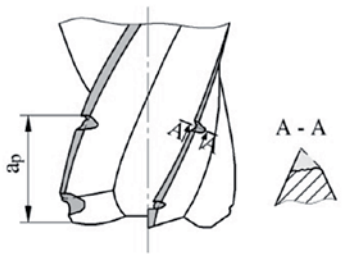	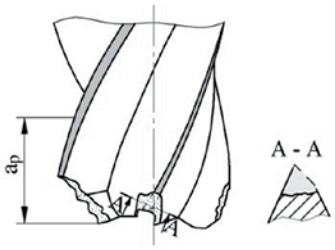
Actual view	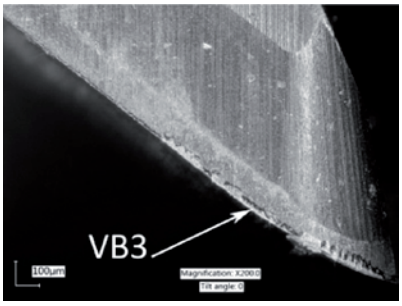	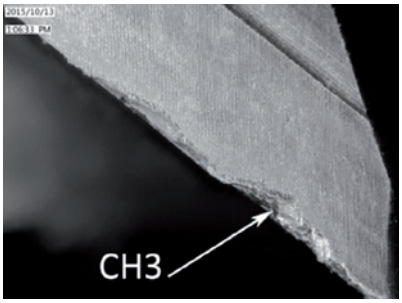	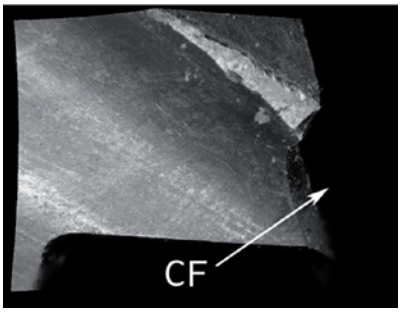

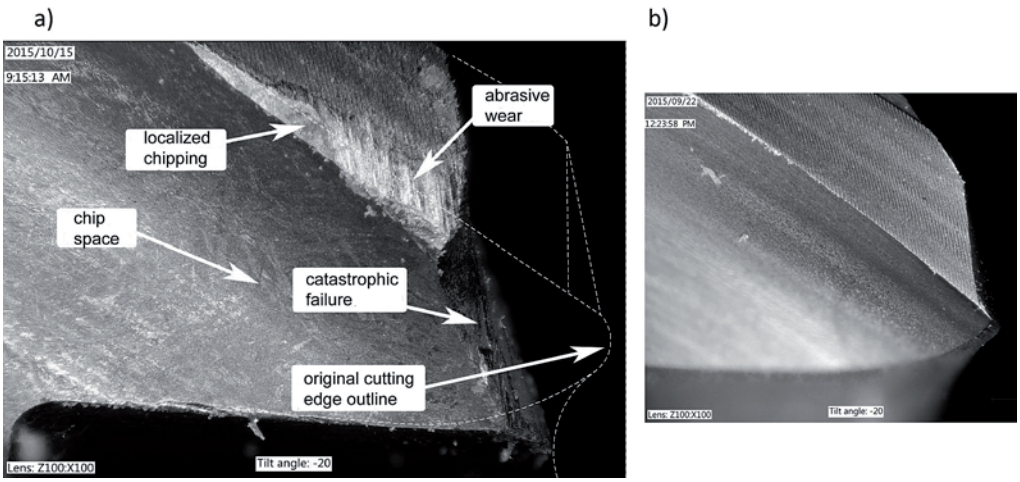

Fig. 2. Tool tooth condition: (a) after machining t = 15 min, (b) new

Fig. 3. Examples of cutters subject to failure

of the workpiece material into a tool with lost teeth causes collision conditions which result in breaking away the entire tool at its held base or over the machined surface plane. An overview of failed cutters is shown in Fig. 3.

Table 4 shows selected photographs of new and worn tool teeth.

Fig. 4 shows a chart of the localized flank wear *VB3* as a function of the machining time. Coarse-grain SC teeth suffered from chipping at the initial stages of the experimental tests; hence, the tool tooth wear measurement results were followed only to the machining time t = 0.5 min. The least worn tool teeth had a fine-grain SC with a mean wear value *VB3* = 0.17 mm after the machining time t = 15 min.

An analysis of the localized flank wear *VB3* did not provide a full insight into the tool tooth service life due to the concurrent presence of other wear types. Fig. 5 shows the percentage of the milling cutters which displayed the chipping wear *CH3*.

12.5% of all ultra fine SC milling cutters were worn out within the last time interval, i.e. t = 12 to 15 min. The population of 87.5% suffered only from localized flank wear *VB3*.

The largest share of localized chipping of fine grain SC milling cutters was occurred at the first minutes of machining. Past the machining time t = 15 min, the total percentage of milling cutters with *CH3* was 100%.

All coarse grain SC milling cutter teeth revealed localized chipping at t = 0 to 3 min.

Table 4. Comparison of new tool teeth to worn tool teeth

	Coarse grain SC	Fine grain SC	Ultra fine grain SC
New	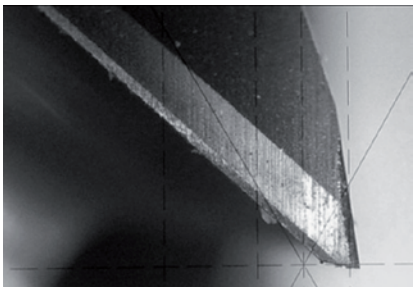	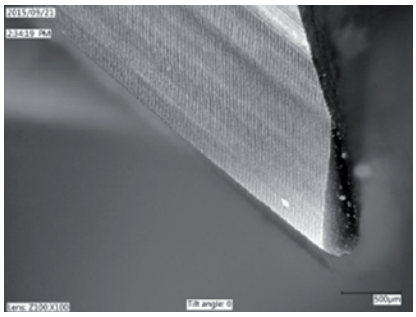	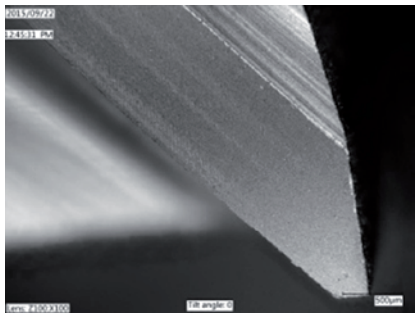
Worn	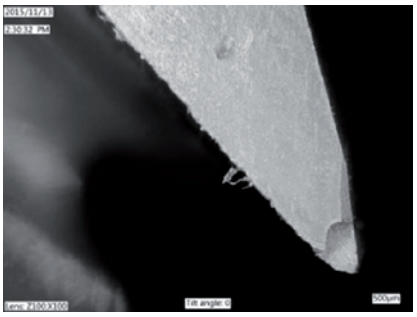	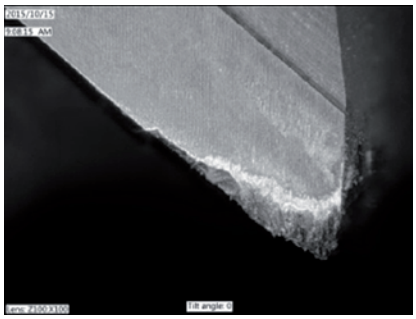	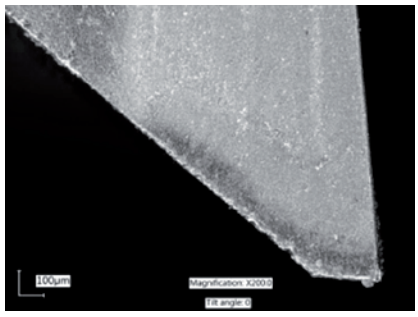

A localized chipping *CH3* is not tantamount to a complete loss of cutting performance of a tool. However, it is often a prelude to a very quick catastrophic failure *CF*.

Fig. 6 shows the distribution of the catastrophic failure *CF* percentage ration in milling cutters of various SC grain sizes. The ultra fine grain SC cutters did not reveal CF across the entire machining time. Catastrophic failure CF is the most undesirable wear type, and a typical problem of automatic CNC machining that requires retooling, stopping the machining program, constant supervision by process operators, etc.

Approximately 85% of fine grain SC cutters failed from wear after t = 15 min.

All coarse grain SC cutters failed from wear at t = 0 to 3 min.

Fig. 7 shows the effect of the SC microstructure on the surface roughness measured at the defined time points at the sample bottom in the process of slot milling. In any study of machined surface roughness, the so-called running-in phase may be found. When a running-in phase occurs, the surface roughness will either be reduced or reveal no discernible growth as the machine time passes. The running-in phase of the ultra fine grain SC cutters was evident from the machining time t = 1 min. One possible cause of the running-in phase emergence was that at the initial stage of machining the sharp cutting edge of a tool, the outline of which was formed within the workpiece, generated large micro irregularities; following the period of initial tool wear with an increase of the cutting edge chamfer radius, the surface roughness began to fall. Fig. 8 shows a comparison between a chamfer radius of a new cutting edge of an ultra fine grain SC cutter and the chamfer radius of the same cutting edge at the machining time t = 1 min. What was evident after this time was a slow increase in surface roughness during the machining time. This was related to the incrementing values of the tool tooth wear indicators. The fine grain SC cutters revealed a shorter running-in phase. After the machining time t = 0.5 min, a gradual increase in surface roughness was evident, whereas its growth rate was higher than in the machining with ultra fine grain SC tools.

The coarse grain SC tools only revealed a fast increase in surface roughness from the initial machining phase. The measurements were continued up to the time of *CF*. The lowest surface roughness was produced with the ultra fine grain SC tools.

Fig. 9 shows a comparison between the surface topography made with the fine grain SC tools and ultra fine SC tools after the machining time *t* = 8 min.

A characteristic periodic arrangement of micro irregularities is evident that follows the cutting edge within the machined workpiece body, and the surface roughness parameters were much higher than produced with fine grain SC tools.

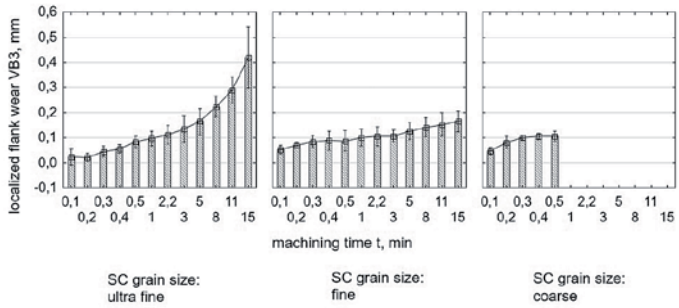

Fig. 4. Localized flank wear vs. machining time

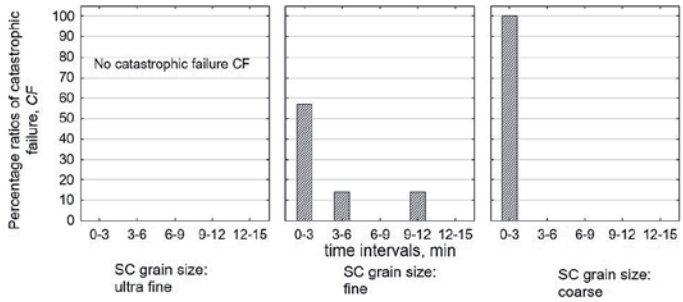

Fig. 6. Percentage ratios of catastrophic failure CF at specific machining time intervals vs. various SC grain sizes

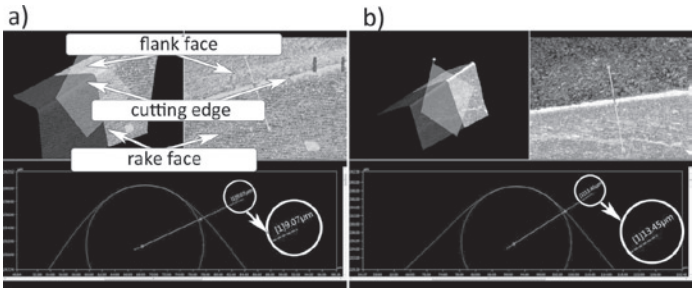

Fig. 8. Comparison between the chamfer radius of the cutting edge of an ultra fine grained SC tool:(a) new cutting edge, (b) after the machining time t = 1 min

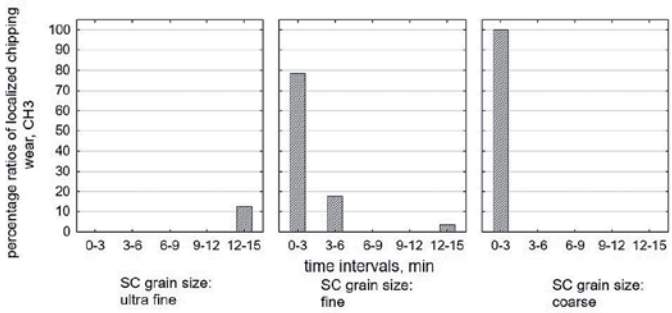

Fig. 5. Percentage ratios of localized chipping wear CH3 at specific machining time intervals vs. various SC grain sizes

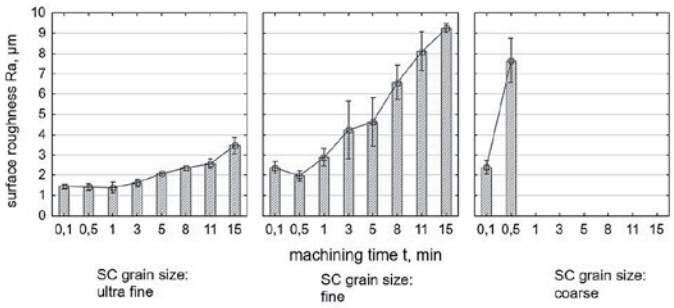

Fig. 7. Impact of the SC structure on surface roughness during slot milling

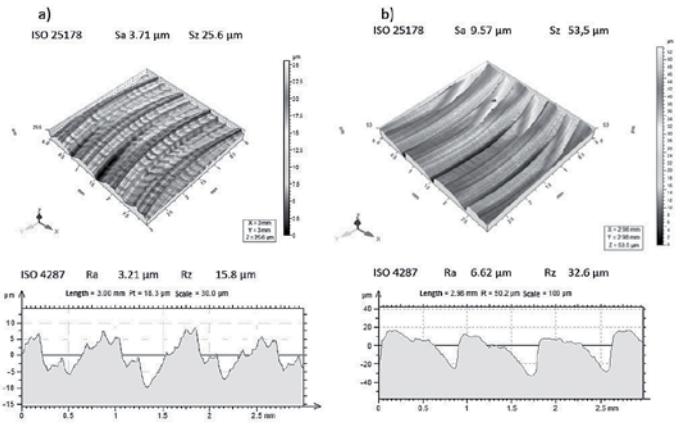

Fig. 9. Comparison of the surface topography at t = 8 min of machining with: (a) ultra fine grain SC tools, (b) fine grain SC tools

4. Summary

These experimental tests of the effect of various SC grain sizes in tools on the tool service life and machined surface roughness during slot milling, with the established machining technological parameters, of Ti6Al4V alloy workpieces allowed formulating several conclusions.

1. Out of the mechanical wear factors, the most frequent wear types witnessed was localized flank wear *VB3*, localized chipping *CH3*, and catastrophic failure *CF*.
2. It is advantageous to adjust the SC grain size to the machined materials as to permit the localized flank wear *VB3* only throughout the cutting tool life. If the machining process parameters are known and set, this helps foresee the time to replace the cutting tool.
3. The lowest values of localized flank wear *VB3* occurred during machining with fine grain SC tools.
4. Ultra fine SC cutting tools are most resistant to localized chipping and failure wear.
5. No catastrophic failure *CF* was witnesses for any ultra fine grain SC cutting tool up to the machining time t = 15 min. All these tools retained their cutting performance.
6. All coarse grain SC tools suffered failure wear *CF* in the first phase of the machining process, t = 0 to 3 min.
7. The best surface roughness was produced with the ultra fine grain SC tools.

Given the tool tooth life and surface roughness, the best performance quality was produced with the ultra fine grain SC tools. Despite the higher localized flank wear *VB3* than in the fine grain SC tools, it is important that all ultra fine grain SC tools retained their cutting performance at the lowest surface roughness of all tested tool groups.

Coarse grain SC tools are not recommended for poorly machinable materials due to the high risk of catastrophic failure *CF*.

On the basis of preliminary research performed milling technological parameters can affect the wear value and percentage of worn mills in particular time intervals, however, the general tendencies connected with the influence of mill structure upon tool life and surface quality will remain on a comparable level.

Acknowledgement

The test were completed under the industry project INNOLOT (abbreviation: AMpHOra) titled "Testing of additive manufacturing technologies and hybrid processing for the development of innovative aerospace manufacturing" and coordinated by Polskie Zakłady Lotnicze Sp. z o.o. – PZL Mielec, and co-financed by the National Centre for Research and Development (NCBiR) and the European Union under the European Regional Development Fund for the Operational Programme: Innovative Economy, OP:IE Priority I, Measure 1.5 Agreement no. INNOLOT /I/6/ NCBR/2013

References

1. Abdel - Aaal H A, Nouari M, Mansori M El. Influence of thermal conductivity on wear when machining titanium alloys. Tribology International 2009; 42: 359-372, https://doi.org/10.1016/j.triboint.2008.07.005.
2. Bach P, Trmal G, Zeman P, Vana J, Maly J. High performance titanium milling at low cutting speed. Procedia CIRP 2012; 1: 226-231, https://doi.org/10.1016/j.procir.2012.04.040.
3. Bławucki S, Zaleski K. The effect of the aluminium alloy surface roughness on the restitution coefficient. Advances in Science and Technology Research Journal 2015; 9(27): 66-71, https://doi.org/10.12913/22998624/59086.
4. Chen L, El-Wardany T I, Harris W C. Modelling of the effects of flank wear land and chip formation on residual stresses. Annals of the CIRP 2004; 53(1): 95-98, https://doi.org/10.1016/S0007-8506(07)60653-2.
5. Ezugwu E O, Wang Z M. Titanium alloys and their machinability - a review. Journal of Materials Processing Technology 1997; 68: 262-274, https://doi.org/10.1016/S0924-0136(96)00030-1.
6. Grzesik W, Małecka J, Zalisz Z, Żak K, Niesłony P. Investigation of friction and wear mechanisms of TiAlN coated carbide against Ti6Al4V titanium alloy using pin – on discs tribometer. Archive of Mechanical Engineering 2016; 63(1): 113-127, https://doi.org/10.1515/meceng-2016-0006.
7. Honghua S U, Peng L I U, Yucan F U, Jiuhua X U. Tool life and surface integrity in high – speed milling of titanium alloy TA15 with PCD/PCBN tools. Chinese Journal of Aeronautics 2012; 25: 784-790, https://doi.org/10.1016/S1000-9361(11)60445-7.
8. Krolczyk G M, Nieslony P, Legutko S. Determination of tool life and research wear during duplex stainless turning. Archives of Civil and Mechanical Engineering 2015; 15(2): 347-354, https://doi.org/10.1016/j.acme.2014.05.001.
9. Krupa K, Sieniawski J, Laskowski P. Zużycie narzędzi skrawających podczas toczenia stopu Ti-6Al-2Sn-4Zr-6Mo. Mechanik 2010; 10: 654-661.
10. Kuczmaszewski J, Pieśko P. Wear of milling cutters resulting from high silicon aluminium alloy cast AlSi21CuNi machining. Eksploatacja i Niezawodnosc – Maintenance and Reliability 2014; 16(1): 37-40.
11. Kuczmaszewski J, Zagórski I, Dziubinska A. Investigation of ignition temperature, time to ignition and chip morphology after the high-speed dry milling of magnesium alloys. Aircraft Engineering and Aerospace Technology: An International Journal 2016; 88(3): 389-396, https://doi.org/10.1108/AEAT-02-2015-0040.
12. Kuczmaszewski J, Zaleski K, Ed. Obróbka skrawaniem stopów aluminium i magnezu. Lublin: Politechnika Lubelska, 2015.
13. Nabhani F. Machining of aerospace titanium alloys. Robotics and Computer Integrated Manufacturing 2001; 17: 99-106, https://doi.org/10.1016/S0736-5845(00)00042-9.
14. Rudawska A, Reszka M, Warda T, Miturska I, Szabelski J, Stancekova D, Skoczylas A. Milling as a method of surface pretreatment of steel for adhesive bonding. Journal of Adhesion Science and Technology 2016; 30(23): 2619-2636, https://doi.org/10.1080/01694243.2016.1191585.
15. Rusinek R, Zaleski K. Dynamics of thin – walled element milling expressed by recurrence analysis. Meccanica 2016; 51(6): 1275-1286, https://doi.org/10.1007/s11012-015-0293-y.
16. Shamato E, Saito A. A novel deep groove machining method utilizing variable – pitch end mill with feed – directional thin support. Precision Engineering 2016; 43: 277-284, https://doi.org/10.1016/j.precisioneng.2015.08.006.
17. Su Y, He N, Li L. An experimental investigation of effects of cooling/lubrication conditions on tool wear in high – speed end milling of Ti-6Al-4V. Wear 2006; 261: 760-766, https://doi.org/10.1016/j.wear.2006.01.013.

18. Twardowski P, Legutko S, Krolczyk G M , Hloch S. Investigation of wear and tool life of coated carbide and cubic boron nitride cutting tools in high speed milling. Advances in Mechanical Engineering 2015; 7(6): 1-9, https://doi.org/10.1177/1687814015590216.
19. Zębala W, Gawlik J, Matras A, Struzikiewicz G, Ślusarczyk Ł. Research of surface finish during titanium alloy turning. Key Engineering Materials 2014; 581: 409-414, https://doi.org/10.4028/www.scientific.net/KEM.581.409.
20. Zareena A R, Rahman M, Wong Y S. Binderless CBN tools, a breakthrough for machining titanium alloys. Journal of Manufacturing Science and Engineering 2005; 127(2): 277-279, https://doi.org/10.1115/1.1852570.
21. Zoya Z A, Krishnamurthy R. The performance of CBN tools in the machining of titanium alloys. Journalof Materials Processing Technology 2000; 100: 80-86, https://doi.org/10.1016/S0924-0136(99)00464-1.

Józef KUCZMASZEWSKI
Kazimierz ZALESKI
Jakub MATUSZAK
Tomasz PAŁKA
Department of Production Engineering
Mechanical Faculty
Lublin University of Technology
ul. Nadbystrzycka, 20-618 Lublin, Poland

Janusz MĄDRY
Polskie Zakłady Lotnicze Sp. z o.o. - PZL Mielec

E-mails: j.kuczmaszewski@pollub.pl, k.zaleski@pollub.pl, j.matuszak@pollub.pl, t.palka@pollub.pl, janusz.madry@lmco.com

Article citation info:
BRZĘCZEK J, MIKRUT S. The use of photogrammetry for special flight tests. Eksploatacja i Niezawodnosc – Maintenance and Reliability 2017; 19 (4): 597–603, http://dx.doi.org/10.17531/ein.2017.4.14.

Józef BRZĘCZEK
Sławomir MIKRUT

THE USE OF PHOTOGRAMMETRY FOR SPECIAL FLIGHT TESTS

WYKORZYSTANIE FOTOGRAMETRII DO PRÓB SPECJALNYCH W LOCIE*

Carrying out flight tests of de-icing systems of aircraft in real or artificial conditions, apart from the measurement of the temperature of the heated areas, requires the verification of the work of the installations in the form assessment of the places of the formation of ice accretions rate and their size. To measure them in the mentioned about tests the authors applied the photogrammetric method, and the obtained results were verified with flight tests, including certified tests. The application of the photogrammetric method in such analyses with the example of processing of the obtained pictures gives base for the assessment of its usefulness and the directions of development in similar applications.

Keywords: *flight tests, photogrametry, de-icing system, temperature measurement.*

Prowadzenie prób w locie instalacji odlodzeniowych statków powietrznych w warunkach rze-czywistych lub sztucznych, oprócz pomiaru temperatury ogrzewanych powierzchni wymaga weryfikacji pracy instalacji w postaci oceny miejsc osadzania się tworów lodowych i ich roz-miarów. Do ich pomiaru w wymienionych próbach autorzy zastosowali metodę fotograme-tryczną, a uzyskane wyniki zweryfikowali próbami w locie, w tym próbami certyfikacyjnymi. Zastosowanie metody fotogrametrycznej do takich analiz z przykładem przetwarzania uzyski-wanych obrazów daje podstawę do oceny jej przydatności oraz kierunków rozwoju w podobnych zastosowaniach.

Słowa kluczowe*: próby w locie, fotogrametria, system odladzania, pomiary temperaturowe.*

1. Introduction

Photogrammetry has a wide application both in documenting geometric figures (the records of construction), making geometric measurements, crash investigation in traffic, etc. The publication refers both to the application of photogrammetry in specific studies of aircraft, such as testing correctness and reliability [1,3] of the work of de-icing system of the airplane[1], on the level accepted by the requirements of the Aviation Regulations, in this specific case, regulations of [2][2]. The presented photogrammetric method for such specific applications can be used, provided the time correlation with other parameters of the flight, including the atmosphere is preserved[3]. The presented in this article method is also useful at the temporary verification of the de-icing system of the aircraft, e.g., after the servicing. Its most important advantage is the possibility of conducting research in the area of the carried out aircraft missions, i.e. from the start to landing. The application of other methods of registering the geometry of ice accretions rate and their changes while moving, e.g., by scanning, does not give satisfactory results due to the occurring dynamic changes in shape and situation. The mentioned already other methods are difficult to implement, mainly because the equipment requirement. The photogrammetric method allows making measurements in any moment of the test flight, without using expensive equipment.

The publication presents the analysis and discussion of the obtained results, based on the carried out examinations of the correctness of the work of de-icing systems of M28 aircraft, made in the framework of the co-operation between AGH University of Science and Technology and PZL Mielec Sp. z o.o.[13]. The goal of the article is to prove the usefulness of the mentioned method to detect and geometrize (define the situation and geometric characteristics) of ice accretions arising on the structure of the airplane in artificial or natural atmosphere icing conditions.

The applied in this type of the flight tests and studies other measurement methods, due to the necessity of landing and the related changes in flight parameters and the changes in the height and atmospheric parameters cause changes e.g., ice melting, which significantly disturbs the assessment of the work of systems and the credibility of the data. The presented method additionally gives the possibility of the assessment of the ice acceration rate and ice melting on the surfaces of aircraft not subdued to de-icing procedures.

The presented in the article results refer to the selected tests of operating de-icing systems and the assessment of the geometry of ice accretions applying advanced image analysis methods. The images used in the article are the property of PZL Mielec [7].

2. Methods of the studies

The planned and carried out researching experiment and the obtained results made the proof of the correct de-icing system of an airplane. The material to provide the evidence was documenting the occurrence of ice accretions (or their lack) on certain areas of the airplane during the flight in artificial or natural icing [4].

In the analyzed case, the airplane de-icing system uses the exausts of hot air from turbine engines[5] which is sent with the ducts alongside the heated – de-iced areas of the aircraft. The proposed and carried out experiment allowed us to show correctness of the work of de-icing system in the aircraft, including thermal changes alongside the heated

1 Examining the compliance with the regulations can be carried out with other methods: e.g., ice tunnels, fights in artificial icy atmosphere, etc. It causes errors of the method and creates specific conditions for the simulation of the phenomenon

2 Requirements of regulations: CS 23. 1419 Ice protection and AMC 23.1419.

3 For these purposes only callibrated sonars are appled for rhe measurement of atmospheric parameters such as: pressure, temperature, humidity, water kontent rate, distribution and size of the water drops, temperature etc.

4 Both the acompanying and tested airplane have the possibility od collecting actual physical parameters of atmosphere during the experiment.

5 The presented method can be applied in other systems de-icing of aircraft, e.g. electric or mechanic.

(*) Tekst artykułu w polskiej wersji językowej dostępny w elektronicznym wydaniu kwartalnika na stronie ***www.ein.org.pl***

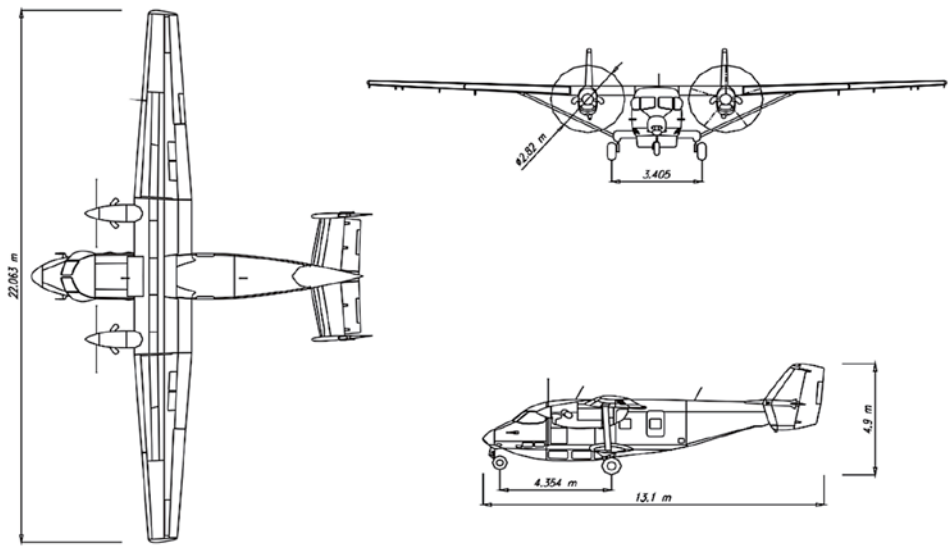

Fig. 1. Based on: http://www.pzlmielec.pl/

areas, determining the characteristic values, and based on them, making the evidence documentation.

The article presents the use images and the analysis of the recorded images of ice accretions and their characteristics. The geometry of the studied airplane was based on the available vector models CAD [12, 13].

2.1. Acquisition of images

The photogrammetric image is made in a central projection. There can be deformation in the picture resulting from radial dislocations caused by the distortion of the lens, and the inclination of the shape. Thus they cannot be used as a map. Their projection transformations can eliminate the inclination, but they cannot remove deformations resulting from drop or the fact that the photographed object is not flat. These deformations cannot exceed the required accuracy of the measurement of the defined characteristic. Radial deviation can be negligible only for the objects, which bias from 2D (flatness) is small.

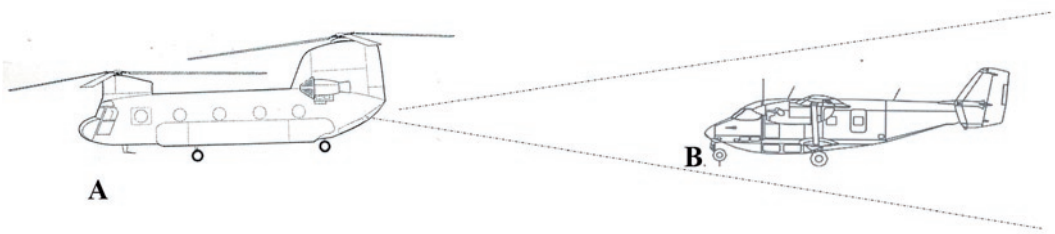

Fig. 2. A scheme of the course of experiments and obtaining the data. Aircraft A (photograph and possible artificial icing), B - tested airplane

In case of other, 3D solids, as aircraft, radial bias can be significant, even making it impossible to make a measurement based on a single photo – so-called one-image photogrammetry.

Aircraft A (leader) and B (the tested plane) (Fig. 2), taking part in the test were subdued to independent dislocations during the flight, caused by gusts, fluctuations of the stability of their movement and steering - reaching several meters, including the vibration [6] of their structures caused by the work of the powerplant and air circulation. The application of very short time of the opening of the shutter allowed avoiding the influence of the mentioned factors i.e. dynamic changes of the situation on the quality of photos. The deflection of the structure of fuselage resulting from the load during the flight regarded in numeric analyses.

In the studies we concentrated on doing the analysis in a single image (one-image photogrammetry), while the analyses referred to the tests carried out in different atmospheric conditions i.e. in natural icing (colourless accretions or white (chyba yellow) accretions in artificial icing). In the tests in artificial icing for better identification of the phenomenon, the sprayed water was dyed yellow. The dye was neutral to the result of the tests. Fig. 2 shows a schematic course of the experiment.

2.2. Data description

Parameters of icing (atmosphere, flight, powerplants and hot air) were recorded in test flights, according to the flight tests plan. The parameters of real atmosphere and air streams with artificially made conditions of icing the aircraft were verified in the flight calibrated with meteorological sonars. Recording icing parameters of natural and artificial atmosphere was carried out in time correlation with photographic documentation.

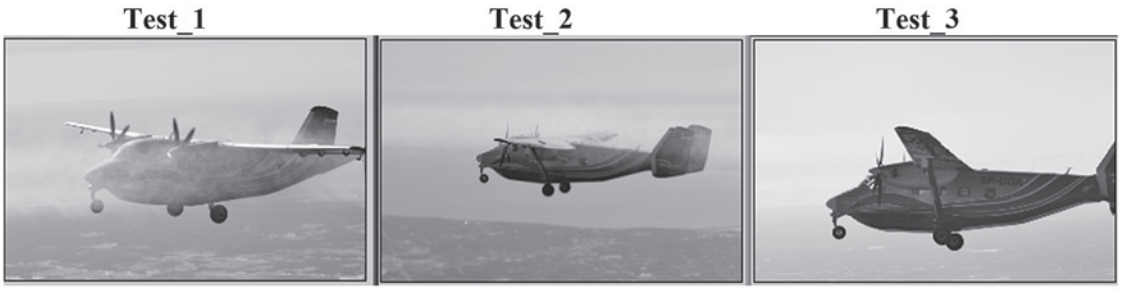

Fig. 3. (Test_1, Test_2, Test_3) the photos defined in the analysis as: Test_1, Test_2, Test_3, (the property of the Polish Aviation Enterprise Ltd. - PZL)

The analyses presented in the article were carried out on the photos taken with amateur photo cameras: Nikon D70 and Nikon D3100 with focal lenses of:

6 Usually the ranges of vibration are within the frequency range of 4Hz to 60Hz, depending on the fight speed.

Fig. 3. (Test 4) The photo used in the experiment defined asTest_4 (the property of the Polish Aviation Enterprise Ltd. - PZL)

f = 18.70 mm and f = 55.300 mm. The base for the analyses was numerical geometry of the airplane An-28 [5] (Fig. 1, 4.) made in the format *. Igs. For the conducted analyses we applied photos used in the flights in w artificial icing tests, of the following parameters:

– digital image of size 4304 x 2850 pixel i.e. about 13 Mega pixel - (Test_1, Test_2, Test_3) of resolution 72 dpi (Fig. 3.)
– digital image of size 4677 x 3307 pixel (Test_4) of resolution 400 dpi (Fig. 3).

The photos were taken from the accompanying aircraft A, during tests in the conditions of artificial and natural icing, according to Fig. 2. The photos were written in format *.jpg and subdued to compression to JPEG format of small degree. The details of the analysis presented in this article refer to the photos of artificial icing, because of better possibilities of the analysis, including the presentation of the possibilities of processing with the use of color.

3. Methods of results processing

At processing and the verification of the methods of the analysis of data in the form of the digital images and the presentation of the results, the following problems were assumed to be necessary to solve:

a) Identification of ice accretions photographed on the airplane structure (in case of tests with artificial icing in yellow),
b) Identification of the accretions of ice photographed on the wing of the airplane in natural color in case of tests in natural icing conditions, at formerly prepared surface of the wing,
c) Defining of the geometry of ice accretions (area of the accretion).

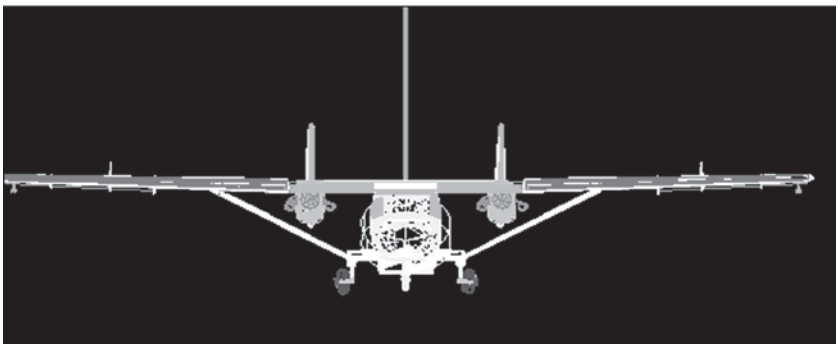

Fig. 4. The applied in the experiment model CAD airplane An-28

The first stage of the carried out analysis and publication was the selection of photos for further processing. Selection referred to the usefulness of the photos in terms of specific fragments of the airplane in the interesting state and during the flight. The article presents the analyses ad and measurements according to the data included in the photo (Fig. 3.) i.e. presenting airplane B seen from the front.

3.1. Image processing to enhance yellow on the wing of the airplane

Image processing was carried out in the Matlab environment and then independently in the Adobe Photoshop environment. Experiments for icing in artificial conditions were meant to confirm, among others, the information on the colors occurring on the devices of the airplane. In the presented case, the task was defining the yellow, occurring as the proof of the occurrence or lack of icing, including so-called thermal bridges. Apart from showing that icing occurred, the task was to define the size of its accretions i.e. the area of the ice, and having time difference in the carried out photographs, define the speed of the growth of icing.

To increase the effect of yellow in the photo, in the first step a simple operation of changes in brightness, contrast was carried out as well as the filtration in the mentioned above specialist software.

The application of these operations gave the effects in the form of selected automatically places of the occurrence of icing. At the enlarged image (Fig. 5.3) the left wing can be seen in the original image, as well as the results image processing to enhance yellow.

The improvement of the quality of images by simple operations on the histogram (changes in contrast and the components of the color of the analyzed image) facilitates underlining the places, where yellow coloration occurs and defining the size of the whole area and icing. An independent experiment was to select the areas of the defined brightness component from the whole image, in the Matlab environment. During the carried out experiments, the conversion of the color model RGB[7] into CMYK model [8] was made for better enhancement of yellow. The results of digital processing were shown in Fig. 5. Light areas are represented by the yellow component. Mathematical bases of the transformation of colors and the implementation in the Matlab environment can be found in the literature [4],[5]. The results of the filtration of the original image in program Adobe Photoshop with various filters was presented in Fig. 5 (b - d). Yellow is the most enhanced with the application of filter Unsharp Mask (Fig. 5d).

In the images transformed in Adobe Photoshop it can be clearly seen that there are also other places of white coloration, which are the effect of the light reflection, and not icing. To eliminate this failure, a subsequent experiment, meaning that the transition from the RGB of the model of colors into CMY model, using Matlab program was carried out. The transformation from RGB environment to CMY (1) and a clear differentiation of yellow channel shows that on the analyzed image light places clearly appeared, thus places of maximal saturation of yellow.

On the other hand, there are no places that were shown earlier in program Abobe Photoshop as the reflection effect.

Transition from RGB color model into CMY was according to:

$$\begin{aligned} R &= 255 - C \\ G &= 255 - M \\ B &= 255 - Y \end{aligned} \tag{1}$$

where:

7 RGB - model of RGB basic colors: Red, Green, Blue.
8 CMYK - model of colors containing complementary components: C-cyan, Y-yellow, M-magenta, K-black.

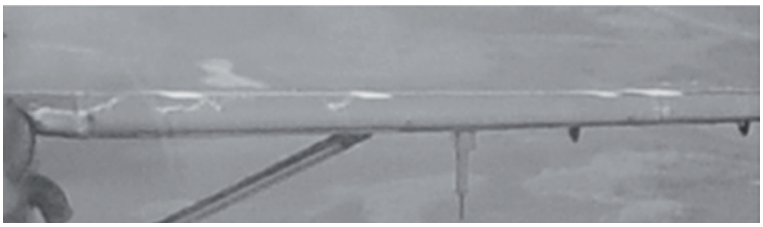

a) Original image

b) Transformation_1

c) Transformation_2

d) Transformation_3

Fig. 5. Results of the original image filtration

RGB – components of the color: R - czerwony, G - zielony, B - niebieski,

CMY – components of the complementary color (C - niebiesko-zielony, M - fioletowy, Y - yellow)

As a result of the analyses digital images obtained in test referring to the measured atmospheric parameters, the occurrence of places with yellow coloration was shown in the image, which proves the correctness of the work of de-icing system and shows the occurrence of ice accretions in non-heated areas of the airplane.

3.2. Geometrization of ice accretions.

To define the situation of ice on the wing and its surface the transformation of the image geometry was made (Fig. 3). The image was recorded from the aircraft flying before the tested airplane. The transformation was made based on the reference model, containing the geometry of airplane written in the vector format. The affine transformation was applied. Its basic parameter of the accuracy assessment is its mean error m_o determined by the formula (2):

$$m_0 = \sqrt{\frac{V^T P V}{r - u}} \tag{2}$$

where:

v – matrix of corrections (v^T – transposed matrix)

p – weights matrix

r – the number of correction equations

u - the number of unknowns

After performing the transformation from the system of raster image to the system of airplane (Fig.1., details of defining in [6, 12, 13]), the size of the pixel was calculated and verified by resampling[9] of the input image. This made basis to calculate the area of ice on not de-iced sections of the airplane. CAD environment (application MicroStation[10]) and the overlay to work with rasters - Image Analyst[11] were applied. To use the CAD model, one had to carry out the transition from 3D model of the airplane (Fig. 1) on the plane parallel to the plane of the taken photo was used. Defined this way 2D system of the model was used as the geometric base for the raster transformation. The view of the image and 2D plane of CAD model, on which the image was transformed, is shown in Fig. 6. By showing the proper characteristic of reference points - on model and digital image the change of geometry of the whole photo. To increase the accuracy of work also other fragments of airplane photo were examined. The applied in the transformation finite elements method[12] allowed obtaining the accuracy of fitting on the level of 3.6 mm.

Fig. 7. presents the fragment of wing subdued to transformation. Despite very unfavorable geometry of the distribution of photo-points (points selected for transformation were almost in one line), relatively good results were obtained, which is proved by the fact that point no. 4 (Fig. 7a) was automatically „proposed" by the program in the place, where on the image there is its equivalent (program after calculating the transformation based on 3 points – prompts the situation of subsequent points, which can be accepted or rejected or corrected manually).

Fig. 8. presents CAD model of the wing in the vector format, which was overlapped by digital image as the effect of transformation, confirming the correctness of the accepted methods. The transformation image on points obtained from CAD model allowed the experiments connected with the measurement of the surface elements with a clear yellow component. To carry out the geometrization of ice accretions, the resampling to the ending pixel was carried out.

The calculation of the area is carried out automatically after marking the borders of the area take for the calculation. In Fig. 9. – 1 pixel has the diameter of 10 mm, the area of the region marked white is 4215 mm^2. In Fig. 10. – 1 pixel has a diameter of 10 mm, the area of the region marked white is 8387 mm^2.

The measurement of the geometry of ice accretions was carried out in the manual way. Using subpixel image analysis and methods of artificial intelligence [7], the accuracy of the processed results can be increased even by one order, i.e. below 1 mm, assuming that the errors of the processing method will not be bigger. The experience of the authors shows that it is reasonable to use subpixel methods, which will mean attributing the image of the gradient value to each pixel. The gradient value is a vector consisting of the amplitude and direction. Then spatial amplitude of the gradient is determined by the equation (3):

$$g(j,k) = \sqrt{g_r\ (j, k)^{\ 2} + g_c\ \ (j, k)^{\ 2}} \tag{3}$$

9 resampling - calculating pixels and giving them another size of the pixel

10 Aplication MicroStation by Bentley

11 Image Analyst – overlay by Intergraph on MicroStaion environment

12 Transformation by finite elements method (FEM) polega means the transformation of the image, after earlier division into the grid.

Fig. 6. The view of the program Image Analyst and MicroStation with CAD model and the image recorded during the flight

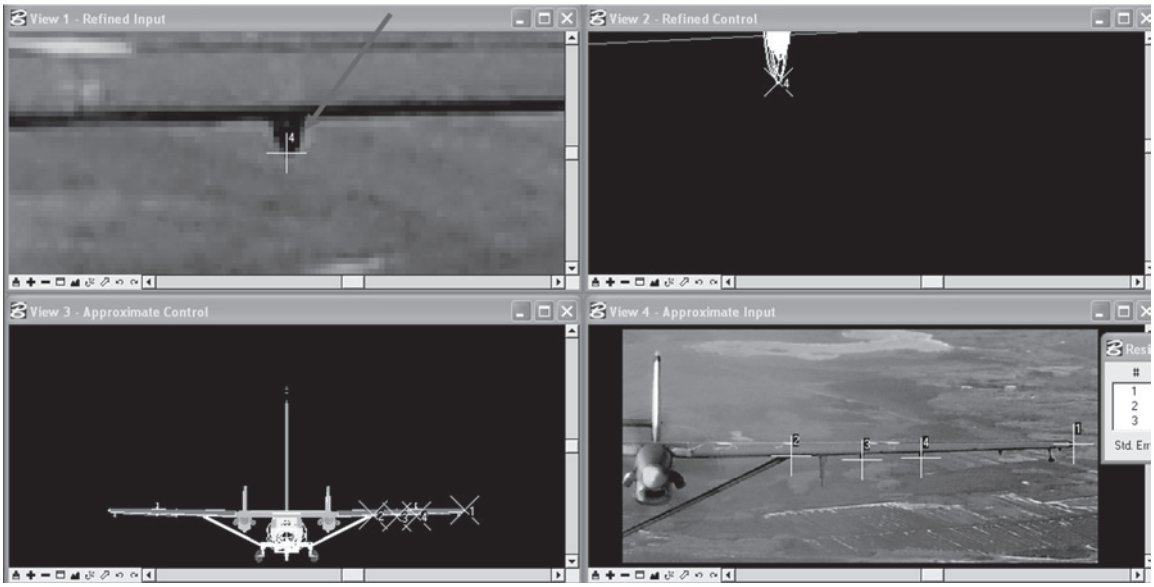

Fig. 7a. Distribution of points for the transformation. Red arrow marks the mentioned in the text point no. 4

Fig. 8. Overlapping the digital image on CAD model

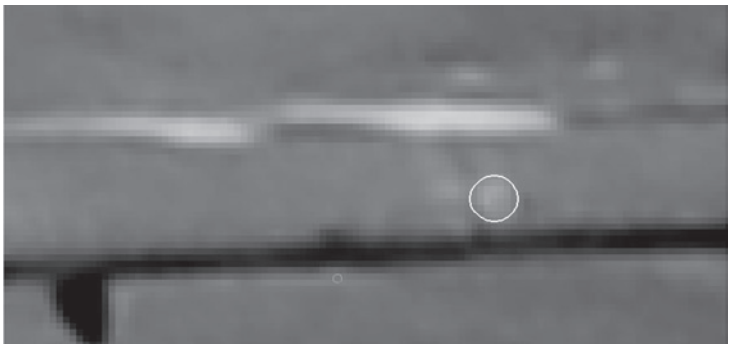

Fig. 9. Augmented fragment of the image

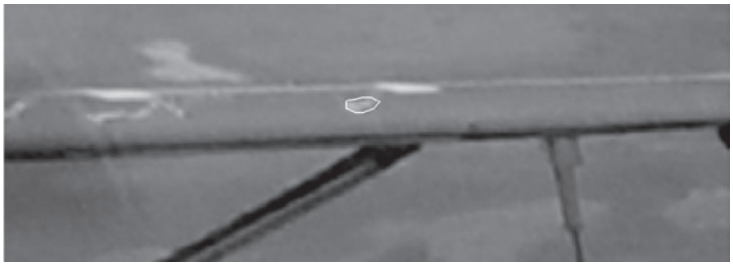

Fig. 10. Augmented fragment of the image

where g_r *(j, k)* and g_c *(j, k)* are gradient calculated towards the rows (r) and columns (c). The direction of the spatial gradient referring to the axis of rows is counted in the following way (4):

$$(j,k) = \arctan \frac{g_c(j,k)}{gr(j,k)} \tag{4}$$

Subpixel edge accuracy is achieved by adjusting the polynomial of the second degree towards the gradient. There, where the function achieves maximum subpixel localization will occur. The essence of subpixel image analysis [8],[9] (application of the second derivative as a method of marking the position of the points on the edge) was

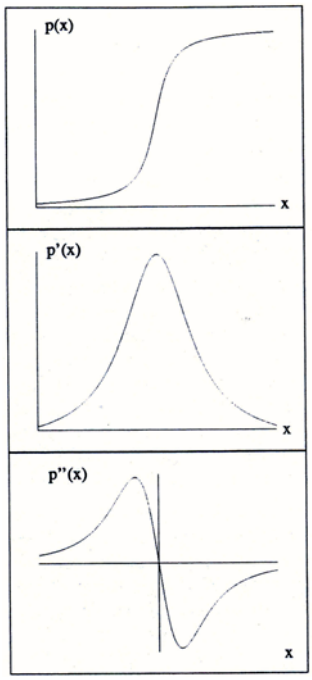

Fig. 11. The essence of subpixel analysis

presented in Fig. 11. where: the inflection point on an exemplified edge as function p(x), its equivalent in the first derivative (maximum function p'(x)) and second derivative (place of zero, function p''(x)).

Formulae (5) and (6) define first and second derivative counted on the digital image.

$$\nabla f = \begin{bmatrix} \frac{\partial f}{\partial x} \\ \frac{\partial f}{\partial y} \end{bmatrix} \tag{5}$$

where:

∇f – is the first derivative of the components in direction x and y $(\frac{\partial f}{\partial x}, \frac{\partial f}{\partial y})$.

The calculation of the second derivative runs according to the formula:

$$\nabla^2 f(x,y) = \frac{\partial^2 f(x,y)}{\partial x^2} + \frac{\partial^2 f(x,y)}{\partial y^2} \tag{6}$$

where:

$\nabla^2 f(x,y)$ - calculation of second derivative towards x and y based on the components :

$$(\frac{\partial^2 f(x,y)}{\partial x^2}, \frac{\partial^2 f(x,y)}{\partial y^2}).$$

In further experiments the authors intend to increase the accuracy of work by the application of the concept of the use of the first and second derivative, which will allow the increase of the quality of the papers of this type.

4. Conclusions

In the carried out experiments the visual assessment and manual measurements of ice accretions due to the improvement of the quality of input images (Fig. 2, 3). The authors of the article can see the possibility of the automation of measurements and the increase of accuracy. The application of results of the analysis, of the character of evidence is in a non-published document, the owner of which is PZL Mielec Sp. z o.o. Sikorsky Company [12, 13].

As a result of the flight tests processing of digital images, it was stated that the application of photogrammetric methods to testing the de-icing systems of airplanes, it is jest reliable and acceptable from the point of view of the information accuracy. The use of neutral substances coloring the water suspension used to sprinkle the airplane during the tests in artificial icing conditions is acceptable and comfortable solution in the understanding of the accuracy of the obtained results, on the level of single millimeters (the accuracy of transformation was calculated on the level ≈ 0,5 pixel and such accuracy was accepted as the accuracy of manual vectorization of theplaces of icing).

Comparison to the geometry of the airplane (pt. 3.2) confirmed the correctness of the approach connected with the processing of the image and geometrization of its details.

It was found sensible to apply subpixel image analysis in the future, which will improve the accuracy of the results. For the discussed case it was the accuracy below 1 mm (0.1 pixel). This refer to all the elements of the geometry of the solid and their situation in the struc-

ture of the airplane. An important element of preparing the airplane for tests in natural conditions is painting the surfaces interesting for us with dark and mat paint, which will decisively increase the accuracy of the analysis. A subsequent element decisively improving the quality of the obtained results is higher number of photos, including the ones taken by the conjugated cameras.

In the indicated improvements the authors of the article can see the possibility of further increase of the accuracy of the carried out analyses by the development and implementation of the methods of artificial intelligence [7] and subpixel image analysis [8].

In subsequent experiments one can apply photo cameras with the image sensor of higher resolution, which should additionally increase the accuracy of the work. Independent research can be carried out on the optimization of the distance of photographing to the studied airplane or the application of experiments with UAV technology, which becomes more and more popular [10, 11].

Icing on the surfaces of the airplane can occur in several forms: white porous ice, transparent ice, cracked ice, etc. Some forms of icing will allow seeing the painting of airplane, and other will reflect the light. In case of testing de-icing systems of the airplane in natural conditions, painting the de-iced surfaces in dark mat paints is suggested.

The authors also believe in the meaning of studies extending the scope of the application of sensors with modern techniques of laser scanning, which in recent years has been gaining more and more popularity and scope [11]. The authors wish to thank the Board of the Polskie Zakłady Lotnicze Sp. z o.o. in Mielec for making available the results of tests and photos to write this article.

References

1. Brzeczek J., Pietruszka J., Polskie Zakłady Lotnicze Sp. z o.o.; Flemming R.J., Bernstein B.,C., Leading Edge Atmospherics. "Certification Flight Tests in Natural Icing of the PZL Mielec M28 Commuter Turboprop Airplane" Praha SAE 2015 International Conference on Icing of Aircraft, Engines, and Structures 22-25 June 2015 Prague, Czech Republic.
2. Certification Specifications CS-23 (Normal, Utility, Aerobatic, and Commuter Category Aeroplanes) with AMC, GM, Amendment 4, 15 July 2015,
3. Golec P., Brzęczek J., Meeting Reliability Requirements for Rotor Ice Protection Systems Design, Diagnostyka 2014; 15 (1): 22-31.
4. Gonzalez R. C., Woods R. E., Eddins S.L., Digital Image Processing Using MATLAB, 2nd edition, Gatesmark Publishing 2009.
5. Gonzalez R. C., Woods R. E., Digital Image Processing (3rd Edition). Prentice Hall Upper Saddle River, New Jersey 2007.
6. Instrukcja Użytkowania w Locie Samolotu M 28.
7. Mikrut S. (praca zbiorowa - Czechowicz A., , Gryboś P., Jachimski J., Mikrut S., Mikrut Z. , Pawlik P., Tadeusiewicz R. pod redakcją naukową dr inż. Sławomir Mikrut) Sieci neuronowe w procesach dopasowania zdjęć lotniczych. Wydawnictwa AGH - AGH University of Science and Technology Press, Kraków 2010.
8. Mikrut S. Przydatność algorytmów podpikselowej detekcji cech w wybranych zagadnieniach fotogrametrycznych. Archiwum Fotogrametrii, Kartografii i Teledetekcji - Archives of Photogrammetry, Cartography and Remote Sensing 2009; 19: 299-308.
9. Mikrut S., Wpływ skanowania i kompresji według standardu JPEG na wykrywanie obiektów liniowych i punktowych na obrazach cyfrowych. Rozprawa doktorska AGH, Kraków 2003. Unpublished.
10. Mikrut S., 2016, : Classical Photogrammetry and UAV – Selected Ascpects. Int. Arch. Photogramm. Remote Sens. Spatial Inf. Sci., XLI-B1, 947-952.
11. Mikrut S., Kohut P., Pyka K., Tokarczyk R., Barszcz T., Uhl T. : Mobile Laser Scanning Systems for Measuring the Clearance Gauge of Railways: State of Play, Testing and Outlook. Sensors 2016; 16(5): 683, https://doi.org/10.3390/s16050683.
12. Opracowanie zbiorowe, Raport AGH, pt. "Analysis of Digital Images Concerning PZL-M28 SP-DAA Airplane" wykonany przez AGH dla PZL Mielec 2014. Unpublished.
13. Opracowanie zbiorowe, Raport AGH, pt. "Wykonanie testów i analiz w zakresie określania geometrii zewnętrznej płatowca metodami fotogrametrii i skaningu" wykonany przez AGH dla PZL Mielec 2015. Unpublished.

Józef BRZĘCZEK
State Higher Vocational School them. Stanislaw Pigon in Krosno
Polytechnic Institute
Department of Mechanics and Mechanical Engineering
ul. Wyspiańskiego 20, 38-400 Krosno, Poland

Sławomir MIKRUT
Faculty of Mining Surveying and Environmental Engineering
AGH University of Science and Technology
Department of Geoinformation, Photogrammetry
and Environmental Remote Sensing
al. Mickiewicza 30, 30-059 Cracow, Poland

E-mails: jbrzeczek@gmail.com, smikrut@agh.edu.pl

Article citation info:
SHEN G, ZENG W, ZHANG Y, HAN C, LIU P. Determination of the average maintenance time of CNC machine tools based on type II failure correlation. Eksploatacja i Niezawodnosc – Maintenance and Reliability 2017; 19 (4): 604–614, http://dx.doi.org/10.17531/ein.2017.4.15.

Guixiang SHEN
Wenbin ZENG
Yingzhi ZHANG
Chenyu HAN
Peng LIU

DETERMINATION OF THE AVERAGE MAINTENANCE TIME OF CNC MACHINE TOOLS BASED ON TYPE II FAILURE CORRELATION

OKREŚLENIE ŚREDNIEGO CZASU KONSERWACJI OBRABIAREK CNC W OPARCIU O KORELACJĘ AWARII TYPU II

An average maintenance time calculation method based on components failure correlation analysis is proposed to revise the traditional system maintenance time. This paper focus on complex system type II fault correlation, using the Decision-making trial and evaluation laboratory / Interpretative structural model method to divide the fault level of components. And the copula connection function is introduced to calculation of failure rate function of failure correlation components. In addition, the system maintenance time model is established by synthesizing the failure rate function of each unit of the system. Moreover, the average maintenance time under the minimum number of failures is determined. This method shows that the minimum average maintenance time of the proposed system is more reasonable than the traditional one and provides the basis for system and component reliability design.

***Keywords**: CNC machine tools, Average maintenance time, Type II failure correlation, DEMATEL/ISM, Copula function.*

W artykule zaproponowano metodę obliczania średniego czasu konserwacji, opartą na analizie korelacji uszkodzeń elementów składowych systemu. Metoda ta ma na celu rewizję tradycyjnego czasu konserwacji systemu. Głównym tematem pracy jest korelacja awarii typu II występujących w systemach złożonych. Elementy systemu podzielono ze względu na poziom uszkodzenia przy użyciu metody DEMATEL w połączeniu z interpretacyjnym modelowaniem strukturalnym. Funkcję intensywności skorelowanych uszkodzeń elementów systemu obliczono za pomocą funkcji łączącej (kopuły). Dodatkowo, opracowano model czasu konserwacji systemu poprzez syntezę funkcji intensywności uszkodzeń każdej jednostki systemu. Ponadto, określono średni czas konserwacji dla minimalnej liczby uszkodzeń. Metoda ta pokazuje, że minimalny średni czas konserwacji proponowanego systemu jest korzystniejszy niż tradycyjnie przyjęty i stanowi podstawę do projektowania niezawodności systemu i jego składowych.

***Słowa kluczowe**: obrabiarki CNC, średni czas konserwacji, korelacja awarii typu II, DEMATE /ISM, funkcja kopuła.*

1. Introduction

Maintenance is an important attribute of product quality. It refers to the prescribed procedures and methods that a product undergoes under specified conditions and time to maintain or restore its regular state [5, 24]. A maintenance program analyzes, predicts, and evaluates the quality of the product and establishes a variety of physical and mathematical models. The program is essential and strongly influences the product maintenance level [1,14,17].

Research on maintenance models is divided into qualitative description and quantitative analysis. Qualitative description includes a descriptive model, flow chart, and graphic model. Literature shows that research on the quantitative analysis of repair time is relatively weak [4,7,13,18,19]. More research has focused on the replacement time and, average repair time for model assumptions, parameters estimation, and hypothesis testing. [3] showed that the maintenance time of CNC machine tools could be statistically analyzed. Assuming that the system maintenance time possesses a lognormal distribution, the maximum likelihood method can be used to estimate the parameters, and the skewness–-kurtosis test can be conducted to obtain the maintenance time distribution. In [25], we use the Origin 8 drawing function to plot the probability density function graph of an NC machining center and judge its possible distribution rule. Then, we use a MATLAB programming function to estimate the parameters and obtain the maintenance time model. In [3] and [25], the maintenance time of all components was indiscriminately based on experience, and the system maintenance time was assumed to follow a certain distribution model. The distribution model was determined by model hypothesis, parameter estimation, and hypothesis testing. Finally, the average maintenance time of the system is determined by point estimation. Most modern mechanical systems comprise the key system units. System failure must be closely related with the system unit; thus, the maintenance time modeling process should consider the role of the system unit.

In [22], a maintenance operation comprised multiple maintenance tasks. Maintenance operation was divided into serial maintenance operations, parallel repair operations, and serial parallel maintenance operations according to the relationship between the maintenance operations; in turn, the maintenance time calculation model was given. In [8], the system maintenance time comprised different maintenance times. Therefore, the subsystem maintenance activity indivisible was defined as the basic maintenance event. The system maintenance work sequence is divided into serial, parallel and hybrid, and the final formula was based on the whole probability of the system to obtain

the average maintenance time. In [9], three kinds of logical relations existed between the system maintenance operations: serial, parallel, and selection. These logical relations then built the maintenance process model based on Colored Stochastic Petri Net (CSTPN). The model was used to propose a maintenance time simulation algorithm using the Monte Carlo method. the maintenance time of the subsystem is considered in [8], [9], and [22], and the corresponding system maintenance time model was established according to the different logical relations among the subsystems. However, a huge error was encountered in the system average maintenance time due to the failure in the correlation between the subsystems. This phenomenon resulted in the failure of, the maintenance cycle plan to satisfy actual project requirements, thereby affecting maintenance efficiency.

System maintenance time function is constituting by the component failure rate and maintenance time. Therefore, this paper studies the type II fault correlation [11,26], which is when a component in the system fails, it will affect the failure rate of other components. And aiming at the serial system, establishing the component failure correlation model by considering the failure rate of the system components. In addition, the average maintenance time model with the minimum failure rate of the system is obtained by weighting the subsystem failure rate. Taking CNC machine tools as an example, the concrete modeling process is introduced to provide a theoretical basis for the system maintenance time design and maintenance plan formulation.

2. Modeling principle of system average maintenance time based on fault correlation

2.1. Implementation of component-level division based DEMATEL / ISM method

Decision-making trial and evaluation laboratory (DEMATEL) is a systematic method of analysis using graph theory and matrix tools. The method studies the complex relationship between the systems converted to visualize the structure of the model, and thus the complex system dependencies between the elements, to make a quantitative analysis, and clarify the key factors [21].

Interpretive structural modeling (ISM) system is used for the analysis of complex issues related to the socio-economic system and development. The idea of this method is to divide the complex system into several sub-systems, draw the relation graph, reflect the direct relationship between the system elements using adjacency matrix, and then transform the adjacency matrix into a reachable matrix. The reachable matrix decomposition is then transformed into a complex system that constitutes a clear multi-level hierarchical structure model [10]; thus, a professional explanation and interpretation of the completion of the structural model are achieved.

This article uses the integrated DEMATEL / ISM method combined with machine fault correlation analysis to clarify the relationship between the system elements and to simplify ISM modeling of large and complex matrix operations. First, a subsystem failure correlation network is established based on the subsystem failure correlation data. Second, the DEMATEL is used to calculate calculated the comprehensive influence matrix of the system to obtain the correlation order of the fault subsystem and discover the key subsystems. Moreover, the overall influence matrix of the system (is unit matrix) is determined, then the reachability matrix $\mathbf{M}$ is obtained. Finally, the ISM method of grading system and domain decomposition is used to analyze the complex issues of hierarchical relationships between the subsystems. The integration of the two methods clarifies the effect of the failure of the subsystem as well as the mechanism of fault transmission.

The procedure in determining the reachability matrix using the DEMATEL method is presented as follows:

1) Determine the correlation matrix, represents the number of impact of influencing factors and; $i = j$, gives $y_{ij} = 0$.
2) Normalized correlation matrix to obtain Normalized matrix $\mathbf{X}$:

$$\mathbf{X} = \frac{\mathbf{Y}}{\max\limits_{1<i<n} \sum_{j=1}^{n} y_{ij}} \tag{1}$$

3) Determine the comprehensive influence matrix $\mathbf{T}$:

$$\mathbf{T} = \lim_{k\to\infty}\left(\mathbf{X} + \mathbf{X}^2 + \cdots + \mathbf{X}^k\right) = \mathbf{X}\left(\mathbf{I} - \mathbf{X}\right)^{-1} \tag{2}$$

$$\mathbf{T} = [t_{ij}]_{n\times n}, i, j = 1, 2, \cdots, n \tag{3}$$

$\mathbf{I}$ is the identity matrix, and t_{ij} is the integrated effect of component i and component j, including direct and indirect effect.

4) Determine the overall system impact matrix $\mathbf{H}$:

$$\mathbf{H} = \mathbf{T} + \mathbf{I} \tag{4}$$

Then the reachability matrix $\mathbf{M}$ is obtained by the overall system impact matrix $\mathbf{H}$.

Finally, the failure to obtain the hierarchical relationships between the subsystems using the ISM method classification system and domain decomposition is shown in Figure 1.

Fig. 1. Hierarchy relationship of system component

2.2. Reliability modeling of system components based on Copula function

First, the reliability of each system component is modeled based on time correlation. Then consider the fault correlation and the transmission of the hierarchy subsystem shown in Figure 1. Moreover, the joint distribution function is established using the copula connection function to determine the fault correlation coefficients among system components, thereby establishing a system reliability model based on fault related components.

2.2.1. Time-dependent system component reliability modeling

A two-parameter Weibull distribution [12] for reliability modeling is introduced in this paper. After the establishment of a system component failures time model, considering the small sample size of each system component, the maximum likelihood estimation method (MLE) is used to estimate the parameters to improve the accuracy of parameter estimation.

$t_1, t_2, \cdots, t_n$ are set up for fault interval time order statistics, using MLE. The shape parameter $\hat{\beta}$ and scale parameter $\hat{\alpha}$ can satisfy the following equation:

$$\hat{\alpha}=\left(\frac{1}{n}\sum_{i=1}^{n}t_i^{\hat{\beta}}\right)^{1\hat{\beta}}\quad \frac{1}{\hat{\beta}}=\frac{\sum_{i=1}^{n}t_i^{\hat{\beta}}lnt_i}{\sum_{i=1}^{n}t_i^{\hat{\beta}}}-\frac{1}{n}\sum_{i=1}^{n}lnt_i \tag{5}$$

$\hat{\beta}_k$–$\hat{\beta}$ is obtained after k times iterations;

As the iteration number increases, its value approaches the optimal solution. The iterative algorithm is shown as follows:

$$\begin{cases}\hat{\beta}_{k+1}=\frac{1}{2}\hat{\beta}_k+\frac{1}{2}\left[h\left(\hat{\beta}_k\right)-\bar{X}\right]^{-1}\\ \hat{\beta}_0=1.0\end{cases} \tag{6}$$

$$\bar{X}=\frac{1}{n}\sum_{i=1}^{n}t_i^{\hat{\beta}_k}\ ;\ h\left(\hat{\beta}_k\right)=\frac{\sum_{i=1}^{n}t_i^{\hat{\beta}}lnt_i}{\sum_{i=1}^{n}t_i^{\hat{\beta}}}$$

The decreased number of system component fault data results in a small sample problem. Result obtained using the MLE have certain deviations, thereby requiring parameter estimation based on the results of a deviation correction.

$$\beta^*=\gamma_\beta(n)\hat{\beta} \tag{7}$$

$\gamma_\beta(n)$ is known as $\hat{\beta}$ of the correction coefficient and calculated by the following formula:

(8)

When n is an even number and $n\geq 4$:

$$\gamma_\beta(n)=\sqrt{\frac{\pi}{n}}\times\frac{1\times3\times\cdots\times(\mathrm{n}-3)}{2^{\frac{\mathrm{n}-3}{2}}\left(\frac{\mathrm{n}}{2}-2\right)!} \tag{9}$$

When n is an odd number and $\mathrm{n}\geq 5$:

$$\gamma_\beta(n)=\frac{2^{\frac{n}{2}-1}}{\sqrt{n\pi}}\times\frac{\left(\frac{\mathrm{n}-3}{2}\right)!}{1\times3\times\cdots\times(\mathrm{n}-4)} \tag{10}$$

For any $n\geq 3$, $\gamma_\beta(n)<1$ and $\lim_{n\to\infty}\gamma_\beta(n)=1$; thus, $\beta^*<\hat{\beta}$, and using formula (9) to correct the deviation of shape parameter β.

The deviation correction formula of scale parameter α is:

$$\alpha^*=\gamma_\alpha\left(n,\beta^*\right)\hat{\alpha} \tag{11}$$

$$\gamma_\alpha\left(n,\beta^*\right)=\frac{n^{\frac{1}{\beta^*}}(n-1)!}{\Gamma\left(n+\frac{1}{\beta^*}\right)}$$

After the parameters are estimated, the d test method is used to test the system component failure of the time interval distribution function and goodness-of-fit test.

2.2.2. Reliability model based on failure rate correlation subsystem

(1) Fault correlation coefficient modeling of system components based on copula function

Considering the failure time correlation of system components to establish the time-dependent reliability model. Then the fault correlation and transfer of the system components are considered, and the copula connection function is used to calculate the failure correlation coefficient.

The copula theory was proposed by Sklar in 1959. This theory can decompose a joint distribution function into a Copula function and k marginal distribution [15,27]. In addition, this theory follows the Sklar theorem:

$H(\cdot,\cdot)$ is a joint distribution function of $F(\cdot)$ and $G(\cdot)$. A function of copula $C(\cdot,\cdot)$ satisfies $H(x,y)=C(F(x),G(y))$. If $F(\cdot)$ and $G(\cdot)$ are continuous, then $C(\cdot,\cdot)$ is the only; otherwise, if $F(\cdot)$ and $G(\cdot)$ are a univariate distribution function and $C(\cdot,\cdot)$ is a corresponding copula function, then the function $H(\cdot,\cdot)$ is the joint distribution function with marginal distribution $F(\cdot)$ and $G(\cdot)$.

Based on experience, the system component time between failure obeys Weibull distribution is generally uses the Gumbel-copula function and is expressed as follows:

$$C\left(R_1(t),R_2(t),\ldots,R_n(t)\right)=exp\left\{-\left[\sum_{i=1}^{n}\left(-lnR_i(t)\right)^{1/\theta}\right]^{\theta}\right\},\theta\in(0,1] \tag{12}$$

$R_i(t)$ is component time-dependent reliability model, $\mathrm{i}=1,2,\ldots,\mathrm{n}$.

And θ is a random variable, where $\theta=1$, if n system components are independent of each other; on the contrary, θ is closer to 0, if n system components have a stronger reliability correlation. Thus, the random variable θ is also known as the correlation coefficient. As a result, how to calculate θ is the key to the establishment of system model.

Based on the relationship between the system components, the correlation between the system components can be established, and the correlation coefficient θ shown as follow:

Figure 2 shows that the system can be divided into three levels with an associated system component failure. And the components of the fault source subsystem and intermediate fault subsystem as well as their reliability marginal distribution function. In addition, the copula connection function is introduced and the joint distribution function is established to determine the fault correlation coefficients among system components, thereby establishing the system reliability model based on failure rate correlation components.

In the system with k failure rate correlation components, suppose the reliability function of each system component, $R_i(t_i)$, $\mathrm{i}=1,2,\ldots,\mathrm{k}$; a copula function $C\left(R_1(t_1),R_2(t_2),\ldots,R_k(t_k)\right)$, such

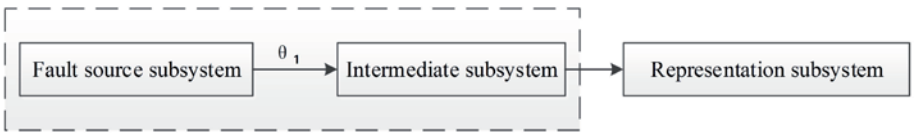

Fig. 2. Fault source subsystem and intermediate subsystem failure associated schematic

that $R(t_1,t_2,\ldots,t_k)=C(R_1(t_1),R_2(t_2),\ldots,R_k(t_k))$, can be uniquely identified. Among the $R(t_1,t_2,\ldots,t_k)$ is the $R_i(t_i)$ of the reliability joint distribution function of k failure rate correlation components.

Each system component in the event of failure needs to be shut down for maintenance, then system can be regarded as a series system. The system components of the fault are both independent and non-independent; thus, the system reliability function is solved as:

$$R(t)=\prod_{i=1}^{n_1}C_i(t)\prod_{j=1}^{n_2}R_j(t) \tag{13}$$

$$n=n_1+n_2$$

Where:

n is the number of system components;

n_1 is the number of components with fault correlation;

n_2 is the number of components with fault independent;

$C_i(t)$ is the integrated reliability of the component i;

$R_j(t)$ is the reliability of the component j.

(2) Failure rate modeling of system components based on failure rate correlation

According to [16], when a subsystem j is affected by subsystem i, the comprehensive failure rate is:

$$\begin{aligned}\lambda_j(t)&=\phi_j\left[\lambda_{Ij}(t),\lambda_{i_j}(t)_g,t\right]\\&=\lambda_{Ij}(t)+\sum_{i_j}\varphi_{i_j}\lambda_{i_j}(t)_g\end{aligned} \tag{14}$$

Where $\lambda_j(t)$ is the comprehensive failure rate of component j;

$\lambda_{Ij}(t)$ is the independent failure rate of component j;

$\varphi_{i_j}(t)$ is the correlation coefficient of component i on component j;

$\lambda_{i_j}(t)_g$ is the correlation failure rate of components i related to component j.

$\lambda_j(t)$ is generally obtained from the field failure data; $\lambda_{Ij}(t)$ is determined by the inherent reliability, usually through factory testing or production data. If relevant effect is not considered, then theoretically $\lambda_j(t)=\lambda_{Ij}(t)$. On the contrary, the copula theory is expressed in this article as $\varphi_{i_j}(t)\in[0,1]$, where $\varphi=0$, indicates no correlation, and $\varphi=1$ indicates completely relevance. That is, a failure of subsystem i will inevitably induce failure of components j; thus, j can be replaced by using $(1-\theta)$.

The integrated failure rate of each subsystem level can be obtained as:

$$\lambda_F(t)=\lambda_1(t)\lambda_I(t)=\lambda_2(t)+(1-\theta_1)\lambda_1(t)$$

Where $\lambda_F(t)$ and $\lambda_I(t)$ are the failure rate of fault source subsystem and intermediate fault subsystem respective with failure rate correlation; $\lambda_1(t)$ and $\lambda_2(t)$ are the failure rate of fault source subsystem and intermediate fault subsystem respective with fault independent; θ_1 is the correlation coefficient between fault source subsystem and intermediate fault subsystem.

Given that the representation subsystem is affected by the failure of the source subsystem and the intermediate subsystem as a whole, the integrated failure rate must be obtained:

$$\lambda_{12}(t)=-\frac{R'_{12}(t)}{R_{12}(t)}$$

$$\lambda_R(t)=\lambda_3(t)+(1-\theta_2)\lambda_{12}(t)$$

Where $\lambda_{12}(t)$ is the integrated failure rate of fault source subsystem and intermediate fault subsystem; $R_{12}(t)$ is the integrated reliability function of fault source subsystem and intermediate fault subsystem; $R'_{12}(t)$ is the partial derivative of $R_{12}(t)$; $\lambda_3(t)$ is the failure rate of representation subsystem with fault independent; $\lambda_R(t)$ is the failure rate of representation subsystem with failure rate correlation; θ_2 is the correlation coefficient between representation subsystem and the whole of fault source subsystem and intermediate fault subsystem.

2.3. Maintenance time modeling of system components based on small sample

In the modeling process of system component maintainability, the small sample features of the system components are considered, using the normal distribution of small sample data processing and the particle swarm optimization algorithm. These procedures are conducted to optimize the parameters estimation, to determine the maintenance time model and calculate the average repair time of the system components, which provide the basis for the maintenance time calculation of the system component failure correlation.

Fault repair time τ is subject to a lognormal distribution $LN(\mu,\sigma^2)$. Its logarithm $ln\,\tau$ satisfies the normal distribution $N(\mu,\sigma^2)$.

The probability density function of repair time τ is expressed as:

$$m(\tau)=\frac{1}{\sigma t\sqrt{2\pi}}exp\left\{-\frac{1}{2}\left(\frac{ln\tau-\mu}{\mu}\right)^2\right\} \tag{15}$$

The cumulative distribution function is expressed as:

$$M(\tau)=\int_0^{\tau}\frac{1}{\sigma x\sqrt{2\pi}}exp\left\{-\frac{1}{2}\left(\frac{lnx-\mu}{\sigma}\right)^2\right\}dx \tag{16}$$

Where σ and μ are parameters to be estimated.

Parameters σ and μ are estimated. Samples $\tau_1,\tau_2,\ldots\tau_n$ are set as the maintenance time data for a hierarchical system components. The maintenance probability estimate value $\hat{p}_i$ at sample τ_i is expressed as:

$$\hat{p}_i=t_{n-1}\left(\sqrt{\frac{n}{n+1}\cdot\frac{X_i-\bar{X}}{S}}\right) \tag{17}$$

$$X_i=ln\tau_i,\ \bar{X}=\frac{1}{n}\sum_{i=1}^{n}ln\tau_i$$

$$S=\frac{1}{n-1}\sqrt{\left(X_i-\bar{X}\right)^2}$$

The repair probability estimate $\hat{p}_i$ is obtained through $X_i = ln\tau_i$, each of which can be further obtained as $\left(\tau_i, \hat{p}_i\right)$ point. Moreover, the maintenance level of the subsystem parameters of the model estimates can be obtained when combined with the least squares method.

The constraint criterion of the least squares method is expressed as:

$$Q = \sum_{i=1}^{n}\left[\int_0^{\tau_i} \frac{1}{\sigma x\sqrt{2\pi}} exp\left\{-\frac{1}{2}\left(\frac{lnx-\mu}{\tilde{A}}\right)^2\right\} dx - \hat{p}_i\right]^2 = min \quad (18)$$

In (18), the parameter of constrained least squares method is solved using particle swarm optimization (PSO) [20, 23, 6] under the guidelines of the optimization problem. The PSO optimization algorithm flow chart is shown in Fig. 3.

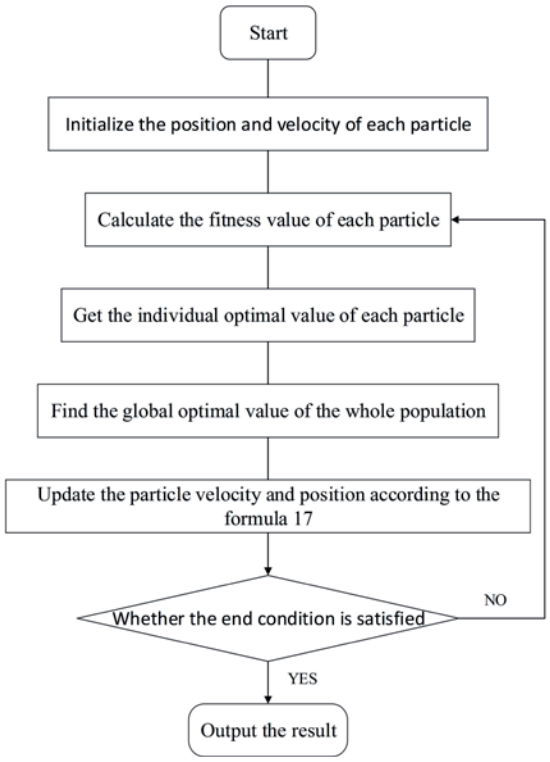

Fig. 3. PSO algorithm flowchart

2.4. System average maintenance time modeling

The system maintenance time can be expressed as a function of its components maintenance time; thus, the integrated maintenance time of the system can be obtained by calculating the components average maintenance time. System *MTTR* (Mean time to repair) can be calculated by system components *MTTR*, and the weighting factor is related to the number of failures of the system components [2].

$$MTTR = \frac{\sum_{i=1}^{n} q_i f_i MTTR_i}{\sum_{i=1}^{n} q_i f_i} \quad (19)$$

Where $MTTR_i$ is average maintenance time of component i,f_i ,is the number of faults in the system design life cycle for component i, q_i is the number of component i.

Given that the number of failures of the system components is closely related to the failure rate of all components and the failure dependencies between the system components makes the weighting factor more accurate and reasonable, the use of λ_i is possible instead of f_i. In other general system, system components are relatively in unique division; thus, q_i=1, and the average system maintenance time can be rewritten as:

$$MTTR = \frac{\sum_{i=1}^{n} \lambda_i MTTR_i}{\sum_{i=1}^{n} \lambda_i} \quad (20)$$

Where λ_i is failure rate for system components in all levels.

The model comprehensively considers the failure time correlation and fault transfer of each component, that is, the corresponding weight maintenance coefficient is given to different system components for repair time calculation and engineering practice.

3. Application example

In this paper, modular methods for the whole function of subsystems are used in combination with the main structure and working process of CNC machine tools, as shown in Table 1.

Table 1 shows five CNC machine tools tracked by the task group from July 1, 2012 to December 31, 2012 in time-truncated mode. The cumulative working time was 2,668 hours (two shifts). The collection and analysis of CNC machine tools used to collate the failure data are shown in Table 2.

The above associated failure statistics is presented as a fault directed graph in Fig. 4.

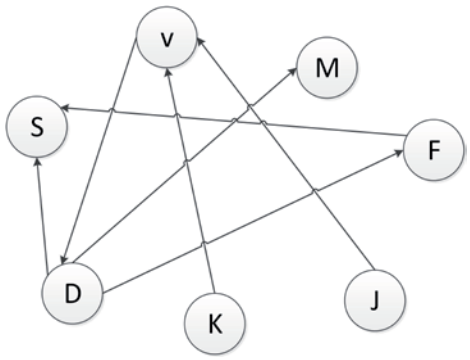

Fig. 4. Fault directed graph of CNC machine tools

3.1. Hierarchical division of CNC machine tools subsystem

The subsystem failure analysis is conducted, the influence matrix **Y** is directly affected, and the comprehensive influence matrix **T** is determined using the DEMATEL method.

$$\mathbf{Y} = \begin{array}{c} S \\ V \\ D \\ M \\ J \\ F \\ K \end{array} \begin{bmatrix} 0 & 0 & 0 & 0 & 0 & 0 & 0 \\ 0 & 0 & 1 & 0 & 0 & 0 & 0 \\ 2 & 0 & 0 & 2 & 0 & 3 & 0 \\ 0 & 0 & 0 & 0 & 0 & 0 & 0 \\ 0 & 1 & 0 & 0 & 0 & 0 & 0 \\ 2 & 0 & 0 & 0 & 0 & 0 & 0 \\ 0 & 2 & 0 & 0 & 0 & 0 & 0 \end{bmatrix}$$

Table 1 CNC machine tools subsystem partition

Site code	system name	Contains components
S	Active system	Including power cutting head, power box, spindle assembly, tools clamping mechanism and its main moving parts
J	Feed system	Including power slide, rail, screw and so on
F	Fixture	Including a positioning element (support nail, support plate and positioning pin, etc.) and positioning device (operating mechanism), clamping mechanism, fixture body, fixture base, table, etc.
NC	CNC system	Including PLC input and output interfaces, hardware, CNC system, servo system, the axis of the motor and its control circuit
V	Electrical System	Including the addition to the power outside the various sockets, switches, relays, contactors, fuses, power distribution boxes, etc.
D	Hydraulic system	Including hydraulic cylinders, fuel tanks, seals, one-way valve
P	Pneumatic system	Including the cylinder, one-way valve, pipeline and so on
Q	Protective device	Including the overall protection of the machine
C	Support member	Including column, column base, middle base, side base and so on
K	Cooling removal system	Mainly include coolant tank, pump, spiral chip conveyor and so on
W	Lubrication system	Mainly include pumps, pressure gauges, tubing and so on
M	Manipulator	Mainly including loading and unloading device

Table 2. Associated fault data of CNC machine tools

Cause of failure	Subsequent failure site	Cause of failure	Subsequent failure site
Fixture	Active system	Cooling chip removal system	Electrical System
Hydraulic system	Active system	Feed system	Electrical System
Cooling chip removal system	Electrical System	Hydraulic system	Active system
Hydraulic system	Fixture	Hydraulic system	Fixture
Hydraulic system	Manipulator	Fixture	Active system
Hydraulic system	Manipulator	Electrical System	Hydraulic system
Hydraulic system	Fixture		

$$\mathbf{T} = \begin{array}{c} S \\ V \\ D \\ M \\ J \\ F \\ K \end{array} \begin{bmatrix} 0 & 0 & 0 & 0 & 0 & 0 & 0 \\ 0.0583 & 0 & 0.1428 & 0.0408 & 0 & 0.0612 & 0 \\ 0.4082 & 0 & 0 & 0.2857 & 0 & 0.4286 & 0 \\ 0 & 0 & 0 & 0 & 0 & 0 & 0 \\ 0.0086 & 0.1428 & 0.0204 & 0.0058 & 0 & 0.0087 & 0 \\ 0.2857 & 0 & 0 & 0 & 0 & 0 & 0 \\ 0.0167 & 0.2857 & 0.0408 & 0.0117 & 0 & 0.0175 & 0 \end{bmatrix}$$

By comparing the row and column sum of the subsystems in $\mathbf{T}$, the ranking of correlation is sorted into hydraulic system, jig, active system, electric system and cooling system. Thus, the system overall impact matrix is:

$$\mathbf{H} = \mathbf{T} + \mathbf{I} = \begin{array}{c} S \\ V \\ D \\ M \\ J \\ F \\ K \end{array} \begin{bmatrix} 1 & 0 & 0 & 0 & 0 & 0 & 0 \\ 0.0583 & 1 & 0.1428 & 0.0408 & 0 & 0.0612 & 0 \\ 0.4082 & 0 & 1 & 0.2857 & 0 & 0.4286 & 0 \\ 0 & 0 & 0 & 1 & 0 & 0 & 0 \\ 0.0086 & 0.1428 & 0.0204 & 0.0058 & 1 & 0.0087 & 0 \\ 0.2857 & 0 & 0 & 0 & 0 & 1 & 0 \\ 0.0167 & 0.2857 & 0.0408 & 0.0117 & 0 & 0.0175 & 1 \end{bmatrix}$$

$m_{ij} = \begin{cases} 1 & \mathrm{h_{ij}} > \lambda \\ 0 & \mathrm{h_{ij}} \le \lambda \end{cases} \left(\mathrm{i, j} = 1, \cdots, \mathrm{n}\right)$ to determine the element values in the reachable matrix, which λ is a given threshold for system simplification. For systems with a small value of n, set $\lambda = 0$. Then, the reachable matrix $\mathbf{M}$ is:

$$\mathbf{M} = \begin{array}{c} S \\ V \\ D \\ M \\ J \\ F \\ K \end{array} \begin{bmatrix} 1 & 0 & 0 & 0 & 0 & 0 & 0 \\ 1 & 1 & 1 & 1 & 0 & 1 & 0 \\ 1 & 0 & 1 & 1 & 0 & 1 & 0 \\ 0 & 0 & 0 & 1 & 0 & 0 & 0 \\ 1 & 1 & 1 & 1 & 1 & 1 & 0 \\ 1 & 0 & 0 & 0 & 0 & 1 & 0 \\ 1 & 1 & 1 & 1 & 0 & 1 & 1 \end{bmatrix}$$

The subsequent operation is simple, with S_1 on behalf of S, S_2 on behalf of V, S_3 on behalf of D, S_4 on behalf of M, S_5 on behalf of J, S_6 on behalf of F, and S_7 on behalf of K. Define the reachable set $R(S_i)$, antecedent set $A(S_i)$, common set $C(S_i)$, and initial set $B(S_i)$ of the factors, as shown in Table 3.

Table 3. Reachable sets, Antecedent sets, Common sets, and Initial sets

S_i	$R(S_i)$	$A(S_i)$	$C(S_i)$	$B(S_i)$
1	1	1,2,3,5,6,7	1	
2	1,2,3,4,6	2,5,7	2	
3	1,3,4,6	2,3,5,7	3	
4	4	2,3,4,5,7	4	
5	1,2,3,4,5,6	5	5	5
6	1,6	2,3,5,6,7	6	
7	1,2,3,4,6,7	7	7	7

Given that $B(S)=\{S_5,S_7\}$, and $R(S_5)\cap R(S_7)\neq\varnothing$, the system can only be divided into a region $P=\{S_1,S_2,S_3,S_4,S_5,S_6,S_7\}$. The same region P, in turn, is used to meet the elements of $R(S_i)\cap A(S_i)=R(S_i)$ to identify and define the highest levels of collection and the second level of the collection until the division is completed. See Table 4 for the details of the classification process.

Table 4. Level division process

Feature set	S_i	$R(S_i)$	$A(S_i)$	$R(S_i)\cap A(S_i)$	$E(S)$	$\prod(P)$
$P-L_0$	1	1	1,2,3,5,6,7	1	1	$L_{1=}\{S_1, S_4\}$
	2	1,2,3,4,6	2,5,7	2		
	3	1,3,4,6	2,3,5,7	3		
	4	4	2,3,4,5,7	4	4	
	5	1,2,3,4,5,6	5	5		
	6	1,6	2,3,5,6,7	6		
	7	1,2,3,4,6,7	7	7		
$P-L_0-L_1$	2	2,3,6	2,5,7	2	6	$L_{2=}\{S_6\}$
	3	3,6	2,3,5,7	3		
	5	2,3,5,6	5	5		
	6	6	2,3,5,6,7	6		
	7	2,3,6,7	7	7		
$P-L_0-L_1-L_2$	2	2,3	2,5,7	2	3	$L_{3=}\{S_3\}$
	3	3	2,3,5,7	3		
	5	2,3,5	5	5		
	7	2,3,7	7	7		
$P-L_0-L_1-L_2-L_3$	2	2	2,5,7	2	2	$L_{4=}\{S_2\}$
	5	2,5	5	5		
	7	2,7	7	7		
$P-L_0-L_1-L_2-L_3$	5	5	5	5	5	$L_{5=}\{S_5, S_7\}$
	7	7	7	7	7	

Termination set $E(S)$ in table 4 represent output elements show that the system can be divided into five levels: $L_{1=}\{S_1, S_4\}$, $L_{2=}\{S_6\}$, $L_{3=}\{S_3\}$, $L_{4=}\{S_2\}$, and $L_{5=}\{S_5, S_7\}$. Determine the reachable matrix **M**(L) and remove the leapfrog binary relations among the elements to obtain **M**(L):

$$\mathbf{M}(\mathbf{L})=\begin{array}{c}1\\4\\6\\3\\2\\5\\7\end{array}\begin{bmatrix}1&0&0&0&0&0&0\\0&1&0&0&0&0&0\\1&0&1&0&0&0&0\\1&1&1&1&0&0&0\\1&1&1&1&1&0&0\\1&1&1&1&1&1&0\\1&1&1&1&1&0&1\end{bmatrix}$$

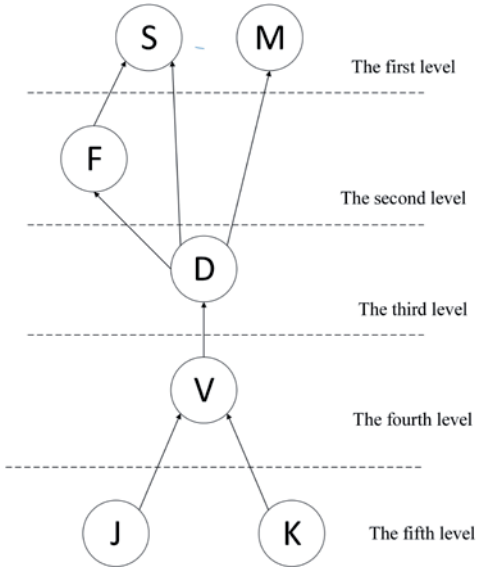

Fig. 5. Hierarchical structure model

$$\mathbf{M}'(\mathbf{L})=\begin{array}{c}1\\4\\6\\3\\2\\5\\7\end{array}\begin{bmatrix}1&0&0&0&0&0&0\\0&1&0&0&0&0&0\\1&0&1&0&0&0&0\\1&1&1&1&0&0&0\\0&0&0&1&1&0&0\\0&0&0&0&1&1&0\\0&0&0&0&1&0&1\end{bmatrix}$$

Further remove the unit matrix of **M'**(L), and obtain the skeleton matrixwith binary relations:

$$\mathbf{A}'=\mathbf{M}'(\mathbf{L})-\mathbf{I}=\begin{array}{c}1\\4\\6\\3\\2\\5\\7\end{array}\begin{bmatrix}0&0&0&0&0&0&0\\0&0&0&0&0&0&0\\1&0&0&0&0&0&0\\1&1&1&0&0&0&0\\0&0&0&1&0&0&0\\0&0&0&0&1&0&0\\0&0&0&0&1&0&0\end{bmatrix}$$

A hierarchical structure of system elements model can be established, as shown in Fig. 5.

The model is a five-level hierarchical structure. The fifth-level elements influence the fourth level, the third level, the second level, the first level, and the final effect on machine reliability through a hierarchical relationship. The division of each subsystem level based on the abovementioned analysis is shown in Table 5.

Table 5. Subsystems division

System level	Contains subsystems
Fault source subsystem	Feed system, cooling chip removal system
Intermediate fault subsystem	Fixtures, hydraulic systems, electrical systems
Representation Subsystem	Active system, manipulator

3.2. CNC machine tools subsystem failure rate modeling

The data in this paper comprise a group of users in CNC machine tools, the collection and accumulation of five CNC machine tools, the on-site operation of the failure of data 28, and the censored time data 5, with a tracking cycle of six months. Fault data belongs to the fault source subsystem analysis, as presented in Table 6.

The absence of a "+" in the table represents the failure source data. The iterative calculation and failure of the source subsystem parameters while running the MATLAB program to conduct 100 iterations are also shown. The estimated values of the parameters are:

$$\hat{\alpha} = 367.4772\ ,\ \hat{\beta} = 1.4973$$

Similarly, the parameters of the remaining subsystems as well as the deviation correction can be estimated. The results are shown in Table 7.

Table 7. Modified parameter values of subsystem reliability model

Hierarchical subsystem	β^*	α^*
Fault source subsystem	1.1492	370.8794
Intermediate fault subsystem	0.9585	353.1728
Representation Subsystem	0.7771	449.5970

The failure time distribution function of CNC machine tools is tested by *d*, the observed value is $D_n = 0.4078$ .Take the significant level $\alpha = 0.10$, check list $D_{n,\alpha} = 1.22/\sqrt{6} = 0.498$. Since $D_n < D_{n,\alpha}$, the original hypothesis is accepted. The model passes the goodness-of-fit test, and the CNC machine tools fault time follows the Weibull distribution.

Therefore, the type of CNC machine tools fault source subsystem failure time function $\lambda_1(t)$:

$$\lambda_1(t) = \frac{1.1492}{370.8794}\left(\frac{t}{370.8794}\right)^{0.1492}$$

Likewise, the failure rate function of the intermediate failure subsystem can be obtained:

$$\lambda_2(t) = \frac{0.9585}{353.1728}\left(\frac{t}{353.1728}\right)^{-0.0415}$$

Failure rate function of representation subsystem:

$$\lambda_3(t) = \frac{0.7771}{449.5970}\left(\frac{t}{449.5970}\right)^{-0.2229}$$

Based on the characteristics of the Gumbel-copula function, combined with the fault data of the intermediate subsystem and the failure source subsystem, using MATLAB software programming, and called the maximum likelihood estimation to obtain $\theta_1 = 0.254$. Similarly, the failure correlation coefficient of the representation subsystem with other two subsystems can be calculated as $\theta_2 = 0.198$.

At this point, considering the fault transfer and correlation, the overall reliability function:

$$R_{123}(t) = exp\left\{-\left[\left[\left[\left(\frac{t}{370.8794}\right)^{1.1492}\right]^{1/\theta_1} + \left[\left(\frac{t}{353.1728}\right)^{1.1492}\right]^{1/\theta_1}\right]^{\theta_1}\right]^{1/\theta_2} + \left[\left(\frac{t}{449.5970}\right)^{0.7771}\right]^{1/\theta_2}\right]^{\theta_2}\right\}$$

$$= exp\left\{-\left[\left[\left(\frac{t}{370.8794}\right)^{4.5244} + \left(\frac{t}{353.1728}\right)^{3.7736}\right]^{1.2828} + \left(\frac{t}{449.5970}\right)^{2.349}\right]^{0.1980}\right\}$$

Therefore, the integrated failure rate of each subsystem is:

$$\lambda_F(t) = \lambda_1(t) = \frac{1.1492}{370.8794}\left(\frac{t}{370.8794}\right)^{0.1492}$$

$$\lambda_I(t) = \lambda_2(t) + (1-\theta_1)\lambda_1(t) = \frac{0.9585}{353.1728}\left(\frac{t}{353.1728}\right)^{-0.0415} + \frac{0.8573}{370.8794}\left(\frac{t}{370.8794}\right)^{0.1492}$$

$$\lambda_R(t) = \lambda_3(t) + (1-\theta_2)\lambda_{12}(t) = \frac{0.7771}{449.5970}\left(\frac{t}{449.5970}\right)^{-0.2229} + 0.802\times\left(\frac{t^{4.5244}}{370.8794^{4.5244}} + \frac{t^{3.7736}}{353.1728^{3.7736}}\right)^{-0.749}$$

$$\times\left(\frac{1.1492t^{3.5244}}{370.8794^{4.5244}} + \frac{0.9585t^{2.7736}}{353.1728^{3.7736}}\right)$$

3.3. CNC machine tools subsystem maintenance time modeling

The fault repair time information analysis and the finishing of CNC modular machine tools are shown in Table 8.

In the table, „*" represents the fault source subsystem maintenance time data, "#" represents the representation fault subsystem maintenance time data and the rest for the intermediate fault subsystem maintenance time data.

An example of the fault source subsystem to repair time processing is shown in Table 9.

Table 9. Fault source subsystem maintenance time processing

i	τ_i	X_i	$\bar{X}$	$\sqrt{\frac{n}{n+1}}\cdot\frac{X_i-\bar{X}}{S}$	$t_{n-1}\left(\sqrt{\frac{n}{n+1}}\cdot\frac{X_i-\bar{X}}{S}\right)$	$\hat{p}_i$
1	0.79	-0.2357			-1.4609	0.1019
2	2.00	0.6931			-0.6334	0.2772
3	3.98	1.3813	1.4042	1.0393	-0.0204	0.4922
4	6.62	1.8901			0.4328	0.6584
5	7.71	2.0425			0.5686	0.7029
6	14.21	2.6539			1.1133	0.8419

Table 8. CNC machine tools failure repair time

Numbering	Maintenance time τ/h						
1	10.62#	3.00	0.79*	1.37#	6.00	2.50	
2	8.00#	16.69#	2.00*	6.00#			
3	3.98*	7.71*	2.20	6.30	6.62*	11.00#	
4	14.21*	2.50	2.00#	0.13#	3.00		
5	10.00	1.58	8.81	5.00#	3.00	2.60	8.83

Table 10. Test results

Hierarchical subsystem	$M(t)=\int_0^t \frac{1}{\sigma x\sqrt{2\pi}}\exp\left\{-\frac{1}{2}\left(\frac{\ln x-\mu}{\sigma}\right)^2\right\}dx$	$m(t)=\frac{1}{\sigma t\sqrt{2\pi}}\exp\left\{-\frac{1}{2}\left(\frac{\ln t-\mu}{\sigma}\right)^2\right\}$
Fault source subsystem	$\int_0^t \frac{1}{0.9488x\sqrt{2\pi}}\exp\left\{-\frac{1}{2}\left(\frac{\ln x-1.4042}{0.9488}\right)^2\right\}dx$	$\frac{1}{0.9488t\sqrt{2\pi}}\exp\left\{-\frac{1}{2}\left(\frac{\ln t-1.4042}{0.9488}\right)^2\right\}$
Intermediate fault subsystem	$\int_0^t \frac{1}{0.5259x\sqrt{2\pi}}\exp\left\{-\frac{1}{2}\left(\frac{\ln x-1.4609}{0.5259}\right)^2\right\}dx$	$\frac{1}{0.5259t\sqrt{2\pi}}\exp\left\{-\frac{1}{2}\left(\frac{\ln t-1.4609}{0.5259}\right)^2\right\}$
Representation Subsystem	$\int_0^t \frac{1}{1.1165x\sqrt{2\pi}}\exp\left\{-\frac{1}{2}\left(\frac{\ln x-1.336}{1.1165}\right)^2\right\}dx$	$\frac{1}{1.1165t\sqrt{2\pi}}\exp\left\{-\frac{1}{2}\left(\frac{\ln t-1.336}{1.1165}\right)^2\right\}$

Table 11. Subsystem maintenance time distribution function

Hierarchical subsystem	$M(t)=\int_0^t \frac{1}{\sigma x\sqrt{2\pi}}exp\left\{-\frac{1}{2}\left(\frac{lnx-\mu}{\sigma}\right)^2\right\}dx$	$m(t)=\frac{1}{\sigma t\sqrt{2\pi}}exp\left\{-\frac{1}{2}\left(\frac{lnt-\mu}{\sigma}\right)^2\right\}$
Fault source subsystem	$\int_0^t \frac{1}{0.9488x\sqrt{2\pi}}exp\left\{-\frac{1}{2}\left(\frac{lnx-1.4042}{0.9488}\right)^2\right\}dx$	$\frac{1}{0.9488t\sqrt{2\pi}}exp\left\{-\frac{1}{2}\left(\frac{lnt-1.4042}{0.9488}\right)^2\right\}$
Intermediate fault subsystem	$\int_0^t \frac{1}{0.5259x\sqrt{2\pi}}exp\left\{-\frac{1}{2}\left(\frac{lnx-1.4609}{0.5259}\right)^2\right\}dx$	$\frac{1}{0.5259t\sqrt{2\pi}}exp\left\{-\frac{1}{2}\left(\frac{lnt-1.4609}{0.5259}\right)^2\right\}$
Representation Subsystem	$\int_0^t \frac{1}{1.1165x\sqrt{2\pi}}exp\left\{-\frac{1}{2}\left(\frac{lnx-1.3360}{1.1165}\right)^2\right\}dx$	$\frac{1}{1.1165t\sqrt{2\pi}}exp\left\{-\frac{1}{2}\left(\frac{lnt-1.3360}{1.1165}\right)^2\right\}$

After using the PSO algorithm and programming with MATLAB, the parameter estimation values of the maintenance model of the fault source subsystem can be obtained $\hat{\mu}_1=1.4042$, $\hat{\sigma}_1=0.9488$. Similarly, the parameters of intermediate failure subsystems are estimated to be $\hat{\mu}_2=1.3553$, $\hat{\sigma}_2=0.5912$, and the parameters of representation failure subsystems are estimated to be $\hat{\mu}_3=1.3360$, $\hat{\sigma}_3=1.1165$.

The *d* test was carried out to test the goodness-of-fit test, and the results are shown in Table 10 (using a significant level $\alpha=0.10$).

All $D_n<D_{n,\alpha}$, the maintenance time distribution function of each level subsystems was shown in Table 11.

Using $MTTR=\int_0^\infty tm(t)dt=exp\left(\mu+\frac{\sigma^2}{2}\right)$, the estimated values of $MTTR$ of each subsystem are obtained, as shown in Table 12.

Table 12. MTTR point estimates for subsystems

Hierarchical subsystem	MTTR（unit：h）
Fault source subsystem	6.387
Intermediate fault subsystem	4.618
Representation Subsystem	7.094

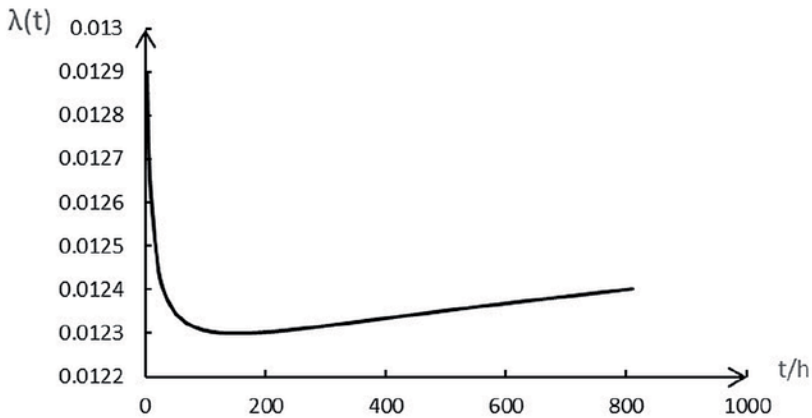

Fig. 6. Failure rate curve of CNC machine tools

3.4. Determination of average maintenance time of CNC machine tools

1) Based on the series relation and the subsystem comprehensive failure rate function, the failure rate curve of CNC machine tools system as shown in Fig. 6.

Figure 6 shows that the minimum fault rate of this type of CNC machine tools is λ_{min}=0.0123, corresponding to the fault time t=100 h, and corresponding failure rate of the subsystems are as follows:

$$\lambda_F(t) = \lambda_F(100) = 0.00255$$

$$\lambda_I(t) = \lambda_I(100) = 0.00476$$

$$\lambda_R(t) = \lambda_R(100) = 0.00499$$

The machine tools maintenance time is determined as follows:

$$MTTR_{(t=100)} = \frac{\sum \lambda_i MTTR_i}{\sum \lambda_i} = \frac{\lambda_F(100) \bullet MTTR_1 + \lambda_I(100) \bullet MTTR_2 + \lambda_R(100) \bullet MTTR_3}{\lambda_F(100) + \lambda_I(100) + \lambda_R(100)} = 5.99\ h$$

Therefore, the average maintenance time of CNC machine tools with the minimum failure rate is 5.99 h.

2) Experience has shown that the maintenance time data mostly follow the lognormal distribution. The maintenance time in Table 8 is assumed to follow the lognormal distribution. Then, using the MLE method to estimate the parameters μ and σ^2, and the probability density function of maintenance time is obtained. Finally, the test results show that the maintenance time follows a lognormal distribution. Therefore, the probability density function and the average maintenance time for the whole machine can be obtained as:

$$f_{ln}(t) = \frac{1}{1.01\sqrt{2\pi}} exp\left[-\frac{1}{2}\left(\frac{lnt - 1.36}{1.01}\right)^2\right] \quad MTTR = \int_0^\infty tm(t)dt = exp\left(\mu + \frac{\sigma^2}{2}\right) = 6.42h$$

3.5. Comparative analysis

Using the minimum failure rate and considering the number of subsystem failures and the corresponding average maintenance time, the subsystem maintenance time is obtained as

$$RT_i = MTTR_i \times \lambda_i(t) \times t_{min}$$

where RT_i is the maintenance time of each subsystem; i=1,2,3 is the fault source subsystem, the intermediate fault subsystem, and the representation subsystem, respectively; and t_{min}=100h is the minimum failure rate occurrence time.

The results are shown in Table 13.

Table 13. Subsystem maintenance time

Hierarchical subsystem	RT(unit: h)
Fault source subsystem	1.627
Intermediate fault subsystem	2.198
Representation Subsystem	3.539

Table 13 shows:

1) $$\begin{cases} RT_R > RT_I > RT_F \\ \sum RT_i = MTTR_{(t=100)} \times \lambda_{min} \times t_{min} \end{cases}$$

where λ_{min}=0.0123 is the minimum failure rate of time t=100. Formula (22) shows that the average maintenance time of the entire machine is equal to the sum of each subsystem repair time, which is in line with actual engineering practices; however, the traditional modeling method is required to determine the failure rate and the number of occurrences. The average maintenance time is not equal to the total maintenance time of all subsystems, which is contrary to actual applications.

2) The failure rate of the representation subsystem is the highest and its maintenance time is the longest because of the long fault location time. The fault source subsystem has the shortest maintenance time followed by the middle fault subsystem; the same applies for the total maintenance time. These results are consistent with the actual diagnosis and troubleshooting.

Therefore, the maintenance time requires a more reasonable design that considers the failure rate and fault frequency of the subsystem.

4. Conclusion

(1) (1) Considering the failure correlation, the DEMATEL-ISM method was introduced. DEMATEL method was used to construct the reachable matrix, and the ISM method is used to decompose the reachable matrix. The complexity of the system was transformed into a clear multi-level hierarchical structure model. Finally, the level of CNC machine tools in the subsystem division were determined.

(2) Using the time-dependent reliability model of each level as the edge distribution, the copula function was used to establish the system joint reliability distribution function to determine the correlation coefficient of each subsystem.

(3) The failure rate function model of each subsystem is established based on the failure rate correlation. Moreover, the average maintenance time model of the CNC machine tools was established under the minimum failure rate of the system.

(4) The average maintenance time of the whole system was determined while considering the number of failures and average maintenance time of each subsystem. Comparative analysis between the traditional maintenance modeling method and the average maintenance time showed that the latter equal to the sum of the maintenance time of each subsystem. This result is consistent with actual applications. The research also provides a basis for the subsystem maintenance time design, and has obtained a more reasonable design scheme for the average maintenance time of CNC machine tools.

Acknowledgment

The research work was financially supported by the National Science and Technology Major Project of China (Project No.2015ZX04003002), Natural Science Foundation of Jilin Province (Project No. 20150101025JC and 20170101212JC).

References

1. Bu Yingyong, Zhang Huailiang. The preliminary attempt to develop preventive-predictive maintenance. Journal of Central South University 1995: 2(2):32-36, https://doi.org/10.1007/BF02652004.
2. Charles E. Ebeling. An Introduction to Reliability and Maintainability Engineering. Tsinghua University Press 2010; 1:157-158.
3. Cheng Xiao-min, Jia Ya-zhou, Shu Ze. Statistical research on maintenance time of CNC machine tools. Machine Tools & Hydraulics 1992;

02:83-85.
4. Ebeling C E. An introduction to reliability and maintainability engineering. McGraw-Hill Education, New York 2004.
5. Huang Xi-li, Han Xi-an. Method for fuzzy maintainability index demonstration in lognormal distribution. Journal of Systems Engineering and Electronics 2008; 30(2): 375-378.
6. Kai Zhang, Jinchun Song, Guangan Ren, Jia Shi. Particle swarm optimization algorithm with multi methods argument. AI Communications 2016; P: 1-15.
7. Lam Y. A geometric Process Maintenance Model with Preventive Repair.European Journal of Operational Research 2007; 182: 806-819, https://doi.org/10.1016/j.ejor.2006.08.054.
8. Liu Duan, Hu Jian Bo, Ge Xiao Kai, el at. Monte Carlo Simulation of Maintenance Time Based on System Maintenance Work Procedure. Fire Control & Command Control 2014; 39 (7): 119-123.
9. Lu Zhong, Sun You Chao, Wu Hai Qiao. System Maintainability Modeling Method Based on Colored Stochastic Time Petri Net. Journal of Mechanical Engineering 2011; 47 (10): 185-191, https://doi.org/10.3901/JME.2011.10.185.
10. Ma Zhan-Fei. ISM-based architecture for network security system. ICEIT 2010 -2010 International Conference on Educational and Information Technology Proceedings 2010:1969-2014.
11. Murthy D N P, Nguyen D G. Study of a multi-component system with failure interaction. Eu J Oper Res 1985; 21: 330-338, https://doi.org/10.1016/0377-2217(85)90153-5.
12. Radiša Djurić, Vladimir Milisavljević. Investigation of the relationship between reliability of track mechanism and mineral dust content in rocks of lignite open pits. Eksploatacja i Niezawodnosc – Maintenance and Reliability 2016; 18 (1): 142–150, https://doi.org/10.17531/ein.2016.1.19.
13. Shahannaghi K, Babaei H, Bakhsha A et al. A New Condition Based Maintenance Model with Random Improvements on the System After Maintenance Actions:Optimizing by Monte Carlo Simulation].World Journal of Modeling and Simulation 2008; 4(3): 230-236.
14. Shey-Huei Sheuab, Chin-Chih Changc, Yen-Luan Chend, Zhe George Zhangef. Optimal preventive maintenance and repair policies for multi-state systems. Reliability Engineering and System Safety 2015; 140: 78-87, https://doi.org/10.1016/j.ress.2015.03.029.
15. Sklar A. Fonctions de repartition an dimensions et leurs marges. Paris: Publication Institute Statist University 1959; 8: 229-231.
16. Sun Y, Ma L, Mathew J, et al. An analytical model for interactive failure. Reliability Engineering& System Safety 2006; 91(5): 495-504, https://doi.org/10.1016/j.ress.2005.03.014.
17. U.S. Department of Defense. MIL-STD-470B Maintainability program requirements for systems and equipment. Ohio: Aeronautical system Center 1989.
18. Wang H Z, Pham H. Reliability and Optimal Maintenance. Springer-Verlag London: Springer Series in Reliability Engineering Series, 2006.
19. Wang L, Hu H J, Wang Y Q, et al. The Availability Model and Parameters Estimation Method for the Delay Time Model with Imperfect Maintenance at Inspection. Applied Mathematical Modeling 2011; (35): 2855-2863, https://doi.org/10.1016/j.apm.2010.11.070.
20. Wu Jingmin, Zuo Hongfu, Chen Yong. An estimation method for direct maintenance cost of aircraft components based on particle swarm optimization with immunity algorithm. Journal of Central South University 2005; 12(2): 95-101, https://doi.org/10.1007/s11771-005-0018-9.
21. Wu W W. Choosing knowledge management strategies by using a combined ANP and DEMATEL approach. Expert Systems and Applications 2008; 35(3): 828-835, https://doi.org/10.1016/j.eswa.2007.07.025.
22. Wu Xi, Xu Da, Mu Ge, Li Chuang. Research on verification method of equipment maintenance time based on digital prototyping. Manufacturing Technology & Machine Tool 2013; 12: 63-66.
23. Y. G. Petalas; K. E. Parsopoulos; M. N. Vrahatis. Memetic particle swarm optimization. Annals of Operations Research 2007; 155(1): 99-127, https://doi.org/10.1007/s10479-007-0224-y.
24. Zhang Deng-Feng, Fei Sheng-Wei, Liu Yuan-Wei, Sun Yu. Approach on failure diagnosis knowledge acquisition in beginning stage of maintenance for complex equipments. Journal of Central South University (Science and Technology) 2009; 40(S1): 284-289.
25. Zhang Hai-bo, Liu Liang, Huang Yang-yang. Maintain Time Model of CNC Machining Center. Modular Machine Tools & Automatic Manufacturing Technique 2014; 05:158-160.
26. Zhuoqi Zhang, Su Wu, Binfeng Li. Opportunistic maintenance policy for a two-unit system with failure interactions. Journal of Tsinghua University(Science and Technology) 2012; 52(1):122-127.
27. Zuo F-J, Yu L, Mi J, Liu Z, Huang H-Z. Reliability analysis of gear transmission with considering failure correlation. Eksploatacja i Niezawodnosc – Maintenance and Reliability 2015; 17 (4): 617–623, https://doi.org/10.17531/ein.2015.4.19.

Guixiang SHEN
Wenbin ZENG
Chenyu HAN
NC equipment credibility Engineering Research Institute
College of Mechanical Science and Engineering
Jilin University
People str., 5988 Changchun, 130022, China

Peng LIU
Yingzhi ZHANG

Department of Industrial Engineering
College of Mechanical Science and Engineering
Jilin University
People str., 5988 Changchun, Jilin 130022, China

Emails: 313442341@qq.com, zengwb15@yeah.net, 1094267138@qq.com, 969929715@qq.com, 569679064@qq.com

Article citation info:
EPLER I, SOKOLOVIĆ V, MILENKOV M, BUKVIĆ M. Application of lean tools for improved effectiveness in maintenance of technical systems for special purposes. Eksploatacja i Niezawodnosc – Maintenance and Reliability 2017; 19 (4): 615–623, http://dx.doi.org/10.17531/ein.2017.4.16.

Igor EPLER
Vlada SOKOLOVIĆ
Marjan MILENKOV
Milan BUKVIĆ

APPLICATION OF LEAN TOOLS FOR IMPROVED EFFECTIVENESS IN MAINTENANCE OF TECHNICAL SYSTEMS FOR SPECIAL PURPOSES

ZASTOSOWANIE NARZĘDZI SZCZUPŁEGO UTRZYMANIA RUCHU DO POPRAWY EFEKTYWNOŚCI OBSŁUGI SYSTEMÓW TECHNICZNYCH SPECJALNEGO PRZEZNACZENIA

Today, executives from the system of maintenance of technical systems for special purposes (military combat vehicles), are trying to improve their organizational processes and create competitive advantage through increasing the quality of maintenance services (increase effectiveness), reducing the total cost (increase efficiency) and reduce the maintenance cycle-time. One of the possible ways for improvements in the maintenance system is the application of lean concept of maintenance, by usage of different tools as 5S, Layout, Visual systems, Kanban and new developed "Technical system maintenance" tool. In order to gain a better understanding of this concept, the paper presents a new developed maintenance model for the application of the lean concept in the real maintenance system. The results of empirical and experimental testing of the proposed model are analysed based on Analysed of methods and effects of improvements (IMEA), Benchmarking methods and multi-criteria, 22 analysis by using the statistical software application MINITAB. The special character of experimental testing are obtained regression equations that describe the changes of the duration of the maintenance cycle, depending on the applied lean tools. The obtained results show that the duration of maintenance cycle is reduced for about 23%, the improvement of maintenance effectiveness is around 14% and the efficiency is showing an upward trend.

***Keywords**: effectiveness, efficiency, lean tools, maintenance, readiness, technical system.*

W dzisiejszych czasach, kadra kierownicza zarządzająca systemami utrzymania ruchu układów technicznych specjalnego przeznaczenia (np. wojskowych pojazdów bojowych) stara się usprawniać procesy organizacyjne i tworzyć przewagę konkurencyjną poprzez podniesienie jakości usług serwisowych (zwiększenie efektywności), redukcję kosztów całkowitych (zwiększenie wydajności) oraz skrócenie czasu trwania cyklu eksploatacyjnego. Jednym z możliwych sposobów udoskonalenia systemu utrzymania ruchu jest zastosowanie pojęcia szczupłego utrzymania ruchu z wykorzystaniem różnych narzędzi, takich jak 5S, Layout, Visual systems, kanban oraz nowo opracowanego narzędzia "Obsługi Ruchu Systemu Technicznego". Aby lepiej zrozumieć tę koncepcję, w artykule przedstawiono nowo opracowany model obsługi technicznej, który pozwala na zastosowanie koncepcji szczupłego utrzymania ruchu w rzeczywistym systemie obsługi. Wyniki empirycznych i eksperymentalnych badań proponowanego modelu analizowano na podstawie analizy metod i efektów doskonalenia IMEA, metod benchmarkingowych oraz analizy wielokryterialnej 22 przy użyciu oprogramowania statystycznego MINITAB. W badaniach eksperymentalnych otrzymano równania regresji, które opisują zmiany czasu trwania cyklu eksploatacyjnego w zależności od zastosowanych narzędzi. Uzyskane wyniki wskazują, że przy zastosowaniu proponowanej metody czas trwania cyklu eksploatacyjnego ulega skróceniu o około 23%, efektywność utrzymania ruchu wzrasta o około 14%, a wydajność wykazuje tendencję wzrostową.

***Słowa kluczowe**: efektywność, wydajność, narzędzia szczupłego utrzymania ruchu, utrzymanie ruchu, gotowość, system techniczny.*

1. Introduction

Today there are a lot of uncertainties in the maintenance management systems which are based on implementing the principles of those traditional maintenance concepts and which generate constant losses during the maintenance process [12]. Existing manuals and other documentation for the maintenance is "poor" from the maintenance management & control point of view. For this reason, the preparation of data for the maintenance information systems is very difficult, because it relies only on current information available from the technological process of maintenance. Therefore, the financial and time losses are recognized as the main problems in existing maintenance systems.

The lean concept of organizational management systems is a way of managing the production, development of products and services, which generates precisely defined and the desired product or service according customers' needs, [5, 18, 21]. The aim of the mentioned concept is to achieve the required quality of products or services by using fewer financial and other resources, whereby a synergy between the lean and "green" production or provision of services is achieved [17, 23]. Even though the lean application is not easy [22], the possibilities of the lean approach are multiple. There are many examples of successful applications in all types of manufacturing [7], in industry and services [13]. The model of lean production system as hierarchical structure consisted of requirements, design parameter and variables of the process is presented by Housmand at. al. in [9].

There are many different lean strategies as in [24] and various maintenance performances measurement frameworks [15]. Although the "lean" management concept has its roots in the automotive industry, it has been successfully used in insurance and IT companies, health care, in public activities such as the civil service and education [16], aircraft maintenance and repair [3], and many industrial branches as described in [6].

The researches related to the application of lean philosophy in maintenance have been mainly based on findings that lean concept leads to the identification and elimination of activities that are harmful to the maintenance process and in same time increase the profit of the organizational systems [20]. The great application of the lean philosophy in maintenance is achieved in the airline branch [3]. Amir Mahmud Sahrabi et al. has shown the possibility of AHP method and Expert Choice as lean software tools that helps to decision makers to find out the possible cause of the failure and to determine activities to be undertaken in order to solve the problem, [19]. Ayad Yusuf et al. in their work [2], described the steps named DMAIC (Define, Measure, Analyze, Improve and Control), that should be applied in the large industrial systems during introduction of Lean Six Sigma maintenance, which would improve the quality and increase the profits. Alireza Irajpur at. al. in their work [11] provided a framework for the evaluation of the effectiveness achieved by applying the lean in maintenance system. They carried out a comparative analysis of maintenance performances based on TOPSIS method.

Military organizations represent very interesting and important field for research. Successful implementation of the lean methodology in the military organizations has been confirmed in the US Army, where savings reached tens of millions of dollars, while the overhaul time was reduced by more than 50%, [1]. In conditions of the limited financial resources, and the required effectiveness in the maintenance of the weapons systems, the lean methodology is the way to reduce costs and maintenance cycle-time. Bearing in mind that reducing maintenance cycle-time the operational availability of weapons systems is greater and in the same time the operational capability of the whole military units is improved. The main problem in this research is to implement lean methodology in maintenance cycle of technical systems for special purposes (TSSP) in order to improve the effectiveness and the efficiency in maintenance process. In this research the attention is paid to the maintenance management of the military combat vehicles (armoured personal carriers and howitzer SH 122 mm DS1), which are named TSSP.

In Serbian Armed Forces the maintenance program divides maintenance into three levels: depot level (strategic level), intermediate level (operational command level), and organizational level (tactical level). Tactical level assumes a basic maintenance activities at the battalion level and the technical maintenance at the brigade level. The technical maintenance involves repairs or the replacement of the modules and based on experience it covers about 60% percent of maintenance activities in the whole maintenance program. Therefore, the technical maintenance is very important and it is the subject of the research presented in this paper. As it is organized at the brigade level (the highest tactical unit in our case), the technical maintenance provides maintenance support for up to ten battalions equipped with above mentioned TSSP with different number of pieces.

The main aim of the presented research was to develop a maintenance model based on the lean methodology that could provide a high level of flexibility and to increase the effectiveness and efficiency of the maintenance. In accordance with the aim an original "lean" tool, software application, is developed and named „Technical systems maintenance" (TSM), for the management of the workshop' documentation, material and spare parts, and reporting of TSSP maintenance, [8] and the new maintenance management model is proposed.

The improvement is reflected in the reduction of the duration of maintenance cycle (*Tc*) [7], increasing the effectiveness (E) [7] and the efficiency (E_f) [21] of TSSP maintenance at tactical level. The proposed maintenance model is based on application of adequate different lean tools, and new developed TSM toll, flexible enough and suitable for practical application and verification. It does not require additional investments in equipment, and it is oriented more to the maintenance management and less to the technology.

The performances of proposed model are numerical values that depend on the applied lean tools and regression equation. The empirical and experimental testing data are analysed by using the statistical software application MINITAB. The results obtained by proposed maintenance management model show the reducing of duration of maintenance cycle, improvement of maintenance effectiveness and upward trend of efficiency.

2. Applied methods and tools

During the development of the maintenance model the following methods are used: failure modes and effects analyses (FMEA), Benchmarking method and multi factor analysis 2^k. Failure modes and effects analyses is an adequate method for systematic process of identification and preventing the occurrence of problems in processes or in the exploitation of products before they are generated. For the purposes of verification of the developed model the base FMEA of the process is used, [14].

Benchmarking is one of a growing and modern management tool, developed in order to improve the characteristics of the organizational systems (business excellence), [25]. Benchmarking can be defined as the tendency of the organizational system (in this paper hereinafter referred to as maintenance system) to achieve higher performances, based on successful experiences. To reach business excellence, maintenance system is to take over the best experience from some other organization system. There are no universal models. Each system must find solution to get competitive advantage.

To verify the performances of the proposed lean maintenance management model, the check list is used, that is defined by Teri Vajerman and is given in detail in [25].

Factor analysis is often used in experiments which involve testing the influence of various factors (in this paper, lean tools) to the value of the observed characteristics (in this paper, *Tc*), or for acceptance or rejection of the hypothesis of the influence of factors on the observed characteristic. There are a few special cases of the factor analysis. One of them is the analysis of *k* factors, where each one has exactly two levels, [4]. For instance, levels could be the presence or absence of some factor, as it is the case in this research.

The simplest form of the factor analysis is the case with only two factors and each of them with two levels. Mathematical model of multi factor analysis is an integral part of the software tool MINITAB, [4].

For the experimental verification of the proposed maintenance management model the MINITAB software tool is used. As "lean" tools, "5S", „Layout" of equipment and tools (LO), visual system (VS), TSM and "Kanban" (KAN) are applied.

Description of mentioned tools:

5S - The objective of this tool is to perform adequate workplace of each labor with the aim to maximize an efficiency, and to accelerate the work of the labors. The unnecessary movements of labors are eliminated by setting tools and equipment at the appropriate position, clearly visible, clean and at any moment ready for usage. A TSSP is to be complete and prepared for the maintenance in every point of view.

Layout - The goal of this tool is the drive to eliminate of movements of labor, technical system etc. that do not contribute to the making of a new value. Therefore, it is suitable to perform "U" form of workplace organization where the mechanic is in the middle and everything is around its hands, [13].

Visual Systems - Represents the continued application of procedures in the execution of maintenance activities, safe usage and maintenance of equipment, mandatory usage of the necessary protective equipment as well as the safety signs for the tools, materials, pathways of the employees, etc. [13].

Kanban - is some kind of card for monitoring storage of spares and supplies for the TSSP maintenance, [13, 20].

TSM – a newly developed "lean" tool, software application created in MS Office Access for the management of the workshop documentation, material and spare parts, and reporting of TSSP maintenance. The TSM represents a unique lean tool that is developed as a small, but very important segment of the maintenance information system. The TSM includes the data collection and activities monitoring from the reception of TSSP in workshop until the end of the maintenance, and drafting of the reports on the maintenance activities. The TSM as a lean tool is adapted to technical level of maintenance and details are given in [8]. It is similar to the lean tool, which is often used in the manufacturing organization systems called Computerized maintenance management system (CMMS). As the The Plant Maintenance Resource Center, [10], published the SAP, Maximo, MP2, i MIMS are the most often used software applications in practice. The all of those applications are defined and built for commercial usage but not suitable for maintenance systems in the military organizations. Mentioned CMMS usually defined the ordering parameters as: spares delivering address, fee instructions, supplier selection, spares selection with the defined amount, which is not sufficient for high-quality maintenance management in military organizations.

Conditions that have great impact on the maintenance management in the military organizational systems are: unscheduled requests for maintenance, hostile conditions of TSSP usage, required reliability and readiness of TSSP, unique spare parts supply system within the maintenance system, strict control of the pare part inventory conditions and strict defined maintenance activities. For the successful maintenance management under these circumstances, it is necessary to have the appropriate information available to the authorities at all levels of maintenance system. This ensures centralized maintenance management, unified purchasing and payment services at a certain level of organization, spares inventory management and their rational use, monitoring of the uniform norms and the maintenance documentation, maintenance resource management, creation of the conditions for the analysis of TSSP reliability and as well as reducing the maintenance cycle-time.

The TSM is application developed in Microsoft Access 2003 software package. It consists of a database, in which are stored all the data necessary for the application operation, and lines of interconnections between the user and the database. The logical link tables of the TSM, as a hurt of developed application, is shown in figure 1.

The database is realized of interrelated tables:

tblTS – the identification and the codification numbers of TSSP,

tblTS1 – contains data related to a specific TSSP (registration number, chassis and engine number, the code of tactical units),

tblTI – a type of the corrective and the preventive maintenance with the description of the technological activates and their estimated duration (TH),

tblSparepart – provides information about the stocks of the spare parts and the consumables in storage and their minimum and maximum amount (necessary for the preparation of requisitions),

tblWorkshopSheet- provides data for the inventory records (workshop operations lists): the number and the date of the first record, required completion date, work hours achieved by the specific specialty, and the name of the person who has received (delivered) the item,

tblNecessarySpareparts – a necessary spares list (with codification number) for the maintenance activity for the particular item,

tblMaintenance – provides information about the type of the maintenance for the specific item.

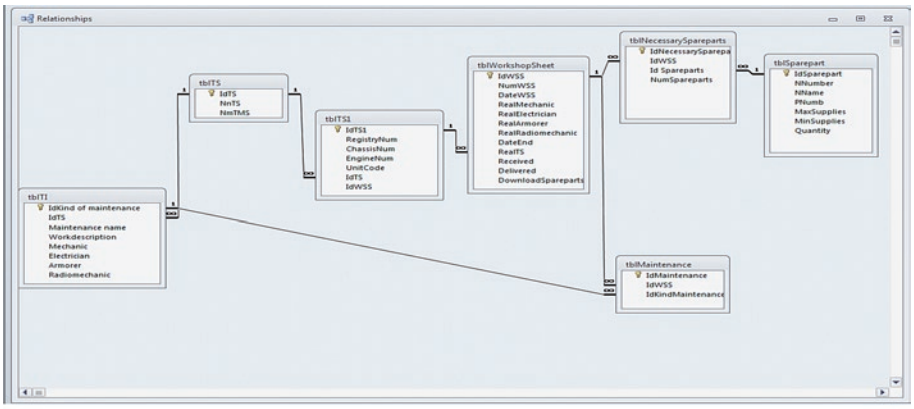

Fig. 1. Logical link of tables within the TSM

Developed TSM application provides the more flexible approach to the TSSP maintenance management than already known CMMS that have not found a direct application in the TSSP maintenance management. A more flexible approach to maintenance management of TSSP, that provides TSM, is possible because the logical data connection in the database is already known. In addition, the TSM is easy for usage and requires a standard MS Office software package, which is another important advantage compared to the other CMMS applications and do not require additional permissions for usage.

3. The proposed maintenance management model

The existing concept of TSSP maintenance is focused on maintenance technology and maintenance staff at all levels within all prescribed forms of maintenance, and less on the optimal organization of resources and the changing demands of users. In situations of a higher risk and uncertainty, it makes the maintenance system inflexible, which reduces readiness of the TSSP. Based on this reasons here is the proposed maintenance model based on the "lean" methodology.

The characteristics of the proposed TSSP maintenance management model are:

- the repair process is initiated at the request of the user or based on data of usage TSSP,
- it is a predictive maintenance model, because of the lean towards maximum maintenance capacity utilization,
- the model monitors the human potential, from the request to the end of the repair process.

In the proposed model, firstly, the analysis of the impact of certain "lean" tools is conducted, which in a relatively short period of time, could lead to reducing the repair time, improvement of effectiveness and efficiency of the TSSP maintenance system.

Components of this proposed model are the following subsystems: capacity planning, workshop scheduling, maintenance processes control and reporting.

The algorithm of planning and management process based on the lean methodology is shown in figure 2.

In case that, in analyzing the current state of the maintenance system, the other lean tools are required, it is possible to extend group

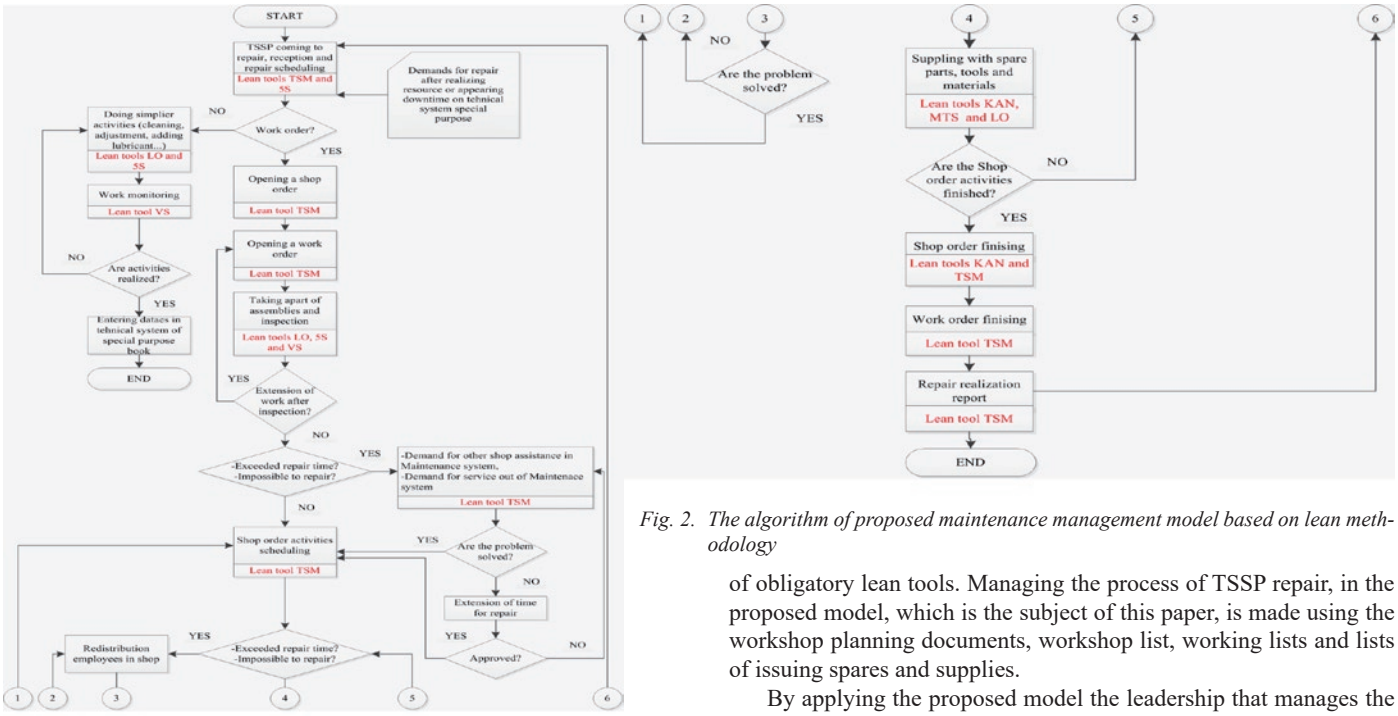

Fig. 2. The algorithm of proposed maintenance management model based on lean methodology

of obligatory lean tools. Managing the process of TSSP repair, in the proposed model, which is the subject of this paper, is made using the workshop planning documents, workshop list, working lists and lists of issuing spares and supplies.

By applying the proposed model the leadership that manages the maintenance can monitor the data that are constantly changing: capac-

Table 1. Maintenance cycle-times after the lean application for TSSP1

Maintenance cycle	Activity	Responsibility	Average maint. cycle-time before lean (in hours)	Average maint. cycle-time after lean (in hours)	
				tool	duration
Shipping and processing	Washing and cleaning	User	1.5	5S VS	0.00
	Item documents control	User	0.33	TSM	0.10
	Shipping a TSSP in workshop	User	0.5		0.5
	Opening of the workshop documentation and handing over assets	User / Workshop manger	0.5	TSM	0.1
repair	TSSP visual inspection	Mechanic	17.9	5S VS LO	16.00
	TSSP dismantling	Mechanic			
	Assemblies cleaning	Mechanic			
	Assemblies checking and testing	Mechanic			
	Assemblies dismantling	Mechanic			
	Parts ordering and receiving	Mechanic			
	Assemblies repairing	Mechanic			
	Assembling	Mechanic			
	Testing of Assemblies	Mechanic			
	Mounting	Mechanic			
	Testing of TSSP	Mechanic			
	Data records and item delivering	Mechanic			
Parts delivering	Parts ordering	Workshop manger	0.67	TSM KAN	0.1
	Parts inventory management	warehouse clerk/ Workshop manger	0.5	TSM KAN	0.1
Documentation control and reporting	Workshop documentation control	Workshop manger	0.25	TSM	0.0
	Completion of the workshop documentation	Workshop manger	0.08	TSM	0.0
	Report writing	Workshop manger	0.17	TSM	0.02
Σ			22.4		19.92

ity, performance workers... The proposed model can be considered as modern, because compared to the conventional methods applied in maintenance management, do not consider maintenance system as a priori disordered and in much of activities impossible to manage.

The greatest achievement of the proposed model is its holistic approach to the maintenance management, which is reflected in the consistent application of selected appropriate "lean" tools and principles in all functions and the activities within the maintenance cycle, in order to achieve a greater improvement compared to the previous state.

4. Maintenance management model verification for two technical systems for special purposes

For the verification of the proposed model the empirical and experimental testing with the results analysis is performed. Empirical and experimental verification of the TSSP maintenance management model were made in the workshop for technical (tactical level) maintenance.

Two independent technical systems for special purposes (armoured personal carrier-TSSP1 and howitzer SH 122 mm DS1-TSSP2) are observed for the three years. The 102 work orders for each TSSP were registered during observing time. The described lean tools are applied in a real workshop for technical maintenance for both TSSP (in a selected group of activities of technical maintenance), and the results are applied in similar activities of technical maintenance in all other work orders, using the general scientific methods of induction.

The observed characteristics of the empirical and experimental testing of the developed "lean" model are: maintenance cycle time (T_c), effectiveness expressed by coefficient of availability (R) and efficiency (E_f), which is based on the following equations, respectively:

$$T_c = t_{pf} + t_{re} + t_s \tag{1}$$

$$R = \frac{t_u}{t_u + t_d} \tag{2}$$

$$E_f = \frac{T_{rc}}{T_{pc}} \tag{3}$$

where t_{pf}– time for the preparation and finilyzing work, t_{re} – time for repair execution, t_s – time for the supply with spares and expendable materials, t_u – uptime, t_d – downtime, T_{rc} – real maintenance cycle, T_{pc} – planed maintenance cycle.

Table 2. Maintenance cycle-times after the lean application for TSSP2.

Maintenance cycle	Activity	Responsibility	Average maint. cycle-time before lean (in hours)	Average maint. cycle-time after lean (in hours)	
				tool	
Shipping and processing	Washing and cleaning	User	1.5	5S VS	0.00
	Item documents control	User	0.33	TSM	0.1
	Shipping a TSSP in workshop	User	0.5		0.5
	Opening of the workshop documentation and handing over assets	User / Workshop manger	0.5	TSM	0.1
repair	TSSP visual inspection	Mechanic	11.1	5S VS LO	10.20
	TSSP dismantling	Mechanic			
	Assemblies cleaning	Mechanic			
	Assemblies checking and testing	Mechanic			
	Assemblies dismantling	Mechanic			
	Parts ordering and receiving	Mechanic			
	Assemblies repairing	Mechanic			
	Assembling	Mechanic			
	Testing of Assemblies	Mechanic			
	Mounting	Mechanic			
	Testing of TSSP	Mechanic			
	Data records and item delivering	Mechanic			
Parts delivering	Parts ordering	Workshop manger	0.67	TSM KAN	0.1
	Parts inventory management	warehouse clerk/ Workshop manger	0.5	TSM KAN	0.1
Documentation control and reporting	Workshop documentation control	Workshop manger	0.25	TSM	0.0
	Completion of the workshop documentation	Workshop manger	0.08	TSM	0.0
	Report writing	Workshop manger	0.17	TSM	0.02
Σ			15.60		11.12

Table 3. Obtained results of the application of the proposed model

TSSP	T_c (h) before lean	T_c (h) after lean	$E_{before\ lean}$		$E_{after\ lean}$		E_f (before lean) / E_f (after lean)
			R (0-1)	Number of points* before lean	R (0-1)	Number of points* after lean	
TSSP1	22.4	16.9	0.98	228	0.99	265	0.89/0.75 increased
IMPROVEMENT	lowered 5.5 (23 %)		increased 14%				
TSSP2	15.6	11.7	0.98	228	0.99	265	0.86/0.75 increased
IMPROVEMENT	lowered 3.8 (24 %)		increased 14 %				

** -based on benchmarking method*

Table 4. Results obtained by application lean tools LO, 5S, VS, TSM and Kanban for TSSP1

Functions of maintenance system	applied „lean" tool	T_c (h) before „lean" pre	T_c (h) after „lean"	IMPROVEMENT
preparation of repair	„5S", VS, TSM	2,83	0,7	lowered 2,13 (75%)
realization of repairs	„5S", VS, L	17,9	16	lowered 1,9 (11%)
spares supply	TSM, KAN	1,17	0,2	lowered 0,97 (8%)
finalization	TSM	0,5	0,02	lowered 0,48 (96%)

Table 5. Results obtained by application lean tools LO, 5S, VS, TSM and Kanban for TSSP2

Functions of maintenance system	applied „lean" tool	T_c (h) before „lean" pre	T_c (h) after „lean" FF	IMPROVEMENT
preparation of repair	„5S", VS, TSM	2,83	0,7	lowered 2,13 (75%)
realization of repairs	„5S", VS, L	11,1	10,2	lowered 0,9 (8%)
spares supply	TSM, KAN	1,17	0,2	lowered 0,97 (8%)
finalization	TSM	0,5	0,02	lowered 0,48 (96%)

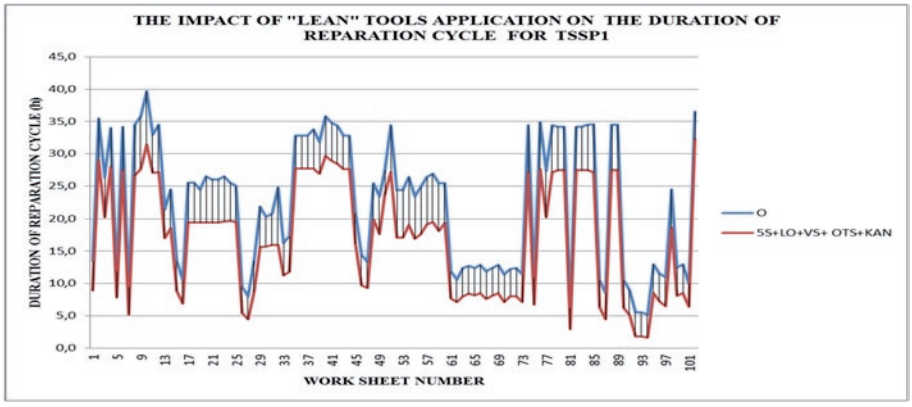

Fig. 3. The duration of technical maintenance, before (the blue line) and after (the red line) lean tools application (LO+5S+VS+TSM+KAN) for TSSP1

4.1. The empirically obtained results

Based on workshop documents analysis, and the measurement of the maintenance cycle-time in real maintenance system an average maintenance cycle-time (t_{mc}) for the TSSN1 and the TSSN2 is defined. The results of the application of specific lean tools for two independent TSSP are shown in the following tables.

Reducing the T_{rc} is slightly higher in the case of technical maintenance of TSSP1 compared to TSSP2 although the technical maintenance tasks take place in the same facility by the same workforce. This is due to the different content and scope of activities of technical maintenance prescribed in technical documentation.

The graphical representation of the results for TSSP1 and TSSP2 are shown in following figures.

The final results of the application of the proposed maintenance model and its improvement compared to the current situation (before lean) are shown in table 3.

Reducing the T_{rc} is slightly higher in the case of technical maintenance of TSSP1 compared to TSSP2 although the technical maintenance tasks take place in the same facility by the same workforce. This is due to the different content and scope of activities of technical maintenance prescribed in technical documentation.

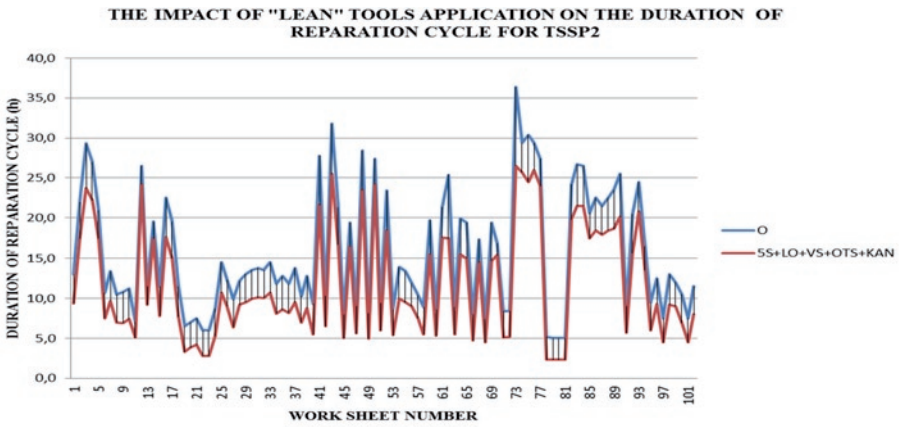

Fig. 4. The duration of technical maintenance, before (the blue line) and after (the red line) lean tools application (LO+5S+VS+TSM+KAN) for TSSP2

Table 6. Maintenance cycle-time T_c for TSSP1

T_c for TSSP1 (armoured personal carrier M80) in hours	LEAN concept TSSP1				
	without LEAN tools	with LEAN tools			
		5S	5S+VS	5S+VS+ TSM	5S+VS+ TSM+KAN
"LAYOUT"	23.16	20.07	18.94	17.69	17.27
	22.45	20.05	18.92	17.67	17.25
	22.20	20.00	18.87	17.62	17.20
	21.80	19.74	18.61	17.36	16.94
"LAYOUT" ("LEAN")	21.55	19.85	18.70	17.47	17.05
	21.25	19.70	18.55	17.32	16.90
	21.00	19.50	18.35	17.12	16.70
	20.09	18.70	17.55	16.32	15.90

Table 7. Maintenance cycle-time T_c for TSSP2

T_c for TSSP2 (howitzer SH 122 mm DS1) in hours	LEAN concept TSSP2				
	without LEAN tools	with LEAN tools			
		5S	5S+VS	5S+VS+ TSM	5S+VS+ TSM+KAN
"LAYOUT"	15.80	14.50	13.65	12.42	12.00
	15.60	14.35	13.50	12.27	11.85
	15.40	14.33	13.48	12.25	11.83
	15.30	14.31	13.46	12.23	11.81
"LAYOUT" ("LEAN")	15.20	14.30	13.45	12.22	11.80
	15.10	14.22	13.37	12.14	11.72
	14.90	14.00	13.15	11.92	11.35
	14.60	13.85	13.00	11.77	11.15

Table 8. Regression analysis and the analysis of variance influence of factors on T_c for TSSP1

```
The regression equation is
          Tc = 23,5 - 0,712 LAYOUT - 1,20 LEAN TOOLS

Predictor        Coef  SE Coef       T      P
Constant      23,4883   0,3505   67,01  0,000
LAYOUT        -0,7120   0,1841   -3,87  0,000
LEAN TOOLS   -1,19525  0,06509  -18,36  0,000

Analysis of Variance for Tc, using Adjusted SS for Tests
Source              DF    Seq SS    Adj SS   Adj MS       F      P
LAYOUT               1     5,069     5,069    5,069   27,17  0,000
LEAN TOOLS           4   119,943   119,943   29,986  160,69  0,000
LAYOUT*LEAN TOOLS    4     1,289     1,289    0,322    1,73  0,170
Error               30     5,598     5,598    0,187
Total               39   131,900
S = 0,431974   R-Sq = 95,76%   R-Sq(adj) = 94,48%
```

The graphical representation of the results for TSSP1 and TSSP2 are shown in following figures.

In figures 3 and 4 is shown the trend of decreasing the duration of maintenance cycle for TSSP1 and TSSP2 after lean tools application. The reduction of the maintenance cycle-time is achieved successively by 5S, TSM, LO, VS and KAN. The maximum effect is obtained when all five lean tools are applied at the same time.

4.2. The experimentally obtained results

After empirical tests of proposed model for TSSP maintenance, the 22 analysis of the impact of described lean tools is performed. The analysis of influence factors is considered in relation to the duration of the maintenance cycle time T_c, using the statistical software MINITAB.

For this experiment lean tools are grouped as:

– Factor 1: LAYOUT with two levels: 1.0 – current state and 2.0 – future state

– Factor 2: group of LEAN TOOLS with the following levels: 1.0 - 5S; 2.5 – 5S+VS; 4.0 – 5S+VS+TSM; and 5.5 – 5S+VS+TSM+KAN.

The data of duration of maintenance cycle T_c after two factors application for the all levels and for both TSSP are given in following tables.

Tables 6 and 7 are the basis for the formation of the starting matrices for regression analysis and analysis of variance influence of factors on T_c which is for both TSSP given in tables 8 and 9 respectively. In following tables the value "F" represents a Fisher criterion of statistical significance of T_c changes after the application of the described factors. The values of "P" represent a criterion for evaluating the impact of factors on T_c. The value of "R-Sq" represents the degree of approximation of empirical data based on linear model.

From statistically obtained result for TSSN1 (Tab. 8), it could be seen that criterion for evaluating the impact of factors on T_c, („LAYOUT" and „LEAN" TOOLS) is P=0. That means that those factors have impact on maintenance cycle-time. In a case of interaction of those factor („LAYOUT*LEAN" TOOLS) the value for criterion is P=0,170, and that means that in this case the factors do not have impact on maintenance cycle-time.

For test evaluation a statistical impact of α=0,05 and degrees of freedom k_2=4 (for LEAN TOOLOS) and k_1=1 (for „LAYOUT"), the critical value for criterion of statistical significance is F_c=8,71. Based on above represented results it is obvious that criterion of statistical significance F is higher than its critical value (for factors („LAYOUT" and „LEAN" TOOLS) which is proved that those factors have the impact on maintenance cycle-time

Table 9. Regression analysis and the analysis of variance influence of factors on T_c for TSSP2

```
The regression equation is
Tc = 16,6 - 0,357 LAYOUT - 0,918 LEAN Tools

Predictor        Coef  SE Coef       T      P
Constant      16,6268   0,1450  114,68  0,000
LAYOUT       -0,35650  0,07615   -4,68  0,000
LEAN TOOLS   -0,91775  0,02692  -34,09  0,000

Analysis of Variance for Tc, using Adjusted SS for Tests

Source              DF   Seq SS   Adj SS   Adj MS       F      P
LAYOUT               1   1,2709   1,2709   1,2709   34,33  0,000
LEAN TOOLS           4  68,2852  68,2852  17,0713  461,08  0,000
LAYOUT*LEAN TOOLS    4   0,1308   0,1308   0,0327    0,88  0,486
Error               30   1,1107   1,1107   0,0370
Total               39  70,7976

S = 0,192417   R-Sq = 98,43%   R-Sq(adj) = 97,96%
```

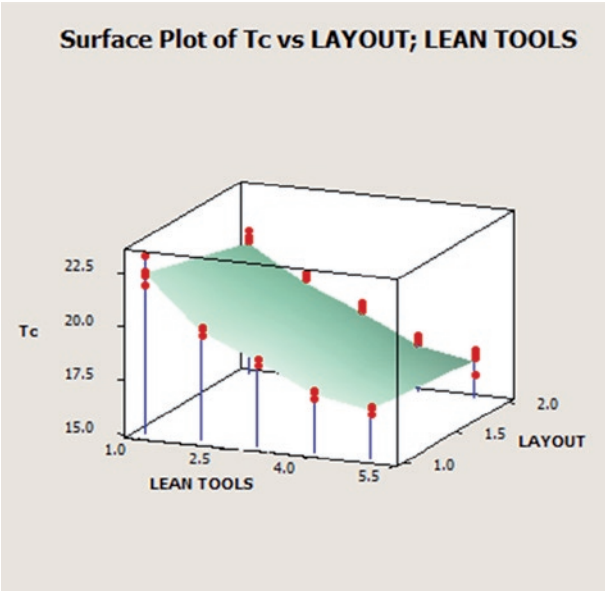

Fig. 5. Influence of LAYOUT and LEAN tools on T_c for TSSP1

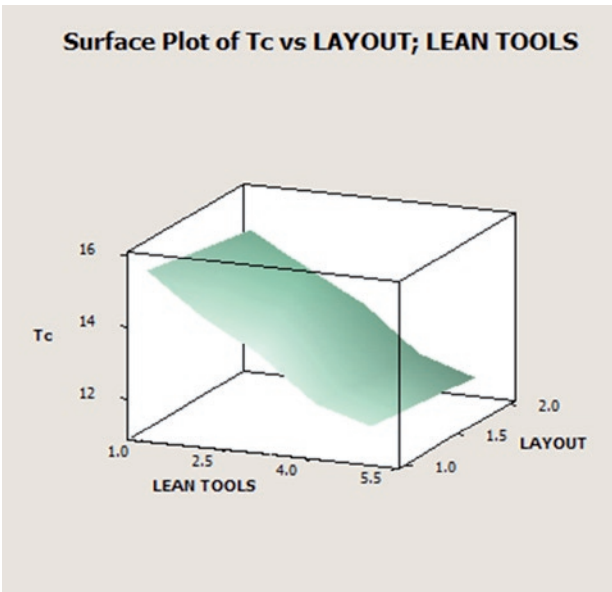

Fig. 6. Influence of LAYOUT and LEAN tools on T_c for TSSP2

T_c. The statistical test evaluation in the case of interaction of those factors („LAYOUT*LEAN" TOOLS) the criterion of statistical significance F is lover than its critical value which means that statistical test was correct or those factors do not have impact on maintenance cycle-time. The degree of approximation of empirical data based on linear model R-Sq = 95,76% shows that mathematical model, which describes statistical rule of changes of maintenance cycle-time T_c, has a high adequacy.

From statistically obtained result for TSSN2 (Tab. 9), it could be seen that criterion for evaluating the impact of factors on T_c, („LAYOUT" and „LEAN" TOOLS) is P=0, which means that those factors have impact on maintenance cycle-time. In a case of interaction of those factor („LAYOUT*LEAN" TOOLS) the value for criterion is P=0,486, and that means that in this case the factors do not have impact on maintenance cycle-time.

As in previous case, the criterion of statistical significance F is higher than its critical value (for factors („LAYOUT" and „LEAN" TOOLS) and lover than its critical value (for „LAYOUT*LEAN" TOOLS) which means that statistical tests were correct.

The degree of approximation of empirical data based on linear model R-Sq = 98,43% shows that mathematical model, which describes statistical rule of changes of maintenance cycle-time T_c, has a high adequacy.

The data in the tables show that factors LAYOUT and LEAN TOOLS affect the change of T_c, that this influence is statistically significant, and that their interaction does not change T_c. In addition to this, the data show that the mathematical models designed for TSSP1 and TSSP2 have a high level of adequacy.

The special significance of developed model is the regression analysis, the outputs of which are equations that mathematically describe the changes of the T_c depending on the applied lean tools (Tab. 6 and 7) and the possibility of their spatial graphics representation as it is shown in the following figures respectively. The regression equations enables to see the magnitude of impact of specific factors on maintenance cycle time T_c, that it is possible to influence them.

The graphics in figures 5 and 6 show that with every new application of "lean" tools, going from LAYOUT 1.0 to LAYOUT 2.0 the duration of T_c is reduced. In addition, it is unambiguously confirmed that the concomitant use of described lean tools in the maintenance system led to a maximal decrease of the T_c.

5. Conclusion

By applying the proposed TSM and maintenance model for the technical maintenance of TSSP it is possible to track maintenance processes and the realization of workshop and work sheets, to have control under the inventories of spares and supplies, and to automatically generate requests for procurement when resources fall below the defined minimal amount.

The presented solution also enables the obtaining reports on performed maintenance activities per individual TSSP, spent spares and supplies, the required procurements of them and the achieved efficiency for the selected period of time. The research described in this paper has special value because of the fact that the experiment was conducted in a real workshop for the technical maintenance of TSSP, after which the results of research are confirmed based on statistical analysis.

The obtained results show that it is possible to develop and implement the lean concept and tools in each function of the maintenance cycle the influence of which is reflected in the reduction of maintenance cycle-time, which is around 23%, depending on the applied function. The improvement of the maintenance effectiveness is around 14%.

Implementation of research, in real terms, contributed to changing the mindset of management and employees in real workshop for technical maintenance, in the direction of accepting the change in a positive way. The present lean model for technical maintenance of TSSP is a good basis for further research into the possibility of applying lean principles, methods and tools in all levels of maintenance, not only on technical maintenance.

References

1. Apte U, Kang K. Lean six sigma for reduced cycle costs and improved readiness. Acquisition Research Sponsored Report Series, Naval Postgraduate School, Monerey, California, 2006.
2. Ayadi Y, Chaib R, Verzea I. Contribution to the optimization of strategy of maintenance by lean six sigma. Physics procedia 2014; 55(2014): 512-518.
3. Ayeni P, Baines T, Lightfoot H, Ball P. State of the art of "Lean" in the aviation maintenance repair overhaul industry. Journal of Engineering Manufacture 2011; 225(11): 2108-2123, https://doi.org/10.1177/0954405411407122.
4. Basilevsky A T. Statistical factor analysis and related methods: theory and applications, Vol. 418. John Wiley & Sons, 2009.
5. Bhasin S, Burcher P. Lean viewed as a philosophy. Journal of Manufacturing Technology Management 2006; 17(1): 56–72, https://doi.org/10.1108/17410380610639506.
6. Biswas S, Chowdhury B. Industrial Applications and Practices of Six Sigma – A Literature Review. International Advanced Research Journal in Science, Engineering and Technology 2016; 3(3): 176-179, https://doi.org/10.17148/IARJSET.2016.3337
7. Božičković R, Radošević M, Ćosić I, Soković M, Rikalović A. Integration of simulation and lean tools in effective production systems – case study. Journal of Mechanical Engineering 2012; 58 (11): 642-652, https://doi.org/10.5545/sv-jme.2012.387.
8. Epler I. "Lean" concep of special purpose technical system maintenance. PhD thesis, University of East Sarajevo, East New Sarajevo, 2016. (In serbian)
9. Houshmand M, Jamshidnezhad B. An extended model of design process of lean production systems by means of process variables. Robotics and Computer: Integrated Manufacturing 2006; 22(1): 1-16, https://doi.org/10.1016/j.rcim.2005.01.004.
10. http://www.plant-maintenance.com/articles/CMMS_survey_2004.shtml
11. Irajpour A, Fallahian-Najafabadi A, Ali Mahbod M, Karimi M. A framework to determine the effectiveness of maintenance strategies lean thinking approach. Mathematical Problems in Engineering 2014, https://doi.org/10.1155/2014/132140
12. Legutko S. Development trends in machines operation maintenance. Eksploatacja i Niezawodnosc-Maintenance and Reliability 2009; 2: 8-16.
13. Marić B, Božičković R, Jašarević S. Softver tool for project management as support to lean concept in the process of technical systems overhaul. Proceedings 18th International Research Expert Conference "Trends in the Development of Machinery and Associated Technology", TMT 2014, Budapest, 2014; 177-180.
14. McDermott R E, Mikulak R J, Beauregard M R. The Basics of FMEA. New York: Productivity Press, 2009.
15. Muchiri P, Pintelon L, Gelders L, Martin H. Development of maintenance function performance measurement framework and indicators. International Journal of Production Economics 2011; 131(1): 295–302, https://doi.org/10.1016/j.ijpe.2010.04.039.
16. Nadeau S. Lean, Six Sigma and Lean Six Sigma in Higher Education: A Review of Experiences around the World. American Journal of Industrial and Business Management, 2017; 7: 591-603, https://doi.org/10.4236/ajibm.2017.75044.
17. Nash M, Poling S R, Ward S. Using Lean for faster Six Sigma results: A synchronized approach. Florida: CRC Press, 2006.
18. Shah R, Ward P T. Lean manufacturing: context, practice bundles, and performance. Journal of Operations Management 2003; 21(2): 129–149, https://doi.org/10.1016/S0272-6963(02)00108-0.
19. Shahrabi M, Shojaie A. Application of FMEA and AHP in lean maintenance. International Journal of Modern Engineering Sciences 2014; 3(1): 61-73.
20. Smith R, Hawkins B. Reduce costs, improve quality and increase market share. Oxford: Elsevier Butterworth-Heinemann, 2004.
21. Štefanić N, Gjeldim N, Mikac T. Lean concept application in production business. Tehnical Gazette 2010; 17 (3): 353-356.
22. Thangarajoo Y, Smith A. Lean Thinking: An Overview. Industrial Engineering & Management 2015; 4(2), https://doi.org/10.4172/2169-0316.1000159.
23. Veza I, Mladineo M, Gjeldum N. Selection of basic lean tools for development of croatian model of innovative smart enterprise. Tehnički vjesnik 2016; 23(5): 1317-1324.
24. Vinodh S, Chintha S K. Leanness assessment using multigrade fuzzy approach. International Journal of Production 2011; 49(2): 431-445, https://doi.org/10.1080/00207540903471494.
25. Wireman T. Benchmarking BEST practices in maintenance management. New York: Industrial Press, 2004.

Igor EPLER
Vlada SOKOLOVIĆ
Marjan MILENKOV
Milan BUKVIĆ
Military Academy, University of Defense in Belgrade
Generala Pavla Jurišića Šturma str.No. 33, 11000 Belgrade, Serbia

E-mails: igor.epler@va.mod.gov.rs, vlada.sokolovic@va.mod.gov.rs, marjan.milenkov@va.mod.gov.rs, milan.bukvic@vs.rs

Article citation info:
POGAČNIK B, DUHOVNIK J, TAVČAR J. Aircraft fault forecasting at maintenance service on the basis of historic data and aircraft parameters. Eksploatacja i Niezawodnosc – Maintenance and Reliability 2017; 19 (4): 624–633, http://dx.doi.org/10.17531/ein.2017.4.17.

Borut POGAČNIK
Jože DUHOVNIK
Jože TAVČAR

AIRCRAFT FAULT FORECASTING AT MAINTENANCE SERVICE ON THE BASIS OF HISTORIC DATA AND AIRCRAFT PARAMETERS

PROGNOZOWANIE USZKODZEŃ STATKÓW POWIETRZNYCH DLA CELÓW OBSŁUGI KONSERWACYJNEJ NA PODSTAWIE ICH PARAMETRÓW ORAZ DANYCH Z EKSPLOATACJI

Aircraft maintenance and repair organizations (MROs) have to be competitive and attractive for both existing and new customers. The aircraft ground time at MROs should be as short as possible and cost effective without reducing the quality of the work. Process optimization in MROs requires the continuous improvement of processes and the elimination of non-value-added activities during maintenance checks. There is, on the one hand, an obligation to follow the prescribed procedures and, on the other hand, pressure for time and cost reduction. The aircraft servicing process has been analysed according to a lean methodology. The optimization of logistics processes is recognized as the most promising method for reducing the maintenance service time and costs of spare parts. The probability of aircraft faults is calculated on the basis of historic data from previously completed service projects. Aircraft parameters, such as aircraft type, operator, aircraft age, flight hours, flight cycles, engine type and operation location, are taken into consideration in the fault forecasting. The fault probability is used as an indicator for defining a priority list for the accomplishment of jobs included in the aircraft maintenance service. The proposed methodology was validated and confirmed on four different projects.

***Keywords**: aircraft maintenance, fault forecasting, lean methods, machine learning, spare parts logistics.*

Organizacje zajmujące się konserwacją i naprawami statków powietrznych (MRO) muszą dbać o swoją konkurencyjność i atrakcyjność zarówno dla istniejących jak i nowych klientów. Czas trwania obsługi naziemnej w MRO powinien być jak najkrótszy a konserwacja powinna pociągać za sobą jak najmniejsze koszty, bez konieczności obniżania jakości pracy. Optymalizacja procesów przeprowadzanych w MRO wymaga ciągłego doskonalenia oraz eliminacji nieuzasadnionych czynności przeglądowych. Z jednej strony pracownicy MRO muszą przestrzegać określonych procedur, z drugiej zaś strony, ciąży na nich presja redukcji czasu i kosztów obsługi. Proces obsługi statku powietrznego analizowano zgodnie z metodologią szczupłego utrzymania ruchu. Optymalizację procesów logistycznych uznaje się za najbardziej obiecujący sposób redukcji czasu obsługi serwisowej oraz kosztów części zamiennych. Prawdopodobieństwo wystąpienia uszkodzeń statku powietrznego obliczano na podstawie danych historycznych z uprzednio przeprowadzonych prac obsługowych. W prognozowaniu uszkodzeń, uwzględniano takie parametry statku powietrznego, jak typ statku, jego operator, wiek, liczba godzin w powietrzu, liczba cykli lotów, typ silnika oraz miejsce stacjonowania. Prawdopodobieństwo wystąpienia uszkodzeń wykorzystano jako wskaźnik do hierarchizacji zadań obsługi technicznej statku powietrznego. Przydatność proponowanej metodologii zweryfikowano i potwierdzono na przykładzie czterech różnych projektów.

***Słowa kluczowe**: konserwacja statków powietrznych, prognozowanie uszkodzeń, metody szczupłego utrzymania ruchu, systemy uczące się, logistyka części zamiennych.*

1. Introduction

Service at a maintenance and repair organization (MRO) should be as short and as cost-effective as possible, while taking into account all safety standards. Regular inspections and preventive maintenance keep aircraft safety at an expected level [28]. Aircraft maintenance is a general term that includes aircraft checks that help assess aircrafts and the condition of their component parts. It can include short pre-flight checking or longer detailed checks of the aircraft and its component parts. Unplanned maintenance downtime causes flight service disruption, resulting in the loss of customer satisfaction for on-time performance [21]. Some component parts have a limited life, and when they expire, they should be replaced by new ones. Maintenance intervals and procedures are specified by the aircraft manufacturer and verified by aviation authorities. MROs have to follow strictly the prescribed procedures.

Aircraft maintenance is based on project-type work. Each aircraft that is being checked is regarded as an independent project. The customer who is bringing the aircraft in for maintenance wants all the work required based on the aircraft age, flight hours and cycles to be completed. All the required work is assembled in a work-package (WP), defined by the customer on the basis of aircraft manufacturer maintenance procedures. WP consists of job cards (JC) and job cards consist of task cards (TC). When an inspector performs some inspection, he signs off the respective task card. When all task cards of a particular job card are signed off, the job card can also be signed off. When all job cards are completed, the work-package is completed. New faults are often found during the aircraft inspection and need to be addressed during aircraft inspection. The number of discovered faults depends on the quality of previous maintenance activities, flight hours and cycles, the aircraft's usual operation location and other factors. Newly discovered faults most often dictate the work performed

on a project. Repairing the faults within the project time frame requires additional spare parts and special tools. Any lack of spare parts or tools can cause a delay in a project in the range of several days or an increase of project costs, caused by urgent supply, which is unacceptable for both the customer and the MRO.

The maintenance service analysis according to lean methodology was conducted on a 10-day C-check [31]. C-check typically has to be performed after 7500 flight hours or 5000 flight cycles or 24 months from the previous check, whatever occurs first. It typically consists of 300 to 600 job cards. A systematic analysis of aircraft maintenance processes revealed that spare parts and tool logistics have a significant impact on the costs and time course of aircraft service activities [31]. Some other researchers report on similar conclusions [2, 13 and 23]. Additional analyses have shown that early information on faults is the main leverage for improved spare parts logistics. The assumption was that fault forecasts can be made from historic data on maintenance services in the past aircraft projects. With respect to aircraft parameters, such as aircraft age, flight hours and cycles, operator, aircraft type, engine type and operation location, it is possible to forecast some of the faults to a certain degree and prepare for them. With this objective in mind, an algorithm has been developed for fault forecasting and it was integrated into spare parts logistics and the whole aircraft maintenance projects.

2. Literature survey

2.1. Aircraft maintenance

A maintenance plan is made for the faults that reduce flight safety and incur high maintenance costs. It includes checks for safe and reliable component functioning [11 and 28]. Several authors focused on aircraft health monitoring and optimum maintaining periods planning [5, 9, 29, 34 and 43]. Aircraft maintenance is split into different types of inspection, consisting of specific tasks, depending on flight hours, flight cycles and how much time has passed since the latest check [28]. Optimizing aircraft maintenance planning is – among others – discussed in the works of [16, 30 and 40]. In their aircraft inspection planning model [4] Baohui takes into account factors such as the human factor, type of inspection, type of aircraft, operation location and MRO. Bruno and co-authors compare the use of different aircraft maintenance planning techniques [6]. They share their focus on aircraft inspection planning, i.e., when a plane should be stopped and what checks should be performed during the forthcoming inspection. Maintenance of complex systems, such as aircraft, benefits vastly from an integrated approach to planning and scheduling of multiple activities, materials and resources. Investigations into current practices have shown that around 50 per cent of the total heavy maintenance workload is typically identified as part of inspections carried out during lay-up [36]. Li and co-authors propose innovative condition-based maintenance scheduling methodologies by integrating complex data processing, feature extraction, prognostic algorithm, and maintenance scheduling optimization. A numerical example shows how the aircraft reliability and health information can be integrated into the maintenance scheduling and planning optimization [26]. There are some specific ERP (Enterprise Resource Planning) software solutions that are upgraded for MRO specific needs [24].

Galar et al [12] propose a combined data mining-based methodology for condition-based maintenance considering condition monitoring data and historical maintenance management data. Gu, Zhang and Li present a non-linear programming model that forecasts demands, based on the aging of parts and the failure of installed parts [14]. Wang and Pham describe various models of maintaining and replacing component parts [42]. They mention replacement due to aging, periodic replacement, replacement due to failure, cost-limited repairs, time-limited repairs, scheduled maintenance, ad hoc maintenance and group maintenance. Each of the above models has its advantages and disadvantages. It has been demonstrated that a branch-and-price approach can be used to solve operational aircraft maintenance routing problem that the airlines face on a daily basis [37]. Lu et al propose a virtual maintenance environment, in which maintenance task virtual simulation can be conducted to support maintainability concurrent design of aircraft system [27].

Some of the authors have focused on the logistics of spare parts. MROs usually have expendable materials in stock. Due to differences in aircraft configurations and modification statuses, different contracts between customers and spare parts suppliers, and customers' wishes, components and other parts are borrowed or exchanged when they are required and as the need arises [31]. Due to the unpredictable nature of aircraft maintenance repair parts demand, MRO (Maintenance, Repair, Overhaul) business experience difficulties in forecasting and are currently looking for a superior forecasting solution. Several authors deal with techniques applicable to predicting spare parts demand [2, 13 and 23]. Most of the literature shows inefficiency of conventional forecasting methods, based on time series, for predicting such phenomena. Conventional methods inadequately reflect nonlinearity in the data, while artificial neural networks or a single artificial neuron do it well. Artificial intelligence techniques, artificial neural networks in particular, are the logical choice for further research [9].

The three main participants in air transport (aircraft manufacturers, operators and maintenance services) have mutually conflicting interests in making profit. Together with technological improvements, the use of new technology should bring economic benefits when compared to existing technologies [16]. Cohen and Wille propose a coordinated, data-driven approach for managing parts throughout the entire MRO service supply chain to improve the management of service part logistics. Improved part consumption forecasts for scheduled maintenance can be developed by taking into account causal factors, such as the plane and part age/history, as well as the known maintenance schedule of tasks for future checks of each airplane in the fleet [10]. The development of autonomic logistics, prognostic health management and distributed information systems are means of cost reduction and improving the maintenance of aircraft [7]. The framework proposed by Lee et al integrates simulation, multi-objective computing budget allocation and multi-objective evolutionary algorithms. The computational results show that, for the aircraft spare parts allocation problem, the framework is capable of finding non-dominated inventory and replacement policies with low average costs and high service levels [25]. Rasuo and Duknic report on a research, based on data, collected at general maintenance of military aircraft with the goal of reducing costs and shortening the overhaul cycle. Proposals for process optimization actions are primarily about improving the overhaul technology and supply system [33].

2.2. Lean methods and aircraft maintenance

The introduction of lean methods into aircraft maintenance requires the introduction of constant changes and the optimization of the aircraft maintenance process. The key is a comprehensive understanding of the processes and the maintenance processes. Lean thinking provides a systematic approach to identifying and eliminating waste through pull strategy in order to remain competitive in the global market [38 and 28]. In this context, any losses caused by the activities that generate direct or indirect costs, while not adding a value to the product and/or service from the point of view of the client, are designated as "waste" [38]. Womack and Jones [45] provide directions to set up guidelines, to cater the challenges that are encountered when a non-lean industrial organization tries to convert itself into a lean organization by means of five lean principles: value, value stream, flow, pull, and perfection, as the framework for an organization to understand the strategic approach of lean transformation. The terms are divided

into "value adding" and "non-value adding activities" (waste): (1) Value adding activities (VAA) convert materials and/or information in the search to meet client's requirements and (2) Non-value adding activities (NVAA) are attributed to time, resource or space consuming, which do not add value to the product and/or service that shall be delivered to the client. Hence, it is essential to minimize NVAA within maintenance by implementing the lean tools [18 and 22]. The two key segments of introducing lean processes are: (i) to understand what represents added value for the end customer and (ii) creating added value. Lean maintenance is a method of discovering and eliminating unnecessary activities, as well as a method of improving the efficiency of processes [19 and 35].

There are some applications of lean methods into aircraft maintenance service. Stadnicka et al. demonstrate the use of the VSM-based (value stream mapping) methodology together with other tools in aircraft maintenance processes in minimizing the lead-time of maintenance services and, subsequently, minimizing the costs of maintenance services [41]. Based on VSM of the current state of the maintenance service process the following solutions were proposed: (i) Analyses of these activities that can be carried out in parallel; (ii) Creating a safety stock on the basis of a statistical analysis of unit's failures in the service company [41]. Kasava analysed the process of line maintenance and four main activities were identified. These were broken down into smaller sub activities and subsequently categorised into value adding and non-value adding activities [20]. Eliminating the unnecessary activities also contributes to cost reduction [3] because the main objective is to respond to the requirements and desires of the end customer as efficiently and economically as possible and with minimal effort, minimal workforce, minimal facilities and in the shortest possible time [17]. Lean thinking first requires specifying the value of a product or service. All processes not contributing to the end value of the product or service are considered waste. The key of lean thinking is eliminating waste and adding value for the customer [28].

A typical project in MRO organization was analysed through LEAN eyes. The results of this analysis encouraged the authors to conduct the research on aircraft fault forecasting. A 10-day C-check on Airbus A321 aircraft was taken as a sample check for lean analysis. The check itself was planned approximately a month in advance. Work-orders were checked and spare material was ordered one week before the start of the check [31]. The project analysis consist of: (i) Estimation of time-schedule for project milestones and project phases within the time given to the project. (ii) The existing main tasks were analysed in the sense of their duration and the ratio between VAA / NVAA was calculated. (iii) A survey was carried out with the main mechanics and heads of each work-shop. They were also asked about possible improvements for each waste or project deficiencies. During the project analysis all the implemented work activities were divided into two groups: VAA and NVAA group. It was found that almost two thirds of all the work is NVAA and just one third of the implemented work is VAA.

The following activities were put into VAA group:

- Inspections – On the basis of these activities the customer is allowed to extend the aircraft airworthiness.
- Modifications – After the accomplishment of the requested modification the customer expects positive impact and consequently lover operational costs and therefore these activities also represent VAA.
- Eliminating incoming defects – At the time of the check the customer knew about them and would like to eliminate them.
- Eliminating of new findings / defects, discovered during the check

Into NVAA group belong all activities in following sub-groups:

- Acceptance
- Preparation
- Close-up
- Tests

Further on, unnecessary project events, which have a negative impact on the used working hours and consequently on the final project price, were analysed. The most exposed events, irrespective of the group into which they belong, were:

- Tooling loan was planned for the first day of the check, although it was eventually needed on the third day of the check.
- Due to simultaneous start of several projects (aircraft checks) on the same day, there was a lack of manpower on the first days of the project.
- Due to the aircraft position in a wrong hangar some work-shops were not close to the aircraft. As a result, much transportation of parts and man-power motions were required during the inspection and the re-assembly phase of the project.
- A lack of some consumable material was found in the middle of the check, which had to be additionally ordered on a higher priority level and was consequently more expensive.
- In the re-installation phase of the project a few man-hours were lost due to the waiting for the material. The particular material could not be released from the store due to certificate issues.
- Due to the aircraft flight hours/flight cycles and job cards (inspections), known prior to the project, some spare material was ordered in advance on the basis of previous experiences and expectations, but was later not used during the project.

The analysis has shown that spare parts logistics has potential for improvement. When spare parts and tools are required, the required shipping speed depends on the time available to finish the project. In terms of the available time, orders are placed according to the following priority list: (5) – Normal, (4) – Urgent, (3) – Critical, (2) –Work on Project Aborted (work on the aircraft has been stopped due to a shortage of material), (1) – Aircraft on Ground (AOG -aircraft has been grounded due to a shortage of material). Higher priority means faster and more expensive shipping. When there is enough time to remedy a fault (a fault was found at the beginning of the inspection), the order is given the 5 – Normal priority and the delivery will be cheaper. The MRO's and the customer's objective is to order materials soon enough with the 5 – Normal priority. However, this is only possible when information on the required material is recognized quickly and the material is ordered sufficiently soon. It is possible to obtain early information on the required material with an early inspection check.

The inspectors' personal experiences are the easiest but usually less optimal way to set the order of jobs to be completed within an aircraft check. As such, this way is limited by the person's abilities. Because the inspector himself or herself sets the order of tasks – without taking into account all aircraft parameters – the discovery of faults is distributed along the entire working process. Often, some faults are found at the beginning of the inspection, which is then followed by a period of finding no faults. At the end of the prescribed tasks, the number of discovered faults increases again.

With the implementation of some tools for optimization, such as fault forecasting, some of the significant wastes can be eliminated from the process and spare material, the required tooling and manpower can be planned in advance more reliably. Aircraft fault forecasting of maintenance service on the basis of historic data and aircraft parameters is presented in the next sections of this paper. Some other long-term activities for waste reduction, related to investments into hanger infrastructure and improved internal logistics, are not included in this report.

3. Research methodology

The analysis of maintenance process has shown the potential for service time and cost reduction in improving the supply of spare parts and tooling. The newly found faults represent a major variable in planning and executing service activities. Better forecasting of these faults offers the potential for quicker execution of aircraft service activities and lower logistics costs. The hypothesis is: historic data of maintenance services in recent years and aircraft parameters can be used for improved prediction on what faults will be found during the service. Early information on requested spare parts and tooling will enable prompt and more cost-efficient spare parts logistics. The solution shall enable continuous learning and incremental model upgrade with new cases of maintenance services. The initial model for the fault forecast algorithm is presented in the Fig. 1.

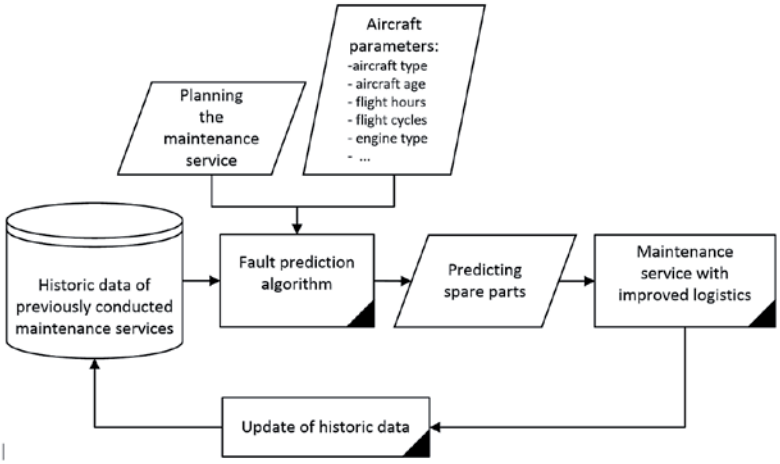

Fig. 1. The initial model for the fault prediction algorithm

At the beginning of the research project, there was a question what kind of machine learning tool shall be applied to a reliable prediction model. The presented model is the result of several iterations and data analyses. Already at the beginning there was a request that the model usability had to be validated by data from several new maintenance services. The initial prediction was that aircraft parameters, such as aircraft age, flight hours and cycles will contribute to the reliability of the model. The data analysis and validation will show a more detailed influence of particular aircraft parameters.

The surveyed literature is focused in most cases on the monitoring and planning of inspections, i.e., when to stop an airplane and what inspections to perform during the check. This article focuses on performing the maintenance project in the shortest and cheapest way. The aircraft parameters and probability factors were introduced, and historical data were processed by means of machine learning. The possibility of using regression analysis, neural networks [32] and genetic algorithms [39] was analysed first. Regression analysis is not suitable due to attribute data (operation location, engine types, operators, aircraft type). Some of the authors report on promising results using neural networks for predicting spare parts at maintenance service [9 and 23]. In our case we have got good results by applying relatively simple calculation of probability. Our wish was to do make spare part prediction model transparent and with traceability from historic data to predictions. In his work, Carbonneau et al investigated the applicability of advanced machine learning techniques for supply chain demand forecasting; the conclusion was that machine learning techniques do not show significantly better performance than linear regression [8]. On the basis of literature review, a generally applicable method for spare parts prediction cannot be specified. The optimal solution depends on the nature of the problem; whether it is linear or non-linear.

Witten defines system learning as a change in system behaviour in the direction that enables an easier/better execution of a task in the future [44]. Machine learning methods are used to forecast faults on aircrafts on the basis of previous checks - data is transformed into information [15]. Many machine learning studies cover the development of algorithms for specific problems and specific data [1]. Machine learning can be divided into supervised learning, unsupervised learning and reinforcement learning.

In his work, Harrington [15] states seven steps of machine learning:

1) collecting data (collecting data and patterns vital to achieve the goal),
2) preparing input data (data processing and selecting appropriate data format),
3) analysing input data (data analysis, recognizing patterns in the data, and recognizing exceptions),
4) validating data correctness (in the case of non-automated systems, to prevent incorrect data entering the system),
5) algorithm learning (inputting the available data into the algorithm),
6) algorithm testing (testing the performance of the algorithm), and
7) applying the knowledge (practical use).

The suggested steps of machine learning were used to forecast faults during aircraft service checks.

3.1. Aircraft parameters and probability factors

Aircraft parameters provide the aircraft's basic features, therefore it was assumed that they represent the key link to fault forecasting. They were selected together with the assistance of experts and are based on years of aircraft maintenance experience. The selected aircraft parameters are as follows:

Aircraft type
Operator
Aircraft age
Flight hours
Flight cycles
Engine type
Operation location – the area where the aircraft spends most of the time

The aircraft parameters served as a basis for defining probability factors. A probability factor represents the ratio between the number of discovered faults and the number of performed checks for the particular job.

$$p = \frac{N_1}{N_2}, \tag{1}$$

Where:

N_1 – number of findings on particular job card
N_2 – number of issued job cards

Probability factor p values can be expressed as follows:

a) »-« – a particular part/area has not been checked yet, so no fault has been discovered yet.
b) »p=0« – a particular part/area has been checked, but no faults were discovered during previous checks.
c) »0<p<1« – a particular part/area has been checked, and faults were discovered during previous checks.

d) »p>1« – a particular part/area has been checked, and several faults were discovered within a single check.

Factor values are used to set the order of jobs to do. Factor values are defined according to the parameters of the aircraft that is being inspected. Seven probability factors have been defined, and they are shown in Table 1. Using equation 2, the aggregate probability factor is calculated from partial probability factors. In principle each probability factor contributes an equal share to the aggregate factor, therefore $1/7$ ue to seven probability factors.

$$p = \frac{p_1 + p_2 + p_3 + p_4 + p_5 + p_6 + p_7}{N_3}, \tag{2}$$

Where:

p_1 – Probability factor for aircraft type
p_2 – Probability factor for operator
p_3 – Probability factor for aircraft age
p_4 – Probability factor for aircraft flight hours
p_5 – Probability factor for aircraft flight cycles
p_6 – Probability factor for engine type
p_7 – Probability factor for operation location
N_3 – number of probability factors ($N_3 = 7$)

Table 1. Probability factors

No.	Probability factor	Mark	Note
1	Aircraft type	p_1	$\frac{N_{11}}{N_{21}}$
2	Operator	p_2	$\frac{N_{12}}{N_{22}}$
3	Aircraft age	p_3	$\frac{N_{13}}{N_{23}}$
4	Aircraft flight hours	p_4	$\frac{N_{14}}{N_{24}}$
5	Aircraft flight cycles	p_5	$\frac{N_{15}}{N_{25}}$
6	Engine type	p_6	$\frac{N_{16}}{N_{26}}$
7	Operation location	p_7	$\frac{N_{17}}{N_{27}}$

Where:

N_{11} – number of findings on particular job card for specific aircraft type
N_{21} – number of issued job cards for specific aircraft type
N_{12} – number of findings on particular job card for specific operator
N_{22} – number of issued job cards for specific operator
N_{13} – number of findings on particular job card for specific aircraft age
N_{23} – number of issued job cards for specific aircraft age
N_{14} – number of findings on particular job card for specific flight hours
N_{24} – number of issued job cards for specific flight hours
N_{15} – number of findings on particular job card for specific flight cycles
N_{25} – number of issued job cards for specific flight cycles
N_{16} – number of findings on particular job card for specific engine type
N_{26} – number of issued job cards for specific engine type
N_{17} – number of findings on particular job card for specific flight location
N_{27} – number of issued job cards for specific flight location

In the next section, the proposed methodology is integrated into the fault prediction model and later the model is validated.

4. Fault forecasting model and job cards priority list setting

The fault forecasting model is integrated into the aircraft maintenance project as presented in Fig. 2. The contract with the customer and the work package are the background for project planning – for the job cards priority list. The fault forecasting algorithm enables fine project scheduling and optimized spare parts logistics.

Maintenance jobs are conducted according to the job cards priority list. Several jobs can be executed concurrently by several inspec-

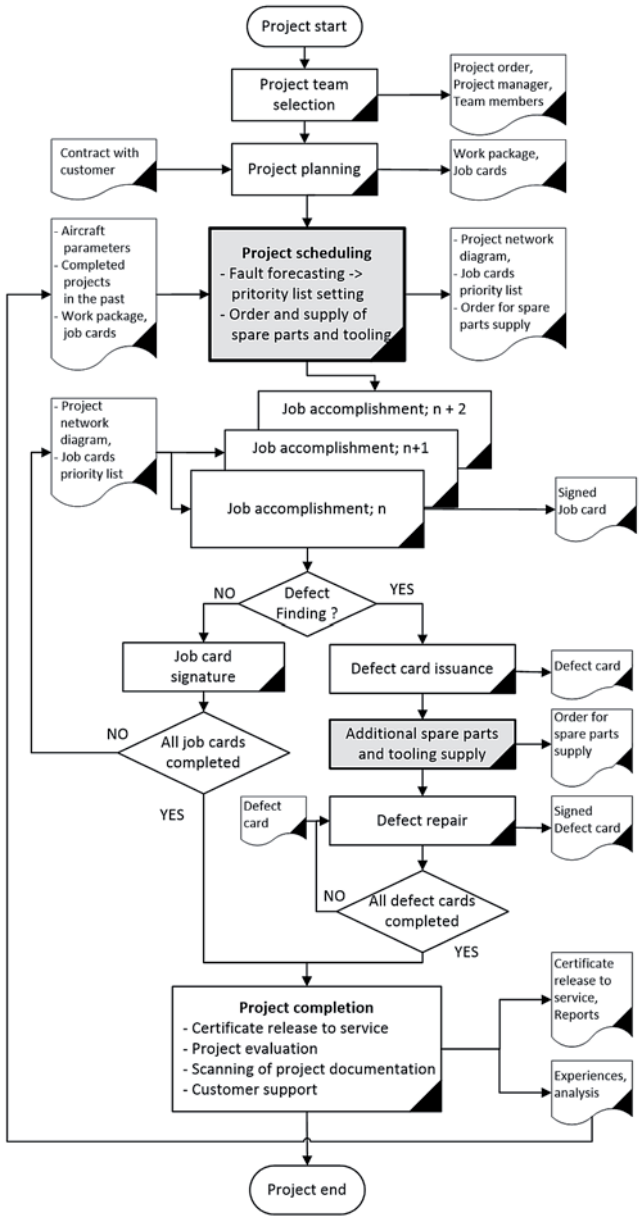

Fig. 2. Position of the fault forecasting in the aircraft maintenance service project process model

tors. If an inspector finds a defect, a defect card is issued and in some cases additional spare parts and tooling need to be supplied before the defect is repaired. Early information on requested spare parts is essential; therefore it is important to do the job cards with higher fault probability first. Once all defects have been repaired and all job cards are completed the activities for project conclusion can start. At the end of the project new findings (newly discovered faults) are included in the history database, which teaches the system for future projects (Fig. 2).

4.1. Model for fault forecasting and calculating the order of job priorities

A model for fault forecasting and setting the order of job priorities is shown in Fig. 3. In Fig. 2, this activity is called "Project scheduling". Input data for the calculation model are as follows:

- Aircraft manufacturer's list of job cards – list of all job cards prescribed by the aircraft manufacturer,
- Historic data from previous projects – information on the number of issued job cards and the number of discovered faults during previous projects,
- Aircraft parameters for each project – basic project data that include seven parameters (aircraft type, operator, aircraft age, aircraft flight hours, aircraft flight cycles, engine types and operation location), the project work order number and the date of the completion of the service project,
- Work-package – list of selected job cards from the manufacturer's list of cards that should be completed within the project according to the aircraft flight hours, flight cycles and aircraft age. This job cards list is defined by the customer.

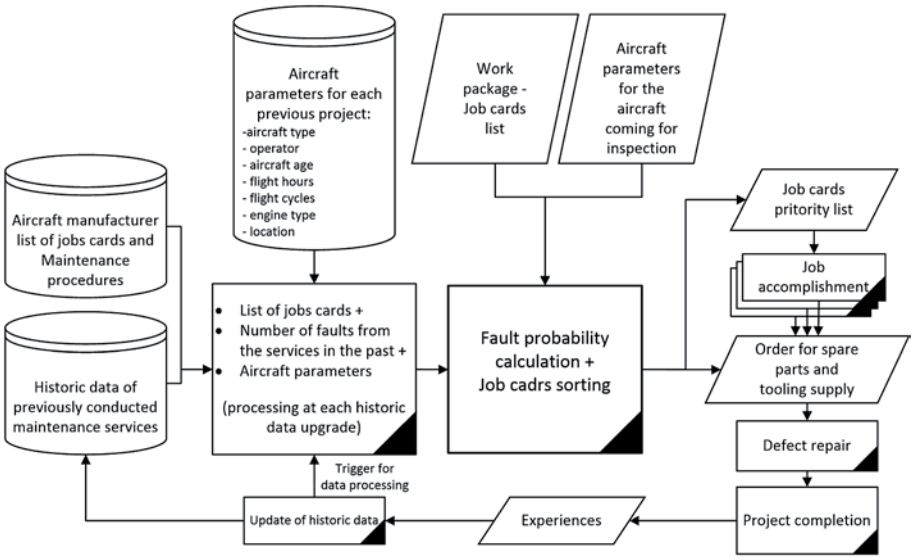

Fig. 3. Model for fault forecasting and calculating the job priority list

Job priority list is created in two steps, as shown in Fig. 3. In the first step the data from the first three databases need to be processed. For each job card, it is counted how many times it has been issued and how many faults have been discovered during the maintenance services in the past. This operation needs to be done each time when history database is upgraded with the data from one or several finished projects.

In the step two the fault probability is calculated for each job card. Work package is available already before the aircraft arrives, so the pre-described job cards are also available in advance. This process is followed by calculating the order in which the jobs will be performed on a particular project. The input data for calculation are as follows: (i) Work package with job cards list, (ii) Parameters of the aircraft coming for inspection, and (iii) the pre-processed data from previous projects prepared in step one (Fig. 3). Considering the number of discovered faults on previous projects the software calculates factors for the probability of discovering a fault within a particular job card. Job cards are then classified according to the size of the probability factor. Those with the highest probability of discovering faults are placed at the beginning of the job cards priority list.

Once a project has finished, the new data on the recently completed project are analysed and attached to the "History" database. The database is updated after each project, which allows the system to learn and offers more accurate solutions. The volume of data will increase with the number of completed projects. This will update the calculation system and improve it.

4.2. Attaching values to probability factors

An analysis of the accuracy model for calculating the aggregate probability factor was performed. The analysis was conducted on four completed projects that were not included in the "History" database. Following a systematic variation of weights and checking the target function the weights for individual parameters were optimized. The weights for each parameter were varied in the programmed calculation experiment in the range between 0 and 3 with step 0.5. The best results according to equation 4 were obtained using the equation with the following weights for individual parameters:

- Weight for the probability factor "Aircraft type": 2.0
- Weight for the probability factor "Operator": 1.0
- Weight for the probability factor "Age": 1.0
- Weight for the probability factor "Flight hours": 0.5
- Weight for the probability factor "Flight cycles": 0.5
- Weight for the probability factor "Engine type": 2.0
- Weight for the probability factor "Operation location": 1.0

The new equation 3 for the calculation of the aggregate probability factor is as follows:

$$p = \frac{2p_1 + p_2 + p_3 + 0.5p_4 + 0.5p_5 + 2p_6 + p_7}{N_3}. \quad (3)$$

Target function that evaluates the job cards priority list is calculated according to the equation 4. Sequence (Job_card_i) represents the sequence position of the Job_card_i in the sorted priority list which is the result of the fault forecasting algorithm. Function Fault (Job_card_i) has value 1 if a fault is found and value 0 if a fault at Job_card_i is not found. Function Fault values are determined after the completion of the maintenance project. It is preferred that the job cards where the fault has been found are in the first third of the priority list. Lower value of the target function means that the fault forecasting was good.

$$Target\_function = \sum_{i=1}^{N} Sequence(Job\_card_i) \bullet Fault(Job\_card_i) \quad (4)$$

At first sight, the result is surprising because it is expected that the (i) "Flight hours" and (ii) Flight cycles" parameters would yield

the best result, which means that the jobs with the highest number of discoveries would be performed at the beginning of the inspections. However, these two parameters perform the worst in the calculation of the sum of job order numbers – the jobs with a higher number of discoveries were performed later in the inspection phase. As a result, the probability factors of the above two parameters were weakened by a weight of 0.5. Calculating the sum of the job order numbers showed that the best results were obtained from the (i) "Aircraft type" and (ii) "Engine type" parameters. As a result, these two parameters were given a weight of 2.

If the best results were obtained by the "Flight hours" and "Flight cycles" parameters, it would mean that more flight hours and more flight cycles (within a particular job card) result in a larger number of discovered faults. However, because aircraft inspection schedules are based on the number of flight hours, flight cycles and the period since the previous inspection, the faults – associated with these two parameters – are fixed promptly and do not accumulate with an increasing number of flight hours and flight cycles. Consequently, it makes sense not to strengthen these two parameters. In contrast, the "Aircraft type" and "Engine type" parameters are strengthened because the obtained results show that they have the most significant effect on the sum of job order numbers.

Table 2. Parameters of the analysed projects

PROJECT	AIRCRAFT TYPE	OPERA-TOR	AGE	FLIGHT HOURS	FLIGHT CYCLES	ENGINE TYPE	LOCATION
I	Type C	J	3	5262	1722	Engine B	Europe
II	Type B	J	5	14264	5486	Engine A	Europe
III	Type A	E	16	42617	31586	Engine B	Europe
IV	Type B	E	24	58904	47370	Engine B	Europe

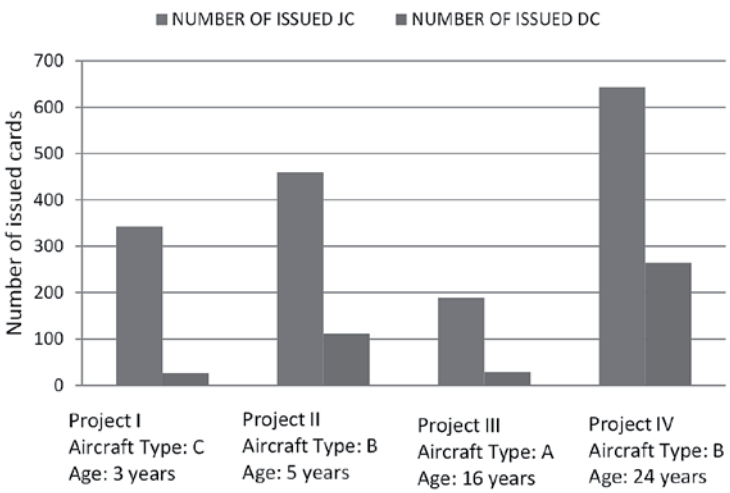

Fig. 4. Number of issued job cards (JC) and defect cards (DC) for each project

5. Algorithm validation

To analyse the current condition with an emphasis on the timeline of fault discovery, four completed projects were included in the analysis. The four projects are named "Project I", "Project II", "Project III" and "Project IV". The parameters of the analysed projects are shown in Table 2.

Figure 4 shows the number of issued job cards and defect cards in relation to aircraft age and aircraft type in the analysed projects.

Figures 5 and 7 show the timeline of discovering faults (issuing defect cards), according to the current method of completing jobs, as determined by inspectors, based on their experience. Figures 6 and 8 show the timeline of discovering faults (issuing defect cards) according to the new, optimized method of completing jobs using probability factors. The x-axis shows the sequence of the accomplished jobs. The y-axis shows the number of issued defect cards per job card. An analysis of the current situation in completing jobs revealed that faults are being discovered along the entire timeline of work. Using probability factors, the discovered faults move to the left, closer to the beginning of work. Figures 5, 6, 7 and 8 graphically present Projects II and IV. Significant improvements were achieved in Projects I and III as well. Validation confirmed the efficiency of the algorithm; the fault forecast is accurate in all four examples of airplanes aged between 3 and 24 years.

6. Conclusion

An aircraft fault forecasting model has been developed on the basis of aircraft parameters and previously completed service projects. The model makes it possible to set the order of inspections according to the criterion of the highest probability of discovering a fault. Its use reduces the total time required to complete the service on an aircraft and reduces logistics costs for spare parts and the required tools. The collected data on the frequency of faults also serve as important feedback for aircraft manufacturers.

Probability factors are the ratio between the number of discovered faults and the number of executed inspections. They are the basis for a fault forecasting model. To calcu-

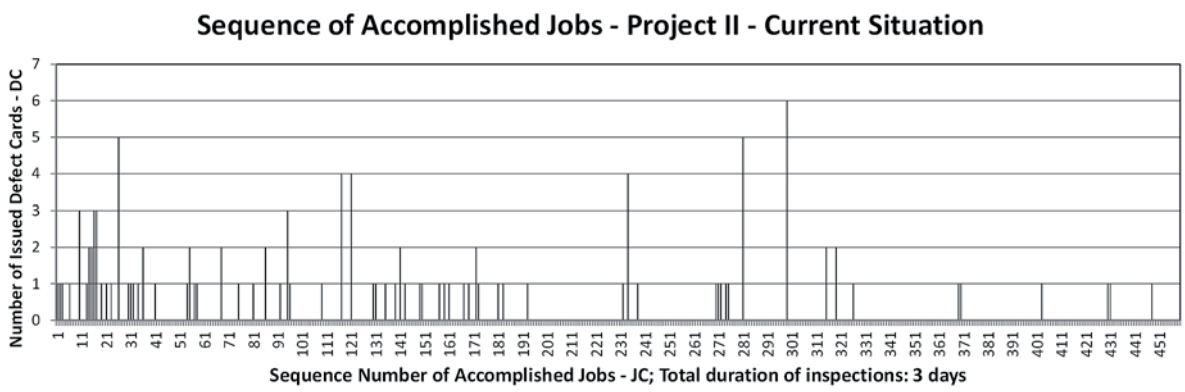

Fig. 5. Comparison of the timeline of issuing defect cards for the analysed project II. Sequence of accomplished jobs as determined by inspectors

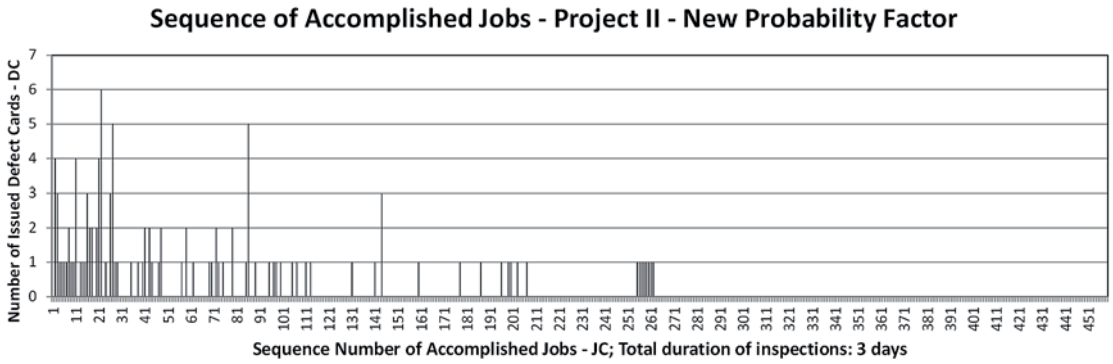

Fig. 6. Comparison of the timeline of issuing defect cards for the analysed project II. Sequence of accomplished jobs according to optimized method, using probability factor.

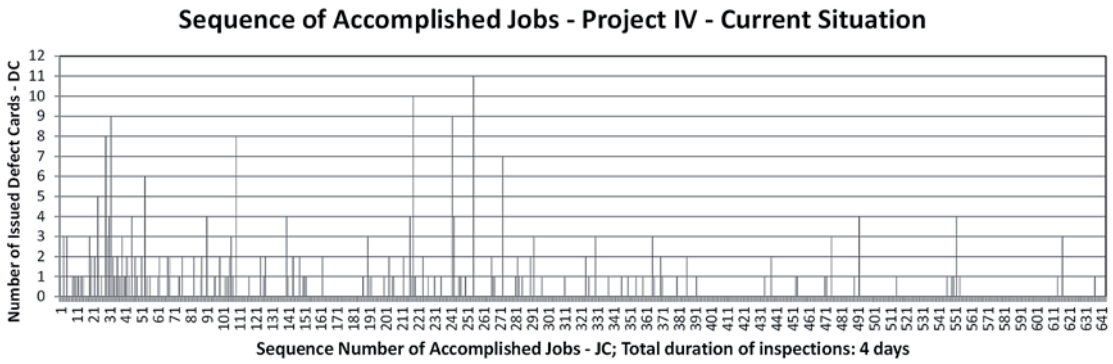

Fig. 7. Comparison of the timeline of issuing defect cards for the analysed project IV. Sequence of accomplished jobs as determined by inspectors

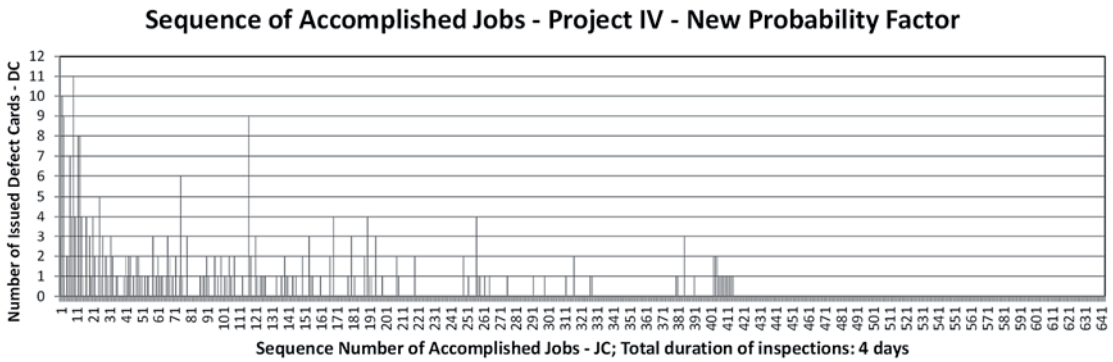

Fig. 8. Comparison of the timeline of issuing defect cards for the analysed project IV. Sequence of accomplished jobs according to the optimized method, using probability factor

late probability factors, an algorithm has been developed. It takes into account aircraft parameters and information on the number of discovered faults on previously completed maintenance projects. The sequence of jobs is determined by the aggregate probability factor, composed of the probability factors of individual parameters, such as flight hours, flight cycles, operators, aircraft age, engine type, aircraft type and the location the aircraft spent most of its operation time, and is further optimized with aircraft parameters weights. The sequence of jobs is determined by the size of the aggregate fault forecasting probability factor. The model for calculating the execution of jobs includes a feedback loop, which allows model learning with new information from the most recently completed maintenance projects. In this way, the calculation method is updated after each completed project, which in turn provides more accurate results. Taking into account a typical seven-day aircraft C check, consisting of approximately 300 jobs, algorithm validation revealed that arranging the jobs can shorten the project by one day, which is 14% of the total duration of the project. Earlier orders of materials and consequently lower shipping costs also significantly reduce the costs of the project. The presented machine learning methodology is therefore a significant tool for more efficient operational management of aircraft maintenance projects.

Acknowledgment

The authors would like to thank the company Adria Airways Tehnika, Aircraft Maintenance, part of Linetech, Poland for support of the research project.

References

1. Allison L. Types and Classes of Machine Learning and Data Mining. Clayton, Victoria: Monash University, 2003.
2. Altay N., Litteral L.A. (ed.) Service parts management: Demand forecasting and Inventory Control, Springer–Verlag, London 2011, https://doi.org/10.1007/978-0-85729-039-7.
3. Amirjabbari B., Bhuiyan N. An Application of a Cost Minimization Model in Determining Safety Stock Level and Location. World Academy of Science, Engineering and Technology 2011; 79: 797-806.
4. Baohui J., Chunhui X., Yaohua L. Study on Optimization Method of Aircraft Maintenance Plan Based on Longest Path. Journal of Applied Sciences 2013; 13(16): 3354-3357, https://doi.org/10.3923/jas.2013.3354.3357.
5. Bazargan M. An optimization approach to aircraft dispatching strategy with maintenance cost - A case study. Journal of Air Transport Management 2015; 42: 10-14, https://doi.org/10.1016/j.jairtraman.2014.07.008.
6. Bruno V., Garcia L., Nocco S., Quer S. Stressing Symbolic Scheduling Techniques within Aircraft Maintenance Optimization. Journal on Satisfiability, Boolean Modeling and Computation 2008; 5: 83-110.
7. Byer B., Hess A., Fila L. Writing A Convincing Cost Benefit Analysis to Substantiate Autonomic Logistics. IEEE Aerospace Conference, 2001; 6: 3095-3103, https://doi.org/10.1109/AERO.2001.931327.
8. Carbonneau R., Laframboise K., Vahidov R. Application of machine learning techniques for supply chain demand forecasting. European Journal of Operational Research 2008; 184: 1140–1154, https://doi.org/10.1016/j.ejor.2006.12.004.
9. Chen D., Wang X., Zhao J. Aircraft Maintenance Decision System Based on Real-time Condition Monitoring. IWIEE, Procedia Engineering 2012; 29: 765 – 769, https://doi.org/10.1016/j.proeng.2012.01.038.
10. Cohen M. A., Wille J.-H. Implications for Service Parts Management in the Rapidly Changing Aviation MRO Market. Hamburg: Helmut Schmidt University, 2006.
11. Dekker R. Applications of maintenance optimization models: a review and analysis. Reliability Engineering and System Safety 1996; 51: 229-240, https://doi.org/10.1016/0951-8320(95)00076-3.
12. Galar D., Gustafson A., Tormos B., Berges L. Maintenance Decision Making based on different types of data fusion. Eksploatacja i Niezawodnosc – Maintenance and Reliability 2012; 14 (2): 135–144.
13. Ghobbar A.A., Friend C.H., Evaluation of forecasting methods for intermittent parts demand in the field of aviation: a predictive model, Computers & Operation research, 2003: 2097–2114, https://doi.org/10.1016/S0305-0548(02)00125-9.
14. Gu J., Zhang G., Li K. W. Efficient aircraft spare parts inventory management under demand uncertainty. Journal of Air Transport Management 2015; 42:101-109, https://doi.org/10.1016/j.jairtraman.2014.09.006.
15. Harrington P. Machine Learning in Action. Shelter Island: Manning, 2012.
16. Hölzel N. B., Schröder C., Schilling T., Gollnick V. A Maintenance Packaging and Scheduling Optimization Method for Future Aircraft. Air Transport and Operations Symposium, 2012; 1-11.
17. Jasiulewicz – Kaczmarek M. Integrating Lean and Green Paradigms in Maintenance Management, The International Federation of Automatic Control, Cape Town, South Africa. August 24-29, 2014: 4471-4476.
18. Jasiulewicz-Kaczmarek M. Sustainability: Orientation in maintenance management: Case study. In: Golinska P, editor. EcoProduction and logistics, London: Springer; 2013: 135–154, https://doi.org/10.1007/978-3-642-23553-5_9.
19. Johnson M. E., Dubikovsky S. I. Incorporating Lean Six Sigma into an Aviation Technology Program. West Lafayette, Indiana: Purdue University, 2008.
20. Kasava N. K., Yusof N. M., Khademi A., Saman M.Z.M. Sustainable Domain Value Stream Mapping (SdVSM) Framework Application in Aircraft Maintenance: A Case Study. 12th Global conference on sustainable manufacturing: Procedia CIRP 2015; 26: 418-423.
21. Kipli J, Toyli J, Vepsalainen A. Cooperative Strategies for the Availability Service of the Repairable Aircraft Components. International Journal of Production Economics 2009; 117(2): 360-370, https://doi.org/10.1016/j.ijpe.2008.12.001.
22. Kolanjiappan S., Maran K. Lean Philosophy in Aircraft Maintenance. Journal of Management Research and Development (JMRD) 2011; 1 (1): 27-41.
23. Kozik P., Sęp J. Aircraft engine overhaul demand forecasting using ANN, Management and Production Engineering Review 2012; 3 (2): 21–26.
24. Lam MD. ERP for MRO: An Alternative Perspective from Package Programs to Niche Providers. Overhaul and Maintenance 2008; 14(5): 36-43.
25. Lee L. H., Chew E. P., Teng S., Chen Y. Multi-objective simulation-based evolutionary algorithm for an aircraft spare parts allocation problem. European Journal of Operational Research 2008; 189: 476–491, https://doi.org/10.1016/j.ejor.2007.05.036.
26. Li Z., Guo J., Zhou R. Maintenance Scheduling Optimization Based on Reliability and Prognostics Information. Conference: 2016 Annual Reliability and Maintainability Symposium (RAMS), https://doi.org/10.1109/RAMS.2016.7448069.
27. Lu Z., Zhou J., Li N. Maintainability fuzzy evaluation based on maintenance task virtual simulation for aircraft system. Eksploatacja i Niezawodnosc – Maintenance and Reliability 2015; 17 (4): 504–512, https://doi.org/10.17531/ein.2015.4.4.
28. Murphy S. The Status of Lean Implementation within South African Aircraft Maintenance Organizations. Johannesburg: University of the Witwatersrand, 2011.
29. Papakostas N., Papachatzakis P., Xanthakis V., Mourtzis D., Chryssolouris G. An approach to operational aircraft maintenance planning. Decision Support Systems 2010; 48: 604–612, https://doi.org/10.1016/j.dss.2009.11.010.
30. Pleumpirom Y., Amornsawadwatana S. Multiobjective Optimization of Aircraft Maintenance in Thailand Using Goal Programming: A Decision-Support Model, Advances in Decision Sciences. 2012; 2012: 1-17.
31. Pogačnik B., Tavčar J., Duhovnik J. Application of lean methods into aircraft maintenance processes. Transdisciplinary lifecycle analysis of systems: ISPE Inc. Int. Con. on CE. Delft: 2015; 259-268.
32. Potočnik P., Strmčnik E., Govekar E. Linear and Neural Network-based Models for Short-Term Heat Load Forecasting. Strojniški vestnik - Journal of Mechanical Engineering 2015; 61 (9): 543-550.
33. Rasuo B., Duknic G. Optimization of the aircraft general overhaul process. Aircraft engineering and aerospace technology 2013; 85 (5):

343-354, https://doi.org/10.1108/AEAT-02-2012-0017.
34. Rodrigues L. R., Pordeus Gomes J. P., Bizarria C. de O., Harrop Galvão R. K. Using Prognostic System and Decision Analysis Techniques in Aircraft Maintenance Cost-Benefit Models. IEEE Aerospace Conference, 2010; 1-7.
35. Sahay C., Shetty D., Ghosh S., Islam M., Turner M. Optimization of Assembly and Disassembly of GP7200 Engine. ASME International Mechanical Engineering Congress and Exposition 2013; 3: 1815-1826.
36. Samaranayake P, Kiridena S. Aircraft Maintenance Planning and Scheduling: An Integrated Framework. Journal of Quality in Maintenance Engineering 2012; 18(4): 432-453, https://doi.org/10.1108/13552511211281598.
37. Sarac A., Batta R., Rump C. M. A branch-and-price approach for operational aircraft maintenance routing. European Journal of Operational Research 2006; 175, 1850–1869, https://doi.org/10.1016/j.ejor.2004.10.033.
38. Savhnay R, Kannan S, Li X. Developing a value stream map to evaluate breakdown maintenance operations. Int J Industrial and Systems Engineering 2009; 4(3): 229–240, https://doi.org/10.1504/IJISE.2009.023539.
39. Slak A., Tavčar J., Duhovnik J. Application of Genetic Algorithm into Multicriteria Batch Manufacturing Scheduling. Strojniški vestnik - Journal of Mechanical Engineering 2011; 57, 2: 110-124.
40. Sriram C., Haghani A. An optimization model for aircraft maintenance scheduling and re-assignment. Transportation Research Part A 2003; 37: 29–48, https://doi.org/10.1016/S0965-8564(02)00004-6.
41. Stadnicka D., Ratnayake R.M.C. Enhancing aircraft maintenance services: a VSM based case study. Procedia Engineering, 2017; 182: 665-672, https://doi.org/10.1016/j.proeng.2017.03.177.
42. Wang H., Pham H. Reliability and Optimal Maintenance. Springer Series in Reliability Engineering series, London: Springer, 2006.
43. Wazny M., Wojtowicz K. The analysis of the military aircraft maintains system and the modernization proposal. Eksploatacja i Niezawodnosc – Maintenance and Reliability 2008; 3: 4-11.
44. Witten I.H., Frank E., Hall M.A. Data Mining, Practical Machine Learning Tools and Techniques. Third Edition. Burlington: Morgan Kaufmann Publishers, 2011.
45. Womack JP, Jones DT. Lean thinking: Banish waste and create wealth in your corporation. New York: Simon and Schuster, 2010.

Borut POGAČNIK
Adria Airways tehnika
Zg. Brnik 130h
SI-4210 Brnik, Slovenia

Jože DUHOVNIK
Jože TAVČAR
University of Ljubljana
Faculty of Mechanical Engineering
Aškerčeva 6
SI-1000 Ljubljana, Slovenia

E-mail: Joze.Duhovnik@lecad.fs.uni-lj.si, Borut.Pogacnik@aateh.si, Joze.Tavcar@lecad.fs.uni-lj.si

Article citation info:
CELIK N, GULOKSUZ CT. A new lifetime distribution. Eksploatacja i Niezawodnosc – Maintenance and Reliability 2017; 19 (4): 634–639, http://dx.doi.org/10.17531/ein.2017.4.18.

Nuri CELIK
Cigdem Topcu GULOKSUZ

A NEW LIFETIME DISTRIBUTION

NOWY ROZKŁAD CYKLU ŻYCIA

The well-known statistical distributions such as Exponential, Weibull and Gamma distributions have been commonly used for analysing the different types of lifetime data. In this paper, following the idea of the extension of T-X family of distributions, we propose a new type of exponential distribution. We define the survival function, the hazard function and the mean time to failure related to this new distribution. Type II censoring procedure is also considered for this distribution. Additionally, stress-strength reliability and the maximum likelihood (ML) estimators of the unknown parameters are obtained. As an application, a real data set is used to show that the proposed distribution gives best fit than the alternative ones.

Keywords: *T-X family of distributions, Reliability Function, Hazard Rate, Type II Censoring, Stress-Strength Probability.*

Powszechnie znane rozkłady statystyczne, takie jak rozkład wykładniczy, Weibulla czy rozkład Gamma znajdują szerokie zastosowanie w analizie różnych typów danych dotyczących cyklu życia. W niniejszym artykule, zaproponowano nowy typ rozkładu wykładniczego, w oparciu o rozszerzenie rodziny rozkładów TX. Zdefiniowano funkcję przeżycia, funkcję ryzyka (hazardu) oraz średni czas do uszkodzenia w odniesieniu do proponowanego rozkładu. Rozpatrywano także procedurę ucinania typu II dla nowego rozkładu. Dodatkowo określono niezawodność wytrzymałościową oraz estymatory największej wiarygodności nieznanych parametrów. Sposób wykorzystania proponowanego rozkładu zilustrowano wykorzystując rzeczywisty zbiór danych. Wykazano, że daje on lepsze dopasowanie niż modele alternatywne.

Słowa kluczowe: *rodzina rozkładów TX, funkcja niezawodności, współczynnik ryzyka, ucinanie typu II, prawdopodobieństwo wytrzymałości.*

1. Introduction

Exponential distribution has been broadly applied in the context of reliability. One reason for the popularity of the exponential distribution in reliability modeling is that it is the limiting lifetime distribution of a series system of substantially similar components [18]. The exponential distribution is also important for its "memoryless" property.

The probability density function (pdf) and the cumulative distribution function (cdf) of the exponential distribution are given by:

$$f(x) = \lambda e^{-\lambda x},\ x > 0 \tag{1}$$

$$F(x) = 1 - e^{-\lambda x},\ x > 0 \tag{2}$$

respectively, where λ is the shape parameter, which is also known as the rate parameter (failure, death, arrival or transition). The reliability function and the hazard function of the exponential distribution are given by:

$$R(x) = 1 - F(x) = e^{-\lambda x},\ \ x > 0 \tag{3}$$

$$h(x) = \frac{f(x)}{R(x)} = \lambda, x > 0 \tag{4}$$

However, the exponential distribution does not provide a significant fitting for some real life applications, where the failure rates are not constant. In recent years, many authors have proposed different types of generalization of the exponential distribution to overcome this problem, see [1, 4, 5, 8 and 11]. Some of these proposed life-time distributions have decreasing failure rate, which are common tools in biology and engineering, while the others have increasing failure rate which have been used in risk analysis. In this paper, we propose a new generalization of exponential distribution, which includes both increasing and decreasing failure rate. This property yields a great flexibility to fit the life time data obtained by any field of subject.

In literature, there are various types of extensions of the exponential distribution. [8-9] proposed an extension of the exponential distribution, which is called the generalized exponential (GE) distribution. Following the idea of the GE distribution, lots of extension procedures for exponential distribution has been introduced, [3], [7], [14] and [15].

Recently, [2] proposed a new technique to generate continuous probability distributions. The methodology proceeds as follows; Let X be arandom variable whose pdf is $f(x)$ and cdf is $F(x)$ and let T be continuous random variable with pdf $h(x)$ defined on the interval $[a, b]$. The cdf of new family of distribution can be obtained by:

$$G(x) = \int_a^{W[F(x)]} h(y)dy \tag{5}$$

where $W[F(x)]$ is differentiable and monotonically non-decreasing on the interval $[a,b]$. It should be also noted that $W[F(x)] \to a$ as $x \to -\infty$ and $W[F(x)] \to b$ as $x \to \infty$. The corresponding pdf of X can be written as:

$$g(x)=\left\{\frac{d}{dx}W\left[F(x)\right]\right\}h\left\{W\left[F(x)\right]\right\}. \tag{6}$$

The random variable T is called "transformed" into a new cdf $G(x)$ through the function $W\left[F(x)\right]$ known as "transformer". So, $G(x)$ is called "Transformed-Transformer" or "$T-X$" distribution.

We propose a new $W\left[F(x)\right]$ described in (5) with additional parameter θ. We define $W\left[F(x)\right]$ as follows:

$$W\left[F(x)\right]=\frac{e^{-\theta F(x)}-1}{e^{-\theta}-1} \tag{7}$$

where $\theta\in\mathcal{R}$. It can be seen that $W\left[F(x)\right]\to 0$ as $x\to-\infty$ and $W\left[F(x)\right]\to 1$ as $x\to-\infty$. Therefore, in order to use such a function defined in (6), it must be used a random variable, whose pdf is defined on the interval $[0,1]$. We use uniform distribution whose pdf is $h(y)=1, 0<y<1$.

Definition: Let $X(a<X<b)$ be a random variable, whose pdf is $f(x)$ and cdf $F(x)$. Let Y be a uniform random variable defined on the interval $[0,1]$. Then:

$$G(x)=\int_0^{\frac{e^{-\theta F(x)}-1}{e^{-\theta}-1}} dy=\frac{e^{-\theta F(x)}-1}{e^{-\theta}-1} \tag{8}$$

is a cdf of new family of "$T-X$" distribution. The corresponding pdfof this new family can be defined as:

$$g(x)=\frac{\theta f(x)e^{-\theta F(x)}}{1-e^{-\theta}},\ a<x<b. \tag{9}$$

In this paper, we propose a new life time distribution by using the pdf and the cdf of the exponential distribution.

2. Uniform-Exponential Distribution

Consider the exponential distribution with parameter λ and let $f(x)$ and $F(x)$ be the pdf and the cdf of exponential distribution, corresponding to the definition,

$$g(x)=\frac{\theta\lambda e^{-\lambda x}e^{-\theta\left(1-e^{-\lambda x}\right)}}{\left(1-e^{-\theta}\right)},\ x>0 \tag{10}$$

is defined as uniform-exponential (UE) distribution. The cdf of X can be written as:

$$G(x)=\frac{e^{-\theta\left(1-e^{-\lambda x}\right)}-1}{e^{-\theta}-1},\ x>0. \tag{11}$$

Figure 1 shows the pdfs of the UE distributions for different θ values. It can be seen that if θ tends to 0, the pdf becomes the original distribution. Additionally, if θ>0, then the pdf becomes more positively skewed and by the same way if θ<0, then the pdf becomes more negatively skewed. From now on, we call θ as the skewness parameter, since it determines the shape (skewness) of the distribution. It should be also noted that, the location parameter μ may be added to the distribution.

The moment generating function (mgf) of the UE distribution can be found as:

$$M_X(t)=\int_0^{\infty}e^{tx}\frac{\theta\lambda e^{-\lambda x}e^{-\theta\left(1-e^{-\lambda x}\right)}}{\left(1-e^{-\theta}\right)}dx \tag{12}$$

To solve (12) firstly, take $u=-e^{-\lambda x}$, then the integral becomes

$$\frac{\theta}{\left(1-e^{-\theta}\right)}\int_{-1}^{0}e^{-\theta(1+u)}(-u)^{-\frac{t}{\lambda}}du \tag{13}$$

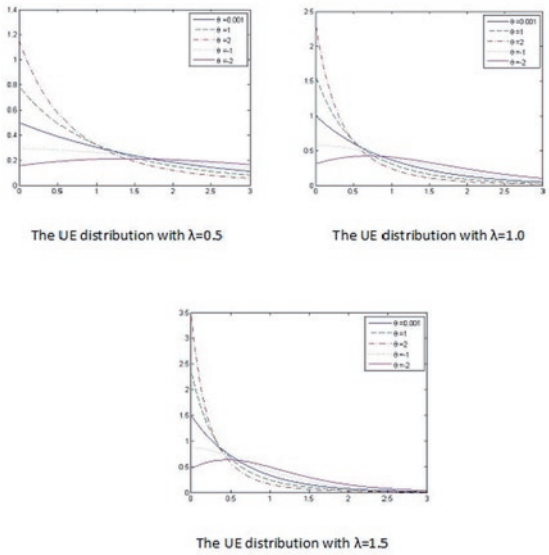

Fig. 1. The pdfs of UE distribution

By transforming $1+u=w$, (13) returns:

$$\frac{\theta}{\left(1-e^{-\theta}\right)}\int_0^1 e^{-\theta w}(1-w)^{-\frac{t}{\lambda}}dw \tag{14}$$

Using the below expansion:

$$e^{-t}=\sum_{i=0}^{\infty}\frac{(-1)^i t^i}{i!} \tag{15}$$

we get:

$$\frac{\theta}{\left(1-e^{-\theta}\right)}\sum_{i=0}^{\infty}\frac{(-1)^i\theta^i}{i!}\int_0^1 w^i(1-w)^{-\frac{t}{\lambda}}dw \tag{16}$$

The integral in (16) is a typical beta function. Therefore, the mgf of UE distribution can be obtained as:

$$M_X(t)=\frac{\theta}{\left(1-e^{-\theta}\right)}\sum_{i=0}^{\infty}\frac{(-1)^i\theta^i}{i!}B\left(i+1,-\frac{t}{\lambda}+1\right) \tag{17}$$

The expected value of UE distribution can be obtained by differentiating the mgf and taking $t=0$.

$$\frac{\theta}{\left(1-e^{-\theta}\right)}\left[\frac{1}{\lambda}-0.75\frac{\theta}{\lambda}+0.31\frac{\theta^2}{\lambda}-0.09\frac{\theta^3}{\lambda}+0.02\frac{\theta^4}{\lambda}+o(\theta,\lambda)\right]=\frac{\theta\Psi(\theta)}{\lambda\left(1-e^{-\theta}\right)} \tag{18}$$

The Ψ(θ) values are given in Table 1. It can be noticed that $\lim_{\theta\to 0}E(X)\to\frac{1}{\lambda}$ which is the expected value of the exponential distribution.

The quantile function $Q(p)$ and the median $Q(0.5)$ of the UE distribution are defined as

$$Q(p)=-\frac{1}{\lambda}\ln\left\{1+\frac{\ln\left[1+p\left(e^{-\theta}-1\right)\right]}{\theta}\right\} \tag{19}$$

Table 1. The Ψ(θ)values

θ	0	0.1	0.2	0.3	0.4	0.5	0.6
Ψ(θ)	1.000	0.9280	0.8617	0.8006	0.7443	0.6924	0.6445
θ	0.7	0.8	0.9	1.0	1.5	2.0	2.5
Ψ(θ)	0.6003	0.5594	0.5216	0.4867	0.3448	0.2344	0.1140

$$Q(0.5)=-\frac{1}{\lambda}\ln\left\{1+\frac{\ln\left[1+0.5\left(e^{-\theta}-1\right)\right]}{\theta}\right\} \tag{20}$$

respectively.

3. Reliability Analysis for UE distribution

In this section, the UE distribution is applied to the well-known reliability procedures.

3.1. Reliability Function

The reliability function means, the probability over duration, based on the time. The reliability function is also known as the survival function. The term reliability indicates the systems or devices in the engineering problems whereas survival is a term used for humans or animals in actuarial analysis. The reliability function is monotonically decreasing and right continuous.

The reliability function for UE distribution is defined by:

$$R(t)=1-F(t)=\frac{e^{-\theta}-e^{-\theta\left(1-e^{-\lambda t}\right)}}{e^{-\theta}-1}. \tag{21}$$

Figure 2 shows the reliability functions of UE distribution for some representative θ values. It should be also noted that $\lim_{\theta\to 0}R(t)\to e^{-\lambda t}$, which is the reliability function of standard exponential distribution.

3.2. Hazard Function

The hazard rate means instantaneous rate of occurrence of the event and is also known as the failure rate. The hazard function of UE

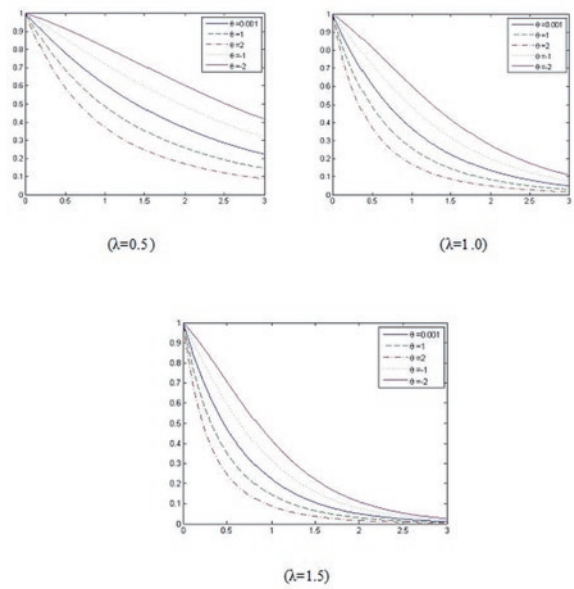

Fig. 2. The reliability functions of the UE distribution

distribution can be determined as follows

$$h(t)=\frac{\theta\lambda e^{-\lambda t}e^{-\theta\left(1-e^{-\lambda t}\right)}}{e^{-\theta\left(1-e^{-\lambda t}\right)}-e^{-\theta}}. \tag{22}$$

Taking $\lim_{\theta\to 0}h(t)\to\lambda$ into account, we can obtain the failure rate of exponential distribution. Figure 3 shows the hazard functions of UE distribution for some θ values. It is clear from the figure, when the parameter θ is greater than 0, then the failure rate function has a decreasing form. On the other hand, if the parameter θ is less than 0, then the failure rate function becomes increasing.

3.3. Mean Time to Failure

Mean time to failure (MTTF) is a measure of the length of the time a system is failed. It is usually used for nonrepairable systems. MTTF of UE is defined

$$MTTF=\int_0^{\infty}tf(t)dt=\frac{\theta^{\cdot\cdot}(\theta)}{\lambda\left(1-e^{-\theta}\right)}. \tag{23}$$

It should be remembered that the Ψ(θ) values are given in Table 1 for some representative θ values.

3.4. Censoring

Censoring is a condition in which some data cannot be observed precisely due to various reasons. There are many censoring schemes in literature. The most frequently encountered censoring is Type II. In the context of Type II censored data, the smallest r observations can-

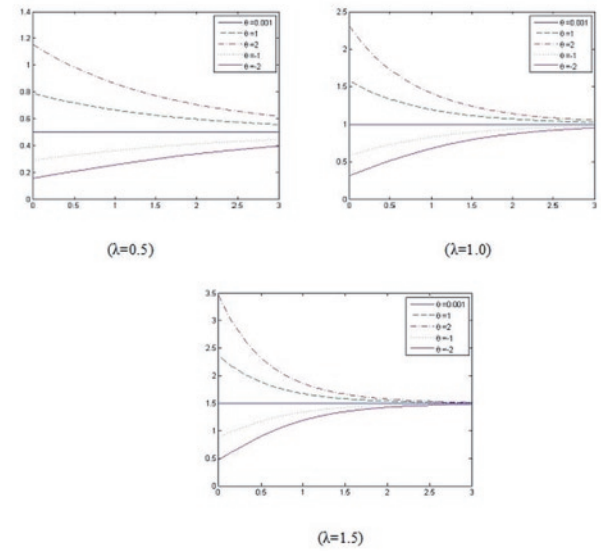

Fig. 3. The hazard functions of the UE distribution.

not be observed. Therefore, we have $n-r$ observations, where n is the number of observations. Let $X_1, X_2, \ldots, X_n$ be lifetimes of the sample. By ordering the sample we get $X_{(1)}, X_{(2)}, \ldots, X_{(n)}$. In type II censoring, we only have $X_{(1)}, X_{(2)}, \ldots, X_{(r)}$. ML estimation method is based on maximizing the likelihood function. The likelihood function of Type II censored data is:

$$L = \frac{n!}{(n-r)!}\prod_{i=1}^{r} f(x_i)\left[1-F(x_i)\right]^{n-r}$$
$$= \frac{n!}{(n-r)!}\prod_{i=1}^{r}\frac{\theta\lambda e^{-\lambda x_i} e^{-\theta\left(1-e^{-\lambda x_i}\right)}}{\left(1-e^{-\theta}\right)}\left[\frac{e^{-\theta\left(1-e^{-\lambda x_r}\right)}-1}{e^{-\theta}-1}\right]^{n-r}. \tag{24}$$

The log-likelihood function can be obtained by taking natural logarithm of (24) as:

$$\ln L = r\ln(\theta) + r\ln(\lambda) - r\ln\left(1-e^{-\theta}\right) - \lambda\sum_{i=1}^{r} x_i - \theta\sum_{i=1}^{r}\left(1-e^{-\lambda x_i}\right)$$
$$+(n-r)\ln\left[e^{-\theta} - e^{-\theta\left(1-e^{-\lambda x_r}\right)}\right] - (n-r)\ln\left(e^{-\theta}-1\right). \tag{25}$$

By differentiating the log-likelihood function with respect to the unknown parameters, we obtain the following likelihood equations

$$\frac{\partial \ln L}{\partial \lambda} = \frac{r}{\lambda} - \sum_{i=1}^{r} x_i - \theta\sum_{i=1}^{r}\left(x_i e^{-\lambda x_i}\right) + \frac{(n-r)e^{-\theta\left(1-e^{-\lambda x_r}\right)}\theta e^{-\lambda x_i} x_r}{e^{-\theta} - e^{-\theta\left(1-e^{-\lambda x_r}\right)}} \tag{26}$$
$$\frac{\partial \ln L}{\partial \theta} = \frac{r}{\theta} - \frac{re^{-\theta}}{1-e^{-\theta}} + \frac{(n-r)e^{-\theta}}{e^{-\theta}-1} - \sum_{i=1}^{r}\left(1-e^{-\lambda x_i}\right) + \frac{(n-r)\left[e^{-\theta\left(1-e^{-\lambda x_r}\right)}\left(1-e^{-\lambda x_i}\right) - e^{-\theta}\right]}{e^{-\theta} - e^{-\theta\left(1-e^{-\lambda x_r}\right)}}.$$

Because of the intractable functions in the likelihood equations, it is not possible to find the closed form expressions for the ML estimators. Therefore, we have to resort to iterative methods to solve them numerically.

3.5. Stress-Strength Probability

The stress-strength probability $R = P(Y < X)$ is a measure of the system reliability with strength X and stress Y. In a stress-strength model the system fails, when the applied stress to the system is greater than its strength. Several distributions have been applied to the stress-strength reliability models, see [6, 10, 13, 16 and 17].

Let X be the strength of a system distributed UE with the parameters (λ_1, θ_1) and Y be the stress, whose distribution is UE with the parameter (λ_2, θ_2). Therefore, stress-strength probability can be derived as:

$$P(Y<X) = \int P(Y<X) f_X(x)dx = \int F_Y(x) f_X(x)dx$$
$$= \int_0^\infty \frac{\left(e^{-\theta_2\left(1-e^{-\lambda_2 x}\right)}-1\right)}{e^{-\theta_2}-1}\frac{\theta_1\lambda_1 e^{-\lambda_1 x} e^{-\theta_1\left(1-e^{-\lambda_1 x}\right)}}{1-e^{-\theta_1}}dx \tag{27}$$
$$= \int_0^\infty \frac{e^{-\theta_2\left(1-e^{-\lambda_2 x}\right)}\left(\theta_1\lambda_1 e^{-\lambda_1 x} e^{-\theta_1\left(1-e^{-\lambda_1 x}\right)}\right)}{e^{-\theta_2}-1\left(1-e^{-\theta_1}\right)}dx - \frac{1}{e^{-\theta_2}-1}.$$

By taking $u = -e^{-\lambda_1 x}$, we get:

$$\frac{\theta_1\left(e^{-\theta_2-\theta_1}\right)}{e^{-\theta_2}-1\left(1-e^{-\theta_1}\right)}\int_{-1}^{0} e^{\theta_2(-u)^{\frac{\lambda_2}{\lambda_1}}} e^{-\theta_1 u}du - \frac{1}{e^{-\theta_2}-1}. \tag{28}$$

Then taking $t = \theta_1 u$, the integral becomes:

$$\frac{\left(e^{-\theta_2-\theta_1}\right)}{e^{-\theta_2}-1\left(1-e^{-\theta_1}\right)}\int_{-\theta_1}^{0} e^{-\left(\frac{t\theta_2}{\theta_1}\right)^{\frac{\lambda_2}{\lambda_1}}} e^{-t}dt - \frac{1}{e^{-\theta_2}-1}. \tag{29}$$

Using the property,

$$e^{-\left(\frac{t\theta_2}{\theta_1}\right)^{\frac{\lambda_2}{\lambda_1}}} = \sum_{i=0}^{\infty}\frac{(-1)^i}{i!}\left[\left(\frac{t\theta_2}{\theta_1}\right)^{\frac{\lambda_2}{\lambda_1}i}\right] \tag{30}$$

we get:

$$\left\{\frac{\left(e^{-\theta_2-\theta_1}\right)}{e^{-\theta_2}-1\left(1-e^{-\theta_1}\right)}\sum_{i=0}^{\infty}\frac{(-1)^i}{i!}\left[\left(\frac{t\theta_2}{\theta_1}\right)^{\frac{\lambda_2}{\lambda_1}i}\right]\int_{-\theta_1}^{0} t^{\frac{\lambda_2}{\lambda_1}i} e^{-t}dt\right\} - \frac{1}{e^{-\theta_2}-1} \tag{31}$$

and by the help of below expansion:

$$e^{-t} = \sum_{k=0}^{\infty}\frac{(-1)^k t^k}{k!} \tag{32}$$

we finally find the reliability as:

$$\left\{\frac{\left(e^{-\theta_2-\theta_1}\right)}{e^{-\theta_2}-1\left(1-e^{-\theta_1}\right)}\sum_{i=0}^{\infty}\frac{(-1)^i}{i!}\left[\left(\frac{t\theta_2}{\theta_1}\right)^{\frac{\lambda_2}{\lambda_1}i}\right]\sum_{k=0}^{\infty}\frac{(-1)^k}{k!}\frac{(-\theta)^{\frac{\lambda_2}{\lambda_1}i+k+1}}{\left(\frac{\lambda_2}{\lambda_1}i+k+1\right)}\right\}-\frac{1}{e^{-\theta_2}-1}. \tag{33}$$

If we take $\lambda_1=\lambda_2$ we can find stress strength reliability as:

$$P(Y<X)=\int P(Y<X)f_X(x)dx=\int F_Y(x)f_X(x)dx$$
$$=\frac{\theta_1}{e^{-\theta_2}-1\left(1-e^{-\theta_1}\right)}\left(\frac{1}{\theta_1+\theta_2}-\frac{\left(e^{-\theta_2-\theta_1}\right)}{\theta_1+\theta_2}\right)-\frac{1}{e^{-\theta_2}-1}. \tag{34}$$

Let $X_1,X_2,\ldots,X_{n_1}$ and $Y_1,Y_2,\ldots,Y_{n_2}$ be two independent random samples from the UE distribution with parameters (λ_1,θ_1) and (λ_2,θ_2) respectively. Assuming θ_1 and θ_2 are known. To obtain the ML estimatorsfor R, we have to find the ML estimators for λ_1 and λ_2. The ML estimators for λ_1 and λ_2 can be obtained by using the following formulas numerically.

$$\hat{\lambda}_1=\frac{n_1}{\sum_{i=1}^{n_1}x_i+\theta_1\sum_{i=1}^{n_1}x_ie^{-\lambda_1x_i}}$$
$$\hat{\lambda}_2=\frac{n_2}{\sum_{i=1}^{n_1}y_i+\theta_1\sum_{i=1}^{n_1}y_ie^{-\lambda_2y_i}} \tag{35}$$

If θ_1 and θ_2 are not known, we can also find the ML estimators of these parameter by:

$$\frac{n_1\left(1-e^{-\theta_1}-\theta_1e^{-\theta_1}\right)}{\theta_1\left(1-e^{-\theta_1}\right)}=\sum_{i=1}^{n_1}\left(1-e^{-\lambda_1x_i}\right)$$
$$\frac{n_2\left(1-e^{-\theta_2}-\theta_2e^{-\theta_2}\right)}{\theta_2\left(1-e^{-\theta_2}\right)}=\sum_{i=1}^{n_2}\left(1-e^{-\lambda_2y_i}\right) \tag{36}$$

solving (36) iteratively. [17] proved that the ML estimators for this reliability are more efficient than the UMVUE and Bayes estimators with respect to MSE values. For this reason, we only obtain ML estimators for stress-strength reliability. One can also find the UMVUE and Bayes estimators. Table 2 shows the reliabilities and ML estimators of these reliabilities calculated from some representative distribution parameters. The MLEs are considered according to the n_1 and n_2 respectively. Table 2 shows stress-strength probabilities and their ML estimations for some representative parameters.

It should be also noted that $\lim_{\theta_1,\theta_2\to 0}R=\frac{\lambda_2}{\lambda_1+\lambda_2}$. This is also the stress-strength probability of the exponential distribution. Additionally, if the other parameters remain stable the following remarks can be obtained

Table 2. The stress-strength probabilities of UE distribution

λ_1	λ_2	θ_1	θ_2	R	MLE(R)
	0.5			0.5000	0.5008
0.5	1.0	0.5	0.5	0.6593	0.6544
	2.0			0.7901	0.7923
	0.5			0.5438	0.5465
0.5	1.0	0.5	1.0	0.6928	0.6956
	2.0			0.8132	0.8139
	0.5			0.6139	0.6175
0.5	1.0	0.5	2.0	0.7530	0.7549
	2.0			0.8539	0.8599
	0.5			0.3407	0.3388
1.0	1.0	0.5	0.5	0.5000	0.5034
	2.0			0.6593	0.6601
	0.5			0.3814	0.3786
1.0	1.0	0.5	1.0	0.5408	0.5501
	2.0			0.6928	0.7004
	0.5			0.4609	0.4692
1.0	1.0	0.5	2.0	0.6169	0.6234
	2.0			0.7530	0.7601
	0.5			0.2099	0.1982
2.0	1.0	0.5	0.5	0.3407	0.3387
	2.0			0.5000	0.5091
	0.5			0.2432	0.2387
2.0	1.0	0.5	1.0	0.3814	0.3785
	2.0			0.5408	0.5472
	0.5			0.3114	0.3006
2.0	1.0	0.5	2.0	0.4609	0.4646
	2.0			0.6169	0.6204
	0.5			0.4592	0.4633
0.5	1.0	1.0	0.5	0.6186	0.6231
	2.0			0.7568	0.7612
	0.5			0.3831	0.3756
0.5	1.0	2.0	1.0	0.5391	0.5454
	2.0			0.6886	0.6934
	0.5			0.3072	0.2994
1.0	1.0	1.0	2.0	0.4592	0.4643
	2.0			0.6186	0.6232
	0.5			0.2470	0.2388
1.0	1.0	2.0	0.5	0.3831	0.3736
	2.0			0.5391	0.5423
	0.5			0.1868	0.1776
2.0	1.0	1.0	1.0	0.3072	0.2991
	2.0			0.4592	0.4665
	0.5			0.1461	0.1387
2.0	1.0	2.0	2.0	0.2470	0.2395
	2.0			0.3831	0.3799

- If θ_1 increases the probability decreases,
- If θ_2 increases the reliability also increases,
- If λ_1 increases the probability decreases,
- If λ_2 increases the reliability also increases.

4. Numerical Example

In this section, we consider the data given by [12]. The data is about the number of million revolutions before failure for each 23 ball bearings in the life test. [8] proposed the *GE* distribution and subsequently compared this with Weibull and gamma distributions. The data are as follows: 17.88; 28.92; 33; 41.52; 42.12; 45.60; 48.40; 51.84; 51.96; 54.12; 55.56; 67.80; 68.64; 68.64; 68.88; 84.12; 93.12;

98.64; 105.12; 105.84; 127.92; 128.04; 173.40. We propose the UE distribution for this data set. We obtain the ML estimators of the parameters and calculate the log-likelihood values and AIC statistics. The results are:

$\hat{\lambda} = 0.0147$ $\hat{\theta} = -1.5410$ $\hat{\mu} = 25.998$ $\ln L = -112.428$ and $AIC = 230.857$

while the ML estimators, log-likelihood values and AIC statistics for Weibull, gamma and generalized exponential distributions with three parameters are obtained as:

$\hat{\alpha} = 1.5979$ $\hat{\lambda} = 0.0156$ $\hat{\mu} = 14.8479$ $\ln L = -112.976$ and $AIC = 231.952$

$\hat{\alpha} = 2.7316$ $\hat{\lambda} = 0.0441$ $\hat{\mu} = 10.2583$ $\ln L = -112.850$ and $AIC = 231.700$

and

$\hat{\alpha} = 4.1658$ $\hat{\lambda} = 0.0314$ $\hat{\mu} = 14.8479$ $\ln L = -112.766$ and $AIC = 231.532$.

The UE distribution has the largest log-likelihood value and the smallest AIC statistics. This indicates that UE distribution provides a much better fit and more reliable inferences than other proposed distributions.

5. Conclusion

In this paper, we propose a new lifetime distribution with both increasing and decreasing failure rates. We define the reliability function, hazard function and MTTF for this new distribution. Furthermore, Type II censoring procedure is also considered for this distribution. We obtain stress-strength probability and ML estimators of this reliability for the proposed distribution. A real data example shows the proposed distribution gets better fit and more reliable solutions from other alternatives.

References

1. Alizadeh M, Bagheri S F, Alizadeh M, Saralees N. A new four-parameter lifetime distribution. Journal of Applied Statistics 2017; 44(5): 767-797, https://doi.org/10.1080/02664763.2016.1182137.
2. Alzaatreh A, Lee C, Famoye F. A new method for generating families of continuous distributions. METRON 2013; 71: 63-79, https://doi.org/10.1007/s40300-013-0007-y.
3. Barreto-Souza W, Santos A H S, Corderio G M. The beta generalized exponential distribution. Journal of Statistical Computation and Simulation 2000; 80(2): 159-172, https://doi.org/10.1080/00949650802552402.
4. Barreto-Souza W, Cribari-Neto F. A generalization of the exponential-Poisson distribution. Statistics and Probability Letters 2009; 79: 2493-2500, https://doi.org/10.1016/j.spl.2009.09.003.
5. Canchoa V G, Louzada-Neto F, Barriga G D C. The Poisson-exponential lifetime distribution. Computational Statistics and Data Analysis 2011; 55: 677-686, https://doi.org/10.1016/j.csda.2010.05.033.
6. Constantine K, Karson M. Estimators of P(Y < X) in the gamma case. Communication in Statistics Simulation and Computation 1986; 15: 365-388, https://doi.org/10.1080/03610918608812513.
7. Gomez Y M, Bolfarine H, Gomez H W. A New Extension of Exponential Distribution. RevistaColombiana de Estadistica 2014; 37: 25-34, https://doi.org/10.15446/rce.v37n1.44355.
8. Gupta R D, Kundu K. Generalized Exponential Distributions. Australian and New Zealand Journal of Statistics 1999; 41(2): 173-188, https://doi.org/10.1111/1467-842X.00072.
9. Gupta R D, Kundu D. Generalized exponential distributions: different methods of estimation. Journal of Statistical Computation and Simulation 2001; 69(4): 315-338, https://doi.org/10.1080/00949650108812098.
10. Kundu D, Gupta R D. Estimation of P(Y < X) for the generalized exponential distribution. Metrika 2005; 61(3): 291-308, https://doi.org/10.1007/s001840400345.
11. Kus C. A New Lifetime Distribution. Computational Statistics and Data Analysis 2007; 51: 4497-4509, https://doi.org/10.1016/j.csda.2006.07.017.
12. Lawless J F. Statistical Models and Methods for Lifetime Data. New York: Wiley, 1982.
13. Mokhlis N A. Reliability of a stress-strength model with Burr Type III distributions. Communication in Statistics Theory and Methods 2005; 34 (7): 1643-1657, https://doi.org/10.1081/STA-200063183.
14. Nadarajah S, Kotz S. The beta exponential distribution. Reliability Engineering and System Safety 2005; 91: 689-697, https://doi.org/10.1016/j.ress.2005.05.008.
15. Nadarajah S, Haghighi F. An extension of the exponential distribution. Statistics: A Journal of Theoretical and Applied Statistics 2011; 45(6): 543-558, https://doi.org/10.1080/02331881003678678.
16. Raqab M Z, Kundu D. Comparison of different estimators of P(Y < X) for a scaled Burr type X distribution. Communication in Statistics Simulation and Computation 2005; 34(2): 465-483, https://doi.org/10.1081/SAC-200055741.
17. Saracoglu B, Kaya M F, Ald-Elfattah A M. Comparison of Estimator for Stress Strength Reliability in the Gompertz Case. Hacettepe Journal of Mathematics and Statistics 2009; 38(3): 339-349.
18. Tortorella M, Reliability, Maintainability and Supportability, John and Wiley, 2015, https://doi.org/10.1002/9781119058823.

Nuri CELIK
Cigdem Topcu GULOKSUZ

Department of Statistics
Bartin University
KutlubeyKampusu 74100, Bartin, Turkey

Emails: ncelik@bartin.edu.tr, ctopcu@bartin.edu.tr

Article citation info:
SHIM J, RYU H, LEE Y. Availability analysis of series redundancy models with imperfect switchover and interrupted repairs. Eksploatacja i Niezawodnosc – Maintenance and Reliability 2017; 19 (4): 640–649, http://dx.doi.org/10.17531/ein.2017.4.19.

Jaechan SHIM
Hoyong RYU
Yutae LEE

AVAILABILITY ANALYSIS OF SERIES REDUNDANCY MODELS WITH IMPERFECT SWITCHOVER AND INTERRUPTED REPAIRS

ANALIZA GOTOWOŚCI MODELI REDUNDANCJI KASKADOWEJ UWZGLĘDNIAJĄCYCH NIEDOSKONAŁE PRZEŁĄCZANIE ORAZ PRZERWANE NAPRAWY

This paper considers N + 1 series redundancy, where N components are active and 1 component is standby in normal state. The active components execute the service, while the standby component is ready to take over the active role if the active components fail. When an active component fails, the standby, if available, automatically takes over system operations. However, the automatic switchover of the standby component to active mode might not be possible due to hardware or software issues. When a component failure or an imperfect switchover occurs, it immediately begins to be repaired. However, the repair process is possible to be interrupted. The most existing literature of redundancy models has focused on Markovian systems with uninterrupted repairs. This paper considers a non-Markovian redundancy model with interrupted repairs, where the repair time, the non-automatic switchover time, and the interrupted time are generally distributed. Using supplementary variable method and integro-differential equations, we obtain the steady-state availability for the redundancy model.

Keywords: *availability, series redundancy, imperfect switchover, interrupted repair, general repair time.*

W niniejszym artykule rozważano przypadek redundancji kaskadowej typu N + 1, w której liczba N elementów pozostaje aktywnych, a jeden komponent jest w trybie gotowości w stanie normalnym. Elementy aktywne wykonują usługę, podczas gdy składowa rezerwowa pozostaje w stanie gotowości do przejęcia roli aktywnej w przypadku, gdyby składniki aktywne uległy uszkodzeniu. Gdy element aktywny przestaje działać, element zastępczy, jeśli jest dostępny, automatycznie przejmuje operacje systemowe. Jednak automatyczne przełączenie komponentu zastępczego na tryb aktywny nie zawsze jest możliwe z powodu problemów ze sprzętem lub oprogramowaniem. Jeśli wystąpi awaria komponentu lub niedoskonałe przełączenie, natychmiast rozpoczyna się naprawa. Proces naprawy może jednak zostać przerwany. Większośćistniejącej literatury na temat modeli nadmiarowości koncentruje się na systemach Markowa, w których nie dochodzi do przerwania naprawy. W niniejszym artykule rozważano niemarkowowski model nadmiarowości uwzględniający możliwość przerwania naprawy, w którym czas naprawy, czas nieautomatycznego przełączenia oraz czas przerwany mają rozkład ogólny. Wykorzystując metodę dodatkowej zmiennej oraz równania całkowo-różniczkowe otrzymano gotowość stacjonarną dla omawianego modelu redundancji.

Słowa kluczowe: *gotowość, redundancja kaskadowa, niedoskonałe przełączenie, naprawa przerwana, ogólny czas naprawy.*

1. Introduction

The availability of a system is defined as the probability that the system is operational at a point in time [16, 25]. High availability is becoming a must in various domains such as telecommunication networks, power plants, and industrial and manufacturing systems [5, 16, 27]. During the past years, many efforts have been made to improve system availability.

Redundancy is a common approach to improve system availability [6]. The redundancy service can offer different levels of availability depending on its redundancy model. Availability Management Framework [16] defines the following four redundancy models: 2N, N+M, N-way, and N-way active. The 2N redundancy model ensures one standby replica for each component in active mode. The active components execute the service, while the standby components are ready to take over the active role if the active components fail. The N+M redundancy model extends the 2N redundancy by allowing more than two components to be active or standby. In the N+M redundancy, N represents the number of components in active mode and M represents the number of components in standby. The N-way redundancy model extends the N+M redundancy allowing a component to be simultaneously active and standby for different services. Lastly, the N-way active redundancy model differs from the 2N, N+M, and N-way redundancy, as it does not support standby service assignments, but allows a service to be assigned active to several components [16].

The availability analysis of a redundancy model is based on analyzing the various states that the model undergoes during its lifespan [21]. The analysis mainly focuses on capturing the failures that cause the system to switch to a faulty state and the repairs that shift the system back to a healthy state [6]. Since the occurrence of failures is erratic by nature, stochastic models have been used to conduct the availability analysis [20]. Markovian models have been extensively used for this purpose because of their expressiveness and their capability of capturing the complexity of real systems [1, 23-25]. One of the major problems of using Markovian models is that a large number of states are required to represent the model accurately [1]. As an alternative, Kanso et al. [6] used Stochastic Reward Nets (SRNs) to model

various redundancy models and evaluated the availability by using the Stochastic Petri Net Package (SPNP). Kim et al. [9] analyzed the networking service availability of 2N redundancy model with non-stop forwarding by using the SPNP. The analytic-numeric methods of SPNP provide the capabilities of solving the Markovian SRNs but fail for non-Markovian SRNs. Actually there is no reason to assume Markov property in modeling of repairable systems [11]. Recently, modeling and analysis of repairable systems with general repair time have drawn a lot of attention. Kuznetsov [11] evaluated the availability of repairable networks with general repair time distribution by a simulation method. However, because of the mathematical complexity of non-Markovian redundancy models, the closed form solutions of the models are extremely difficult to obtain.

In redundancy models with standby components, one of the standby components takes over the active role if an active component fails [16]. This process is called a switchover from standby mode into active mode. However, the switchover process is not always perfect [14]. That is, the switchover process may fail during the transition of a standby component to active mode. Lewis [14] first brought the concept of imperfect switchover in the availability analysis of redundancy models. Wang et al. [22] studied the availability of four different repairable systems with imperfect switchover. Ke et al. [7] used a Laplace transform method to study the availability of a Markovian repairable system. Hsu et al. [3] considered the profit analysis of a repairable system with imperfect switchover. Sadjadi and Soltani [18] considered a series-parallel system with the choice of redundancy strategy. In the above-mentioned works, the repair times have been assumed to be exponentially distributed. However, the assumption of exponential repair time distribution limits its use for solving real problems. In this paper, we consider non-Markovian model with imperfect switchover.

We consider a N+1 redundancy model. This is a special case of the N+M redundancy [16]. The classic "k-out-of-N" model [26], which is a very popular type of redundancy in fault-tolerant systems, can be seen as a special case of N+M redundancy if it is assumed that the switchover is perfect and instantaneous and the failure rate of a standby component is equal to the failure rate of an active component. Actually, the standby component may be different from the active component normally operating and may have a different failure rate in the operational mode [6]. In N+1 redundancy model, a single component acts as a standby for all components in active mode. In operation, the active components provide their service while the standby component is prepared to become backup to any of the active components, should one of them fails [16]. The N+1 redundancy itself has many real-world applications. One of the examples is a network device, DSLAM (Digital Subscriber Line Access Multiplexer), which connects the customer's end to the Internet through NICs (Network Interface Cards) [4, 10]. There may be multiple primary NICs and one standby NIC on DSLAM. When one of the primary NICs is faulty, services can be switched to the standby NIC. The switchover of the standby NIC to primary mode may fail due to hardware or software issues [10]. The failed NICs can be fixed through the remote server, which may also function wrongly [10]. Other examples include: Servers designed with multiple power supplies with one reserved as a cold backup [15]; A bank website deployed to a cloud platform, which has a dynamic number of active instances with a running backup always ready to replace a failed instance [19]; A factory having multiple industrial robots and one backup [17].

When a component failure or an imperfect switchover occurs, it immediately begins to be repaired. In realistic environments the repair process is possible to be interrupted [10]. Therefore, considering an interrupted repair in a repairable system is practical and imperative. The most existing literature of redundancy models has focused on uninterrupted repairs with exponentially distributed repair time. Little attention has been given to redundancy models with interrupted repairs and generally distributed repair time. Lee [12] analyzed the steady-state availability of a simple parallel 1+1 redundancy model with one active and one standby component. Bosse et al. [2] estimated the availability of a redundancy model with imperfect switchovers and interrupted repairs by using a Petri net Monte Carlo simulation. Kuo and Ke [10] and Lee [13] studied the steady-state availability of series systems with switching failures, interrupted repairs, and generally distributed repair time. However, they did not distinguish between the repairs of the component failures and the imperfect switchovers.

This paper focuses on the analytical expression of the availability for N+1 series redundancy model with imperfect switchovers, generally distributed repair times, and interrupted repairs. Furthermore, we distinguish between the repairs of the component failures and the imperfect switchovers. Using supplementary variable method and integro-differential equations governing the steady-state behavior of the model, we obtain the analytical expression of the steady-state availability. Some numerical examples for the steady-state availability of the redundancy model are presented.

2. Models

We describe a redundant system with one repairer and $N+1$ components, among which N components are active and 1 component is standby in normal state. The components in active mode operate normally and the component in standby mode is ready to assume the active role should the active components fail. The system is available only when there are N active components. It is assumed that the components in active mode operate independently from each other and their position in the serial structure of the system is not important. When the system is available, each component may fail independently of the state of the others. When the system is unavailable, it is shutdown and the additional failures do not occur. Components are repaired on a 'first come first served' basis. After the repair of a component is completed, the fixed component becomes standby if there are already N active components; otherwise, it becomes active. If one of the active components fails and there is a standby component, then the standby component automatically takes over system operations with neglibile switchover time and becomes active. The automatic switchover from standby to active may fail due to hardware or software issues. In this case, the repairer first switchs over non-automatically the standby component to active, then repairs the failed component. Moreover, the repairer may function wrongly or fail sometimes in its busy period, i.e., when it is repairing a failed component or it is switching over non-automatically a standby component. When the repairer is not available, its ongoing repair or non-automatic switchover process is interrupted. Once the repairer becomes available again, it resumes the interrupted process.

Let the time-to-failure of the active and the standby components be exponentially distributed with rate λ and μ, respectively. The repair time X is generally distributed with probability density function (PDF) $f(x)$ and cumulative distribution function (CDF) $F(x)$. The automatic switchover is assumed to fail with probability p and the non-automatic switchover time Y is generally distributed with PDF $g(y)$ and CDF $G(y)$. Moreover, the repairer may fail in its busy period with an exponential failure rate δ. The interrupted time Z is generally distributed with PDF $h(z)$ and CDF $H(z)$.

For mathematical analysis, we define some supplementary variables. The random process $X\_(t)$ denotes the amount of repair time already received by a failed component in repair at time t. We call $X\_(t)$ the elapsed repair time. The random processes $Y\_(t)$ and $Z\_(t)$ denote the elapsed non-automatic switchover time and the elapsed interrupted time, respectively, at time t. We also introduce:

$$\alpha(x) \equiv \frac{f(x)}{1-F(x)}, \tag{1}$$

$$\beta(y) \equiv \frac{g(y)}{1-G(y)}, \tag{2}$$

$$\gamma(z) \equiv \frac{h(z)}{1-H(z)}. \tag{3}$$

The function $\alpha(x)$ is the PDF for the repair time X on condition that $X>x$:

$$\alpha(x)dx = \mathrm{P}\{x < X < x+dx | X > x\}. \tag{4}$$

Note that the function $\alpha(x)$ is called the hazard rate or the age-specific failure rate in renewal theory. The functions $\beta(y)$ and $\gamma(z)$ are the hazard rates of the random variables Y and Z, respectively:

$$\beta(y)dy = \mathrm{P}\{y < Y < y+dy | Y > y\}, \tag{5}$$

$$\gamma(z)dz = \mathrm{P}\{z < Z < z+dz | Z > z\}. \tag{6}$$

Throughout this paper, $b^*(s)$ is the Laplace transform of a function $b(t)$.

3. Availability analysis

Let $M(t)$ and $K(t)$ be the state of the N+1 components and the state of the repairer, respectively, at time t:

$$M(t) = \begin{cases} 0 & \text{if there are } N-1 \text{ active and 2 failed components at time } t, \\ 1 & \text{if there are } N-1 \text{ active, 1 standby, and 1 failed component at time } t, \\ 2 & \text{if there are } N \text{ active and 1 failed component at time } t, \\ 3 & \text{if there are } N \text{ active and 1 standy component at time } t, \end{cases} \tag{7}$$

$$K(t) = \begin{cases} 0 & \text{if the repairer is idle at time } t, \\ 1 & \text{if the repairer is busy at time } t, \\ 2 & \text{if the repairer is in failed state at time } t. \end{cases} \tag{8}$$

Note that when $M(t)=0$, the system is unavailable and the repairer, if available, is repairing one of the two failed components; when $M(t)=1$, the system is unavailable and the repairer, if available, is switching over non-automatically the standby component to active; when $M(t)=2$, the system is available and the repairer, if available, is repairing the failed component; and when $M(t)=3$, the system is available and the repairer is idle. Let us define

$$P_0(x,z)dxdz \equiv \lim_{t\to\infty} \mathrm{P}\{M(t)=0, K(t)=2, x < X_-(t) < x+dx, z < Z_-(t) < z+dz\},$$

$$P_1(x,z)dxdz \equiv \lim_{t\to\infty} \mathrm{P}\{M(t)=1, K(t)=2, x < Y_-(t) < x+dx, z < Z_-(t) < z+dz\},$$

$$P_2(x,z)dxdz \equiv \lim_{t\to\infty} \mathrm{P}\{M(t)=2, K(t)=2, x < X_-(t) < x+dx, z < Z_-(t) < z+dz\},$$

$$Q_0(x)dx \equiv \lim_{t\to\infty} \mathrm{P}\{M(t)=0, K(t)=1, x < X_-(t) < x+dx\},$$

$$Q_1(x)dx \equiv \lim_{t\to\infty} \mathrm{P}\{M(t)=1, K(t)=1, x < Y_-(t) < x+dx\},$$

$$Q_2(x)dx \equiv \lim_{t\to\infty} \mathrm{P}\{M(t)=2, K(t)=1, x < X_-(t) < x+dx\},.$$

$$Q_3 \equiv \lim_{t\to\infty} \mathrm{P}\{M(t)=3, K(t)=1\},$$

$$P_m \equiv \int_0^\infty\int_0^\infty P_m(x,z)dxdz, \quad m=0,1,2,$$

$$Q_m \equiv \int_0^\infty Q_m(x)dx, \quad m=0,1,2.$$

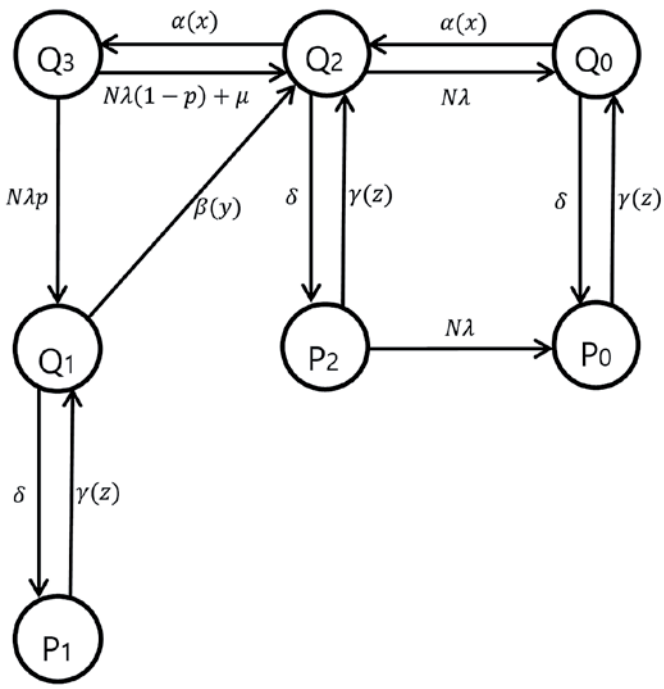

Fig. 1. State transition diagram

We construct the following integro-differential equations governing the steady-state behavior of the model by using supplementary variables:

$$\frac{dP_0(x,z)}{dz} = -\gamma(z)P_0(x,z) + N\lambda P_2(x,z), \tag{9}$$

$$\frac{dP_1(x,z)}{dz} = -\gamma(z)P_1(x,z), \tag{10}$$

$$\frac{dP_2(x,z)}{dz} = -\left[N\lambda + \gamma(z)\right]P_2(x,z), \tag{11}$$

$$\frac{dQ_0(x)}{dx} = -\left[\delta + \alpha(x)\right]Q_0(x) + N\lambda Q_2(x) + \int_0^\infty \gamma(z)P_0(x,z)dz, \tag{12}$$

$$\frac{dQ_1(x)}{dx} = -\left[\delta + \beta(x)\right]Q_1(x) + \int_0^\infty \gamma(z)P_1(x,z)dz, \tag{13}$$

$$\frac{dQ_2(x)}{dx} = -\left[N\lambda + \delta + \alpha(x)\right]Q_2(x) + \int_0^\infty \gamma(z)P_2(x,z)dz, \quad (14)$$

$$0 = -(N\lambda + \mu)Q_3 + \int_0^\infty \alpha(x)Q_2(x)dx. \quad (15)$$

We solve the above equations with boundary conditions:

$$P_m(x,0) = \delta Q_m(x), \quad m = 0,1,2, \quad (16)$$

$$Q_0(0) = 0, \quad (17)$$

$$Q_1(0) = N\lambda p Q_3, \quad (18)$$

$$Q_2(0) = \left[N\lambda(1-p) + \mu\right]Q_3 + \int_0^\infty \alpha(x)Q_0(x)dx + \int_0^\infty \beta(x)Q_1(x)dx. \quad (19)$$

Solving the above integro-differential equations, we obtain

$$P_2(x,z) = \delta e^{-N\lambda z}\bar{H}(z)Q_2(x), \quad (20)$$

$$P_1(x,z) = \delta \bar{H}(z)Q_1(x), \quad (21)$$

$$P_0(x,z) = \delta \bar{H}(z)Q_0(x) + \delta\left(1 - e^{-N\lambda z}\right)\bar{H}(z)Q_2(x). \quad (22)$$

Note that:

$$\bar{H}(z) \equiv 1 - H(z) \quad (23)$$

for CDF $H(z)$. Then, we get:

$$Q_2(x) = e^{-C_{N\lambda}x}\bar{F}(x)Q_2(0), \quad (24)$$

$$Q_1(x) = \bar{G}(x)Q_1(0), \quad (25)$$

$$Q_0(x) = \left(1 - e^{-C_{N\lambda}x}\right)\bar{F}(x)Q_2(0), \quad (26)$$

where $\bar{F}(x) \equiv 1 - F(x)$ and:

$$C_{N\lambda} \equiv N\lambda + \delta - \delta h^*(N\lambda). \quad (27)$$

Thus, we obtain:

$$Q_3 = \frac{1}{N\lambda + \mu} f^*(C_{N\lambda})Q_2(0), \quad (28)$$

$$Q_1(0) = \frac{N\lambda p}{N\lambda + \mu} f^*(C_{N\lambda})Q_2(0). \quad (29)$$

From (20)–(29), $P_m(x,z)$, $Q_m(x)$, $m = 0,1,2$, and Q_3 can be clearly expressed by $Q_2(0)$. Now we need to find the expression of $Q_2(0)$. From (26), we obtain:

$$Q_0 \equiv \int_0^\infty Q_0(x)dx = \int_0^\infty \left(1 - e^{-C_{N\lambda}x}\right)\bar{F}(x)Q_2(0)dx = \left[\mathrm{E}(X) - \bar{F}^*(C_{N\lambda})\right]Q_2(0). \quad (30)$$

From (25) and (29),

$$Q_1 \equiv \int_0^\infty Q_1(x)dx = \int_0^\infty \bar{G}(x)Q_1(0)dx$$
$$= \int_0^\infty \bar{G}(x)\frac{N\lambda p}{N\lambda + \mu} f^*(C_{N\lambda})Q_2(0)dx = \mathrm{E}(Y)\frac{N\lambda p}{N\lambda + \mu} f^*(C_{N\lambda})Q_2(0). \quad (31)$$

From (24),

$$Q_2 \equiv \int_0^\infty Q_2(x)dx = \int_0^\infty e^{-C_{N\lambda}x}\bar{F}(x)Q_2(0)dx = \bar{F}^*(C_{N\lambda})Q_2(0). \quad (32)$$

From (22), (30), and (32),

$$P_0 \equiv \int_0^\infty\int_0^\infty P_0(x,z)dxdz = \int_0^\infty\int_0^\infty \left[\delta \bar{H}(z)Q_0(x) + \delta\left(1 - e^{-N\lambda z}\right)\bar{H}(z)Q_2(x)\right]dxdz$$
$$= \int_0^\infty \delta \bar{H}(z)dz \int_0^\infty Q_0(x)dx + \int_0^\infty \delta\left(1 - e^{-N\lambda z}\right)\bar{H}(z)dz \int_0^\infty Q_2(x)dx$$
$$= \delta \mathrm{E}(Z)Q_0 + \delta\left[\mathrm{E}(Z) - \bar{H}^*(N\lambda)\right]Q_2. \quad (33)$$

Similarly, from (20), (21), (31), and (32), we obtain:

$$P_1 = \int_0^\infty\int_0^\infty \delta \bar{H}(z)Q_1(x)dxdz = \int_0^\infty \delta \bar{H}(z)dz \int_0^\infty Q_1(x)dx = \delta \mathrm{E}(Z)Q_1, \quad (34)$$

$$P_2 = \int_0^\infty\int_0^\infty \delta e^{-N\lambda z}\bar{H}(z)Q_2(x)dxdz = \delta \bar{H}^*(N\lambda)Q_2. \quad (35)$$

By normalization condition:

$$\sum_{m=0}^{2}(P_m + Q_m) + Q_3 = 1, \quad (36)$$

we obtain:

$$Q_2(0) = \frac{N\lambda + \mu}{f^*(C_{N\lambda}) + \left[1 + \delta E(Z)\right]\left[E(X)(N\lambda + \mu) + E(Y)N\lambda p f^*(C_{N\lambda})\right]}, \quad (37)$$

from which Q_m, $m = 0,1,2,3$, and P_m, $m = 0,1,2$, are obtained. Then, the steady-state availability Av_{N+1} can be obtained as:

$$Av_{N+1} = Q_2 + Q_3 + P_2$$
$$= \frac{f^*(C_{N\lambda}) + (N\lambda+\mu)\left[\bar{F}^*(C_{N\lambda}) + \delta\bar{H}^*(N\lambda)\right]}{f^*(C_{N\lambda}) + \left[1+\delta E(Z)\right]\left[E(X)(N\lambda+\mu) + E(Y)N\lambda p f^*(C_{N\lambda})\right]}. \tag{38}$$

4. Numerical examples

Table 1. Values of parameters

Case	Parameters	Variables
1	$\lambda\in[0,1]$, μ=.2λ, δ=.5, p=.1, $E(X)$=1, $E(Y)$=.5, $E(Z)$=1	λ, μ
2	λ=.5, μ=.2λ, $\delta\in[0,1]$, p=.1, $E(X)$=1, $E(Y)$=0.5, $E(Z)$=1	δ
3	λ=.5, μ=.2λ, δ=.5, p=.1, $E(X)$=1, $E(Y)$=.5, $E(Z)\in[1,5]$	E(Z)
4	λ=.2, μ=.2λ, δ=.2, $p\in[0,1]$, $E(X)$=1, $E(Y)$=.5, $E(Z)$=.2	p
5	λ=.7, μ=.2λ, δ=.7, $p\in[0,1]$, $E(X)$=1, $E(Y)$=.5, $E(Z)$=4	p
6	λ=.2, μ=.2λ, δ=.2, p=.1, $E(X)\in[1,5]$, $E(Y)$=.5, $E(Z)$=.2	E(X)
7	λ=.7, μ=.2λ, δ=.7, p=.1, $E(X)\in[1,5]$, $E(Y)$=.5, $E(Z)$=4	E(X)
8	λ=.2, μ=.2λ, δ=.2, p=.1, $E(X)$=1, $E(Y)\in[.1,1]$, $E(Z)$=.2	E(Y)
9	λ=.7, μ=.2λ, δ=.7, p=.1, $E(X)$=1, $E(Y)\in[.1,1]$, $E(Z)$= 4	E(Y)

For numerical examples, we consider three different models: 1 active and 1 standby($1+1$); 2 active and 1 standby($2+1$); and 3 active and 1 standby($3+1$). As shown in Table 1, nine cases are provided for illustration purposes. We consider three different distributions: Exponential (M), Deterministic (D), and Weibull (W) with shape parameter 2. We will compare the steady-state availability among three different redundancy models with five different triads of the repair time, the non-automatic switchover time, and the interrupted time distribution: MMM, DDD, DDW, WWD, and WWW, where the notation ABC represents that the repair time distribution is A, the non-automatic switchover time distribution is B, and the interrupted time distribution is C. For example, MMM represents that the three random variables are all exponentially distributed and WWD represents that the repair time and the non-automatic switchover time follow a Weibull distribution with shape parameter 2 and the interrupted time is deterministic. Note that all parameters can be modified to reflect other situations.

Table 2 shows the effect of parameter λ on the steady-state availability for three different models with five different triads of the repair time, the non-automatic switchover time, and the interrupted time distribution. Under our numerical environments given in Case 1, we find that:

$$Av(\text{DDD}) > Av(\text{DDW}) > Av(\text{WWD}) > Av(\text{WWW}) > Av(\text{MMM}).$$

Table 3 shows the effect of parameter δ on the steady-state availability for Case 2.

For the $1+1$ model:

$$Av(\text{DDD}) > Av(\text{DDW}) > Av(\text{WWD}) > Av(\text{WWW}) > Av(\text{MMM})$$

if $\delta \le 0.6$;

$$Av(\text{DDD}) > Av(\text{DDW}) > Av(\text{WWD}) > Av(\text{MMM}) > Av(\text{WWW})$$

if $0.7 \le \delta \le 1.0$.

For the $2+1$ and $3+1$ models:

$$Av(\text{DDD}) > Av(\text{DDW}) > Av(\text{WWD}) > Av(\text{WWW}) > Av(\text{MMM})$$

if $\delta \le 0.5$;

$$Av(\text{DDD}) > Av(\text{DDW}) > Av(\text{WWD}) > Av(\text{MMM}) > Av(\text{WWW})$$

if $0.6 \le \delta \le 1.0$.

Table 4 shows the effect of parameter $\text{E}(Z)$ on the steady-state availability for Case 3. For the $1+1$ model:

$$Av(\text{DDD}) > Av(\text{DDW}) > Av(\text{WWD}) > Av(\text{WWW}) > Av(\text{MMM})$$

if $1.0 \le \text{E}(Z) \le 1.5$;

Table 2. Steady state availability versus λ for Case 1

λ		0.1	0.2	0.3	0.4	0.5	0.6	0.7	0.8	0.9	1.0
1+1	MMM	.9788	.9399	.8930	.8440	.7958	.7501	.7075	.6681	.6320	.5989
	DDD	.9858	.9614	.9305	.8960	.8597	.8231	.7869	.7517	.7180	.6858
	DDW	.9851	.9592	.9264	.8900	.8519	.8137	.7762	.7400	.7055	.6727
	WWD	.9811	.9460	.9024	.8559	.8095	.7651	.7235	.6849	.6493	.6166
	WWW	.9804	.9436	.8981	.8495	.8013	.7553	.7124	.6728	.6365	.6033
2+1	MMM	.9426	.8495	.7569	.6752	.6057	.5472	.4978	.4559	.4201	.3891
	DDD	.9628	.8992	.8272	.7560	.6898	.6300	.5769	.5299	.4885	.4520
	DDW	.9607	.8934	.8181	.7445	.6769	.6165	.5633	.5167	.4759	.4401
	WWD	.9482	.8605	.7705	.6901	.6213	.5630	.5135	.4712	.4347	.4031
	WWW	.9460	.8544	.7610	.6783	.6082	.5493	.4999	.4580	.4222	.3913
3+1	MMM	.8989	.7594	.6415	.5495	.4780	.4218	.3767	.3400	.3095	.2840
	DDD	.9338	.8286	.7236	.6313	.5536	.4892	.4359	.3916	.3544	.3230
	DDW	.9299	.8196	.7114	.6178	.5402	.4766	.4244	.3813	.3454	.3151
	WWD	.9073	.7725	.6561	.5645	.4927	.4357	.3896	.3517	.3201	.2934
	WWW	.9033	.7631	.6436	.5509	.4793	.4232	.3782	.3416	.3112	.2856

Table 3. Steady state availability versus δ for Case 2

δ		0.0	0.1	0.2	0.3	0.4	0.5	0.6	0.7	0.8	0.9	1.0
1 + 1	MMM	.8312	.8228	.8152	.8082	.8017	.7958	.7903	.7852	.7805	.7761	.7719
	DDD	.8829	.8774	.8724	.8678	.8636	.8597	.8562	.8529	.8498	.8470	.8443
	DDW	.8829	.8756	.8688	.8627	.8571	.8519	.8472	.8427	.8386	.8348	.8313
	WWD	.8652	.8519	.8398	.8288	.8187	.8095	.8012	.7936	.7866	.7803	.7746
	WWW	.8652	.8501	.8362	.8235	.8119	.8013	.7916	.7827	.7746	.7672	.7603
2 + 1	MMM	.6462	.6360	.6270	.6191	.6120	.6057	.6000	.5948	.5901	.5858	.5818
	DDD	.7154	.7088	.7031	.6981	.6937	.6898	.6862	.6831	.6802	.6775	.6752
	DDW	.7154	.7055	.6969	.6894	.6828	.6769	.6716	.6668	.6625	.6585	.6549
	WWD	.6888	.6709	.6555	.6424	.6310	.6213	.6129	.6056	.5993	.5938	.5891
	WWW	.6888	.6676	.6494	.6337	.6200	.6082	.5979	.5889	.5810	.5741	.5680
3 + 1	MMM	.5123	.5034	.4958	.4891	.4832	.4780	.4734	.4693	.4655	.4621	.4590
	DDD	.5717	.5669	.5628	.5593	.5563	.5536	.5513	.5492	.5473	.5456	.5440
	DDW	.5717	.5633	.5563	.5502	.5449	.5402	.5361	.5324	.5291	.5262	.5235
	WWD	.5479	.5324	.5196	.5090	.5001	.4927	.4864	.4812	.4767	.4730	.4698
	WWW	.5479	.5290	.5132	.4999	.4888	.4793	.4713	.4644	.4585	.4534	.4490

Table 4. Steady state availability versus E(Z) for Case 3

E(Z)		1.0	1.5	2.0	2.5	3.0	3.5	4.0	4.5	5.0
1 + 1	MMM	.7958	.7583	.7193	.6815	.6460	.6131	.5828	.5549	.5293
	DDD	.8597	.8290	.7937	.7569	.7204	.6851	.6515	.6199	.5905
	DDW	.8519	.8167	.7781	.7393	.7018	.6663	.6332	.6024	.5740
	WWD	.8095	.7719	.7324	.6930	.6551	.6191	.5855	.5543	.5255
	WWW	.8013	.7587	.7156	.6740	.6350	.5990	.5659	.5356	.5079
2 + 1	MMM	.6057	.5590	.5152	.4760	.4415	.4112	.3845	.3609	.3399
	DDD	.6898	.6411	.5908	.5437	.5012	.4637	.4306	.4015	.3759
	DDW	.6769	.6253	.5750	.5292	.4887	.4531	.4218	.3942	.3698
	WWD	.6213	.5716	.5231	.4788	.4396	.4052	.3752	.3489	.3259
	WWW	.6082	.5555	.5069	.4640	.4267	.3943	.3661	.3415	.3198
3 + 1	MMM	.4780	.4333	.3934	.3592	.3299	.3048	.2830	.2641	.2474
	DDD	.5536	.5009	.4509	.4073	.3703	.3389	.3122	.2893	.2695
	DDW	.5402	.4876	.4398	.3986	.3636	.3339	.3084	.2863	.2672
	WWD	.4927	.4428	.3970	.3577	.3245	.2965	.2728	.2526	.2351
	WWW	.4793	.4295	.3859	.3489	.3178	.2915	.2690	.2496	.2328

$Av(\mathrm{DDD}) > Av(\mathrm{DDW}) > Av(\mathrm{WWD}) > Av(\mathrm{MMM}) > Av(\mathrm{WWW})$ if $2.0 \le \mathrm{E}(Z) \le 4.0$;

$Av(\mathrm{DDD}) > Av(\mathrm{DDW}) > Av(\mathrm{MMM}) > Av(\mathrm{WWD}) > Av(\mathrm{WWW})$ if $4.5 \le \mathrm{E}(Z) \le 5.0$.

For the $2+1$ model,

$Av(\mathrm{DDD}) > Av(\mathrm{DDW}) > Av(\mathrm{WWD}) > Av(\mathrm{WWW}) > Av(\mathrm{MMM})$ if $\mathrm{E}(Z) = 1.0$;

$Av(\mathrm{DDD}) > Av(\mathrm{DDW}) > Av(\mathrm{WWD}) > Av(\mathrm{MMM}) > Av(\mathrm{WWW})$ if $1.5 \le \mathrm{E}(Z) \le 2.5$;

$Av(\mathrm{DDD}) > Av(\mathrm{DDW}) > Av(\mathrm{MMM}) > Av(\mathrm{WWD}) > Av(\mathrm{WWW})$ if $3.0 \le \mathrm{E}(Z) \le 5.0$.

For the $3+1$ model,

$Av(\mathrm{DDD}) > Av(\mathrm{DDW}) > Av(\mathrm{WWD}) > Av(\mathrm{WWW}) > Av(\mathrm{MMM})$ if $\mathrm{E}(Z) = 1.0$;

$Av(\mathrm{DDD}) > Av(\mathrm{DDW}) > Av(\mathrm{WWD}) > Av(\mathrm{MMM}) > Av(\mathrm{WWW})$

Table 5. Steady state availability versus p for Case 4

p		0.0	0.1	0.2	0.3	0.4	0.5	0.6	0.7	0.8	0.9	1.0
1+1	MMM	.9627	.9551	.9476	.9402	.9329	.9257	.9186	.9117	.9048	.8980	.8914
	DDD	.9788	.9710	.9634	.9559	.9485	.9413	.9341	.9271	.9201	.9133	.9065
	DDW	.9787	.9710	.9634	.9559	.9485	.9412	.9341	.9270	.9201	.9132	.9065
	WWD	.9729	.9652	.9576	.9502	.9429	.9356	.9285	.9215	.9146	.9078	.9011
	WWW	.9728	.9652	.9576	.9501	.9428	.9356	.9285	.9215	.9146	.9078	.9011
2+1	MMM	.8916	.8804	.8696	.8589	.8486	.8385	.8286	.8189	.8095	.8003	.7913
	DDD	.9308	.9194	.9084	.8975	.8870	.8766	.8665	.8567	.8470	.8376	.8284
	DDW	.9307	.9193	.9082	.8974	.8868	.8765	.8664	.8565	.8469	.8375	.8283
	WWD	.9148	.9036	.8927	.8820	.8716	.8614	.8515	.8417	.8322	.8230	.8139
	WWW	.9146	.9034	.8925	.8818	.8714	.8613	.8513	.8416	.8321	.8228	.8138
3+1	MMM	.8119	.7998	.7881	.7767	.7656	.7549	.7444	.7343	.7244	.7147	.7053
	DDD	.8681	.8560	.8443	.8328	.8217	.8109	.8004	.7901	.7801	.7703	.7608
	DDW	.8678	.8557	.8440	.8326	.8214	.8106	.8001	.7898	.7798	.7701	.7605
	WWD	.8431	.8312	.8196	.8084	.7974	.7868	.7764	.7663	.7565	.7469	.7375
	WWW	.8428	.8309	.8193	.8081	.7971	.7865	.7761	.7660	.7562	.7466	.7373

Table 6. Steady state availability versus p for Case 5

p		0.0	0.1	0.2	0.3	0.4	0.5	0.6	0.7	0.8	0.9	1.0
1+1	MMM	.4501	.4409	.4322	.4237	.4156	.4078	.4003	.3931	.3861	.3794	.3729
	DDD	.5123	.5033	.4946	.4862	.4780	.4702	.4626	.4552	.4481	.4412	.4345
	DDW	.4954	.4867	.4783	.4702	.4623	.4547	.4474	.4403	.4334	.4267	.4202
	WWD	.4400	.4346	.4293	.4241	.4191	.4141	.4093	.4046	.4000	.3955	.3911
	WWW	.4224	.4172	.4121	.4071	.4023	.3975	.3929	.3884	.3840	.3796	.3754
2+1	MMM	.2731	.2683	.2637	.2593	.2550	.2509	.2469	.2430	.2392	.2356	.2320
	DDD	.3021	.2989	.2958	.2927	.2897	.2867	.2838	.2810	.2782	.2755	.2728
	DDW	.2970	.2939	.2908	.2877	.2848	.2819	.2790	.2762	.2735	.2708	.2682
	WWD	.2582	.2559	.2537	.2515	.2493	.2472	.2452	.2431	.2411	.2391	.2372
	WWW	.2531	.2508	.2487	.2465	.2444	.2423	.2403	.2383	.2363	.2344	.2325
3+1	MMM	.1938	.1910	.1883	.1857	.1832	.1807	.1782	.1759	.1736	.1714	.1692
	DDD	.2090	.2079	.2067	.2056	.2044	.2033	.2022	.2011	.2000	.1989	.1979
	DDW	.2073	.2061	.2049	.2038	.2027	.2016	.2005	.1994	.1983	.1972	.1962
	WWD	.1824	.1813	.1801	.1790	.1779	.1769	.1758	.1747	.1737	.1727	.1716
	WWW	.1806	.1795	.1784	.1773	.1762	.1751	.1741	.1730	.1720	.1710	.1700

if $1.5 \le \mathrm{E}(Z) \le 2.0$;

$$Av(\mathrm{DDD}) > Av(\mathrm{DDW}) > Av(\mathrm{MMM}) > Av(\mathrm{WWD}) > Av(\mathrm{WWW})$$

if $2.5 \le \mathrm{E}(Z) \le 5.0$.

Table 5, 7, and 9 show the effect of p, $\mathrm{E}(X)$, and $\mathrm{E}(Y)$, respectively, on the steady-state availability when λ, δ, and $\mathrm{E}(Z)$ are small: $\lambda = 0.2$, $\delta = 0.2$, and $\mathrm{E}(Z) = 0.2$. Under our numerical environments given in Case 4, 6, and 8, we find that:

$$Av(\mathrm{DDD}) > Av(\mathrm{DDW}) > Av(\mathrm{WWD}) > Av(\mathrm{WWW}) > Av(\mathrm{MMM}).$$

Table 6, 8, and 10 show theeffect of p, $\mathrm{E}(X)$, and $\mathrm{E}(Y)$, respectively, on the steady-state availability when λ, δ, and $\mathrm{E}(Z)$ are large: $\lambda = 0.7$, $\delta = 0.7$, and $\mathrm{E}(Z) = 4$. Under our numerical environments given in Case 5, we find the followings:

For the $1+1$ model:

$$Av(\mathrm{DDD}) > Av(\mathrm{DDW}) > Av(\mathrm{WWD}) > Av(\mathrm{WWW}) > Av(\mathrm{MMM})$$

if $p \ge 0.9$;

$$Av(\mathrm{DDD}) > Av(\mathrm{DDW}) > Av(\mathrm{WWD}) > Av(\mathrm{MMM}) > Av(\mathrm{WWW})$$

if $0.3 \le p \le 0.8$;

Table 7. Steady state availability versus E*(X) for Case 6*

E(X)		1.0	1.5	2.0	2.5	3.0	3.5	4.0	4.5	5.0
1 + 1	MMM	.9551	.9164	.8734	.8291	.7855	.7436	.7040	.6671	.6327
	DDD	.9710	.9562	.9417	.9266	.9108	.8942	.8767	.8584	.8393
	DDW	.9710	.9562	.9417	.9266	.9108	.8942	.8767	.8584	.8393
	WWD	.9652	.9339	.8972	.8577	.8172	.7770	.7380	.7007	.6654
	WWW	.9652	.9338	.8972	.8576	.8171	.7770	.7380	.7007	.6654
2 + 1	MMM	.8804	.7957	.7156	.6445	.5830	.5302	.4849	.4458	.4120
	DDD	.9194	.8754	.8302	.7835	.7360	.6883	.6413	.5957	.5522
	DDW	.9193	.8752	.8301	.7834	.7359	.6882	.6412	.5956	.5521
	WWD	.9036	.8266	.7487	.6763	.6117	.5552	.5062	.4638	.4270
	WWW	.9034	.8264	.7486	.6762	.6116	.5551	.5061	.4637	.4270
3 + 1	MMM	.7998	.6842	.5885	.5119	.4506	.4012	.3608	.3273	.2992
	DDD	.8560	.7786	.7027	.6300	.5623	.5011	.4468	.3996	.3589
	DDW	.8557	.7784	.7025	.6298	.5622	.5009	.4467	.3995	.3588
	WWD	.8312	.7174	.6175	.5353	.4687	.4148	.3709	.3346	.3044
	WWW	.8309	.7171	.6173	.5351	.4685	.4147	.3707	.3345	.3043

Table 8. Steady state availability versus E*(X) for Case 7*

E(X)		1.0	1.5	2.0	2.5	3.0	3.5	4.0	4.5	5.0
1 + 1	MMM	.4409	.3223	.2531	.2081	.1765	.1531	.1352	.1210	.1095
	DDD	.5033	.3890	.3149	.2614	.2211	.1900	.1655	.1461	.1304
	DDW	.4867	.3775	.3059	.2541	.2149	.1846	.1608	.1418	.1266
	WWD	.4346	.2999	.2267	.1815	.1511	.1294	.1131	.1004	.0903
	WWW	.4172	.2876	.2172	.1738	.1447	.1239	.1082	.0961	.0864
2 + 1	MMM	.2683	.1874	.1435	.1161	.0974	.0839	.0737	.0656	.0592
	DDD	.2989	.2127	.1621	.1297	.1076	.0919	.0802	.0711	.0639
	DDW	.2939	.2092	.1595	.1276	.1059	.0904	.0788	.0699	.0629
	WWD	.2559	.1727	.1297	.1037	.0864	.0740	.0647	.0575	.0517
	WWW	.2508	.1692	.1271	.1016	.0846	.0725	.0634	.0563	.0507
3 + 1	MMM	.1910	.1311	.0995	.0801	.0670	.0576	.0505	.0449	.0405
	DDD	.2079	.1425	.1071	.0855	.0711	.0609	.0533	.0473	.0426
	DDW	.2061	.1413	.1062	.0848	.0705	.0604	.0528	.0469	.0422
	WWD	.1813	.1216	.0913	.0730	.0608	.0521	.0456	.0405	.0365
	WWW	.1795	.1204	.0904	.0723	.0602	.0516	.0451	.0401	.0361

$Av(\mathrm{DDD}) > Av(\mathrm{DDW}) > Av(\mathrm{MMM}) > Av(\mathrm{WWD}) > Av(\mathrm{WWW})$
if $p \le 0.2$.

For the $2+1$ model:

$Av(\mathrm{DDD}) > Av(\mathrm{DDW}) > Av(\mathrm{WWD}) > Av(\mathrm{WWW}) > Av(\mathrm{MMM})$
if p=1.0;
$Av(\mathrm{DDD}) > Av(\mathrm{DDW}) > Av(\mathrm{WWD}) > Av(\mathrm{MMM}) > Av(\mathrm{WWW})$
if $0.7 \le p \le 0.9$;
$Av(\mathrm{DDD}) > Av(\mathrm{DDW}) > Av(\mathrm{MMM}) > Av(\mathrm{WWD}) > Av(\mathrm{WWW})$
if $p \le 0.6$.

For the $3+1$ model:

$Av(\mathrm{DDD}) > Av(\mathrm{DDW}) > Av(\mathrm{WWD}) > Av(\mathrm{WWW}) > Av(\mathrm{MMM})$
if p=1.0;
$Av(\mathrm{DDD}) > Av(\mathrm{DDW}) > Av(\mathrm{WWD}) > Av(\mathrm{MMM}) > Av(\mathrm{WWW})$
if $0.8 \le p \le 0.9$;
$Av(\mathrm{DDD}) > Av(\mathrm{DDW}) > Av(\mathrm{MMM}) > Av(\mathrm{WWD}) > Av(\mathrm{WWW})$
if $p \le 0.7$.

Under our numerical environments given in Case 7 and 9, we find that:

$Av(\mathrm{DDD}) > Av(\mathrm{DDW}) > Av(\mathrm{MMM}) > Av(\mathrm{WWD}) > Av(\mathrm{WWW})$.

Table 9. Steady state availability versus E*(Y) for Case 8*

E(Y)		0.1	0.2	0.3	0.4	0.5	0.6	0.7	0.8	0.9	1.0
1+1	MMM	.9612	.9597	.9581	.9566	.9551	.9536	.9521	.9506	.9491	.9476
	DDD	.9772	.9757	.9741	.9726	.9710	.9695	.9680	.9665	.9649	.9634
	DDW	.9772	.9756	.9741	.9725	.9710	.9695	.9679	.9664	.9649	.9634
	WWD	.9713	.9698	.9683	.9667	.9652	.9637	.9622	.9607	.9591	.9576
	WWW	.9713	.9698	.9682	.9667	.9652	.9636	.9621	.9606	.9591	.9576
2+1	MMM	.8894	.8871	.8849	.8827	.8804	.8783	.8761	.8739	.8717	.8696
	DDD	.9285	.9262	.9240	.9217	.9194	.9172	.9150	.9128	.9106	.9084
	DDW	.9284	.9261	.9238	.9215	.9193	.9171	.9148	.9126	.9104	.9082
	WWD	.9125	.9103	.9080	.9058	.9036	.9014	.8992	.8970	.8948	.8927
	WWW	.9124	.9101	.9079	.9057	.9034	.9012	.8990	.8968	.8947	.8925
3+1	MMM	.8095	.8070	.8046	.8022	.7998	.7975	.7951	.7928	.7904	.7881
	DDD	.8656	.8632	.8608	.8584	.8560	.8536	.8513	.8489	.8466	.8443
	DDW	.8653	.8629	.8605	.8581	.8557	.8533	.8510	.8486	.8463	.8440
	WWD	.8407	.8383	.8359	.8335	.8312	.8288	.8265	.8242	.8219	.8196
	WWW	.8404	.8380	.8356	.8332	.8309	.8285	.8262	.8239	.8216	.8193

Table 10. Steady state availability versus E*(Y) for Case 9*

		0.1	0.2	0.3	0.4	0.5	0.6	0.7	0.8	0.9	1.0
1+1	MMM	.4482	.4464	.4445	.4427	.4409	.4391	.4374	.4356	.4339	.4322
	DDD	.5105	.5086	.5068	.5050	.5033	.5015	.4998	.4980	.4963	.4946
	DDW	.4937	.4919	.4902	.4884	.4867	.4850	.4833	.4816	.4800	.4783
	WWD	.4389	.4379	.4368	.4357	.4346	.4335	.4325	.4314	.4303	.4293
	WWW	.4214	.4203	.4193	.4182	.4172	.4162	.4151	.4141	.4131	.4121
2+1	MMM	.2721	.2711	.2702	.2692	.2683	.2674	.2665	.2655	.2646	.2637
	DDD	.3015	.3008	.3002	.2995	.2989	.2983	.2976	.2970	.2964	.2958
	DDW	.2964	.2958	.2951	.2945	.2939	.2932	.2926	.2920	.2914	.2908
	WWD	.2577	.2573	.2568	.2564	.2559	.2555	.2550	.2546	.2541	.2537
	WWW	.2526	.2522	.2517	.2513	.2508	.2504	.2500	.2495	.2491	.2487
3+1	MMM	.1933	.1927	.1921	.1916	.1910	.1905	.1900	.1894	.1889	.1883
	DDD	.2088	.2086	.2083	.2081	.2079	.2076	.2074	.2072	.2069	.2067
	DDW	.2070	.2068	.2066	.2063	.2061	.2059	.2056	.2054	.2052	.2049
	WWD	.1822	.1819	.1817	.1815	.1813	.1810	.1808	.1806	.1804	.1801
	WWW	.1804	.1802	.1799	.1797	.1795	.1793	.1790	.1788	.1786	.1784

As expected, we also find in the tables that $Av_{1+1}>Av_{2+1}>Av_{3+1}$ for all parameter values given in Case 1–9.

4. Conclusions

By using supplementary variables and integro-differential equations, we have obtained the analytical expression of the steady-state availability for series redundancy model with imperfect switchovers, generally distributed repair times, and interrupted repairs. Numerical examples have been provided for 1+1, 2+1, and 3+1 models.

The drawback of this paper is to focus only on computing steady-state availability due to non-Markovian assumptions. Although the study of steady-state availability is important to understand the characteristics of redundancy models, it is more interesting to have the system availability at any time than steady state availability. However, it is difficult to obtain a transient solution in explicit form for system availability of the N+1 model because of complex structure due to non-Markovian assumptions. The analysis considering transient availability may constitute a challenging research topic and draw research interests. Steady-state analysis for availability of N+M redundancy models with more than one standby component is also not an easy task. Further studies are necessary in order to obtain the transient availability of N+M redundancy models.

Acknowledgement

This work was partially supported by the ICT R&D program of MSIP/IITP [R0101-16-0070, Development of The High Availability Network Operating System for Supporting NonStop Active Routing] and by Basic Science Research Program through the National Research Foundation of Korea(NRF) funded by the Ministry of Education (2017R1A2B1009504).

References

1. Ambuj G, Stephen L. Modeling and analysis of computer system availability. IBM Journal of Research and Development 1987; 31(6): 651-664, https://doi.org/10.1147/rd.316.0651.
2. Bosse S, Splieth M, Turowski K. Multi-objective optimization of IT service availability and costs. Reliability Engineering and System Safety 2016; 147: 142-155, https://doi.org/10.1016/j.ress.2015.11.004.
3. Hsu Y L, Ke J C, Liu T H, Wu C H. Modeling of multi-server repair problem with switching failure and reboot delay and related profit analysis. Comput. Ind. Eng. 2014; 69: 21-28, https://doi.org/10.1016/j.cie.2013.12.003.
4. Huawei. Planning Guide: iManager U2000 Unified Network Management System, Huawei Technologies Co., Ltd. 2010.
5. Kadyan M S. Reliability and profit analysis of a single-unit system with preventive maintenance subject to maximum operation time. Eksploatacja i Niezawodnosc – Maintenance and Reliability 2013;5(2):176-181.
6. Kanso A, Khendek F, Mishra A, Toeroe M. Integrating legacy applications for high availability: a case study. Proc. 13th IEEE International Symposium on High-Assurance Systems Engineering 2011; 83-90, https://doi.org/10.1109/HASE.2011.39.
7. Ke J B, Chen J W, Wang K H. Reliability measures of a repairable system with standby switching failures and reboot delay. Qual. Technol. Quant. Manag. 2011; 8(1): 15-26, https://doi.org/10.1080/16843703.2011.11673243.
8. Ke J C, Lin C H. A Markov repairable system involving an imperfect service station with multiple vacations. Asia-Pacific Journal of Operational Research 2005; 22(4): 555-582, https://doi.org/10.1142/S021759590500073X.
9. Kim D, Shim J, Ryu H, Lee Y. Networking service availability analysis of 2N redundancy model with non-stop forwarding. Lecture Notes in Electrical Engineering 2015; 339: 1063-1069, https://doi.org/10.1007/978-3-662-46578-3_126.
10. Kuo C C, Ke J C. Comparative analysis of standby systems with unreliable server and switching failure. Reliability Engineering and System Safety 2016; 145: 74-82, https://doi.org/10.1016/j.ress.2015.09.001.
11. Kuznetsov N Y. Evaluation of the reliability of repairable (s-t) networks by fast simulation method. Journal of Automation and Information Sciences 2014; 46(5): 1-14, https://doi.org/10.1615/JAutomatInfScien.v46.i5.10.
12. Lee Y. Availability analysis of redundancy model with generally distributed repair time, imperfect switchover, and interrupted repair. Electronics Letters 2016; 52(22): 1851-1853, https://doi.org/10.1049/el.2016.2114.
13. Lee Y. Comments on "Comparative analysis of standby systems with unreliable server and switching failure"[RelibEngSystSaf 2016; 145: 74–82]. Reliability Engineering and System Safety 2017; 160: 98-100, https://doi.org/10.1016/j.ress.2016.11.005.
14. Lewis E E. Introduction to Reliability Engineering, John Wiley & Sons, New York, 1996.
15. Marks H. Specifying Servers based on Needs and Growth. [IN:] Gilbert H.(ed.) Server Management, Auerbach, 1996.
16. OpenSAF foundation, http://www.opensaf.org, accessed Sep. 9. 2016.
17. Piotrowski J A, Randolph W T. Robotic Welding: A Guide to Selection and Application, Robotics International of SME, Publications Development Dept., 1987.
18. Sadjadi S J, Soltani R. Minimum-maximum regret redundancy allocation with the choice of redundancy strategy and multiple choice of component type under uncertainty. Comput. Ind. Eng. 2015; 79: 204-213, https://doi.org/10.1016/j.cie.2014.10.021.
19. Schedule automatic website backups. https://backup-guard.com/.
20. Toeroe M, Tam F. Service Availability: Principles and Practice, John Wiley & Sons, 2012, https://doi.org/10.1002/9781119941378.
21. Veeramany A. Multi-State Reliability Analysis of Nuclear Power Plant Systems, Ph.D. Thesis, University of Waterloo, 2012.
22. Wang K H, Dong W L, Ke J B. Comparison of reliability and the availability between four systems with warm standby components and standby switching failures. Appl. Math. Comput. 2006; 183: 1310-1322, https://doi.org/10.1016/j.amc.2006.05.161.
23. Wang K H Ke J C. Probabilistic analysis of a repairable system with warm standbys plus balking and reneging. Applied Mathematical Modelling 2003; 27: 327-336, https://doi.org/10.1016/S0307-904X(02)00133-6.
24. Wang K H, Sivazlian B D. Reliability of a system with warm standbys and repairmen. Microelectronic and Reliability 1989; 29: 849-860, https://doi.org/10.1016/0026-2714(89)90184-4.
25. Wood A. Availability modeling. IEEE Circuits and Devices Magazine 1994; 10(3): 22-27, https://doi.org/10.1109/101.283651.
26. Zhang Y, Wu W, Tang Y. Analysis of a k-out-of- n: G system with repairman's single vacation and shut off rule. Operations Research Perspectives 2017; 4: 29–38, https://doi.org/10.1016/j.orp.2017.02.002.
27. Zhou Y, Zhang Z. Optimal maintenance of a series production system with two multi-component subsystems and an intermediate buffer. Eksploatacja i Niezawodnosc – Maintenance and Reliability 2015;17(2): 314–325, https://doi.org/10.17531/ein.2015.2.20.

Jaechan SHIM
Hoyong RYU
Hyper-connected Communication Research Laboratory
Electronics and Telecommunications Research Institute
Daejeon 34129, Republic of Korea

Yutae LEE
Department of Information and Communications Engineering
Dongeui University
176 Eomgwangno, Busanjin, Busan 47340, Republic of Korea

E-mail: jcshim@etri.re.kr, hyryu@etri.re.kr, ylee@deu.ac.kr

Article citation info:
FUQING Y, BARABADI A, JINMEI L. Reliability modelling on two-dimensional life data using bivariate weibull distribution: with case study of truck in mines. Eksploatacja i Niezawodnosc – Maintenance and Reliability 2017; 19 (4): 650–659, http://dx.doi.org/10.17531/ein.2017.4.20.

Yuan FUQING
Abbas BARABADI
Lu JINMEI

RELIABILITY MODELLING ON TWO-DIMENSIONAL LIFE DATA USING BIVARIATE WEIBULL DISTRIBUTION: WITH CASE STUDY OF TRUCK IN MINES

MODELOWANIE NIEZAWODNOŚCIOWE DWUWYMIAROWYCH DANYCH DOTYCZĄCYCH OKRESU EKSPLOATACJI Z WYKORZYSTANIEM DWUWYMIAROWEGO ROZKŁADU WEIBULLA. Z BADAŃ NAD WYWROTKAMI KOPALNIANYMI

An engineering system can exhibit two- or multi-dimensions in its lifetime. As the classical univariate distribution cannot model this multi-dimensional characteristic, it is necessary to extend it to multivariate distribution in order to capture the multi-dimensional characteristics. This paper proposes a bivariate Weibull distribution that combines two classical Weibull models by a common exponent. The common exponent can represent the correlation between the two dimensions. A ratio likelihood test is proposed to test the significance of the correlation between the two dimensions. To solve the parameter estimation problem, this paper suggests a Bayesian method. Moreover, a goodness of fit test method is developed to visually check the fitness of the model. A case study considering mining trucks is presented to apply the bivariate Weibull distribution to model the two-dimensional life data.

Keywords: *bivariate Weibull; life data; reliability modelling; Bayesian method; mining truck.*

Systemy inżynieryjne można charakteryzować za pomocą dwóch lub więcej wymiarów dotyczących okresu ich eksploatacji (np. przebieg i czas pracy pojazdu). Ponieważ klasyczny rozkład jednowymiarowy nie wystarcza do zamodelowania tej wielowymiarowej charakterystyki, konieczne jest wykorzystanie rozkładu wielowymiarowego, który pozwala uchwycić wielowymiarowość cyklu życia systemu. W artykule zaproponowano dwuwymiarowy rozkład Weibulla, który łączy w sobie dwa klasyczne modele Weibulla za pomocą wspólnego wykładnika. Wspólny wykładnik może reprezentować korelację między dwoma wymiarami. Zaproponowano test ilorazu wiarygodności, który umożliwia badanie istotności korelacji pomiędzy dwoma wymiarami. Do rozwiązania problemu estymacji parametrów zastosowano metodę bayesowską. Ponadto opracowano metodę badania dopasowania modelu do danych empirycznych służącą do wizualizacji dopasowania modelu. Przedstawiono studium przypadku dotyczące wywrotek kopalnianych, w którym dwuwymiarowy rozkład Weibulla zastosowano do modelowania dwuwymiarowych danych dotyczących okresu eksploatacji tych pojazdów.

Słowa kluczowe: *dwuwymiarowy rozkład Weibulla; dane z okresu eksploatacji; modelowanie niezawodności; metoda Bayesa; wywrotka kopalniana.*

1. Introduction

It is not rare for engineering systems exhibiting binary- or even multi-dimensional lifetimes. The life of an airplane can be described by both calendar time and the total flight hours; the life of rail track life can be described according to both age and the total gross load it has carried [2], while an automobile's usage also corresponds with calendar time and distance travelled [12]. Binary-dimensional or multi-dimensional failure times are also practical when a system comprises several dependent components. For example, for the railway bogie, the failures of a wheel, an axle or a spring are essentially dependent on each other. The reliability of the bogie should address the dependency of the load, torque or other mechanic measurement on each other. Each measurement is a dimension corresponding to the lifetime. Multi-dimensional distribution is also practical when a system has multiple dependent failure modes. Each failure mode corresponds one dimension in the lifetime.

Classic life-data analysis in reliability considers only one dimension [4, 24, 26, 28]. A typical example is Weibull analysis, which considers time as the sole variate. The covariate-based model, such as the Proportional Hazard Model (PHM), can accommodate multi-dimensional variates to some extend [3, 7, 14, 15]. The main dimension, usually calendar time, is in the baseline function. The other dimensions are accommodated in the covariate function. However, covariates are not one dimension of the distribution. The PHM is essentially a one-dimensional model.

It is thus necessary to develop multivariate lifetime distribution model, applicable for reliability analysis. In the desired multi-dimensional model, each dimension of the lifetime is considered equal, instead of as covariate as in the PHM model. In order to apply the model to reliability analysis, the corresponding parameter estimation and goodness of fit test method should also be proposed. This paper is organized as follows: Section 2 presents the literature survey and discusses some properties of the bivariate Weibull model concerned with reliability. Section 3 presents the methods for parameter estimation and the reliability evaluation, while Section 4 discusses the case of the mining transportation truck and the application of the Bivariate Weibull model to the case. Finally, Section 5 presents the discussion and conclusion of the paper.

2. Bivariate Weibull model

Weibull distribution can characterize an increasing, decreasing and constant failure rate. The desirable bivariate distribution is designated to retain this advantage.

2.1. Bivariate Distribution Model

Various state-of-the-art bivariate distributions have been developed. Copula models are some of them. The Copula model uses a copula function to connect two or more cumulative distribution functions [27]. For different Copula functions and cumulative distribution, there are the Gaussian Copula model, the Gumbel Copula model, the Frank Copula model, the Joe Copula model, etc. [8]. The Copula model can model the dependence of the multi-variant distribution and is especially suitable for mechanical system reliability analysis. However, Copula models require an explicit expression of the marginal distribution for each variate. For example, for the bivariate situation, suppose the marginal distribution is u and v. The Gumbel Copula function is defined as:

$$C(u,v;\theta)=\exp\left\{-\left[(-\ln u)^{\frac{1}{\theta}}+(-\ln v)^{\frac{1}{\theta}}\right]^{\theta}\right\} \tag{1}$$

The dependency of the two marginal distributions is contained in the Copula parameter θ. In the univariate distribution, the exponential and Weibull distributions are intensively investigated. It is preferable to have a bivariate distribution of exponential or Weibull forms. The bivariate distribution is designated to inherit the good properties from the univariate exponential or Weibull distribution. For most exponential or Weibull distribution-based bivariate distributions, in general, the cumulative density function of the bivariate distribution can be written in the form:

$$R(t,s)=\exp\left[-f(t,s)\right] \tag{2}$$

State-of-the-art models, with the bivariate Marshall-Olkin model being one of the most famous among them, differ in the definition of the function $f(t,s)$ [23]. The bivariate Marshall-Olkin model considers the two variates to be exponentially distributed. The two variates are competing to fail. The Marshall-Olkin takes the form:

$$R(t,s)=exp\left[-\lambda_1 \mathrm{t}-\lambda_2 \mathrm{s}-\lambda_0 \mathrm{Max}(\mathrm{t},\mathrm{s})\right]. \tag{3}$$

Hanagal (1996) extended Model (3) to bivariate or multivariate Weibull distribution by replacing the exponential distribution of (3) by Weibull distribution [6]:

$$R(t,s)=exp\left[-\alpha_1 t^{\mathrm{c}}-\alpha_2 s^{\mathrm{c}}-\alpha_3 Max(t,s)^{\mathrm{c}}\right]. \tag{4}$$

Ryu (1993) developed another bivariate Weibull distribution that extends the classical bivariate Marshall-Olkin. The model is as follows [32]:

$$R(t_1,t_2)=\begin{cases} exp\left[-\alpha_1 t_1^{\beta_1}-\alpha_{12}t_2-\alpha_2 t_2^{\beta_2}+\frac{\alpha_{12}}{\gamma_2}\left(1-e^{-\gamma_2(t_2-t_1)}\right)+\frac{\alpha_{12}}{\gamma_2-\gamma_1}\left(e^{-\gamma_2(t_2-t_1)}-e^{-\gamma_1 t_1-\gamma_2 t_2}\right)\right]; t_1\le t_2 \\ exp\left[-\alpha_1 t_1^{\beta_1}-\alpha_{12}t_1-\alpha_2 t_2^{\beta_2}+\frac{\alpha_{12}}{\gamma_1}\left(1-e^{-\gamma_2(t_2-t_1)}\right)+\frac{\alpha_{12}}{\gamma_2-\gamma_1}\left(e^{-\gamma_1(t_1-t_2)}-e^{-\gamma_1 t_1-\gamma_2 t_2}\right)\right]; t_1>t_2 \end{cases} \tag{5}$$

This model is much more complex than the model developed by Hanagal (1996), which complicates the parameter estimation. Other available models such as the Nataf model, the 2D Nagao-Kadoya-Rice model and the Placket model are derived from univariate Weibull distribution [18]. These models are simpler than (5) but still have complex analytical expressions. We prefer the simple model with fewer parameters and a simple reliability function or probability density function. Roy (1994) developed another bivariate Weibull distribution with a simpler form of reliability function [30]:

$$R(t,s)=exp\left[-\alpha_1 t^{\beta_1}-\alpha_2 s^{\beta_2}-\alpha_3 t^{\beta_1}s^{\beta_2}\right]. \tag{6}$$

In that model, the dependence of two variates is described by the term $\alpha_3 x^{\beta_1} y^{\beta_2}$. Hougaard (1986), Lu and Bhattacharyya (1990) and Joy (1998) developed a bivariate Weibull model by combining the two bivariates by means of a common exponent [10, 17, 20, 31, 34]. This model is simple, and it can be derived from physical model:

$$\frac{\partial h(s,t)}{\partial t}=\gamma^2\alpha_1^{-2}\beta_1(\beta_1-1)\left(\frac{t}{\alpha_1}\right)^{\beta_1-2}\alpha_2^{-1}\beta_2\left(\frac{s}{\alpha_2}\right)^{\beta_2-1}\left[\left(\frac{t}{\alpha_1}\right)^{\beta_1}+(s/\alpha_2)^{\beta_2}\right]^{\gamma-2}\left\{\frac{1}{\gamma}-1+\left[\left(\frac{t}{\alpha_1}\right)^{\beta_1}+(s/\alpha_2)^{\beta_2}\right]^{\gamma}\right\}+$$
$$\gamma^2\alpha_1^{-1}\beta_1\left(\frac{t}{\alpha_1}\right)^{\beta_1-1}\alpha_2^{-1}\beta_2\left(\frac{s}{\alpha_2}\right)^{\beta_2-1}\left\{\left(\frac{1}{\gamma}-1\right)(\gamma-2)\alpha_1^{-1}\beta_1\left(\frac{t}{\alpha_1}\right)^{\beta_1-1}\left[\left(\frac{t}{\alpha_1}\right)^{\beta_1}+(s/\alpha_2)^{\beta_2}\right]^{\gamma-3}+(2\gamma-2)\alpha_1^{-1}\beta_1\left(\frac{t}{\alpha_1}\right)^{\beta_1-1}\left[(t/\alpha_1)^{\beta_1}+(s/\alpha_2)^{\beta_2}\right]^{2\gamma-3}\right\} \tag{7}$$

This paper follows Model (7), but with a slight modification. This bivariate Weibull model considered by this paper is of this form:

$$R(t,s)=exp\left[-\left(\alpha_1 t^{\beta_1}+\alpha_2 s^{\beta_2}\right)^{\gamma}\right]. \tag{8}$$

The same model as (8) is also shown in [10, 17]. The model is the simplest state-of-the-art model for bivariate Weibull distribution derived from univariate Weibull distribution. This paper uses this model due to its simplicity.

2.2. Bivariate hazard function

In the case of a univariate case, for example where only time is under consideration, the hazard function describes the conditional probability that a system will fail per time unit, given that the system has survived until time t. Provided the failure distribution function is first-order continuous, the hazard function can be defined as:

$$\mathrm{r}(t)=\frac{\lim\limits_{\Delta t\to 0}\frac{F(t+\Delta t)-F(t)}{\Delta t}}{R(t)}=\frac{f(t)}{R(t)} \tag{9}$$

Extending (9), we can derive the hazard function of the bivariate case as:

$$\mathrm{r}(t,s)=\frac{\lim\limits_{\substack{\Delta t\to 0\\ \Delta s\to 0}}\frac{F(t+\Delta t,s+\Delta s)-F(t,s)}{\Delta t\Delta s}}{R(t,s)}=\frac{\partial F(t,s)/\partial t+\partial F(t,s)/\partial s}{R(t,s)} \tag{10}$$

This formula implies the bivariate failure rate and its distribution function can be converted from each other. For the univariate case, a simple and flexible hazard function is of the power form $\Lambda(t)=\int r(t)\,dt=(t/\alpha)^{\beta-1}$). This is the hazard function of the two-parameter Weibull distribution. This form can describe a monotonically increasing, decreasing and constant hazard function. This monotonicity

describes the physical characteristics of the system. The desired hazard function of model (8) for bivariate-dimensional distribution also retains this advantage. This cumulative hazard function of model (8) is a combination of the cumulative hazard function of the two variates:

$$B = (t/\alpha_1)^{\beta_1} + (s/\alpha_2)^{\beta_2} \tag{11}$$

where $\gamma>0$; $\alpha_1, \alpha_2 \geq 0$; $\beta_1, \beta_2 \geq 0$; $\alpha_1, \alpha_2, \beta_1, \beta_2, \gamma \in R$, and α_1, α_2 cannot both be zero. This condition ensures the $\lim_{\substack{t\to\infty \\ s\to\infty}} r(t,s) = +\infty$. Equation (11) is the desired cumulative hazard function of binary Weibull distribution. The cumulative hazard function is linear when all shape parameters and γ are equal to 1. For simplicity of notation, we let $B = (t/\alpha_1)^{\beta_1} + (s/\alpha_2)^{\beta_2}$.

This (11) is similar but simplifies the cumulative hazard function described by Lu and Hougaard [9-11, 20]. This model implicitly assumes the two variates s and t are influenced by the unknown common factor γ The variates t and s are independent only when γ =1. By binomial series expansion, Equation (11) expands into a series as:

$$\Lambda(t,s) = (t/\alpha_1)^{\beta_1} + \gamma(s/\alpha_2)^{\beta_2} + \frac{\gamma(\gamma-1)}{2!}(t/\alpha_1)^{\beta_1}.(s/\alpha_2)^{\beta_2} + \frac{\gamma(\gamma-1)(\gamma-2)}{3!}\frac{\left((s/\alpha_2)^{\beta_2}\right)^3}{\left((t/\alpha_1)^{\beta_1}\right)^2}\ldots.. \tag{12}$$

when $(s/\alpha_2)^{\beta_2} < (t/\alpha_1)^{\beta_1}$. Equation (12) reveals that Model (11) degenerates into a linear model where variates s and t are independent. Model (6) is also a special case of (11). Model (6) only considers the first three terms of (11). It is also revealed from (11) that, when γ<1, Model (11) is nonlinear and the interaction of s and t are considered.

The reliability function corresponding to hazard function (11) is $R = \exp[-\Lambda(t,s)]$. The corresponding probability density function (PDF) is:

$$f(s,t) = \gamma^2\alpha_1^{-1}\beta_1(t/\alpha_1)^{\beta_1-1}\alpha_2^{-1}\beta_2(s/\alpha_2)^{\beta_2-1}\left[(t/\alpha_1)^{\beta_1} + (s/\alpha_2)^{\beta_2}\right]^{\gamma-2}\left\{1/\gamma - 1 + \left[(t/\alpha_1)^{\beta_1} + \right.\right.$$
$$\left.\left. + (s/\alpha_2)^{\beta_2}\right]^{\gamma}\right\}\exp\left(-\left[(t/\alpha_1)^{\beta_1} + (s/\alpha_2)^{\beta_2}\right]^{\gamma}\right) \tag{13}$$

As $\gamma \in (0,1]$ $\gamma \in (0,1]$, the $f(s,t)f(s,t)$ is positive, which ensures (13) is a legitimate PDF function. The corresponding hazard function is:

$$h(s,t) = \frac{f(t)}{R(t)} = \gamma^2\alpha_1^{-1}\beta_1(t/\alpha_1)^{\beta_1-1}\alpha_2^{-1}\beta_2(s/\alpha_2)^{\beta_2-1}\left[(t/\alpha_1)^{\beta_1} + (s/\alpha_2)^{\beta_2}\right]^{\gamma-2}\left\{1/\gamma - 1 + \left[(t/\alpha_1)^{\beta_1} + (s/\alpha_2)^{\beta_2}\right]^{\gamma}\right\} \tag{14}$$

as:

$$\frac{\partial h(s,t)}{\partial t} = \gamma^2\alpha_1^{-2}\beta_1(\beta_1-1)\left(\frac{t}{\alpha_1}\right)^{\beta_1-2}\alpha_2^{-1}\beta_2\left(\frac{s}{\alpha_2}\right)^{\beta_2-1}\left[\left(\frac{t}{\alpha_1}\right)^{\beta_1} + (s/\alpha_2)^{\beta_2}\right]^{\gamma-2}\left\{\frac{1}{\gamma} - 1 + \left[\left(\frac{t}{\alpha_1}\right)^{\beta_1} + (s/\alpha_2)^{\beta_2}\right]^{\gamma}\right\} +$$
$$\gamma^2\alpha_1^{-1}\beta_1\left(\frac{t}{\alpha_1}\right)^{\beta_1-1}\alpha_2^{-1}\beta_2\left(\frac{s}{\alpha_2}\right)^{\beta_2-1}\left\{\left(\frac{1}{\gamma} - 1\right)(\gamma-2)\alpha_1^{-1}\beta_1\left(\frac{t}{\alpha_1}\right)^{\beta_1-1}\left[\left(\frac{t}{\alpha_1}\right)^{\beta_1} + (s/\alpha_2)^{\beta_2}\right]^{\gamma-3} + (2\gamma-2)\alpha_1^{-1}\beta_1\left(\frac{t}{\alpha_1}\right)^{\beta_1-1}\left[(t/\alpha_1)^{\beta_1} + (s/\alpha_2)^{\beta_2}\right]^{2\gamma}\right. \tag{15}$$

as: $0 < \gamma \leq 1$, when:

$$\begin{cases} \beta_1 = 1; \dfrac{\partial h(s,t)}{\partial t} \neq 0 \\ \beta_1 > 1; \dfrac{\partial h(s,t)}{\partial t} \text{ is not monotonic} \\ 0 < \beta_1 < 1; \dfrac{\partial h(s,t)}{\partial t} < 0 \end{cases} \tag{16}$$

A similar situation is for $\frac{\partial h(s,t)}{\partial s}$. The (16) reveals a weakness of Model (8): the failure rate is not always monotonic. When $\beta_1 = 1$, the hazard function for the bivariate Weibull is not the constant. Some desired properties for the univariate Weibull has not retained in the multi-dimensional model.

3. Parameter estimation of bivariate Weibull model

The bivariate Weibull model should overcome the parameter estimation issue in order for it to be applied to reliability. This section firstly derives the likelihood function of the bivariate model. This likelihood function will be used for parameter estimation and for optimal model selection among various bivariate models.

3.1. Likelihood function

When observed failure data are given as pairwise (s_i, t_i) $i = 1,2,..$, the likelihood function corresponding to (13) is:

$$L = \prod_{i=1}^{n} f(s_i, t_i) \tag{17}$$

The marginal distributions are $R(s,0) = \exp(-(s/\alpha_1)^{\gamma\beta_1})$ and $R(0,t) = \exp(-(t/\alpha_2)^{\gamma\beta_2})$, where the model have degenerated into two univariate Weibull distributions.

$$\ln L = n\left(-\ln a_1 - \ln a_2 + 2\ln g + \ln b_1 + \ln b_2\right) + (b_1 - 1)\sum t_i / a_1 + (\beta_2 - 1)\sum s_i / \alpha_2 + (\gamma - 2)\sum \ln B_i + \sum \ln\left(1/\gamma - 1 + B_i^{\gamma}\right) - \sum B_i^{\gamma} \tag{18}$$

The maximum likelihood estimate method can be used to estimate the parameters. There are no explicit analytical solutions by maximizing (18). One has to resort to a numerical method to find a solution. This numerical computation is heavy to find the solution by maximizing (18). However, the computation can be simplified, as the likelihood function (17) has a special property: the maximum likelihood estimator of γ is unique when B_i is known. The proof is shown as follows. The computation can be simplified if the parameters in the two individual Weibull distributions are known.

Theory 1: The likelihood function in (17) has a unique global maximum when $B_i \geq 0$.

Proof: Rewrite (11) as B and we consider the B as a variable. The PDF corresponding to Model (8) can then be written as $f(B) = \gamma B^{\gamma-1}\exp\left(-B^{\gamma}\right)$. It is a continuous function for $B \in R$. A likelihood function can then be written as:

$$\ln L = f(\gamma) = n\ln\gamma + (\gamma - 1)\sum \ln B_i - \sum B_i^{\gamma}. \tag{19}$$

The function is continuous and has a second derivative as:

$$\frac{\partial^2 \ln L}{\partial \gamma^2} = -\left[\frac{n}{\gamma^2} + \sum B_i^{\gamma}\left(\ln B_i\right)^2\right] \tag{20}$$

Then $\frac{\partial^2 \ln L}{\partial \gamma^2} \leq 0$ when $B_i \geq 0$, i.e. the $\ln L$ is a concave function when $B_i \geq 0$. The local maximum will be the global maximum. The maximum likelihood estimate obtained by setting the first derivative to zero has a unique and global solution. This property facilitates the parameter estimation. Once the B_i is known, one can find the optimal γ.

3.2. Test the significance of correlation

When $\gamma = 1$, Model (8) degenerates to a classic competing model. The γ contains the information about correction between the two variates s,t. The likelihood ratio test can be used to test the significance of γ. The hypothesis is:

$$H_0 : \gamma = 1; H_1 : \gamma \neq 1 \tag{21}$$

The statistics for test $T = \frac{L_{\gamma \neq 1}}{L_{\gamma = 1}}$. The H_0 is accepted when the $\chi^2(1) \geq T$.

The PDF of (8) for $\gamma = 1$ degenerates into $f(s,t) = f(s).f(t)$, i.e. two independent univariate Weibull distributions. The likelihood function is then $L_{\gamma=1} = \max L(s).\max L(t)$. The significance test of γ can facilitate the parameter estimation. If γ is significantly near to 1, the two variates in (8) are considered as independent. One can hence estimate the parameters as univariate Weibull distributions for each dimension.

3.4. Bayesian parameter estimation

As there is no analytical solution to the parameter estimate problem for Model (8), using maximum likelihood estimate when the two variates are significantly correlated, only a numerical method is feasible. For this situation, alternatively, this paper proposes a Bayesian estimate method [5, 19, 25]. The Bayesian method considers the parameter as a random variable. The distribution of the random variable (prior distribution) should be specified. For the univariate Weibull model, when the shape parameter is known, Gamma distribution can be used as the prior distribution for the scale parameter [16]. However, practically, the shape parameter is unknown in a more general situation. This paper uses the general Gamma and Beta distribution as the prior distribution.

As $\alpha_1, \alpha_2, \beta_1, \beta_2$ >0, this paper assumes their prior distributions follow Gamma distribution. The γ is assumed to be Beta distribution since it is confined in (0,1). The case with $\gamma = 1$ can be considered separately. The full Bayesian expression is then:

$$\pi(\alpha_1, \alpha_2, \beta_1, \beta_2, \gamma | Data) \propto L(Data) \times \frac{1}{\Gamma(a_1) b_1^{a_1}} \alpha_1^{a_1 - 1} e^{-\frac{\alpha_1}{b_1}} \times \frac{1}{\Gamma(a_2) b_2^{a_2}} \alpha_1^{a_2 - 1} e^{-\frac{\alpha_2}{b_2}} \times \frac{1}{\Gamma(a_3) b_3^{a_3}} \beta_1^{a_3 - 1} e^{-\beta_1 / b_3} \times \frac{1}{\Gamma(a_4) b_4^{a_4}} \beta_2^{a_4 - 1} e^{-\beta_2 / b_4} \times \frac{\Gamma(a_5)}{\Gamma(a_5)\Gamma(b_5)} \gamma^{a_5 - 1} (1 - \gamma)^{b_5 - 1} \tag{22}$$

The $a_1, b_1, a_2, b_2, a_3, b_3, a_4, b_4$, a_5, b_5 are hyper-parameters for the corresponding distribution. When there is no expert information or no knowledge regarding the hyper-parameters, the uninformative uni-

form distribution can be used; that is the case in this paper. Alternatively, one can use Jeffreys' prior as prior distribution [1]. However, Jeffreys' prior requires the Fisher information matrix. For our model with five unknown parameters, the Fisher information matrix is complex. Therefore, Jeffreys' prior is not preferable. In order to obtain the posterior distribution of parameters, this papers uses the MCMC (Markov chain Monte Carlo) simulation method with Gibbs sampling [22]. The discussion on the computing method is ignored here, as it is not the main concern of this paper.

3.4. Reliability evaluation using Bayesian method

The reliability can be evaluated once the parameters in Model (8) are known. One advantage of the Bayesian method is that the distribution of the estimator is its posterior distribution. Reliability and its credible interval can be readily derived since each of the distributions of the parameters is known. The point reliability at time t, by integrating (8) and (22), is as follows:

$$\mathrm{R}(t,s)=\int_0^\infty e^{\left((t/\alpha_1)^{\beta_1}+\left(s/\alpha_2\right)^{\beta_2}\right)^{\gamma}}\pi\left(\alpha_1,\alpha_2,\beta_1,\beta_2,\gamma|Data\right)d\alpha_1 d\beta_1 d\alpha_2 d\beta_2 d\gamma \tag{23}$$

The corresponding credible interval for $\mathrm{R}(t,s)$ at significance level α is:

$$\int_0^{\theta_L} e^{\left((t/\alpha_1)^{\beta_1}+\left(s/\alpha_2\right)^{\beta_2}\right)^{\gamma}}\pi\left(\alpha_1,\alpha_2,\beta_1,\beta_2,\gamma|Data\right)d\alpha_1 d\beta_1 d\alpha_2 d\beta_2 d\gamma=\alpha/2$$
$$\int_0^{\theta_U} e^{\left((t/\alpha_1)^{\beta_1}+\left(s/\alpha_2\right)^{\beta_2}\right)^{\gamma}}\pi\left(\alpha_1,\alpha_2,\beta_1,\beta_2,\gamma|Data\right)d\alpha_1 d\beta_1 d\alpha_2 d\beta_2 d\gamma=1-\alpha/2 \tag{24}$$

where $\theta=f\left(\alpha_1,\beta_1,\alpha_2,\beta_2,\gamma\right)$. The lower and upper bound of $\mathrm{R}(t,s)$ given parameter θ is:

$$\mathrm{R}(t,s)=\left[\inf\left(R\left(t,s;\theta_L\right)\right),\sup\left(R\left(t,s;\theta_u\right)\right)\right] \tag{25}$$

It is hard to obtain the analytical expression of θ_L and θ_U. The (25) can be derived using the MCMC simulation method. The MCMC method is a standard method to find the solution in Bayesian analysis. One can refer to [21] for detail.

4. Case study

The case study addresses the reliability analysis of trucks at Jajarm Bauxite Mine in Iran. Jajarm Bauxite Mine is an open-pit mine, where the ore rock and waste is hauled by truck from the mine to the allocated deposition places. In this mine, the ore rock is diasporic bauxite and the waste is flysch, which is characterized by the rhythmic alternations of sandstone and fine-grained layers. The fine-grained layers contain siltstone, silty shales, clay shales, and, rarely, limestone beds or an ophiolitic mass may be found close to its margins. Based on the percentage of diaspora, ore rock is divided into three groups: Hard Bauxite (HB), Kaolin Bauxite (KB) and Shale Bauxite (SB). Waste and ore deposition are located in different places, at varying distances from the mine. The waste rock and ore rock depots are around 4 and 15 kilometres outside the mine pit, respectively. The trucks transfer the ore rock during the day shift, and, during the night shift, they work on the waste rock. This mine is the biggest bauxite mine in Iran, at a length of 11 kilometres. It is divided into 12 different sections, each section working independently with its own allocated trucks. Currently, two types of trucks work in this mine: truck Type A and Type B. The capacity of Type A is 14 tons and of Type B is 35 tons. The truck

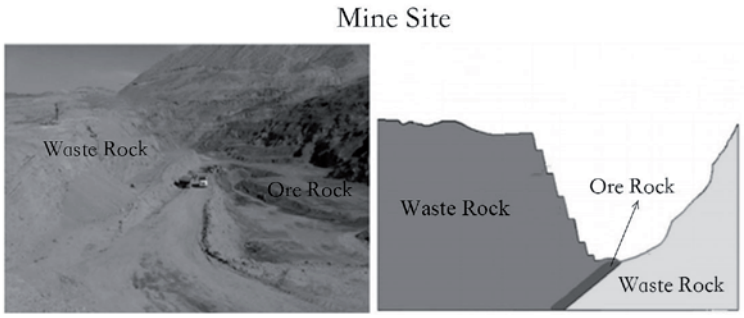

Fig. 1. Mining activities in Jajarm Bauxite Mines

drivers have, on average, 12 years' experience. The mine has its own repair shop, where all maintenance is carried out by mine employees. The mine follows the preventive maintenance plan recommended by the truck manufacturing company. Fig. 1 shows a picture and a geological section of Jajarm Bauxite Mine.

4.1. Data description

Data are collected from the maintenance database for two trucks. The database records the total tons carried by the trucks between two failure times. During operation, the trucks carry SB, KB, HB and waste. The travel distance from the original location to the destination varies for iron ore or waste, as they are located in different spots. This paper defines the product of tonnage and travelled distance in km, abbreviated as Tons×kM, as the work load, as the failure depends on both the tonnage and the distance travelled. After sorting out the data, the total number of failures observed for each truck is 49 and 32, respectively. Table 1 shows all the Time To Failure (TTFs) and the workload.

4.2. Fitting data to bivariate Weibull model

Considering TTF as one dimension (variate) and the workload as another dimension (variate), the bivariate Weibull models are used as reliability models. In order to compare the performance, this paper uses three models as the bivariate Weibull models: the simple bivariate Weibull model, where the two dimensions are independent; the model (6) in Section 2; and the desired model (8) also in Section 2.

4.2.1. Model 1: Simple bivariate Weibull model

The first model uses the simple model of cumulative hazard function, assuming γ=1 for $\Lambda(t,s)=\left((t/\alpha_1)^{\beta_1}+\left(s/\alpha_2\right)^{\beta_2}\right)^{\gamma}$. This implicitly assumes the two variates are independent of each other. We estimate the scale and shape parameters for the classical univariate Weibull distribution for each variate. The maximum likelihood method is used for each univariate Weibull distribution to estimate the parameters. The results are shown in Table 2.

4.2.2. Model 2: Linear bivariate Weibull model

Model (6) is also applied to analyse the data. In order to differentiate it from the other models, we name it the linear bivariate Weibull model. Let t in the bi-Weibull denote the calendar time and s denote the work load, Ton×kM. The probability density function for Model (6) is written as:

Table 1. Failure Data Collected from Field for Truck 1 and Truck 2

Truck 1			Truck 2		
No.	TTF (In hours)	Workload (Ton*km)	No.	TTF (In hours)	Workload (Ton*km)
1	18.55	2013	1	225.15	21997.8
2	31.15	3501.3	2	255.35	26485.8
3	67.05	6986.1	3	109.4	10840.5
4	10.4	1511.4	4	52.1	6754
5	26.55	2963.4	5	44.4	6664.9
6	292.5	29494.3	6	280.11	34886.5
7	10.3	1217.7	7	39.2	4527.6
8	20.4	2992	8	180.55	24619.1
9	101.15	10906.5	9	254.1	26753.1
10	85	6705.6	10	22.45	2821.5
11	46.05	5009.4	11	45.4	6695.7
12	266.29	31519.4	12	252.1	28967.4
13	21.3	5544	13	33.5	4664
14	35	3375.9	14	9.2	3483.7
15	11	1230.9	15	56.25	6496.6
16	243.15	26690.4	16	22.15	3465
17	120.55	13084.5	17	31.35	4048
18	34.1	5359.2	18	44.2	12698.4
19	42.05	4775.1	19	169.41	34491.6
20	136.35	16525.3	20	20.45	2079
21	10.2	2420	21	149.05	14813.7
22	19.3	10351	22	326.3	47537.6
23	22.15	10997.8	23	61.35	11809.6
24	61.15	6755.1	24	33.55	4818
25	28.45	3177.9	25	17.55	1570.8
26	39.45	4492.4	26	37.35	3036
27	29.15	3831.3	27	203.2	29823.2
28	2.1	653.4	28	97.55	11267.3
29	10.4	2051.5	29	110.25	16124.9
30	5	1100	30	45.25	6211.7
31	22.05	2607	31	86.45	13818.2
32	39.45	5643	32	85.1	18590
33	67.21	14032.7			
34	34.15	8911.1			
35	94.3	13212.1			
36	195.4	23562			
37	32.4	5984			
38	69.5	16434			
39	19.25	3410			
40	56.45	10609.5			
41	17.25	3421			
42	89.1	15446.2			
43	143.4	48605.7			
44	4.1	920.7			
45	3.2	742.5			
46	81.2	8434.8			
47	87	10611.7			
48	279.5	51966.2			
49	10.1	1007.6			

Table 2. Maximum Likelihood Estimator for γ=1

Truck	Variable	Parameter	Estimator	$-\ln L$	Total
Truck 1	Workload	α_1	9496	498.5	752
		β_1	0.96		
	Time	α_2	63.4	253.5	
		β_2	0.95		
Truck 2	Workload	α_1	15202	336.8	517.4
		β_1	1.2328		
	Time	α_2	112.97	180.6	
		β_2	1.1845		

$$f(t,s)=\left(\alpha_3\beta_1\beta_2 t^{\beta_1-1}s^{\beta_2-1}+\alpha_2\alpha_3\beta_1\beta_2 t^{\beta_1-1}s^{2\beta_2-1}+\alpha_1\alpha_3\beta_1\beta_2 t^{2\beta_1-1}s^{\beta_2-1}+\alpha_3^2\beta_1\beta_2 t^{2\beta_1-1}s^{2\beta_2-1}\right)exp\left[-\alpha_1 t^{\beta_1}-\alpha_2 s^{\beta_2}-\alpha_3 t^{\beta_1}s^{\beta_2}\right] \tag{26}$$

We apply the Bayesian method discussed in Section 3.3 to estimate the parameters. The prior distribution chooses the uniform distribution for the hyper parameters in the Gamma prior distribution. The MCMC method is applied to compute the posterior distribution. After 10,000 iterations, the results converge. The mean of the posterior distribution, which is also the Bayesian estimator of the model, is shown in Table 3.

Table 3. Bayesian Estimator for Linear Bivariate Model

Truck	Parameter	Estimator	$-\ln L$
Truck 1	α_1	4.61*10-4	713.4
	β_1	0.534	
	α_2	0.01387	
	β_2	0.5591	
	α_3	0.001233	
Truck 2	β_1	0.5853	
	α_2	0.01394	
	β_2	0.5893	
	α_3	5.608*10-4	

4.2.3. Model 3: Exponent bivariate Weibull model

Similarly to the linear bivariate Weibull model, the paper also let t in the bi-Weibull denote the calendar time and s denote the work load, Ton×kM in Model (8). The prior distribution chooses the Gamma distribution as prior. The results are shown in Table 4.

4.3. Model selection

When γ=1 for Model (8), two variates in the bivariate Weibull model are independent. The bivariate Weibull model is degenerated into two ordinary univariate Weibull models, and the classic parameter estimation for univariate Weibull distribution can be used. Section 3.2 in this paper proposes a likelihood ratio test for the significance of γ=1. If the hypothesis of γ=1 is accepted, the simple bivariate model should be chosen. Firstly, we use the maximum likelihood method to estimate the parameter to obtain the likelihood function for Model (8). Table 5 shows the results of maximizing (13) in Section 3.1 by using the constrained optimization method in Matlab for the data from Trucks 1 and 2. The results are close to the Bayesian estimators in Table 4.

Table 4. Bayesian Estimator for Exponent Bivariate Model

Truck	Parameter	Estimator	$-\ln L$
Truck 1	α_1	11.210	701.2
	β_1	4.526	
	α_2	79.33	
	β_2	4.224	
	γ	0.2237	
Truck 2	α_1	15760	480.5
	β_1	5.861	
	α_2	119.3	
	β_2	5.823	
	γ	0.214	

Table 5. Maximum Likelihood Estimator for $\mathrm{g} \neq 1$

Truck	Parameter	Estimator	$-\ln L$
Truck 1	α_1	10000	700.5
	β_1	4.514	
	α_2	70.55	
	β_2	4.224	
	g	0.219	
Truck 2	α_1	15019	480.4
	β_1	6.002	
	α_2	113.9	
	β_2	5.9708	
	γ	0.2035	

At significant level α=0.98, the $\chi^2(1)$=5.41. The hypothesis T is $2\times\left(-\ln\frac{L_{\gamma\neq1}}{L_{\gamma=1}}\right)=104$ for Truck 1 and 218 for Truck 2. For both trucks, $\chi^2(1)$=5.41<5.41. The calculations are shown in Table 6. Therefore, the hypothesis is rejected for both trucks.
Conclusively, for both trucks, work load and time are not independent. The bivariate Weibull model with γ=1 is out of consideration for both trucks.

Table 6. Hypothesis Test for $\gamma = 1$

Truck	Likelihood of $\gamma = 1$	Likelihood of $\gamma \neq 1$	T	Result
Truck 1	752	700.5	103	Rejected
Truck 2	517.4	480.4	218	Rejected

A more general model selection uses the AIC (Akaike Information Criterion) and BIC (Bayes Information Criterion) [13, 29, 33]. BIC and AIC are defined as:

$$AIC = -\ln L + 2p \quad \text{and} \quad BIC = -\ln L + p\ln n \tag{27}$$

where L is the likelihood value, p is the number of parameters, and n is the data size. The model with lower AIC or BIC value is considered to be better. A complex model with more parameters has the potential to be more flexible than the simpler one to fit the data. However, the more complex model tends to have greater uncertainty. The AIC and BIC can balance the complexity and the model uncertainty. The AIC and BIC for the three models are shown in Table 7.

Table 7. BIC and AIC of Models

Truck	Model	BIC	AIC
Truck 1	Simple Model	1519.6	1512
	Model (5)	1446.3	1436.8
	Model (8)	1421.9	1412.4
Truck 2	Simple Model	1048.7	1042.8
	Model (5)	1196.0	1188.7
	Model (8)	978.1	970.8

It can be seen from Table 7 that the exponent bivariate Weibull Model (8) has the lowest BIC and AIC values for both trucks and it is therefore considered the best model among the three. The linear bivariate Weibull model has the same number of parameters in the models. However, the BIC and AIC values are higher than the exponent bivariate Weibull. The simple bivariate Weibull shows the worst performance for both trucks. This paper thus selects the exponent bivariate Weibull for both trucks.

4.4. Analysis using exponent bivariate Weibull

The model selected is the exponent bivariate Weibull Model (8). The results of parameter estimation by the Bayesian method are elaborated in Table 8. "Std" denotes the standard deviation. The lower and upper bounds of the credible interval are derived from the posterior distribution (22).

Table 8. Bayesian Parameter Estimator for Trucks with Credible Interval

Truck	Parameter	Estimator	Std	Lower	Upper
Truck 1	α_1	11210	929	10050	13430
	β_1	4.526	0.5585	3.504	5.663
	α_2	79.33	7.76	66.28	96.07
	β_2	4.224	0.5055	3.295	5.263
	γ	0.2237	0.034	0.1637	0.2972
Truck 2	α_1	15760	2143	11510	19660
	β_1	5.861	0.922	4.149	7.907
	α_2	119.3	16.59	88.03	153.6
	β_2	5.823	0.921	4.144	7.879
	γ	0.214	0.04282	0.1439	0.3031

Table 8 shows that the γ of the data for both trucks is below 0.5; the credible bounds of γ are far below 1. The results also showed the hypothesis of γ should be rejected. This result is consistent with the results from the likelihood ration test described in Table 6.

4.5. Goodness of fit test

The assumption of the data fitting the bivariate Weibull model should be validated by the goodness of fit test. The reliability function for Model (8) has the form $R(\Lambda)=\gamma\Lambda^{\gamma-1}\exp\left(-\Lambda^{\gamma}\right)$. This is a univariant Weibull distribution with scale parameter 1 and shape parameter γ. The proposed goodness of fit test is based on this special structure. Each Λ_i can be computed from the given data and the estimated

parameter. This paper proposes a simple goodness of fit test based on the plot. Let $B = \alpha_1 t^{\beta_1} + \alpha_2 s^{\beta_2}$, since:

$$\ln R(t) = -\mathrm{B}^{\gamma} \tag{28}$$

The (28) can be converted to a linear function, the linearity can be used to test goodness of fit. The $R(t)$ is approximated by median rank $R(i) = 1-(\mathrm{i}-0.3)/(\mathrm{n}+0.4)$. The B^{γ} can be calculated by using the parameters in Table 8. Some of B^{γ} are tabulated in Table 9 for Truck 1.

The task is to check whether $\ln R(t)$ and B^{γ} is a linear function of form, as y=−x. If the model fits the data, the data will scatter around the straight line y=−x. Figure 3 presents the $\ln R(t)$ against B^{γ} for Trucks 1 and 2. For Truck 1, the empirical values (red dots) are around the theoretical values (the blue line in Figure 2). For Truck 2, the empirical data deviate more from the expected value than in the case of Truck 1. The model is considered unable to fit the data for Truck 2.

Table 9. Cumulative Hazard Function and Empirical Reliability

i	1	2	3	4	5	6	7	8	9	10	..
B^{γ}	0.058	0.068	0.084	0.10	0.146	0.152	0.1607	0.1632	0.1934	0.2196	..
$\ln R(t)$	0.0142	0.035	0.0562	0.078	0.10	0.123	0.146	0.170	0.194	0.219	..

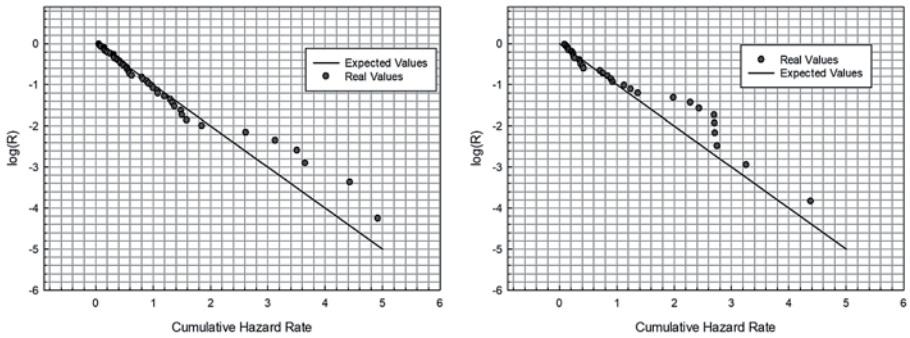

Fig. 2. Goodness of Fit Test for Truck 1 (Left) and Truck 2 (Right)

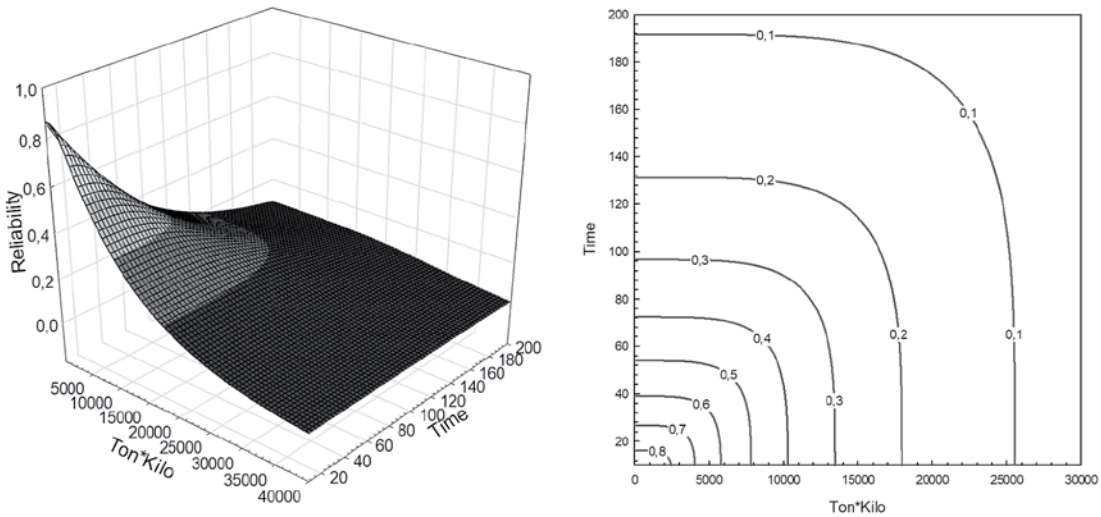

Fig. 3. Reliability Function of Mining Truck 1

4.6. Reliability evaluating

The bivariate Weibull model can be applied to the data from Truck 1. Substitute the estimated parameters into Model (8); the reliability function against calendar time and work load is:

$$\mathrm{R}(t.s) = \left((t/11{,}210)^{4.526} + \left(s/79.33\right)^{4.224}\right)^{0.2237} \tag{29}$$

Model (29) is plotted in Figure 3 in three dimensions.

Table 10. Reliability for Some Points for Truck 1

(T.S)	R	Std	Lower	Upper
(20.2000)	0.7165	0.05052	0.6129	0.8097
(100.10000)	0.2359	0.04949	0.1491	0.342
(30.10000)	0.3628	0.05484	0.2604	0.4729
(30.5000)	0.5556	0.05654	0.4438	0.6659
(300.30000)	0.02118	0.01495	0.003495	0.06009

It is usually of interest to find the reliability for a given time. The reliability and its lower and upper bounds of the credible interval are also computed by the MCMC method described in Section 3.5. Table 10 gives a demonstration of the reliability for some lifetime points.

The reliability function (29) can be further used to schedule the maintenance activities in respect of cost and available resources. This paper omits this, as the maintenance optimization is outside the paper's scope.

5. Discussion and conclusion

In the truck data, the work load and the calendar time show significant correlation. The simple bivariate Weibull model is thus not suitable for the data. In this case study, according to the AIC and BIC model selection criteria, the exponent model has the best performance, as it has the lowest AIC and BIC values. Moreover, with reference to our discussion in Section 3, the exponent model is the most general among the three models. The linear bivariate Weibull model only considers the first two orders of the exponent bivariate model. The simple bivariate model does not have the interaction part of the linear bivariate model. The exponent model is more general than the simple model and the linear model.

The reliability of the mining trucks depends on

two dimensions: calendar time and work load. The bivariate Weibull model is proposed to accommodate this two-dimensional life data for reliability modelling. Three bivariate models – simple bivariate Weibull model, linear bivariate Weibull model and the exponent bivariate model – are selected to model the reliability. The exponent model shows the best performance among the three models, and so, in the case study, the reliability model chooses the exponent model. The likelihood ratio test proposed in the paper is used to test whether the correlation of the two dimensions of the data are significant. In the case study, it found the correlation significant. If they are not correlated, the simple bivariate is preferred, as the model can be simplified and the traditional parameter estimation method can be used, since each independent variant can be considered as a univariate Weibull distribution. The case study found that the Bayesian method is effective by using the Gamma distribution as prior-distribution. The disadvantage is that obtaining the results requires simulation, which is time-consuming. Future work will focus on the development of a more efficient parameter estimation method.

References

1. Ahmed A M, Ibrahim N A. Bayesian Estimator for Weibull Distribution with Censored Data using Extension of Jeffrey Prior Information. Procd Soc Behv 2010; 8: 663-669, https://doi.org/10.1016/j.sbspro.2010.12.092.
2. Are N. LCC for Switches and Crossings at the Swedish Railway – A case study. International Journal of Condition Monitoring and Diagnostic Engineering Management 2009; 12: 10-19.
3. Barker K, Baroud H. Proportional hazards models of infrastructure system recovery. Reliab Eng Syst Safe 2014; 124: 201-206, https://doi.org/10.1016/j.ress.2013.12.004.
4. Barlow R E, Proschan F, Hunter L C. Mathematical theory of reliability. Philadelphia: SIAM, 1996, https://doi.org/10.1137/1.9781611971194.
5. Berger J O, Sun D C. Bayesian-Analysis for the Poly-Weibull Distribution. J Am Stat Assoc 1993; 88: 1412-1418, https://doi.org/10.1080/01621459.1993.10476426.
6. D.Hanagal D. A multivariate Weibull distribution. Economic Quality Control 1996; 11: 193-200.
7. Drury M R, Walker E V, Wightman DW, Bendell A. Proportional Hazards Modeling in the Analysis of Computer-Systems Reliability. Reliab Eng Syst Safe 1988; 21: 197-214, https://doi.org/10.1016/0951-8320(88)90121-4.
8. Genest C, Rivest L P. Statistical-Inference Procedures for Bivariate Archimedean Copulas. J Am Stat Assoc 1993; 88: 1034-1043, https://doi.org/10.1080/01621459.1993.10476372.
9. Hanagal D A. Bivariate Weibull regression model based on censored samples. Stat Pap 2006; 47: 137-147, https://doi.org/10.1007/s00362-005-0277-4.
10. Hougaard P. A Class of Multivariate Failure Time Distributions. Biometrika 1986; 73: 671-678, https://doi.org/10.2307/2336531.
11. Hougaard P. Modeling Multivariate Survival. Scand J Stat 1987; 14: 291-304.
12. Jack N, Iskandar B P, Murthy D N P. A repair-replace strategy based on usage rate for items sold with a two-dimensional warranty. Reliab Eng Syst Safe 2009; 94: 611-617, https://doi.org/10.1016/j.ress.2008.06.019.
13. Kim Y, Park J, Jung W, Jang I, Seong P H. A statistical approach to estimating effects of performance shaping factors on human error probabilities of soft controls. Reliab Eng Syst Safe 2015; 142: 378-387, https://doi.org/10.1016/j.ress.2015.06.004.
14. Kumar D, Klefsjo B. Proportional Hazards Model - a Review. Reliab Eng Syst Safe 1994; 44: 177-188, https://doi.org/10.1016/0951-8320(94)90010-8.
15. Kumar D, Westberg U. Proportional hazards modeling of time-dependent covariates using linear regression: A case study. IEEE T Reliab 1996; 45: 386-392, https://doi.org/10.1109/24.536990.
16. Kundu D, Gupta A K. Bayes estimation for the Marshall-Olkin bivariate Weibull distribution. Comput Stat Data An 2013; 57: 271-281, https://doi.org/10.1016/j.csda.2012.06.002.
17. Lee L. Multivariate Distributions Having Weibull Properties. J Multivariate Anal 1979; 9: 267-277, https://doi.org/10.1016/0047-259X(79)90084-8.
18. Leira B J. A comparison of some multivariate weibull distributions. Proceedings of the ASME 2010 29th Internatinal conference on Ocean, offshore and arctic Engineering, 2010, Shanghai, China, https://doi.org/10.1115/OMAE2010-20678.
19. Lu J-C. Bayes Paramter Estimation for the Bivariate Weibull Model of Marshall-Olkin for censored data. Ieee T Reliab 1992; 41: 608-615, https://doi.org/10.1109/24.249597.
20. Lu J C, Bhattacharyya G K. Some New Constructions of Bivariate Weibull Models. Ann I Stat Math 1990; 42: 543-559, https://doi.org/10.1007/BF00049307.
21. Lunn D, Jackson C, Best N, Thomas A, Spiegelhalter D. The BUGS book : a practical introduction to Bayesian analysis. London: CRC Press, 2013.
22. Lynch S M. Introduction to applied Bayesian statistics and estimation for social scientists. New York: Springer, 2007, https://doi.org/10.1007/978-0-387-71265-9.
23. Marshall A W, Olkin I. A Multivariate Exponential Distribution. J Am Stat Assoc 1967; 62: 30-44, https://doi.org/10.1080/01621459.1967.10482885.
24. Meeker WQ, Escobar LA (1998) Statistical methods for reliability data. New York: Wiley,1998.
25. Mostafa B, Celeux G. Bayesian estimation of a Weibull distribution in a highly censored and small sample setting. Institut National De Recherche En Informatque Et Automatique. 1996.
26. Murthy D N P, Xie M, Jiang R. Weibull models. J. New Jersey: Wiley, 2004.
27. Nelsen RB. Copulas and quasi-copulas: An introduction to their properties and applications. Logical, Algebraic, Analytic, and Probabilistic Aspects of Triangular Norms 2005; 391-413.
28. Hryniewicz O, Kaczmarek K, Nowak P. Bayes statistical decisions with random fuzzy data – an application for the Weibull distribution. Eksploatacja i Niezawodnosc – Maintenance and Reliability 2015; 17 (4): 610–616, http://dx.doi.org/10.17531/ein.2015.4.18.
29. Posada D, Buckley T R. Model selection and model averaging in phylogenetics: Advantages of akaike information criterion and Bayesian

approaches over likelihood ratio tests. Syst Biol 2004; 53: 793-808, https://doi.org/10.1080/10635150490522304.
30. Roy D. Classification of Life Distributions in Multivariate Models. IEEE T Reliab 1994; 43: 445-445, https://doi.org/10.1109/24.294995.
31. Roy D, Mukherjee S P. Multivariate extensions of univariate life distributions. J Multivariate Anal 1998; 67: 72-79, https://doi.org/10.1006/jmva.1998.1754.
32. Ryu K. An extension of Marshall and Olkin multivariate exponential distribution. Journal of American Statistical Association 1993; 88: 1458–1465, https://doi.org/10.1080/01621459.1993.10476434
33. Sarhan A M, Hamilton D C, Smith B. Statistical analysis of competing risks models. Reliab Eng Syst Safe 2010; 95: 953-962, https://doi.org/10.1016/j.ress.2010.04.006.
34. Wen M-J, Lee C K. A. Multivariate Weibull Distribution. Pakistan Journal of Statistical operation research 2009; 5: 55-66.

Yuan FUQING
Abbas BARABADI
Lu JINMEI
Department of Engineering and Safety
University of Tromsø
N-9037 Tromsø, Norway

E-Mails: yuan.fuqing@uit.no, abbas.b.abadi@uit.no, jinmei.lu@uit.no

INFORMATION FOR AUTHORS

Eksploatacja i Niezawodnosc – Maintenance and Reliability – the journal of the Polish Maintenance Society, under the scientific supervision of the Polish Academy of Sciences (Branch in Lublin), published four times a year.

The scope of the Quarterly

The quarterly *Eksploatacja i Niezawodnosc – Maintenance and Reliability* publishes articles containing original results of experimental research on the durability and reliability of technical objects. We also accept papers presenting theoretical analyses supported by physical interpretation of causes or ones that have been verified empirically. *Eksploatacja i Niezawodność – Maintenance and Reliability* also publishes articles on innovative modeling approaches and research methods regarding the durability and reliability of objects.

The following research areas are particularly relevant to the journal:

1. degradation processes of mechanical and biomechanical systems,
2. diagnosis and prognosis of operational malfunctions and failures.
3. analysis of failure risk/wear,
4. reliability-and-environmental-safety engineering in the design, manufacturing and maintenance of objects,
5. management and rationalization of object maintenance,
6. risk management in the processes of operation and maintenance,
7. the human factor and human reliability in operation and maintenance systems.

Terms and Conditions of Publication

The quarterly *Eksploatacja i Niezawodnosc – Maintenance and Reliability* publishes only original papers written in English or in Polish with an English translation. Translation into English is done by the Authors after they have received information from the Editorial Office about the outcome of the review process and have introduced the necessary modifications in accordance with the suggestions of the referees! Acceptance of papers for publication is based on two independent reviews commissioned by the Editor.

The quarterly *Eksploatacja i Niezawodnosc – Maintenance and Reliability* proceeds entirely online at submission.ein.org.pl

Technical requirements

- After receiving positive reviews and after acceptance of the paper for publication, the text must be submitted in a Microsoft Word document format.
- Drawings and photos should be additionally submitted in the form of high resolution separate graphical files in the TIFF, SVG, AI or JPG formats.
- A manuscript should include: names of authors, title, abstract, and key words that should complement the title and abstract (in Polish and in English), the text in Polish and in English with a clear division into sections (please, do not divide words in the text); tables, drawings, graphs, and photos included in the text should have descriptive two-language captions, if this can be avoided, no formulae and symbols should be inserted into text paragraphs by means of a formula editor; references (written in accordance with the required reference format); author data – first names and surnames along with scientific titles, affiliation, address, phone number, fax, and e-mail address.

The Editor reserves the right to abridge and adjust the manuscripts. All submissions should be accompanied by a submission form.

Detailed instructions to Authors, including evaluation criteria can be found on the journal's website: www.ein.org.pl

Editor contact info

Editorial Office of „Eksploatacja i Niezawodnosc - Maintenance and Reliability"
Nadbystrzycka 36, 20-618 Lublin, Poland
e-mail: office@ein.org.pl

INFORMATION FOR SUBSCRIBERS

Fees

Yearly subscription fee (four issues) is 100 zloty and includes delivery costs. Subscribers receive any additional special issues published during their year of subscription free of charge.

Orders

Subscription orders along with authorization to issue a VAT invoice without receiver's signature should be sent to the Editor's address.

Note

In accordance with the requirements of citation databases, proper citation of publications appearing in our Quarterly should include the full name of the journal in Polish and English without Polish diacritical marks, i.e.,

Eksploatacja i Niezawodnosc – Maintenance and Reliability.

Wydawca:
Polskie Naukowo Techniczne
Towarzystwo Eksploatacyjne
Warszawa

Publisher:
Polish Maintenance Society
Warsaw

Członek:
Europejskiej Federacji
Narodowych Towarzystw
Eksploatacyjnych

Member of:
European Federation of National
Maintenance Societies

Patronat naukowy:
Polska Akademia Nauk
Oddział Lublin

Scientific Supervision:
Polish Academy of Sciences
Branch in Lublin